

MSC-PA-R-68-1



75N741050

NATIONAL AERONAUTICS AND SPACE ADMINISTRATION

Copy No. 259

EB (2)

Travis

EB3 (9)

EB2 (2)

EB5

Rec'd 4/15/68

## APOLLO 4 MISSION REPORT

CLASSIFICATION CHANGED TO

**UNCLASSIFIED**BY AUTHORITY OF Memo, MSC,Bm4/R.C. Puffer, 12-12-69DATE SEP 20 1971 en

## GROUP 4

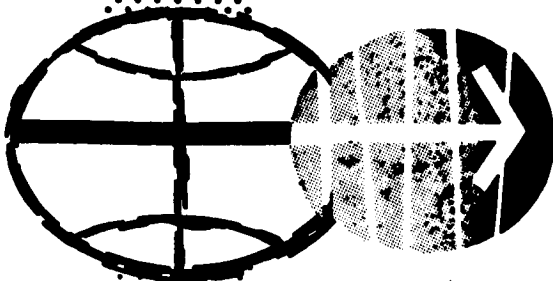
Downgraded at 3-year  
intervals; declassified  
after 12 years

## CLASSIFIED DOCUMENT - TITLE UNCLASSIFIED

This material contains information affecting the national defense of the United States within the meaning of the espionage laws, Title 18, U.S.C., Secs. 793 and 794, the transmission or revelation of which in any manner to an unauthorized person is prohibited by law.

## DISTRIBUTION AND REFERENCING

This paper is not suitable for general distribution or referencing. It may be referenced only in other working correspondence and documents by participating organizations.



MANNED SPACECRAFT CENTER

HOUSTON, TEXAS

January 1968

EB-68-1/13

~~CONFIDENTIAL~~

APOLLO SPACECRAFT FLIGHT HISTORY

<u>Mission</u>	<u>Spacecraft</u>	<u>Description</u>	<u>Launch date</u>	<u>Launch site</u>
PA-1	BP-6	First pad abort	Nov. 7, 1963	White Sands Missile Range, N. Mex.
A-001	BP-12	Transonic abort	May 13, 1964	White Sands Missile Range, N. Mex.
AS-101	BP-13	Nominal launch and exit environment	May 28, 1964	Cape Kennedy, Fla.
AS-102	BP-15	Nominal launch and exit environment	Sept. 18, 1964	Cape Kennedy, Fla.
A-002	BP-23	Maximum dynamic pressure abort	Dec. 8, 1964	White Sands Missile Range, N. Mex.
AS-103	BP-16	Micrometeoroid experiment	Feb. 16, 1965	Cape Kennedy, Fla.
A-003	BP-22	Low-altitude abort (planned high- altitude abort)	May 19, 1965	White Sands Missile Range, N. Mex.
AS-104	BP-26	Micrometeoroid experiment and service module RCS launch environment	May 25, 1965	Cape Kennedy, Fla.
PA-2	BP-23A	Second pad abort	June 29, 1965	White Sands Missile Range, N. Mex.
AS-105	BP-9A	Micrometeoroid experiment and service module RCS launch environment	July 30, 1965	Cape Kennedy, Fla.
A-004	SC-002	Power-on tumbling boundary abort	Jan. 20, 1966	White Sands Missile Range, N. Mex.
AS-201	SC-009	Supercircular entry with high heat rate	Feb. 26, 1966	Cape Kennedy, Fla.
AS-202	SC-011	Supercircular entry with high heat load	Aug. 25, 1966	Cape Kennedy, Fla.
Apollo 4	SC-017 LTA-10R	Supercircular entry at lunar return velocity	Nov. 9, 1967	Cape Kennedy, Fla.

~~CONFIDENTIAL~~



APOLLO 4 MISSION REPORT

CLASSIFICATION CHANGED TO  
**UNCLASSIFIED**  
BY AUTHORITY OF \_\_\_\_\_

DATE SEP 20 1971

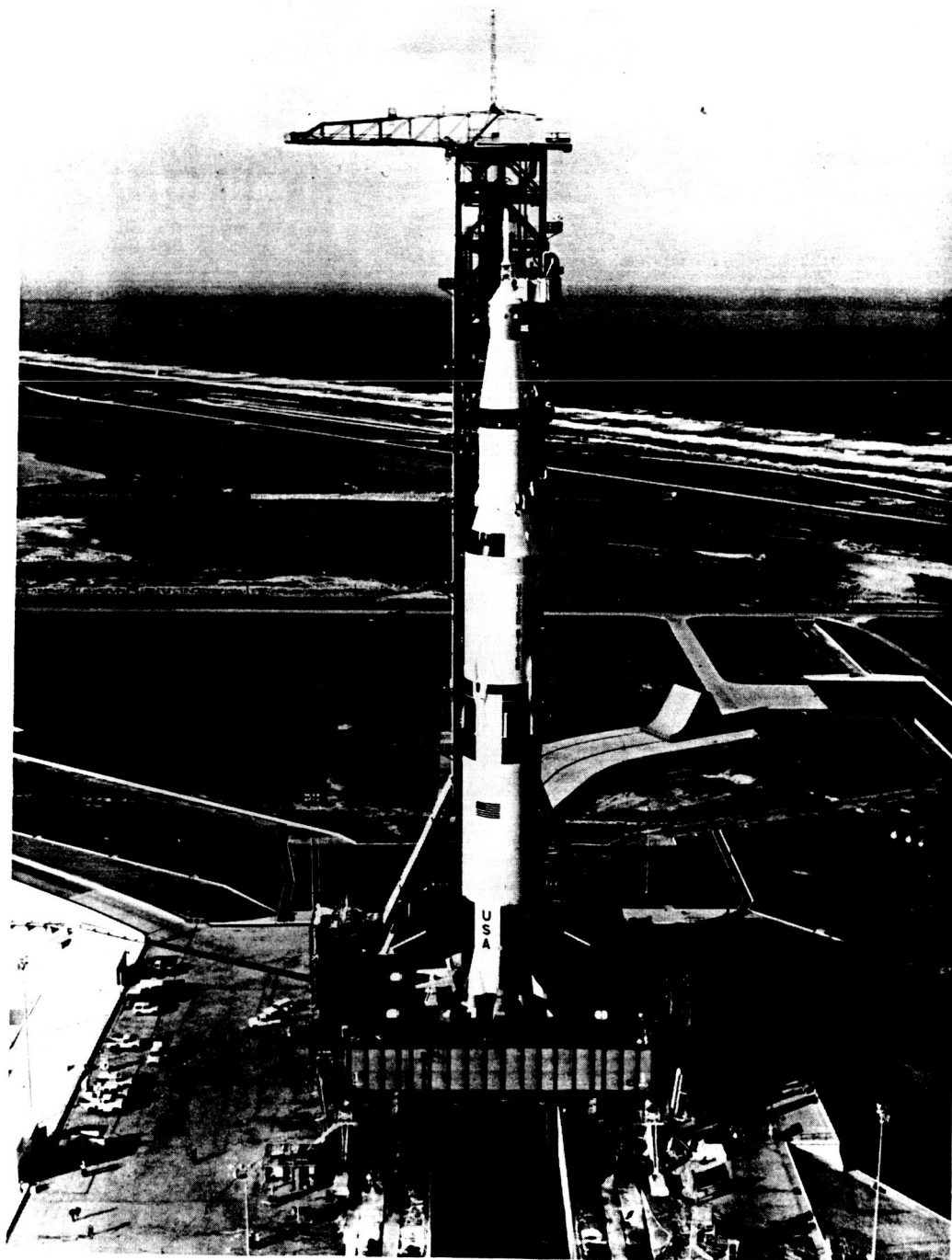
Prepared by: Apollo 4 Mission Evaluation Team

Approved by:

George M. Low  
George M. Low  
Manager  
Apollo Spacecraft Program

NATIONAL AERONAUTICS AND SPACE ADMINISTRATION  
MANNED SPACECRAFT CENTER  
HOUSTON, TEXAS  
January 7, 1968

~~CONFIDENTIAL~~



APOLLO 4 SPACE VEHICLE.

~~CONFIDENTIAL~~

~~CONFIDENTIAL~~

iii

CONTENTS

Section		Page
	TABLES . . . . .	
	FIGURES . . . . .	
1.0	<u>MISSION SUMMARY</u> . . . . .	1-1
2.0	<u>MISSION DESCRIPTION AND OBJECTIVES</u> . . . . .	2-1
2.1	MISSION DESCRIPTION . . . . .	2-1
2.2	MISSION OBJECTIVES . . . . .	2-4
3.0	<u>TRAJECTORY DATA</u> . . . . .	3-1
3.1	APOLLO 4 MISSION . . . . .	3-1
3.1.1	Launch . . . . .	3-1
3.1.2	Parking Orbit . . . . .	3-1
3.1.3	Coast Ellipse . . . . .	3-3
3.1.4	Entry . . . . .	3-6
3.2	DUAL MISSION . . . . .	3-35
4.0	<u>LAUNCH VEHICLE PERFORMANCE</u> . . . . .	4-1
5.0	<u>COMMAND AND SERVICE MODULE PERFORMANCE</u> . . . . .	5.1-1
5.1	SPACECRAFT STRUCTURE . . . . .	5.1-1
5.1.1	Spacecraft Interface Loads . . . . .	5.1-1
5.1.2	Mission Phase Loads . . . . .	5.1-2
5.1.3	Spacecraft Modifications . . . . .	5.1-4
5.1.4	Internal Loads . . . . .	5.1-5
5.1.5	Low Frequency Vibration . . . . .	5.1-8
5.1.6	High Frequency Vibrations . . . . .	5.1-9

~~CONFIDENTIAL~~

~~CONFIDENTIAL~~

Section	Page
5.2 AERODYNAMICS . . . . .	5.2-1
5.2.1 Summary . . . . .	5.2-1
5.2.2 Aerodynamics Predictions . . . . .	5.2-1
5.2.3 Flight-Derived Aerodynamics . . . . .	5.2-2
5.2.4 Comparison of Predictions With Flight-Derived Aerodynamic Data . .	5.2-2
5.3 THERMAL STRUCTURES . . . . .	5.3-1
5.3.1 Launch Phase . . . . .	5.3-1
5.3.2 Orbital Flight . . . . .	5.3-3
5.4 AEROTHERMODYNAMICS AND HEAT PROTECTION SUBSYSTEM . . . . .	5.4-1
5.4.1 Aerothermodynamics . . . . .	5.4-1
5.4.2 Heat Protection Subsystem . . . . .	5.4-6
5.5 EARTH LANDING SUBSYSTEM (ELS) . . . . .	5.5-1
5.5.1 Performance . . . . .	5.5-1
5.5.2 Postflight Test Activity . . . . .	5.5-2
5.6 MECHANICAL SUBSYSTEMS . . . . .	5.6-1
5.6.1 Summary . . . . .	5.6-1
5.6.2 Performance . . . . .	5.6-1
5.7 ELECTRICAL POWER SUBSYSTEM . . . . .	5.7-1
5.8 FUEL CELLS . . . . .	5.8-1
5.8.1 Summary . . . . .	5.8-1
5.8.2 Prelaunch Operation . . . . .	5.8-1
5.8.3 Performance . . . . .	5.8-1

~~CONFIDENTIAL~~

~~CONFIDENTIAL~~

v

Section	Page
5.9 SEQUENTIAL EVENTS CONTROL SUBSYSTEM . . . . .	5.9-1
5.10 PYROTECHNIC SUBSYSTEM . . . . .	5.10-1
5.11 LAUNCH ESCAPE SUBSYSTEM . . . . .	5.11-1
5.12 EMERGENCY DETECTION SUBSYSTEM . . . . .	5.12-1
5.12.1 Summary . . . . .	5.12-1
5.12.2 Description . . . . .	5.12-1
5.12.3 Performance . . . . .	5.12-1
5.13 COMMUNICATIONS SYSTEM PERFORMANCE . . . . .	5.13-1
5.13.1 Summary . . . . .	5.13-1
5.13.2 Communications Subsystem Performance . . . . .	5.13-2
5.13.3 Performance During Launch Phase . . .	5.13-4
5.13.4 Performance During Near-Earth Parking Orbit . . . . .	5.13-8
5.13.5 Performance During Translunar Injection and High Ellipse Phase . .	5.13-11
5.14 INSTRUMENTATION . . . . .	5.14-1
5.15 GUIDANCE AND CONTROL SUBSYSTEM . . . . .	5.15-1
5.15.1 Summary . . . . .	5.15-1
5.15.2 Integrated Subsystem Performance . . .	5.15-1
5.15.3 Guidance and Navigation Subsystem Performance . . . . .	5.15-7
5.15.4 Stabilization and Control Subsystem Performance . . . . .	5.15-10
5.15.5 Mission Control Programmer Performance . . . . .	5.15-11

~~CONFIDENTIAL~~

~~CONFIDENTIAL~~

Section	Page
5.16 REACTION CONTROL SUBSYSTEM . . . . .	5.16-1
5.16.1 Service Module Reaction Control Subsystem . . . . .	5.16-1
5.16.2 Command Module Reaction Control Subsystem . . . . .	5.16-6
5.17 SERVICE PROPULSION SUBSYSTEM . . . . .	5.17-1
5.17.1 Subsystem Description . . . . .	5.17-1
5.17.2 Propellant Loading . . . . .	5.17-2
5.17.3 Service Propulsion Subsystem Mission Description . . . . .	5.17-2
5.17.4 Steady-State Performance and Analysis . . . . .	5.17-3
5.17.5 Normalized Performance . . . . .	5.17-5
5.17.6 Gauging Subsystem Analysis . . . . .	5.17-5
5.17.7 Pressurization Subsystems . . . . .	5.17-6
5.17.8 Engine Transient Analysis . . . . .	5.17-7
5.18 CRYOGENIC SUBSYSTEM . . . . .	5.18-1
5.18.1 Summary . . . . .	5.18-1
5.18.2 Prelaunch Operations . . . . .	5.18-1
5.18.3 Performance . . . . .	5.18-2
5.19 ENVIRONMENTAL CONTROL SUBSYSTEM . . . . .	5.19-1
5.19.1 Launch Phase . . . . .	5.19-1
5.19.2 Earth Orbital Phase . . . . .	5.19-2
5.19.3 Entry Phase . . . . .	5.19-3
5.19.4 Postrecovery Observations . . . . .	5.19-4

~~CONFIDENTIAL~~

Section	Page
5.20 CREW STATION PERFORMANCE . . . . .	5.20-1
5.20.1 Crew Visibility . . . . .	5.20-1
5.20.2 Crew Related Dynamics . . . . .	5.20-3
5.20.3 Radiation Monitoring . . . . .	5.20-4
6.0 <u>LUNAR MODULE TEST ARTICLE</u> . . . . .	6-1
6.1 STRUCTURE . . . . .	6-1
6.1.1 Loads . . . . .	6-1
6.1.2 Low Frequency Vibration . . . . .	6-2
6.1.3 Vibro-Acoustics . . . . .	6-3
6.2 INSTRUMENTATION . . . . .	6-21
7.0 <u>FLIGHT CREW</u> . . . . .	7-1
8.0 <u>BIOMEDICAL EVALUATION</u> . . . . .	8-1
9.0 <u>MISSION SUPPORT</u> . . . . .	9-1
9.1 FLIGHT CONTROL . . . . .	9-1
9.1.1 Prelaunch . . . . .	9-1
9.1.2 Launch Phase . . . . .	9-3
9.1.3 Earth Orbit - Revolution 1 . . . . .	9-4
9.1.4 Earth Orbit - Revolution 2 . . . . .	9-5
9.1.5 Translunar Injection - Revolution 3 . . . . .	9-6
9.1.6 Entry . . . . .	9-10
9.2 NETWORK PERFORMANCE . . . . .	9-11
9.2.1 Apollo/Range Instrumentation Aircraft . . . . .	9-11

~~CONFIDENTIAL~~

Section		Page
	9.2.2 Telemetry . . . . .	9-11
	9.2.3 Tracking . . . . .	9-11
	9.2.4 Command . . . . .	9-12
	9.2.5 Goddard Space Flight Center Central Processors . . . . .	9-13
	9.2.6 Real Time Computer Complex . . . . .	9-13
9.3	RECOVERY OPERATIONS . . . . .	9-15
	9.3.1 Recovery Force Deployment . . . . .	9-15
	9.3.2 Spacecraft Location and Retrieval . . . . .	9-16
	9.3.3 Recovery Force Electronic Reception . . . . .	9-18
	9.3.4 Spacecraft Recovery Inspection . . . . .	9-20
	9.3.5 Spacecraft Deactivation . . . . .	9-22
	9.3.6 S-IC and Camera Capsule Recovery . . . . .	9-22
10.0	<u>EXPERIMENTS</u> . . . . .	10-1
11.0	<u>CONCLUSIONS</u> . . . . .	11-1
12.0	<u>ANOMALY SUMMARY AND POSTFLIGHT TESTING</u> . . . . .	12-1
	12.1 MISSION ANOMALIES . . . . .	12-1
	12.2 COUNTDOWN ANOMALIES . . . . .	12-6
	12.3 TEST AND CHECKOUT ANOMALIES . . . . .	12-7
	12.4 POSTFLIGHT TESTING . . . . .	12-8
	12.4.1 Heat Protection Subsystem . . . . .	12-8
	12.4.2 Earth Landing Subsystem . . . . .	12-8

~~CONFIDENTIAL~~



~~CONFIDENTIAL~~

ix

Section		Page
	12.4.3 Mechanical Subsystems . . . . .	12-8
	12.4.4 Electrical Power Subsystem . . . . .	12-8
	12.4.5 Environmental Control Subsystem . . . . .	12-9
	12.4.6 Communications . . . . .	12-9
	12.4.7 Pyrotechnics . . . . .	12-9
	12.4.8 Instrumentation . . . . .	12-9
	12.4.9 Guidance and Control Subsystems . . . . .	12-10
	12.4.10 Reaction Control Subsystem . . . . .	12-10
13.0	<u>VEHICLE AND SYSTEMS DESCRIPTION</u> . . . . .	13-1
13.1	COMMAND AND SERVICE MODULE . . . . .	13-3
	13.1.1 Structures . . . . .	13-3
	13.1.2 Earth Landing System . . . . .	13-4
	13.1.3 Mechanical Subsystem . . . . .	13-5
	13.1.4 Electrical Power Subsystem . . . . .	13-7
	13.1.5 Sequential Events Control Subsystem . . . . .	13-9
	13.1.6 Pyrotechnic Devices . . . . .	13-10
	13.1.7 Emergency Detection Subsystem . . . . .	13-10
	13.1.8 Communications Subsystem . . . . .	13-11
	13.1.9 Instrumentation Subsystem . . . . .	13-11
	13.1.10 Guidance and Control . . . . .	13-12
	13.1.11 Reaction Control Subsystem . . . . .	13-15
	13.1.12 Service Propulsion Subsystem . . . . .	13-17
	13.1.13 Environmental Control Subsystem . . . . .	13-18

~~CONFIDENTIAL~~

~~CONFIDENTIAL~~

Section	Page
13.2 LUNAR MODULE TEST ARTICLE . . . . .	13-40
13.2.1 General Description . . . . .	13-40
13.2.2. Instrumentation and Communication . . . . .	13-40
13.3 LAUNCH VEHICLE DESCRIPTION . . . . .	13-43
13.4 WEIGHT AND BALANCE DATA . . . . .	13-47
14.0 <u>SPACECRAFT HISTORIES</u> . . . . .	14-1
14.1 COMMAND MODULE AND SERVICE MODULE . . . . .	14-1
14.2 LUNAR MODULE TEST ARTICLE . . . . .	14-4
15.0 <u>REFERENCES</u> . . . . .	15-1
16.0 <u>DISTRIBUTION</u> . . . . .	16-1

~~CONFIDENTIAL~~

~~CONFIDENTIAL~~

xi

TABLES

Table		Page
2.1-I	APOLLO 4 MISSION EVENTS . . . . .	2-3
2.2-I	DETAILED TEST OBJECTIVES . . . . .	2-5
3.1-I	LAUNCH PHASE PLANNED AND ACTUAL TRAJECTORY PARAMETERS . . . . .	3-7
3.1-II	PARKING ORBIT PLANNED AND ACTUAL TRAJECTORY PARAMETERS . . . . .	3-9
3.1-III	ORBITAL ELEMENTS . . . . .	3-11
3.1-IV	REVOLUTION 1 TRACKING RESIDUAL STATISTICS . . . . .	3-12
3.1-V	REVOLUTION 2 TRACKING RESIDUAL STATISTICS . . . . .	3-13
3.1-VI	COAST ELLIPSE PLANNED AND ACTUAL TRAJECTORY PARAMETERS . . . . .	3-14
3.1-VII	COAST ELLIPSE TRACKING RESIDUAL STATISTICS . . . . .	3-18
3.1-VIII	SPS THRUST AND TARGETING CHARACTERISTICS . . . . .	3-19
3.1-IX	ENTRY INTERFACE PLANNED AND ACTUAL TRAJECTORY PARAMETERS . . . . .	3-20
3.1-X	SUMMARY OF PLANNED AND ACTUAL TRAJECTORY PARAMETERS . . . . .	3-21
5.1-I	MAXIMUM LATERAL LOAD CONDITIONS . . . . .	5.1-10
5.1-II	MAXIMUM SPACECRAFT LOADS AT MAXIMUM $q\alpha$ . . . . .	5.1-11
5.1-III	MAXIMUM SPACECRAFT LOADS AT END OF FIRST-STAGE BOOST . . . . .	5.1-12
5.1-IV	LAUNCH ESCAPE SYSTEM AND COMMAND MODULE LOW FREQUENCY VIBRATION DURING FIRST-STAGE LAUNCH AND BOOST . . . . .	5.1-13
5.2-I	COMMAND MODULE AERODYNAMICS-PREFLIGHT PREDICTIONS . . . . .	5.2-4

~~CONFIDENTIAL~~

~~CONFIDENTIAL~~

Table		Page
5.4-I	LOCATIONS AND RANGES OF PRESSURE SENSORS, CALORIMETERS, AND RADIOMETERS . . . . .	5.4-12
5.4-II	TABLE OF HEAT SHIELD COMPONENT AND EQUIPMENT THERMAL RESPONSE . . . . .	5.4-15
5.4-III	AFT HEAT SHIELD ABLATOR DATA . . . . .	5.4-18
5.4-IV	HEAT SHIELD BONDLINE TEMPERATURES . . . . .	5.4-19
5.8-I	SUMMARY OF FUEL CELL HYDROGEN COMSUMPTION AND WATER PRODUCTION . . . . .	5.8-4
5.13-I	COMMAND EVENTS - BERMUDA AND THE U.S.N.S. VANGUARD . . . . .	5.13-17
5.15-I	STATE VECTOR COMPARISON . . . . .	5.15-13
5.15-II	SERVICE PROPULSION SUBSYSTEM GIMBAL TRIM VALUES . . . . .	5.15-14
5.15-III	COMPARISON OF ATTAINED ORBIT WITH TARGET DURING FIRST SPS BURN . . . . .	5.15-15
5.15-IV	COMPARISON OF ATTAINED ORBIT WITH TARGET DURING SECOND SPS BURN . . . . .	5.15-16
5.15-V	APOLLO GUIDANCE COMPUTED ENTRY NAVIGATION AND GUIDANCE RECONSTRUCTION . . . . .	5.15-17
5.15-VI	PRELIMINARY IMU ERROR COEFFICIENTS . . . . .	5.15-18
5.15-VII	APOLLO GUIDANCE COMPUTER ENTRY NAVIGATION ACCURACY . . . . .	5.15-19
5.15-VIII	INERTIAL MEASUREMENT UNIT PREFLIGHT PERFORMANCE SUMMARY . . . . .	5.15-20
5.15-IX	COMPARISON OF INFLIGHT ACCELEROMETER BIAS WITH PREFLIGHT COMPENSATION . . . . .	5.15-21
5.15-X	APOLLO GUIDANCE COMPUTER MAJOR MODE TIMELINE . . .	5.15-22
5.15-XI	SCS PARAMETER COMPARISON . . . . .	5.15-24

~~CONFIDENTIAL~~

~~CONFIDENTIAL~~

xiii

Table		Page
5.16-I	HELIUM AND PROPELLANT SERVICING . . . . .	5.16-10
5.16-II	RCS SEQUENCE OF EVENTS . . . . .	5.16-11
5.16-III	TYPICAL MANEUVER ACCELERATIONS AND TRANSLATION VELOCITY CHANGES . . . . .	5.16-13
5.16-IV	SERVICE MODULE REACTION CONTROL SUBSYSTEM PROPELLANT CONSUMPTION, ENGINE BURN TIMES, NUMBER OF PULSES, DUTY CYCLES, AND PRESSURE DROPS PER MANEUVER . . . . .	5.16-14
5.16-V	SM-RCS LAUNCH HEATING SUMMARY . . . . .	5.16-18
5.16-VI	SUMMARY OF SM-RCS TEMPERATURES FROM CSM/S-IVB SEPARATION THROUGH CM/SM SEPARATION . . . . .	5.16-19
5.16-VII	THERMAL CONTROL SUBSYSTEM PERFORMANCE SUMMARY DURING COLD-SOAK PERIOD (03:29:00 TO 08:01:00) . . . . .	5.16-20
5.16-VIII	TYPICAL CM-RCS CONTROL CROSS-COUPLING EFFECTS . . .	5.16-21
5.16-IX	CM-RCS PRESSURE TRENDS . . . . .	5.16-22
5.16-X	COMMAND MODULE REACTION CONTROL SUBSYSTEM PROPELLANT CONSUMPTION, ENGINE BURN TIMES, NUMBER OF PULSES, DUTY CYCLES, AND PRESSURE DROPS PER MANEUVER . . . . .	5.16-23
5.16-XI	COMMAND MODULE REACTION SUBSYSTEM THERMAL PERFORMANCE SUMMARY . . . . .	5.16-24
5.17-I	FLIGHT DATA USED IN THE ANALYSIS PROGRAM . . . . .	5.17-8
5.17-II	SERVICE PROPULSION SUBSYSTEM PERFORMANCE SUMMARY, APOLLO 4 MISSION . . . . .	5.17-9
5.17-III	SERVICE PROPULSION SUBSYSTEM ENGINE TRANSIENT ANALYSIS SUMMARY . . . . .	5.17-10
5.20-I	SPACECRAFT WINDOW RESOLUTION CHARACTERISTICS . . .	5.20-6
6.1-I	LUNAR MODULE LOW FREQUENCY VIBRATION DURING FIRST STAGE LAUNCH AND BOOST . . . . .	6-7

~~CONFIDENTIAL~~

~~CONFIDENTIAL~~

Table		Page
9.3-I	RECOVERY SUPPORT . . . . .	9-24
12.4-I	ASHUR's FOR POSTFLIGHT ANOMALY TESTING . . . . .	12-11
13.4-I	SPACECRAFT MASS PROPERTIES AT LAUNCH AND DURING ORBITAL FLIGHT . . . . .	13-49
13.4-II	COMMAND MODULE MASS PROPERTIES AT ENTRY . . . . .	13-52

~~CONFIDENTIAL~~

~~CONFIDENTIAL~~

xv

FIGURES

Figure		Page
3.1-1	Apollo 4 mission ground track . . . . .	3-22
3.1-2	Time history of the launch phase	
	(a) Latitude, longitude, and altitude . . . . .	3-23
	(b) Space-fixed flight-path angle and velocity . . . . .	3-24
	(c) Earth-fixed flight-path angle and velocity . . . . .	3-25
	(d) Mach number and dynamic pressure . . . . .	3-26
3.1-3	Orbital time history of space-fixed flight-path angle, velocity, and altitude	
	(a) Parking orbit . . . . .	3-27
	(b) Coast ellipse . . . . .	3-28
3.1-4	Service propulsion subsystem burn time history of space-fixed flight-path angle, velocity, and altitude	
	(a) First service propulsion subsystem burn . . .	3-29
	(b) Second service propulsion subsystem burn . . .	3-30
3.1-5	Time history of entry phase	
	(a) Latitude, longitude, altitude . . . . .	3-31
	(b) Space-fixed flight-path angle and velocity . . . . .	3-32
	(c) Earth-fixed flight-path angle and velocity . . . . .	3-33
	(d) Load factor . . . . .	3-34
5.1-1	Launch escape system and command module accelerometer locations . . . . .	5.1-14
5.1-2	S-IC engine thrust build-up . . . . .	5.1-15
5.1-3	Spacecraft accelerations at lift-off	
	(a) LA0011A, LA0012A, and CA0001A . . . . .	5.1-16
	(b) CA0007A, CK0036A, and CK0037A . . . . .	5.1-17

~~CONFIDENTIAL~~

~~CONFIDENTIAL~~

Figure		Page
5.1-4	Launch winds	
	(a) Launch winds magnitude . . . . .	5.1-18
	(b) Launch winds direction . . . . .	5.1-19
5.1-5	Comparison of maximum $q\alpha$ command module/service module interface loads with structural capabilities . . . . .	5.1-20
5.1-6	Comparison of maximum $q\alpha$ service module/spacecraft lunar module adapter interface loads with structural capabilities . . . . .	5.1-21
5.1-7	Comparison of maximum $q\alpha$ spacecraft lunar module/instrument unit interface loads with structural capabilities . . . . .	5.1-22
5.1-8	Launch escape tower lateral oscillations during first-stage boost . . . . .	5.1-23
5.1-9	Spacecraft accelerations during high axial acceleration oscillation period	
	(a) LA0011A, LA0012A, and CA0001A . . . . .	5.1-24
	(b) CA0007A, CA0036A, and CK0037A . . . . .	5.1-25
5.1-10	Spacecraft accelerations at first-stage end of boost	
	(a) LA0011A, LA0012A, and LA0001A . . . . .	5.1-26
	(b) CA0007A, CK0036A, and CK0037A . . . . .	5.1-27
5.1-11	Spacecraft accelerations during S-IC/S-II separation	
	(a) LA0011A, LA0012A, and CA0001A . . . . .	5.1-28
	(b) CA0007A, CK0037A, and CK0036A . . . . .	5.1-29
5.1-12	Typical command module/service module tension tie strain gauge location . . . . .	5.1-30
5.1-13	SLA structural measurement locations . . . . .	5.1-31

~~CONFIDENTIAL~~



~~CONFIDENTIAL~~

xvii

Figure	Page
5.1-14	Command module acceleration spectral density
(a)	Prior to ignition . . . . . 5.1-32
(b)	Maximum vibration from 85.0 to 87.5 seconds . . 5.1-33
5.1-15	Comparison of command module internal equipment bay's (Block I) vibration criteria to measured vibration during atmospheric flight . . . . . 5.1-34
5.1-16	Service module acceleration spectral density
(a)	Prior to ignition . . . . . 5.1-35
(b)	Maximum vibration from 77.0 to 79.0 seconds . . 5.1-36
5.1-17	Comparison of service module aft bulkhead vibration criteria to measured vibration during atmospheric flight . . . . . 5.1-37
5.2-1	Command module external configuration . . . . . 5.2-5
5.2-2	Aerodynamic correlation parameters
(a)	Mach number . . . . . 5.2-6
(b)	Reynolds number per foot . . . . . 5.2-7
5.2-3	Command module total lift-to-drag ratio . . . . . 5.2-8
5.2-4	Command module total angle-of-attack . . . . . 5.2-9
5.3-1	Location of service module inner skin thermocouples . . . . . 5.3-6
5.3-2	Peak temperatures measured on spacecraft lunar module adapter outer surface during the launch phase . . 5.3-7
5.3-3	Temperature measured by spacecraft lunar module adaptor sensor AA7863T . . . . . 5.3-8
5.3-4	Temperature measured by spacecraft lunar module adaptor sensor AA7864T . . . . . 5.3-9
5.3-5	Outer surface temperatures of the spacecraft lunar module adapter at S-IC outboard engine cutoff . . 5.3-10

~~CONFIDENTIAL~~

~~CONFIDENTIAL~~

Figure		Page
5.3-6	Temperature sensor locations on command module and predicted maximum temperatures . . . . .	5.3-11
5.3-7	Forward and side heat shield measurement locations and values just prior to entry . . . . .	5.3-12
5.3-8	Spacecraft attitude referenced to the sun during cold-soak period . . . . .	5.3-13
5.3-9	Temperature measured by command module sensor CA1502T during cold-soak period . . . . .	5.3-14
5.3-10	Temperature measured by command module sensor CA1509T during cold-soak period . . . . .	5.3-15
5.4-1	Sketch of Apollo command module showing locations of aerothermodynamic sensors . . . . .	5.4-20
5.4-2	Free-stream density . . . . .	5.4-21
5.4-3	Pressures measured on aft heat shield	
	(a) Location 1 . . . . .	5.4-22
	(b) Location 2 . . . . .	5.4-23
	(c) Location 3 . . . . .	5.4-24
	(d) Location 4 . . . . .	5.4-25
	(e) Location 5 . . . . .	5.4-26
	(f) Location 6 . . . . .	5.4-27
	(g) Location 7 . . . . .	5.4-28
	(h) Locations 12, 13, and 16 . . . . .	5.4-29
	(i) Locations 18, 19, and 20 . . . . .	5.4-30
5.4-4	Distribution of measured pressure ratio with wind tunnel data $\alpha = 25^\circ$ . . . . .	5.4-31
5.4-5	Comparison of measured radiative heating rate with theoretical predictions	
	(a) First heat pulse . . . . .	5.4-32
	(b) Second heat pulse . . . . .	5.4-33
5.4-6	Total radiative heating rate prediction with its components . . . . .	5.4-34

~~CONFIDENTIAL~~

Figure		Page
5.4-7	High range calorimeter wafer temperatures	
(a)	Locations 1, 2, 5, and 6 . . . . .	5.4-35
(b)	Locations 8, 9, and 11 . . . . .	5.4-36
(c)	Top 4 wafers of location 3 . . . . .	5.4-37
(d)	Top 3 wafers of location 7 . . . . .	5.4-38
(e)	Top 3 wafers of location 8 . . . . .	5.4-39
5.4-8	Comparison of aft heat shield heating rate obtained from wafer temperature measurement with theoretical prediction	
(a)	Location 1 . . . . .	5.4-40
(b)	Location 2 . . . . .	5.4-41
(c)	Location 3 . . . . .	5.4-42
(d)	Location 5 . . . . .	5.4-43
(e)	Location 6 . . . . .	5.4-44
(f)	Location 7 . . . . .	5.4-45
(g)	Location 8 . . . . .	5.4-46
(h)	Location 10 . . . . .	5.4-47
5.4-9	Comparison of measured heating rate on the conical section with theoretical predictions	
(a)	Locations 12, 13, and 14 . . . . .	5.4-48
(b)	Locations 16, 17, 21, and 22 . . . . .	5.4-49
(c)	Location 18 . . . . .	5.4-50
(d)	Locations 19 and 20 . . . . .	5.4-51
(e)	Locations 24, 25, 26, and 27 . . . . .	5.4-52
(f)	Locations 15, 23, and 28 . . . . .	5.4-53
(g)	Singularity locations . . . . .	5.4-54
5.4-10	Aft heat shield ablator temperature and char measurements . . . . .	5.4-55
5.4-11	Conical heat shield ablator and astro-sextant area temperature and char measurements . . . . .	5.4-56
5.4-12	Major component thermodynamic measurement locations	
(a)	Umbilical . . . . .	5.4-57
(b)	Parachute compartment . . . . .	5.4-58
(c)	Launch escape system tower well and disconnect . . . . .	5.4-58
(d)	S-band window . . . . .	5.4-59
(e)	Crew compartment (hatch stringer 12-C) . . . .	5.4-60

~~CONFIDENTIAL~~

Figure		Page
	(f) Aft heat shield (tension tie 1) . . . . .	5.4-60
	(g) Command module air vent . . . . .	5.4-61
	(h) Steam vent . . . . .	5.4-61
	(i) Command module stringer . . . . .	5.4-62
	(j) Sidewall heat shield attachment . . . . .	5.4-62
	(k) Command module window . . . . .	5.4-63
	(l) C-band antenna . . . . .	5.4-63
5.4-13	Postflight photograph showing char condition of aft heat shield . . . . .	5.4-64
5.4-14	Aft heat shield temperature measurements at depths indicated	
	(a) Station $Z = +71.82, Y = 0$ . . . . .	5.4-65
	(b) Station $Z = -50.0, Y = -1.99$ . . . . .	5.4-66
	(c) Station $Z = -64.85, Y = -14.68$ . . . . .	5.4-67
5.4-15	Aft heat shield $1050^{\circ}$ F isotherm comparison with char sensor and core char . . . . .	5.4-68
5.4-16	Maximum temperature measured in depth and comparison of char interface with $1050^{\circ}$ F isotherm	
	(a) $Y = 0, Z = +71.82$ . . . . .	5.4-69
	(b) $Y = 0, Z = +50$ . . . . .	5.4-69
5.4-17	Postflight photograph showing details of typical shear compression pad, located at $\phi = 152^{\circ} 45'$ . . . . .	5.4-70
5.4-18	Postflight photograph showing char condition of umbilical ramp . . . . .	5.4-71
5.4-19	Toroidal heat shield temperature measurements at depths indicated	
	(a) Station $X_c = 18.5, \phi = 180^{\circ}$ . . . . .	5.4-72
	(b) Station $X_c = 18.5, \phi = 225^{\circ}$ . . . . .	5.4-73
	(c) Station $X_c = 18.5, \phi = 270^{\circ}$ . . . . .	5.4-74
5.4-20	Postflight photographs of conical heat shield	
	(a) +Z-axis to +Y-axis . . . . .	5.4-75
	(b) +Y-axis to -Z-axis . . . . .	5.4-76

~~CONFIDENTIAL~~

~~CONFIDENTIAL~~

xxi

Figure		Page
	(c) -Y-axis to +Z-axis . . . . .	5.4-77
	(d) -Z lee side of spacecraft . . . . .	5.4-78
	(e) Forward compartment heat shield . . . . .	5.4-79
5.4-21	Conical heat shield temperature measurements at depths indicated	
	(a) Station $X_c = 26$ , $\phi = 90^\circ$ . . . . .	5.4-80
	(b) Station $X_c = 50$ , $\phi = 90^\circ$ . . . . .	5.4-81
	(c) Station $X_c = 84$ , $\phi = 90^\circ$ . . . . .	5.4-82
	(d) Station $X_c = 104$ , $\phi = 90^\circ$ . . . . .	5.4-83
	(e) Station $X_c = 26$ , $\phi = 135^\circ$ . . . . .	5.4-84
	(f) Station $X_c = 50$ , $\phi = 180^\circ$ . . . . .	5.4-85
	(g) Station $X_c = 80$ , $\phi = 180^\circ$ . . . . .	5.4-86
	(h) Station $X_c = 104$ , $\phi = 180^\circ$ . . . . .	5.4-87
	(i) Station $X_c = 80$ , $\phi = 270^\circ$ . . . . .	5.4-88
	(j) Station $X_c = 104$ , $\phi = 270^\circ$ . . . . .	5.4-89
5.4-22	Comparison of Apollo 4 measured and predicted heat shield temperature data at $X_c = 50^\circ$ , $\phi = 180^\circ$ using 0.06-inch thermocouple driver . . . . .	5.4-90
5.4-23	Simulated windward umbilical cavity, located at $\phi = 87^\circ$ . . . . .	5.4-91
5.4-24	Charred astro-sextant area . . . . .	5.4-92
5.4-25	Unified side hatch test panel showing gap and seal . . . . .	5.4-93
5.4-26	Steam vent, air vent, and EVA hand hold . . . . .	5.4-94
5.5-1	Pressure altitude during descent . . . . .	5.5-3
5.5-2	Earth landing subsystem upper deck after recovery	
	(a) Drogue mortar can no. 1 . . . . .	5.5-4
	(b) Drogue mortar can no. 2 . . . . .	5.5-5

~~CONFIDENTIAL~~

~~CONFIDENTIAL~~

Figure		Page
5.7-1	Main DC Bus A voltage and total spacecraft current during gimbal motors start-up . . . . .	5.7-2
5.7-2	Entry battery currents during gimbal motors start-up . . . . .	5.7-3
5.7-3	Entry battery voltages during gimbal motors start-up . . . . .	5.7-4
5.8-1	Load profile . . . . .	5.8-5
5.8-2	Nominal fuel cell performance compared with actual flight data . . . . .	5.8-6
5.8-3	Fuel cell no. 3 temperatures . . . . .	5.8-7
5.12-1	Emergency detection subsystem, angle of attack parameter ( $\Delta P$ ) . . . . .	5.12-3
5.12-2	Angular rates and emergency detection system abort limits during S-II stage burn . . . . .	5.12-4
5.12-3	Angular rates and emergency detection system abort limits during first S-IVB stage burn . . . . .	5.12-5
5.12-4	Angular rates and emergency detection system abort limits during second S-IVB stage burn . . . . .	5.12-6
5.13-1	Apollo 4 communications capabilities . . . . .	5.13-19
5.13-2	Uplink received carrier power at spacecraft, launch phase . . . . .	5.13-20
5.13-3	Downlink received carrier power at Manned Spaceflight Network sites, launch phase . . . . .	5.13-21
5.13-4	Downlink received carrier power at MIL, launch phase . . . . .	5.13-22
5.13-5	Downlink received carrier power at GBM, launch phase . . . . .	5.13-23
5.13-6	Downlink received carrier power at BDA, launch phase . . . . .	5.13-24

~~CONFIDENTIAL~~

~~CONFIDENTIAL~~

xxiii

Figure		Page
5.13-7	Uplink received carrier power at spacecraft, Hawaii coverage of second revolution . . . . .	5.13-25
5.13-8	Downlink received carrier power at Hawaii, second revolution . . . . .	5.13-26
5.13-9	Downlink received carrier power at MIL, first and second revolution . . . . .	5.13-27
5.13-10	Unified S-band telemetry bit error probability, Hawaii coverage of second revolution . . . . .	5.13-28
5.13-11	VHF telemetry bit error probability, Hawaii coverage of second revolution . . . . .	5.13-29
5.13-12	Uplink received carrier power at spacecraft, ACN and CRO coverage of third revolution . . . . .	5.13-30
5.13-13	Downlink received carrier power at ACN and CRO, third revolution . . . . .	5.13-31
5.13-14	Uplink received carrier power at spacecraft, Guam coverage of third revolution . . . . .	5.13-32
5.13-15	Downlink received carrier power at Guam, third revolution . . . . .	5.13-33
5.13-16	Uplink received carrier power at spacecraft, A/RIA 3 coverage of entry . . . . .	5.13-34
5.13-17	Unified S-band telemetry bit error probability, ascension coverage of third revolution . . . . .	5.13-35
5.13-18	Unified S-band telemetry bit error probability, Guam coverage of third revolution . . . . .	5.13-36
5.15-1	Boost monitor phase, pitch error . . . . .	5.15-25
5.15-2	Spacecraft dynamics, ascent phase . . . . .	5.15-26
5.15-3	S-IVB separation and service propulsion subsystem burn number 1 sequence of events . . . . .	5.15-27
5.15-4	Velocity accumulation, S-IVB/CSM separation . . . . .	5.15-28

~~CONFIDENTIAL~~

~~CONFIDENTIAL~~

Figure		Page
5.15-5	Spacecraft dynamics, S-IVB/CSM separation and maneuver to service propulsion subsystem first burn attitude . . . . .	5.15-29
5.15-6	Spacecraft dynamics, service propulsion subsystem first burn . . . . .	5.15-30
5.15-7	Velocity to be gained ( $V_G$ ), service propulsion subsystem first burn . . . . .	5.15-31
5.15-8	Spacecraft dynamics, maneuvers to cold-soak attitude . . . . .	5.15-32
5.15-9	Spacecraft dynamics, typical coast phase limit cycle . . . . .	5.15-33
5.15-10	Spacecraft dynamics, maneuver to service propulsion subsystem second burn attitude . . . . .	5.15-34
5.15-11	Sequence of events for service propulsion subsystem second burn . . . . .	5.15-35
5.15-12	Spacecraft dynamics, service propulsion subsystem second burn . . . . .	5.15-36
5.15-13	Velocity to be gained ( $V_G$ ), service propulsion subsystem second burn . . . . .	5.15-37
5.15-14	Spacecraft Dynamics, entry	
	(a) 08:18:00 to 08:22:00 . . . . .	5.15-38
	(b) 08:22:00 to 08:26:30 . . . . .	5.15-39
	(c) 08:26:30 to 08:31:00 . . . . .	5.15-40
	(d) 08:31:00 to 08:35:40 . . . . .	5.15-41
5.15-15	Entry sequence plotted against altitude and range . . . . .	5.15-42
5.15-16	Roll command plotted against actual roll (CDUX) . .	5.15-43
5.15-17	Landing point data . . . . .	5.15-44

~~CONFIDENTIAL~~



~~CONFIDENTIAL~~

xxv

Figure

Page

5.15-18	Time histories of guidance and navigation subsystem inertial instrument coefficients errors	
(a)	X, Y, and Z-axis accelerometer bias and scale factor error coefficients . . . . .	5.15-45
(b)	X, Y, and Z-axis gyro acceleration drift spin reference axis (ADSRA) and null bias drift coefficients (NDB) . . . . .	5.15-46
(c)	X, Y, and Z-axis gyro acceleration drift input axis (ADIA) coefficient . . . . .	5.15-47
5.15-19	Ascent velocity residuals . . . . .	5.15-48
5.16-1	Average number of pulses accumulated during service module reaction control subsystem activity . . . .	5.16-25
5.16-2	Average burn time accumulated during service module reaction control subsystem activity . . . . .	5.16-26
5.16-3	Service module reaction control subsystem propellant consumption	
(a)	Quad A consumption . . . . .	5.16-27
(b)	Quad B consumption . . . . .	5.16-28
(c)	Quad C consumption . . . . .	5.16-29
(d)	Quad D consumption . . . . .	5.16-30
(e)	Total consumption . . . . .	5.16-31
5.16-4	Service module reaction control subsystem engine mounting structure temperatures	
(a)	Quads A and B . . . . .	5.16-32
(b)	Quads C and D . . . . .	5.16-33
5.16-5	Service module reaction control subsystem engine injector head temperatures . . . . .	5.16-34
5.16-6	Quad B engine mounting structure temperature during portion of the cold-soak period . . . . .	5.16-35
5.16-7	Effect of engine firing on injector head and engine mounting structure temperatures . . . . .	5.16-36
5.16-8	Command module reaction control subsystem helium tank pressures during entry . . . . .	5.16-37

~~CONFIDENTIAL~~

~~CONFIDENTIAL~~

Figure		Page
5.16-9	Command module reaction control subsystem helium tank temperatures during entry . . . . .	5.16-38
5.16-10	Typical command module reaction control subsystem engine chamber pressure for burns of 0.005, 0.145 and 42.1 seconds . . . . .	5.16-39
5.16-11	Average number of pulses accumulated during command module reaction control subsystem activity . . . .	5.16-40
5.16-12	Average burn time accumulated during command module reaction control subsystem activity . . . . .	5.16-41
5.16-13	Command module reaction control subsystem propellant consumption	
	(a) System A consumption . . . . .	5.16-42
	(b) System B consumption . . . . .	5.16-43
	(c) Total command module reaction control subsystem . . . . .	5.16-44
5.16-14	Typical command module reaction control subsystem engine component temperatures during entry . . . .	5.16-45
5.17-1	Service propulsion subsystem chamber pressure data	
	(a) First burn . . . . .	5.17-11
	(b) Second burn . . . . .	5.17-12
5.17-2	Service propulsion subsystem second burn acceleration match . . . . .	5.17-13
5.18-1	Oxygen tank pressure and events . . . . .	5.18-4
5.19-1	Waste water tank quantity plotted against time . . .	5.19-6
5.19-2	Potable water tank quantity plotted against time . .	5.19-7
5.20-1	Postflight photograph of left-side window after spacecraft had been secured on recovery ship . . .	5.20-7
5.20-2	Shipboard photographs showing postflight condition of spacecraft 017 windows . . . . .	5.20-8

~~CONFIDENTIAL~~

~~CONFIDENTIAL~~

xxvii

Figure		Page
5.20-3	Postflight photographs of spacecraft windows taken after spacecraft arrived at Downey, California . . . . .	5.20-9
5.20-4	Postflight photographs of spacecraft windows showing discoloration due to contaminate . . . . .	5.20-10
5.20-5	Postflight grid photographs of windows taken after spacecraft arrived at Downey, California . .	5.20-11
5.20-6	Postflight resolution photographs taken after spacecraft arrived at Downey, California . . . . .	5.20-12
5.20-7	Acceleration input to command module X-axis at lift-off, measurement CA0001A . . . . .	5.20-13
5.20-8	Spectral density derived from X-axis accelerometer at time of lift-off, measurement CA0001A . . . . .	5.20-14
5.20-9	Spectral density derived from X-axis accelerometer during period of maximum response, measurement CA0001A . . . . .	5.20-15
6.1-1	+Z outrigger strut load typical 5 Hz oscillation . .	6-8
6.1-2	Effect of 5 Hz oscillation on +Z apex X-component of load . . . . .	6-9
6.1-3	Lunar module accelerations at lift-off . . . . .	6-10
6.1-4	Lunar module accelerations during high oscillation period . . . . .	6-11
6.1-5	Lunar module accelerations during first stage center engine cutoff . . . . .	6-12
6.1-6	Lunar module accelerations during first stage outboard engine cutoff . . . . .	6-13
6.1-7	Acceleration spectral density of LTA-10R oxidizer tank vibration . . . . .	6-14
6.1-8	Propellant tank vibration qualification accelerations (a) Random, tank full . . . . .	6-15

~~CONFIDENTIAL~~

~~CONFIDENTIAL~~

Figure		Page
	(b) Sine, tank full . . . . .	6-16
	(c) Sine, tank empty . . . . .	6-17
6.1-9	Comparison of LTA-10R fuel tank acceleration spectral density to qualification criteria . . . . .	6-18
6.1-10	Comparison of LTA-10R descent engine acceleration spectral density to qualification criteria . . . .	6-19
6.1-11	Comparison of LTA-10R to LTA-3 sound pressure levels spectra at lift-off . . . . .	6-20
9.3-1	Apollo 4 launch abort areas and recovery force structure . . . . .	9-27
9.3-2	Booster and camera capsule recovery . . . . .	9-28
9.3-3	Mid-Pacific recovery zone and force deployment . . .	9-29
9.3-4	Primary recovery area and force deployment . . . . .	9-30
9.3-5	Spacecraft and parachute . . . . .	9-31
9.3-6	Forward heat shield . . . . .	9-32
9.3-7	Spacecraft in flotation collar . . . . .	9-33
9.3-8	Spacecraft after recovery . . . . .	9-34
9.3-9	Left rendezvous window (inside view) . . . . .	9-35
9.3-10	Right side window (inside view) . . . . .	9-36
9.3-11	Camera capsules . . . . .	9-37
9.3-12	S-IC/S-II Interstage ullage rocket motor fairings . . . . .	9-38
13.0-1	Apollo space vehicle . . . . .	13-2
13.1-1	Spacecraft 017 . . . . .	13-20
13.1-2	Command module window assembly . . . . .	13-21
13.1-3	Fuel cell power plant flow diagram . . . . .	13-22

~~CONFIDENTIAL~~

~~CONFIDENTIAL~~

xxix

Figure		Page
13.1-4	Command and service module cryogenic schematic . . .	13-23
13.1-5	Electrical power distribution subsystem . . . . .	13-24
13.1-6	Sequential events control subsystem functional block diagram . . . . .	13-25
13.1-7	Debris catcher configuration on spacecraft lunar module adapter . . . . .	13-26
13.1-8	Communications subsystem . . . . .	13-27
13.1-9	Guidance and navigation subsystem functional schematic . . . . .	13-28
13.1-10	Stabilization and control subsystem functional schematic . . . . .	13-29
13.1-11	Service module reaction control subsystem component location . . . . .	13-30
13.1-12	Command module reaction control subsystem . . . . .	13-31
13.1-13	Service module reaction control subsystem propellant feed subsystem . . . . .	13-32
13.1-14	Command module reaction control subsystem propellant distribution . . . . .	13-33
13.1-15	Service propulsion subsystem functional flow diagram . . . . .	13-34
13.1-16	Environmental control subsystem schematic . . . . .	13-35
13.1-17	Glycol coolant circuit . . . . .	13-36
13.1-18	Vapor sensitive tape locations	
	(a) Tape locations 1-5 . . . . .	13-37
	(b) Tape locations 6-9 . . . . .	13-38
	(c) Tape locations 10-15 . . . . .	13-39
13.2-1	LTA-10R, descent stage . . . . .	13-41
13.2-2	LTA-10R, ascent stage . . . . .	13-42

~~CONFIDENTIAL~~

xxx

~~CONFIDENTIAL~~

Figure		Page
13.3-1	Saturn V launch vehicle with Apollo Spacecraft 017 . . . . .	13-46
14.1-1	Factory checkout flow for command and service module at Downey . . . . .	14-2
14.1-2	Prelaunch checkout flow for command and service module at Kennedy Space Center . . . . .	14-3
14.2-1	Factory modification and checkout flow for LTA-10R at Bethpage . . . . .	14-5
14.2-2	Prelaunch checkout flow for LTA-10R for Kennedy Space Center . . . . .	14-5

~~CONFIDENTIAL~~

~~CONFIDENTIAL~~

1-1

## 1.0 MISSION SUMMARY

The Apollo 4 mission was successfully accomplished on November 9, 1967. This was the first Apollo mission utilizing a Saturn V launch vehicle with a lunar module test article (LTA-10R) and a Block I command and service module (Spacecraft 017). The unmanned spacecraft was launched from complex 39A, Cape Kennedy, Florida. Lift-off occurred at 1200:01 G.m.t., one second after the planned time, during the first launch attempt. The spacecraft landed in the primary recovery area in the Pacific Ocean near Hawaii approximately 8-1/2 hours later.

The principal objectives of the Apollo 4 mission were to demonstrate the structural and thermal integrity of the space vehicle and to verify adequacy of the Block II heat shield design for entry at lunar return conditions. These objectives were satisfactorily accomplished.

Performance of the spacecraft was satisfactory in all respects. The launch phase of the flight was normal, with all planned events occurring within allowable limits. Strain gauge data indicated that no structural failures occurred and that structural loading was well within the capability of the vehicle. Vibration data measured in the command module indicated that qualification vibration levels were not exceeded. Sufficient valid data were obtained on the spacecraft structure to enable determination of the thermal response during the launch phase and to verify the adequacy of the thermal analysis prediction techniques.

Performance of the emergency detection subsystem, operating in an open-loop mode, was satisfactory. No conditions approaching manual or automatic abort levels were encountered at any time during the launch phase.

The S-IVB stage inserted the spacecraft into an earth parking orbit after approximately 11 minutes of powered flight. After two revolutions in an earth parking orbit, the S-IVB stage was reignited for a simulated translunar injection burn. Shortly after this burn, the spacecraft separated from the S-IVB stage and the service propulsion subsystem was ignited for a short-duration burn. No adverse effects were noted as a result of starting the service propulsion subsystem, as planned, in a zero-g environment with no reaction control subsystem ullage maneuvers. This burn raised the apogee altitude to 9769 nautical miles.

Following this service propulsion subsystem burn, the spacecraft was aligned to a specific attitude to achieve a thermal gradient across the command module heat shield. This spacecraft thermal orientation attitude, with the command module hatch window directly toward the sun

~~CONFIDENTIAL~~

~~CONFIDENTIAL~~

such that the conical surface of the crew compartment was perpendicular to the sun rays, was maintained for approximately 4-1/2 hours. The objective of thermally conditioning the command module ablator prior to entry to induce circumferential thermal stresses and distortions on the command module was achieved. The cold-soak attitude was maintained properly throughout the coast phase although continuous venting from the environmental control subsystem water boiler produced a disturbance torque which caused unsymmetrical limit cycles in the pitch and yaw axes. Block II thermal control coating degradation did occur, as evidenced by measured data exceeding the Block II nominal coating equilibrium temperatures. This degradation is attributed to materials used in the launch escape tower solid propellant jettison motor.

Following the cold-soak coast phase, the service propulsion subsystem was reignited for a long-duration burn to accelerate the spacecraft to entry conditions that represent the most severe combination of the two extreme operational conditions that could possibly be achieved from a lunar return trajectory. Shortly after this burn, the command module separated from the service module and the command module was oriented to entry attitude. Atmospheric entry, 400 000 feet, occurred at an inertial velocity of 36 629 ft/sec and a flight-path angle of minus 6.93 degrees. The entry interface conditions were 210 ft/sec greater and 0.20 degree shallower than had been predicted. The overspeed condition resulted from a longer than planned second service propulsion subsystem burn. Because of the change in the entry conditions, the peak load factor of 7.27g was lower than the predicted 8.34g. These conditions did not affect the performance of the guidance system in achieving the target.

The flight-derived total lift-to-drag ratio and total angle of attack were well within the predicted uncertainty boundaries for the entire hypersonic flight regime. The flight derived data during the first entry are estimated to be a lift-to-drag ratio of 0.370 and a total angle of attack of 154.6 degrees.

Command module landing occurred within 10 nautical miles of the planned landing point. The command module, the apex cover, and one of the three main parachutes were recovered by the prime recovery ship, U.S.S. Bennington. This was the first recovery of an Apollo parachute.

All spacecraft subsystems operated properly throughout the mission. There is no evidence of any functional anomalies that affected the mission.

The thermal protection subsystem survived the lunar entry environment satisfactorily. Sufficient data were obtained to permit a thorough evaluation of the thermal performance of the Block II thermal protection

~~CONFIDENTIAL~~



~~CONFIDENTIAL~~

1-3

subsystem. Temperature data were within design limits. The maximum calculated heating rate was 430 Btu/ft<sup>2</sup>/sec and the maximum calculated heat load was 38 150 Btu/ft<sup>2</sup>. These values are related to a reference point on the aft heat shield (location S/R = 0.9875,  $\theta$  = 90°). The expected values were 422 Btu/ft<sup>2</sup>/sec and 34 750 Btu/ft<sup>2</sup>, based on the latest prediction method and the preflight trajectory. The expected values before the mission were 594 Btu/ft<sup>2</sup>/sec and 37 777 Btu/ft<sup>2</sup>. The reason for the differences in the expected values is based on the use of updated radiative terms which are approximately 50 percent of those previously used. Temperature data indicated that surface temperatures approached 5000° F. The maximum bondline temperature measured on the aft heat shield was 150° F. The surface erosion in the stagnation area and other points on the aft heat shield was less than expected. Examination of cores taken from the aft heat shield indicated a strong surface char and less-than-expected char penetration. The maximum char penetration was 0.88 inch.

Performance of the guidance and control subsystems was equal to or better than preflight predictions. Analysis of navigation error propagation during ascent, the service propulsion subsystem burns, and entry indicates that inertial measurement unit gyro drifts and accelerometer biases and scale factors remained within specification tolerances. All sequencing and computational operations performed by the Apollo guidance computer have been verified to have been correct.

Sequencing of the mission control programmer was satisfactory throughout the mission.

Operation of the environmental control subsystem was satisfactory. The cabin pressure remained between 5.6 and 5.8 psia during the orbital phase of the mission. The cabin temperature was maintained at a constant 60° F during the mission, increasing to 68° F during entry.

Main dc power was satisfactorily supplied by three Block I fuel cells, augmented by three auxiliary batteries during peak electrical loads. Extended zero-g operation of the fuel cells, inflight fuel cell reactant purge, and thermal control of the fuel cells were demonstrated. The cryogenic storage subsystem operation was also satisfactory. Extended zero-g operation, equal depletion, pressure control, and stratification control were demonstrated.

The electrical power distribution subsystem operation was nominal throughout the mission. All power switching occurred as planned and programmed.

All maneuvers using the reaction control subsystem thrusters were completed as planned. Satisfactory maneuver rates, accelerations, and translation velocity changes were attained.

~~CONFIDENTIAL~~

~~CONFIDENTIAL~~

The spacecraft and Manned Space Flight Network S-band communications and spacecraft vhf communications were satisfactorily demonstrated. General support from the NASA and Department of Defense network stations was excellent.

~~CONFIDENTIAL~~

~~CONFIDENTIAL~~

2-1

## 2.0 MISSION DESCRIPTION AND OBJECTIVES

### 2.1 MISSION DESCRIPTION

The Apollo 4 space vehicle was launched from complex 39A at Cape Kennedy, Florida, at 12:00:01 G.m.t. (07:00:01 a.m. e.s.t.) on November 9, 1967. The launch azimuth was 72.0 degrees from true North. The sequence of the major mission events is shown in table 2.1-I.

S-IC stage cutoff occurred nominally at 00:02:30.8 at an altitude of approximately 34 nautical miles. S-II stage ignition occurred at a nominal time of 00:02:32.2 with the stage burning for a period of 6 minutes 7.6 seconds. The S-IVB stage was ignited and burned for 2 minutes 24.9 seconds to place the spacecraft/S-IVB stage combination into an earth parking orbit having an apogee of 101.1 nautical miles and a perigee of 99.1 nautical miles.

After approximately two orbits (at 03:11:26.6), the S-IVB stage was reignited to place the spacecraft into the simulated translunar trajectory. This burn was for a period of 4 minutes 59.7 seconds.

Approximately 10 minutes after the completion of the second S-IVB burn, a nominal spacecraft separation from the S-IVB was achieved. One minute 38.4 seconds after spacecraft separation, the first burn of the service propulsion subsystem was initiated and, 16 seconds later, was completed satisfactorily. Upon completion of the burn, the spacecraft was oriented to a cold-soak attitude which placed the thickest side of the command module heat shield away from the solar vector. During the approximate 4.5-hour cold-soak period, the spacecraft coasted to its highest apogee, 9769 nautical miles. Also, a 70-mm still camera was photographing the earth's surface once every 10.6 seconds during this period. A total of 715 good-quality, high-resolution photographs were taken during this period.

At 08:10:54.8, the service propulsion subsystem was ignited again to increase the spacecraft inertial velocity. The planned velocity was 34 816 feet per second; however, the velocity achieved was 35 115 feet per second.

Two minutes 27.2 seconds after the completion of the second service propulsion subsystem burn, the command module was separated from the service module, and the command module was oriented to the entry attitude.

~~CONFIDENTIAL~~

~~CONFIDENTIAL~~

The entry phase of the flight was well within the conditions expected. The lift-to-drag ratio obtained was 0.365 ( $\pm 0.015$ ) compared with preflight predictions of 0.350 (0.322 to 0.416). The spacecraft on its main parachutes was sighted from the recovery carrier, the U.S.S. Bennington, approximately 6 to 8 nautical miles from the recovery vessel. Landing occurred at 08:37:09.2 approximately 10 nautical miles from the planned landing point based on postflight reconstruction of the entry data. Swimmers were deployed from helicopters and had a flotation collar secured around the spacecraft within 20 minutes. Recovery of the command module, apex heat shield, and one main parachute was effected approximately 2 hours 28 minutes after landing. This period was somewhat longer than anticipated; however, sea conditions of 8-foot swells were the cause of the longer recovery period.

~~CONFIDENTIAL~~

~~CONFIDENTIAL~~

2-3

TABLE 2.1-I.- APOLLO 4 MISSION EVENTS

Source	Event	Mission elapsed time, hr:min:sec	
		Planned	Actual
LAUNCH PHASE RANGE ZERO 12:00:01 G.m.t.			
MSFC <sup>a</sup>	Lift-off (12:00:01.3 G.m.t.)	00:00:00.	00:00:00.3
	Maximum dynamic pressure	00:01:18.4	00:01:18.5
MSFC <sup>a</sup>	S-IC inboard engine cutoff	00:02:15.5	00:02:15.5
MSFC <sup>a</sup>	S-IC outboard engine cutoff	00:02:31.9	00:02:30.8
MSFC <sup>a</sup>	S-IC/S-II separation command	00:02:32.6	00:02:31.4
MSFC <sup>a</sup>	S-II engine ignition command	00:02:33.3	00:02:32.2
MSFC <sup>a</sup>	S-IC interstage jettison	00:03:02.6	00:03:01.4
CD0105	LES jettison	00:03:08.8	00:03:07.2
MSFC <sup>a</sup>	S-II cutoff	00:08:36.3	00:08:39.8
MSFC <sup>a</sup>	S-II/S-IVB separation	00:08:37.1	00:08:40.5
MSFC <sup>a</sup>	S-IVB engine ignition command (first burn)	00:08:37.3	00:08:40.7
MSFC <sup>a</sup>	S-IVB cutoff (first burn)	00:10:56.0	00:11:05.6
ORBITAL PHASE			
MSFC <sup>a</sup>	Begin earth parking orbit	00:11:06.0	00:11:15.6
Trajectory data	Begin second earth orbit	01:38:20.0	01:38:47
MSFC <sup>a</sup>	S-IVB ignition (second burn)	03:11:33.5	03:11:26.6
MSFC <sup>a</sup>	S-IVB cutoff (second burn)	03:16:39.9	03:16:26.3
CD0127	CSM/S-IVB separation	03:26:42.8	03:26:28.2
CH4320	SPS ignition (first burn)	03:28:20.1	03:28:06.6
CH4320	SPS cutoff (first burn)	03:28:35.1	03:28:22.6
Trajectory data	Apogee (planned 9890 n. mi.) (actual 9769 n. mi.)	05:48:43.1	05:46:49.5
CH4320 and SP0661	SPS ignition (second burn)	08:14:42.7	08:10:54.8
SP0661	SPS cutoff (second burn)	08:19:11.3	08:15:35.4
ENTRY PHASE			
CD0023	CM/SM separation	08:21:45.7	08:18:02.6
Trajectory data	400 000 ft altitude	08:23:12.8	08:19:28.5
CC0228	Drogue parachute deployment	08:35:11.0	08:31:18.6
CD0005	Main parachute deployment	08:36:27.0	08:32:05.8
CH0024	Landing	08:41:25.0	08:37:09.2

<sup>a</sup>Marshall Space Flight Center event times. All other times are from spacecraft measurements or trajectory data.

~~CONFIDENTIAL~~

~~CONFIDENTIAL~~

## 2.2 MISSION OBJECTIVES

The four mission objectives relating to the spacecraft for the Apollo 4 mission as assigned by the Office of Manned Space Flight are listed below. All four have been satisfactorily accomplished.

1. Demonstrate the structural and thermal integrity and compatibility of the launch vehicle and spacecraft. Confirm launch loads and dynamic characteristics.
2. Verify operation of the following subsystems: command module heat shield (adequacy of Block II design for entry at lunar return conditions), service propulsion subsystem (including no ullage start), and selected subsystems.
3. Evaluate the performance of the space vehicle emergency detection subsystem (open-loop configuration).
4. Demonstrate mission support facilities and operations required for launch, mission conduct and command module recovery.

The detailed test objectives developed by MSC to support the four mission objectives are listed in table 2.2-1 along with the degree of accomplishment and appropriate comments.

~~CONFIDENTIAL~~

~~CONFIDENTIAL~~

2- 5

TABLE 2.2-I.- DETAILED TEST OBJECTIVES

No.	Category	Objective description	Degree of accomplishment
1.1	M	Demonstrate CSM/SLA/LTA/Saturn V structural compatibility and determine spacecraft loads in a Saturn V launch environment.	Satisfied.
1.2	M	Determine the dynamic and thermal responses of the SLA/CSM structure in the Saturn V launch environment.	Satisfied.
1.4	M	Determine the force inputs to the simulated LM from the SLA at the spacecraft attachment structure in a Saturn V launch environment.	Partial. Only qualitative data were obtained.
1.5	M	Obtain data on the acoustic and thermal environment of the SLA/simulated LM interface during a Saturn V launch.	Satisfied.
1.7		Determine vibration response of LM descent stage engine and propellant tanks in a Saturn V launch environment.	Satisfied.
3.1	M	Evaluate the thermal and structural performance of the Block II Thermal Protection System, including effects of cold soak and maximum thermal gradient when subjected to the combination of a high heat load and a high heating rate representative of lunar return entry.	Satisfied.
3.2	M	Demonstrate an SPS no ullage start.	Satisfied.
3.3	P	Determine performance of the SPS during a long duration burn.	Satisfied.
3.5	M	Verify the performance of the SM-RCS thermal control subsystem and engine thermal response in the deep space environment.	Satisfied.

M - denotes mandatory

P - denotes primary

~~CONFIDENTIAL~~

~~CONFIDENTIAL~~

TABLE 2.2-I.- DETAILED TEST OBJECTIVES - Continued

No.	Category	Objective description	Degree of accomplishment
3.6	M	Verify the thermal design adequacy of the CM-RCS thrusters and extensions during simulated lunar return entry.	Satisfied.
3.8	M	Evaluate the thermal performance of a gap and seal configuration simulating the unified crew hatch design for heating conditions anticipated during lunar return entry.	Satisfied.
3.9	M	Verify operation of the heat rejection system throughout the mission.	Satisfied.
4	M	Evaluate the performance of the spacecraft emergency detection subsystem (EDS) in the open-loop configuration.	Satisfied.
5.2b	P	Demonstrate the performance of CSM/MSFN S-band communications.	Satisfied.
5.6	P	Measure the integrated skin and depth radiation dose within the command module up to an altitude of at least 2000 nautical miles.	Satisfied.
1	S	Determine the radiation shielding effectiveness of the CM.	Satisfied.
2	S	Demonstrate satisfactory operation of CSM communication subsystem using the Block II type vhf omnidirectional antennas.	Satisfied.
3.1c	S	Verify operation of the G&N system after subjection to the Saturn V boost environment.	Satisfied.
3.1d Part I	S	Verify operation of the EPS after being subjected to the Saturn V launch environment.	Satisfied.
3.1d Part II	S	Verify operation of PGS after being subjected to the Saturn V launch environment.	Satisfied.

M - denotes mandatory  
P - denotes primary  
S - denotes secondary

~~CONFIDENTIAL~~



~~CONFIDENTIAL~~

2-7

TABLE 2.2-I.- DETAILED TEST OBJECTIVES - Concluded

No.	Category	Objective description	Degree of accomplishment
3.2a	S	Verify operation of the G&N in the space environment after S-IVB separation.	Satisfied.
3.2d Part I	S	Verify operation of the EPS in the space environment after S-IVB separation.	Satisfied.
3.2d Part II	S	Verify operation of the PGS in the space environment after S-IVB separation.	Satisfied.
3.3a	S	Verify operation of the CM-RCS during entry and recovery.	Satisfied.
3.3c	S	Verify operation of the G&N/SCS during entry and recovery.	Satisfied.
3.3d	S	Verify operation of the EPS during entry and recovery.	Satisfied.
3.3e	S	Verify operation of the ELS during entry and recovery.	Satisfied.
5	S	Obtain data via CSM-A/RIA communications.	Unknown. Evaluation of signal-to-noise ratios and bit error rate analyses have not yet been accomplished.
6	S	Gather data on the effects of a long duration SPS burn on spacecraft stability.	Satisfied.
7	S	Obtain data on the temperature of the simulated LM skin during launch.	Satisfied.

S - denotes secondary

~~CONFIDENTIAL~~

~~CONFIDENTIAL~~

THIS PAGE INTENTIONALLY LEFT BLANK

~~CONFIDENTIAL~~

~~CONFIDENTIAL~~

3-1

### 3.0 TRAJECTORY DATA

This section contains a comparison of the planned and actual trajectories of the Apollo 4 mission. The launch, orbital, and entry trajectories referred to as planned in this section, are preflight calculated trajectories. The actual trajectories shown in this section are based on the Manned Space Flight Network (MSFN) tracking data and the actual performance and sequences as determined by airborne instrumentation. Marshall Space Flight Center (MSFC) supplied all trajectory data for the launch phase, parking orbit, and second S-IVB burn. An analysis of the Apollo 4 trajectory through the second S-IVB burn may be obtained from the MSFC Apollo 4 Mission Report (ref. 1). The earth model for all trajectories and analyses of the MSFN trackers contained geodetic and gravitational constants representing the Fischer ellipsoid. A ground track of the mission is shown in figure 3.1-1. Time histories of the launch, orbit, and entry trajectories are presented in figures 3.1-2 to 3.1-5.

#### 3.1 APOLLO 4 MISSION

The trajectory analysis presented herein is based on intermediate trajectory data generated 21 days after the end of the mission. The final trajectory data are being prepared at this time and will be released in a supplemental report to this report on January 31, 1968.

##### 3.1.1 Launch

The performance of all launch vehicle (AS 501) stages was reported by MSFC as satisfactory. Mach 1 occurred 0.6 second earlier and 0.1 n. mi. lower than planned. The maximum dynamic pressure was within 3 psf of the expected, and 0.1 second later and 0.05 n. mi. lower than planned. A time history of the launch phase is presented in figure 3.1-2; a comparison of the planned and actual trajectory parameters is contained in table 3.1-I.

##### 3.1.2 Parking Orbit

Insertion.- The first S-IVB cutoff occurred at 00:11:05.6, with the time of insertion defined as 00:11:15.6. The insertion conditions presented in table 3.1-II were obtained from the MSFC orbit determination program which used first revolution tracking data from Bermuda, Carnarvon, and White Sands. Insertion elements are presented in table 3.1-III.

~~CONFIDENTIAL~~

~~CONFIDENTIAL~~

A time history of velocity, flight-path angle, and altitude is presented in figure 3.1-3.

Venting trajectory.- The S-IVB venting polynomials from MSFC have been implemented into the MSC orbit determination program in order to generate the best estimated trajectory during the parking orbit. Orbital fits through the tracking data include revolution 1, revolution 2, and revolution 1 and 2. The state vectors which were solved for from these fits agree within 500 feet in position and 1 ft/sec in velocity. The best trajectory, however, is a combination of fits through revolution 1 and revolution 2, as shown by better agreement with vectors at insertion, lower tracker residuals, and small position and velocity differences (177 feet and 0.5 ft/sec) at revolution interface.

Tables 3.1-IV and 3.1-V contain statistical summaries of the C-band tracking data utilized in the fits. It should be emphasized that because several stations are being considered in each fit, the comparison of actual and theoretical noise, and actual and theoretical bias limits are a qualification of both the tracking data and data fit. An analysis of all data has shown that the noise of the data was generally below the theoretical value. The large values shown in the tables are the result of the data fits and not noisy tracker data; however, the quality of the fit is a function of tracking data biases due to unsolved for parameters, which in these cases show that the fits are actually very good.

An evaluation of the real time computer complex (RTCC) navigation update vector prior to the second S-IVB ignition was performed in order to explain the difference in the actual apogee achieved. The inflight RTCC navigation update vector, prior to the second S-IVB burn, was based on a Bermuda vector at the start of revolution 2 (01:57:49). This vector was integrated to the update time (02:58:30.02) using a preflight venting model which assumes a linear thrust. The postflight vector and the RTCC Bermuda revolution 2 vector agree reasonably well (i.e., the differences were 1433 feet and 1 ft/sec. However, when the postflight vector was integrated to the update time, using the postflight venting polynomials provided by MSFC, the difference increased to 5.6 n. mi. in position and plus 51 ft/sec in velocity. Of the two vectors, the postflight vector is more consistent with subsequent data, and indicates that the update vector was high in velocity. This would make the Apollo guidance computer determine that it had achieved the proper apogee at cutoff (see section 3.1.3). It appears the large difference in the navigation update vector is the result of the predicted venting model and the 1-hour propagation prior to the update.

In general, the unified S-band tracking data for the parking orbit were not as good as expected. No known biases were found on the data by the RTCC, but the high-speed Doppler was considered too noisy to

~~CONFIDENTIAL~~

~~CONFIDENTIAL~~

3-3

be useful. A detailed analysis of the unified S-band tracker data will be contained in a supplement to this report.

Second S-IVB burn.- The S-IVB stage was ignited for the second time at an elapsed time of 03:11:26.6 and burned for 299.7 seconds. The time of injection (10 seconds after cutoff) into the coast ellipse was defined as 03:16:36.3. The injection conditions presented in table 3.1-VI were obtained by MSFC from the launch vehicle instrument unit data and from MSFN tracking data. These conditions agree with those obtained from the MSC preliminary BET within approximately 2 n. mi. in position and 3 ft/sec velocity. Injection elements are presented in table 3.1-III.

### 3.1.3 Coast Ellipse

Injection/separation.- The CSM/S-IVB separation occurred at 03:26:28.2, 602 seconds after the second S-IVB burn. Separation occurred 1.7 seconds after the RCS thrusters came on, followed by 8.4 seconds of +X translation. A comparison of planned and actual separation conditions is presented in table 3.1-VI. The actual conditions were calculated using the Eastern Test Range (ETR) tracking data taken between the time of the second S-IVB burn cutoff and first SPS burn ignition. These conditions were validated by integrating a vector before CSM/S-IVB separation through the normal separation sequence, and comparing the results at the time of ignition for the first SPS burn with a vector obtained after CSM/S-IVB separation. The two solutions agreed within 2640 feet altitude, 0.74 ft/sec velocity, and 0.1 degree flight-path angle, indicating that actual separation was satisfactory. These conditions in table 3.1-VI agree with the MSFC separation conditions within approximately 1 n. mi. in position and 1 ft/sec in velocity.

Tracking analysis and reconstruction.- Tracking data for the coast ellipse was satisfactory. Deviations between the C-band radar data and unified S-band orbit data were small. The best reconstructions have shown position and velocity differences of only 3000 ft and 2 ft/sec, respectively, for the two solutions. Analysis shows that the correction of several small data differences which have appeared during the analysis should bring the two trajectories closer together. Table 3.1-VII presents a statistical summary of the tracking residuals for both the C-band radar and unified S-band radar data.

As noted above, several tracking data differences have been noted; primarily, a 300-foot jump in the C-band range residuals at 03:29:59 and 05:12:29; and secondarily, a Carnarvon elevation bias on C-band radar data, and a time bias on Ascension unified S-band radar data. The analysis has not resolved these problems; however, this will not affect the validity of the BET.

~~CONFIDENTIAL~~

~~CONFIDENTIAL~~

SPS maneuvers and targeting.- The first and second SPS burn maneuvers determined by the onboard guidance logic were nominal for the Apollo guidance computer state vectors indicated at the start of each burn and the respective targeting parameters loaded in the computer erasable memory prior to launch. Each burn was reconstructed by using raw pulsed integrating pendulous accelerometer data to determine the acceleration profiles during the burns, and by using the engine and chamber pressure data to simulate thrust buildup and tail-off. The SPS cases discussed in this analysis each include actual thrust characteristics. The first and second SPS burns (SPS-1 and SPS-2, respectively) were simulated for the navigational state vectors and the actual state vectors established from tracking data. The actual targeted values achieved for semilatus rectum (P) and orbit eccentricity (e) were determined from the trajectories propagated from Eastern Test Range tracking vectors after SPS-1 and from the Guam tracking information after SPS-2. In both burns, it was established that guidance cutoff was indicated for the times when the onboard targeting quantities were satisfied and when the simulated burn times agreed very closely with Apollo guidance computer telemetry information.

Ignition for the first SPS burn occurred at 03:28:06.6 with guidance cutoff occurring 16.0 seconds later. The first SPS maneuver was a posigrade guided burn targeted to an in-plane coast ellipse having an apogee of 9899 n. mi., a P of 32 928 190 feet, and an e of 0.593874991. The spacecraft pitch attitude at SPS-1 ignition was 72.2 degrees up from the local horizontal or 43.9 degrees up from the inertial velocity vector. The difference between actual and planned pitch attitude was about 17 degrees which resulted from the second S-IVB burn providing a lower earth-intersecting coast ellipse. The actual coast ellipse achieved by the guided burn had an apogee of 9769 n. mi., a P of 32 833 060 feet, and an e of 0.59133947. Table 3.1-VI shows a state vector comparison of the planned and actual conditions at SPS-1 ignition, guidance cutoff, and apogee. Figure 3.1-4 presents a time history of the SPS-1 burn for the trajectory parameters inertial velocity, flight-path angle, and altitude.

To explain the differences between the planned and actual ellipses achieved at the end of the first SPS burn, a number of SPS burn simulations were made. The burn characteristics and orbital parameters generated for the various SPS first-burn simulations are presented in table 3.1-VIII.

Case I shows the actual conditions reconstructed from an ETR tracking vector at the end of the first SPS burn. Case II is the best estimate of the first SPS burn which results from integrating an ETR tracking vector through a guidance and navigation subsystem guided burn targeted for the actual P and e determined in Case I. In reconstructing the first SPS burn, the best estimate of the total thrust was calculated to be 21 106 pounds, from the known weight losses, burn duration, and total  $\Delta V$  achieved.

~~CONFIDENTIAL~~

~~CONFIDENTIAL~~

3-5

Because the first SPS burn cutoff occurred when the Apollo guidance computer calculated that the targeting conditions had been achieved, it was apparent that the nominal P and e values loaded in the erasable memory had been satisfied. Cases III and IV show the results of a guidance cutoff on nominal targets for integrated ETR and AGC tracking vectors, respectively. As expected, Case IV indicated that the Apollo guidance computer burn logic yielded the desired P and e values and an apogee of 9890 n. mi. This apogee solution differs by 6.3 n. mi. from the Apollo guidance computer estimated solution. This difference is accounted for by the fact that the apogee solution used in the Case IV simulation of this burn took into account the effects of earth oblateness and did not include any inertial measurement unit errors effective during the burn. Case III indicates that an additional 2.64 seconds of burn time would be required to achieve the planned P and e, if the onboard state vector had agreed with the actual state vector at ignition of the first SPS burn. It follows that the difference between the value that the Apollo guidance computer computed for the state vector and the value of the actual state vector yielded a burn which missed the planned apogee by 121 n. mi. This difference in the actual and the Apollo guidance computer state vectors prior to the first SPS burn is attributed to the combined effects of S-IVB venting, the navigation update, and inertial measurement unit errors.

Ignition for the second SPS burn occurred at 08:10:54.8, with the ground-commanded cutoff occurring 280.6 seconds later. The planned mission called for the second SPS burn to accelerate the spacecraft to an entry interface velocity of 36 333 ft/sec and an entry interface flight-path angle of minus 7.13 degrees. The nominal target orbit parameters loaded in the Apollo guidance computer to accomplish the aforementioned objectives included a semilatus rectum of 41 960 233 ft and an orbit eccentricity of 0.99909924. The actual target orbit achieved at the end of the second SPS burn had a semilatus rectum of 42 488 012 ft and an eccentricity of 1.0221608. The spacecraft pitch attitude at ignition for the second SPS burn was 25.93 degrees below the inertial velocity vector or 49.13 degrees down from the local horizontal. These values agree within 0.7 degree of the planned pitch angles. Table 3.1-V contains a state-vector comparison of planned and actual conditions at second SPS burn ignition, guidance cutoff, and entry interface. Figure 3.1-4 shows the planned and actual velocity, flight-path angle, and altitude during the second SPS burn. It should be noted that the 288-second deviation in planned and actual time of the ignition of the second SPS burn is the result of the lower apogee after the first SPS burn.

Four cases representing the simulated results of the second SPS burn are presented in table 3.1-VIII.

~~CONFIDENTIAL~~

~~CONFIDENTIAL~~

Case V shows the actual conditions reconstructed from a Guam tracking vector at the end of the second SPS burn. The second SPS burn engine cutoff command was accepted about 10.3 seconds after the guidance and navigation engine cutoff command was indicated.

Case VI simulates the second SPS burn and resulted from integrating a tracking vector through a guided burn targeted to the actual P and e determined in Case V. In reconstructing the burn, the best estimate of the actual thrust was calculated in the same manner as that for the first SPS burn. Cases VII and VIII show the results of integrating a tracking vector and an Apollo guidance computer vector, respectively, through a guided burn targeted to the planned P and e. As can be seen from both cases, if a guidance cutoff had been performed, the nominal target orbit and entry conditions would have been achieved.

The entry interface conditions for Case VIII indicated a velocity of 36 332.6 ft/sec and a flight-path angle of minus 7.13 degrees. Actual cutoff represented in Case V yielded a velocity of 36 544.6 ft/sec and flight-path angle of minus 6.93 degrees.

#### 3.1.4 Entry

The planned and actual entry trajectories are shown in figure 3.1-5. As explained in section 3.1.3, the time shift between the actual and planned curves can be attributed to the lower targeting achieved after the first SPS burn. The actual trajectory is based on a post-SPS-2 Guam radar vector, and the entry was generated by correcting the guidance and navigation pulsed integrating pendulous accelerometer data for known inertial measurement unit errors. Table 3.1-IX presents the planned and actual conditions at entry interface.

The entry interface conditions were 212 ft/sec greater and 0.20 degree shallower than planned. The off-nominal conditions did not affect the performance of the guidance system in achieving the target. Table 3.1-X contains a comparison of the planned and actual values of the maximum entry parameters. Because of the change in the entry conditions, the peak load factor of 7.27g was slightly lower than predicted.

The analysis of the guidance and navigation subsystem has shown no anomalies and is discussed in section 5.15 of this report. The guidance and navigation subsystem indicated a 2.2 n. mi. overshoot at drogue parachute deployment. The postflight reconstructed trajectory indicates a 4.6 n. mi. undershoot at drogue parachute deployment.

~~CONFIDENTIAL~~



~~CONFIDENTIAL~~

3-7

TABLE 3.1-I.- LAUNCH PHASE PLANNED AND ACTUAL TRAJECTORY PARAMETERS

Condition	Planned	Actual
S-IC Stage Inboard Engine Cutoff		
Time from range zero, hr:min:sec . . . . .	00:02:15.5	00:02:15.5
Geodetic latitude, deg North . . . . .	28.75	28.75
Longitude, deg West . . . . .	80.08	80.07
Altitude, ft . . . . .	159 006	162 861
Altitude, n. mi. . . . .	26	27
Space-fixed velocity, ft/sec . . . . .	7151	7241
Space-fixed flight-path angle, deg . . . . .	22.96	23.28
Space-fixed heading angle, deg E of N . . .	76.38	75.95
S-IC Stage Outboard Engine Cutoff		
Time from range zero, hr:min:sec . . . . .	00:02:31.9	00:02:30.8
Geodetic latitude, deg North . . . . .	28.83	28.83
Longitude, deg West . . . . .	79.77	79.80
Altitude, ft . . . . .	208 691	208 990
Altitude, n. mi. . . . .	34	34
Space-fixed velocity, ft/sec . . . . .	8896	8831
Space-fixed flight-path angle, deg . . . . .	20.33	20.96
Space-fixed heading angle, deg E of N . . .	75.62	75.29

~~CONFIDENTIAL~~

~~CONFIDENTIAL~~

TABLE 3.1-I.- LAUNCH PHASE PLANNED AND ACTUAL

## TRAJECTORY PARAMETERS - Concluded

Condition	Planned	Actual
S-II Stage Engine Cutoff		
Time from range zero, hr:min:sec . . . . .	00:08:36.3	00:08:39.8
Geodetic latitude, deg North . . . . .	31.70	31.72
Longitude, deg West . . . . .	65.72	65.67
Altitude, ft . . . . .	622 510	631 050
Altitude, n. mi. . . . .	102	104
Space-fixed velocity, ft/sec . . . . .	22 482	22 356
Space-fixed flight-path angle, deg . . . . .	0.523	0.642
Space-fixed heading angle, deg E of N . . .	81.43	81.49
First S-IVB Stage Engine Cutoff		
Time from range zero, hr:min:sec . . . . .	00:10:56.0	00:11:05.6
Geodetic latitude, deg North . . . . .	32.60	32.64
Longitude, deg West . . . . .	55.88	55.43
Altitude, ft . . . . .	628 077	631 936
Altitude, n. mi. . . . .	103	104
Space-fixed velocity, ft/sec . . . . .	25 561	25 557
Space-fixed flight-path angle, deg . . . . .	-0.001	0.015
Space-fixed heading angle, deg E of N . . .	86.97	87.21

~~CONFIDENTIAL~~

~~CONFIDENTIAL~~

3-9

TABLE 3.1-II.- PARKING ORBIT PLANNED AND ACTUAL  
TRAJECTORY PARAMETERS

Condition	Planned	Actual
Insertion (S-IVB Stage Cutoff Plus 10 Seconds)		
Time from range zero, hr:min:sec . . . . .	00:11:06.0	00:11:15.6
Geodetic latitude, deg North . . . . .	32.64	32.67
Longitude, deg West . . . . .	55.12	54.67
Altitude, ft . . . . .	628 117	631 670
Altitude, n. mi. . . . .	103	104
Space-fixed velocity, ft/sec . . . . .	25 570	25 564
Space-fixed flight-path angle, deg . . . . .	0.001	0.014
Space-fixed heading angle, deg E of N. . . . .	87.42	87.65
Second S-IVB Stage Ignition		
Time from range zero, hr:min:sec . . . . .	03:11:33.5	03:11:26.6
Geodetic latitude, deg North . . . . .	31.90	31.95
Longitude, deg West . . . . .	82.07	82.33
Altitude, ft . . . . .	671 568	668 045
Altitude, n. mi. . . . .	110	110
Space-fixed velocity, ft/sec . . . . .	25 551	25 547
Space-fixed flight-path angle, deg . . . . .	-0.008	-0.001
Space-fixed heading angle, deg E of N. . . . .	97.70	97.54

~~CONFIDENTIAL~~

~~CONFIDENTIAL~~

TABLE 3.1-II.- PARKING ORBIT PLANNED AND ACTUAL

TRAJECTORY PARAMETERS - Concluded

Condition	Planned	Actual
Second S-IVB Stage Cutoff		
Time from range zero, hr:min:sec . . . . .	03:16:39.9	03:16:26.3
Geodetic latitude, deg North . . . . .	27.93	28.03
Longitude, deg West . . . . .	58.65	59.36
Altitude, ft . . . . .	1 844 882	1 766 542
Altitude, n. mi. . . . .	304	291
Space-fixed velocity, ft/sec . . . . .	30 840	30 882
Space-fixed flight-path angle, deg . . . .	15.03	14.77
Space-fixed heading angle, deg E of N. . .	102.64	102.38

~~CONFIDENTIAL~~

~~CONFIDENTIAL~~

3-11

TABLE 3.1-III.- ORBITAL ELEMENTS

	Condition	Planned	Actual
Insertion (MSFC data)	Apogee, n. mi. . . . .	101.4	101.1
	Perigee, n. mi. . . . .	100.0	99.1
	Period, min . . . . .	88.2	88.3
	Inclination, deg . . . . .	32.56	32.57
Injection	Apogee, n. mi. . . . .	9410	9292
	Perigee, n. mi. . . . .	-45	-44
	Period, min . . . . .	306.2	303.1
	Inclination, deg . . . . .	30.31	30.31
Coast ellipse	Apogee, n. mi. . . . .	9890	9769
	Perigee, n. mi. . . . .	-41	-45
	Period, min . . . . .	320.2	316.6
	Inclination, deg . . . . .	30.31	30.31

~~CONFIDENTIAL~~

~~CONFIDENTIAL~~

TABLE 3.1-IV.- REVOLUTION 1 TRACKING RESIDUAL STATISTICS

Station	Data type	Theoretical bias ( $\pm$ )	Theoretical noise ( $\pm$ )	Actual bias	Actual noise (rms)
Bermuda	Range, ft . . . . .	60	30	3.3	41.8
	Azimuth, deg . . . . .	0.022	0.011	-0.005	0.007
	Elevation, deg . . . . .	0.022	0.011	-0.018	0.015
Patrick	Range, ft . . . . .	40	20	-75.2	51.6
	Azimuth, deg . . . . .	0.017	0.008	-0.006	0.005
	Elevation, deg . . . . .	0.017	0.008	-0.006	0.008
Carnarvon	Range, ft . . . . .	40	20	0.9	13.3
	Azimuth, deg . . . . .	0.017	0.008	0	0.006
	Elevation, deg . . . . .	0.017	0.008	0.015	0.008
White Sands	Range, ft . . . . .	60	30	15.7	37.8
	Azimuth, deg . . . . .	0.022	0.011	0.015	0.012
	Elevation, deg . . . . .	0.022	0.011	-0.009	0.008
MILA	Range, ft . . . . .	60	30	60.4	32.3
	Azimuth, deg . . . . .	0.022	0.011	-0.004	0.004
	Elevation, deg . . . . .	0.022	0.011	-0.008	0.010
Grand Bahama	Range, ft . . . . .	60	30	152.6	35.9
	Azimuth, deg . . . . .	0.022	0.011	-0.015	0.002
	Elevation, deg . . . . .	0.022	0.011	-0.005	0.007

~~CONFIDENTIAL~~

CONFIDENTIAL

3-13

TABLE 3.1-V.- REVOLUTION 2 TRACKING RESIDUAL STATISTICS

Station	Data type	Theoretical bias ( $\pm$ )	Theoretical noise ( $\pm$ )	Actual bias	Actual noise (rms)
Bermuda	Range, ft . . . . .	60	30	-18.7	40.2
	Azimuth, deg . . . . .	0.022	0.011	-0.013	0.012
	Elevation, deg . . . . .	0.022	0.011	-0.009	0.015
California	Range, ft . . . . .	60	30	-25.4	81.8
	Azimuth, deg . . . . .	0.022	0.011	-0.007	0.006
	Elevation, deg . . . . .	0.022	0.011	-0.015	0.006
White Sands	Range, ft . . . . .	60	30	-30.3	46.0
	Azimuth, deg . . . . .	0.022	0.011	-0.009	0.027
	Elevation, deg . . . . .	0.022	0.011	-0.012	0.029
Hawaii	Range, ft . . . . .	60	30	4.3	36.1
	Azimuth, deg . . . . .	0.022	0.011	0.010	0.010
	Elevation, deg . . . . .	0.022	0.011	-0.030	0.011
Carnarvon	Range, ft . . . . .	40	20	0	16.9
	Azimuth, deg . . . . .	0.017	0.008	-0.002	0.004
	Elevation, deg . . . . .	0.017	0.008	0.015	0.008
Bermuda	Range, ft . . . . .	40	20	17.5	38.2
	Azimuth, deg . . . . .	0.017	0.008	0.003	0.025
	Elevation, deg . . . . .	0.017	0.008	-0.004	0.019
Grand Bahama	Range, ft . . . . .	60	30	48.2	32.2
	Azimuth, deg . . . . .	0.022	0.011	-0.005	0.008
	Elevation, deg . . . . .	0.022	0.011	-0.015	0.015

CONFIDENTIAL

~~CONFIDENTIAL~~

TABLE 3.1-VI.- COAST ELLIPSE PLANNED AND ACTUAL  
TRAJECTORY PARAMETERS

Condition	Planned	Actual
Injection (Second S-IVB Stage Cutoff Plus 10 Seconds)		
Time from range zero, hr:min:sec . . . . .	03:16:49.9	03:16:36.3
Geodetic latitude, deg North . . . . .	27.77	27.87
Longitude, deg West . . . . .	58.08	58.58
Altitude, ft . . . . .	1 925 302	1 845 719
Altitude, n. mi. . . . .	317	304
Spaced-fixed velocity, ft/sec . . . . .	30 786	30 823
Spaced-fixed flight-path angle, deg . . . . .	15.29	15.03
Space-fixed heading angle, deg E of N . . . . .	103.02	102.76
CSM/S-IVB Separation		
Time from range zero, hr:min:sec . . . . .	03:26:42.8	03:26:28.2
Geodetic latitude, deg North . . . . .	15.35	15.43
Longitude, deg West . . . . .	24.94	25.10
Altitude, ft . . . . .	8 082 316	7 948 424
Altitude, n. mi. . . . .	1330	1308
Space-fixed velocity, ft/sec . . . . .	26 185	26 233
Space-fixed flight-path angle, deg . . . . .	26.74	26.53
Space-fixed heading angle, deg E of N . . . . .	116.52	116.46

~~CONFIDENTIAL~~



~~CONFIDENTIAL~~

3-15

TABLE 3.1-VI.- COAST ELLIPSE PLANNED AND ACTUAL  
TRAJECTORY PARAMETERS - Continued

Condition	Planned	Actual
First SPS Ignition		
Time from range zero, hr:min:sec . . . . .	03:28:20.1	03:28:06.6
Geodetic latitude, deg North . . . . .	13.36	13.44
Longitude, deg West . . . . .	21.33	21.46
Altitude, ft . . . . .	9 248 199	9 110 599
Altitude, n. mi. . . . .	1522	1499
Space-fixed velocity, ft/sec . . . . .	25 459	25 504
Space-fixed flight-path angle, deg . . . . .	27.99	27.80
Space-fixed heading angle, deg E of N . . .	117.51	117.46
First SPS Cutoff		
Time from range zero, hr:min:sec . . . . .	03:28:35.1	03:28:22.6
Geodetic latitude, deg North . . . . .	13.06	13.15
Longitude, deg West . . . . .	20.82	20.91
Altitude, ft . . . . .	9 429 496	9 301 402
Altitude, n. mi. . . . .	1552	1531
Space-fixed velocity, ft/sec . . . . .	25 507	25 547
Space-fixed flight-path angle, deg . . . . .	28.44	28.30
Space-fixed heading angle, deg E of N . . .	117.64	117.59

~~CONFIDENTIAL~~

~~CONFIDENTIAL~~

TABLE 3.1-VI.- COAST ELLIPSE PLANNED AND ACTUAL

## TRAJECTORY PARAMETERS - Continued

Condition	Planned	Actual
Apogee		
Time from range zero, hr:min:sec . . . . .	05:48:43.1	05:46:49.5
Geodetic latitude, deg South . . . . .	28.69	28.68
Longitude, deg East . . . . .	36.39	36.87
Altitude, ft . . . . .	60 092 348	59 358 268
Altitude, n. mi. . . . .	9890	9769
Space-fixed velocity, ft/sec . . . . .	8450	8405
Space-fixed flight-path angle, deg . . . . .	0.0	0.0
Space-fixed heading angle, deg E of N . . .	100.38	100.38
Second SPS Ignition		
Time from range zero, hr:min:sec . . . . .	08:14:42.7	08:10:54.8
Geodetic latitude, deg North . . . . .	3.67	3.45
Longitude, deg East . . . . .	116.92	117.49
Altitude, ft . . . . .	5 303 046	5 340 719
Altitude, n. mi. . . . .	873	879
Space-fixed velocity, ft/sec . . . . .	28 235	28 173
Space-fixed flight-path angle, deg . . . . .	-23.14	-23.22
Space-fixed heading angle, deg E of N . . .	59.87	59.85

~~CONFIDENTIAL~~

~~CONFIDENTIAL~~

3-17

TABLE 3.1-VI.- COAST ELLIPSE PLANNED AND ACTUAL

TRAJECTORY PARAMETERS - Concluded

Condition	Planned	Actual
Second SPS Cutoff		
Time from range zero, hr:min:sec . . . . .	08:19:11.3	08:15:35.4
Geodetic latitude, deg North . . . . .	12.64	12.83
Longitude, deg East . . . . .	131.93	133.25
Altitude, ft . . . . .	2 279 663	2 187 530
Altitude, n. mi. . . . .	375	360
Space-fixed velocity, ft/sec . . . . .	34 816	35 115
Space-fixed flight-path angle, deg . . . . .	-17.98	-17.64
Space-fixed heading angle, deg E of N . . . .	62.16	62.21
CM/SM Separation		
Time from range zero, hr:min:sec . . . . .	08:21:45.7	08:18:02.6
Geodetic latitude, deg North . . . . .	18.64	18.62
Longitude, deg East . . . . .	143.84	144.74
Altitude, ft . . . . .	900 749	886 467
Altitude, n. mi. . . . .	148	146
Space-fixed velocity, ft/sec . . . . .	35 912	36 138
Space-fixed flight-path angle, deg . . . . .	-11.25	-11.07
Space-fixed heading angle, deg E of N . . . .	65.55	65.49

~~CONFIDENTIAL~~

~~CONFIDENTIAL~~

TABLE 3.1-VII.- COAST ELLIPSE TRACKING RESIDUAL STATISTICS

Station	Data type	Theoretical bias ( $\pm$ )	Theoretical noise ( $\pm$ )	Actual bias	Actual noise (rms)
Ascension C-band	Range, ft . . . . .	60	30	1.5	9.5
	Azimuth, deg . . . . .	0.022	0.011	0.007	0.004
	Elevation, deg . . . . .	0.022	0.011	-0.001	0.008
Unified S-band	Range, ft . . . . .	60	30	-1.7	44.2
	X, deg . . . . .	0.090	0.040	0.027	0.012
	Y, deg . . . . .	0.090	0.040	-0.012	0.011
	Doppler, Hz . . . . .	0.300	0.150	0.0006	0.0929
Carnarvon C-band	Range, ft . . . . .	40	20	5.9	26.7
	Azimuth, deg . . . . .	0.017	0.008	-0.004	0.005
	Elevation, deg . . . . .	0.017	0.008	0.009	0.010
Unified S-band	Range, ft . . . . .	60	30	3.2	14.7
	X, deg . . . . .	0.090	0.040	-0.043	0.004
	Y, deg . . . . .	0.090	0.040	0.001	0.003
	Doppler, Hz . . . . .	0.300	0.150	-0.0426	0.1524

~~CONFIDENTIAL~~

~~CONFIDENTIAL~~

3-19

TABLE 3.1-VIII.- SPS THRUST AND TARGETING CHARACTERISTICS

Case	Maneuver	Thrust character- istics	Burn time, sec	$\Delta V$ , ft/sec	Apogee, n. mi.	Semilatus rectum, P, ft	Eccentricity, e
I	SPS-1	-	16.00	212.50	9769.11	32 833 060	0.59133947
II	SPS-1	Actual	15.97	213.44	9769.08	32 832 753	0.59134189
III	SPS-1	Actual	18.76	249.56	9890.4	32 928 386	0.59388164
IV	SPS-1	Actual	16.12	217.53	9890.02	32 927 832	0.59387747
V	SPS-2	-	280.6	4824.3	-	42 488 012	1.022161
VI	SPS-2	Actual	279.0	4820.3	-	42 487 421	1.022127
VII	SPS-2	Actual	269.83	4604.6	-	41 959 029	0.9990709
VIII	SPS-2	Actual	269.88	4606.1	-	41 959 365	0.9990709

~~CONFIDENTIAL~~

~~CONFIDENTIAL~~

TABLE 3.1-IX.- ENTRY INTERFACE PLANNED AND ACTUAL  
TRAJECTORY PARAMETERS

Condition	Planned	Actual
Time from range zero, hr:min:sec . . . . .	08:23:12.8	08:19:28.5
Geodetic latitude, deg North . . . . .	21.90	21.86
Longitude, deg East . . . . .	151.58	152.42
Altitude, ft . . . . .	400 000	400 000
Altitude, n. mi. . . . .	66	66
Space-fixed velocity, ft/sec . . . . .	36 333	36 545
Space-fixed flight-path angle, deg . . . . .	-7.13	-6.93
Space-fixed heading angle, deg E of N . . . .	68.35	68.26

~~CONFIDENTIAL~~

~~CONFIDENTIAL~~

3-21

TABLE 3.1-X.- SUMMARY OF PLANNED AND ACTUAL ENTRY PARAMETERS

Entry Conditions		
Parameter	Planned	Actual
Maximum entry velocity, ft/sec . . . . .	36 419	36 629
Maximum entry deceleration, g . . . . .	8.34	7.27
Drogue Parachute Deployment Coordinates		
Time from range zero, hr:min:sec . . . . .	08:35:11.0	08:31:18.6
Latitude, deg North . . . . .	30.00	30.10 <sup>a</sup>
Longitude, deg West . . . . .	172.40	172.52 <sup>a</sup>

<sup>a</sup>Based on recovery data,  
G&N indicated - 172.38, 29.97  
BET indicated - 172.48, 30.02.

~~CONFIDENTIAL~~

~~CONFIDENTIAL~~

NASA-S-68-308

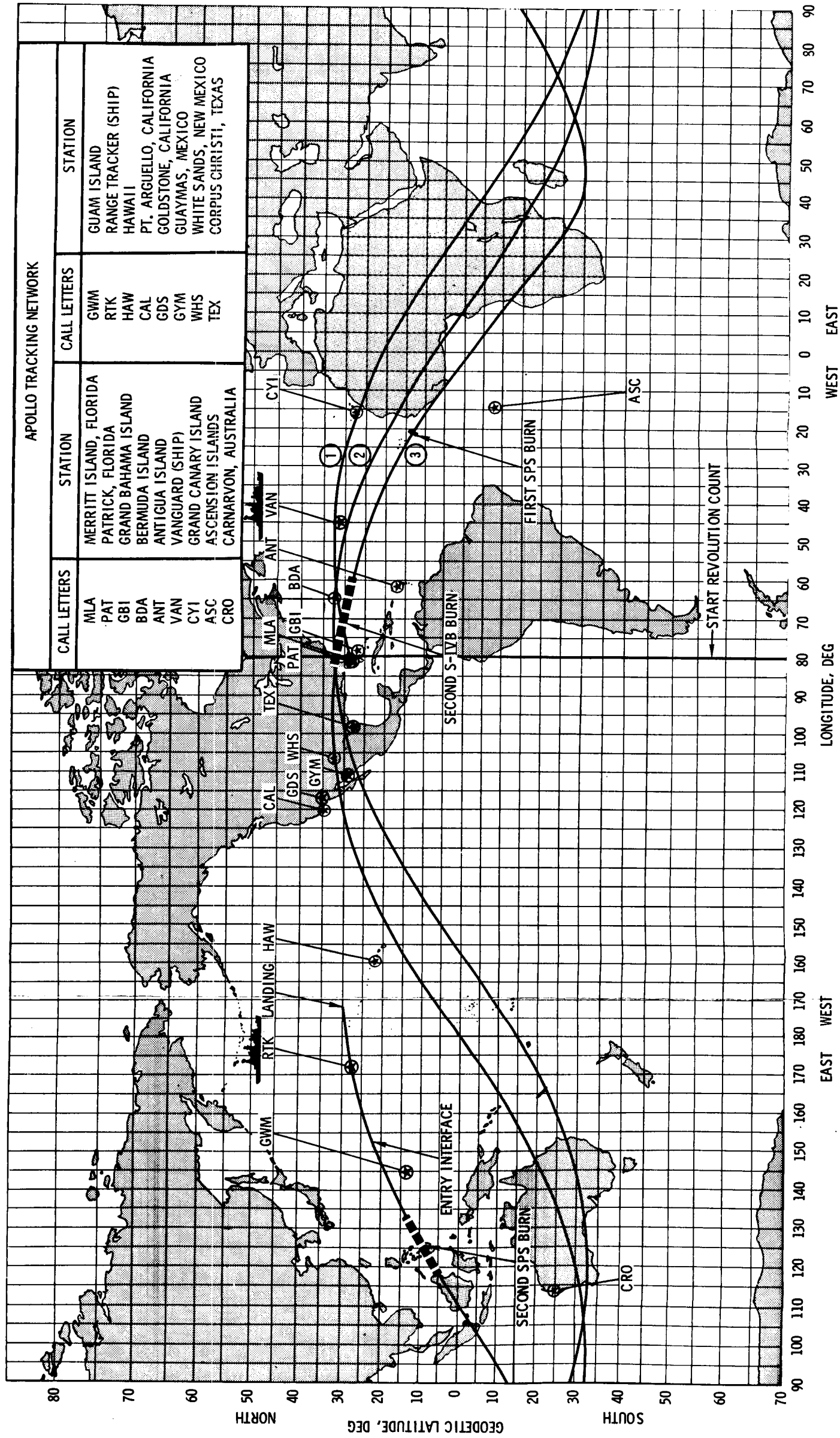


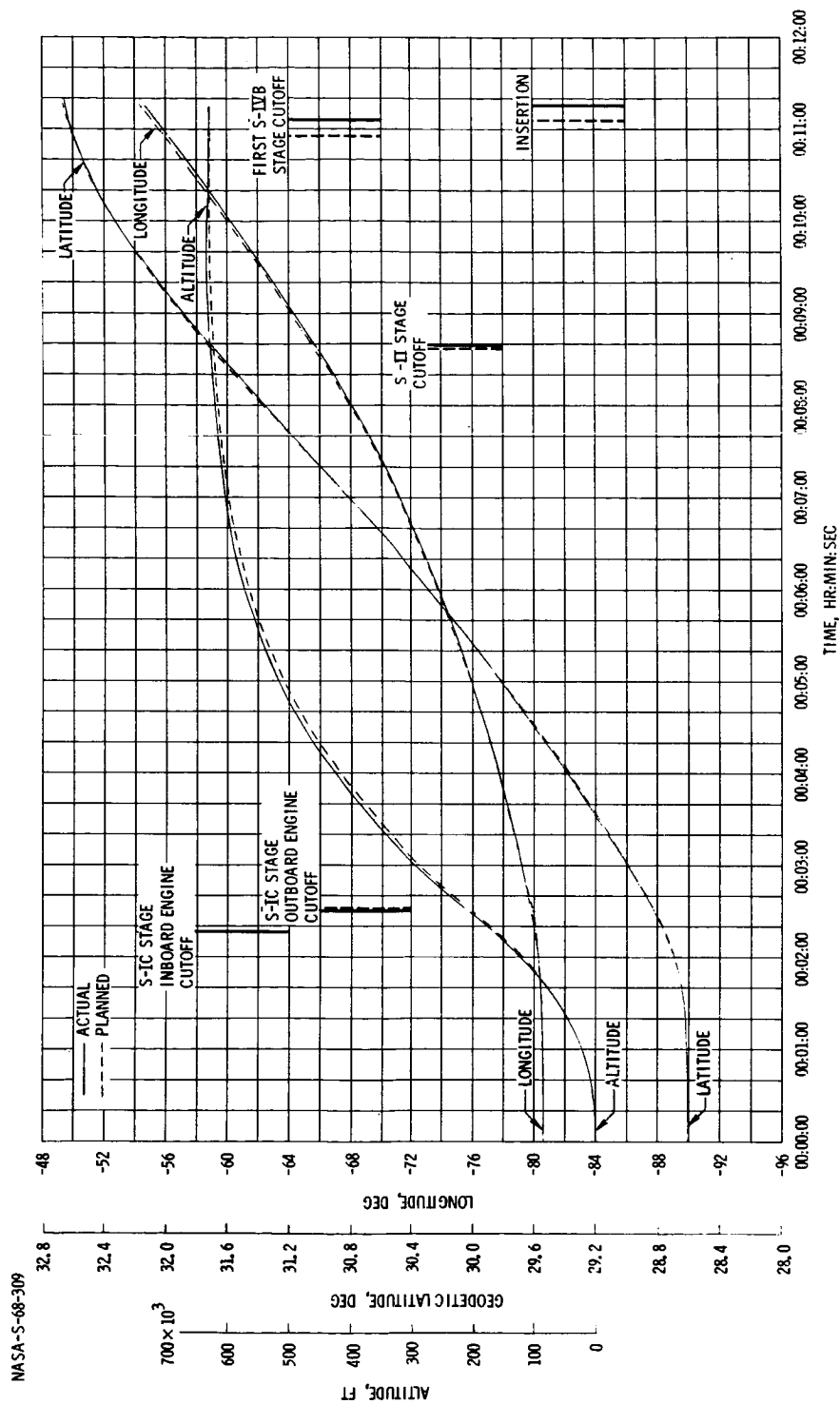
FIGURE 3.1-1.- APOLLO 4 MISSION GROUND TRACK.

~~CONFIDENTIAL~~



~~CONFIDENTIAL~~

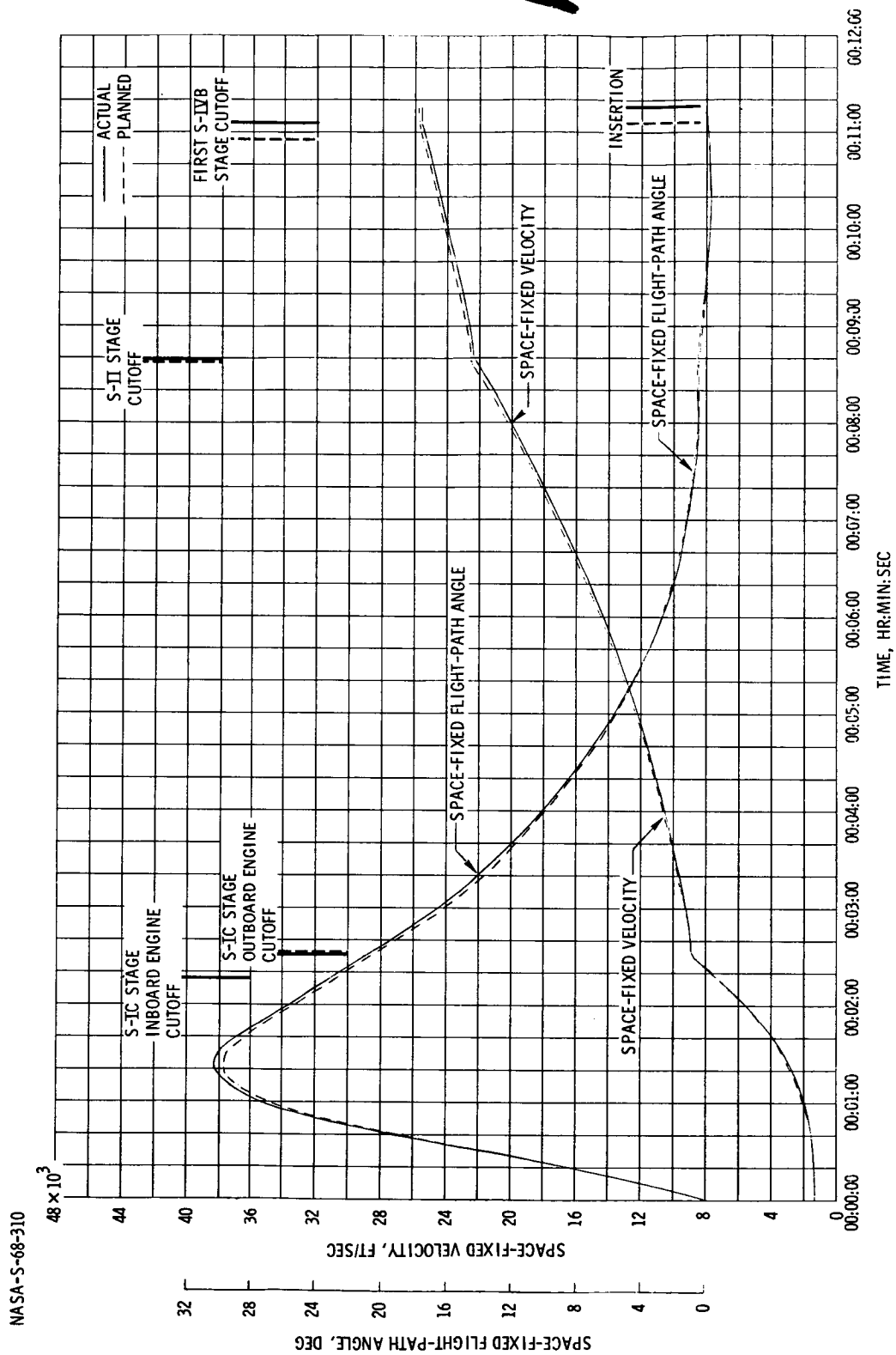
3-23



(A) LATITUDE, LONGITUDE, AND ALTITUDE.

FIGURE 3.1-2. - TIME HISTORY OF THE LAUNCH PHASE.

~~CONFIDENTIAL~~

~~CONFIDENTIAL~~

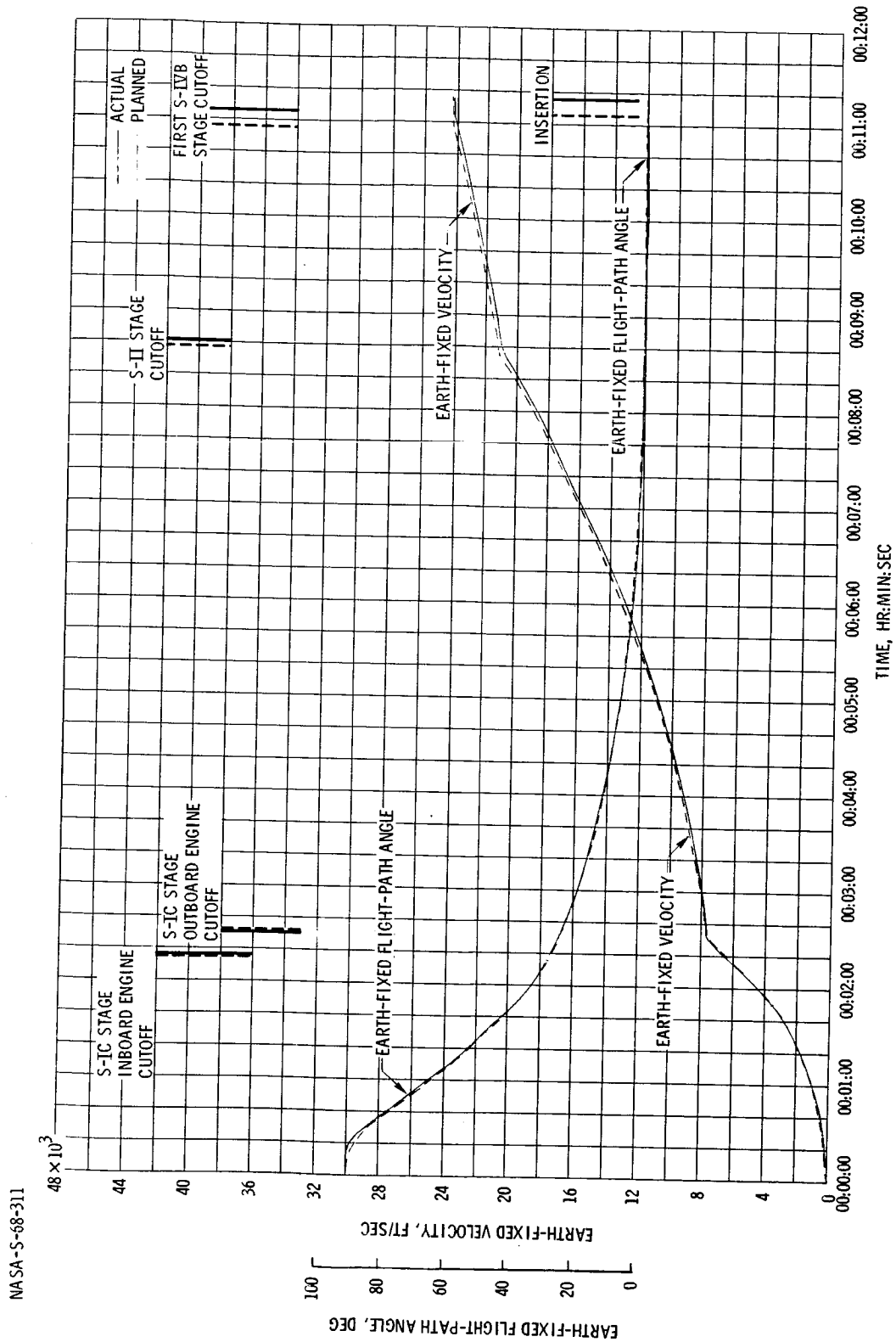
(B) SPACE-FIXED FLIGHT-PATH ANGLE AND VELOCITY.

FIGURE 3.1-2. - CONTINUED.

~~CONFIDENTIAL~~

~~CONFIDENTIAL~~

3-25



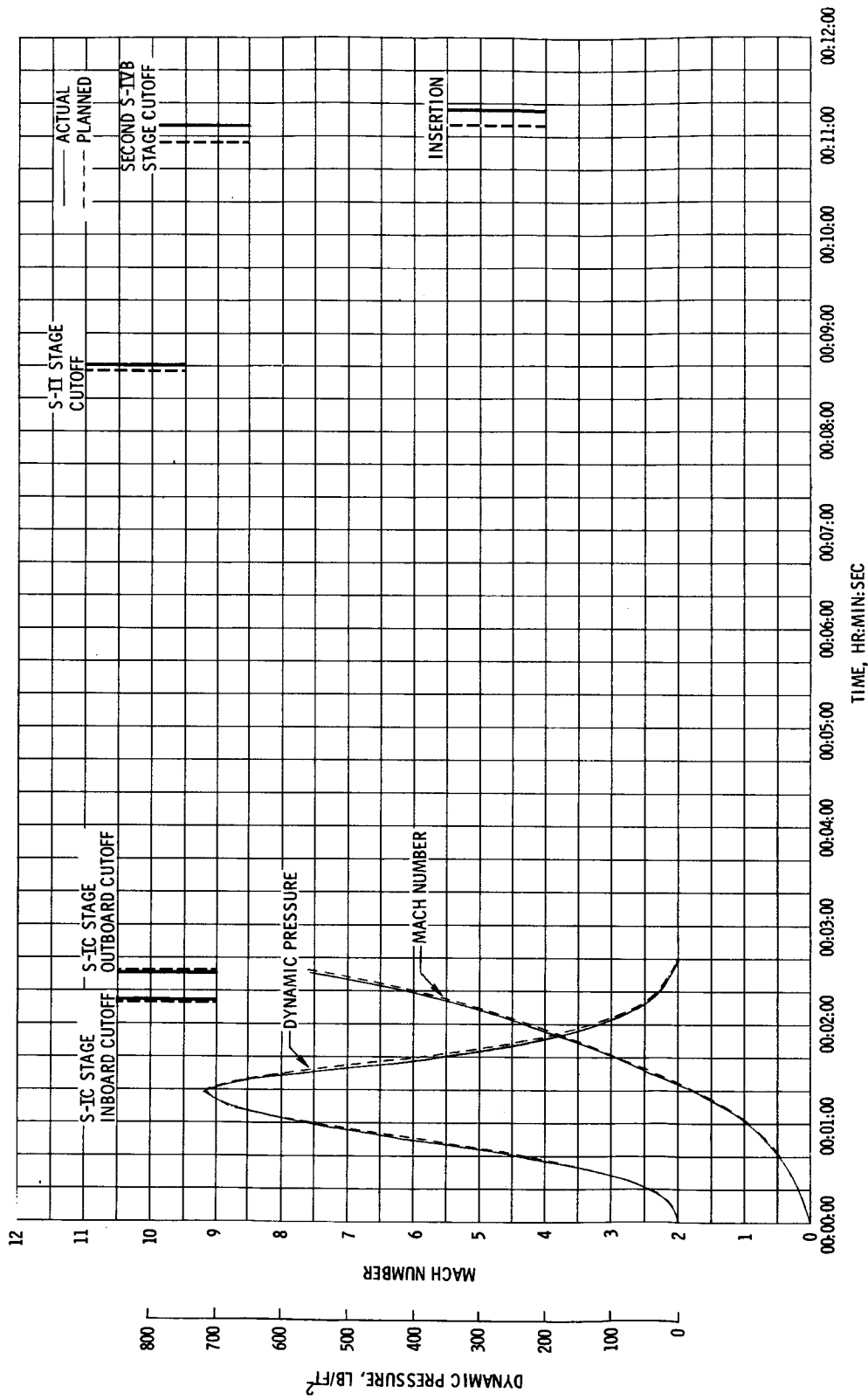
(C) EARTH-FIXED FLIGHT-PATH ANGLE AND VELOCITY.

FIGURE 3.1-2. - CONTINUED.

~~CONFIDENTIAL~~

~~CONFIDENTIAL~~

NASA-S-68-312



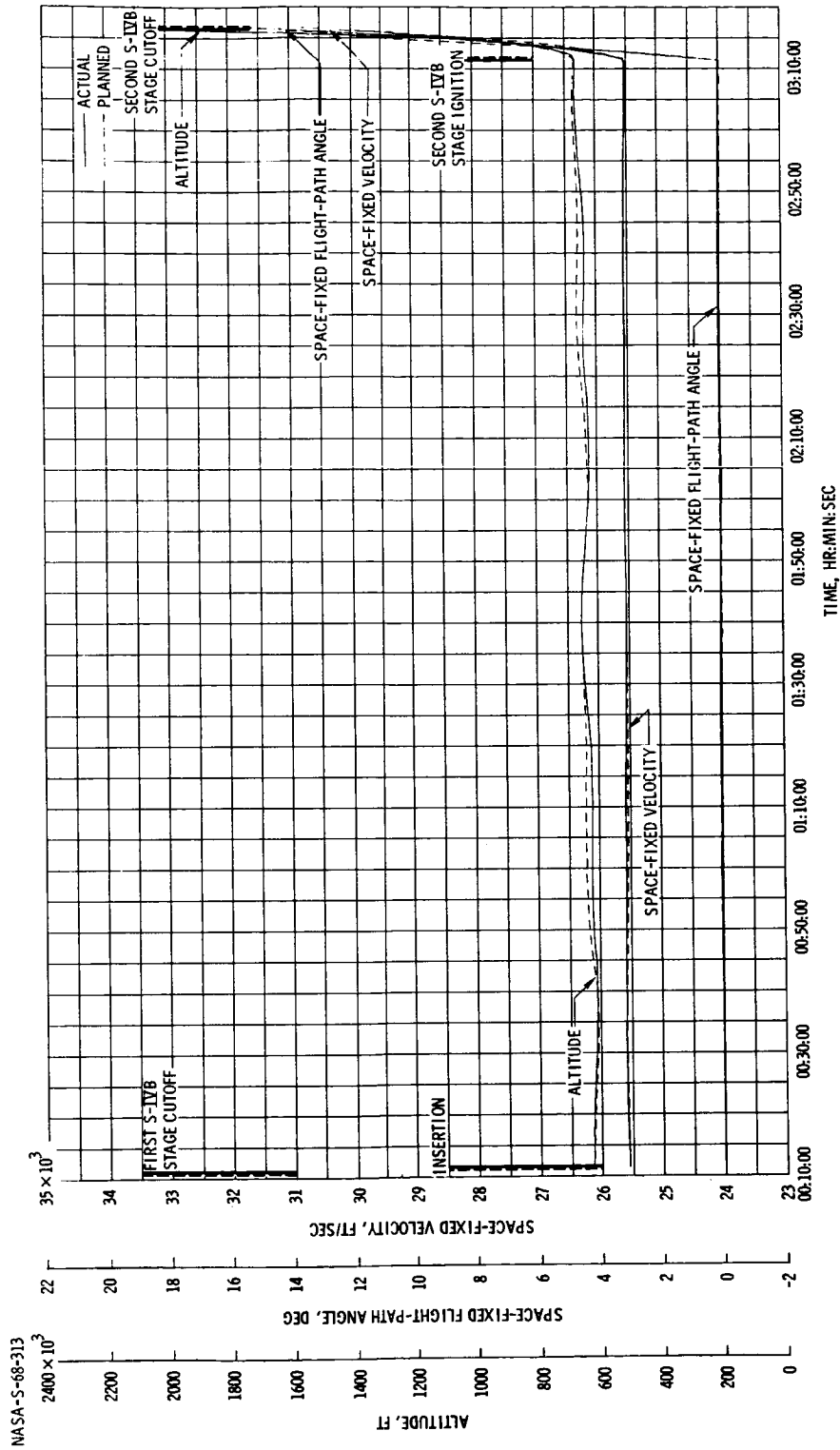
(D) MACH NUMBER AND DYNAMIC PRESSURE.

FIGURE 3.1-2. - CONCLUDED.

~~CONFIDENTIAL~~

~~CONFIDENTIAL~~

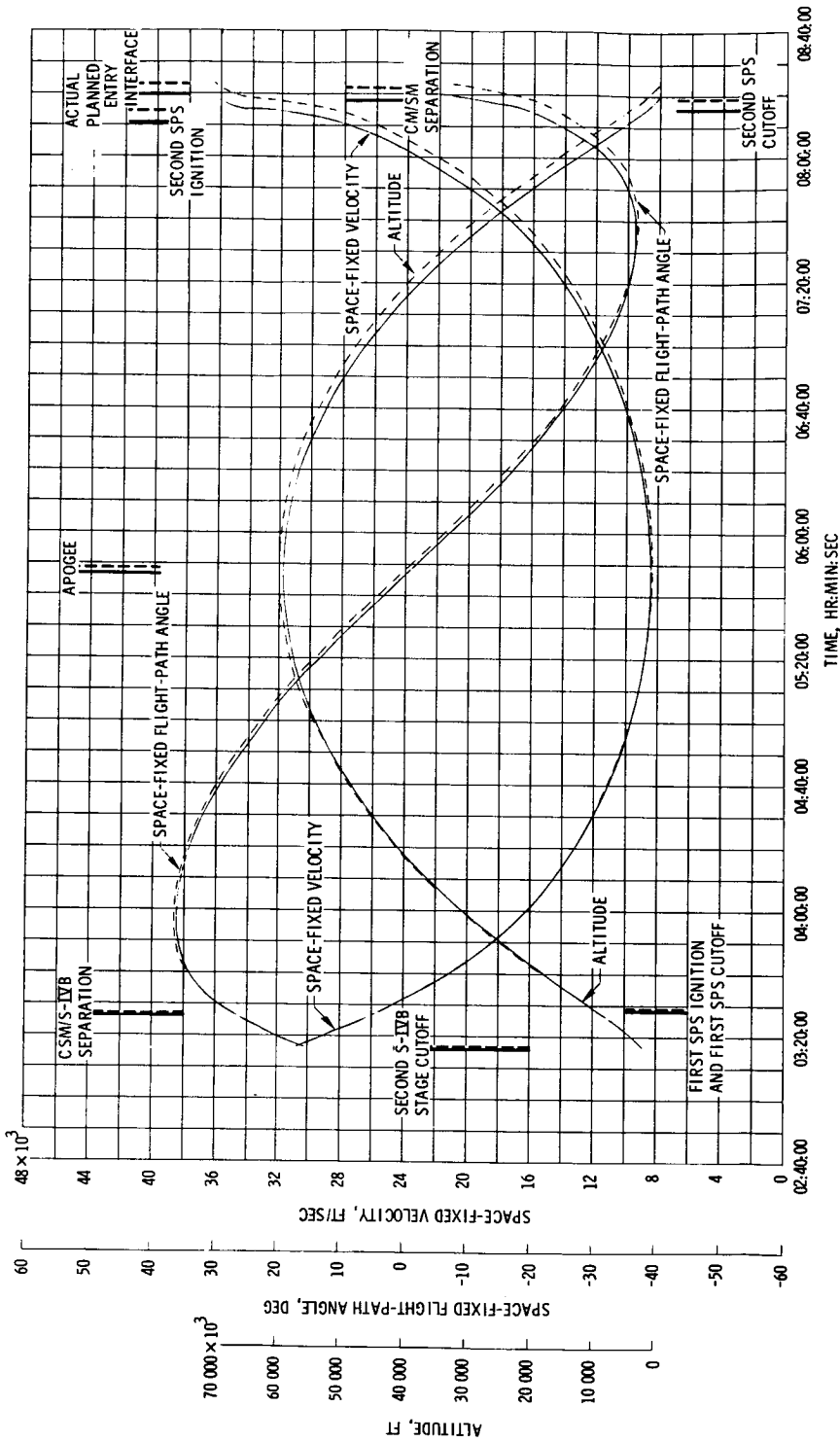
3-27



(A) PARKING ORBIT.

FIGURE 3.1-3. - ORBITAL TIME HISTORY OF SPACE-FIXED FLIGHT-PATH ANGLE, VELOCITY, AND ALTITUDE.

~~CONFIDENTIAL~~

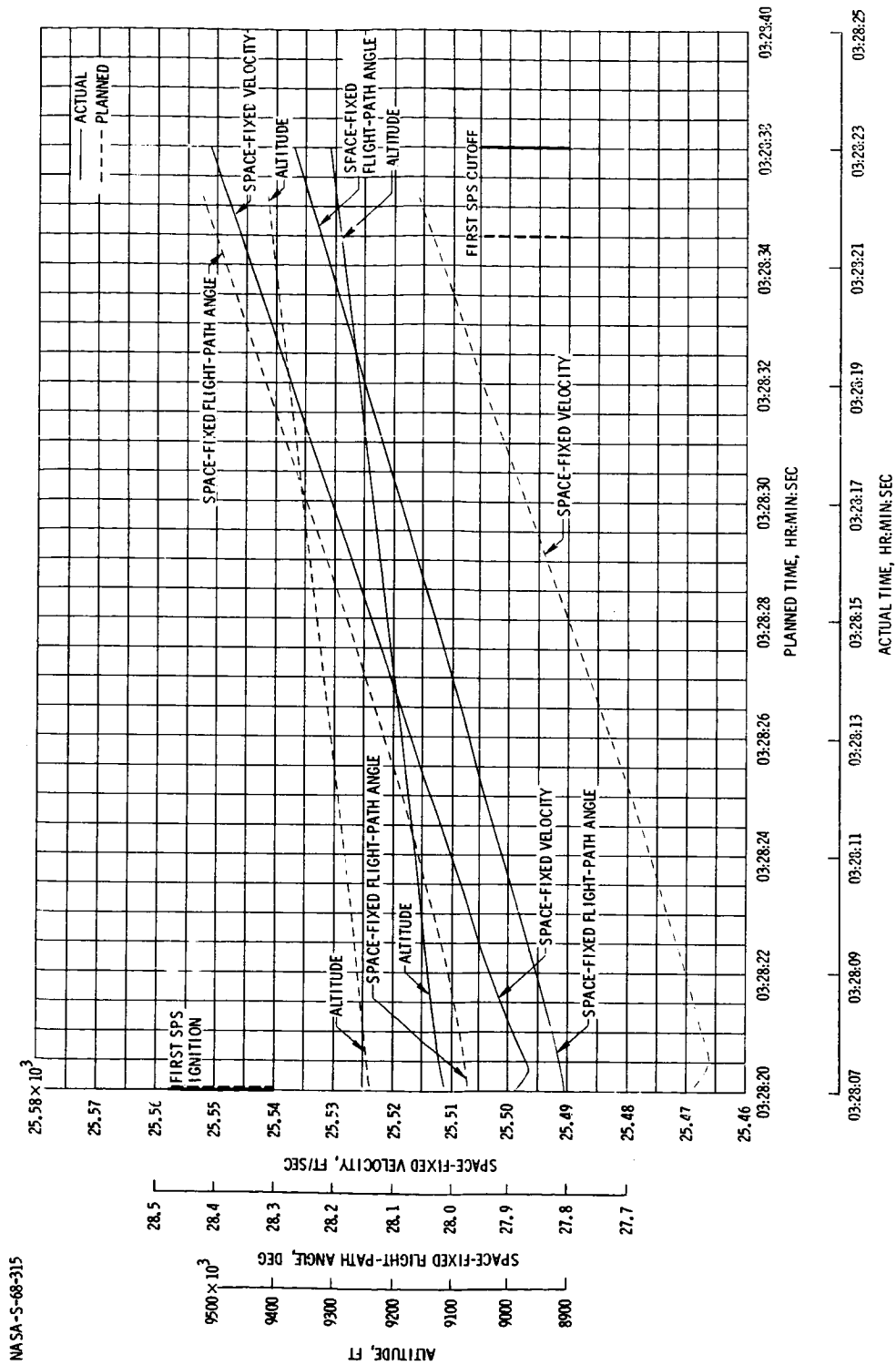
~~CONFIDENTIAL~~

(B) COAST ELLIPSE.

FIGURE 3.1-3. - CONCLUDED.

~~CONFIDENTIAL~~

~~CONFIDENTIAL~~

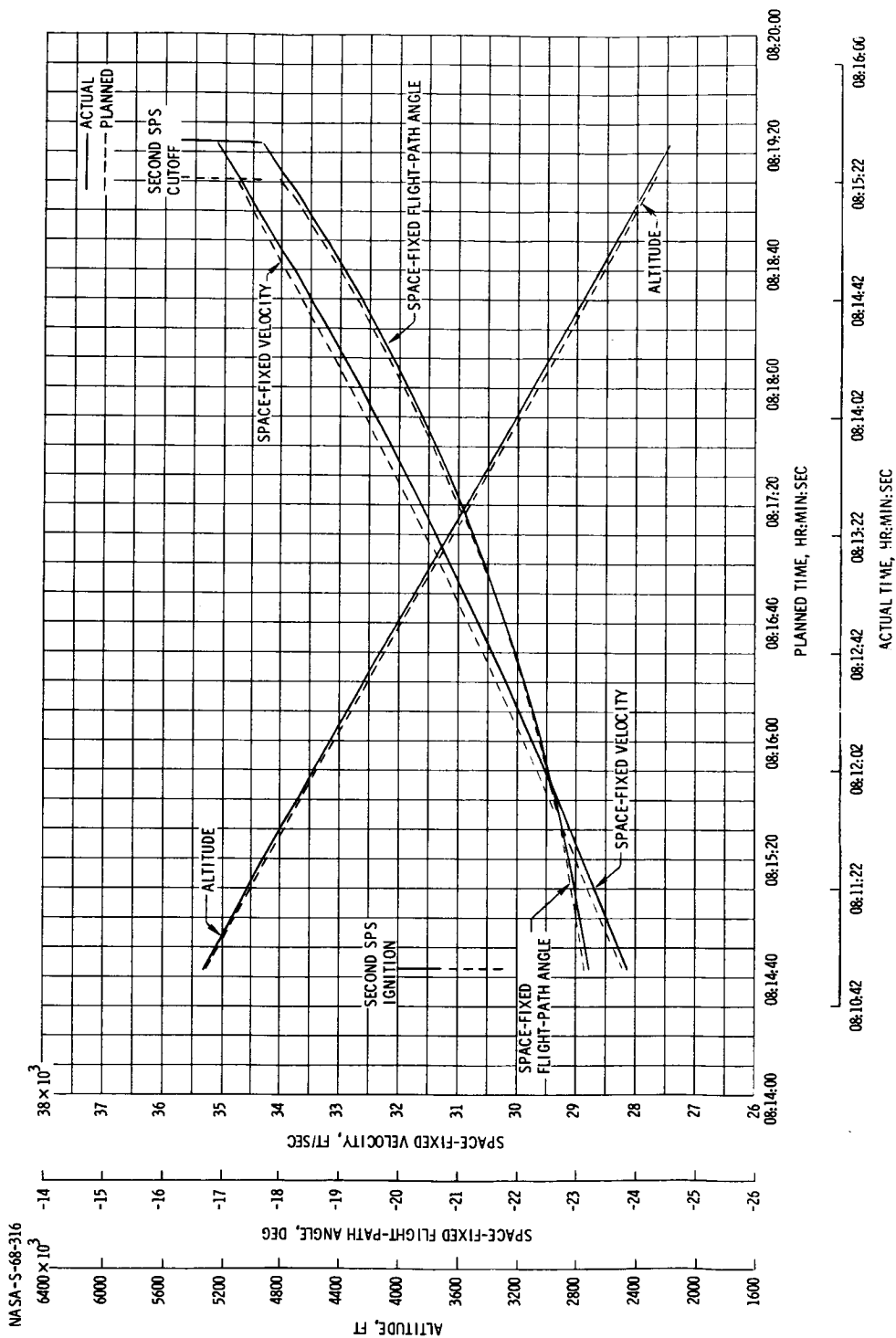


(A) FIRST SERVICE PROPUSSION SUBSYSTEM BURN.

3.1-4. - SERVICE PROPUSSION SUBSYSTEM BURN TIME HISTORY OF SPACE-FIXED FLIGHT-PATH ANGLE, VELOCITY, AND ALTITUDE.

~~CONFIDENTIAL~~

~~CONFIDENTIAL~~



(B) SECOND SERVICE PROPULSION SUBSYSTEM BURN.

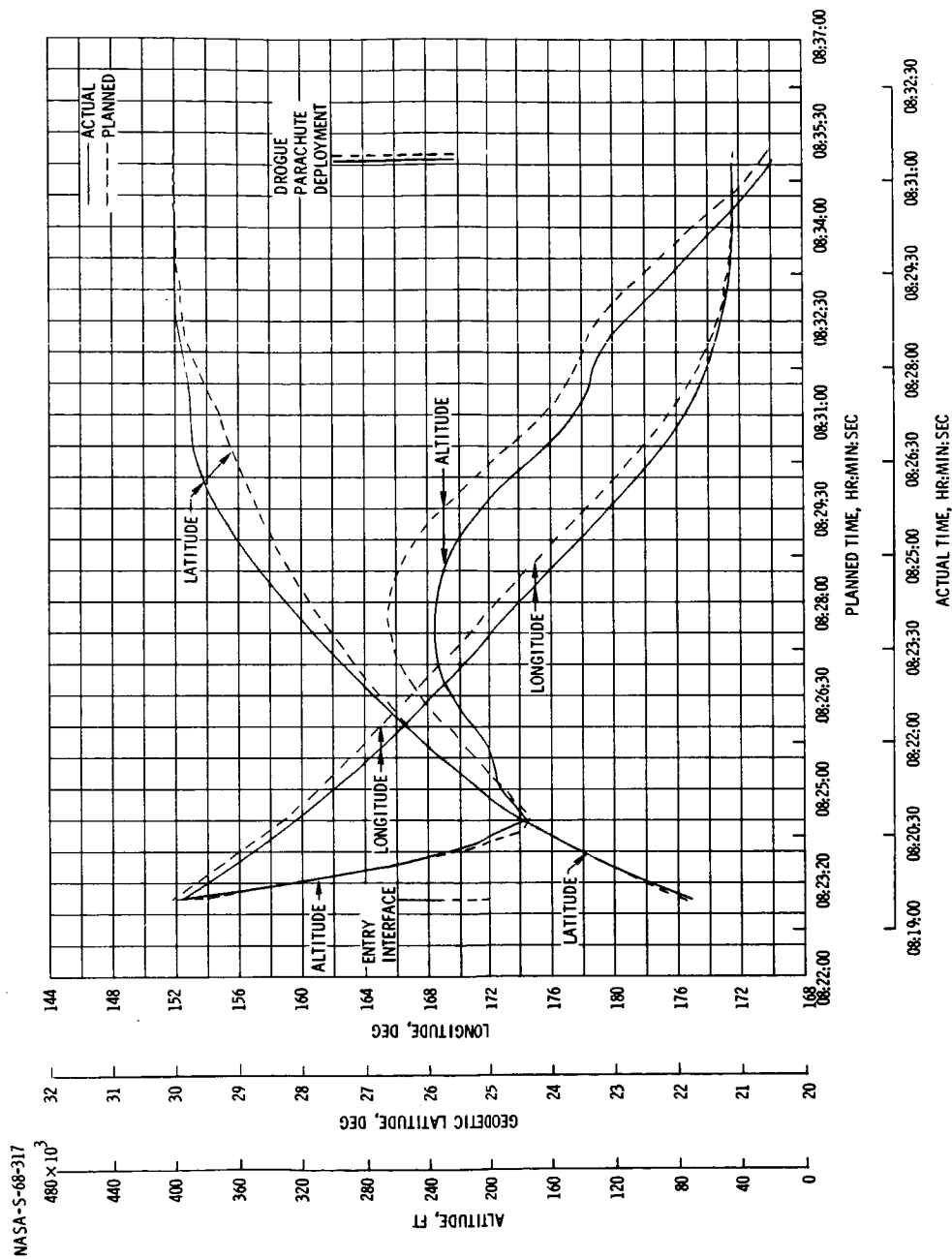
FIGURE 3.1-4. - CONCLUDED.

~~CONFIDENTIAL~~



~~CONFIDENTIAL~~

3-31

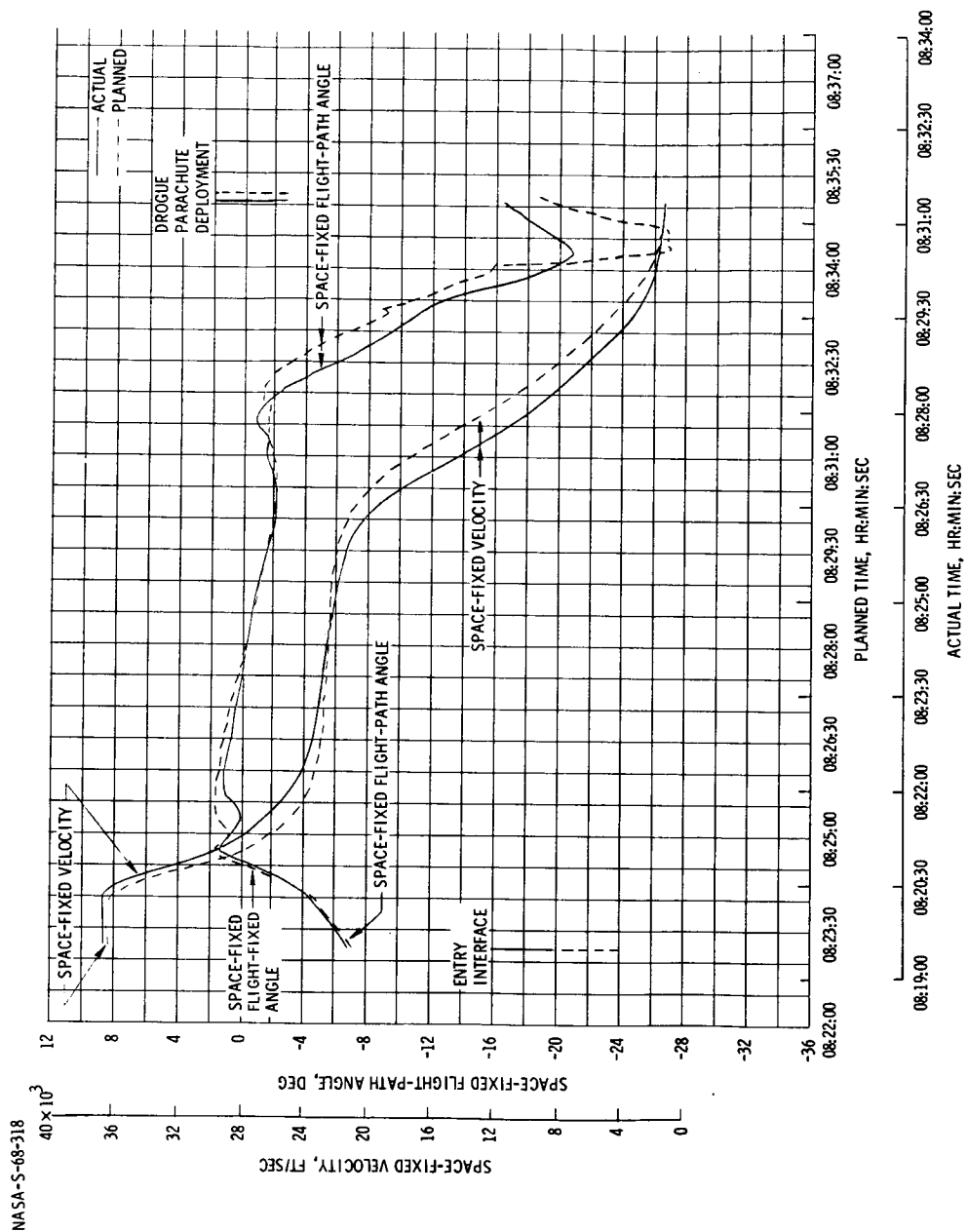


(A) LATITUDE, LONGITUDE, ALTITUDE.

FIGURE 3.1-5. - TIME HISTORY OF ENTRY PHASE.

~~CONFIDENTIAL~~

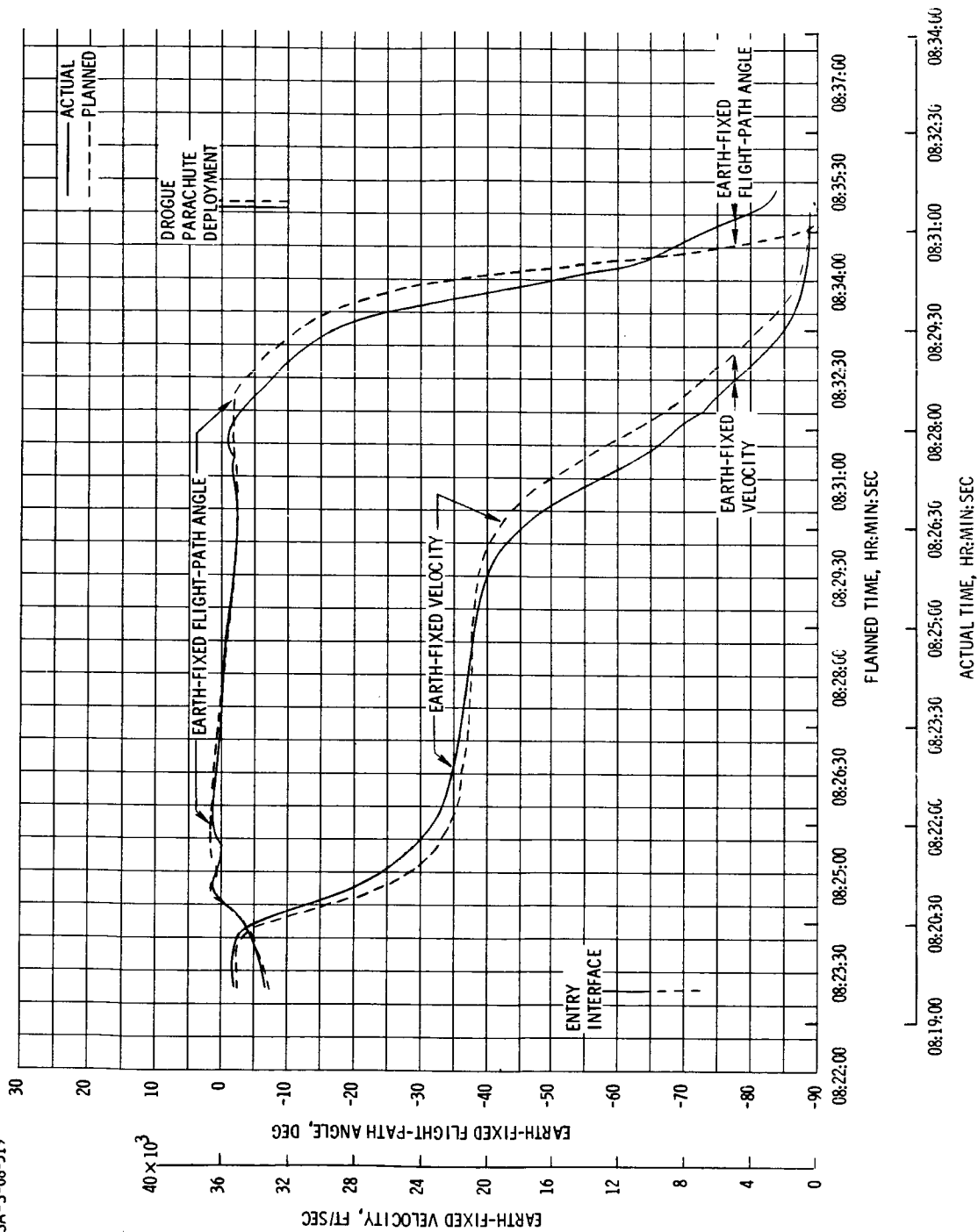
CONFIDENTIAL



(B) SPACE-FIXED FLIGHT-PATH ANGLE AND VELOCITY.

FIGURE 3.1-5. - CONTINUED.

CONFIDENTIAL

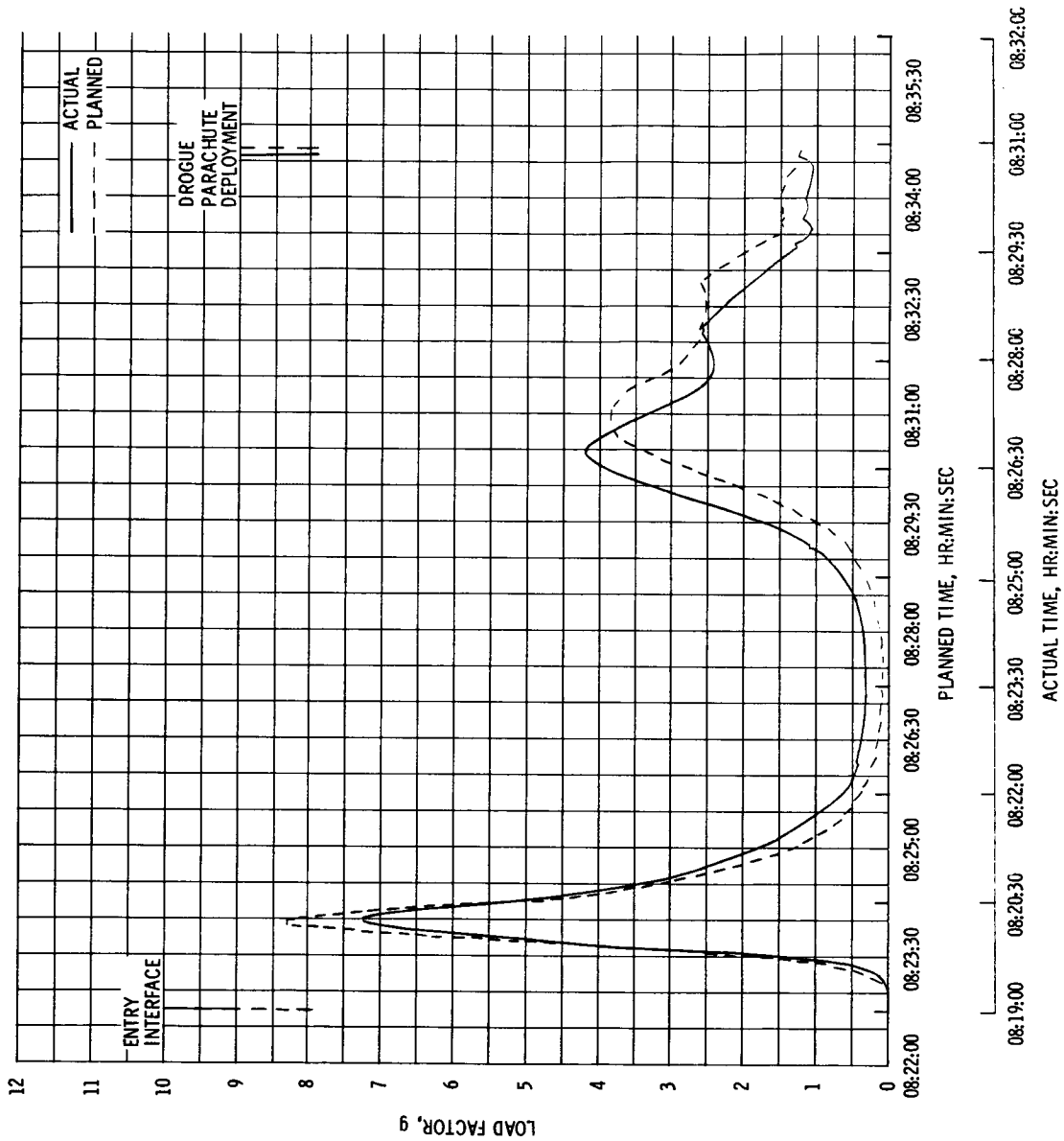


(C) EARTH-FIXED FLIGHT-PATH ANGLE AND VELOCITY.

FIGURE 3.1-5. - CONTINUED.

~~CONFIDENTIAL~~

~~CONFIDENTIAL~~

~~CONFIDENTIAL~~

(D) LOAD FACTOR.

FIGURE 3.1-5. - CONCLUDED.

~~CONFIDENTIAL~~

~~CONFIDENTIAL~~

3-35

### 3.2 DUAL MISSION

This heading is not applicable to this report, but was intended to be used in the event of a dual mission.

~~CONFIDENTIAL~~

~~CONFIDENTIAL~~

THIS PAGE INTENTIONALLY LEFT BLANK

~~CONFIDENTIAL~~

~~CONFIDENTIAL~~

4-1

#### 4.0 LAUNCH VEHICLE PERFORMANCE

The S-IC stage flight was near nominal. The maximum angle of attack during first stage burn was 1.3 degrees and the maximum engine deflections were 0.6 degree. The thrust buildup of the engines is shown in figure 5.1-2.

The Apollo/Saturn V space vehicle reached Mach 1 at 00:01:01.4 at an altitude of 4 n. mi. Maximum dynamic pressure was reached at 00:01:18.5 at an altitude of 7.2 n. mi.

The S-IC inboard engine was cut off by a timer at 00:02:15.5. S-IC outboard engine cutoff occurred because of liquid oxygen depletion at 00:02:30.8 with the vehicle at 34.4 n. mi. altitude, at a velocity of 8831 ft/sec. Cameras on the S-II stage photographed a smooth separation of the S-IC stage and, later, the aft interstage from the S-II stage.

Propulsion and other systems on the S-IC, including the pressurization and the pneumatic control pressure systems, operated within expected tolerances.

S-II engine performance, the stage propellant utilization system, pressurization system, pneumatic control pressure system, camera ejection system, and the helium injection system operated satisfactorily. All five J-2 engines operated properly during the engine start sequence and burn. The S-II stage liquid hydrogen tank external insulation performed satisfactorily with no defects noted during countdown or in flight. S-II stage cutoff occurred because of liquid oxygen depletion at 00:08:39.8.

The third stage (S-IVB) first burn lasted 144.9 seconds. The single J-2 engine was cut off by the guidance system at 00:11:05.6 after achieving insertion conditions for the earth parking orbit. Insertion was 9.6 seconds later than planned, at a velocity of 25 564 ft/sec. The space vehicle was inserted into a nearly circular orbit with an apogee altitude of 101.1 n. mi. and a perigee altitude of 99.1 n. mi.

The vehicle remained in the near earth parking orbit for approximately two revolutions around the earth. During this time a small continuous thrust was provided from the venting of the liquid hydrogen tank to provide a settling force to maintain the propellants in the S-IVB stage in the bottom of the tanks. Restart preparations, which included repressurizing the liquid hydrogen tanks, were started when the vehicle was over the western part of North America. Reignition of the S-IVB stage occurred when the vehicle was back over the Eastern Test Range.

~~CONFIDENTIAL~~

~~CONFIDENTIAL~~

Hydraulic systems on all three stages performed without evidence of out-of-tolerance conditions.

Structurally the launch vehicle performed with no problems. Maximum bending occurred between 00:01:10 and 00:01:20. Longitudinal loads were near nominal throughout the flight, and longitudinal acceleration at S-IC inboard engine cutoff was 4.15g, which was very close to the expected value.

Small oscillations (5 to 6 Hz) in the first longitudinal mode were observed during the first 35 seconds of flight and again during the last half of S-IC boost. The first vehicle longitudinal mode was forced by small engine thrust variations which were close to the first mode frequency. Maximum response in the instrument unit was approximately 0.04g rms and is about the same order of magnitude that had been expected for the Saturn V launch vehicle. There was no sustained buildup in amplitude; therefore, these loads are of no consequence for the launch vehicle structure and should not be a problem for future flights.

The emergency detection subsystem was flown open loop on this flight. All indications were that the subsystem operated satisfactorily.

Both onboard cameras viewing first and second stage separation recorded excellent quality pictures and were recovered shortly after being ejected into the Atlantic.

For a detailed description of the launch vehicle performance, see reference 1.

~~CONFIDENTIAL~~



~~CONFIDENTIAL~~

5.1-1

## 5.0 COMMAND AND SERVICE MODULE PERFORMANCE

### 5.1 SPACECRAFT STRUCTURE

#### 5.1.1 Spacecraft Interface Loads

The primary structural loads objective for the Apollo 4 mission was to demonstrate the structural compatibility of the command and service module (CSM), spacecraft lunar module adapter (SLA), and launch vehicle in the Saturn V launch environment and to determine launch loads. This objective was satisfied.

Spacecraft structural loads have been evaluated for the critical load conditions that occur during portions of the boost phase, which dictate the design of the spacecraft structure. The critical load portions of the boost phase are as follows.

- a. Launch release
- b. Maximum dynamic pressure region
- c. End of first-stage boost
- d. First-stage separation.

Structural loads have been determined for the following interfaces during the boost periods of concern.

- a. Launch release
  - (1) LES/CM
  - (2) CM/SM
- b. Maximum dynamic pressure region (max q)
  - (1) CM/SM
  - (2) SM/SLA
  - (3) SLA/IU

~~CONFIDENTIAL~~

~~CONFIDENTIAL~~

## c. End of first-stage (S-IC) boost

- (1) CM/SM
- (2) SM/SLA
- (3) SLA/IU

## d. First-stage separation — Torsional loads at CM/SM interface

All spacecraft structural loads are based on accelerations measured at the locations shown in figure 5.1-1 and on aerodynamic data.

Loads have also been calculated for the upper portion of the SLA (Apollo station 775) for comparison with loads derived from strain gauge data; this comparison is made in the internal loads paragraph of this section of the report. Preflight predicted loads have also been included for the max q region.

Torsion loads have been determined for lift-off, 120.7 seconds after lift-off, and at first-stage separation.

## 5.1.2 Mission Phase Loads

Lift-off.— Spacecraft lateral loads before launch release result from steady-state winds, gusts, vortex shedding, and S-IC unsymmetric thrust buildup. These external forces also cause a large constraining moment and shear at the base of the launch vehicle. Spacecraft lateral loads immediately after lift-off are caused primarily by the sudden release of this constraining moment and shear.

Only moderate ground winds and gusts were measured before S-IC stage ignition. The average steady-state wind at the 60-foot level was 16.0 knots, with an average peak of 20.1 knots. No vehicle responses could be attributed to vortex shedding; however, vortex shedding was not expected at the measured ground wind velocities. The spacecraft lateral loads and accelerations before and after launch release were about the same magnitude although the sources of excitation were different. Lateral accelerations measured in the spacecraft before launch release were caused primarily by the unsymmetric thrust buildup of the S-IC engines (fig. 5.1-2). Spacecraft accelerations during launch are shown in figure 5.1-3. The lateral accelerations measured immediately after launch release were caused primarily by the sudden release of the shear and bending moment at the base of the vehicle. The maximum torsion at the CM/SM interface was excited during launch release. Torsional loads were also about the same magnitude before and after launch release. LES/CM and CM/SM interface loads are compared to design limit loads and are

~~CONFIDENTIAL~~

~~CONFIDENTIAL~~

5.1-3

shown in table 5.1-I. All launch release load conditions, based upon design loads, had factors of safety greater than the design factor of safety.

Maximum dynamic pressure region.- Large spacecraft interface loads normally occur in the region of flight where the product of dynamic pressure and angle of attack are maximum ( $\max q\alpha$ ).

The shears and magnitude of the winds aloft were moderate in the region of maximum dynamic pressure (fig. 5.1-4). The maximum angle of attack (measured by the q-ball) during the  $\max q$  region of flight was 1.82 degrees. However, a 2-Hz lateral oscillation, which was recorded throughout the first-stage flight, added significantly to the calculated lateral loads in the spacecraft. This oscillation was not caused by the flight winds and had not been included in any analysis for spacecraft design loads.

The spacecraft loads presented in table 5.1-II were derived by three methods.

- a. Predicted loads from MSFC preflight trajectory simulation using lift-off winds (used for the go/no-go determination).
- b. Predicted loads from MSC trajectory simulation using T minus 0 winds.
- c. Calculated loads using measured aerodynamic and acceleration data.

Loads at the forward portion of the SLA at Apollo station 775 were calculated using measured aerodynamic and acceleration data. Values obtained by these methods are compared with the  $\max q\alpha$  design loads in table 5.1-II. The predicted and calculated loads compare favorably and are well below the design values. The 2-Hz lateral oscillation causes a difference between the predicted and calculated loads. The CM/SM, SM/SLA, and SLA/IU loads are also compared with the structural capability of each interface (figs. 5.1-5, 5.1-6, and 5.1-7). The sway brace on radial beam truss no. 6 had a 1.33 factor of safety for the latest Apollo 4 loads. This was known prior to flight and was considered acceptable for this mission. The typical 2-Hz lateral acceleration is shown in figure 5.1-8.

Spacecraft axial acceleration oscillations of approximately 5-Hz were measured through first-stage boost and had the greatest magnitude between 107 seconds of flight time and inboard engine cutoff. This axial oscillation was not predicted nor considered in the prediction of design loads and will cause increased axial loads in the spacecraft

~~CONFIDENTIAL~~

~~CONFIDENTIAL~~

during boost; however, during this flight the oscillation, although causing increased axial loads in the spacecraft, did not cause excessive loads. The maximum CM/SM interface torsion loads, excluding launch release and engine shutdown, were measured at 120.7 seconds of flight time. This torsion load, 87 000 in-lb, was well below the torsional capability of the interface. This torsional load has been attributed to the axial oscillation. Spacecraft accelerations for this period of the flight are shown in figure 5.1-9.

End of first-stage boost.- The maximum axial acceleration and compression loads in the spacecraft were experienced immediately prior to inboard engine cutoff. The 2-Hz lateral acceleration of the spacecraft and the 5-Hz axial acceleration were both present at the end of first-stage boost. These effects had not been included in the analysis for the determination of the design loads. The bending moment at the CM/SM interface was significantly higher than used for design. This interface is not critical for this condition and is within the structural capability even considering this higher bending moment with the design axial load. Interface loads for end of first-stage boost are shown in table 5.1-III, and spacecraft accelerations are shown in figure 5.1-10.

Staging.- S-IC/S-II staging causes maximum tension and minimum acceleration for the spacecraft design. Also, maximum peak-to-peak axial acceleration oscillations occur at this time. During the period of high axial oscillations, torsional acceleration was occurring in the CM. The maximum torsion calculated for this period was 65 700 in-lb and was well below the torsional capability of the interface. Spacecraft accelerations during staging are shown in figure 5.1-11.

S-II stage and S-IVB stage operation.- There are no design conditions during the remainder of S-II stage and S-IVB stage boost phases, and no data were available between tower jettison and CM/SM separation. However, all acceleration levels were at a minimum during the S-II stage operation in which spacecraft data were recorded, and no significant spacecraft loads were experienced.

During the remainder of the period, when no structural data were available, no significant load conditions were expected.

### 5.1.3 Spacecraft Modifications

Shortly before the Apollo 4 mission the CM/SM structural interface was modified by the addition of four radial beam sway braces to the CM/SM interface. This modification was required after analysis revealed that excessive axial-torsional coupling of the spacecraft could be expected. This analysis was verified by testing on the Saturn V Dynamic

~~CONFIDENTIAL~~

~~CONFIDENTIAL~~

5.1-5

Test Vehicle at the Marshall Space Flight Center. The purpose of this modification was to reduce the axial torsional coupling during high amplitude axial transient conditions. The worst axial transient conditions for this flight occurred at lift-off, at 00:02:00.7, and at first stage separation. The resulting torsional loads were a maximum at lift-off. The torsional load at lift-off was 189 000 in-lb compared to the capability of more than 300 000 in-lb. This load is well within the capability of the modified structure, but in excess of the original design load of 100 000 in-lb. Hence, the modification to the CM/SM interface was required and was sufficient to reduce the loads to allowable values.

#### 5.1.4 Internal Loads

Internal loads were determined from strain gauge instrumentation located on the CM tension ties and on the inner and outer skins of the SLA at station 775.

The three CM tension ties were instrumented with strain gauges (fig. 5.1-12) calibrated to indicated forces in the axial direction of the tension tie. The data indicated a 5-Hz oscillation throughout first-stage boost. The averaged forces obtained during significant launch phases are shown in the following table.

Phase	Beam 2, lb	Beam 4, lb	Beam 6, lb
Pre-ignition	6 900	6 900	9 200
Lift-off	13 500	12 200	12 000
Max $q_a$ (00:01:12)	2 400	3 700	6 000
End of first-stage boost	1 700	3 000	4 400
Staging	13 100	13 400	11 200

Peak loads occurred, as expected, during the launch phase and again during S-IC/S-II staging. These loads were well within the 40 000-pound allowable for the structure.

The SLA was instrumented with 16 strain gauges (fig. 5.1-13) to

~~CONFIDENTIAL~~

~~CONFIDENTIAL~~

obtain launch loads. Strains measured during the boost phase were converted to stresses and are presented in the following table.

Gauge location, deg	Lift-off, psi	Max $q\alpha$ , psi	End of first- stage boost, psi	Allowable stress end of first- stage boost, psi
Outer shell, long. 34	3150	-4150	-8 200	-41 000
Outer shell, circ. 34	1475	-1780	-1 580	-10 250
Inner shell, long. 34	-3620	-5070	-2 950	-57 000
Inner shell, circ. 34	-2550	-1830	-6 210	-14 250
Outer shell, long. 124	-3800	-7900	-9 280	-41 000
Outer shell, circ. 124	-3450	-4020	-3 550	-10 250
Inner shell, long. 124	-4040	-7620	1 030	-57 000
Inner shell, circ. 124	-3090	-4780	8 400	-14 250
Outer shell, long. 214	-3620	-8220	-11 600	-41 000
Outer shell, circ. 214	-2860	-5400	-3 280	-10 250
Inner shell, long. 214	-3300	-3510	1 610	-57 000
Inner shell, circ. 214	-2190	-900	8 020	-14 250
Outer shell, long. 304	-8170	-9290	-13 850	-41 000

~~CONFIDENTIAL~~

~~CONFIDENTIAL~~

5.1-7

Gauge location, deg	Lift-off, psi	Max $q_a$ , psi	End of first- stage boost, psi	Allowable stress end of first- stage boost, psi
Outer shell, circ. 304	-5420	-5620	-4 720	-10 250
Inner shell, long. 304	-3670	-4200	-890	-57 000
Inner shell, circ. 304	-1060	-150	9 120	-14 250

These stress levels are compared to the allowable levels at the end of first-stage boost when allowables are reduced by temperature effects. The allowables at lift-off and max  $q_a$  are higher than those shown for end of first-stage boost. At the end of first-stage boost, the maximum temperature measured on the SLA was 290° F; the design temperature is 435° F for this location.

Strains measured during max  $q_a$  were converted to vehicle loads and are presented in the following table for comparison with design limit loads and loads calculated from trajectory data.

Loading	Measured load	Calculated load	Design limit load
Bending moment, in-lb	1 750 000	1 735 000	13 700 000
Axial force, lb	- 190 750	- 180 800	-200 000

Measured and calculated loads compare closely and both are well below the design limit loads at max  $q_a$ .

Determination of vehicle loads for launch and S-IC/S-II staging conditions was not practical because strain gauge sampling rates were too low to determine peak loading during these transient conditions. Loads were not calculated from strain data for end of first-stage boost because it was not possible to separate thermal strains from the total measured strains. Strain gauge data indicated that no structural failures occurred during the launch phase of the mission. Structural loading was well within the structural capability of the vehicle and strain gauge instrumentation provided sufficient data to satisfy the mission objective.

~~CONFIDENTIAL~~

~~CONFIDENTIAL~~

## 5.1.5 Low Frequency Vibration

Low frequency oscillations of significant magnitude were observed during most phases of first-stage launch and boost.

During launch release, the longitudinal, lateral, and torsional oscillations occurred from T minus 3 seconds to approximately T plus 3 seconds (fig. 5.1-3). These oscillations contained frequencies of 1.8, 2.5, 4.5, and 12.0 Hz. The frequencies corresponded closely to the second-bending, third-bending, second-longitudinal, and first-torsional modes, respectively, of the Saturn V launch vehicle. A tabulation of the peak values which occurred at each mode during launch release is presented in table 5.1-IV. The values in table 5.1-IV were derived from a combination of oscillographs and spectral analyses. The effects of accelerations on structural loads are evaluated for all launch phases in section 5.1.1.

Longitudinal oscillations at approximately 5 Hz were predominant in the CM during all phases of first-stage boost and during the first few seconds of second-stage boost. This oscillation is illustrated in figure 5.1-9. The actual frequency at launch release was 4.5 Hz, which corresponds, as stated above, with the second longitudinal mode of the Saturn V vehicle with launch release weights. The frequency increased to approximately 6.8 Hz at first-stage separation due to the decrease in mass of the first stage during boost. The peak values of each mode during midboost are presented in table 5.1-IV. The peak values presented occur at different times during the midboost phase. The 5-Hz oscillation was characterized by a 5-second beat period from maximum amplitude to minimum amplitude and was at minimum amplitude at inboard engine cutoff and outboard engine cutoff.

At first-stage inboard engine cutoff the only significant oscillation occurring was an axial oscillation in the CM (fig. 5.1-10) resulting from the transient response of the second longitudinal mode to the engine thrust decay. The value of the oscillation is given in table 5.1-IV.

The maximum CM axial oscillations (fig. 5.1-11) occurred at first stage outboard engine cutoff. The oscillations were transient in nature and were caused by the second longitudinal mode response to the engine thrust decay as during center engine cutoff. Torsional oscillations also existed at this time and were caused by axial-torsional coupling in the second longitudinal mode of the launch vehicle. The peak values are given in table 5.1-IV.

After first-stage separation the 6.8 Hz oscillations continued for approximately 4 seconds of second-stage boost but were of insignificant amplitude (fig. 5.1-11). The first longitudinal mode of the second

~~CONFIDENTIAL~~



~~CONFIDENTIAL~~

5.1-9

stage at ignition was approximately the same frequency (6.8 Hz) as the second longitudinal mode of the first stage at burn out; therefore, the oscillations continued for a short time during second-stage boost and then decayed due to lack of a forcing function.

There were no significant low frequency vibrations subsequent to those discussed.

#### 5.1.6 High Frequency Vibrations

The CM was instrumented with four vibration accelerometers for the purpose of verifying the CM systems vibration criteria. Comparison of acceleration spectral density from SM vibration measurements at periods of no vibration (noise floor from minus 7.5 to minus 5.5 seconds) to periods of maximum vibration showed energy concentrations at identical frequencies. Data at these frequencies are considered invalid since this comparison shows the energy to be electrical noise. Figure 5.1-14 shows the spectral density distribution at lift-off and at maximum vibration. All CM vibration measurements, with the exception of CA2530D, exhibited rms signal-to-noise ratios less than 3 to 1; therefore, data from these measurements are not usable. Data from CA2530D are compared to existing criteria in figure 5.1-15 without scaling the flight data to design values.

The CM vibration data gave no indication that vibration qualification criteria levels were exceeded.

The SM was instrumented with nine vibration accelerometers for the purpose of verifying SM systems vibration criteria levels. Comparison of acceleration spectral density analyses from all SM vibration measurements at periods of no vibration (minus 7.5 to minus 5.5 seconds) to periods of maximum vibration showed energy concentrations at identical frequencies as did the CM vibration data. Data at these frequencies are considered invalid since this comparison shows the energy to be electrical noise. Figure 5.1-16 shows the spectral density distribution at lift-off and at maximum vibration. All SM vibration measurements, with the exceptions of SA2211D and SA2218D, exhibited rms signal-to-noise ratios less than 4 to 1. Usable SM vibration data indicate that vibration levels were below systems criteria. Acceleration spectral density analysis of aft bulkhead radial vibrations indicate that the flight vibrations approached the Block I criteria vibrations in the high frequency region of the spectrum, as shown in figures 5.1-17. The flight data are plotted without scaling to design values.

~~CONFIDENTIAL~~

~~CONFIDENTIAL~~

TABLE 5.1-1.- MAXIMUM LATERAL LOAD CONDITIONS

Interface	Condition	Before lift-off	After lift-off	Design limit loads
Launch escape subsystem and command module	Bending moment, in-lb . . . .	1 300 000	1 420 000	2 380 000
	Axial force, lb . . . . .	a-7740	a-11 000	-11 000
Command module and service module	Bending moment, in-lb . . . .	1 790 000	1 830 000	3 150 000
	Axial force, lb . . . . .	a-20 500	a-26 600	-27 000
	Torsion, in-lb . . . .	173 000	189 000	b <sub>118</sub> 000

<sup>a</sup>Negative sign indicates compression.<sup>b</sup>Torsional capability exceeds 300 000 in-lb.~~CONFIDENTIAL~~

~~CONFIDENTIAL~~

5.1-11

TABLE 5.1-II.- MAXIMUM SPACECRAFT LOADS AT MAXIMUM  $q_a$ 

Interface	Condition	Predicted from MSFC simulation using lift-off winds	Predicted from MSC simulation using lift-off winds	Calculated from flight data	Design
	Flight time, sec Mach no. Dynamic pressure, psf Angle of attack, deg Max $q_a$ , psf-deg	80 1.75 745 2.2 1639.0	79.6 1.77 735 2.12 1558.2	78 1.74 720 1.8 1296.0	69.6 1.3 713 9.0 6417.0
Command module and service module	Bending moment, in-lb Axial force, lb	500 000 -92 000 <sup>a</sup>	445 000 -90 600 <sup>a</sup>	800 000 -89 600 <sup>a</sup>	2 100 000 -90 600 <sup>a</sup>
Service module and spacecraft lunar module adapter	Bending moment, in-lb Axial force, lb	1 200 000 -176 000 <sup>a</sup>	1 480 000 -176 400 <sup>a</sup>	1 340 000 -176 100 <sup>a</sup>	8 400 000 -192 000 <sup>a</sup>
Apollo station 775	Bending moment, in-lb Axial force, lb	Not predicted	Not predicted	1 735 000 -180 780 <sup>a</sup>	11 000 000 -193 000 <sup>a</sup>
Spacecraft lunar module adapter and launch vehicle instrument unit	Bending moment, in-lb Axial force, lb	5 000 000 -267 000 <sup>a</sup>	4 170 000 -269 000 <sup>a</sup>	4 500 000 -270 000 <sup>a</sup>	26 000 000 -272 000 <sup>a</sup>

<sup>a</sup>Negative sign indicates compression.~~CONFIDENTIAL~~

~~CONFIDENTIAL~~

TABLE 5.1-III.- MAXIMUM SPACECRAFT LOADS AT END  
OF FIRST-STAGE BOOST

Interface	Condition	Calculated from flight data	Design
	Axial acceleration, g	4.2	4.9
Command module and service module	Bending moment, in-lb	835 000	550 000
	Axial force, lb	-86 100 <sup>a</sup>	-97 600 <sup>a</sup>
Service module and spacecraft lunar module adapter	Bending moment, in-lb	1 566 000	3 000 000
	Axial force, lb	-252 500 <sup>a</sup>	-332 000 <sup>a</sup>
Spacecraft lunar module adapter and launch vehicle instru- ment unit	Bending moment, in-lb	1 875 000	4 700 000
	Axial force, lb	-388 000 <sup>a</sup>	-482 000 <sup>a</sup>

<sup>a</sup>Negative sign indicates compression.

~~CONFIDENTIAL~~

CONFIDENTIAL

5.1-13

TABLE 5.1-IV.- LAUNCH ESCAPE SYSTEM AND COMMAND MODULE LOW FREQUENCY

DURING FIRST-STAGE LAUNCH AND BOOST

	Launch release		Midboost		Inboard engine cutoff		Outboard engine cutoff	
	Frequency	Amplitude	Frequency	Amplitude	Frequency	Amplitude	Frequency	Amplitude
Launch escape system lateral	1.8 Hz	$\pm 0.18g$						
	2.5 Hz	$\pm 0.68g$	2.1 Hz	$\pm 0.23g$		(a)		(a)
	4.5 Hz	$\pm 0.064g$						
	12.0 Hz	$\pm 0.20g$	5.5 Hz	$\pm 0.10g$				
Command module lateral	1.8 Hz	$\pm 0.041g$						
	2.5 Hz	$\pm 0.03g$	5.5 Hz	$\pm 0.04g$		(a)		(a)
	4.5 Hz	$\pm 0.032g$						
Command module torsional	12.0 Hz	$\pm 2.5 \frac{\text{rad}}{\text{sec}^2}$	5.6 Hz	$\pm 0.9 \frac{\text{rad}}{\text{sec}^2}$		(a)	6.8 Hz	$\pm 1.125 \frac{\text{rad}}{\text{sec}^2}$
Command module axial	4.5 Hz	$\pm 0.112g$	5.9 Hz	$\pm 0.22g$	6.1 Hz	$\pm 0.28g$	6.8 Hz	$\pm 0.48g$

NOTE: These are peak oscillatory values.

<sup>a</sup> Insignificant.

CONFIDENTIAL

~~CONFIDENTIAL~~

NASA-S-68-326

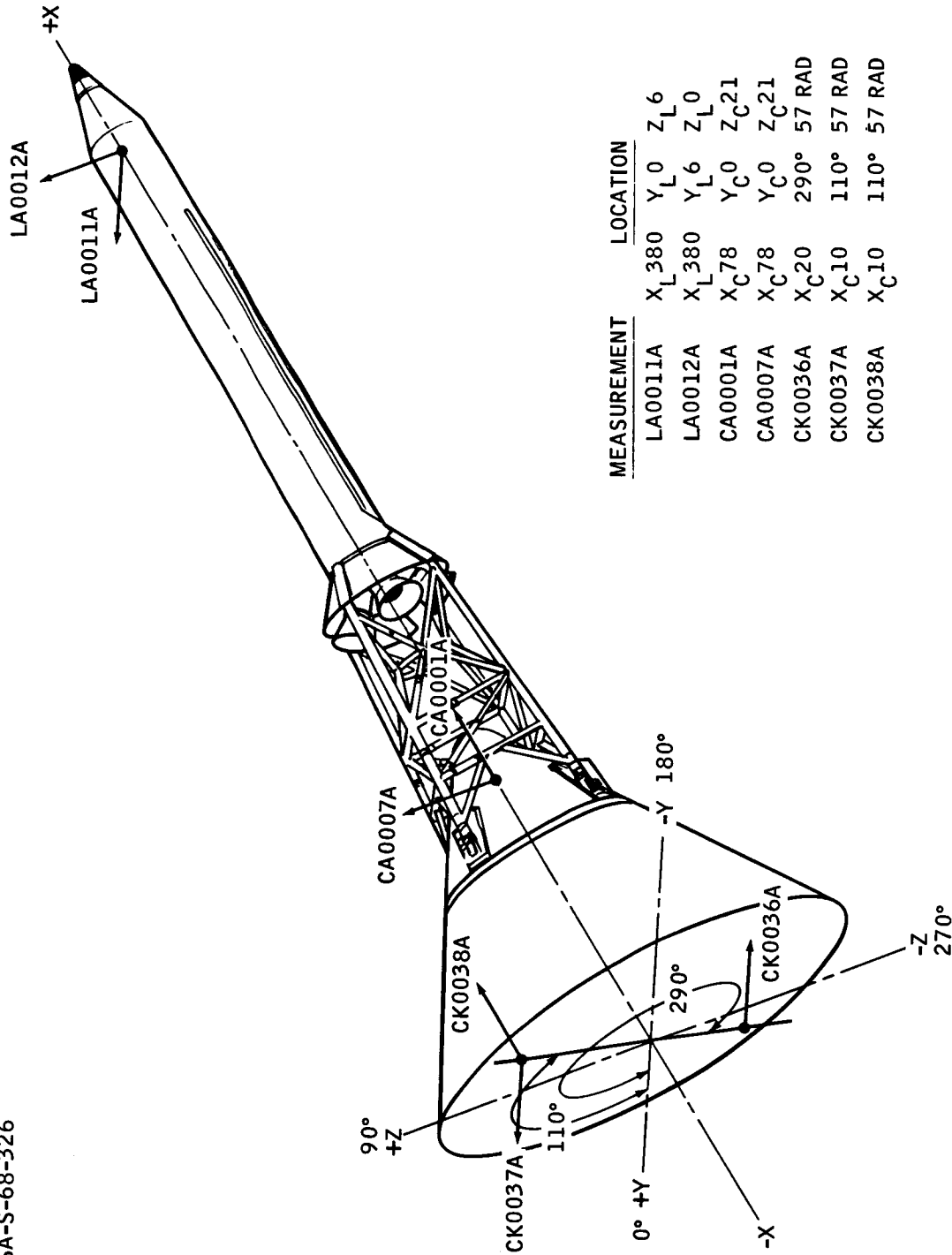


FIGURE 5.1-1.1.- LAUNCH ESCAPE SYSTEM AND COMMAND MODULE ACCELEROMETER LOCATIONS.

~~CONFIDENTIAL~~

~~CONFIDENTIAL~~

5.1-15

NASA-S-68-325

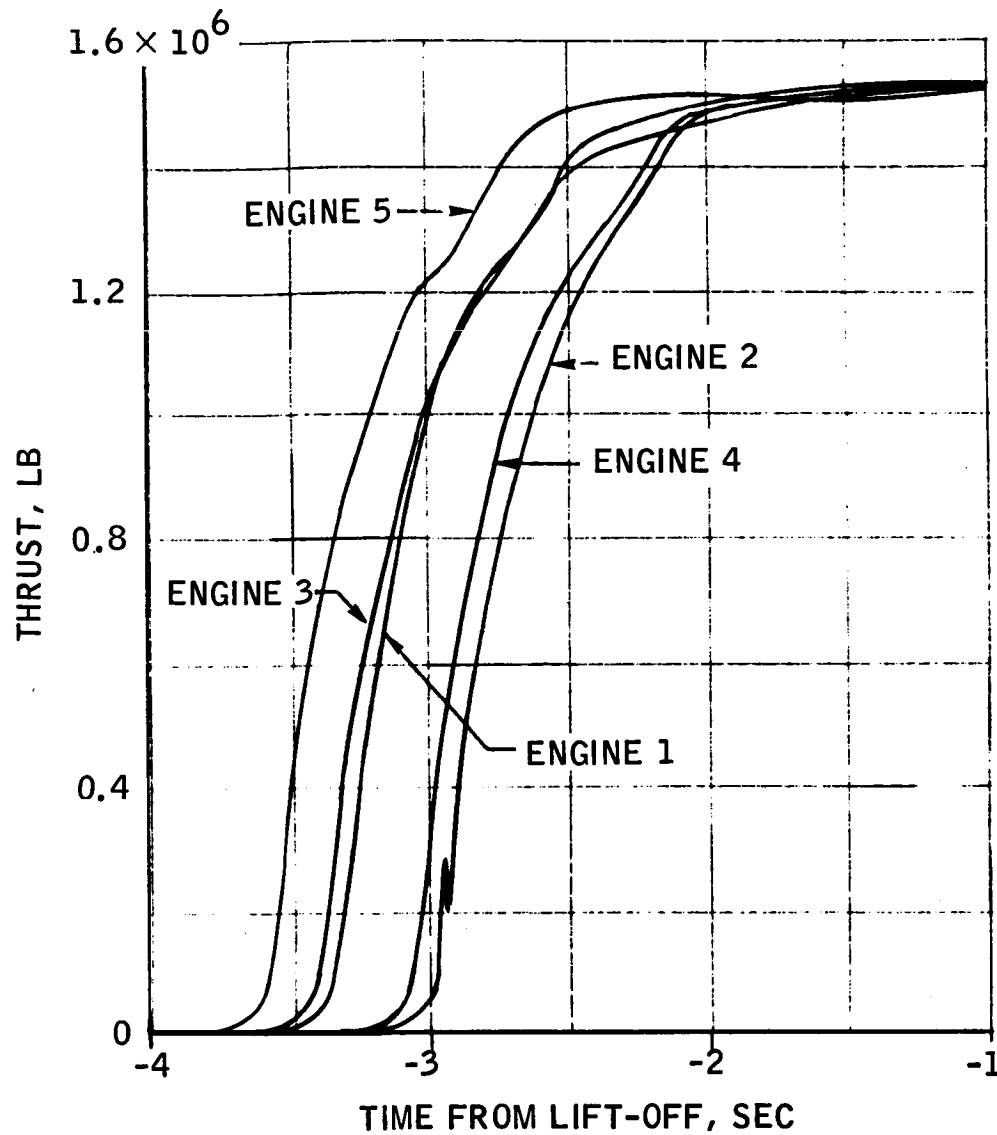
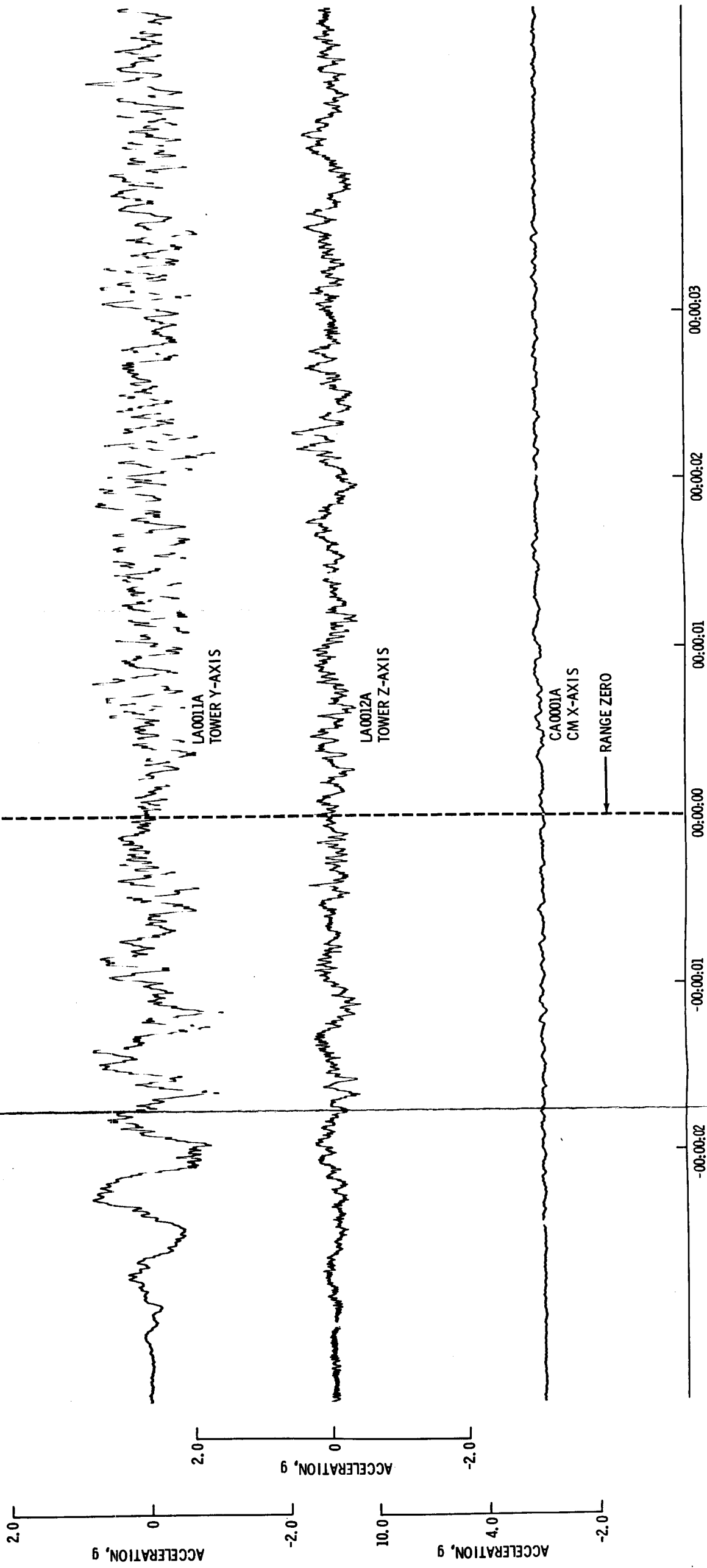


FIGURE 5.1-2.- S-IC ENGINE THRUST BUILDUP.

~~CONFIDENTIAL~~

~~CONFIDENTIAL~~

NASA-S-68-321



(A) LA0011A, LA0012A, and CA0001A.

FIGURE 5.1-3.- SPACECRAFT ACCELERATIONS AT LIFT-OFF.

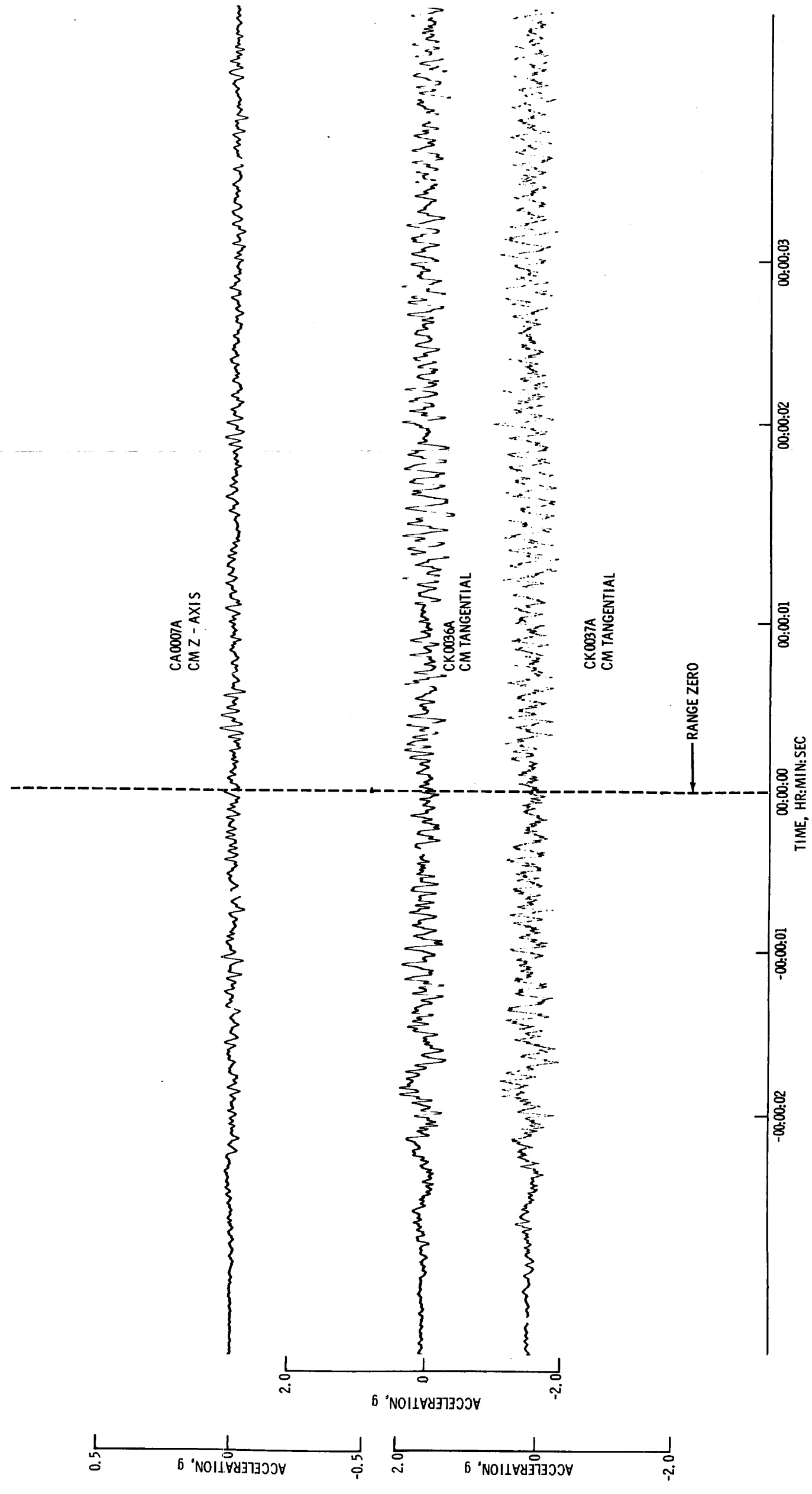
~~CONFIDENTIAL~~



~~CONFIDENTIAL~~

5.1-17

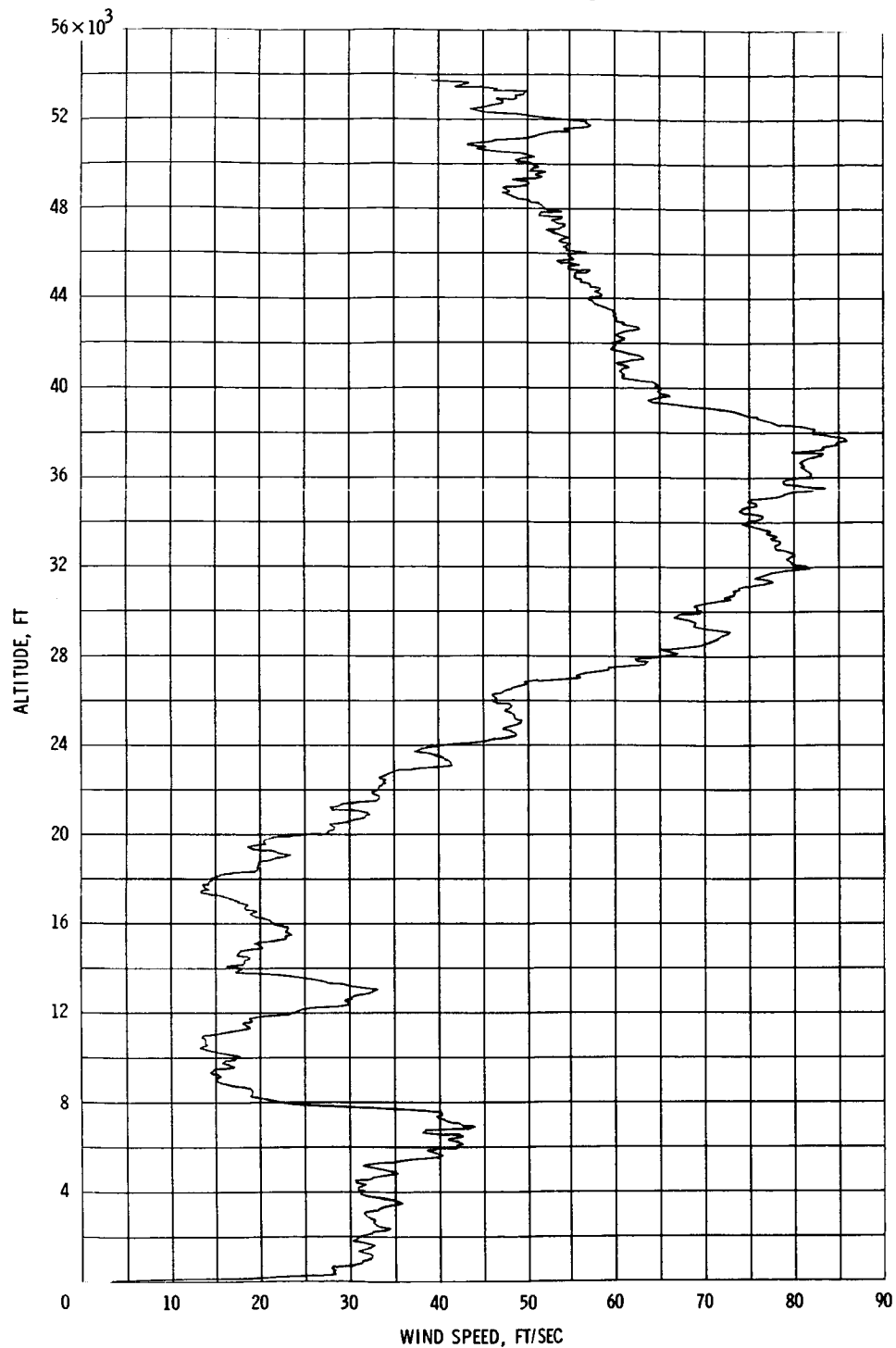
NASA-S-68-322



(B) CA0007A, CK0036A, AND CK0037A.

FIGURE 5.1-3. - CONCLUDED.

~~CONFIDENTIAL~~

~~CONFIDENTIAL~~

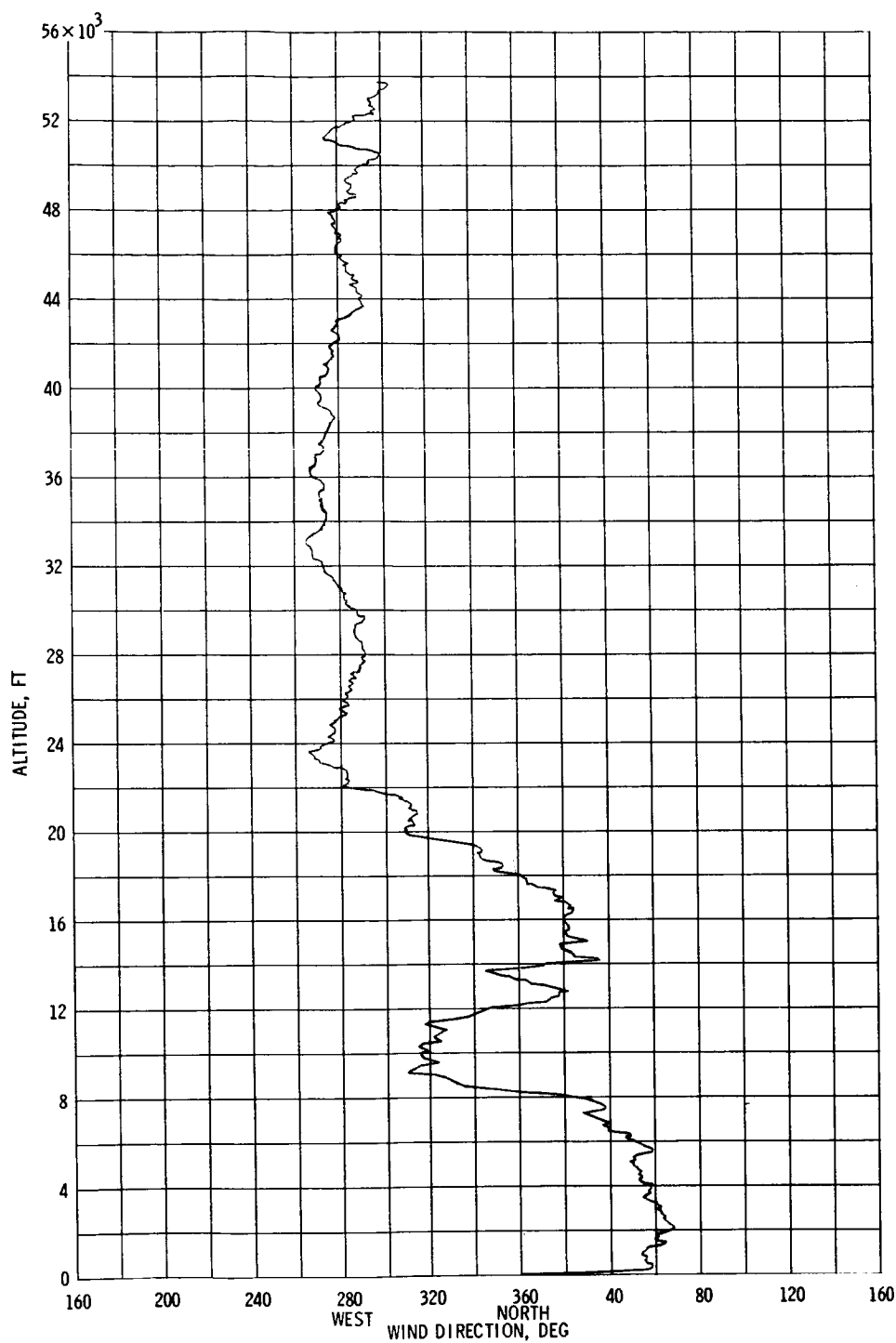
(A) LAUNCH WINDS MAGNITUDE.

FIGURE 5.1-4. - LAUNCH WINDS.

~~CONFIDENTIAL~~

~~CONFIDENTIAL~~

5.1-19



(B) LAUNCH WIND DIRECTION.

FIGURE 5.1-4. - CONCLUDED.

~~CONFIDENTIAL~~

NASA-S-68-324

~~CONFIDENTIAL~~

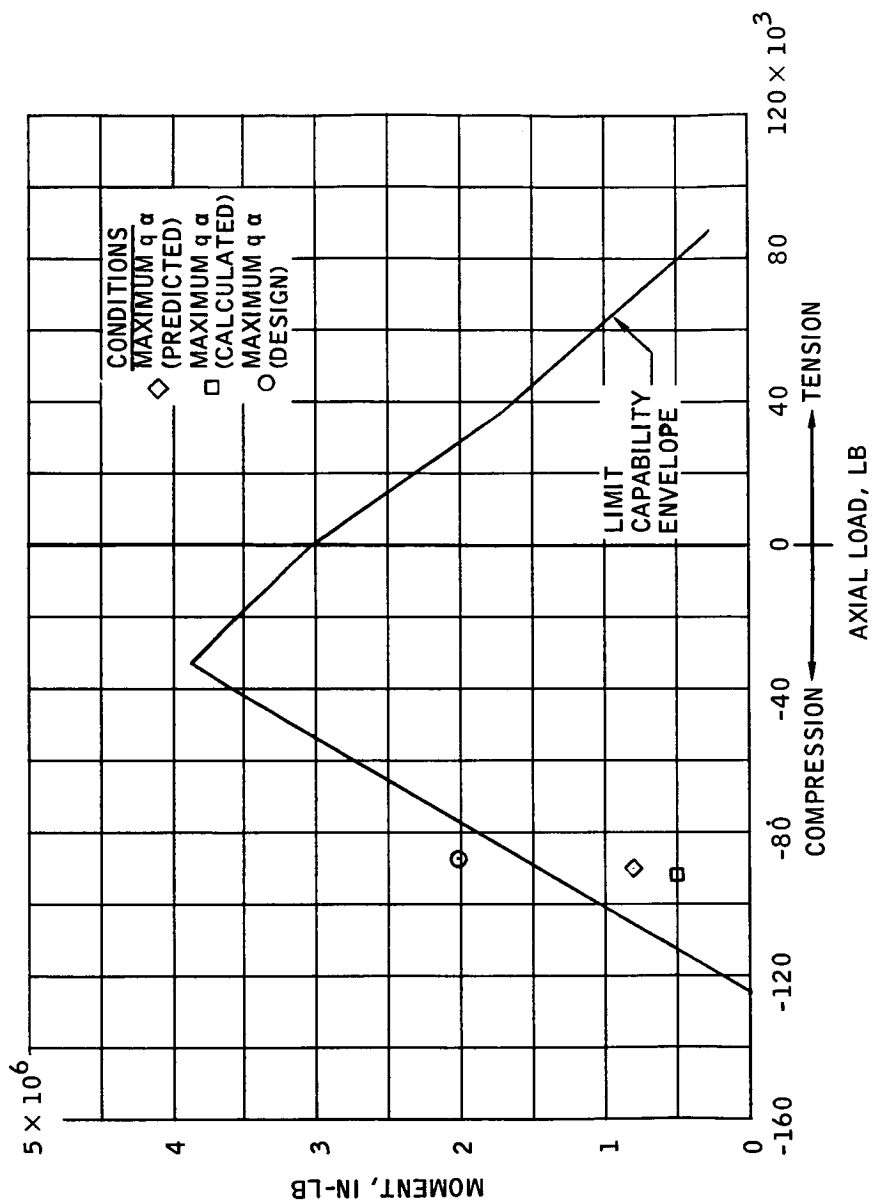


FIGURE 5.1-5.- COMPARISON OF MAXIMUM  $q \alpha$  COMMAND MODULE/SERVICE MODULE INTERFACE LOADS WITH STRUCTURAL CAPABILITIES.

NASA-S-68-327

~~CONFIDENTIAL~~

~~CONFIDENTIAL~~

5.1-21

NASA-S-68-328

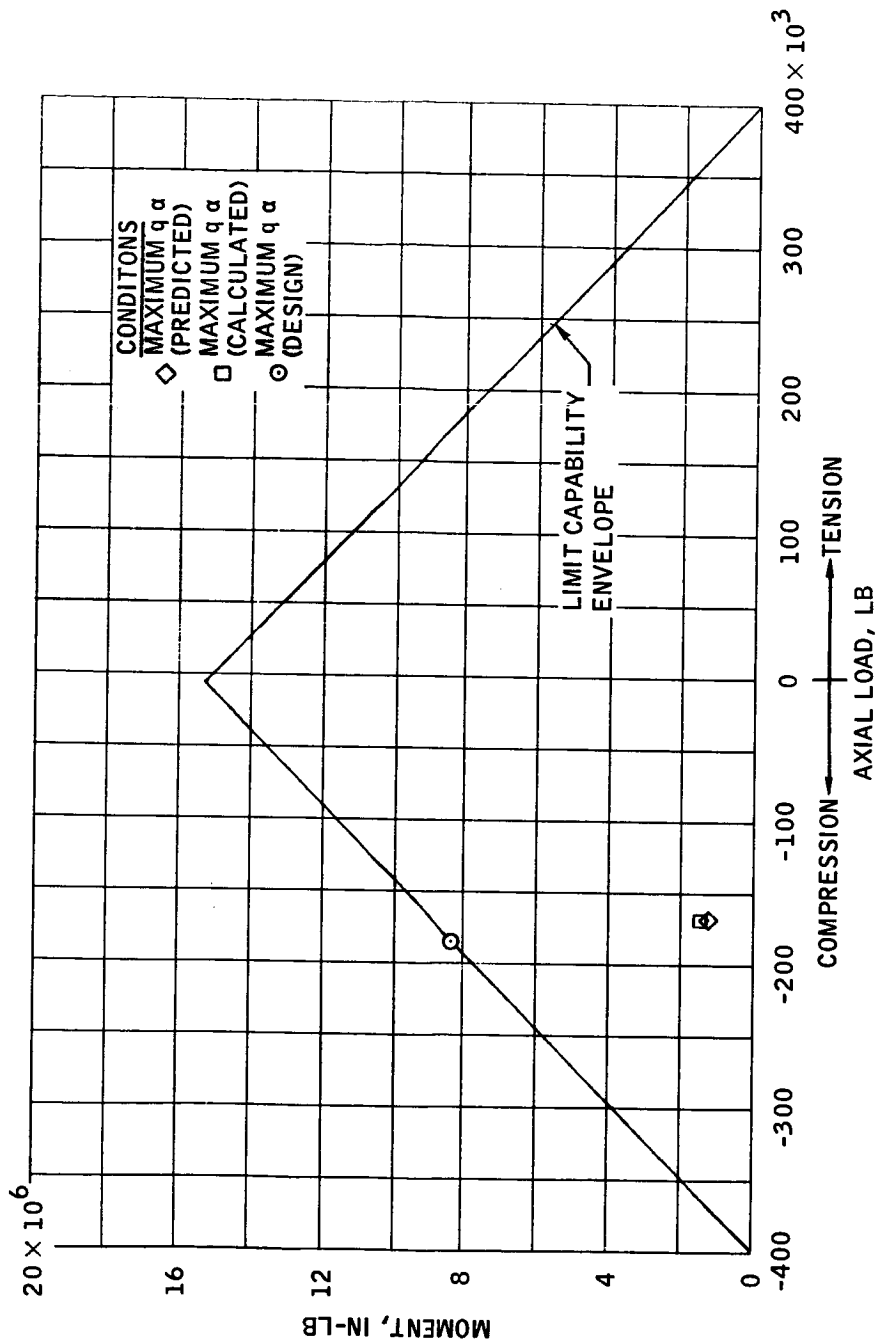


FIGURE 5.1-6.- COMPARISON OF MAXIMUM  $q \alpha$  SERVICE MODULE/SPACECRAFT LUNAR MODULE ADAPTER INTERFACE LOADS WITH STRUCTURAL CAPABILITIES.

~~CONFIDENTIAL~~

~~CONFIDENTIAL~~

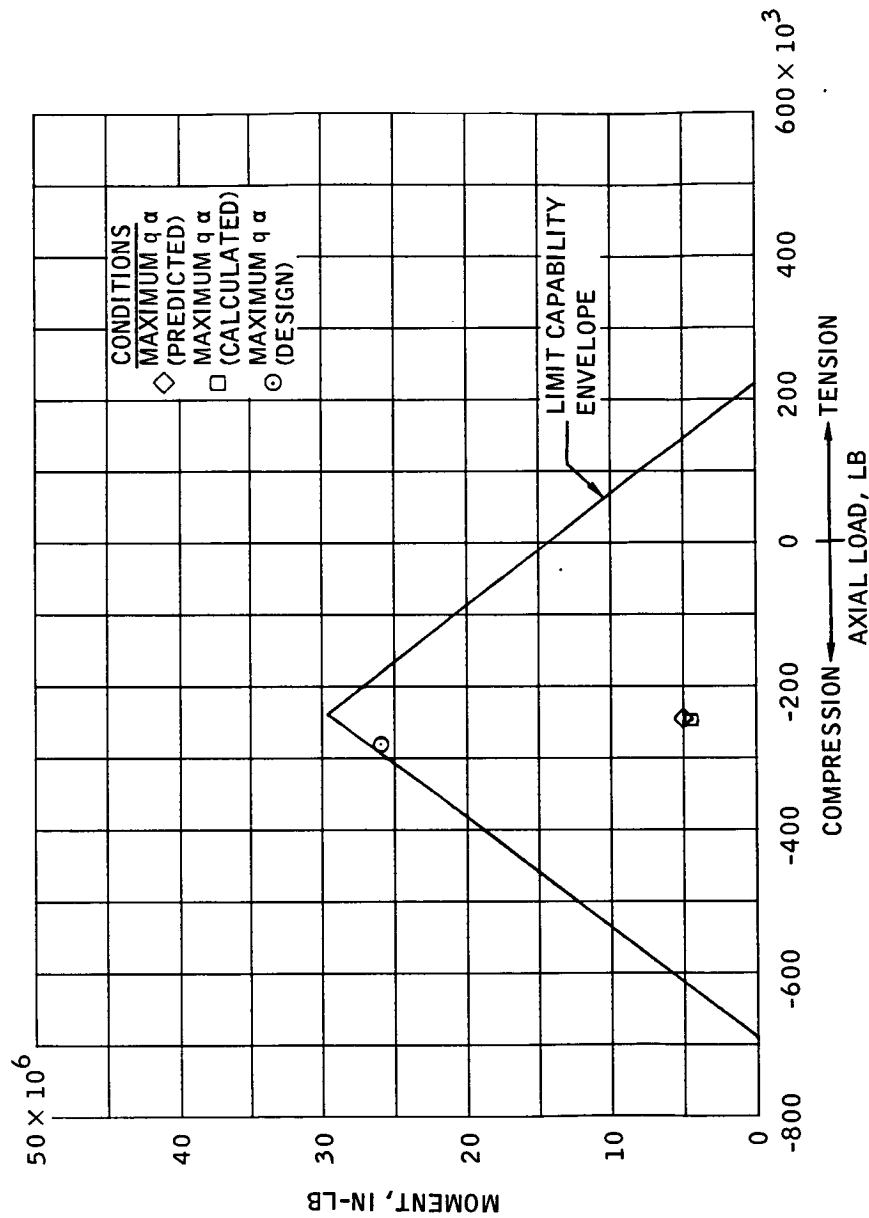


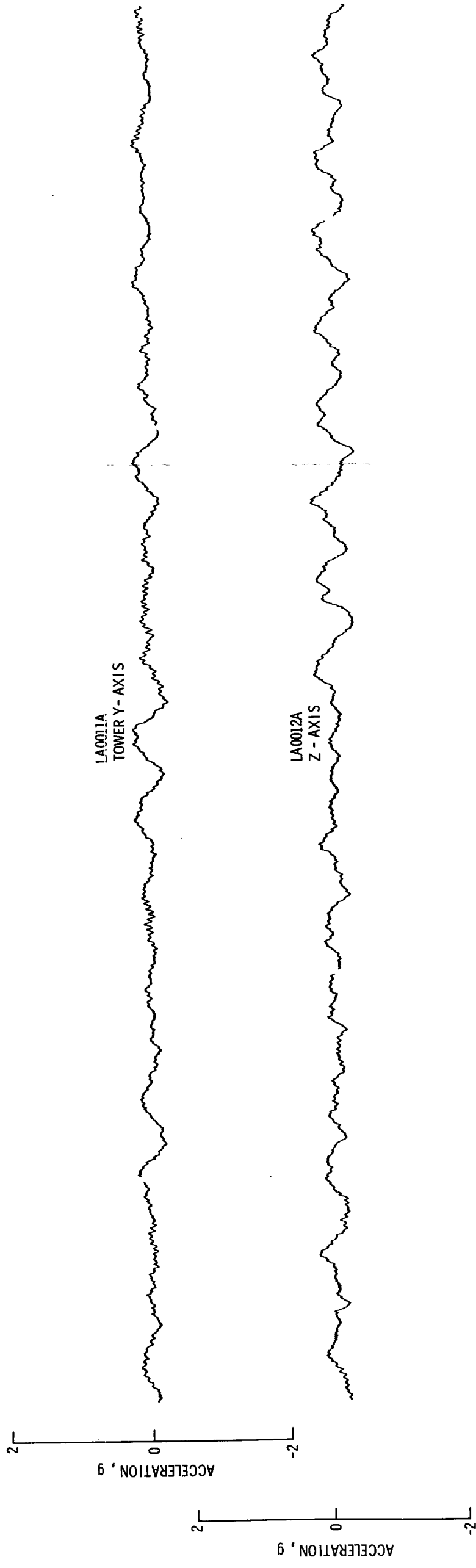
FIGURE 5.1-7.- COMPARISON OF MAXIMUM q α SPACECRAFT LUNAR MODULE ADAPTER/INSTRUMENT UNIT INTERFACE LOADS WITH STRUCTURAL CAPABILITIES.

~~CONFIDENTIAL~~

~~CONFIDENTIAL~~

5.1-23

NASA-S-68-330

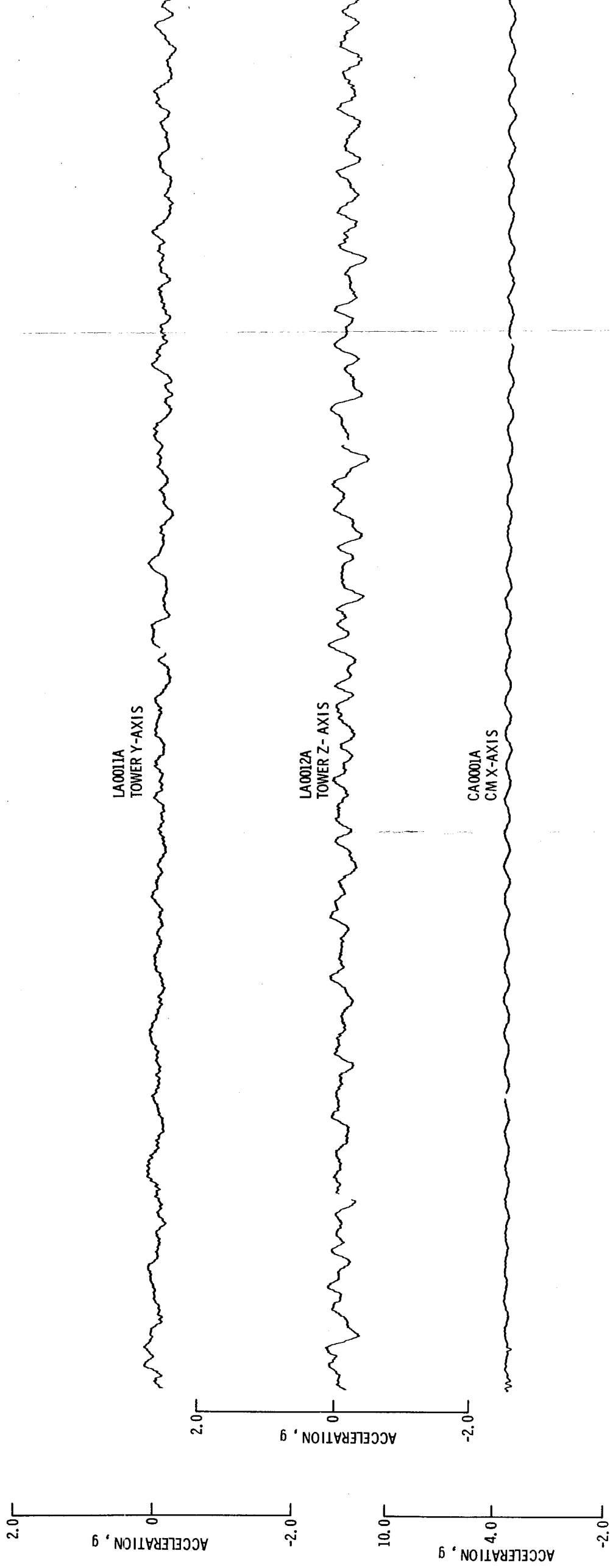


TIME, HR: MIN: SEC

FIGURE 5.1-8. - LAUNCH ESCAPE TOWER LATERAL OSCILLATIONS DURING FIRST-STAGE BOOST.

~~CONFIDENTIAL~~

NASA-S-68-331



(A) LA0011A, LA0012A, AND CA0001A

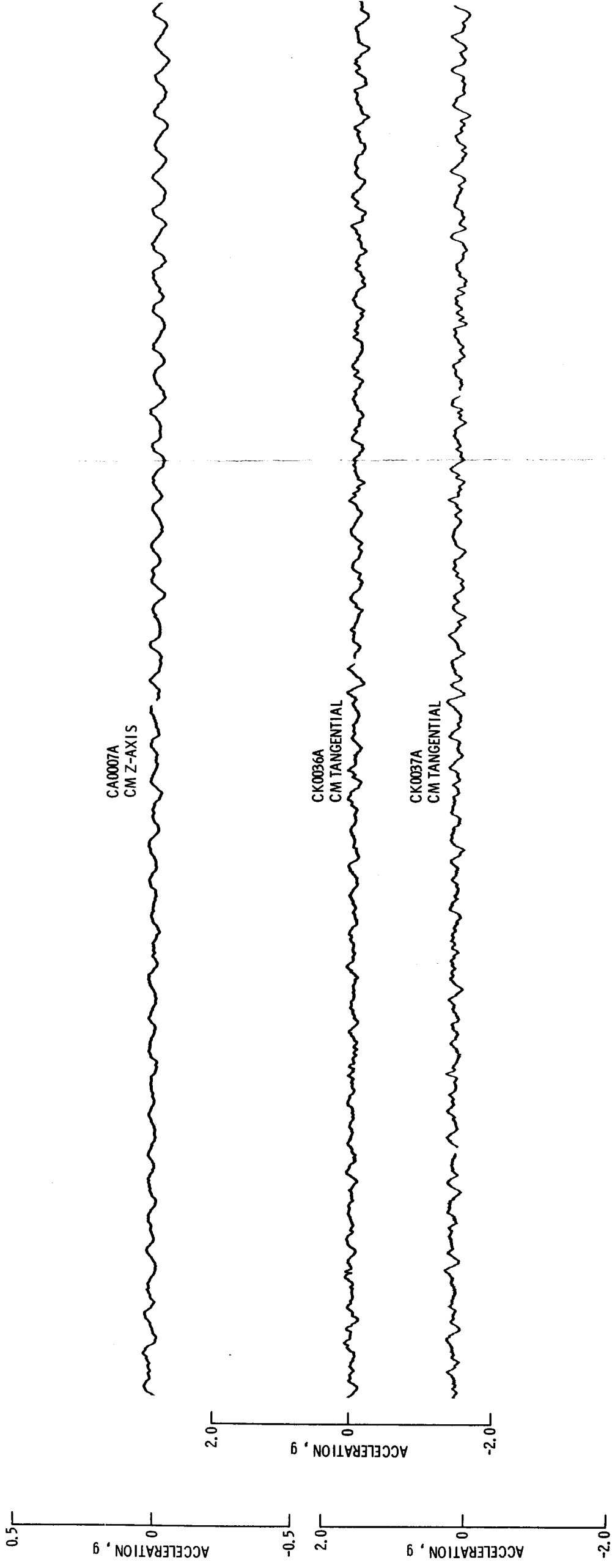
FIGURE 5.1-9. - SPACECRAFT ACCELERATIONS DURING HIGH AXIAL ACCELERATION OSCILLATION PERIOD.



~~CONFIDENTIAL~~

5.1.1-25

NASA-S-68-332



00:01:56.8

TIME, HR:MIN:SEC

00:02:01.75

(B) CA0007A, CA0036A, AND CK0037A

FIGURE 5.1-9. - CONCLUDED.

~~CONFIDENTIAL~~

NASA-S-68-333

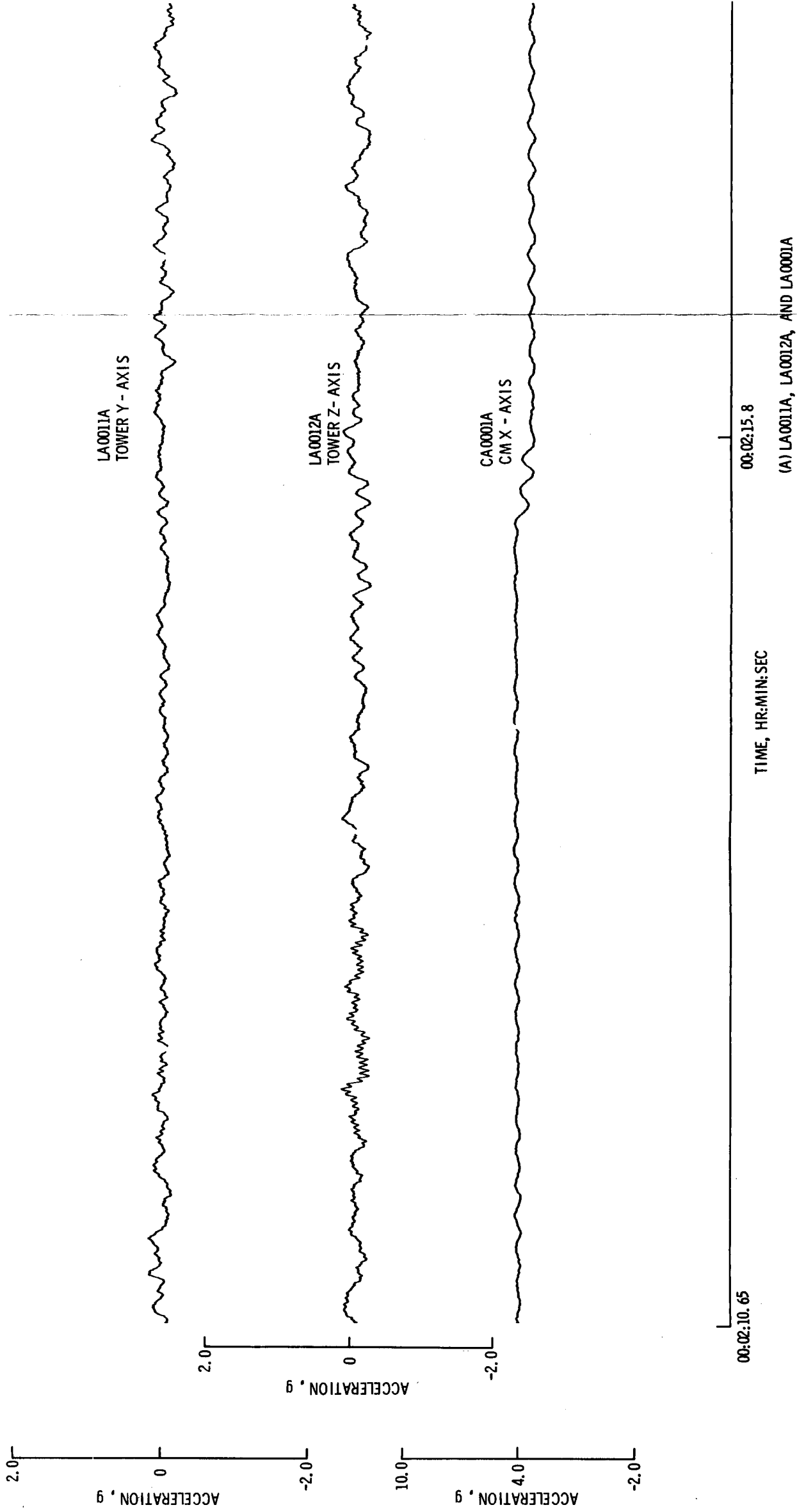
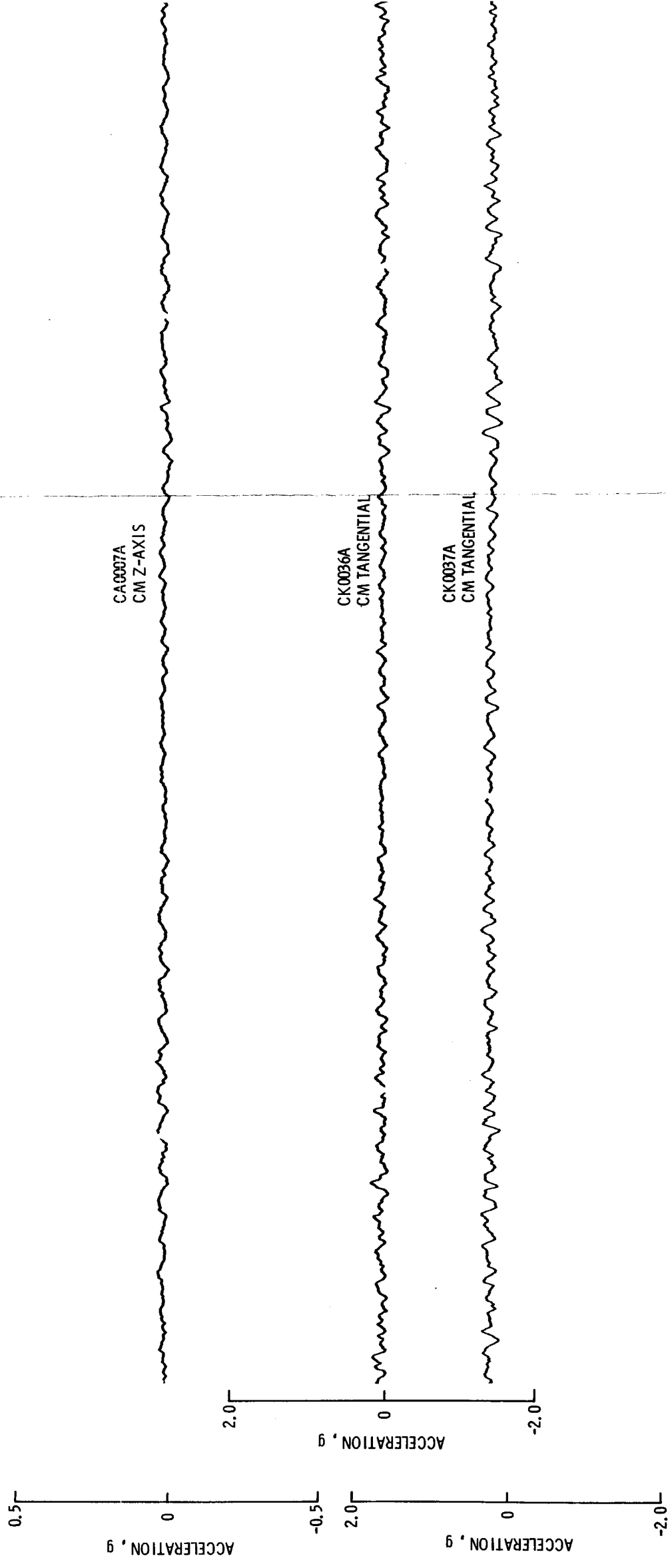


FIGURE 5.1-10. - SPACECRAFT ACCELERATIONS AT FIRST-STAGE END OF BOOST.

~~CONFIDENTIAL~~

5.1-27

NASA-S-68-334



00:02:10.65

TIME, HR:MIN:SEC

00:02:15.8

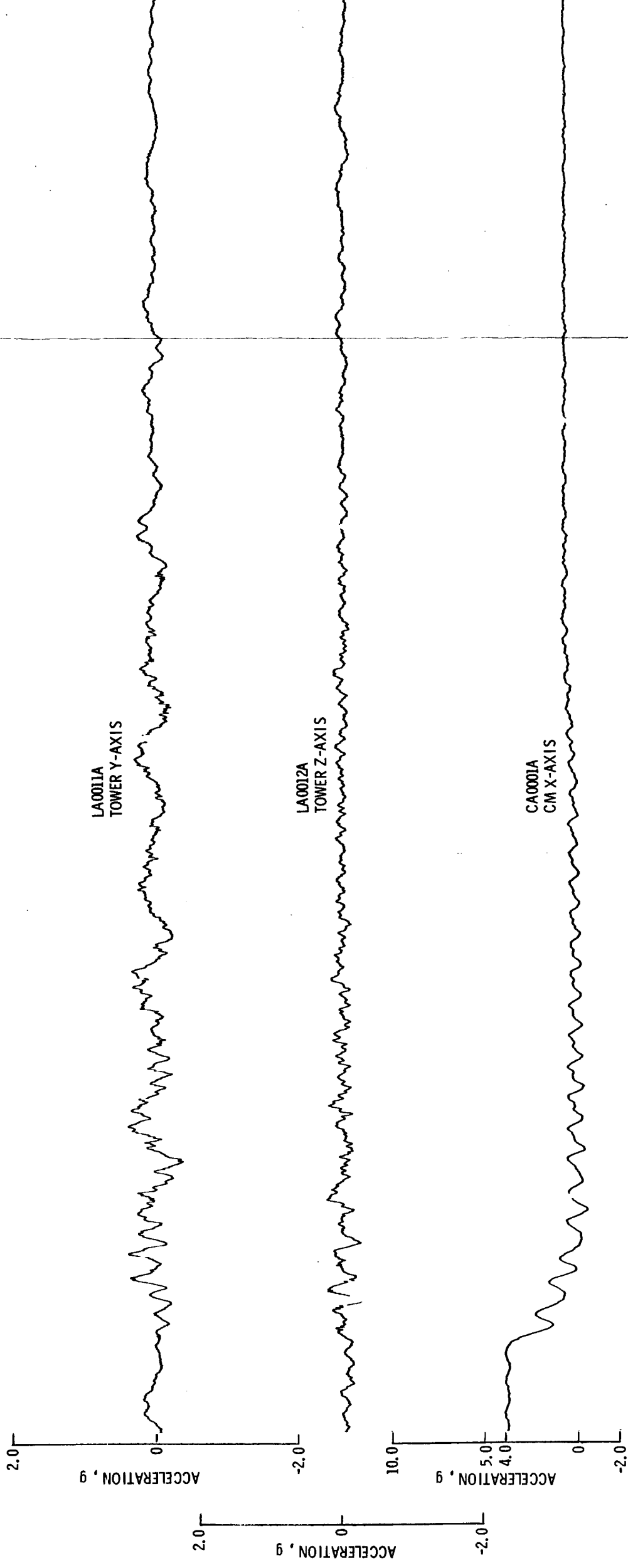
(B) CA0007A, CK0036A, AND CK0037A

FIGURE 5.1-10. - CONCLUDED.

~~CONFIDENTIAL~~

~~CONFIDENTIAL~~

NASA-S-68-335



00:02:31.44

00:02:36.39

TIME, HR:MIN:SEC

(A) LA0011A, LA0012A, AND CA0001A.

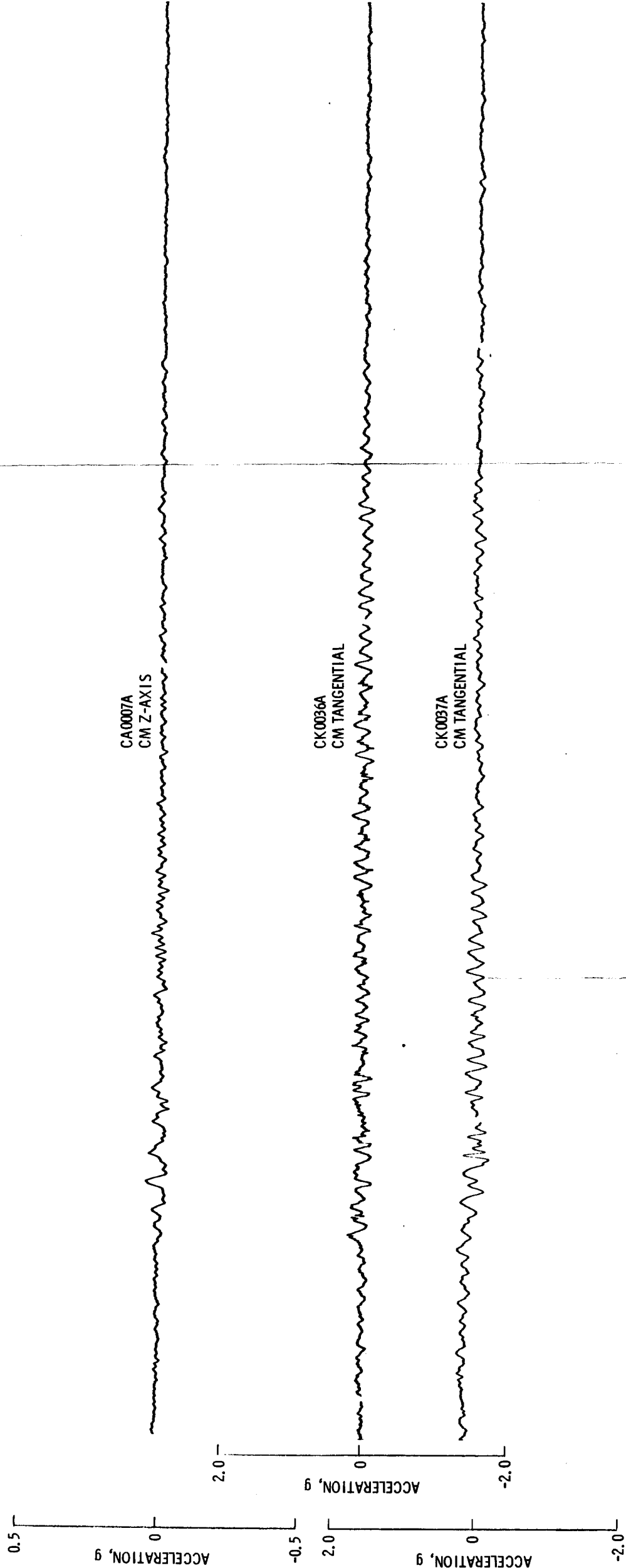
FIGURE 5.1-11. - SPACECRAFT ACCELERATIONS DURING S-IC/S-II SEPARATION.

~~CONFIDENTIAL~~

~~CONFIDENTIAL~~

5.1-29

NASA-S-68-336



TIME, HR:MIN:SEC

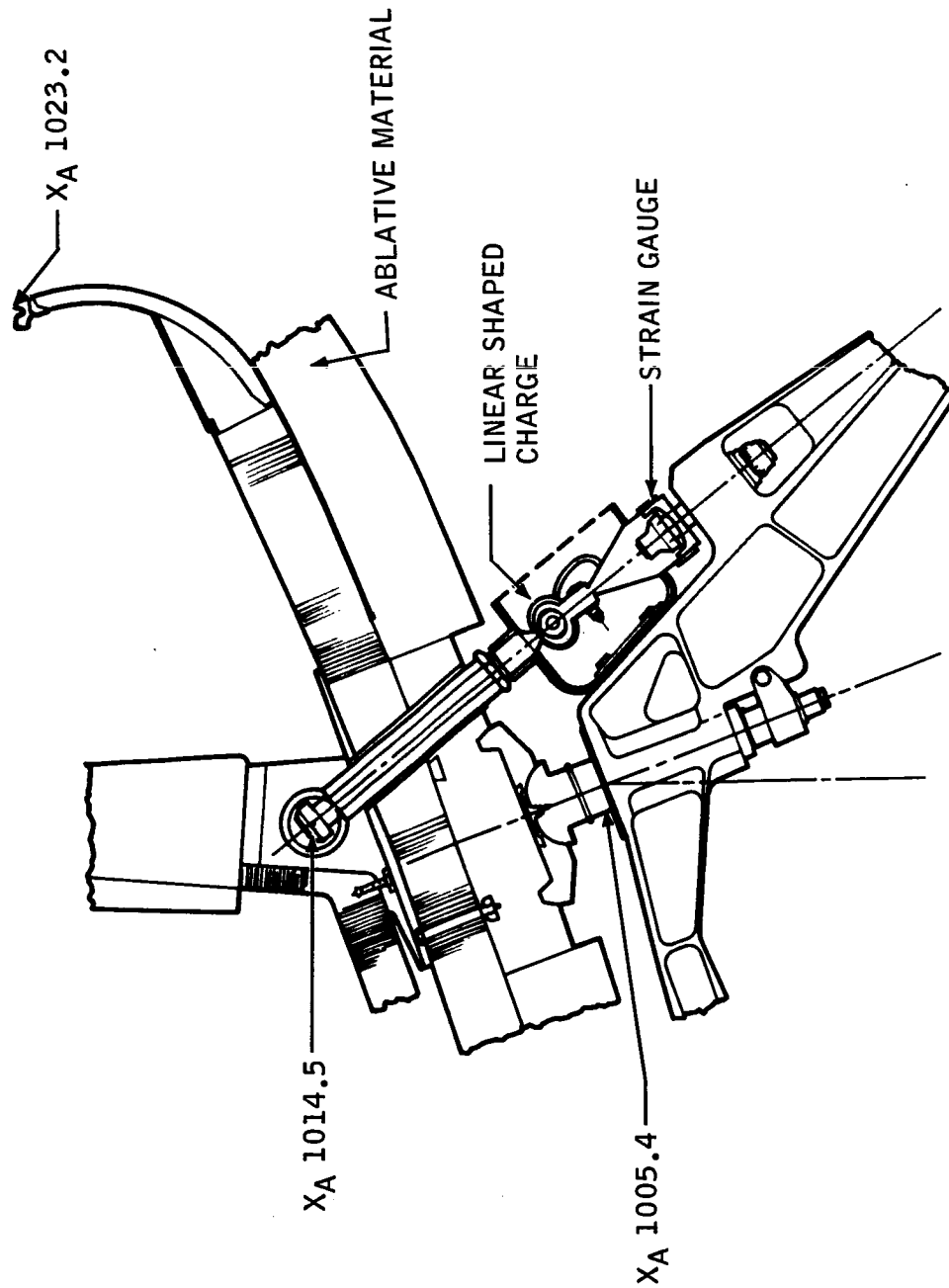
00:02:36.39

00:02:31.44

(B) CA0007A, CK0037A, AND CK0036A.

FIGURE 5.1-11. - CONCLUDED.

~~CONFIDENTIAL~~

~~CONFIDENTIAL~~

NASA-S-68-337

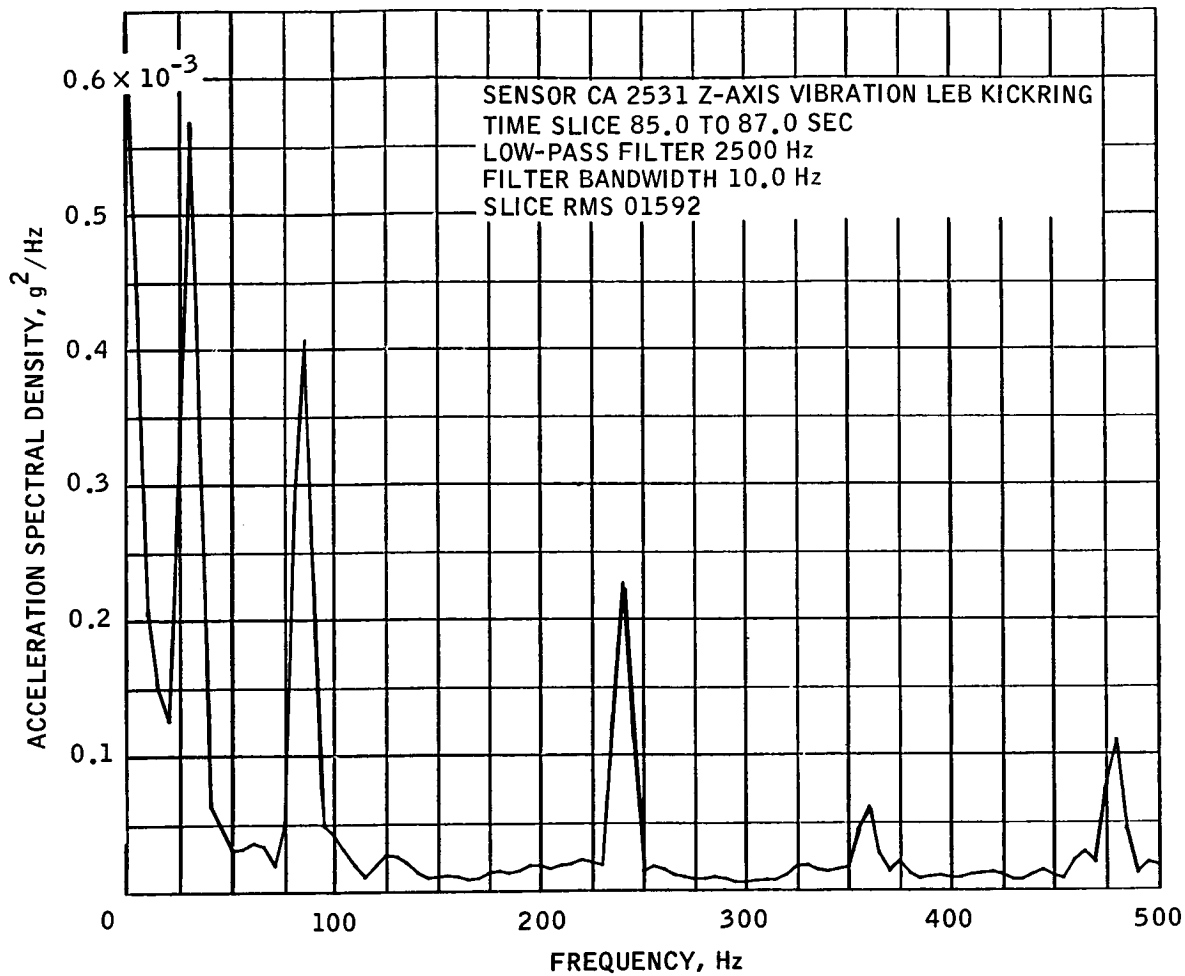
~~CONFIDENTIAL~~

FIGURE 5.1-12.- TYPICAL COMMAND MODULE/SERVICE MODULE TENSION TIE STRAIN GAUGE LOCATION.



~~CONFIDENTIAL~~

NASA-S-68-339



(A) PRIOR TO IGNITION.

FIGURE 5.1-14.- COMMAND MODULE ACCELERATION SPECTRAL DENSITY.

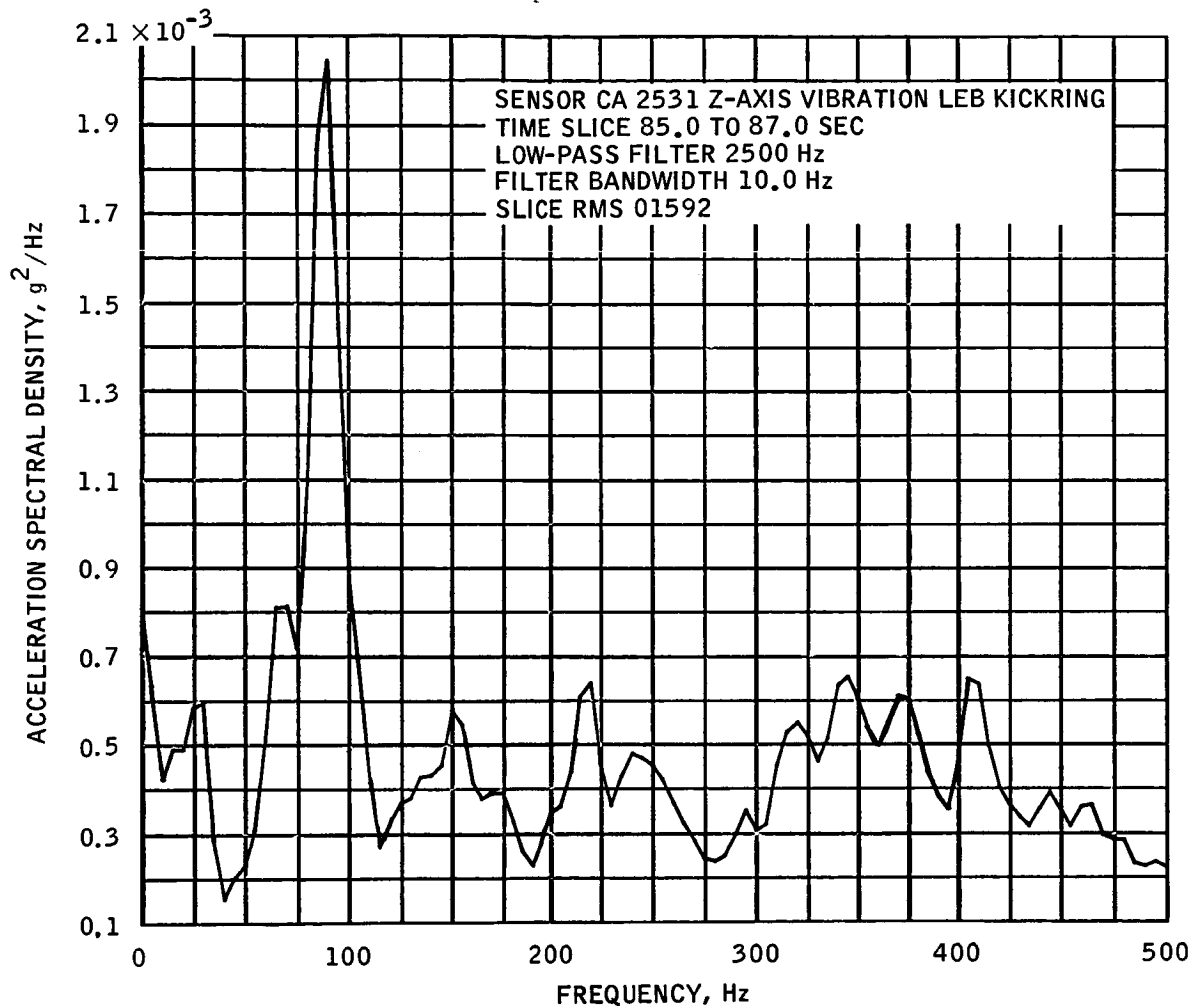
~~CONFIDENTIAL~~



~~CONFIDENTIAL~~

5.1-33

NASA-S-68-340



(B) MAXIMUM VIBRATION FROM 85.0 TO 87.5 SECONDS.

FIGURE 5.1-14.- CONCLUDED.

~~CONFIDENTIAL~~

~~CONFIDENTIAL~~

NASA-S-68-341

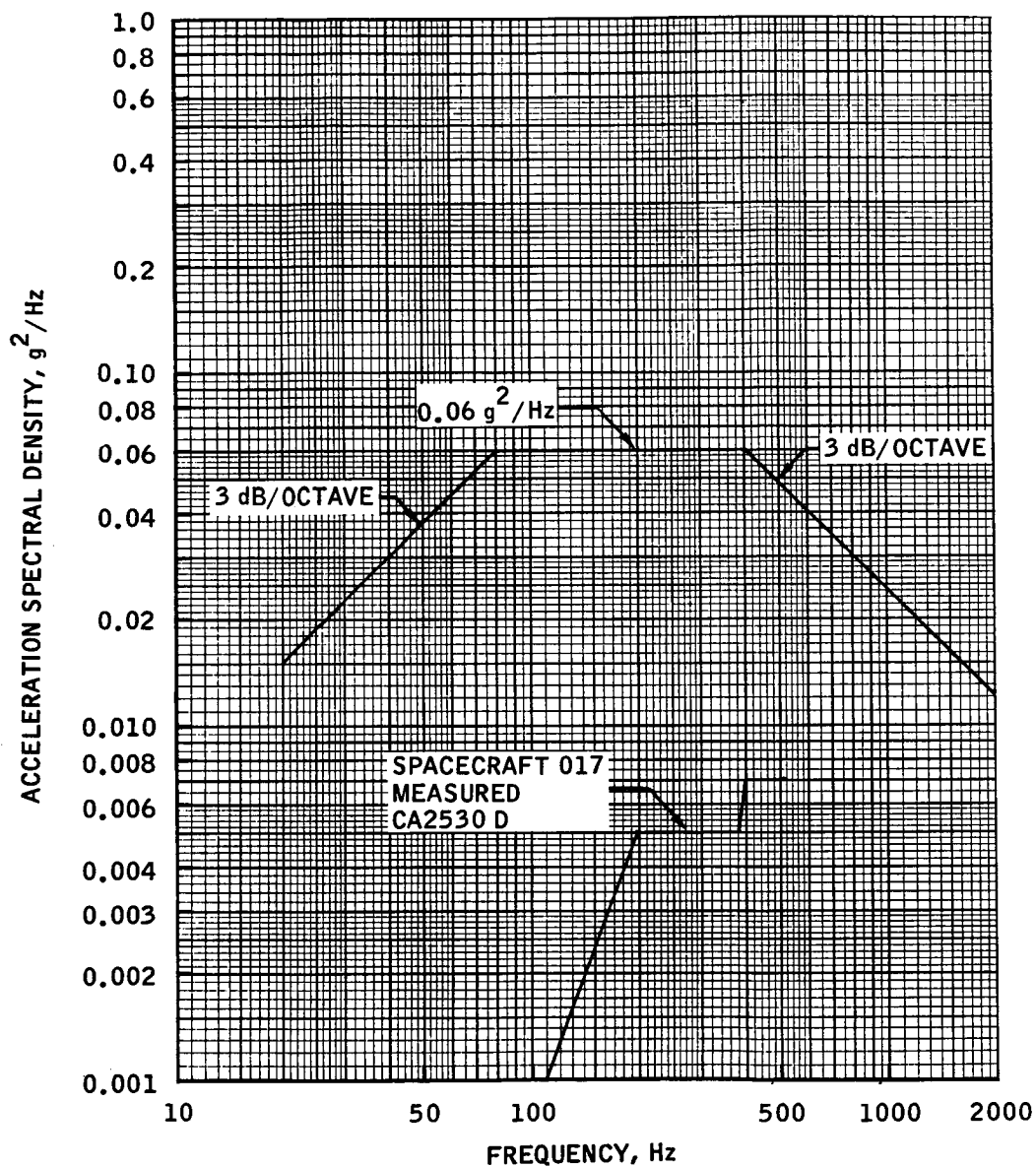


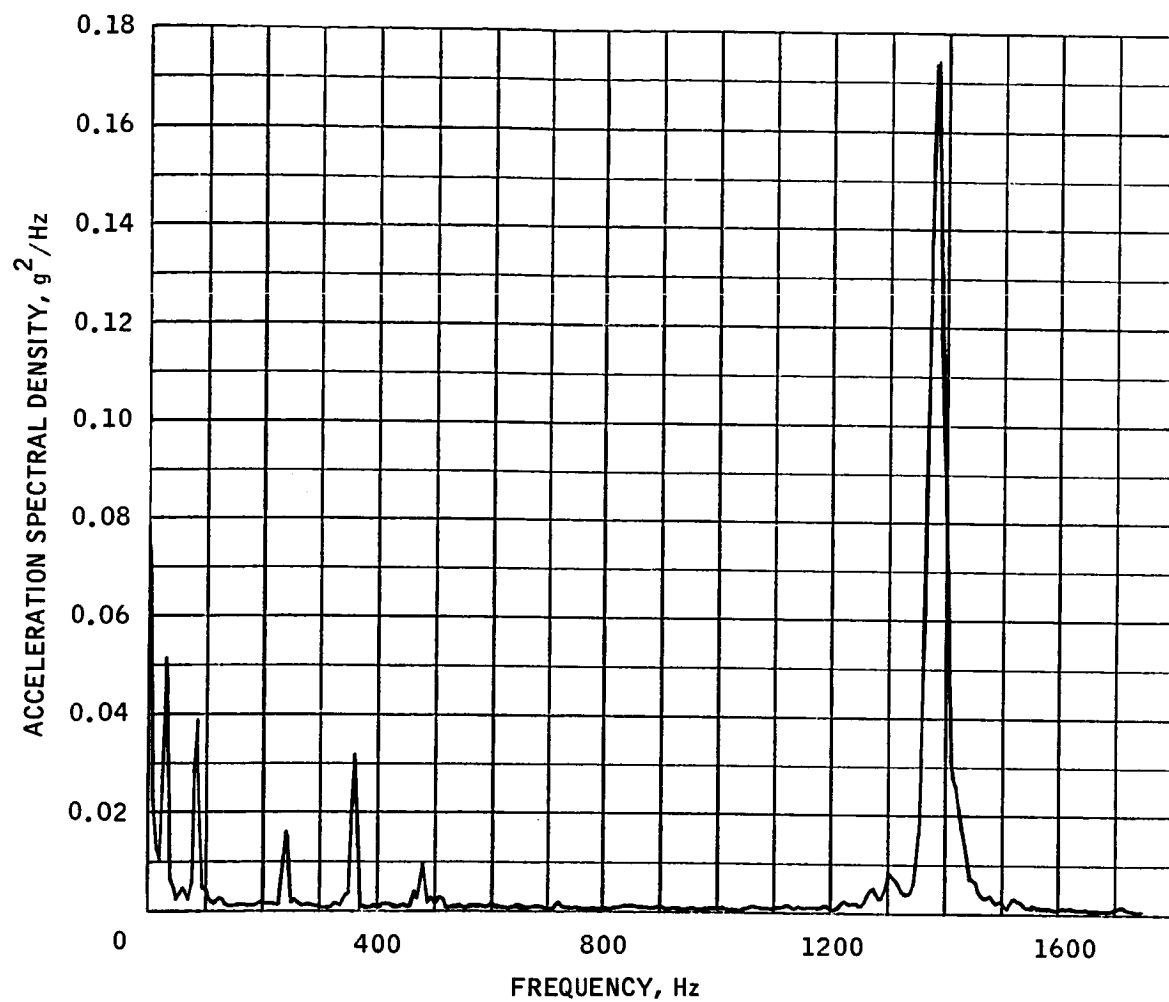
FIGURE 5.1-15.- COMPARISON OF COMMAND MODULE INTERNAL EQUIPMENT BAY'S (BLOCK D) VIBRATION CRITERIA TO MEASURED VIBRATION DURING ATMOSPHERIC FLIGHT.

~~CONFIDENTIAL~~

~~CONFIDENTIAL~~

5.1-35

NASA-S-68-342



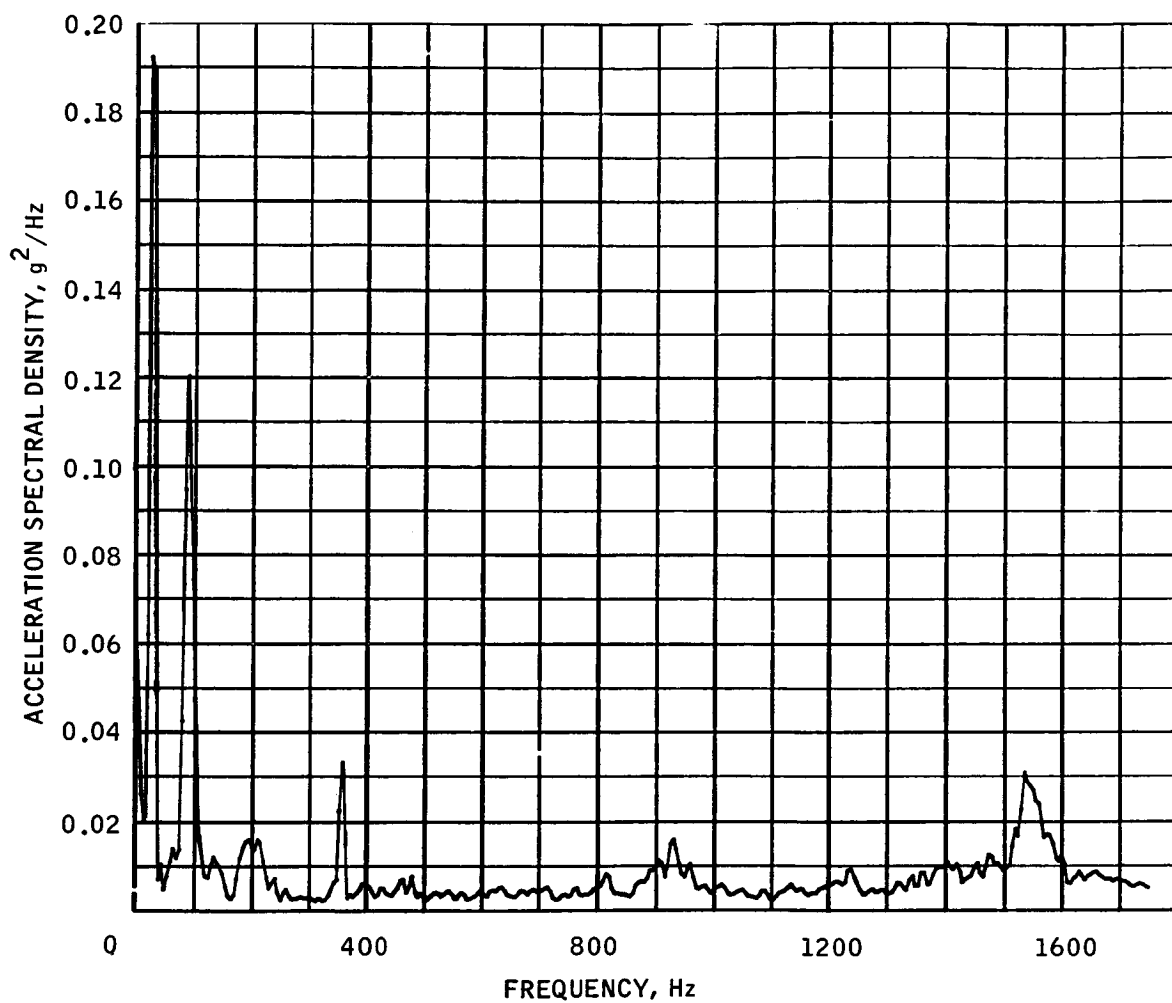
(A) PRIOR TO IGNITION.

FIGURE 5.1-16. - SERVICE MODULE ACCELERATION SPECTRAL DENSITY.

~~CONFIDENTIAL~~

~~CONFIDENTIAL~~

NASA-S-68-343



(B) MAXIMUM VIBRATION FROM 77.0 TO 79.0 SECONDS.

FIGURE 5.1-16. - CONCLUDED.

~~CONFIDENTIAL~~

~~CONFIDENTIAL~~

5.1-37

NASA-S-68-344

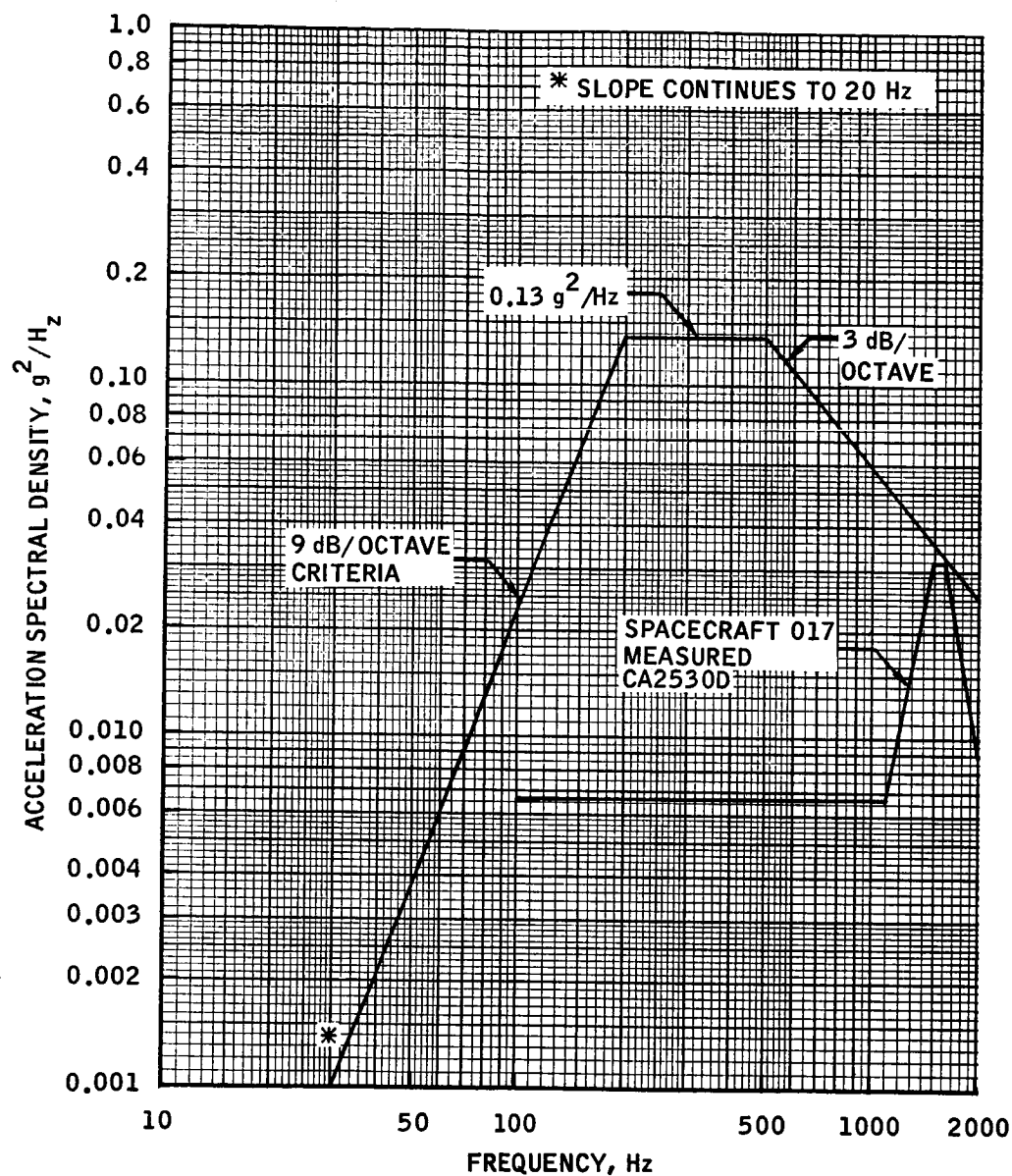


FIGURE 5.1-17.- COMPARISON OF SERVICE MODULE AFT BULKHEAD VIBRATION CRITERIA TO MEASURED VIBRATION DURING ATMOSPHERIC FLIGHT.

~~CONFIDENTIAL~~

~~CONFIDENTIAL~~

THIS PAGE INTENTIONALLY LEFT BLANK

~~CONFIDENTIAL~~

~~CONFIDENTIAL~~

5.2-1

## 5.2 AERODYNAMICS

### 5.2.1 Summary

The flight-derived total lift-to-drag ratio and total angle of attack were well within the predicted uncertainty boundaries for the entire hypersonic flight regime. The flight-derived data during the first entry are estimated to be a lift-to-drag ratio of 0.370 and a total angle of attack of 154.6 degrees. Averaged values for a lift-to-drag ratio equal to 0.365 ( $\pm 0.015$ ) and a total angle of attack equal to 155.5 ( $\pm 1.5$ ) degrees were obtained in the region from entry to final entry phase where most of the maneuvering was accomplished.

### 5.2.2 Aerodynamics Predictions

Preflight predictions of the command module (CM) trim aerodynamics were based on extensive analyses of preflight wind tunnel data, with appropriate modifications, and flight-derived data obtained from the two previous Apollo space-flight tests.

The wind tunnel data were corrected to account for external protuberances (located on or near the aft heat shield) that would affect the aerodynamics. The major effects were caused by the umbilical housing, ramp, and a thicker layer of ablative material (fig. 5.2-1) in the region of the stagnation point. The trim attitude was determined using the latest entry center-of-gravity data, which were then analytically modified during entry to account for flight-measured reaction control subsystem (RCS) usage (section 13.4). Shape change during entry and the effect of ablative material loss on the aerodynamics were found to be negligible.

In addition to these corrections, flight-derived aerodynamic data from previous Apollo missions were taken into consideration. The limited data from the AS 201 mission (Spacecraft 009) were consistent with the preflight predictions at the time of that mission; therefore, no changes were made to predictions for future flights. Flight-derived data from the AS 202 (Spacecraft 011) mission, with an entry configuration and center of gravity similar to that of the AS 201 mission, showed the hypersonic trim lift-to-drag ratio to be 18 percent lower than predicted (reference 2). This resulted in a subsequent correction to the wind tunnel data by adjusting the hypersonic pitching moment data predictions to give a trim point that was approximately 3 degrees higher in angle of attack.

As a consequence of these preflight and flight data analyses, a set of unsymmetrical uncertainty bands, about the predicted nominal trim

~~CONFIDENTIAL~~

~~CONFIDENTIAL~~

values, was determined to be the most realistic method of accounting for uncertainties in both the wind-tunnel data and the results of the two previous flights. In addition, the set of bands included uncertainties in center-of-gravity location, aft heat shield mating alignment, and aft heat shield cant angle determination. Table 5.2-I lists the predicted total lift-to-drag trim and total angle of attack, and their associated uncertainty bands, for conditions at the entry interface (400 000 feet), at the first peak deceleration load (peak g), and at the second peak g (see section 3.1.4 and figure 3.1-5 for the deceleration time history).

### 5.2.3 Flight-Derived Aerodynamics

Flight total angle of attack  $\alpha_T$  referenced to the positive body X-axis of the CM is obtained from the inertial measurement unit (IMU) gimbal angles recorded on board the spacecraft and from position and velocity data obtained from the reconstructed entry trajectory (section 3.1.4). The angles are used to transform the relative velocity into components in the body frame where

$$\alpha_T = \tan^{-1} \left[ \frac{\sqrt{(\text{Y-body velocity})^2 + (\text{Z-body velocity})^2}}{\text{X-body velocity}} \right]$$

Flight total lift-to-drag ratio is obtained from the IMU acceleration data which have been corrected for known preflight bias and scale factor errors and from preliminary reconstructed entry trajectory data. These data are then corrected for platform misalignment (see section 5.15.2) and transformed along, and perpendicular to, the relative velocity vector giving lift and drag proportional terms and, thereby, the total lift-to-drag ratio. Details of the method used are given in reference 2. Time histories of Mach number and free stream Reynolds number per foot are presented in figure 5.2-2 for reference.

The atmospheric model recommended for postflight analysis was the 15 degrees North Annual (reference 3), based on a comparison of Rawinsonde data obtained near the entry path (Eniwetok Atoll, Marshall Islands).

### 5.2.4 Comparison of Predictions With Flight-Derived Aerodynamic Data

Comparisons of flight-derived values with predictions of total lift-to-drag ratio and total angle of attack are presented in figures 5.2-3 and 5.2-4, respectively. The Apollo guidance computer control phases are noted on the lift-to-drag ratio time history for reference. Details

~~CONFIDENTIAL~~



~~CONFIDENTIAL~~

5.2-3

of the guidance and control subsystem performance during entry are discussed in section 5.15.2.

The flight-derived data were well within the predicted uncertainty boundaries for the entire hypersonic flight regime. Shortly after the entry interface at 400 000 feet, the dynamic pressure increased to a level where the CM aerodynamic moments damped the oscillations and a steady-state trim attitude was reached, near 0.05 g. The corresponding lift-to-drag ratio was 0.37, or 0.02 above the predicted value in this region through the first g peak. This level dropped to a low of 0.36 about halfway between the entry interface and the start of the final entry phase. The flight-derived lift-to-drag ratio was then linear from this time, 08:21:50, until the second peak g point, at 08:27:11, when it rose to 0.40.

Most importantly, the agreement of the lift-to-drag ratio was best in the region from the entry interface to the start of the final entry phase. This was the region where any maneuvering necessary to reach the targeted landing point was conducted. The total lift-to-drag ratio averaged out to 0.365 ( $\pm 0.015$ ) for this region. Several shifts in the data were noted, one near the upcontrol guidance phase and a larger one just after the second peak g. These both coincide with large, controlled variations in bank angle (fig. 5.15-16) and can therefore be attributed to the preliminary nature of the flight data used in the calculations rather than to aerodynamic phenomena.

The flight-derived angle-of-attack data showed a trend that was correlated with the lift-to-drag time history with a total angle of attack of 154.6 degrees through the first peak g and an average angle of attack of 155.5 ( $\pm 1.5$ ) degrees in the region to the final entry phase. The shift in total angle of attack near the upcontrol phase was more noticeable than was the lift-to-drag shift; however, the angle-of-attack calculations are generally more susceptible to errors in the flight data. The good agreement between both the total lift-to-drag ratio and the total angle of attack appears to substantiate the adjustment made to the preflight CM aerodynamics for the Apollo 4 mission in which the predicted trim attitude was shifted approximately 3 degrees based on the flight data from the AS 202 mission.

The overall accuracy of these preliminary flight-derived aerodynamic data is estimated to be  $\pm 0.015$  for the lift-to-drag ratio and  $\pm 2.5$  degrees for the total angle of attack. Results of a detailed analysis of the final input data required to calculate the flight-derived aerodynamics will be provided in a supplemental report.

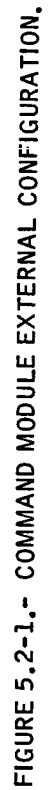
~~CONFIDENTIAL~~

~~CONFIDENTIAL~~

TABLE 5.2-I.- COMMAND MODULE AERODYNAMICS - PREFLIGHT PREDICTIONS

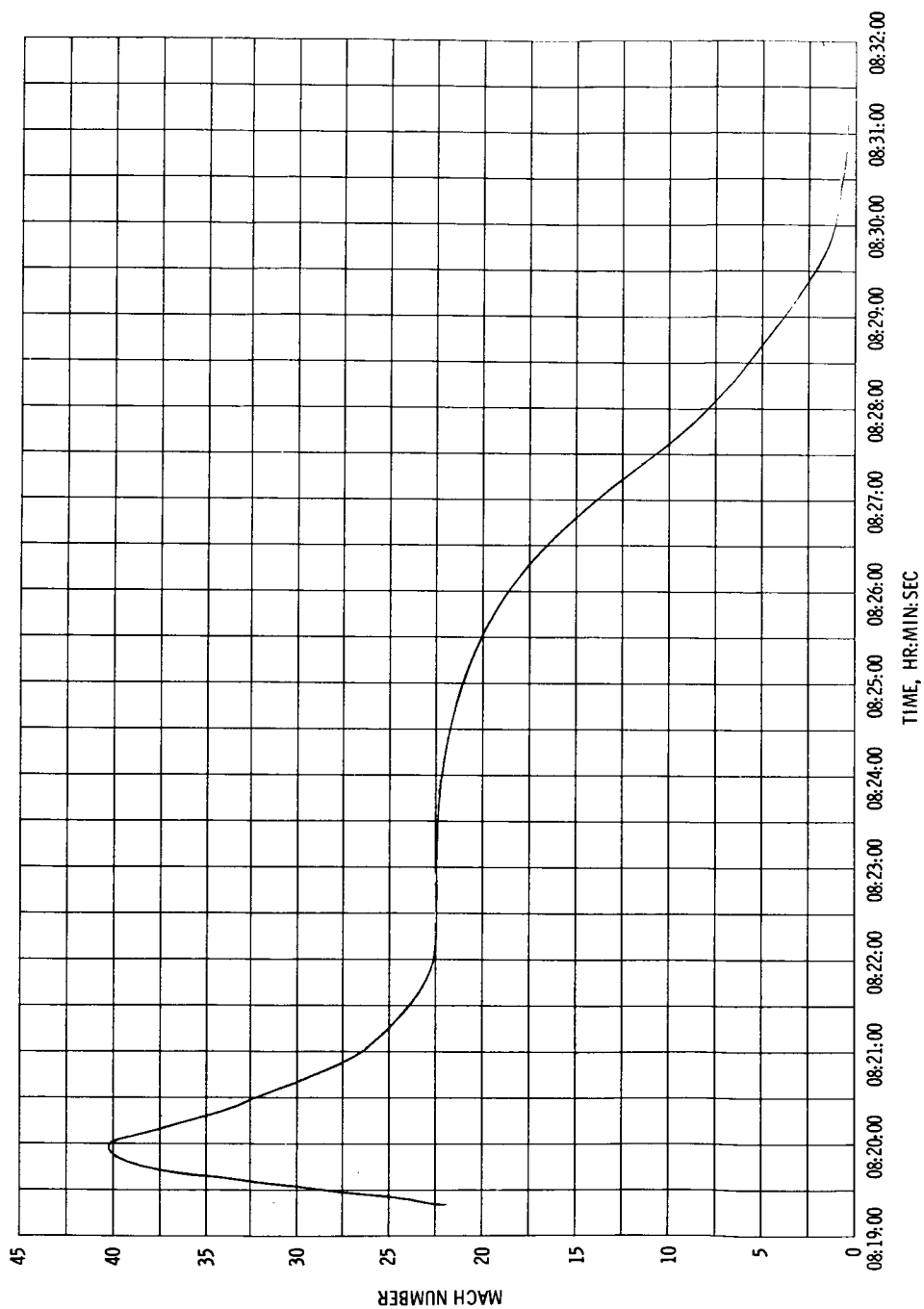
		Total lift-to-drag ratio	Corresponding total angle of attack, deg
Entry interface	High	0.416	152.2
	Nominal	0.350	156.7
	Low	0.322	158.5
First peak g	High	0.415	152.2
	Nominal	0.349	156.8
	Low	0.321	158.6
Second peak g	High	0.410	152.6
	Nominal	0.344	157.1
	Low	0.316	159.0

~~CONFIDENTIAL~~



~~CONFIDENTIAL~~

NASA-S-68-346



(A) MACH NUMBER.

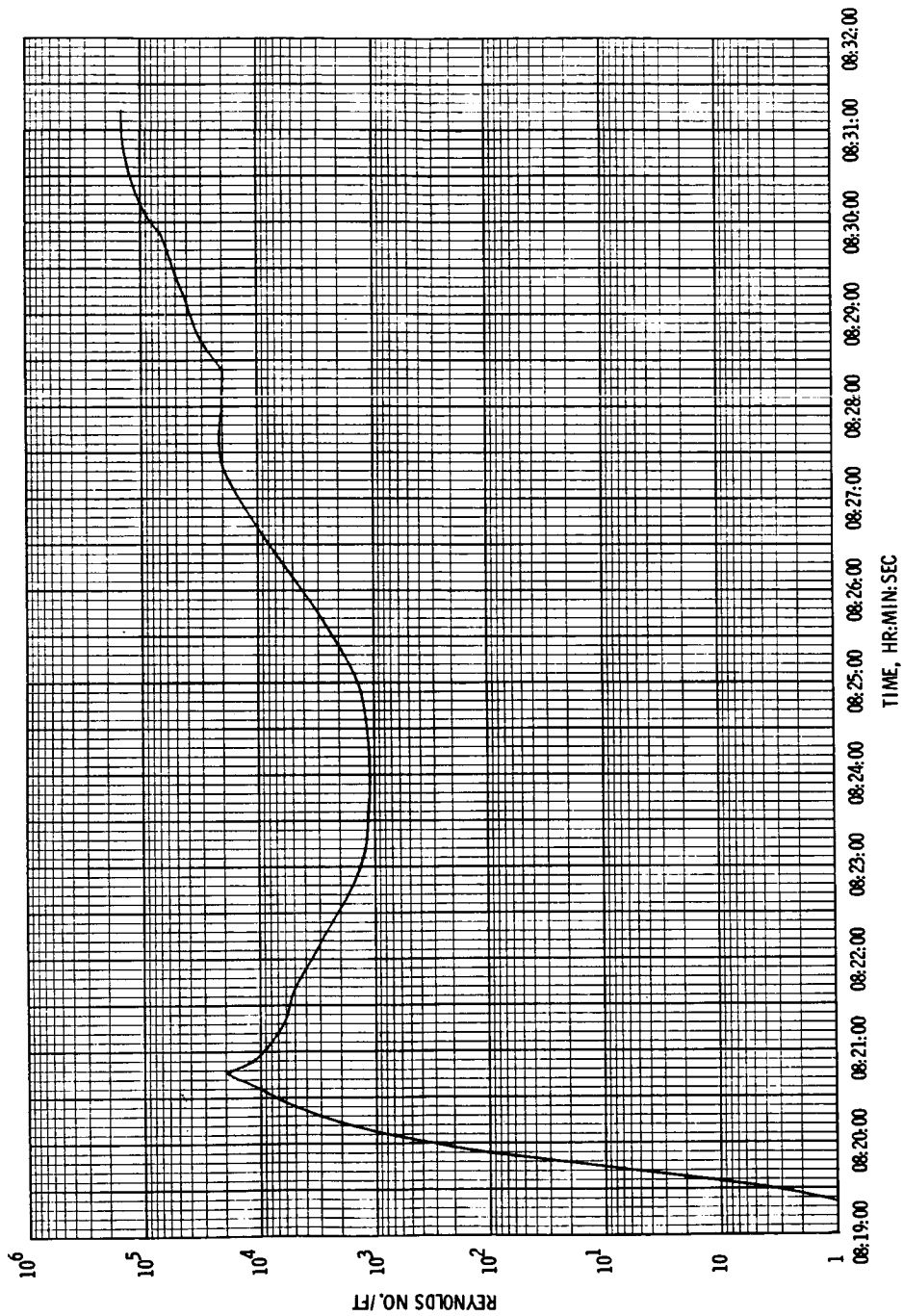
FIGURE 5.2-2. - AERODYNAMIC CORRELATION PARAMETERS.

~~CONFIDENTIAL~~

~~CONFIDENTIAL~~

5.2-7

NASA-S-68-347



(B) REYNOLDS NUMBER PER FOOT.

FIGURE 5.2-2. - CONCLUDED.

~~CONFIDENTIAL~~

~~CONFIDENTIAL~~

NASA-S-68-348

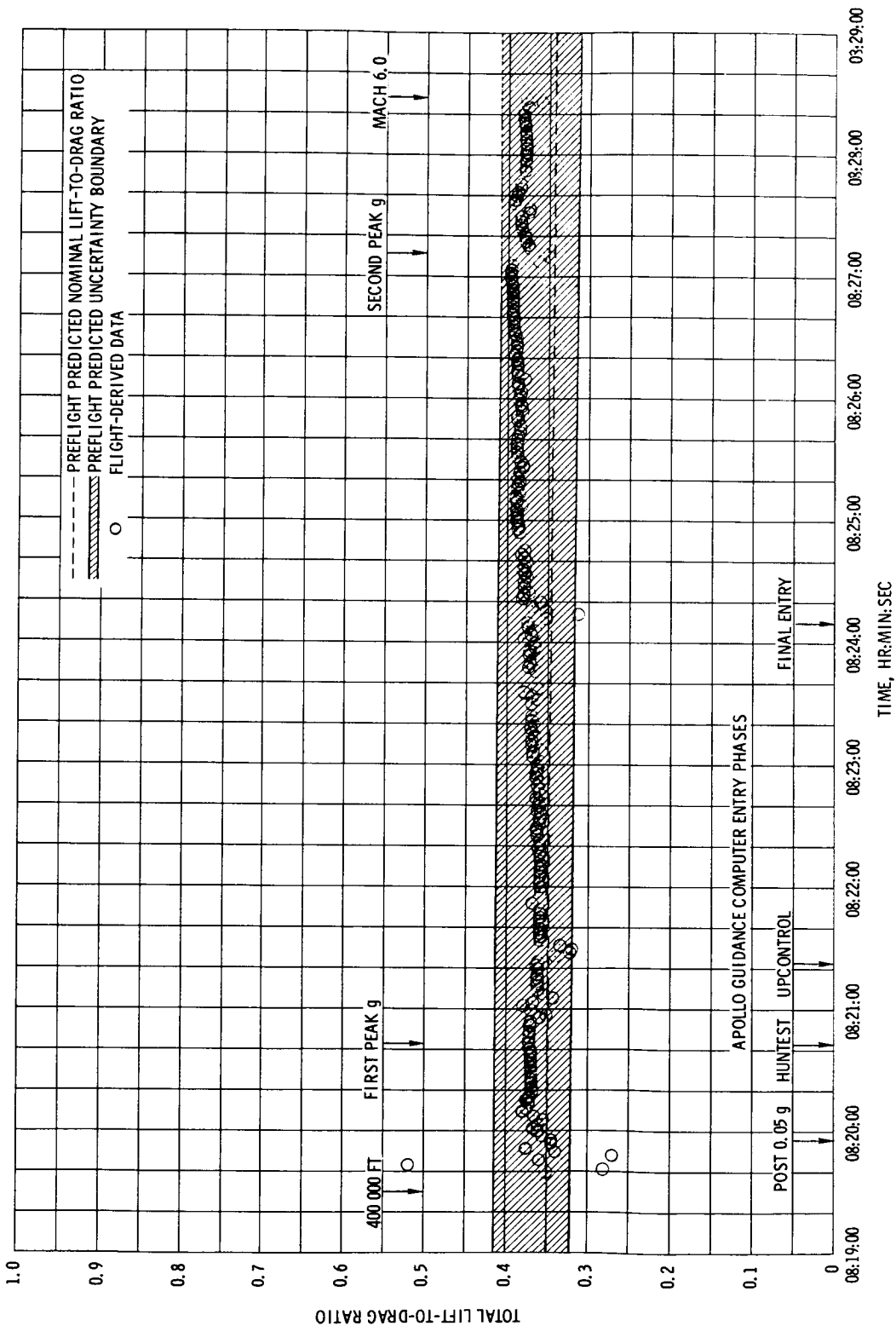


FIGURE 5.2-3. - COMMAND MODULE TOTAL LIFT-TO-DRAG RATIO.

~~CONFIDENTIAL~~

~~CONFIDENTIAL~~

5.2-9

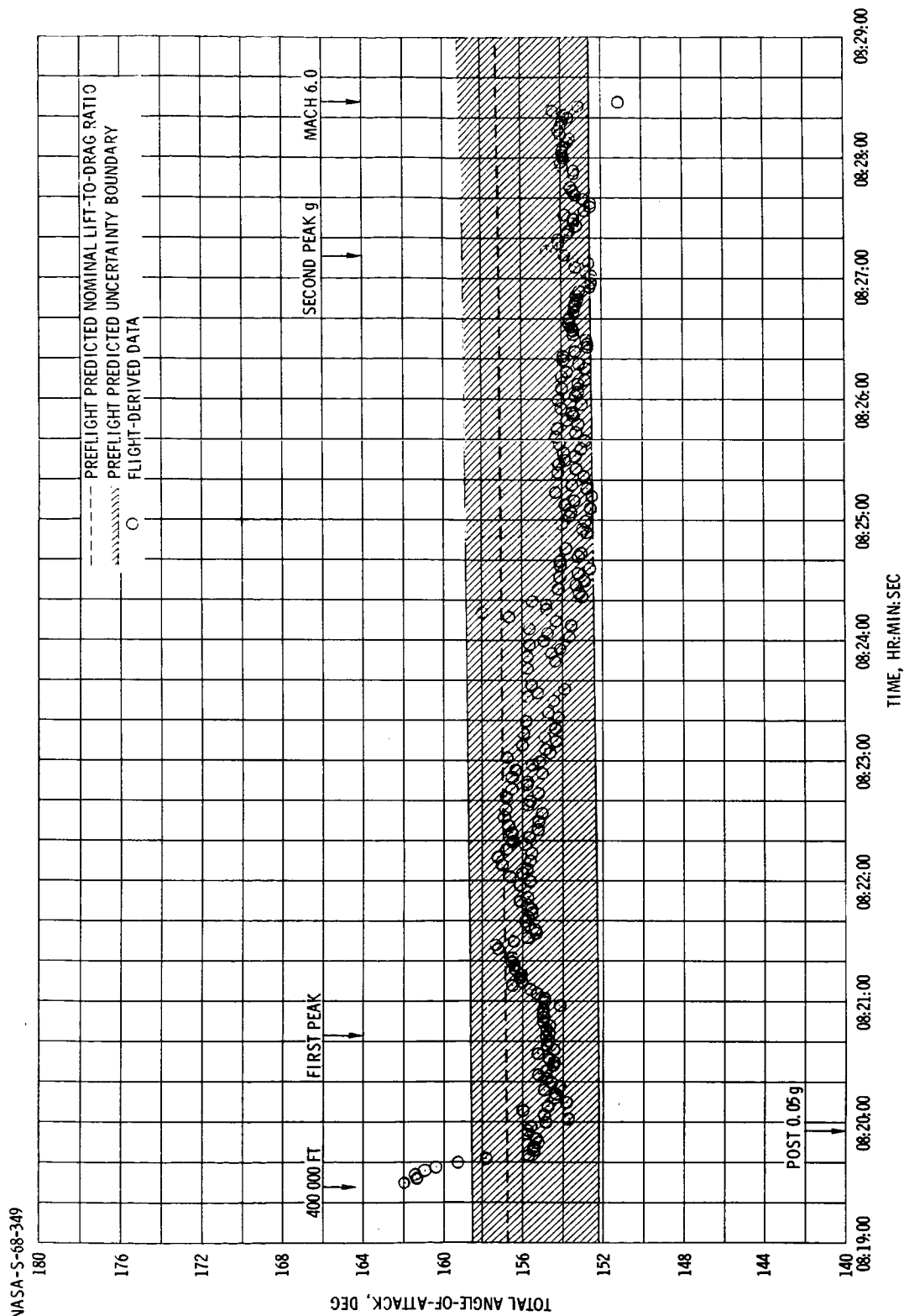


FIGURE 5.2-4. - COMMAND MODULE TOTAL ANGLE-OF-ATTACK.

~~CONFIDENTIAL~~

~~CONFIDENTIAL~~

THIS PAGE INTENTIONALLY LEFT BLANK

~~CONFIDENTIAL~~



~~CONFIDENTIAL~~

5.3-1

### 5.3 THERMAL STRUCTURES

#### 5.3.1 Launch Phase

Thermal structures.- The thermal environment of the Apollo 4 launch phase ascent trajectory has been evaluated for the service module (SM) and the spacecraft/lunar module adapter (SLA). The heating parameters were lower than those predicted for the operational trajectory.

The thermal environment was deduced from the measured temperatures of the outer and inner SM and SLA skins and several internal structure locations during ascent. In the following evaluation of temperatures, the discussion is limited to a representative number of typical temperature locations for the time period from lift-off to about 00:05:00. This is the portion of the trajectory significant for ascent heating.

Service module temperatures.- Figure 5.3-1 shows the locations of the three thermocouples used to measure the inner skin temperature of the SM. The maximum SM temperature of 91° F recorded during the first 300 seconds of ascent was measured by sensor SA2366T on the inner skin at longitudinal station  $X_S$  280 inches and 145 degrees from the +Y-axis.

The low temperatures recorded for the SM inner skin were the result of the protection afforded by the cork insulation on the exterior of the SM skin. Because of the low temperature levels measured and the relatively low temperature levels expected for a completely corked SM structure, the SM inner skin temperatures for the operational launch trajectory were not correlated with analytical predictions.

Spacecraft/lunar module adapter temperatures.- Figure 5.3-2 shows the distribution of peak temperatures measured on the SLA outer skin during ascent. The maximum SLA launch temperature of 290° F was measured by sensor AA7863T on the outer skin at longitudinal station  $X_A$

645 inches and 174 degrees from the positive Y-axis at 00:02:25. Figure 5.3-3 compares the predicted temperature response with the measured temperature time history for this sensor (AA7863T). Figure 5.3-4 compares the predicted temperature response with the measured temperature time history for sensor AA7864T, which was the outer skin thermocouple located at  $X_A$  730 inches and 174 degrees. The maximum predicted response shown was based on SLA radiation interchange with the sun and the earth. The minimum predicted response was based on radiation exchange with space only. The predicted temperatures agree well with the data measured by sensor AA7864T (fig. 5.3-4), but the predicted temperatures for sensor AA7863T (fig. 5.3-3) are seen to fall about 40° F below the measured data band. The higher

~~CONFIDENTIAL~~

~~CONFIDENTIAL~~

temperatures measured by AA7863T are attributed to the flow disturbance caused by the cable way attached to the surface of the SLA (fig. 5.3-2). Sensor AA7864T was located in an undisturbed flow area and was removed from any structure which would act as a heat sink. The thermocouple response therefore compared favorably with the one-dimensional predicted values (fig. 5.3-4).

The predicted response (fig. 5.3-4) falls above the measured data band during the first 80 seconds of ascent. This occurs because the standard atmosphere used in the analytical predictions has higher ambient air temperatures during this period than were actually encountered by the spacecraft. The low initial temperature of 50° F coupled with this somewhat hotter atmosphere, resulted in an increase in the predicted surface temperature rather than the normally expected initial cooldown after lift-off.

Sensors AA7860T, AA7869T, AA7870T, and AA7871T all recorded lower peak temperatures than sensor AA7864 (fig. 5.3-2). All four of these thermocouples are located in the proximity of the SLA vertical separation joints, and the measured temperatures are influenced by the heat sink effect of the separation joint structure.

The low peak temperature of 130° F recorded by sensor AA7866T results from the heat sink effect of the SLA circumferential joint at  $X_A$  838 inches. All outer skin temperature measurements aft of  $X_A$  610 inches show maximum temperatures below 120° F (fig. 5.3-2). The low temperatures were the result of the protection afforded by cork insulation on the surface of the SLA in this area.

The only SLA inner skin thermocouple (AA7874T) was located at longitudinal station  $X_A$  785 inches and 214 degrees from the positive Y-axis. It recorded a peak temperature of 140° F compared with a predicted 200° F maximum using a one-dimensional thermal analysis. This difference is attributed to the heat sink effect of the vertical separation joint structure.

Figure 5.3-5 shows the distribution of surface temperature on the SLA at S-IC outboard engine cutoff. These temperatures are of importance in determining material properties and thermal stresses used in the structural loads evaluation.

Temperature sensors on the simulated lunar module (LM) descent stage skin, which was mounted inside the SLA, recorded no significant temperature increase during ascent. The simulated LM skin decreased from an initial temperature of 50° F to about 40° F and then increased to 60° F by the end of boost.

~~CONFIDENTIAL~~

~~CONFIDENTIAL~~

5.3-3

The measured SLA temperatures were well within the design value maximum temperature of 490° F and verify the adequacy of this design. Sufficient valid data of the CSM/SLA structure were obtained to enable determination of the thermal response during boost and to verify the adequacy of the thermal analysis prediction techniques.

### 5.3.2 Orbital Flight

The command module (CM) heat shield thermal response to the space environment during the orbital portion of the mission was measured by three operational ablator bondline temperature sensors. Three SM temperature measurements located on the SM aluminum honeycomb inner skin were also recorded during the orbital flight period. The time of interest for the orbital flight period was from orbit insertion to entry, approximately 00:11:00 to 08:00:00.

The location of CM sensors CA1502T and CA1509T, for which periods of data were available throughout the orbital flight and for which temperature predictions were made, are shown on figure 5.3-6. Postflight predictions were made based on sun look angles computed from the actual guidance and control gimbal angle data recorded during the orbital portion of the flight. Temperature measurements (fig. 5.3-7) available just prior to entry confirm that the CM positive Z-side heat shield was cold soaked in accordance with the flight plan. The spacecraft orientation with respect to the sun during the elliptical cold-soak third orbit is shown in figure 5.3-8.

The negative Z-side of the CM from positive Y to negative Y was coated with the standard Block II thermal control coating having a nominal solar absorptance of 0.16 and an infrared emittance of 0.4. To obtain a faster cooldown response during the ablator cold-soak period, the positive Z-side of the CM was painted with a coating having a 0.5 solar absorptance and infrared emittance of 0.85.

The CM ablator bondline cold-soak response was measured by sensor 1502T (fig. 5.3-6). Temperature-time histories of the measured data and postflight temperature predictions during the coast ellipse for this location are shown in figure 5.3-9. Because of the scarcity of measured data points and the changing sun attitude relative to the spacecraft during the first two circular earth-parking orbits, comparison of predicted and measured flight data for the parking orbits is excluded. Figure 5.3-8 shows that at 08:00:00 the flight measurements are approximately 20° F higher than predicted. Part of this difference results from the thermal coupling to the adjacent redesigned astro-sextant telescope region and to the substructure stringer. This area will respond thermally slower than other regions because of the higher thermal capacitance of the structure. Uncertainty in the actual conductivity of

~~CONFIDENTIAL~~

~~CONFIDENTIAL~~

the insulation (TG-15000) because of its sensitivity to insulation pressure is an additional factor that affects the thermal response in this region.

Ablator bondline hot-soak response was measured by sensor CA1509T (fig. 5.3-10). Predicted temperatures for a nominal Block II thermal control coating having a solar absorptance and infrared emittance ratio ( $\alpha/\epsilon$ ) of 0.4 and for a degraded  $\alpha/\epsilon$  of 0.54 are shown on this figure. Reasonable correlation is obtained using  $\alpha/\epsilon$  equal to 0.54 which indicates that thermal control coating degradation did occur. Observation of the temperature measurement levels prior to entry (fig. 5.3-7) also shows coating degradation effects. Temperatures of approximately 150° F were measured at locations on the negative Z-side of the CM. The maximum possible steady-state equilibrium temperature that would correspond to the solar vector normal to the non-degraded Block II coating surface is approximately 107° F for  $\alpha/\epsilon$  equal to 0.4. An equilibrium temperature of 150° F would require  $\alpha/\epsilon$  equal to 0.54.

The conclusion that the Block II CM composite coating of oxidized silicon monoxide on aluminized Kapton (Schjeldal coating) was degraded, was further substantiated by postflight microscopic examination of the coating. This examination showed that there was considerable contamination by black and red particles, impacted upon and driven into the polymer matrix of the coating. The black particles appeared angular and sharp edged and are considered to be solid fuel rocket exhaust particles of reduced iron oxide (black FeO). The red particles were red iron oxide particles. This type of contamination is not attributable to the entry products but to the materials used in the solid propellant tower jettison motor.

Degradation of the coating was expected for this flight; however, instrumentation limitations prevented an accurate determination of absolute values. Further evaluation of degradation is planned for the first manned flight through radiator performance tests and on the second manned flight by EVA retrieval of thermal coating specimens located on the external surfaces of the LM, CM, SM, and EPS radiators.

Temperatures on the Block I SM with total cork insulation were measured by sensors SA2360T, SA2361T, and SA2366T (fig. 5.3-1). The inner aluminum honeycomb skin temperatures measured by these sensors remained within the range of 110° F to minus 90° F and were well within the design limits for the aluminum honeycomb panels.

The flight objective of thermally cold conditioning the ablator positive Z-side and hot soaking the negative Z-side of the CM prior to entry to induce circumferential thermal stresses and distortions on the CM was achieved. Block II thermal control coating degradation did occur and is evidenced by the measured data exceeding the Block II nominal

~~CONFIDENTIAL~~

~~CONFIDENTIAL~~

5.3-5

coating equilibrium temperatures; this degradation is attributed to the tower jettison motor.

~~CONFIDENTIAL~~

~~CONFIDENTIAL~~

NASA-S-68-350

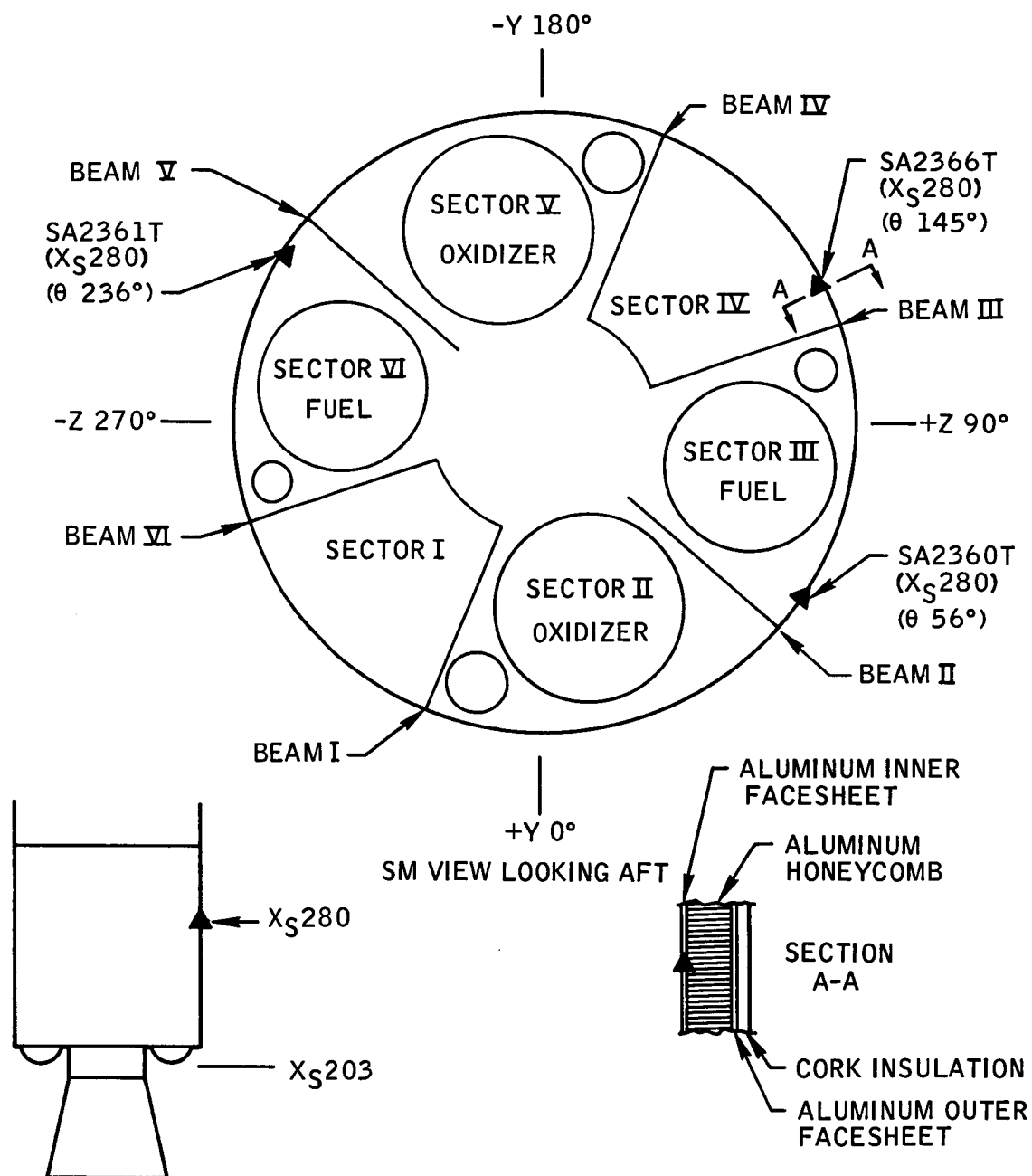


FIGURE 5.3-1.- LOCATION OF SERVICE MODULE INNER SKIN THERMOCOUPLES.

~~CONFIDENTIAL~~

~~CONFIDENTIAL~~

5.3-7

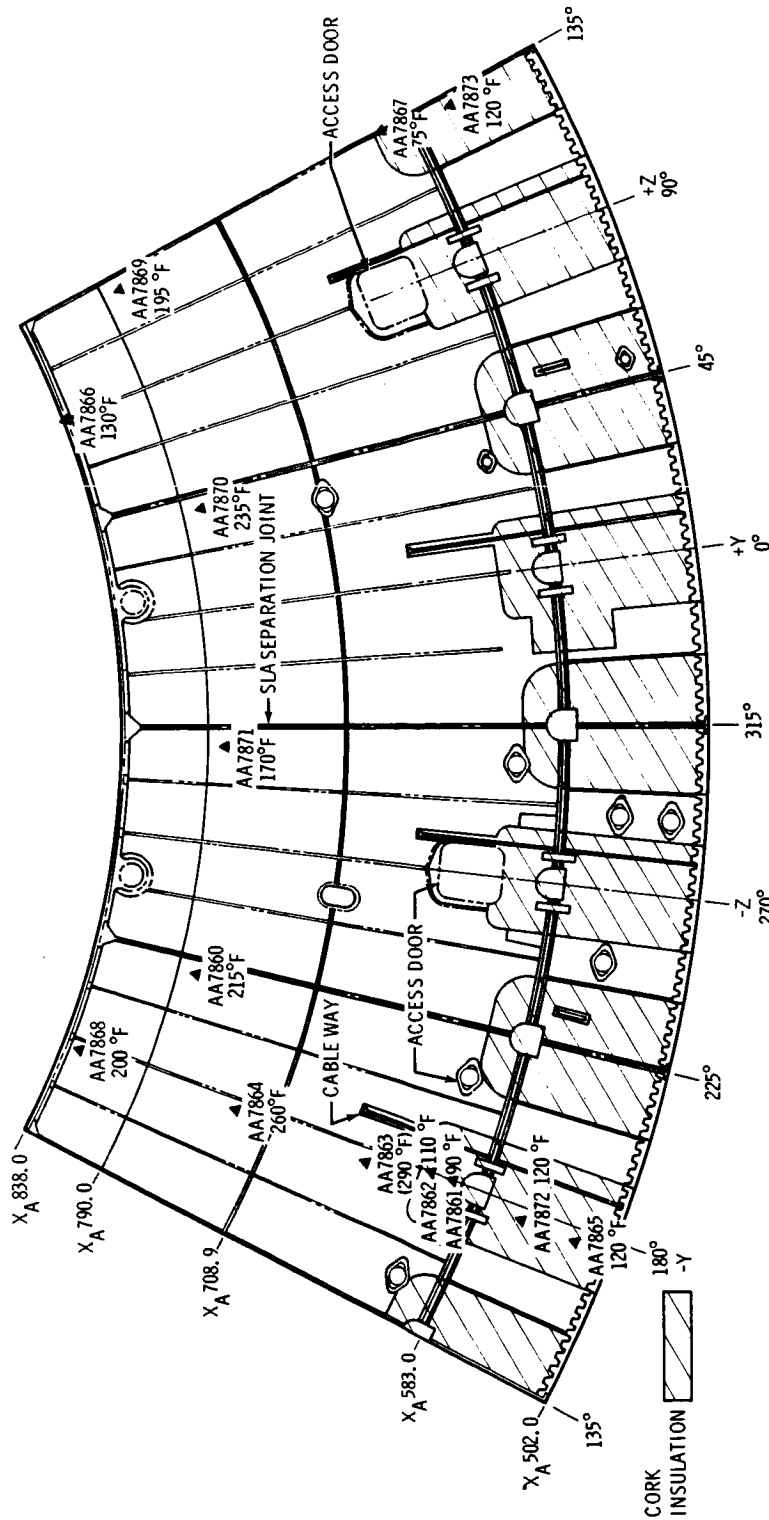


FIGURE 5.3-2. - PEAK TEMPERATURES MEASURED ON SPACECRAFT LUNAR MODULE ADAPTER OUTER SURFACE DURING THE LAUNCH PHASE.

NASA-S-68-351

~~CONFIDENTIAL~~

~~CONFIDENTIAL~~

NASA-S-68-352

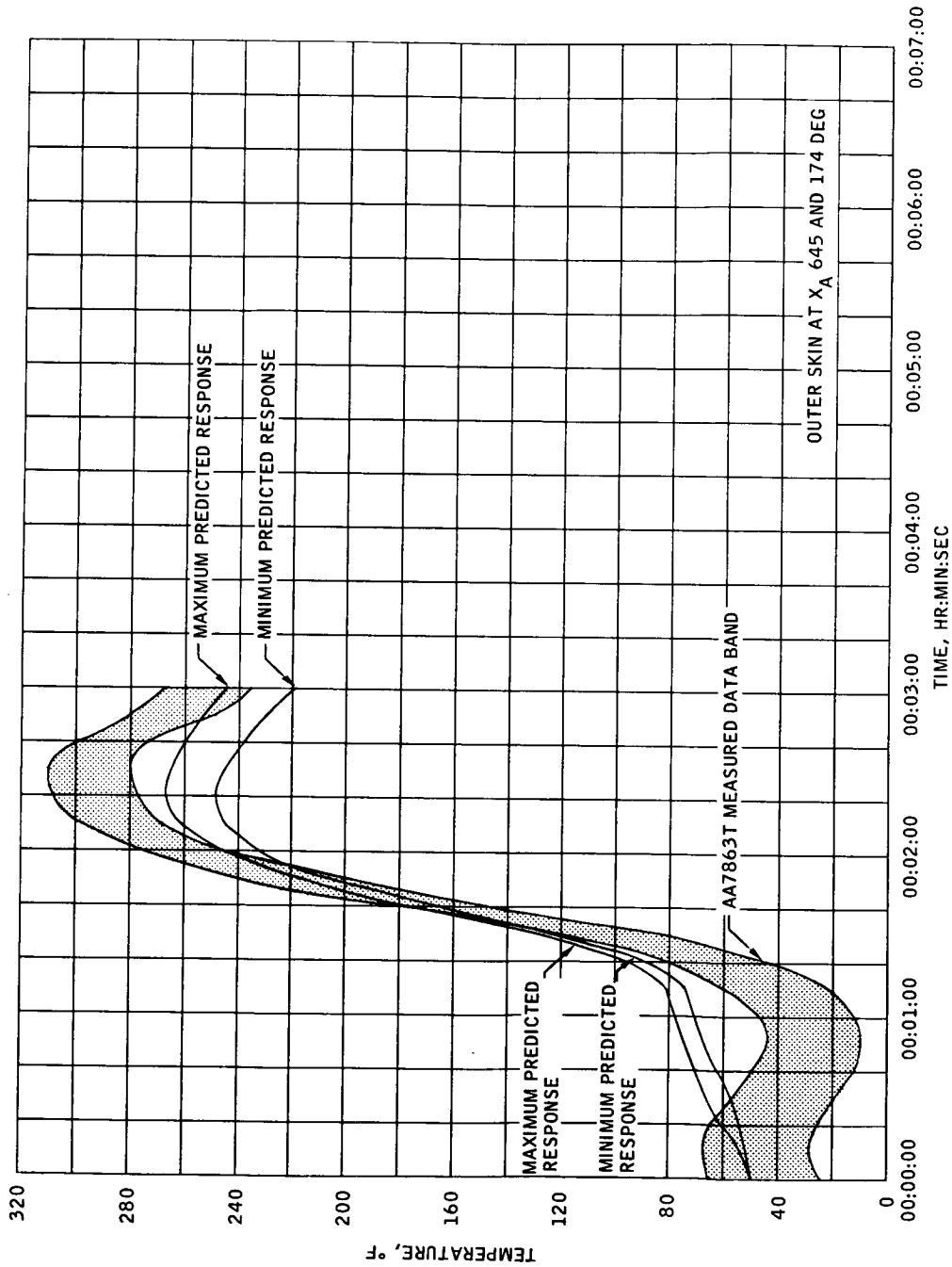


FIGURE 5.3-3.- TEMPERATURE MEASURED BY SPACECRAFT LUNAR MODULE ADAPTER SENSOR AA7863T.

~~CONFIDENTIAL~~



~~CONFIDENTIAL~~

5.3-9

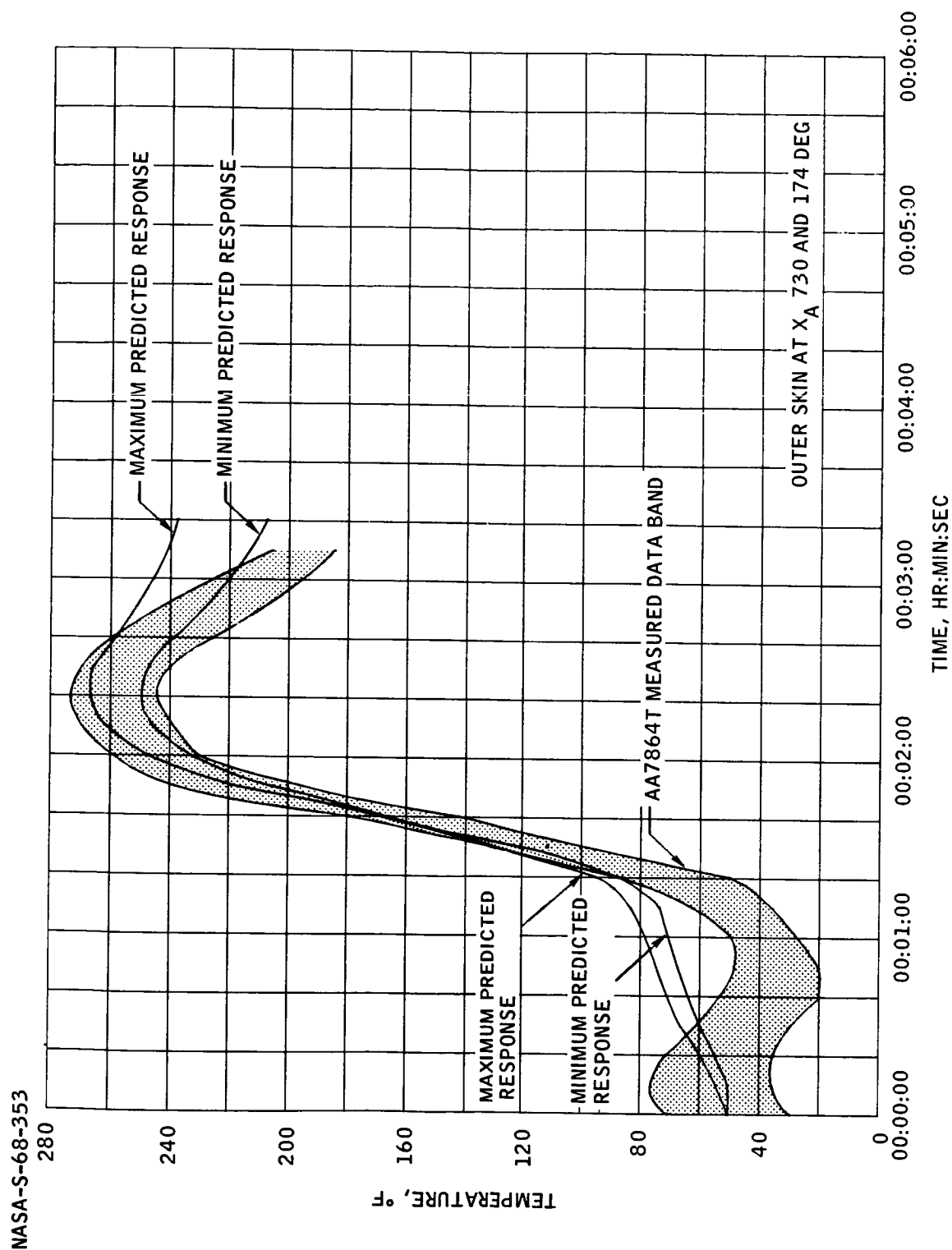


FIGURE 5.3-4.- TEMPERATURE MEASURED BY SPACECRAFT LUNAR MODULE ADAPTER SENSOR AA7864T.

~~CONFIDENTIAL~~

~~CONFIDENTIAL~~

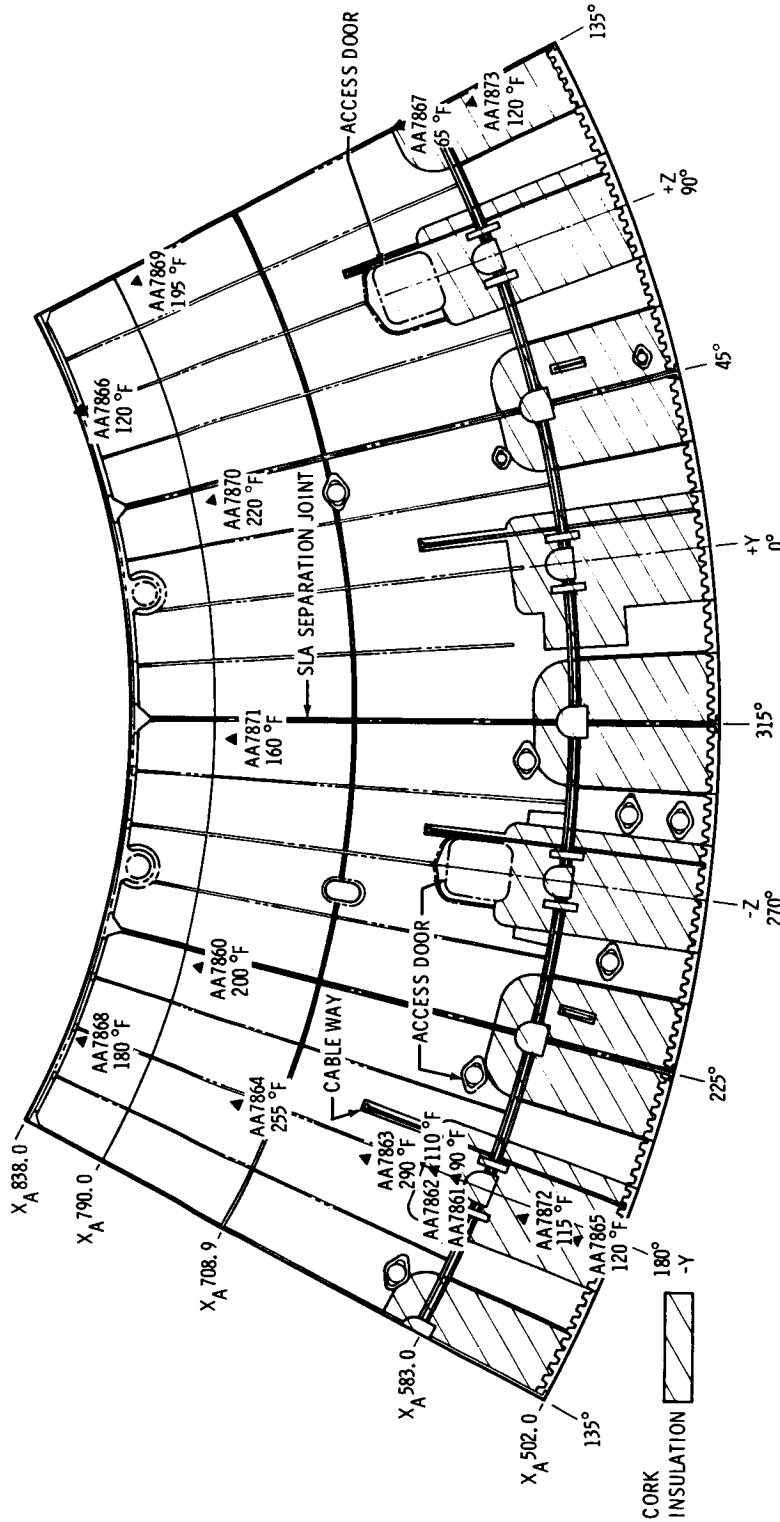


FIGURE 5.3-5. - OUTER SURFACE TEMPERATURES OF THE SPACECRAFT LUNAR MODULE ADAPTER AT S-IC OUTBOARD ENGINE CUTOFF.

~~CONFIDENTIAL~~

~~CONFIDENTIAL~~

5.3-11

NASA-S-68-355

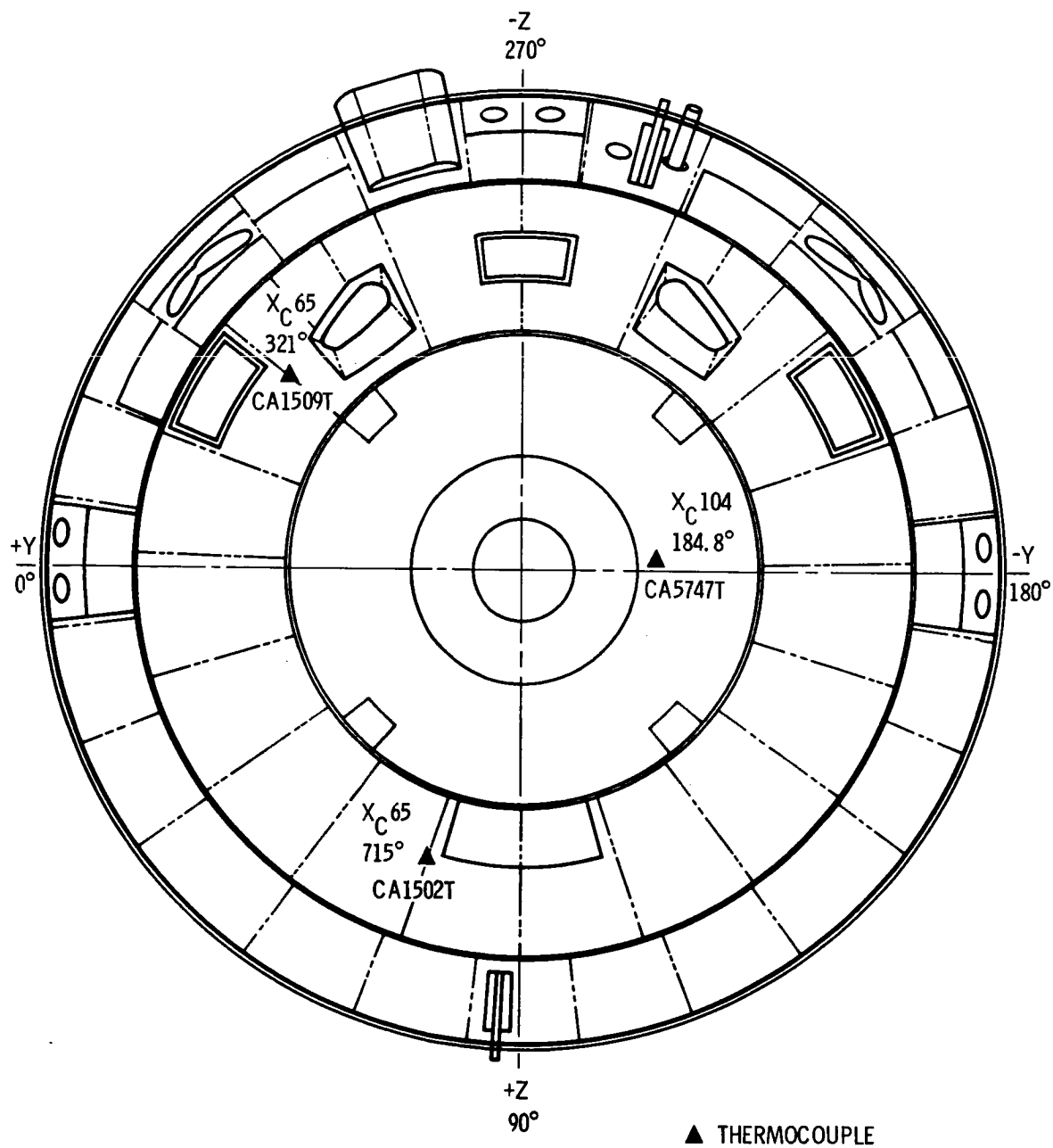


FIGURE 5.3-6. - TEMPERATURE SENSOR LOCATIONS ON COMMAND MODULE AND PREDICTED MAXIMUM TEMPERATURES.

~~CONFIDENTIAL~~

~~CONFIDENTIAL~~

NASA-S-68-356

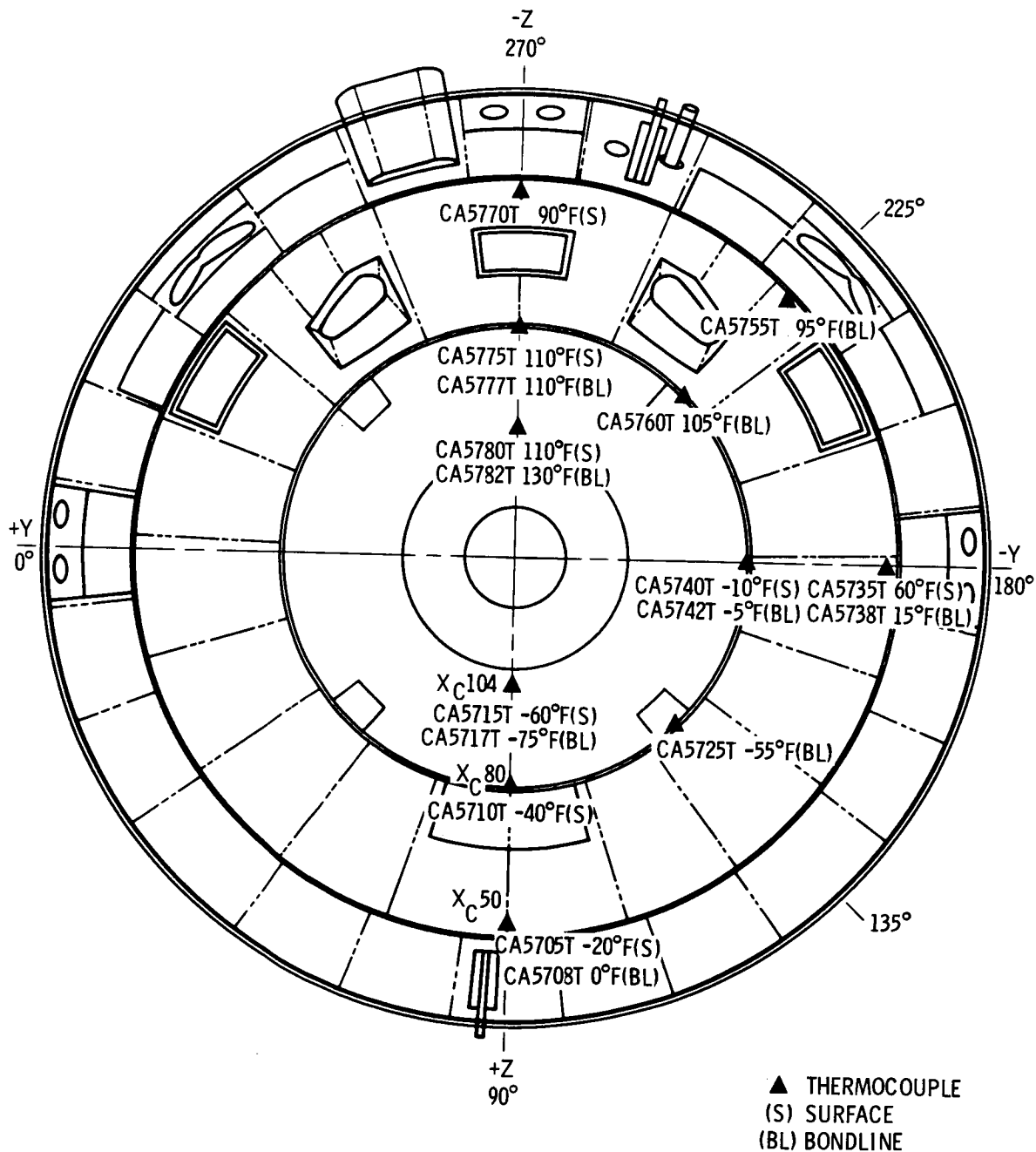


FIGURE 5.3-7. - FORWARD AND SIDE HEAT SHIELD MEASUREMENT LOCATIONS AND VALUES JUST PRIOR TO ENTRY.

~~CONFIDENTIAL~~

~~CONFIDENTIAL~~

5.3-13

NASA-S-68-357

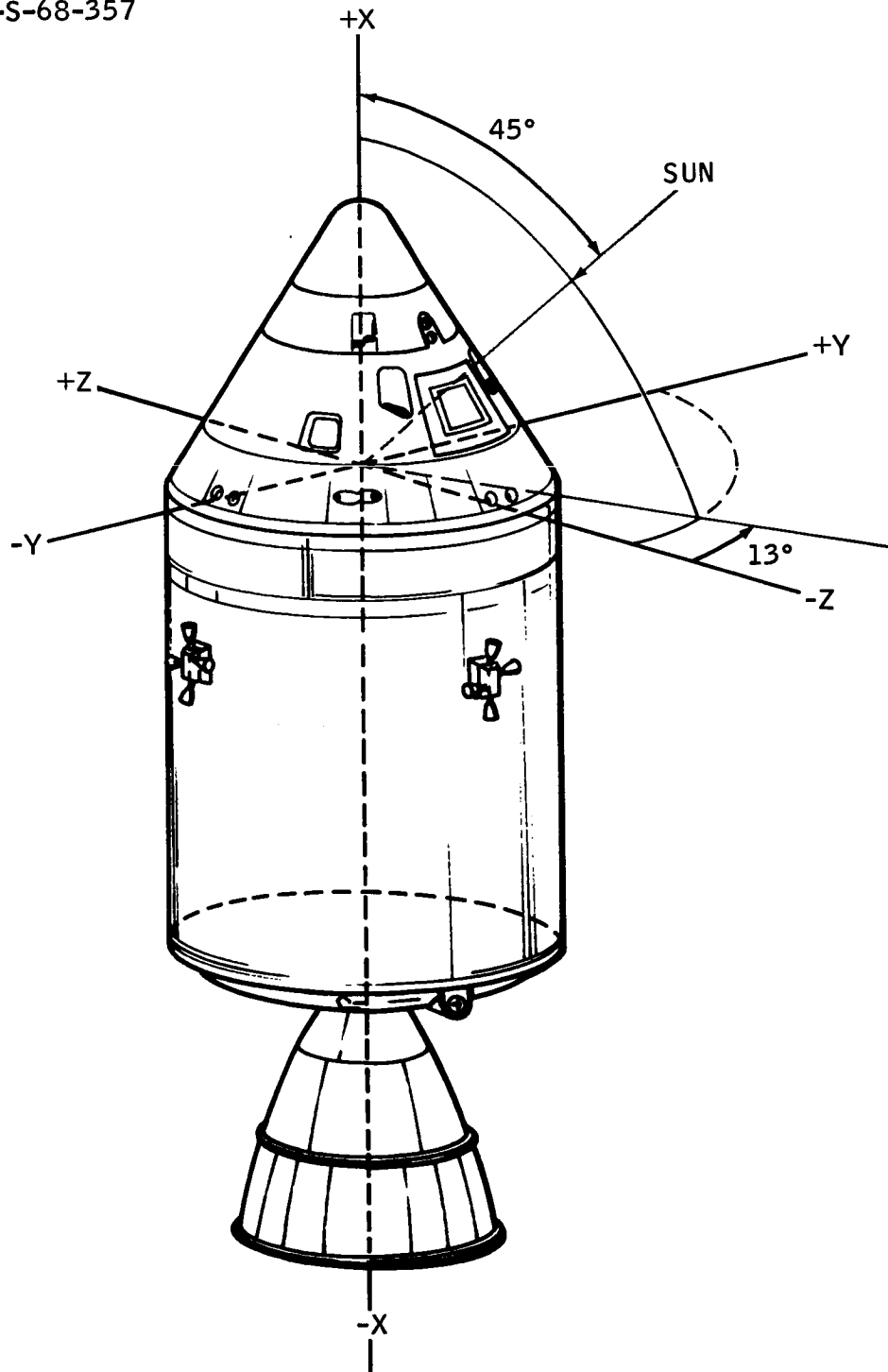


FIGURE 5.3-8.- SPACECRAFT ATTITUDE REFERENCED TO THE SUN  
DURING COLD-SOAK PERIOD.

~~CONFIDENTIAL~~

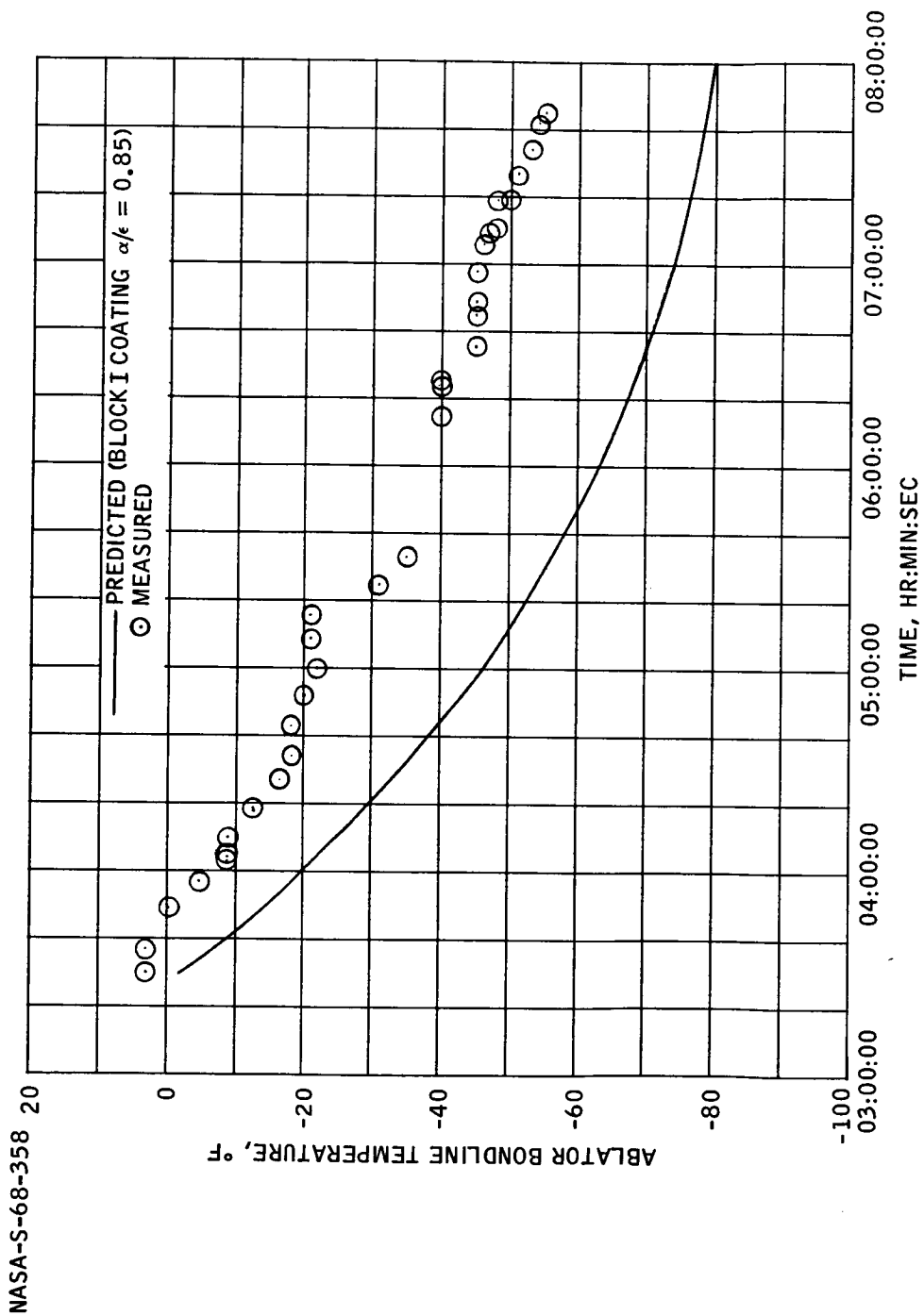
~~CONFIDENTIAL~~

FIGURE 5.3-9.- TEMPERATURE MEASURED BY COMMAND MODULE SENSOR CA1502T DURING COLD-SOAK PERIOD.

~~CONFIDENTIAL~~

~~CONFIDENTIAL~~

5.3-15

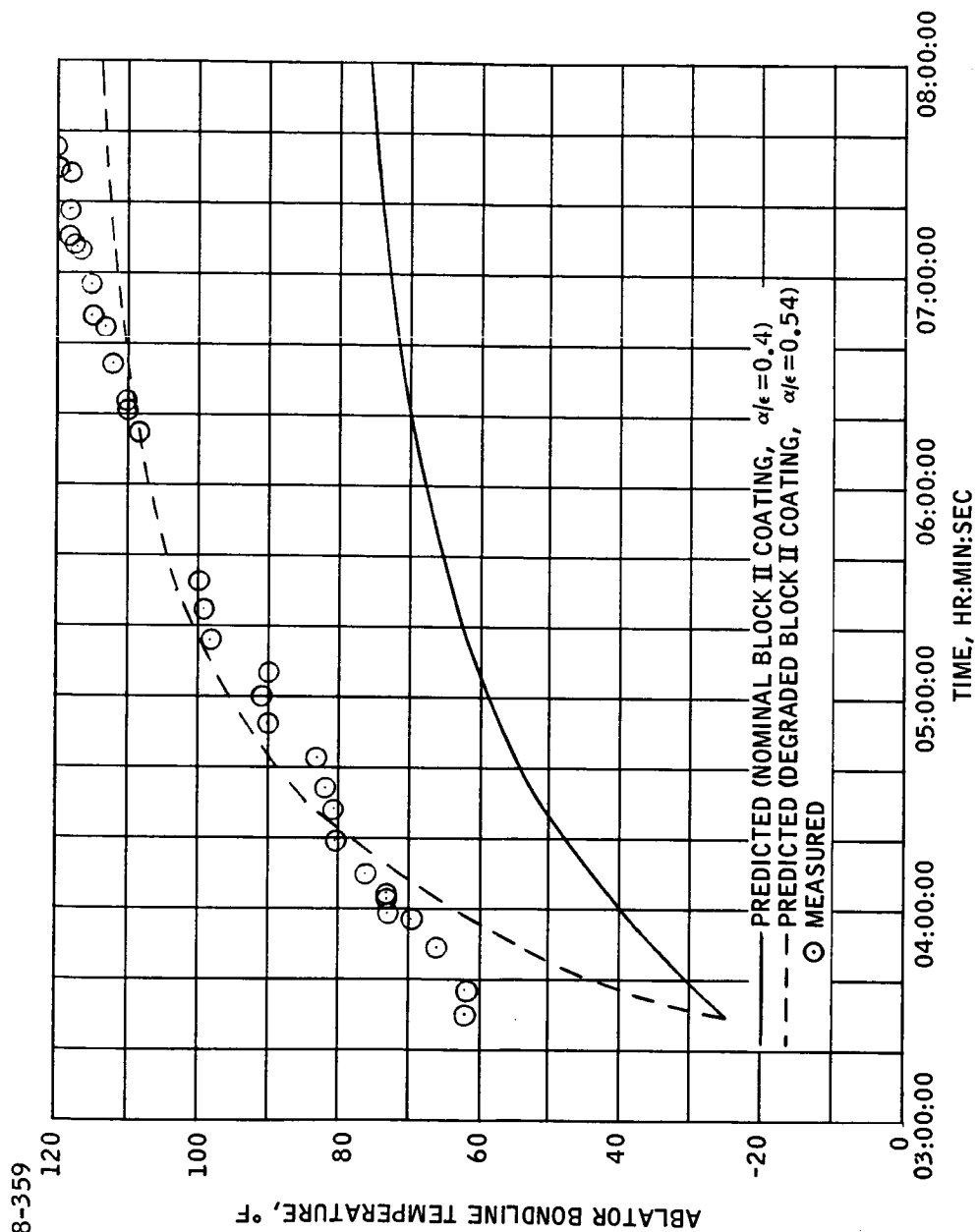


FIGURE 5.3-10.- TEMPERATURE MEASURED BY COMMAND MODULE SENSOR CA1509T DURING COLD-SOAK PERIOD.

~~CONFIDENTIAL~~

~~CONFIDENTIAL~~

THIS PAGE INTENTIONALLY LEFT BLANK

~~CONFIDENTIAL~~



~~CONFIDENTIAL~~

5.4-1

## 5.4 AEROTHERMODYNAMICS AND HEAT PROTECTION SUBSYSTEM

### 5.4.1 Aerothermodynamics

The evaluation of the Apollo heat shield performance during entry into the earth's atmosphere required measurements of the thermal environment of the spacecraft. These measurements consisted of local pressure and heating rates on the command module obtained with pressure transducers, surface-mounted calorimeters, and radiometers. The locations of these sensors are shown in figure 5.4-1 and given in table 5.4-I.

Comparison of the Apollo 4 flight pressure measurements with wind tunnel-based predictions showed good agreement at all aft heat shield stations. On the conical section where the measured values were less than 10 percent of full-scale sensor range, the predicted values exceed the flight measurements.

The aft heat shield radiometer measurement was less than 50 percent of the predictions during the first heating period and considerably in excess of the predictions during the second heating period. The discrepancies are not understood. However, investigations of both instrument and physical phenomena are continuing. The radiometers located on the conical section showed no response, as predicted.

The convective heating rates used for predicting the Apollo flight performance were found to be adequate when local mass injection from ablator pyrolysis was taken into account. Local mass injection significantly influenced calorimeter measurements on both the aft heat shield and the windward conical section.

Heating rates to the aft heat shield were calculated from the wafer calorimeter temperature measurements, which are usable for approximately 50 seconds of initial entry time. Calculated rates were in good agreement with predictions adjusted for local mass injection and including measured radiative heating rates for locations in the stagnation region. Other measurements in leeward areas of the aft heat shield showed heating rates of a transitional or turbulent nature.

Heating rates measured on the conical section were lower than non-blowing heat rate predictions. It was found that local blowing can account for the difference on the windward conical and toroidal sections. The predictions, however, appear to overestimate the lee-side heating. Both ground and flight test measurements in separated flow areas show significant uncorrelated scatter. The potential reduction of leeward conical section heating rates due to aft heat shield mass injection is being investigated.

~~CONFIDENTIAL~~

~~CONFIDENTIAL~~

The maximum calculated heating rate was  $430 \text{ Btu/ft}^2/\text{sec}$  and the maximum calculated heat load was  $38\,150 \text{ Btu/ft}^2$ . These values are related to a reference point on the aft heat shield (location  $S/R = 0.9875$ ,  $\theta = 90^\circ$ ). The expected values were  $422 \text{ Btu/ft}^2/\text{sec}$  and  $34\,750 \text{ Btu/ft}^2$ , based on the latest prediction method and the preflight trajectory. The expected values before the mission were  $594 \text{ Btu/ft}^2/\text{sec}$  and  $37\,777 \text{ Btu/ft}^2$ . The reason for the differences in the expected values is based on the use of updated radiative terms which are approximately 50 percent of those previously used.

Trajectory assessment.- Due to the importance of the knowledge of density in the calculations of radiative and convective heating rates, calculations of free stream density were made using the flight pressure measurements and the relative velocity corrected from the measured inertial velocity. The calculated density is compared with the density used for the trajectory reconstruction in figure 5.4-2. Excellent agreement exists most of the time, but differences of 20 or 30 percent can be seen during the second heating pulse. Good agreement between the flight pressure measurements with those obtained in wind tunnel tests were found for each heat shield sensor location, and the density history derived from the stagnation pressure measurement is used in the aerothermodynamic analysis presented herein.

Pressure measurements.- A total of 17 pressure transducers were installed around the command module (CM): seven of these were on the aft compartment and 10 on the conical section and toroid. All seven of the transducers on the aft heat shield, plus three transducers on the conical section and three on the toroid, gave usable data.

Histories of the measured pressures are compared with those calculated from wind-tunnel measurements in figure 5.4-3. Good agreement is seen on the aft compartment (fig. 5.4-3) throughout the significant entry time. The comparison for the conical and toroid sections (fig. 5.4-3) shows that predictions based on the wind-tunnel results exceed the flight data. However, the output from the transducers on the conical section indicated less than 10 percent of full scale, and the local pressure may be too low to be measured accurately.

Figure 5.4-4 shows the distribution of the pressure measurements on the aft compartment in the pitch plane compared with the 25-degree angle-of-attack wind tunnel distribution. The flight data have been normalized by the maximum pressure measurement at location 3. The bars on the figure indicate the range of pressure ratio at a given location during the period of time that the pressure measurements exceeded half of their maximum value.

~~CONFIDENTIAL~~

~~CONFIDENTIAL~~

5.4-3

Radiometer measurements.- The four radiometers mounted in the CM each consisted of a small hole in the ablator leading to a quartz window and subsequently to a thermopile element. The two radiometers mounted on the crew compartment showed no discernible response. This lack of response agrees with MSC calculations of negligible air and ablation products radiation to the conical section.

The aft heat shield radiometer data from location 7 exhibited a high level of noise through the entire flight. This sensor had required a waiver because of excessive noise prior to launch. The remaining radiometer located near the stagnation point (location 3) exhibited a good response. In figure 5.4-5, the data are compared to MSC postflight predictions and preliminary predictions obtained from the Ames Research Center. The total radiative heating prediction is also shown which includes the ultraviolet radiation that does not penetrate the quartz window of the radiometer. All theoretical radiation curves presented include self-absorption, non-adiabatic, and shock curvature effects. For comparison purposes, the MSC non-adiabatic factors have also been applied to the predictions from the Ames Research Center. At peak radiative heating, the calculated peak non-adiabatic radiative heating is 76 percent of the adiabatic value.

The calculated truncation of the non-equilibrium radiation results in the drastic change of the MSC predictions curve at a time of 30 000 seconds from launch (08:20:00). The level and trend of the data at this time indicate that truncation is completely obscured by collision limiting. Although indications of collision limiting may have been observed in ground tests, the phenomenon has not been quantitatively defined. Collision limiting has not been included in the MSC predictions.

Figure 5.4-6 shows the total radiation predictions for location 3 with a breakdown into the various emission components. The significance of the line radiation hampers the evaluation of collision limiting, non-adiabatic, and absorption effects. Measurements from this radiometer (location 3) only reached 5 percent of the instrument range. A large uncertainty in the data is created by the attenuation effect of 5 centimeters of relatively cold air and ablation products in the radiometer cavity. The data dropped to an unexplained minimum at a time of 08:21:10 and then rose to agree with the prediction. The air emission would not exhibit this behavior; however, attenuation by the cavity gas could account for it.

During the second peak heating period (fig. 5.4-5), the predictions are as low as one-fifth of the data. This large discrepancy must be attributed to an additional source of radiation. It is noted that if the ablator pyrolysis gases undergo combustion in the radiometer cavity, the restricted view of the radiometer could effectively magnify this emission

~~CONFIDENTIAL~~

~~CONFIDENTIAL~~

by two orders of magnitude. There are two other possibilities for the second peak data shown in figure 5.4-5. One is equilibrium ablation products radiation and the other is a boundary layer recombination reaction which produced radiation.

Although the discrepancies between the data and the predictions are not currently understood, ground tests of the sensor and additional analytical work is in progress to resolve the differences. The MSC predictions presented here are from a revision of previous operational radiative heating predictions (implemented in September 1964). The present total radiative predictions represent a reduction to roughly 50 percent of the previous operational radiative heating rates. Approximately 15 percent of this reduction is obtained by improved knowledge of the emission characteristics of air, 20 percent from non-adiabatic effects, and 15 percent from shock curvature effects.

Calorimeters.- Two types of calorimeters were installed around the CM to measure heating rates experienced during atmospheric entry. One type was a high range sensor which consisted of several graphite wafers stacked to allow removal of single wafers by aerodynamic forces when the surrounding heat shield material receded. The other type was an asymptotic calorimeter designed to accommodate the lower range of heating rates expected on the conical and toroidal sections.

Eleven wafer calorimeters were located on the aft compartment and eight of these provided usable measurements for approximately 40 to 50 seconds of initial entry time. Tungsten-rhenium thermocouples embedded in each graphite wafer measured temperatures from which heating rates can be calculated when material properties and conduction losses are known. In an effort to determine the amount of heat conducted to subsequent wafers, simultaneous wafer temperatures were measured for three calorimeters; these included the top four wafers of the calorimeter at location 3 and the top three wafers at locations 7 and 10. Only the top wafer temperature was measured for the other calorimeters. Figure 5.4-7 shows the measured wafer temperatures from initial entry time through the first heat pulse when the data became questionable.

The wafer calorimeter data have been reduced from the temperature histories of the first wafer using:

$$q_{\text{measured}} = C_p \delta \gamma \frac{dT}{dt} + \sigma \epsilon T^4 + q_{\text{losses}}$$

Here the terms on the right side of the equation account for the rate of energy storage in the wafer, the reradiation from the outer surface of

~~CONFIDENTIAL~~

~~CONFIDENTIAL~~

5.4-5

the wafer and the internal radiative and conductive heat losses, respectively. The loss term in the flight data analysis was obtained from a correlation of losses obtained from ground tests.

The heating rates determined from the wafer temperature measurements are shown in figure 5.4-8 along with the cold-wall prediction, which includes the sum of the non-blowing convective heating rate and the predicted radiative heating rates. The predicted heating rates have been adjusted for local blowing and for the predicted radiation and the radiation determined from the radiometer measurement.

These figures show the importance of accounting for the reduction in local heating rates due to local mass injection. The sensors in the vicinity of the stagnation region (locations 1, 2, 3, 5, 6) all show reasonable agreement with the predictions accounting for local mass injection. The surprising agreement of these measurements with the predictions employing the radiometer measurement lends credence to the radiation measurement as well as to laminar convective heating rate prediction methods. The measurements at locations 7 and 10 increase more rapidly than the laminar heat rate predictions suggest. It is believed that transitional or turbulent heating will account for this behavior.

Heating rates on the conical section were measured directly with asymptotic calorimeters having ranges from 50 to 150 Btu/ft<sup>2</sup>/sec, as shown in table 5.4-I. An estimate of their accuracy is  $\pm 2$  percent of full scale. The measured rates are compared with predicted heating rates in figure 5.4-9. The cold wall convective predictions were based on non-dimensional wind tunnel measurements and a stagnation-point heating rate theory. For locations 12 through 20 where the ablator was observed to be charred, the cold wall rates have been corrected for local mass injection. The comparison of the measurements with the adjusted predictions in figure 5.4-9 shows that blowing can account for the low measured rates at these locations. However, the analytical method employed to obtain the blowing corrections is subject to further refinement.

The lee conical portion of the command module did not char during entry and local blowing was not considered in the analysis. At most of the lee side locations 21 through 28, the cold wall predictions exceed the measurements and are considered adequate to describe the heating to this region of the Apollo spacecraft. The potential reduction of leeward conical section heat rates due to upstream (aft heat shield) mass injection is being investigated.

Heating rates measured in the simulated Block II umbilical and the unified hatch gap are also shown in figure 5.4-9. The predictions compared with the umbilical cavity measurement, and the two hatch gap locations were based on half the values predicted for a smooth configuration

~~CONFIDENTIAL~~

~~CONFIDENTIAL~~

and are conservative by an order of magnitude. The umbilical frame predictions were based on a smooth body without consideration of interference effects. The predictions are high for the first heat pulse but low for the second pulse. Again, blowing can account for the low measured values.

#### 5.4.2 Heat Protection Subsystem

The Block II thermal protection subsystem is qualified for lunar return at velocities similar to those experienced by Spacecraft 017. Further analysis of data obtained from Spacecraft 017, together with data expected from Spacecraft 101 during a future mission, should result in complete certification of the Block II thermal protection subsystem for manned lunar return.

Postflight ablator predictions using the actual trajectory and revised heating data are not available to be included in the report at this time. It is intended that a supplemental report showing detailed analysis of the Spacecraft 017 thermal protection subsystem will be published at a later date.

The thermal protection subsystem consisted of the Block II heat shield design with the following exceptions.

- a. The apex was rounded on Spacecraft 017 whereas on Block II spacecraft it will be flat. Qualification of the flat apex will be accomplished on Spacecraft 101 for orbital entry velocity and by analysis for lunar entry.
- b. A fail-safe simulated Block II thermal gap and seal was mounted in place of the hatch window to thermally qualify the unified crew hatch that will be flown on Block II spacecraft.
- c. Two of the six extravehicular activity handrail configurations were flown on the leeward conic for Block II qualification.
- d. Spacecraft 017 was a Block I spacecraft with its umbilical located on the leeward side, and it was necessary to add a ramp in front of the umbilical to alleviate the high aerodynamic shears and heating rates that the umbilical would impose on the spacecraft at lunar return velocities. The umbilical is located on the windward conic on Block II, and a simulated umbilical cavity was flown on Spacecraft 017.

The ablative heat shield and singular components were extensively instrumented. Figure 5.4-10 shows the locations of thermocouples and char sensors on the aft heat shield, and figure 5.4-11 shows the locations of thermocouples and char sensors on the conical heat shield and

~~CONFIDENTIAL~~

~~CONFIDENTIAL~~

5.4-7

astro-sextant area. Thermocouple locations in and around major components are shown in figure 5.4-12. Minimum and maximum temperatures at these locations are presented in table 5.4-II.

Postflight inspection of the recovered Apollo 4 spacecraft indicated that the Block II thermal protection subsystem survived the lunar entry environment satisfactorily. Sufficient flight data were obtained to permit a thorough evaluation of the thermal performance of the Block II thermal protection subsystem. Temperature data were within design limits for the flight.

Aft heat shield.- The aft ablative heat shield was heavily charred over its entire surface (fig. 5.4-13). Temperature data indicated that surface temperatures approached 5000° F, which formed a strong carbonaceous char. There were no visible streamlines emanating from the stagnation area. There were no areas of excessive erosion and no erosion along splice gaps. The surface erosion in the stagnation area and other points on the aft heat shield was less than expected.

Examination of cores taken from the aft heat shield indicated a very strong surface char and less-than-expected char penetration. Table 5.4-III shows the levels of char penetration measured on the aft shield with preflight predictions. The maximum char penetration was 0.88 inch, in close proximity to the previously mentioned reference point used for heating rates and heat loads. The maximum expected char penetration was approximately 1.25 inches. This expected value is not based on the updated prediction method. The temperatures measured in depth in the aft shield are shown in figure 5.4-14. By cross-plotting the 1050° F isotherm as a function of time, reasonable correlation with char sensor data is obtained (fig. 5.4-15).

Maximum temperature measured in depth for two locations on the pitch plane are shown in figure 5.4-16. The depth of the 1050° F isotherm, obtained by interpolating these data, agrees well with the char interface obtained from heat shield cores.

Thermocouples located on the outer mold line at the bolt circle showed no temperature increase at  $\theta=228$  degrees, a 5-degree increase at  $\theta=290$  degrees, and an 80-degree increase at  $\theta=134$  degrees. A 10-degree temperature response was measured at the center of the aluminum aft bulkhead.

Shear-compression and compression pads.- All of the shear compression and compression pads remained recessed, except the ablator downstream of the pads, which eroded to form a 35-degree to 45-degree slope (fig. 5.4-17). Recession in this area varied from 0.12 inch to 0.50 inch. No detectable temperature response was obtained from any of the seven bondline thermocouples located near the pads.

~~CONFIDENTIAL~~

~~CONFIDENTIAL~~

Tension-tie bolts.- The tension-tie bolts located in the shear-compression pads ablated flush or to within 0.25 inch of the pad surface. A maximum temperature rise of 16° F was measured on the base of tension tie 1, near the area of maximum heating.

Umbilical ramp.- The umbilical ramp performed well, protecting the Block I umbilical and the area upstream of the umbilical from erosion (fig. 5.4-18).

Aft heat shield toroid.- The aft heat shield toroidal section was located at the interface between the aft heat shield and the conical heat shield. The maximum heat shield diameter was located in this area. Thermocouples were located in depth in the toroidal section at  $\theta=180$  degrees (-Y),  $\theta=225$  degrees, and  $\theta=270$  degrees (-Z). The temperature responses are shown in figure 5.4-19.

Conical heat shield.- The conical section consisting of the crew compartment and forward compartment heat shields showed little or no evidence of ablation (fig. 5.4-20) and, on the leeward side (-Z), showed little evidence of aerodynamic heating.

The +Z side was charred but paint residue was still visible. The silicone rubber seal at the interface of the crew compartment and aft compartment heat shield was slightly recessed. Thermocouples located 0.05 inch from the surface were not exposed, indicating virtually no surface loss. Char thickness in this area was less than 0.1 inch, based on the 1050° F isotherm penetration.

On the +Y and -Y sides of the crew compartment, the char line started at the bottom of the crew compartment and slanted approximately 45 degrees from the -Y axis and 20 degrees from the +Y axis toward the +Z axis to approximately the center of the crew compartment and then slanted back toward the corresponding axes at the top of the crew compartment. With the exception of the areas around the reaction control nozzles, there was no char on the leeward side of the crew compartment heat shield. Large areas were still covered with the Block II thermal control coating giving a yellow appearance on the upper part of the crew compartment and an aluminized appearance on the lower part. In areas where the coating was missing, the heat shield was white.

The forward compartment was recovered intact and showed very little effect of the entry heating. There was slight char on the +Z side between 45 and 135 degrees. The remainder of the forward compartment had the same appearance as the leeward side of the crew compartment.

The temperatures measured in depth in the ablator on the crew compartment and forward compartment heat shields are shown in figure 5.4-21.

~~CONFIDENTIAL~~



~~CONFIDENTIAL~~

5.4-9

The use of a measured temperature history as the input boundary condition to the ablator program provides for a verification of the thermal properties used in the analysis. This analysis technique decouples the environment and material surface phenomena from the in-depth ablator response. As shown in figure 5.4-22, for a typical location on the conical section, the temperature history of thermocouple CA5735T located at a depth of 0.05 inch below the ablator surface was used as an input boundary condition. The agreement of the in-depth temperatures confirms the material thermal properties used in the analytical model to predict ablator performance.

Bondline temperatures measured on the aft and conical sections of the heat shield are summarized in table 5.4-IV. Included in the table are preflight predictions for selected thermocouple locations. The maximum bondline temperature measured on the aft heat shield was 150° F. For this location, the maximum expected temperature was 438° F. This expected value is not based on the updated prediction method.

Block I umbilical.— Postflight inspection of the Block I umbilical revealed some wires extending a maximum of 0.85 inch from the umbilical face. Hardlines receded from 0.25 to 0.50 inch. Recession on the aft outboard edge of the housing varied from 0.85 to 1.25 inch (fig. 5.4-18).

Block II simulated umbilical cavity.— On the Block II simulated umbilical cavity (fig. 5.4-23), the downstream (forward slot) wire and hardline bundle were slightly degraded with no apparent melting of the wires. Temperatures measured at a depth of 1.5 inches in the forward slot varied from 108° F at the center to 150° F on the hardline. Hardline temperature data were not indicative of in-depth heating because the hardline was partially plugged with potting compound. A slight discoloration of the upstream bundle and downstream edge of the umbilical cavity was noted. An area of light color on the ablator immediately downstream of the umbilical was believed to be absorbed paint which was applied on the unsealed ablator surface.

Astro-sextant.— Nine thermocouples plus temperature-sensitive paint were utilized in and around the astro-sextant to determine the effects of heating in this area. The performance of the astro-sextant configuration met thermal qualification standards for use on Block II spacecraft. The greatest thermocouple response was measured on the heat shield outer mold line where the temperature rose to 94° F from an initial cold soak temperature of minus 48° F at the beginning of entry.

The outer heat shield ablator downstream of the astro-sextant showed signs of significant heating (fig. 5.4-24). When viewed from the outside, visible portions of the primary seal appeared red upstream and blackened downstream. The RTV coating on the optical cones swelled about 0.06 inch.

~~CONFIDENTIAL~~

~~CONFIDENTIAL~~

With the exception of the area downstream of the astro-sextant, no other significant temperatures were recorded.

Unified side hatch test panel.- Postflight examination of this component revealed that the simulated seal was essentially in preflight condition. The ablator in the remaining half of the gap was slightly degraded (fig. 5.4-25).

Air and steam vents.- There was no apparent degradation of either fiberglass duct (fig. 5.4-26). A maximum temperature rise of 27° F was measured on the leading edge of the air vent heat exchanger and a temperature rise of 17° F was measured on the fiberglass mount of the steam vent.

C-band and S-band antennas.- Postflight inspection determined that minimal differential recession occurred at the interfaces between the quartz antenna cylinders and the surrounding ablator. The maximum measured recession was 0.06 inch. Thermocouples located near antenna heat sinks measured temperature increases that varied from 9 degrees at  $\theta=270$  degrees location to 53 degrees at  $\theta=76$  degrees location. The greatest temperature rise of 138 degrees was measured at the ablator-quartz interface of the S-band antenna.

Extravehicular activity handrails.- Both EVA handrails remain intact with little evidence of heating. At least 90 percent of the H-film tape wrap remained. There was no evidence of flow perturbation. White heat shield paint was visible from  $\theta=260$  degrees near the handrail base to 1.25 inches below the  $X_c = 23$  compartment gap (fig. 5.4-26).

Sea anchor attachment ring.- There was little or no recession of the Teflon that covered the ring and no inflight degradation of the ablator ramp. There was a slight discoloration of the Teflon and also upstream on the ramp with approximately 50 percent of Block II thermal control coating remaining on the panel.

Urine dump assembly.- Slight discoloration was present on the hemispherical heat sink and was most noticeable on the side facing the roll engine reaction control subsystem engine nozzles. The small external orifice was undistorted and the surrounding gold coating was intact. A narrow gap remained between the heat sink and the ablator.

Launch escape system tower leg wells.- The leg bolt and the umbilical receptacle for the launch escape system were only slightly discolored. No appreciable temperature rise was measured.

Stringers and attachment rings.- Thermocouples located on stringers and attachment rings measured temperature rises ranging from 10 degrees to 35 degrees.

~~CONFIDENTIAL~~

~~CONFIDENTIAL~~

5.4-11

Windows.- The exterior surfaces of the micrometeoroid pane showed considerable discoloration. The seals between the heat shield panes and the ablator appeared to be in preflight condition.

Forward compartment and equipment.- Thermocouple responses at the command module forward deck and equipment areas indicated very little heating. Temp-plate indicators located on the upper deck showed temperatures of 120° F to 140° F around the spacecraft, and temp-plate indicators on the top of the tunnel also showed temperatures varying from 100° F to 140° F around the spacecraft. Thermocouples located in the main parachute risers cooled after forward heat shield jettison.

~~CONFIDENTIAL~~

~~CONFIDENTIAL~~

TABLE 5.4-I.- LOCATIONS AND RANGES OF PRESSURE SENSORS, CALORIMETERS, AND RADIOMETERS

Aft compartment									
Location no.	Pressure sensor			Wafer calorimeter			Radiometer		
	Y <sub>c</sub> , in.	Z <sub>c</sub> , in.	Range, psia	Y <sub>c</sub> , in.	Z <sub>c</sub> , in.	Range, °F	Y <sub>c</sub> , in.	Z <sub>c</sub> , in.	Range, Btu/ft <sup>2</sup> /sec
1	-2.0	-2.0	10	-0.5	0.5	5000			
2	2.7	39.1	10	0	39.0	5000			
3	1.5	55.0	10	4.2	55.2	5000	-0.5	55.0	1200
4	1.8	65.0	10	0	65.0	<sup>a</sup> 5000			
5	1.5	71.8	10	4.0	71.7	5000			
6	-1.2	75.0	5	1.3	75.0	5000			
7	-10.6	-48.9	5	-4.7	-50.0	5000	1.0	-48.8	<sup>a</sup> 1200
8				12.7	-49.5	5000			
9				13.2	-65.2	5000			
10				50.0	-1.5	5000			
11				-59.6	31.9	5000			

<sup>a</sup>Invalid.~~CONFIDENTIAL~~

~~CONFIDENTIAL~~

5.4-13

TABLE 5.4-I .- LOCATIONS AND RANGES OF PRESSURE SENSORS, CALORIMETERS, AND RADIOMETERS - Continued

Conical section									
Location no.	Pressure sensor			Calorimeter			Radiometer		
	X <sub>c</sub> , in.	θ, deg	Range, psia	X <sub>c</sub> , in.	θ, deg	Range, Btu/ft <sup>2</sup> /sec	X <sub>c</sub> , in.	θ, deg	Range, Btu/ft <sup>2</sup> /sec
12	26.5	91.6	2	26.5	93.7	150	52.3	88.5	50
13	50.0	88.5	2	50.0	85.3	100			
14	83.4	86.9	2	83.4	82.6	100			
15	104.0	94.8	2	104.0	101.5	<sup>a</sup> <sub>75</sub>			
16	26.3	135.8	2	26.3	137.9	100			
17				78.9	137.0	75			
18	18.2	176.6	2	18.2	179.4	75			
19	18.5	229.5	2	18.5	225.1	75			
20	18.5	272.3	2	18.5	264.0	75			
21				52.5	179.0	50			
22	78.9	185.0	<sup>b</sup> <sub>2</sub>	78.9	189.0	50	104.0	228.8	50
23					191.5	50			
24				50.0	228.8	50			
25				78.9	226.2	50			

<sup>a</sup>Invalid.<sup>b</sup>Covered with tape.~~CONFIDENTIAL~~

~~CONFIDENTIAL~~

TABLE 5.4-I.- LOCATIONS AND RANGES OF PRESSURE SENSORS, CALORIMETERS, AND RADIOMETERS - Concluded

Conical section								
Location no.	Pressure sensor			Calorimeter			Radiometer	
	X <sub>c</sub> , in.	θ, deg	Range, psia	X <sub>c</sub> , in.	θ, deg	Range, Btu/ft <sup>2</sup> /sec	X <sub>c</sub> , in.	θ, deg Range, Btu/ft <sup>2</sup> /sec
26				50.0	272.0	50	45.0	270.1 50
27	78.9	263.9	2	78.9	267.8	50		
28				104.0	274.8	50		
Hatch gap				60.0	268.0			
Hatch gap				65.0	270.0			
Umbilical cavity				35.0	90	150		
Umbilical frame				43.0	90	150		

~~CONFIDENTIAL~~

~~CONFIDENTIAL~~

5.4-15

TABLE 5.4-II.- TABLE OF HEAT SHIELD COMPONENT AND EQUIPMENT THERMAL RESPONSE

Component	Measurement no.	Location/Description	Measured temperature, °F	
			Minimum	Maximum
Aft heat shield and bulkhead	CA7608T	$R_c = 58$ , $\theta_c = 290$ ; outer mold line (OML) near bolt no. 48 and pad 5	70	75
	CA7609T	$R_c = 58$ , $\theta_c = 228$ ; OML near bolt no. 38 and pad 4	80	80
	CA7610T	$R_c = 58$ , $\theta_c = 184$ ; OML near bolt no. 31	80	160
	CA7800T	Center of aluminum aft bulkhead	47	57
Shear/compression and compression pads	CA1477T	$Y_c = 16$ , $Z_c = -65$ ; bondline near pad 5	70	70
	CA1478T	$Y_c = -60$ , $Z_c = 29$ ; bondline near pad 3	70	70
	CA1479T	$Y_c = 12$ , $Z_c = -50$ ; bondline near pad 5	70	70
	CA1480T	$Y_c = -59$ , $Z_c = 31$ ; bondline near pad 3	70	70
	CA1481T	$Y_c = 11$ , $Z_c = -50$ ; bondline near pad 5	70	70
	CA5090T	$Y_c = -2$ , $Z_c = 55$ ; bondline vicinity pad 2	80	80
	CA5114T	$Y_c = 2$ , $Z_c = -50$ ; bondline vicinity pad 5	75	75
Tension ties	CA1461T	Aft heat shield OML near tension tie no. 1	60	70
	CA1464T	Longeron, tension tie no. 1	70	75
	CA1465T	Tension tie no. 1 barrel nut	67	83
	CA7801T	Aluminum aft bulkhead near longeron no. 1	74	75
Block II simulated CSM umbilical	CA1441T	On forward slot, depth $\approx 1.5$ in.	0	150
	CA1442T		27	44
	CA1443T		36	42
	CA1445T	Center forward slot, depth $\approx 1.5$ in.	24	108
	CA1446T	Side forward slot, depth $\approx 1.5$ in.	19	119
	CA1447T	Inside bundle	28	57
	CA1448T	Inside bundle	25	57
	CA1449T	Near inboard end of bundle	37	44
	CA1450T	Near inboard end of bundle	38	45
	CA1451T	In fully simulated side heat sink	45	50
	CA1452T	In partially simulated side sink	45	40
	CA1453T	Aft compartment, housing exterior	50	50
	CA1454T	Aft compartment, bundle exterior	55	55
	CA1455T	IML at fully simulated heat sink	55	55

~~CONFIDENTIAL~~

~~CONFIDENTIAL~~

TABLE 5.4-II.- TABLE OF HEAT SHIELD COMPONENT AND EQUIPMENT THERMAL RESPONSE - Continued

Component	Measurement no.	Location/Description	Measured temperature, °F	
			Minimum	Maximum
Astro-sextant	CA1502T	$X_c = 65$ , $\theta_c = 71.5$ ; Heat shield OML near panel	-48	94
	CA5811T	$\theta_c \approx 87$ ; Heat shield (IFOS) downstream	-20	70
	CA5812T	$\theta_c \approx 98$ ; Heat shield downstream of astro-sextant on Z-member	-1	38
	CA5813T	Aluminum honeycomb (IFIS) downstream of astro-sextant	43	48
	CA5814T	Aluminum optical case mount downstream of astro-sextant	43	43
	CA5815T	$\theta_c \approx 72$ ; aluminum honeycomb (IFIS)	43	48
	CA5816T	$\theta_c \approx 108$ ; aluminum honeycomb (IFIS)	43	48
	CA5817T	Aluminum optical case mount on beam	43	48
	CA5818T	Aluminum optical case mount downstream of astro-sextant	23	33
Unified side hatch test panel	CA5548T	$X_c = 60$ , $\theta_c = 275$ ; gap with no seal, $d = 0.05$ in.	31	144
Air and steam vents	CA7603T	Leading edge air vent heat exchanger	74	101
	CA7875T	Aluminum steam vent tube inboard of fiberglass	80	85
	CA7876T	Near OML in fiberglass mount, steam vent	106	123
	CA7877T	Steam vent inner surface near fiberglass elbow	85	79
C-band antennas	CA7446T	$\theta_c = 270$ , near heat sink	94	103
	CA7447T	$\theta_c = 76$ , $X_c = 59$ ; near heat sink	-33	20
S-band antennas	CA8520T	$\theta_c = 135$ ; ablator/quartz interface	-9	129
	CA8521T	$\theta_c = 225$ ; 0.7 in. from quartz surface	77	184
	CA8522T	$\theta_c = 135$ ; near heat sink	2	41
	CA8523T	$\theta_c = 225$ ; near heat sink	80	100
LES tower leg wells	CA0210T	$X_c = 87$ , $\theta_c = 135$ ; well wall	-29	-8
	CA0211T	$X_c = 87$ , $\theta_c = 225$ ; well backwall	97	104
	CA0212T	$\theta_c = 135$ ; leg stud nut in longeron	32	39

IFOS - Inner Face Sheet Outer Surface

IFIS - Inner Face Sheet Inner Surface

~~CONFIDENTIAL~~



~~CONFIDENTIAL~~

5.4-17

TABLE 5.4-II.- TABLE OF HEAT SHIELD COMPONENT AND EQUIPMENT THERMAL RESPONSE - Concluded

Component	Measurement no.	Location/Description	Measured temperature, °F	
			Minimum	Maximum
Stringers and attach ring	CA1509T	$X_c = 65$ , $\theta_c = 321$ ; OML near stringer no. 13	121	156
	CA3600T	$X_c = 42$ , $\theta_c = 90$ ; on attach ring	40	50
	CA3601T	$X_c = 42$ , $\theta_c = 270$ ; on attach ring	80	100
	CA3640T	$X_c = 50$ , $\theta_c = 90$ ; on stringer no. 5	20	40
	CA3641T	$X_c = 50$ , $\theta_c = 182$ ; on stringer no. 10	50	70
	CA3642T	$X_c = 50$ , $\theta_c = 247$ ; on hatch stringer no. 120	100	125
Windows	CA7820T	Left side window at OML	85	123
	CA7821T	Left side heat shield window frame	93	108
	CA7822T	Left side pressure vessel frame	72	77
Forward compartment and equipment	CA7674T	Forward cylinder ring, forward of main parachute pack	51	60
	CA7675T	Forward bulkhead aft of main parachute pack	46	63
	CA7760T	Pilot parachute mortar can	50	50
	CA7761T	Main parachute riser	69	68
	CA7762T	Main parachute pack	-	-

~~CONFIDENTIAL~~

~~CONFIDENTIAL~~

TABLE 5.4-III.- AFT HEAT SHIELD ABLATOR DATA

			Obtained from heat shield cores				
Location		Original ablator thickness, in.	Final ablator thickness, in.	Char thickness, in.	Surface loss, in.	Char penetration, in.	Preflight predicted char penetration, in.
$R_c$ , in.	$\theta$ , deg						
50	1	1.68	1.60	0.54	0.08	0.62	
40	45	1.99	1.94	0.60	0.05	0.65	
62.5	75	2.02	1.93	0.61	0.09	0.70	
70.5	83.5	2.02	1.84	0.70	0.18	0.88	
42	90	2.06	1.98	0.58	0.08	0.66	
20.5	134	1.93	1.88	0.59	0.05	0.64	1.05
40.5	135	1.96	1.87	0.57	0.09	0.66	1.08
63.3	135	1.89	1.84	0.56	0.05	0.61	1.19
70.5	135	1.80	1.70	0.59	0.10	0.69	1.27
50	180	1.67	1.62	0.54	0.05	0.66	1.14
3	225	1.80	1.74	0.60	0.06	0.66	1.11
28.1	225	1.64	1.60	0.54	0.04	0.58	1.12
33.1	225	1.59	1.56	0.52	0.03	0.55	1.12
36.4	225	1.58	1.58	0.53	0	0.53	1.10
63.5	248	1.42	1.42	0.44	0	0.44	
70.5	248	1.43	1.42	0.45	0	0.45	0.83
50.8	261	1.66	1.58	0.44	0.08	0.52	1.03
60.7	309	1.45	1.40	0.48	0.05	0.53	
70.5	309	1.45	1.42	0.54	0.03	0.57	

~~CONFIDENTIAL~~

~~CONFIDENTIAL~~

5.4-19

TABLE 5.4-IV.- HEAT SHIELD BONDLINE TEMPERATURES

Body location	Measured			Preflight predicted		
	Initial bondline temperature, °F	Maximum bondline temperature, °F	ΔT, °F	Initial bondline temperature, °F	Maximum bondline temperature, °F	ΔT, °F
Aft heat shield						
Z = 0, Y = 0	35	90	55	100	319	219
Z = 39, Y = 0	70	95	25			
Z = 55, Y = 0	75	80	5	100	107	7
Z = 65, Y = 0	65	75	10			
Z = 72, Y = 0	55	110	55	100	336	236
Z = 75, Y = 0	35	115	80	100	312	212
Z = -50, Y = 0	70	75	5	100	239	139
Z = 0, Y = 50	70	150	80	100	468	368
Z = -65, Y = 14	70	70	0			
Z = -49, Y = 12	70	75	5	100	239	139
Z = 29, Y = -60	70	70	0			
Z = 30, Y = -59	70	70	0			
Conical heat shield (windward)						
X <sub>c</sub> = 26, θ <sub>c</sub> = 90°	-25	35	60	150	219	69
X <sub>c</sub> = 50, θ <sub>c</sub> = 90°	0	75	75			
X <sub>c</sub> = 104, θ <sub>c</sub> = 90°	-75	100	175			
X <sub>c</sub> = 26, θ <sub>c</sub> = 135°	-45	65	110			
X <sub>c</sub> = 80, θ <sub>c</sub> = 135°	-55	135	190			
X <sub>c</sub> = 18.5, θ <sub>c</sub> = 180°	35	145	110			
X <sub>c</sub> = 18.5, θ <sub>c</sub> = 225°	75	85	10			
X <sub>c</sub> = 18.5 θ <sub>c</sub> = 270°	105	140	35			
Conical heat shield (leeward)						
X <sub>c</sub> = 50, θ <sub>c</sub> = 180°	15	135	120	150	338	188
X <sub>c</sub> = 80, θ <sub>c</sub> = 180°	-5	130	135			
X <sub>c</sub> = 104, θ <sub>c</sub> = 180°	35	--	--			
X <sub>c</sub> = 50, θ <sub>c</sub> = 225°	95	140	45			
X <sub>c</sub> = 80, θ <sub>c</sub> = 225°	105	145	40			
X <sub>c</sub> = 80, θ <sub>c</sub> = 270°	110	150	40	150	331	181
X <sub>c</sub> = 104, θ <sub>c</sub> = 270°	130	195	65			

~~CONFIDENTIAL~~

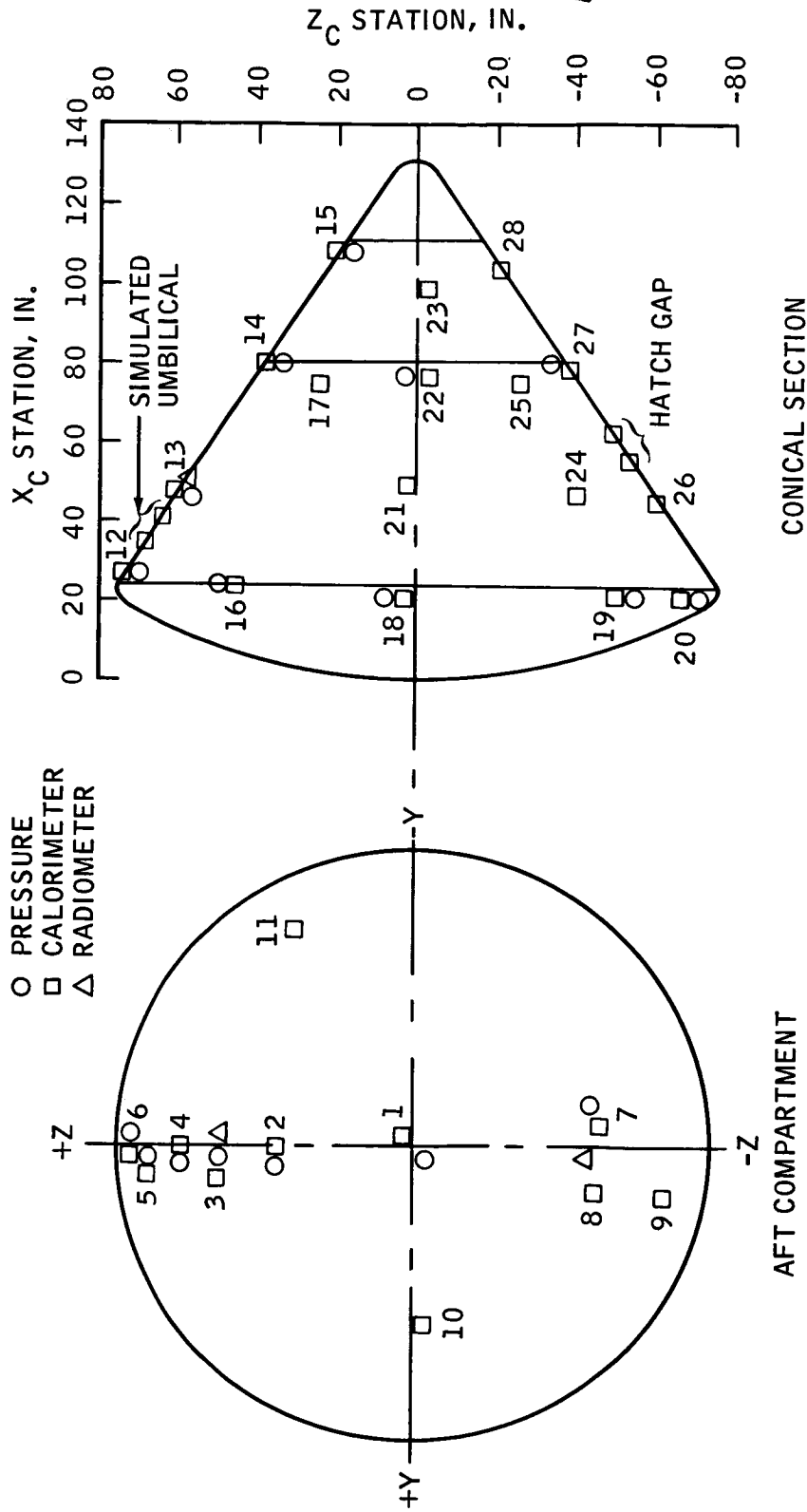
~~CONFIDENTIAL~~

FIGURE 5.4-1.- SKETCH OF APOLLO COMMAND MODULE SHOWING LOCATIONS OF AEROTHERMODYNAMIC SENSORS.

~~CONFIDENTIAL~~

~~CONFIDENTIAL~~

5.4-21

NASA-S-68-361  
10<sup>-2</sup>

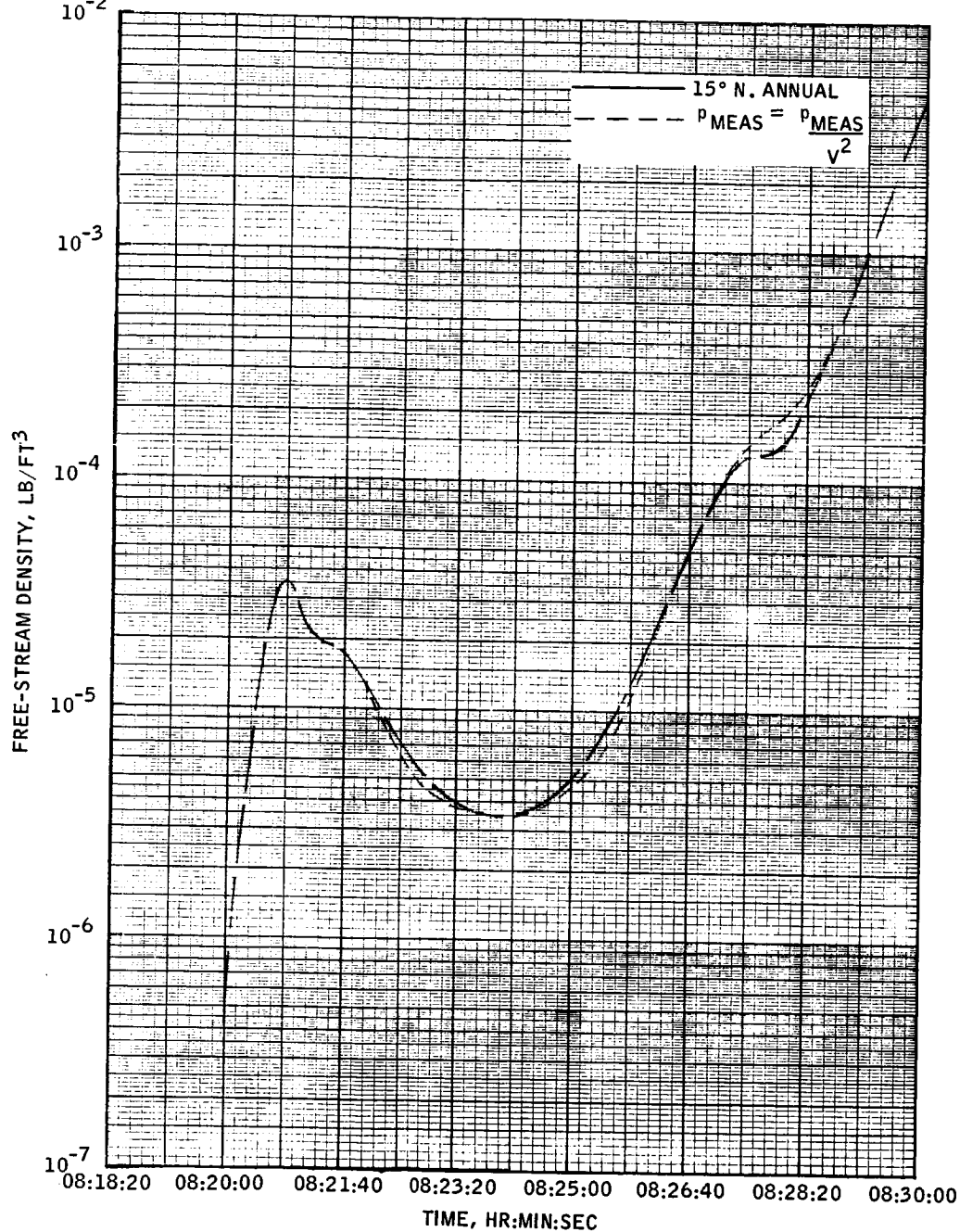
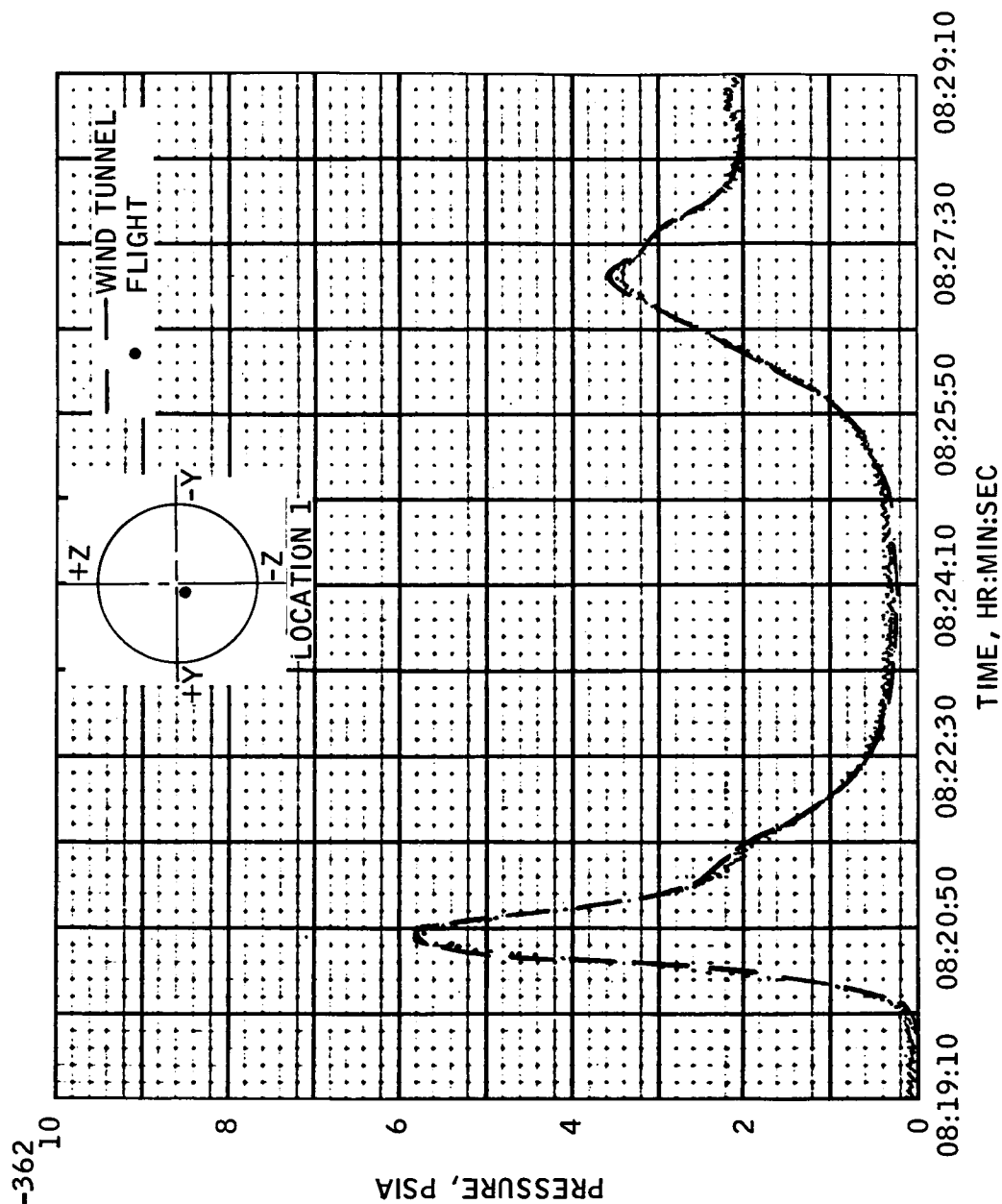


FIGURE 5.4-2.- FREE-STREAM DENSITY.

~~CONFIDENTIAL~~

~~CONFIDENTIAL~~

(A) LOCATION 1.

FIGURE 5.4-3.- PRESSURES MEASURED ON AFT HEAT SHIELD.

~~CONFIDENTIAL~~

5.4-23

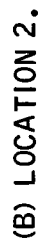
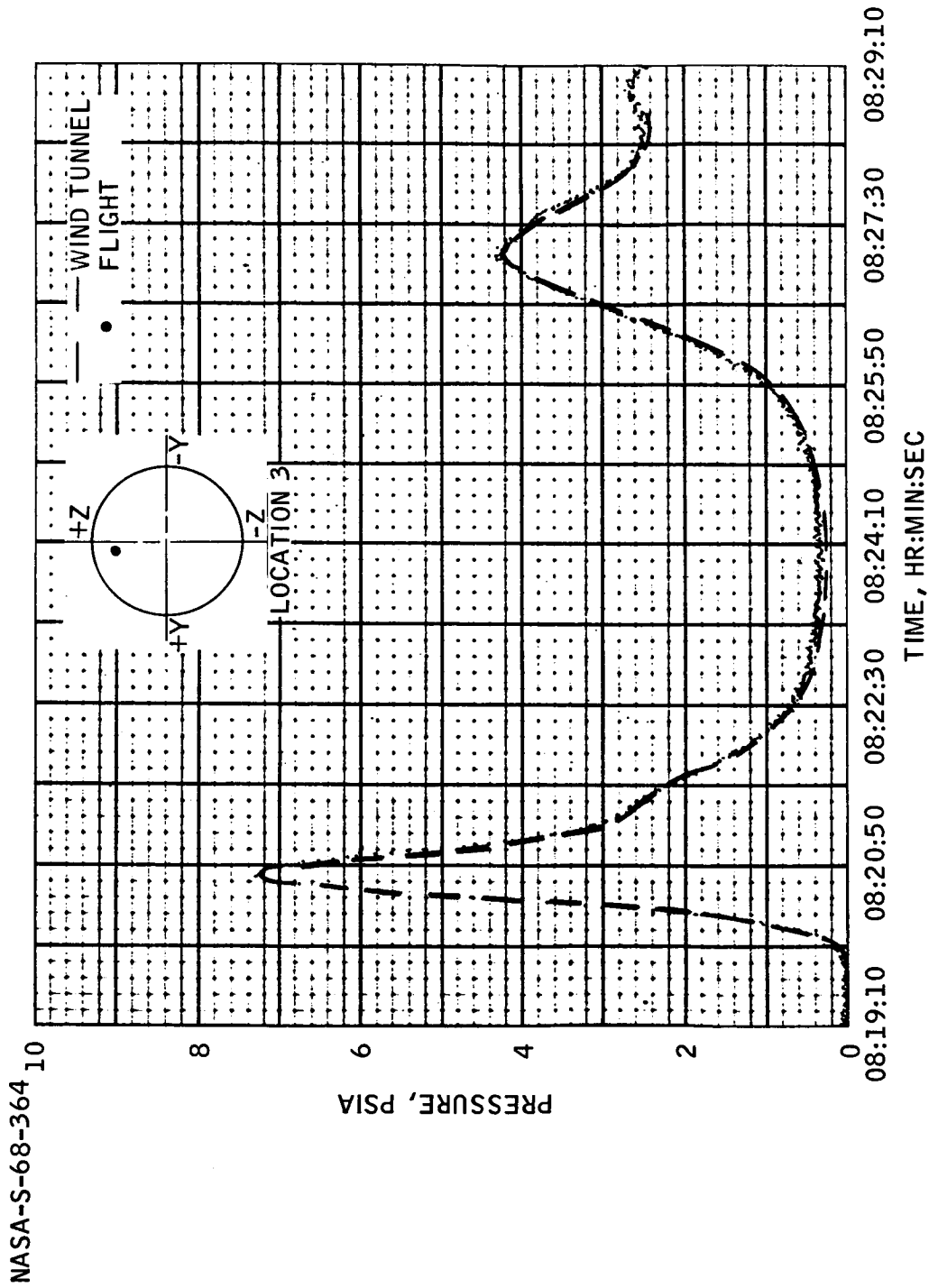


FIGURE 5.4-3.- CONTINUED.

~~CONFIDENTIAL~~

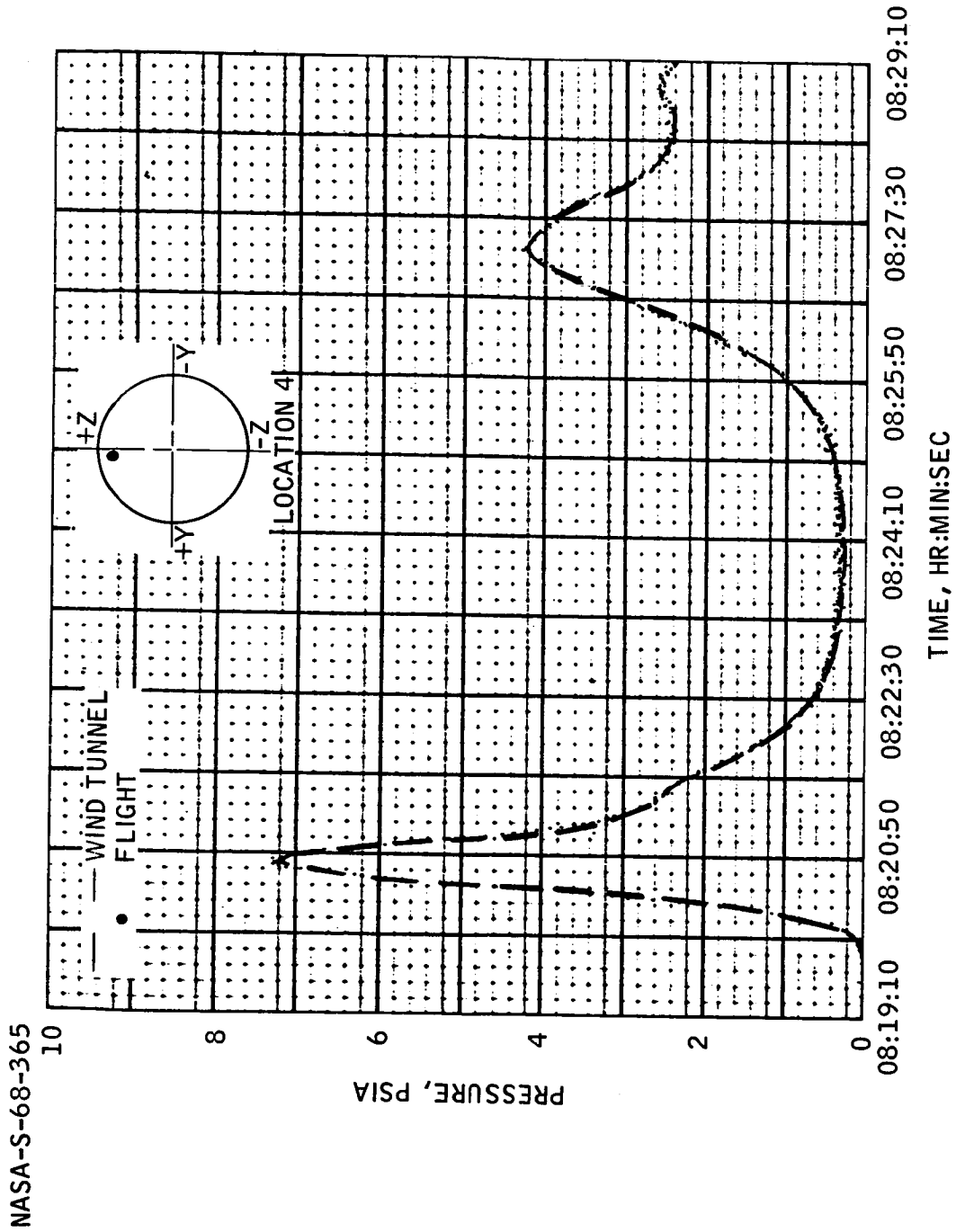
(C) LOCATION 3.

FIGURE 5.4-3.- CONTINUED.



~~CONFIDENTIAL~~

5.4-25

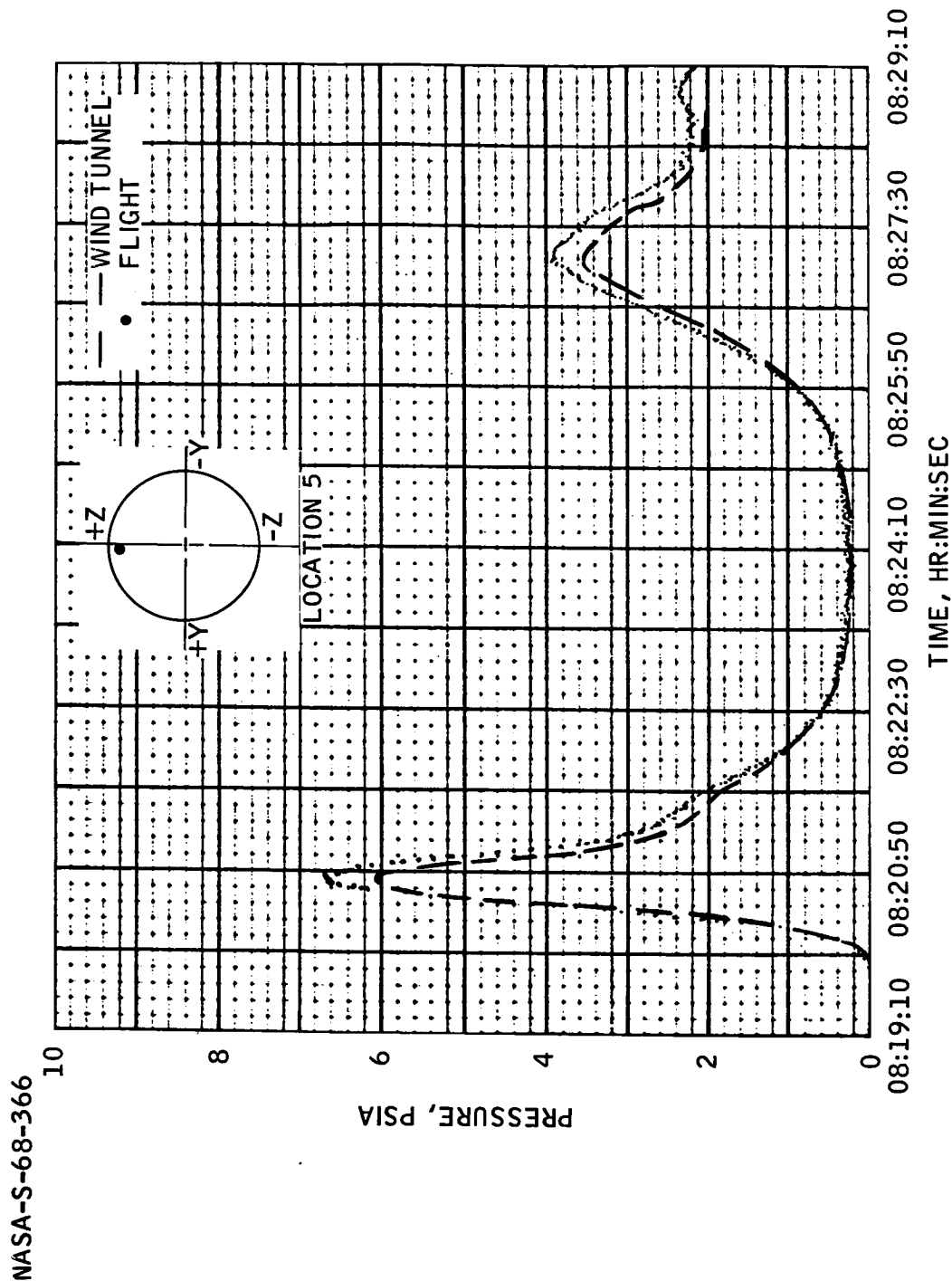


(D) LOCATION 4.

FIGURE 5.4-3.- CONTINUED.

~~CONFIDENTIAL~~

~~CONFIDENTIAL~~



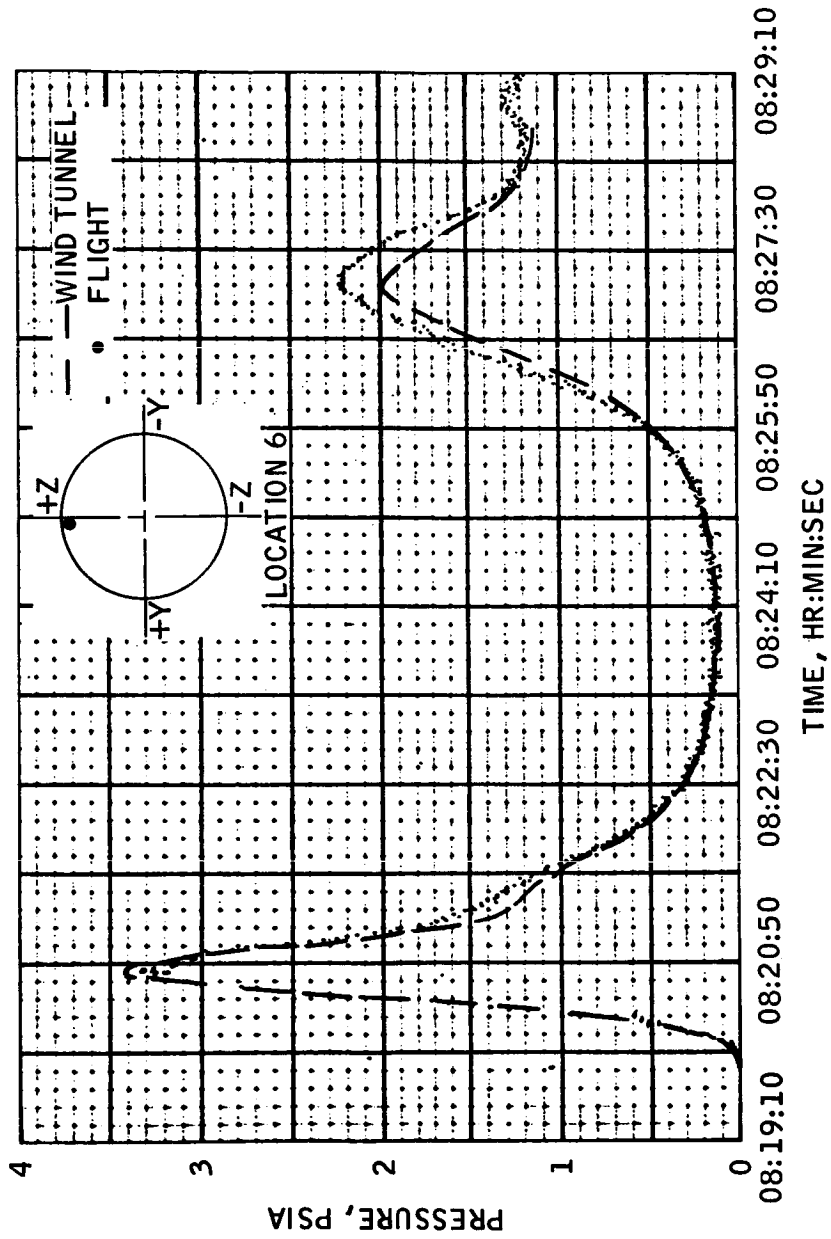
(E) LOCATION 5.

FIGURE 5.4-3.- CONTINUED.

~~CONFIDENTIAL~~

~~CONFIDENTIAL~~

5.4-27

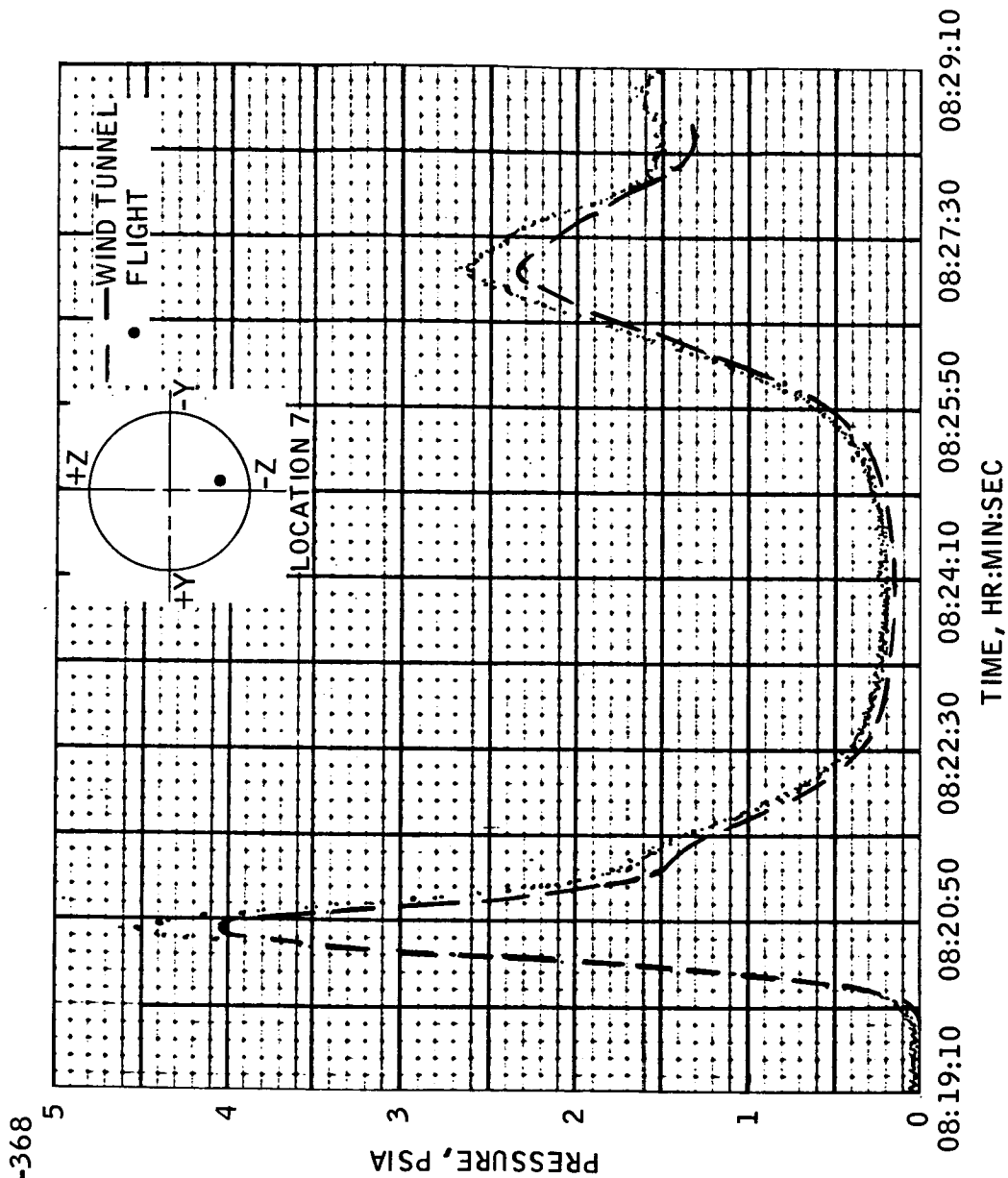


(F) LOCATION 6.

FIGURE 5.4-3.- CONTINUED.

~~CONFIDENTIAL~~

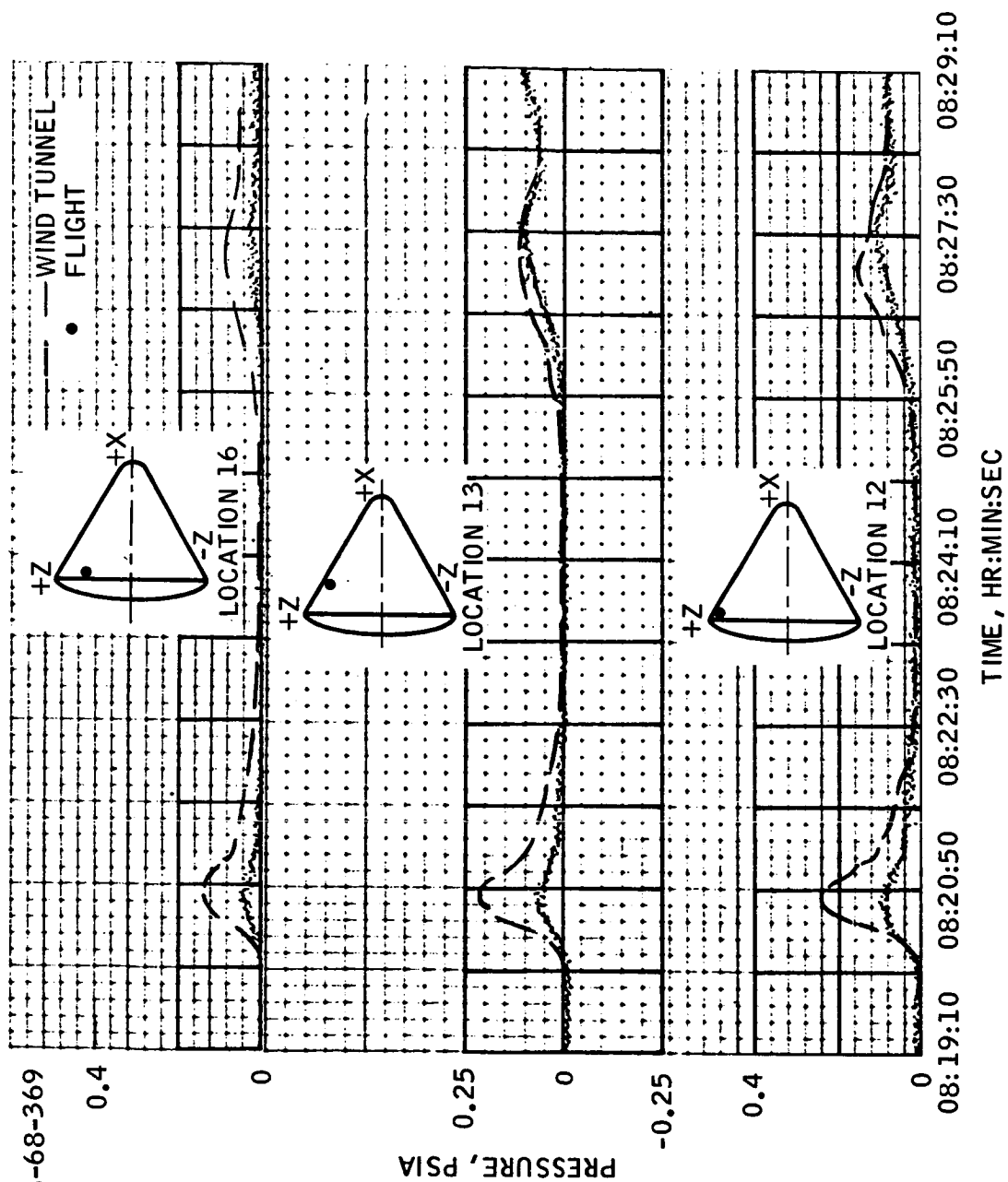
~~CONFIDENTIAL~~



(G) LOCATION 7.

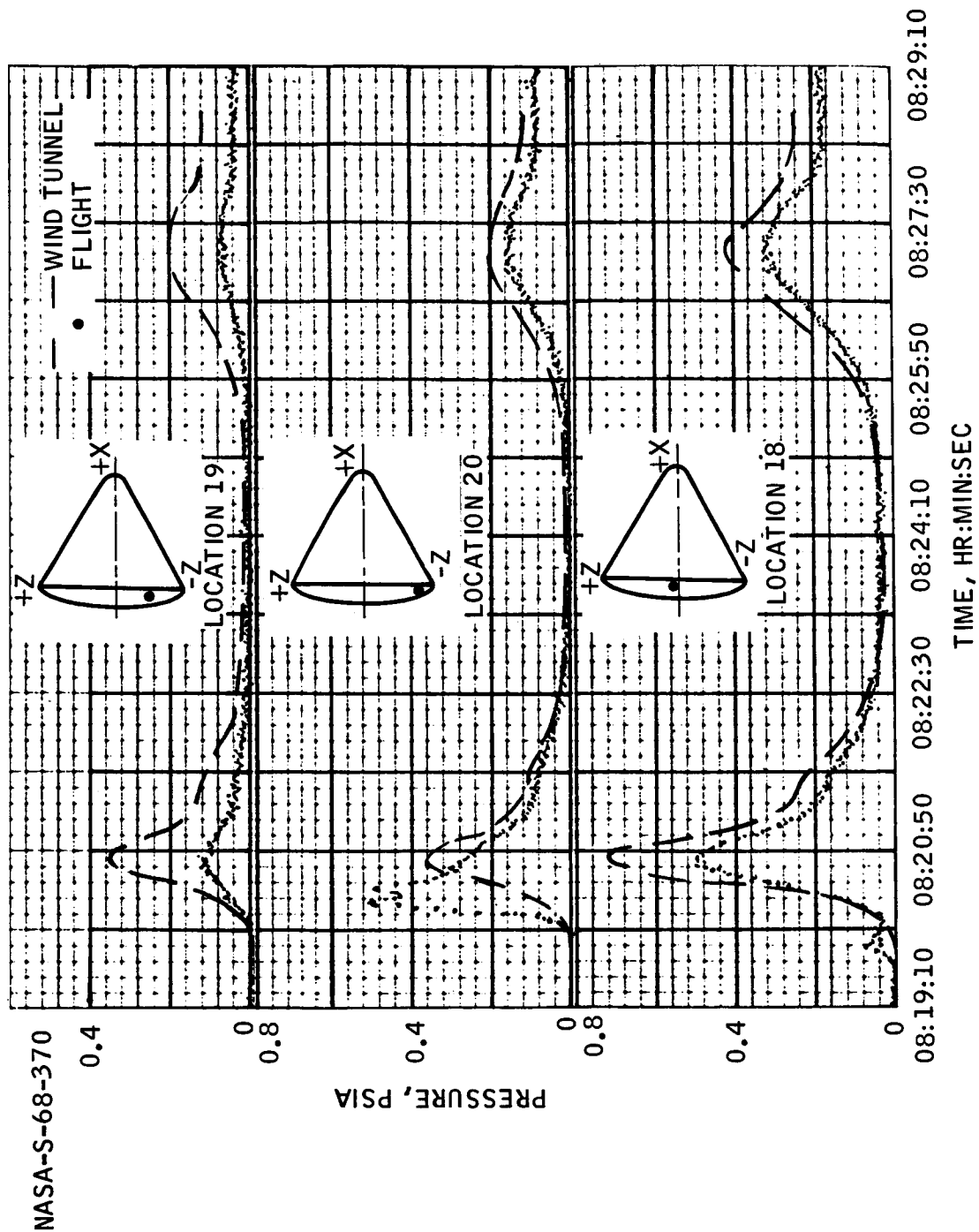
FIGURE 5.4-3.- CONTINUED.

~~CONFIDENTIAL~~



**(H) LOCATIONS 12, 13, AND 16.**

FIGURE 5.4.3- CONTINUED.

~~CONFIDENTIAL~~

(1) LOCATION 18, 19, AND 20.

FIGURE 5.4-3.- CONCLUDED.

~~CONFIDENTIAL~~

~~CONFIDENTIAL~~

5.4-31

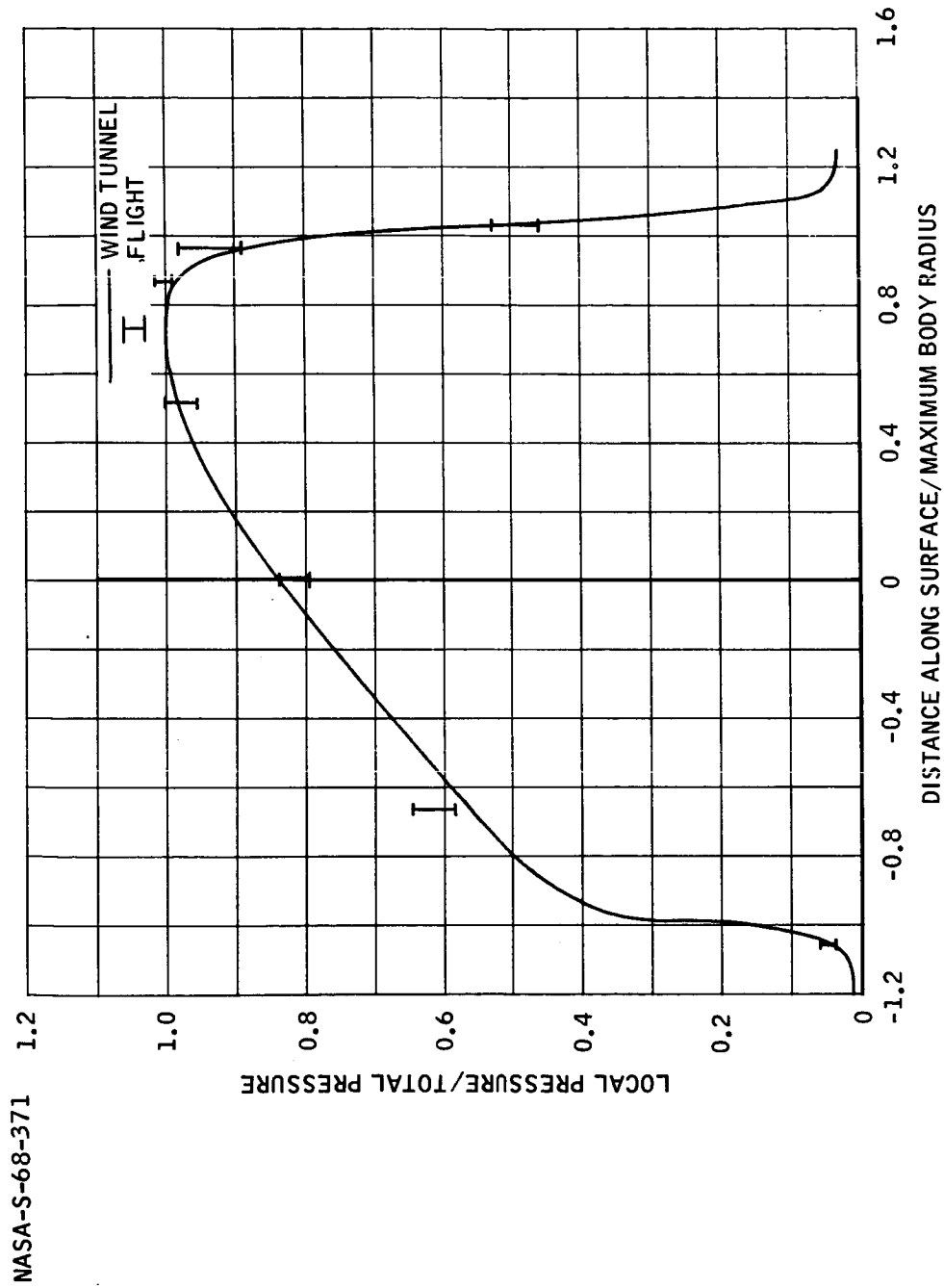
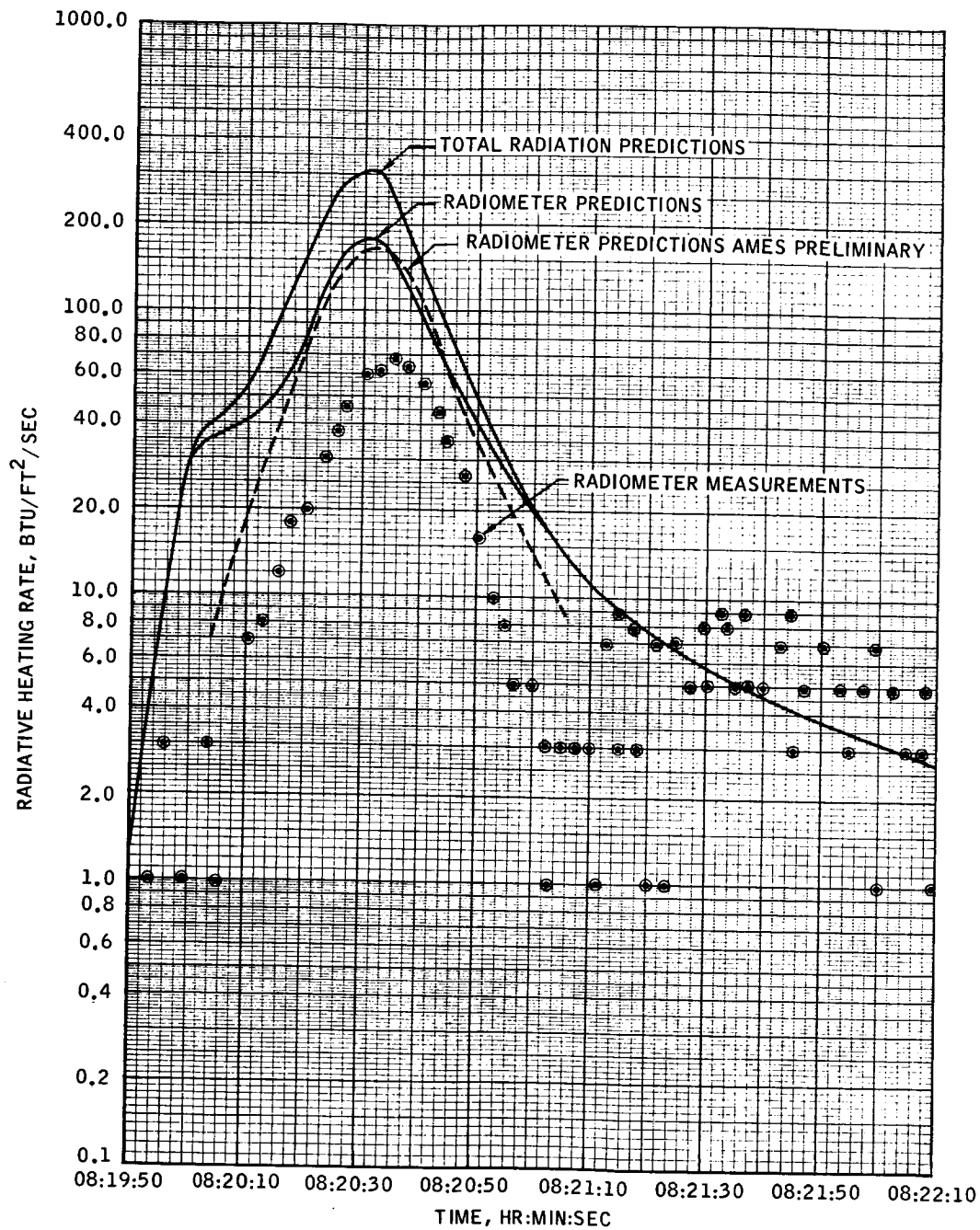


FIGURE 5.4-4.- DISTRIBUTION OF MEASURED PRESSURE RATIO WITH WIND TUNNEL  
DATA  $\alpha = 25^\circ$ .

~~CONFIDENTIAL~~

~~CONFIDENTIAL~~

NASA-S-68-372



(A) FIRST HEAT PULSE.

FIGURE 5.4-5.- COMPARISON OF MEASURED RADIATIVE HEATING RATE WITH THEORETICAL PREDICTIONS.

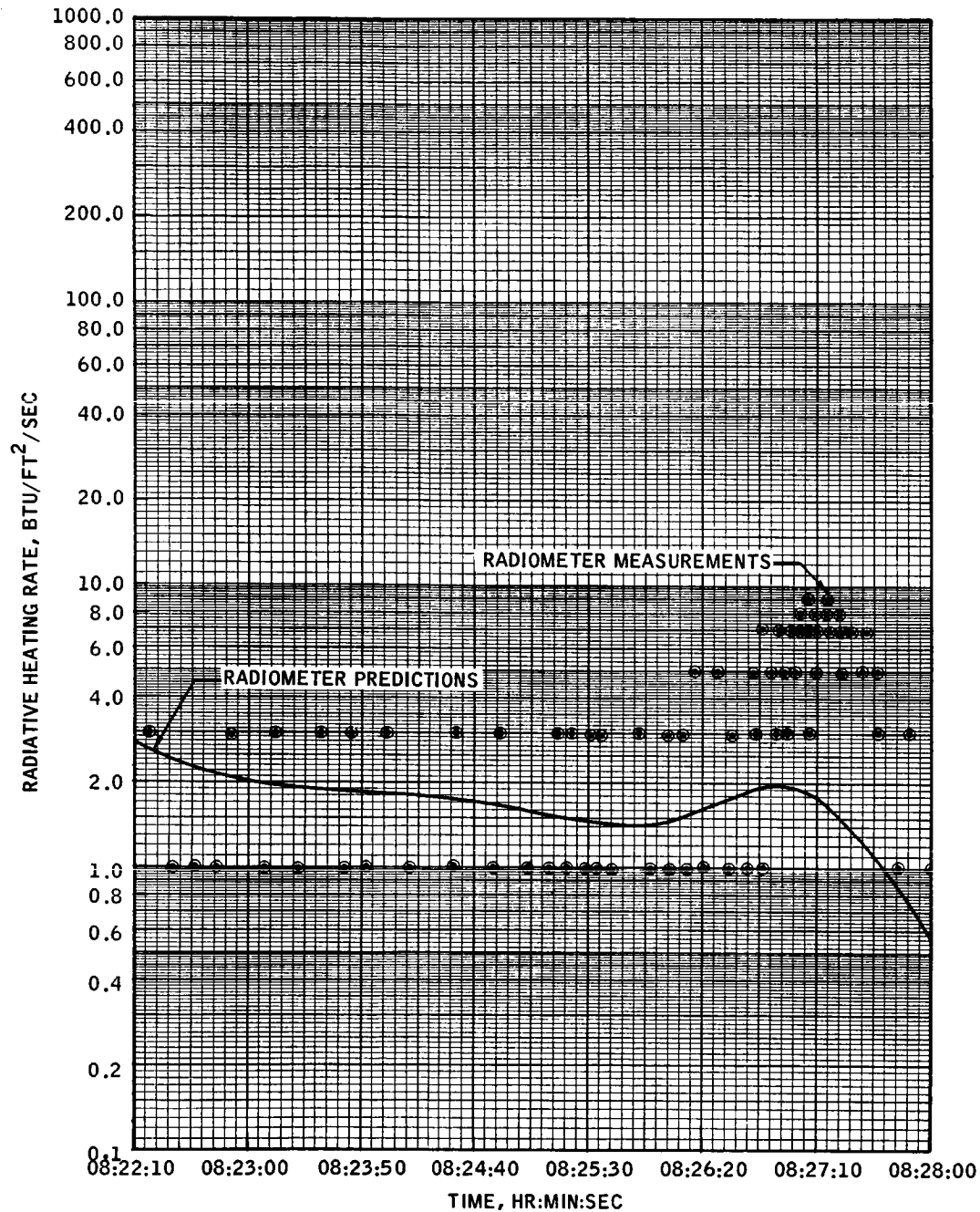
~~CONFIDENTIAL~~



~~CONFIDENTIAL~~

5.4-33

NASA-S-68-373



(B) SECOND HEAT PULSE.

FIGURE 5.4-5.- CONCLUDED.

~~CONFIDENTIAL~~

~~CONFIDENTIAL~~

NASA-S-68-374

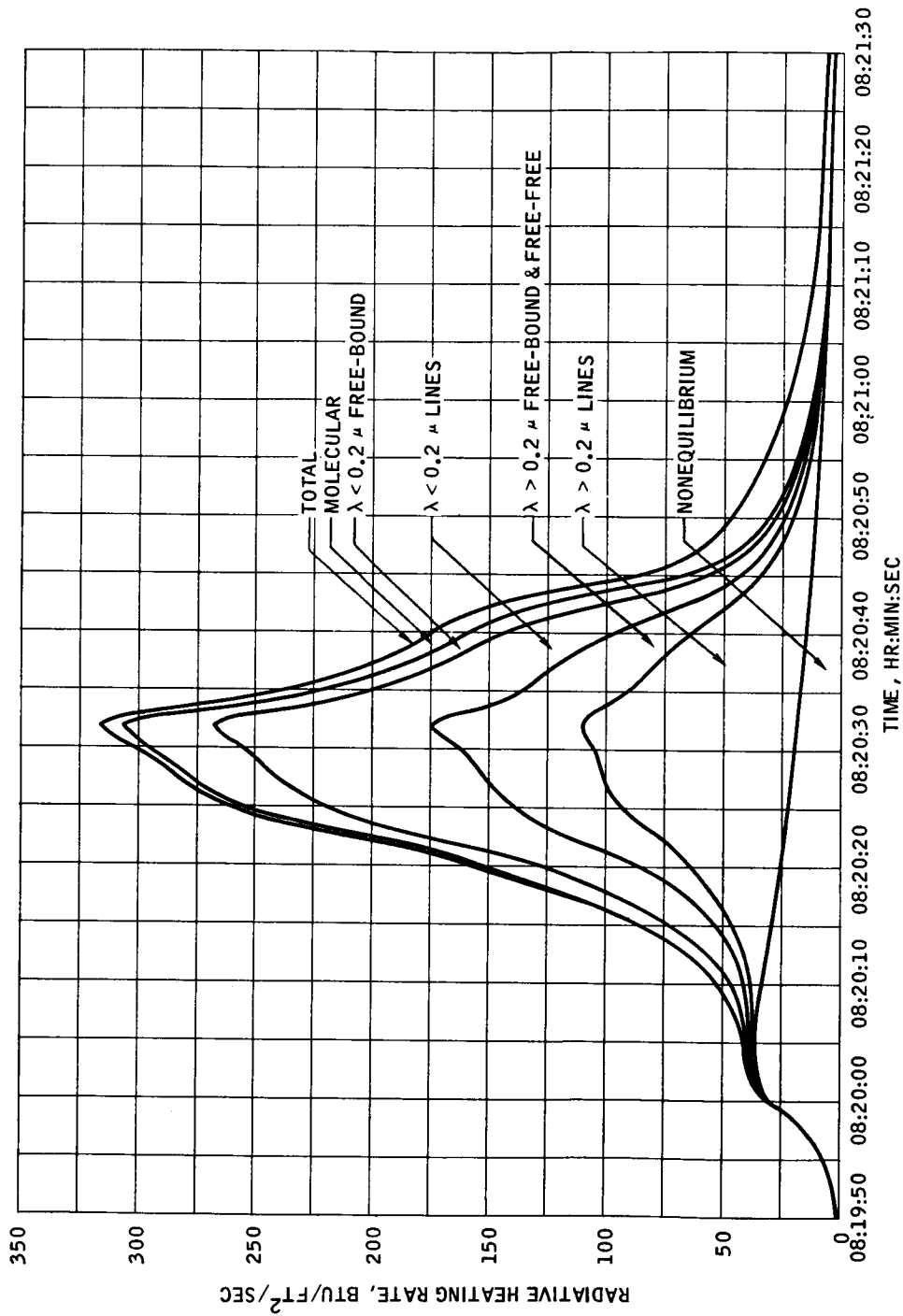
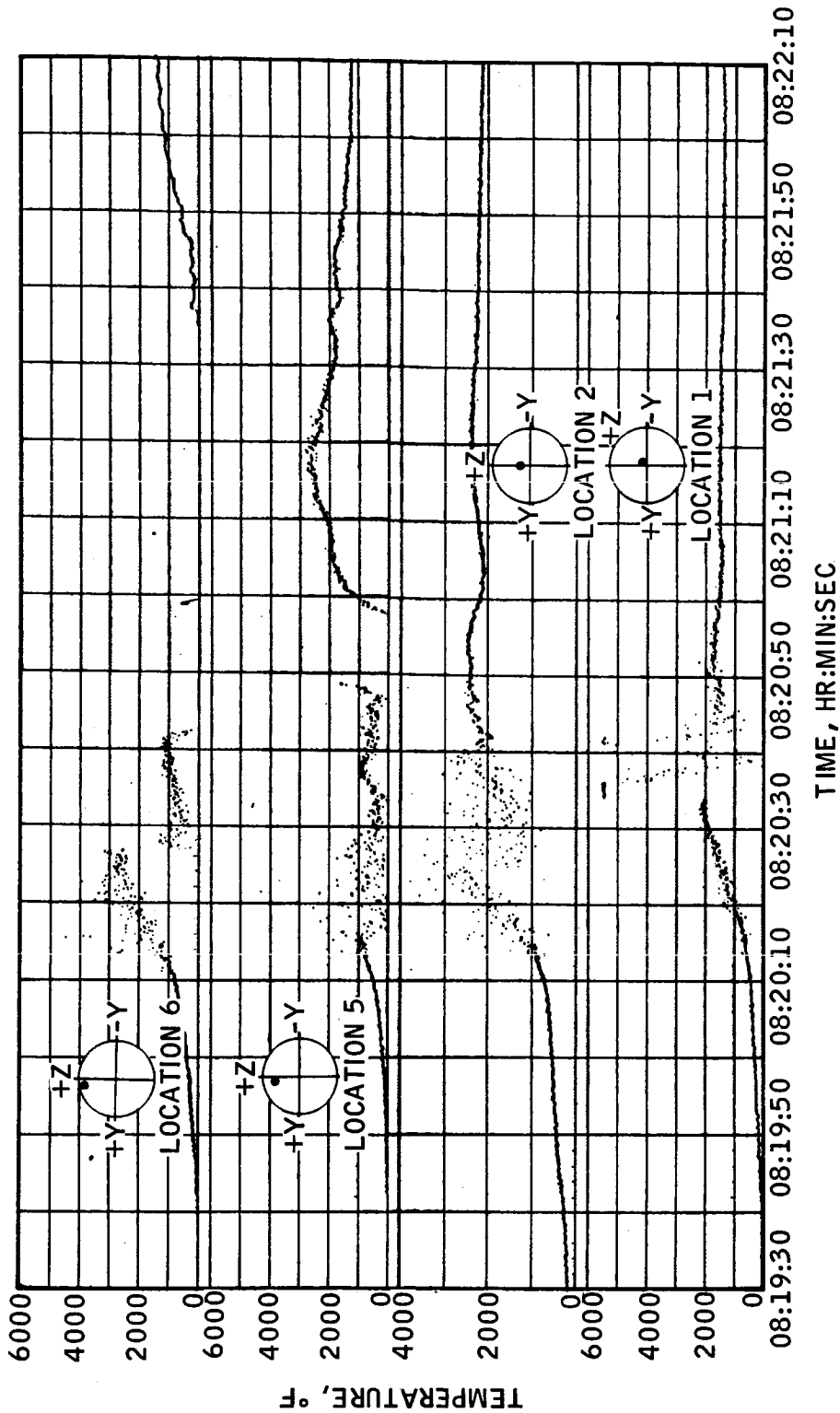


FIGURE 5.4-6.- TOTAL RADIATIVE HEATING RATE PREDICTION WITH ITS COMPONENTS.

~~CONFIDENTIAL~~

NASA-S-68-375



(A) LOCATIONS 1, 2, 5, AND 6.

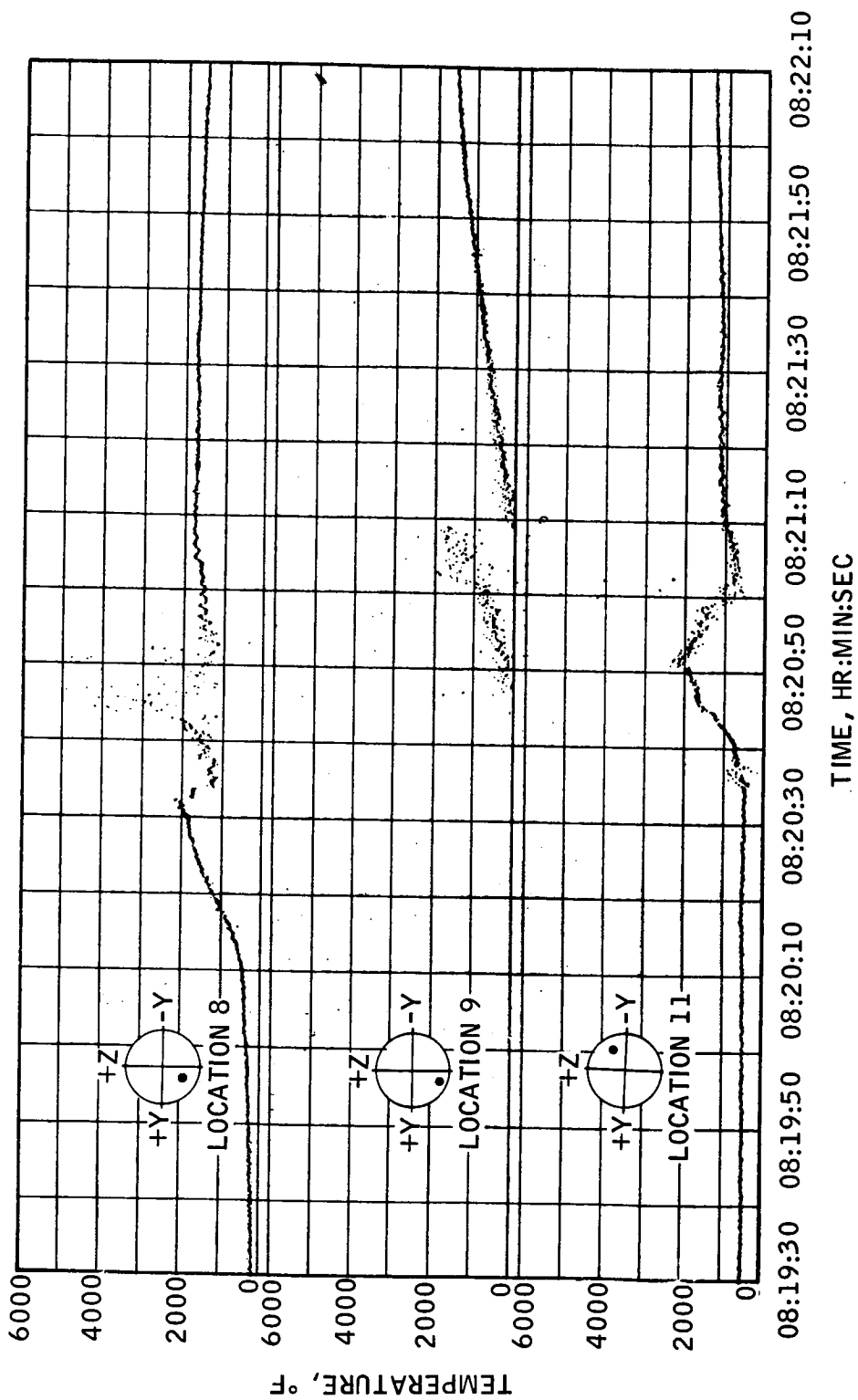
FIGURE 5.4-7.- HIGH RANGE CALORIMETER WAFER TEMPERATURES.

5.4-35

~~CONFIDENTIAL~~

~~CONFIDENTIAL~~

NASA-S-68-376



(B) LOCATIONS 8, 9, AND 11.

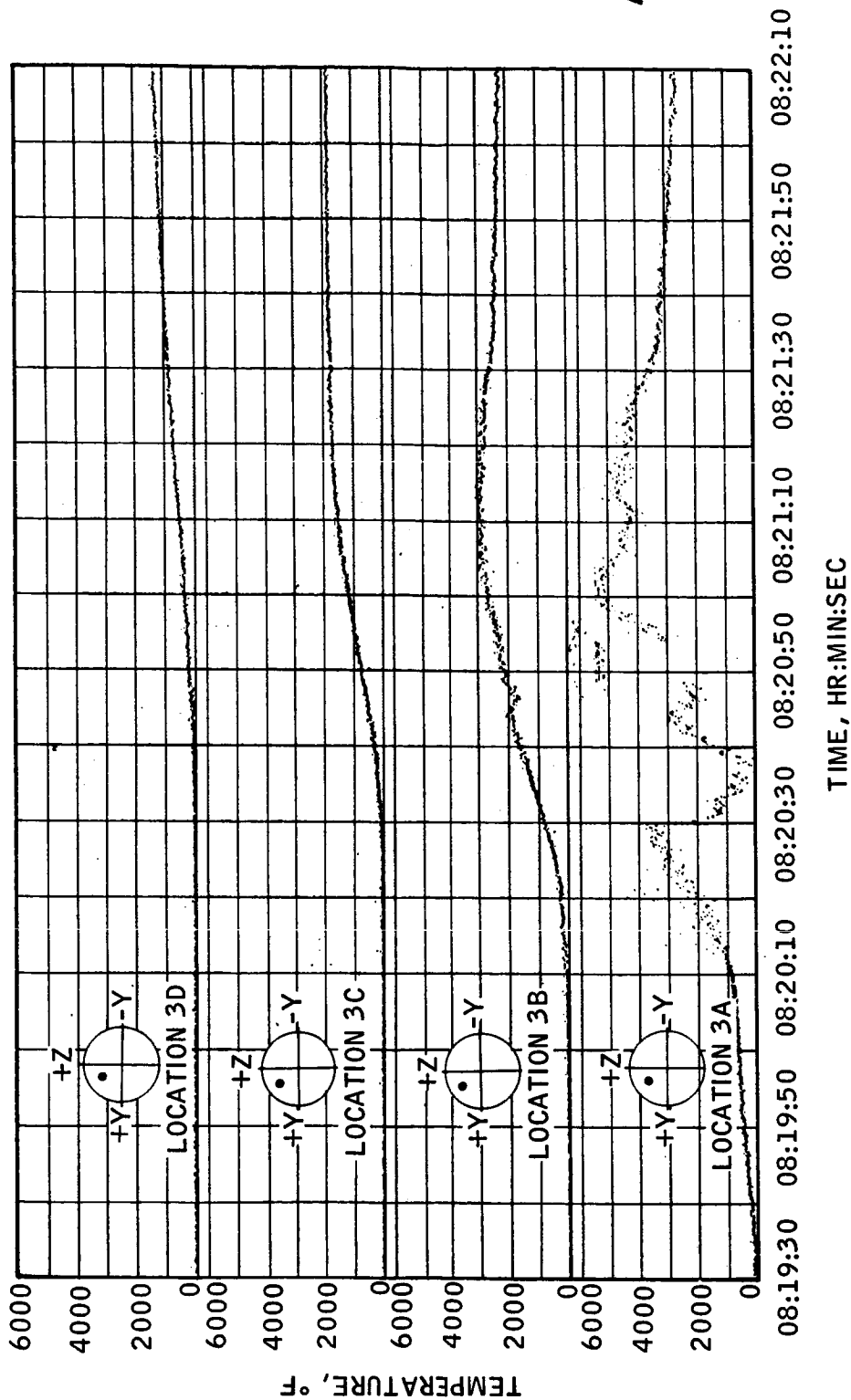
FIGURE 5.4-7.- CONTINUED.

~~CONFIDENTIAL~~

~~CONFIDENTIAL~~

5.4-37

NASA-S-68-377



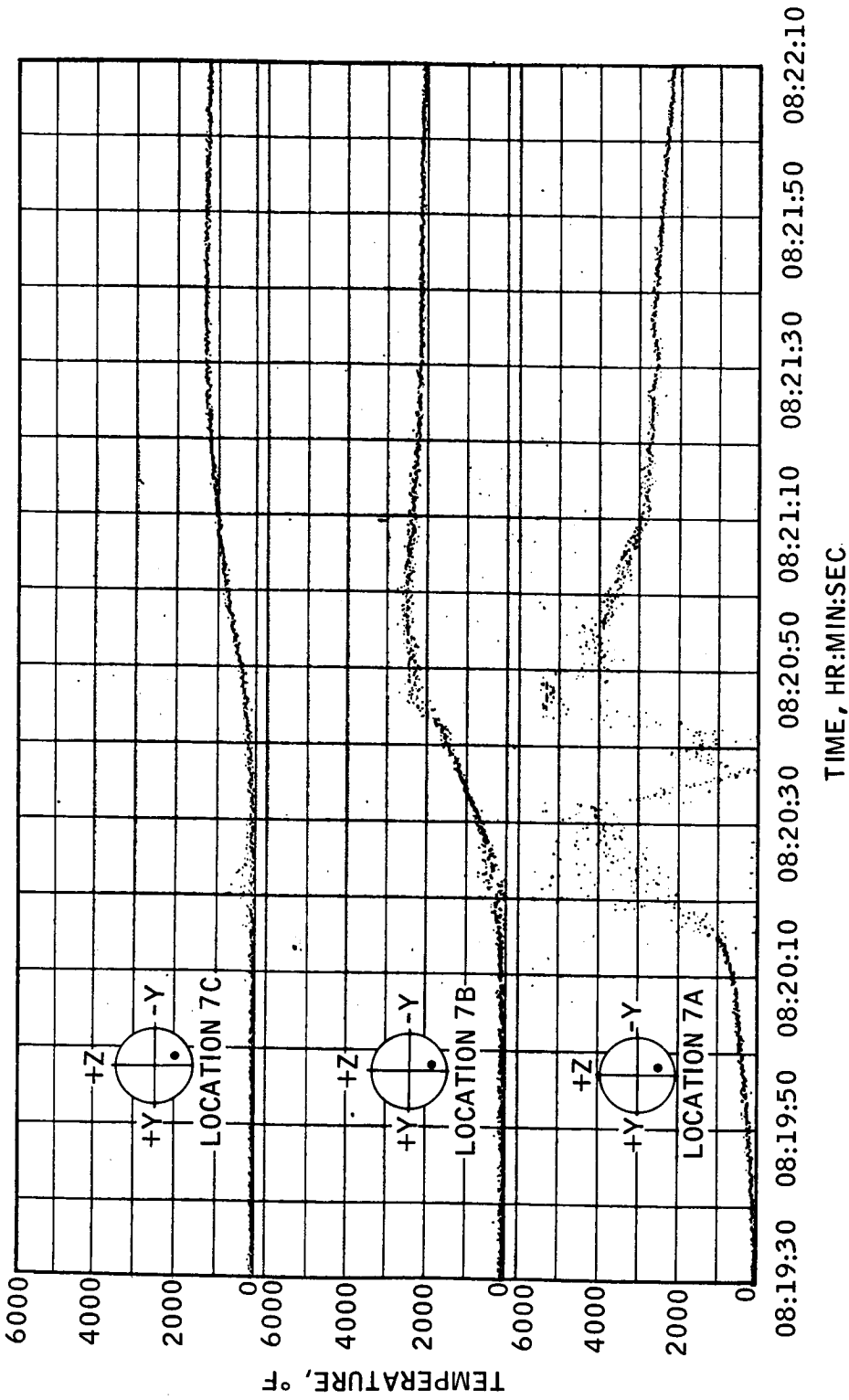
(C) TOP 4 WAFERS OF LOCATION 3.

FIGURE 5.4-7. - CONTINUED.

~~CONFIDENTIAL~~

~~CONFIDENTIAL~~

NASA-S-68-378



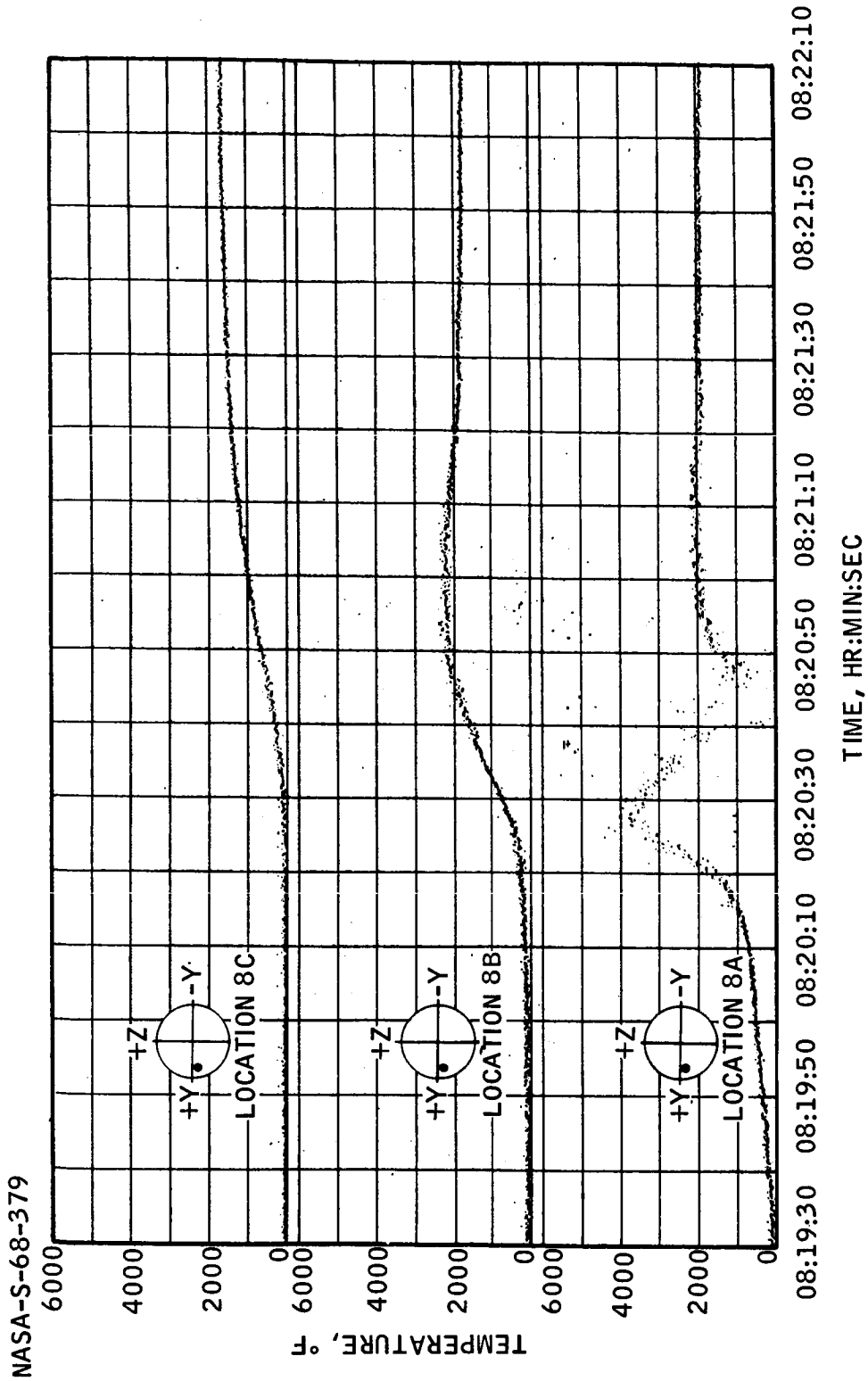
(D) TOP 3 WAFERS OF LOCATION 7.

FIGURE 5.4-7.- CONTINUED.

~~CONFIDENTIAL~~

~~CONFIDENTIAL~~

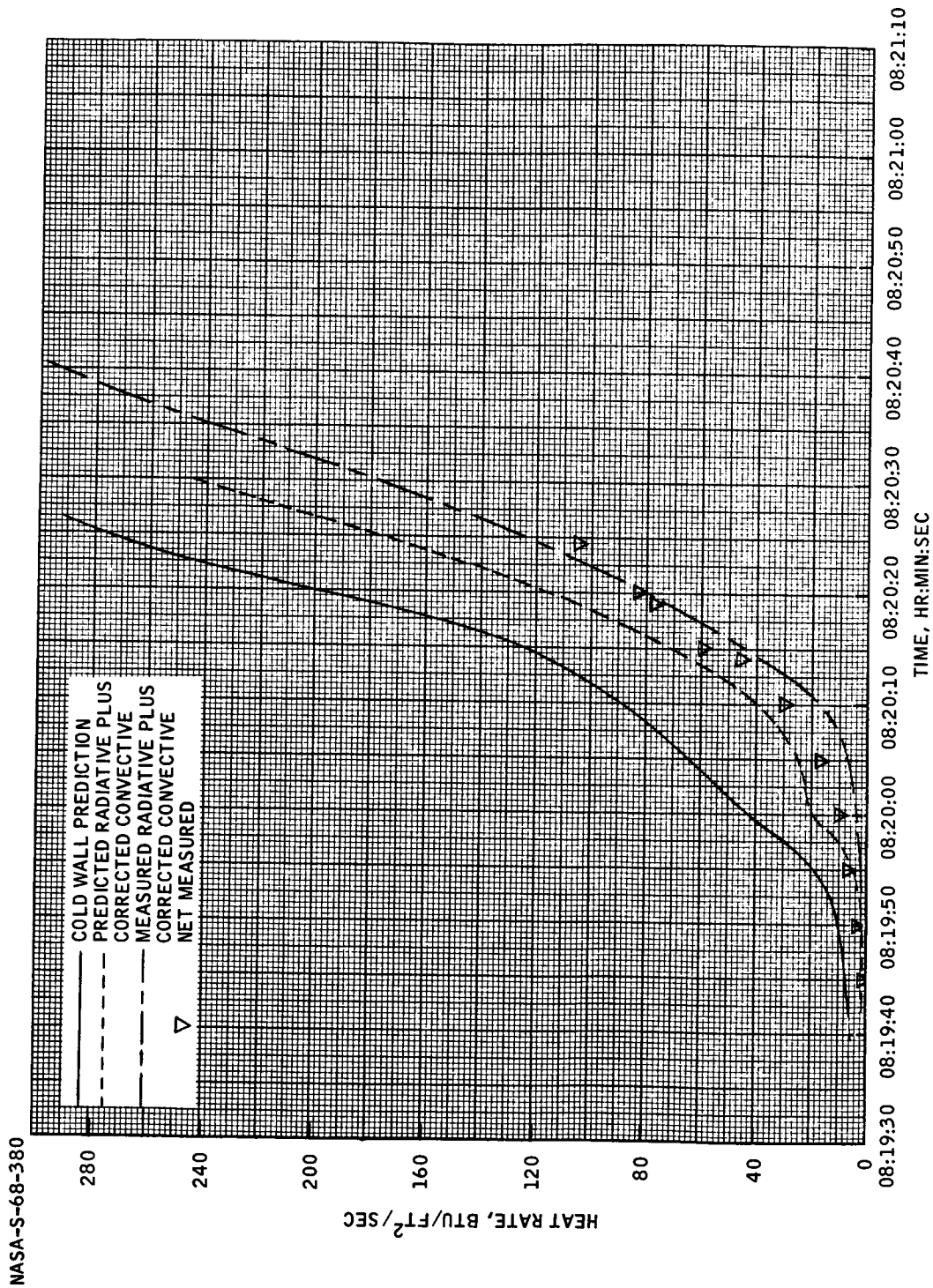
5.4-39



~~CONFIDENTIAL~~

(E) TOP 3 WAFERS OF LOCATION 8.

FIGURE 5.4-7.- CONCLUDED.

~~CONFIDENTIAL~~

(A) LOCATION 1.

FIGURE 5.4-8.- COMPARISON OF AFT HEAT SHIELD HEATING RATE OBTAINED FROM WAFER TEMPERATURE MEASUREMENT WITH THEORETICAL PREDICTION.

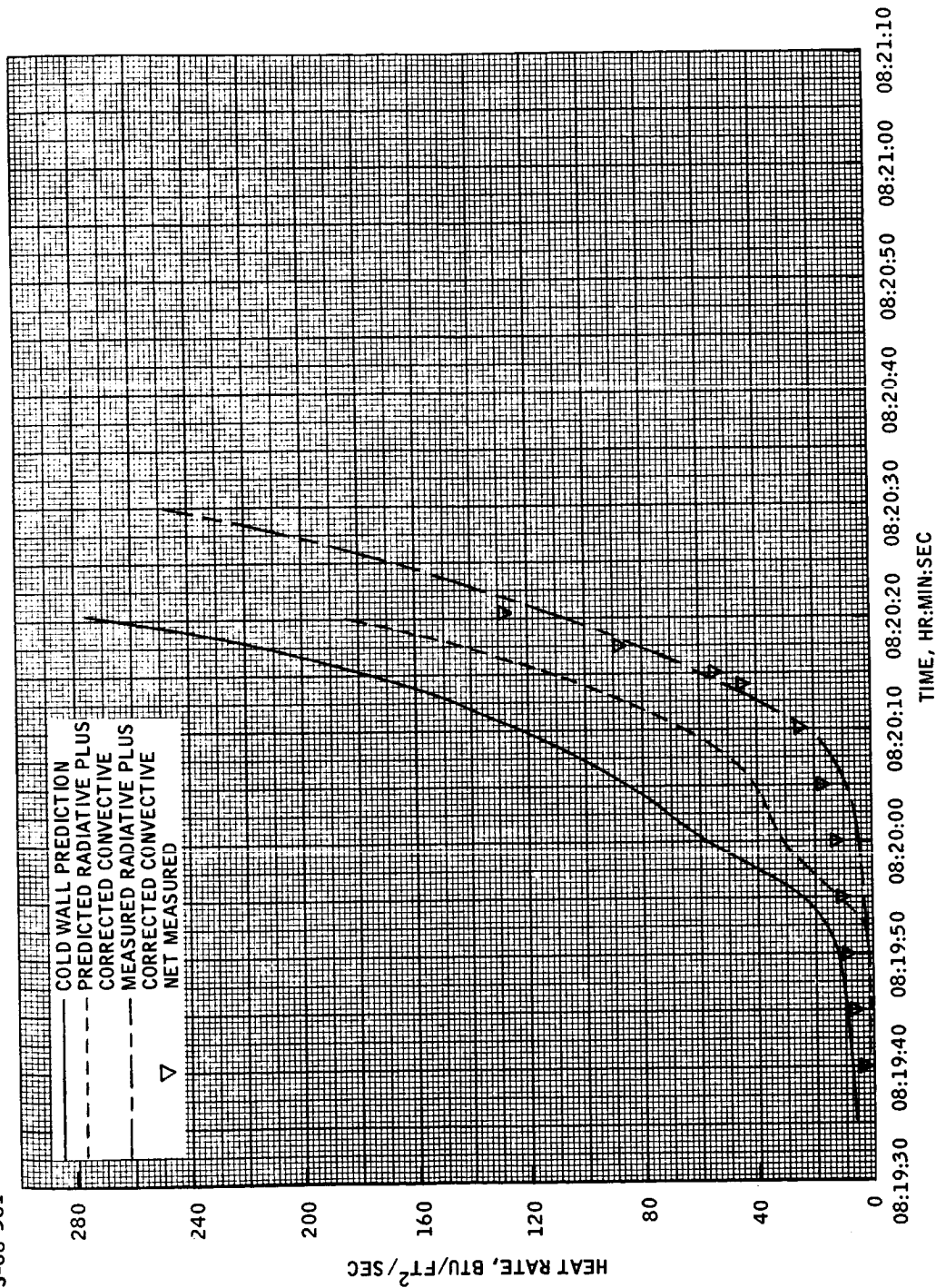
~~CONFIDENTIAL~~



~~CONFIDENTIAL~~

5.4-41

NASA-S-68-381



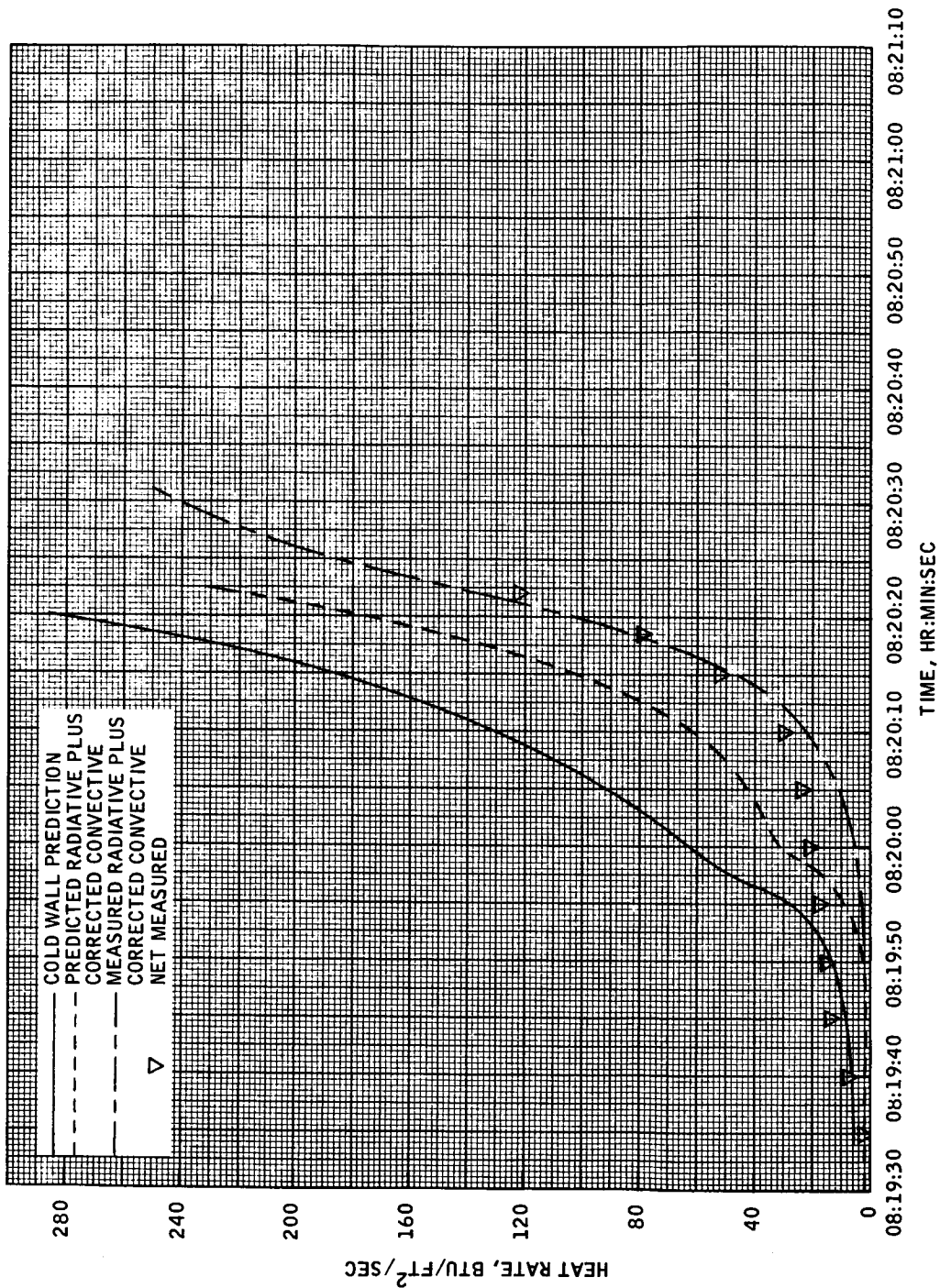
(B) LOCATION 2.

FIGURE 5.4-8.- CONTINUED.

~~CONFIDENTIAL~~

~~CONFIDENTIAL~~

NASA-S-68-382



(C) LOCATION 3.

FIGURE 5.4-8.- CONTINUED.

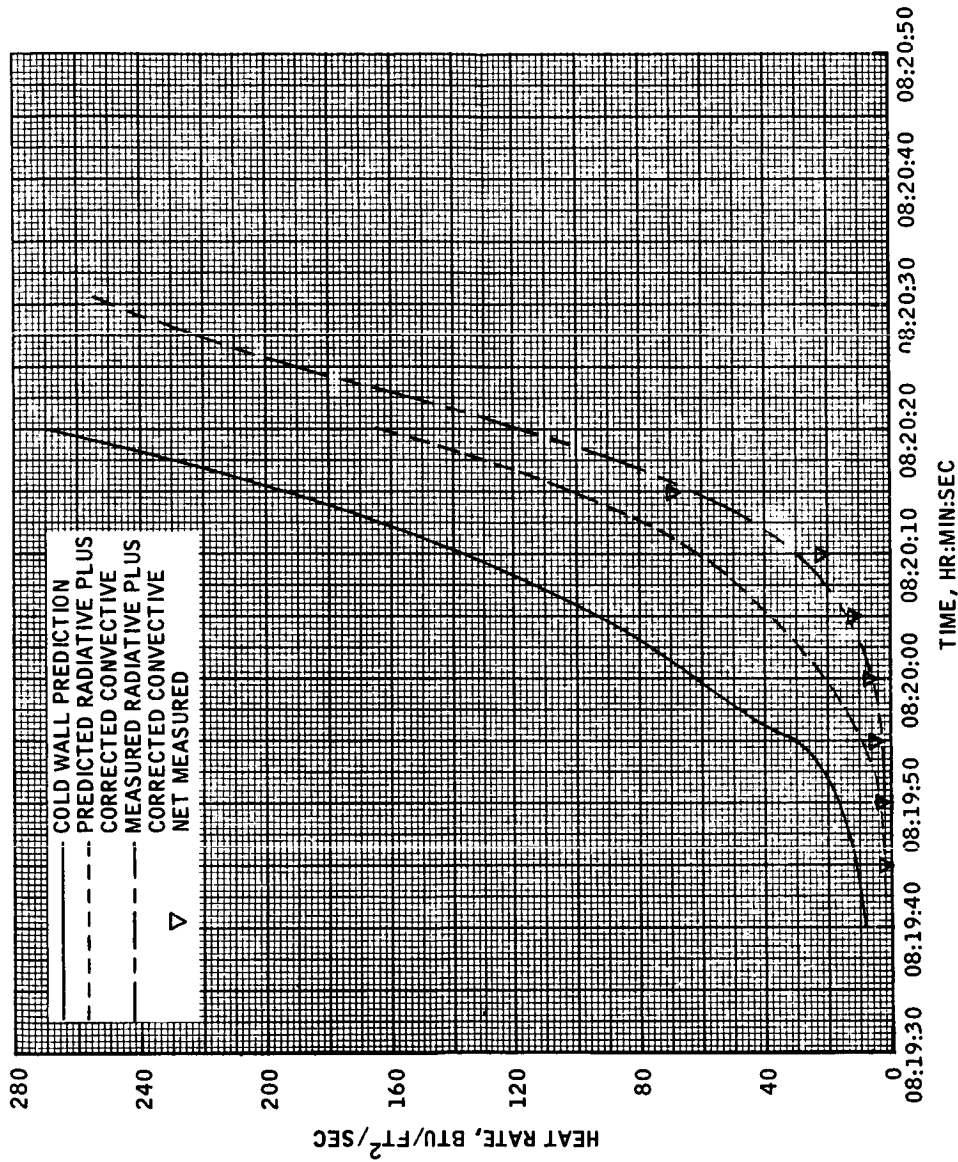
~~CONFIDENTIAL~~

~~CONFIDENTIAL~~

5.4-43

NASA-S-68-383

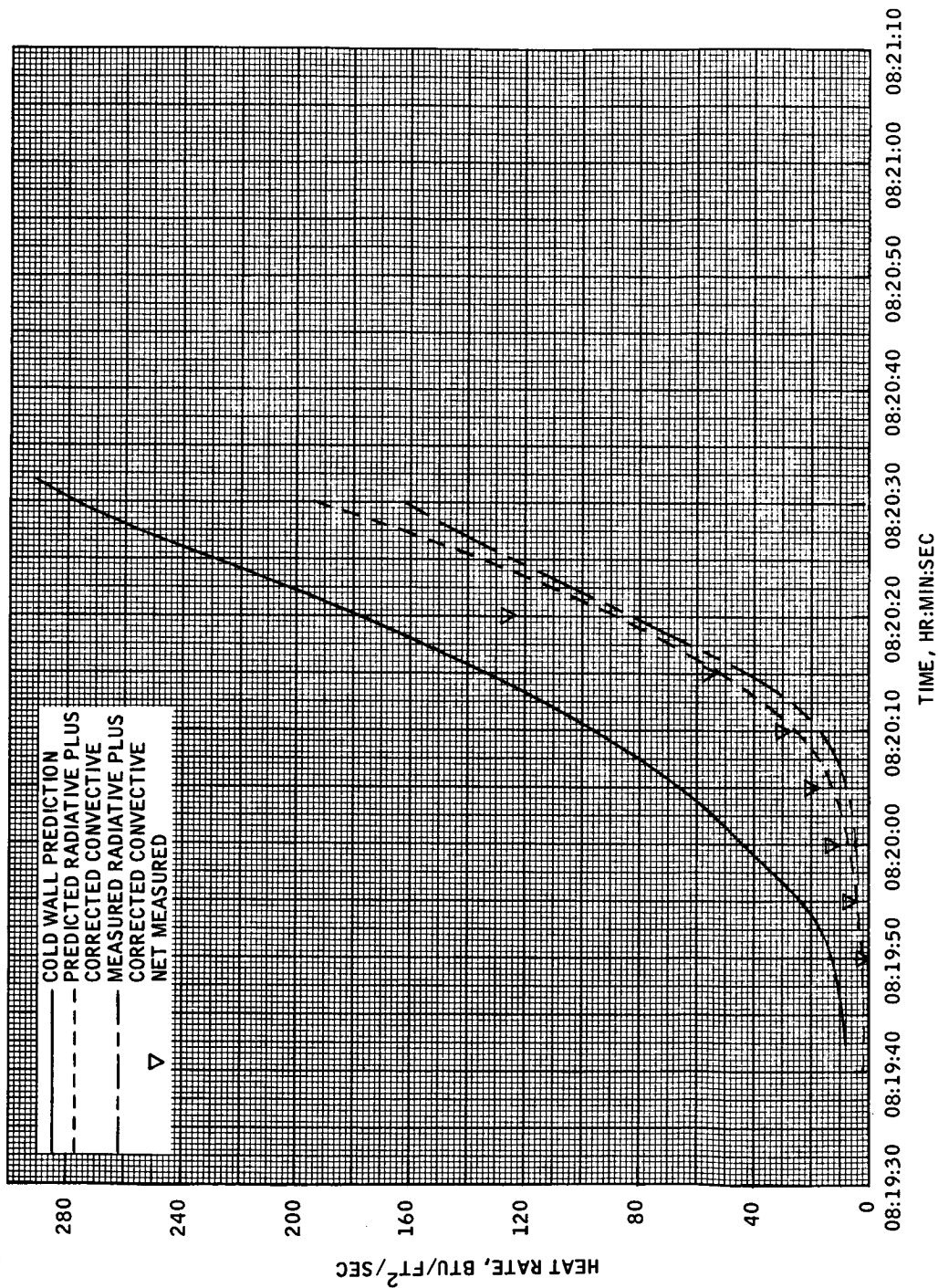
~~CONFIDENTIAL~~



(D) LOCATION 5.  
FIGURE 5.4-8.- CONTINUED.

~~CONFIDENTIAL~~

NASA-S-68-384



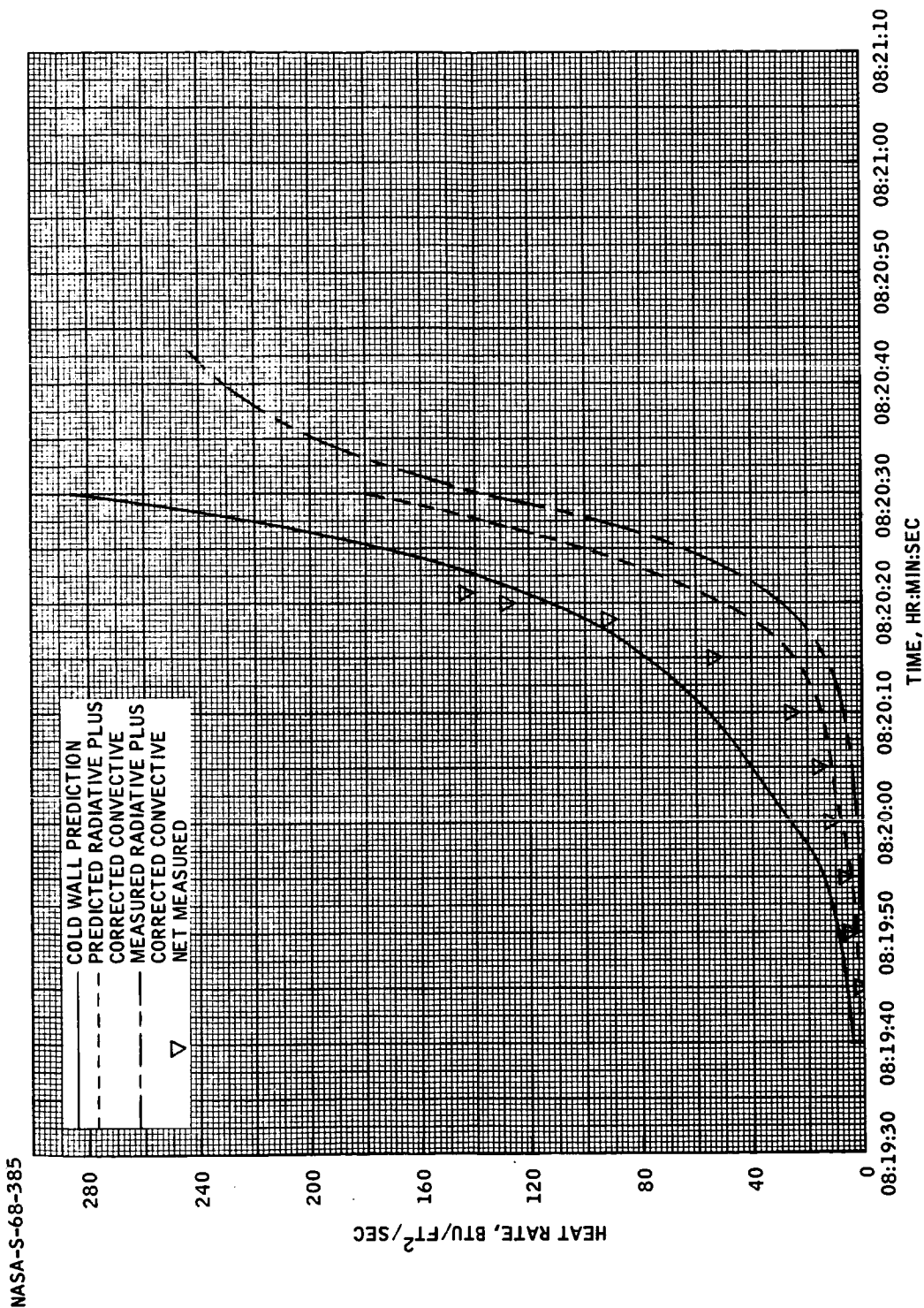
(E) LOCATION 6.

FIGURE 5.4-8.- CONTINUED.

~~CONFIDENTIAL~~

~~CONFIDENTIAL~~

5.4-45



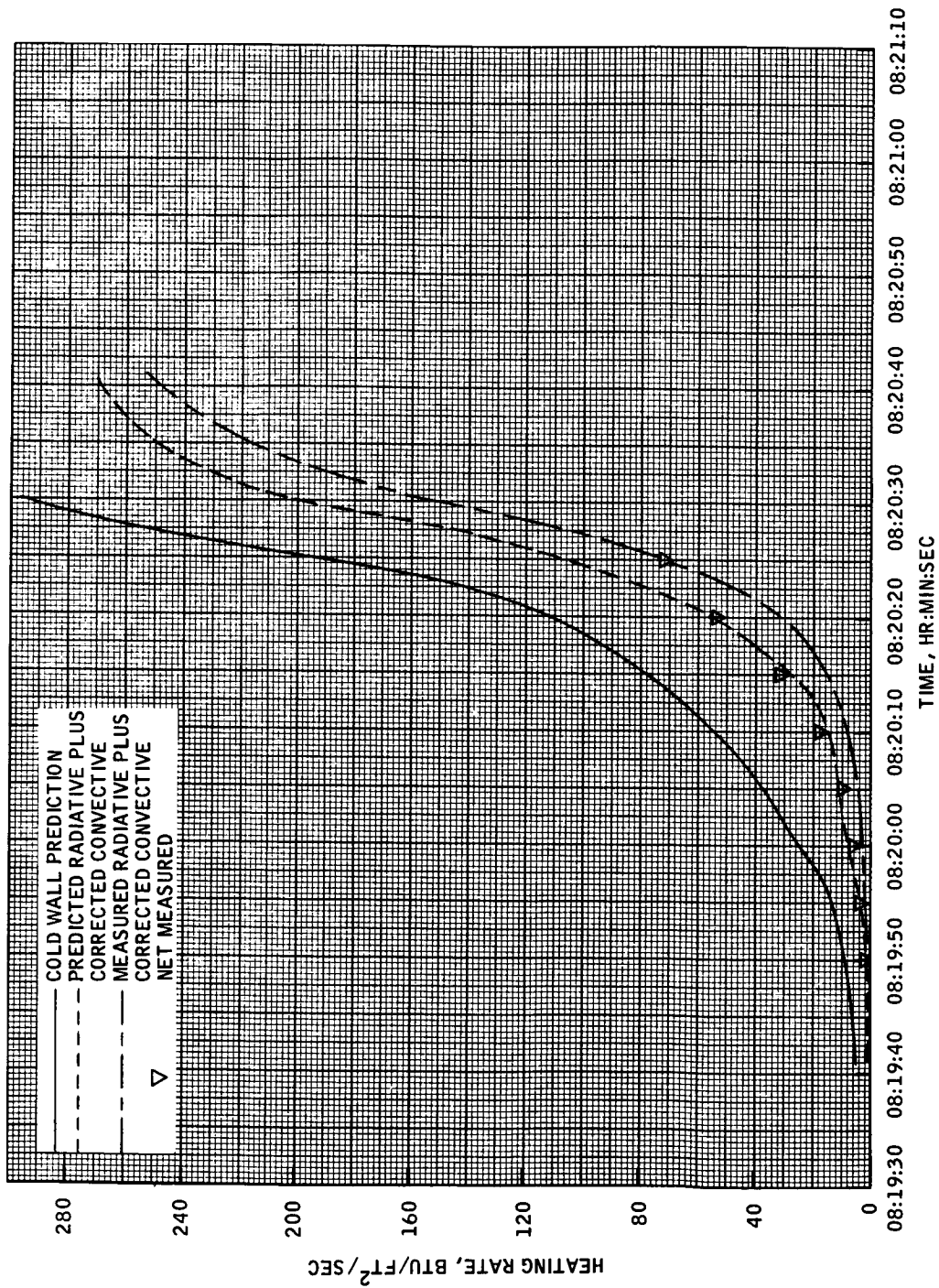
(F) LOCATION 7.

FIGURE 5.4-8.- CONTINUED.

~~CONFIDENTIAL~~

~~CONFIDENTIAL~~

NASA-S-68-386

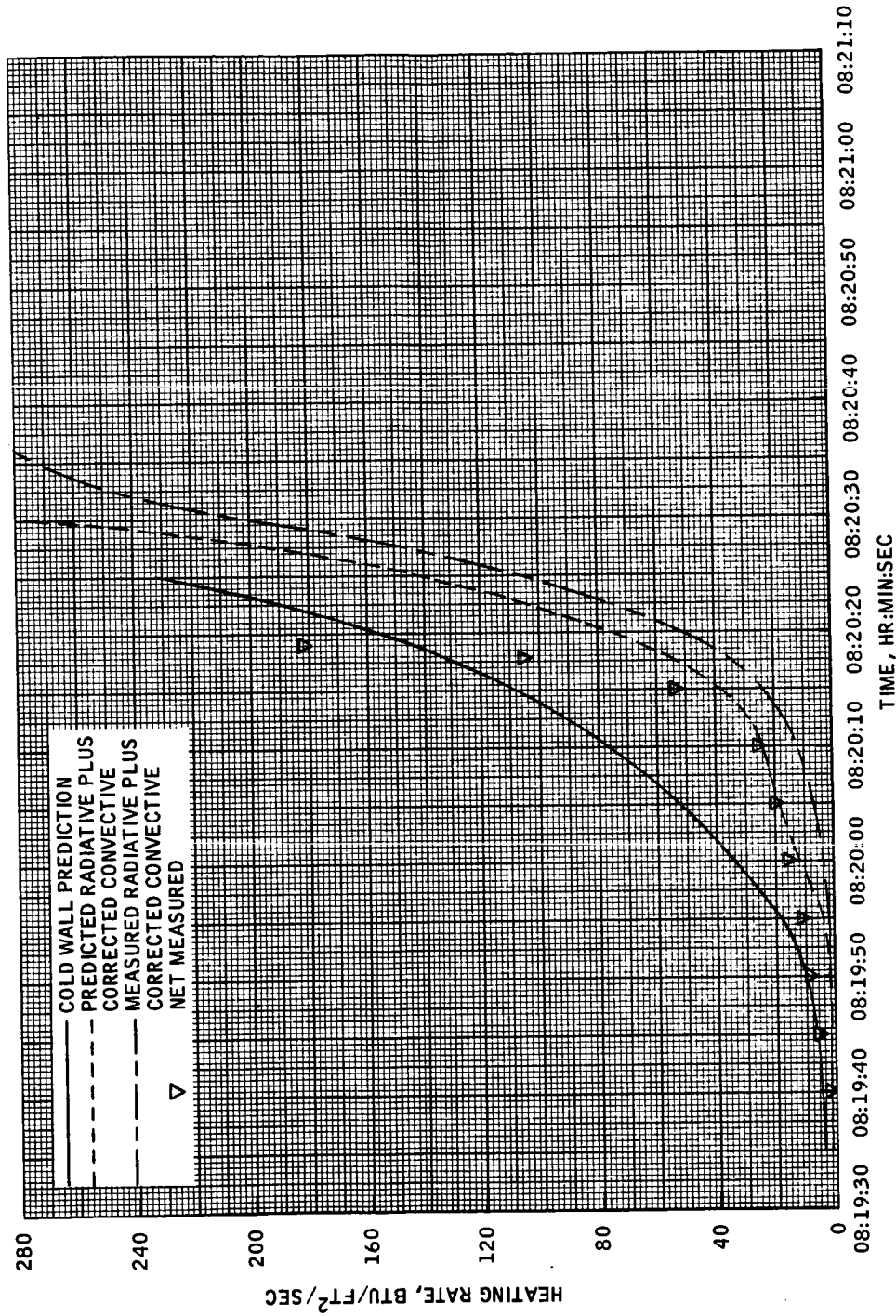


(G) LOCATION 8.

FIGURE 5.4-8.- CONTINUED.

~~CONFIDENTIAL~~





(H) LOCATION 10.

FIGURE 5.4-8.- CONCLUDED.

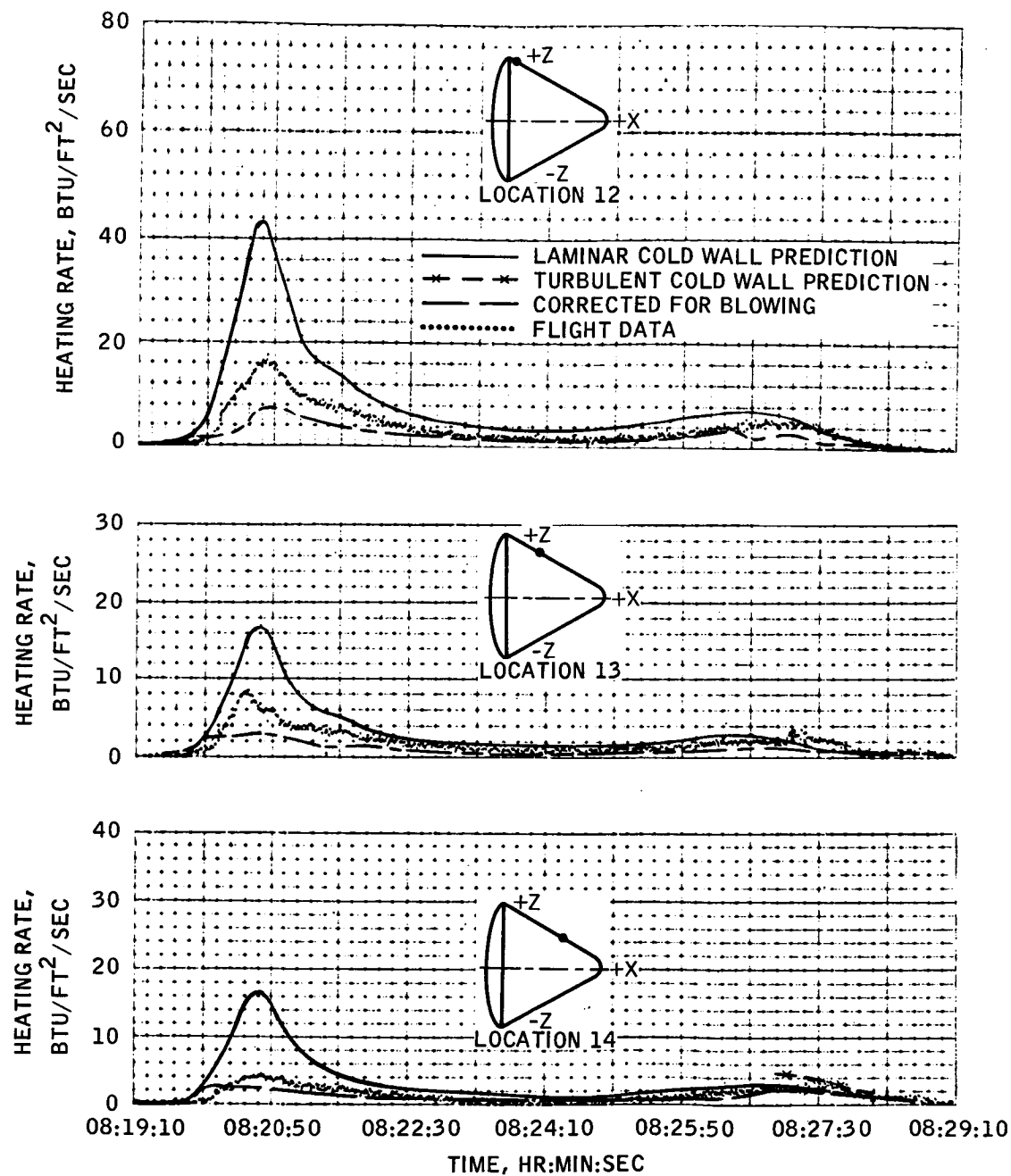
~~CONFIDENTIAL~~

5.4-47

~~CONFIDENTIAL~~

~~CONFIDENTIAL~~

NASA-S-68-388



(A) LOCATIONS 12, 13, AND 14.

FIGURE 5.4-9.- COMPARISON OF MEASURED HEATING RATE ON THE CONICAL SECTION WITH THEORETICAL PREDICTIONS.

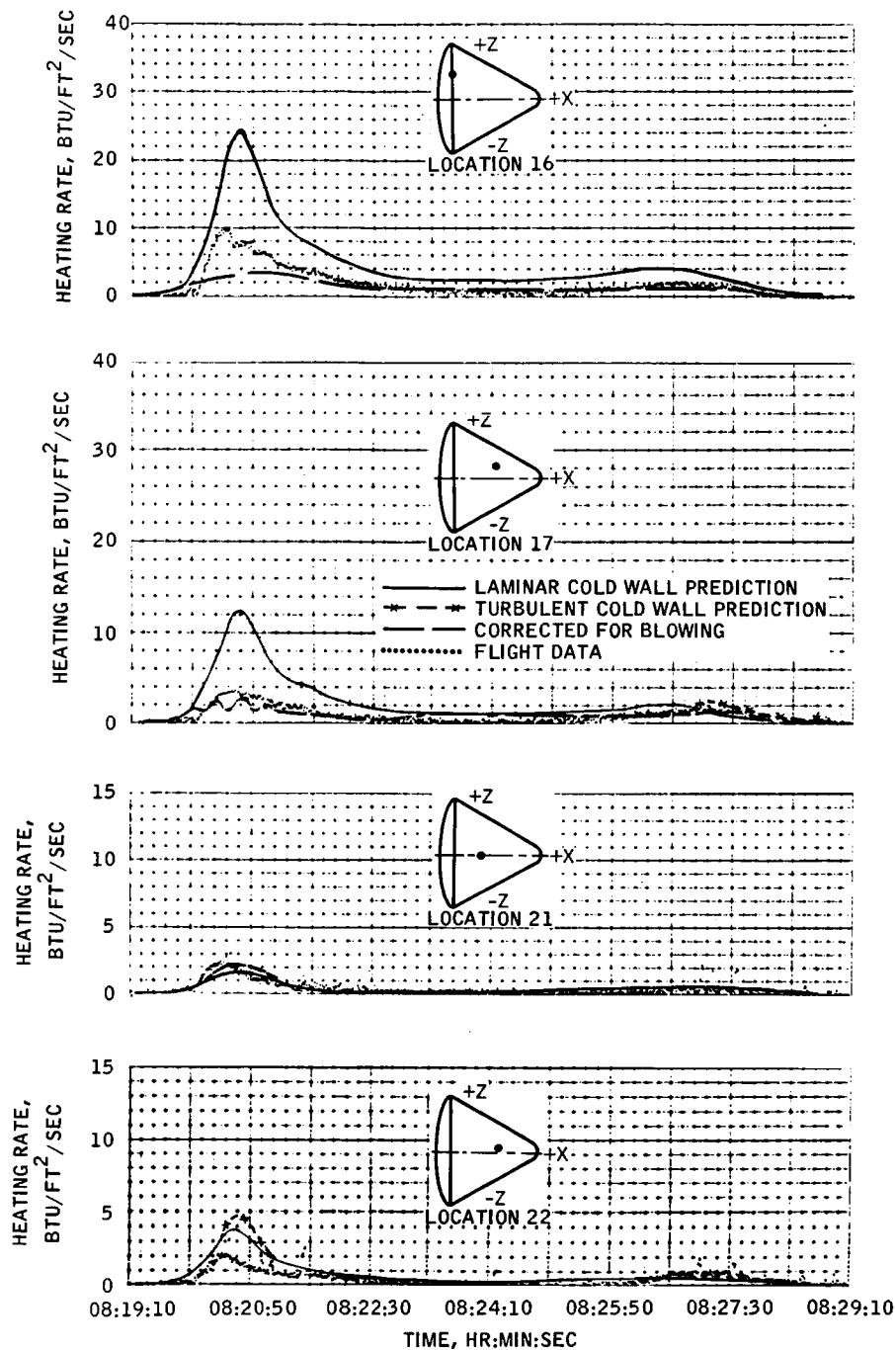
~~CONFIDENTIAL~~



~~CONFIDENTIAL~~

5.4-49

NASA-S-68-389



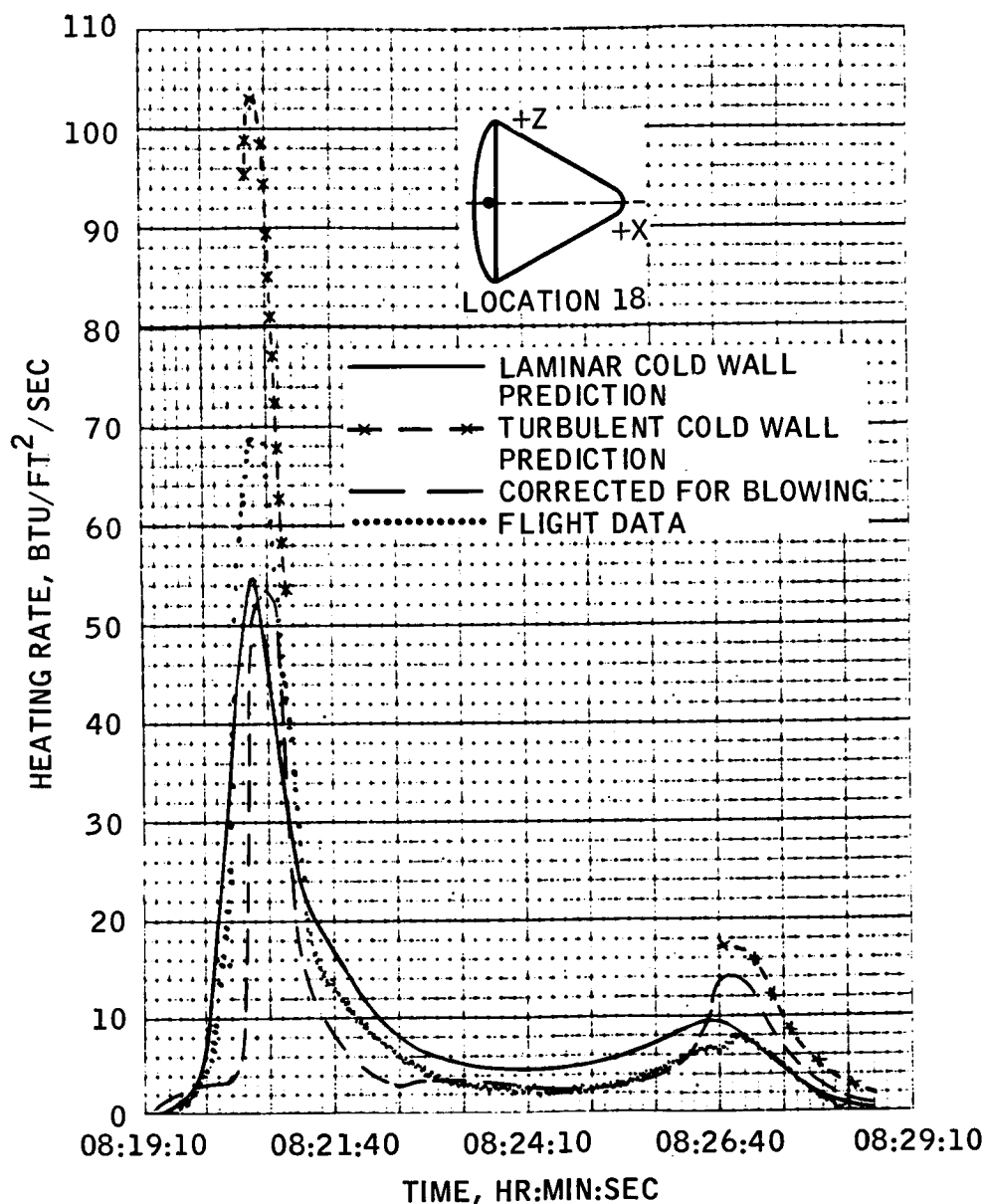
(B) LOCATIONS 16, 17, 21, AND 22.

FIGURE 5.4-9.- CONTINUED.

~~CONFIDENTIAL~~

~~CONFIDENTIAL~~

NASA-S-68-390



(C) LOCATION 18.

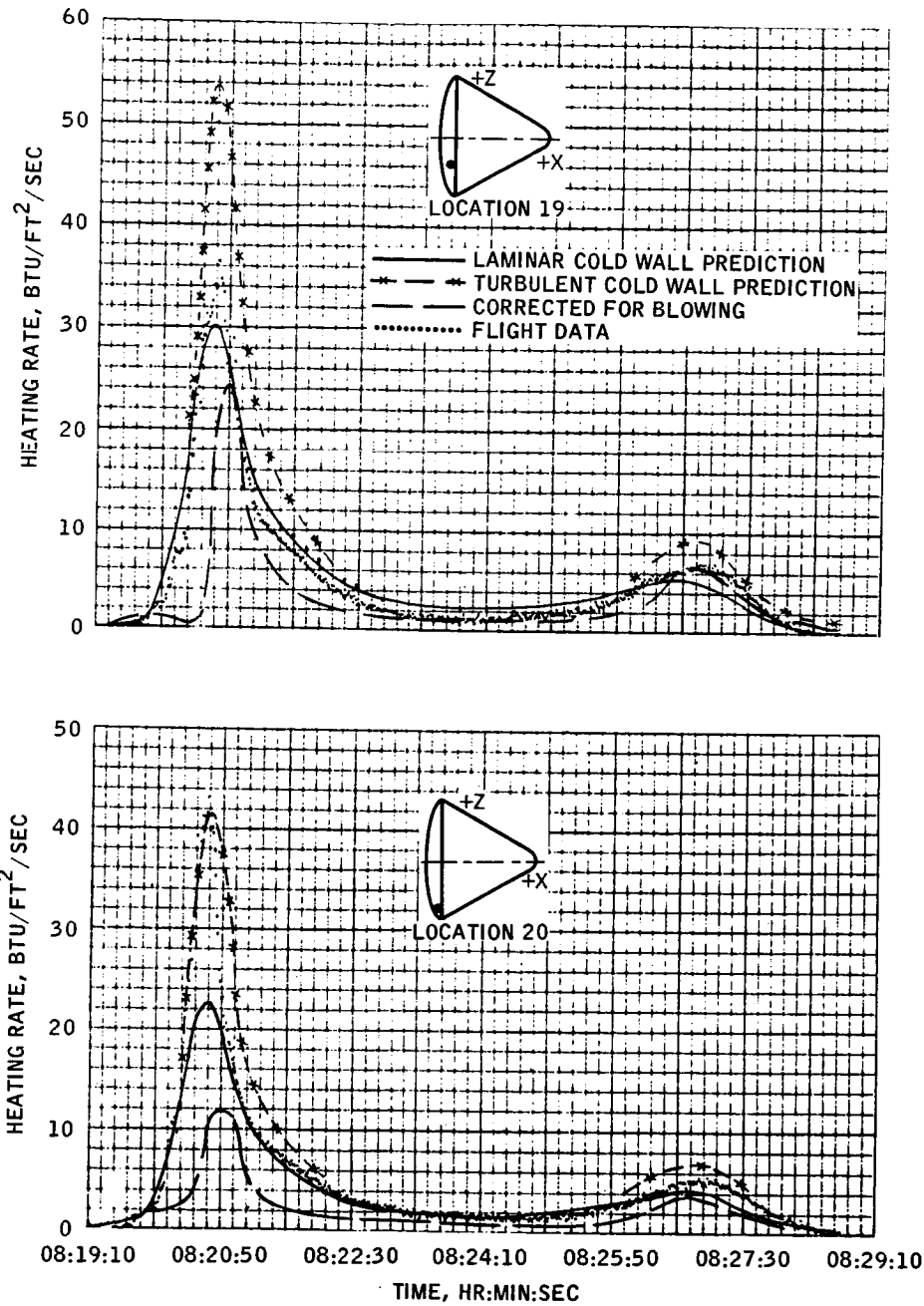
FIGURE 5.4-9.- CONTINUED.

~~CONFIDENTIAL~~

~~CONFIDENTIAL~~

5.4-51

NASA-S-68-391



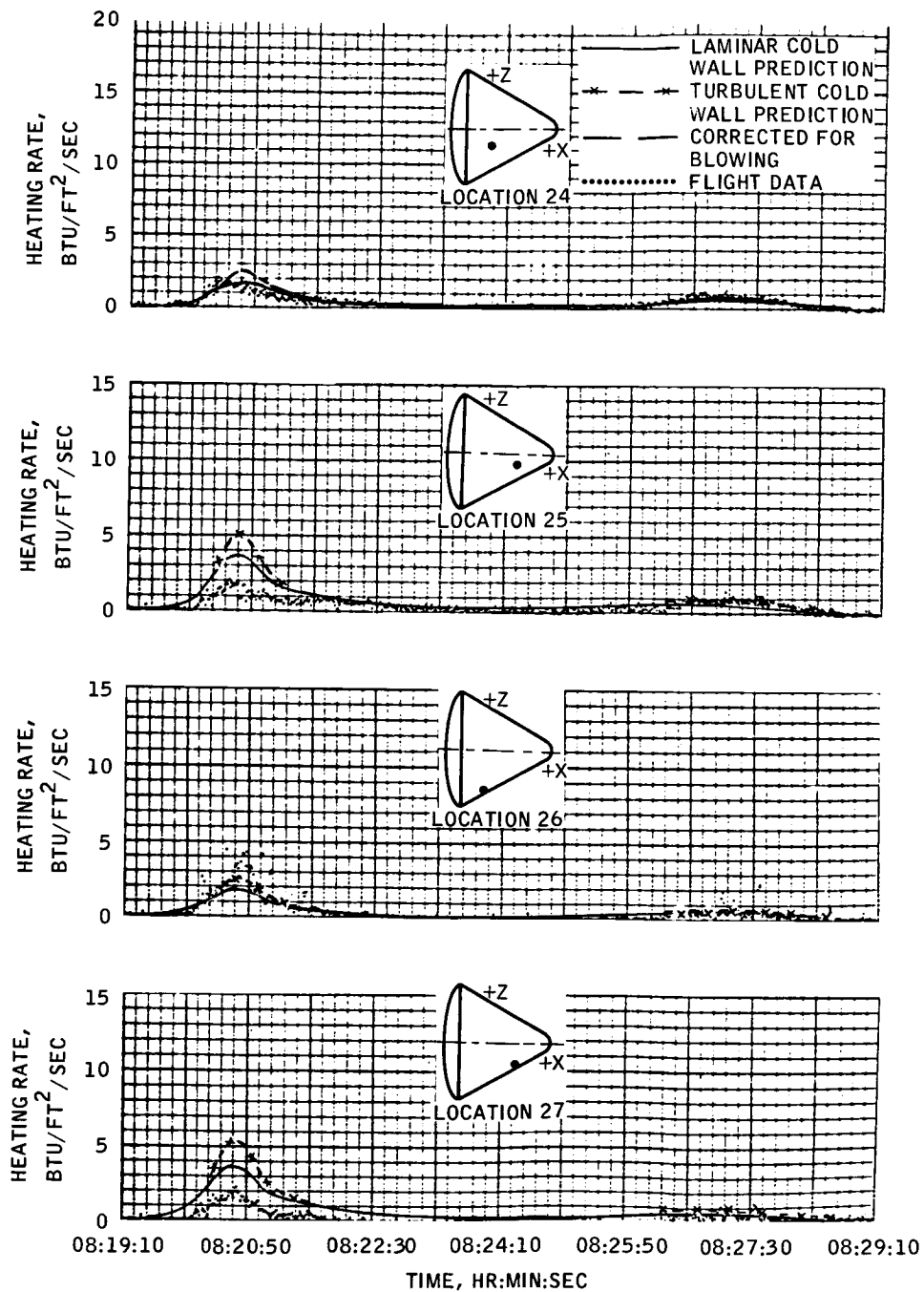
(D) LOCATIONS 19 AND 20.

FIGURE 5.4-9.- CONTINUED.

~~CONFIDENTIAL~~

~~CONFIDENTIAL~~

NASA-S-68-392



(E) LOCATIONS 24, 25, 26 AND 27.

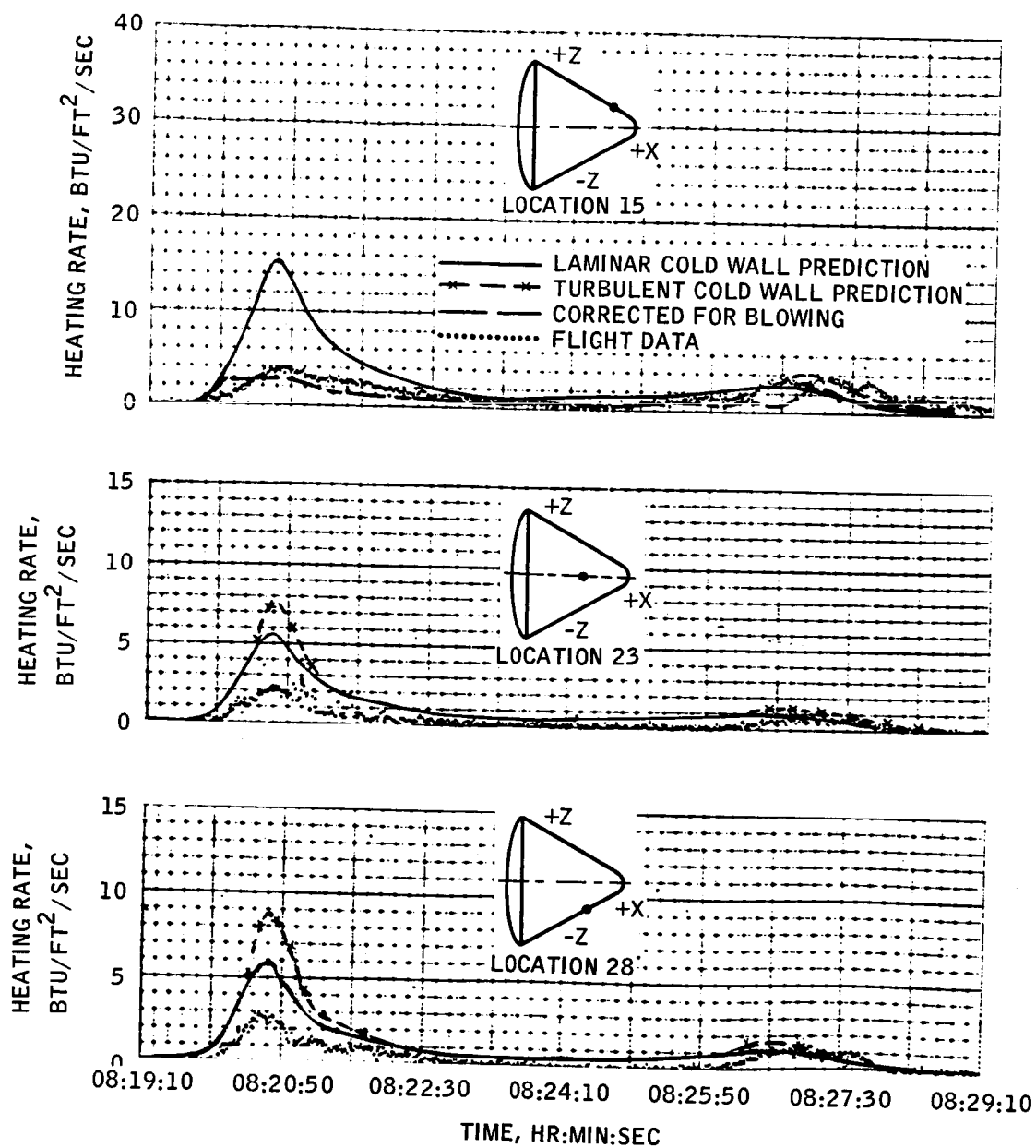
FIGURE 5.4-9.- CONTINUED.

~~CONFIDENTIAL~~

~~CONFIDENTIAL~~

5.4-53

NASA-S-68-393



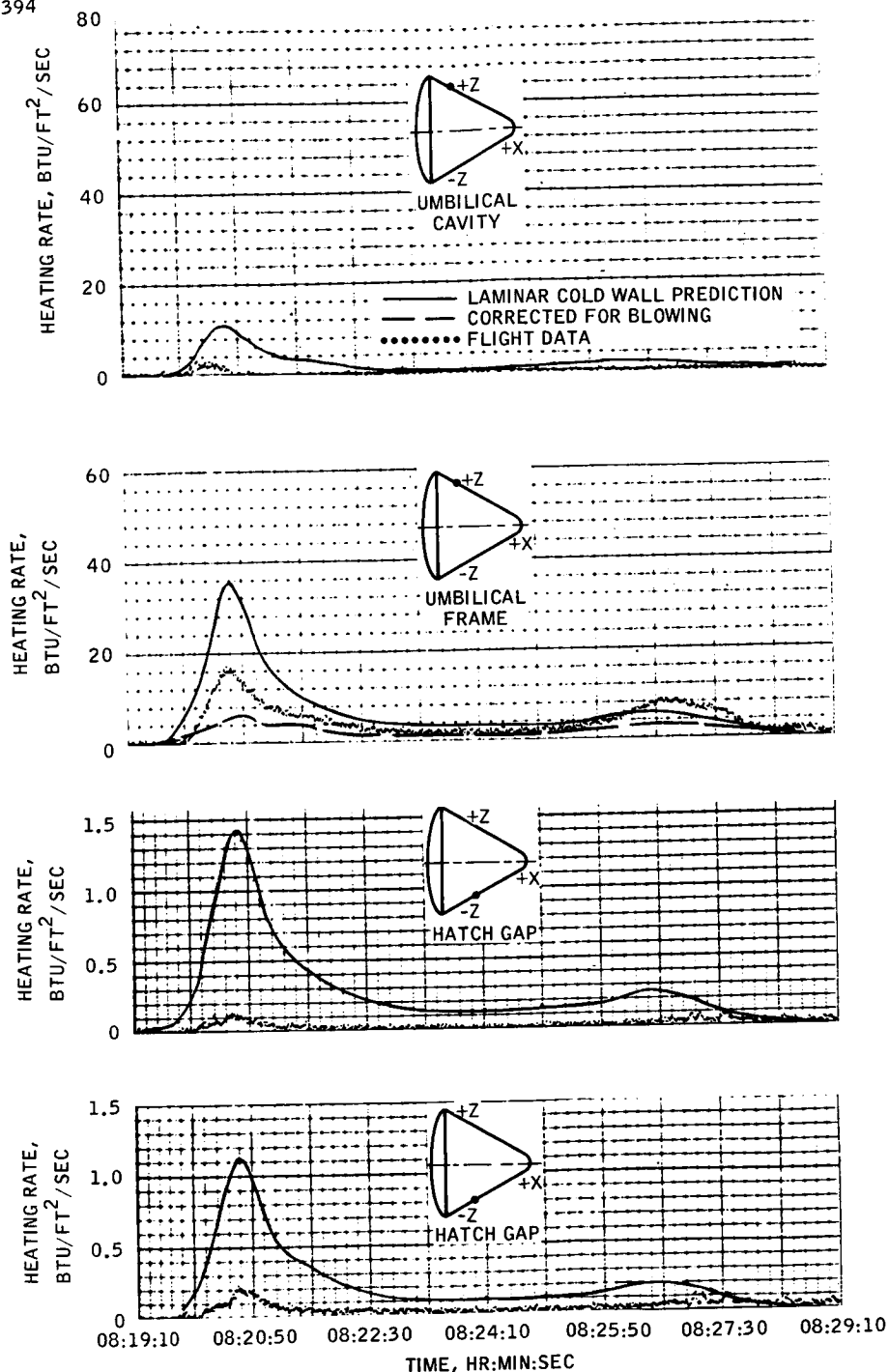
(F) LOCATIONS 15, 23 AND 28.

FIGURE 5.4-9.- CONTINUED.

~~CONFIDENTIAL~~

~~CONFIDENTIAL~~

NASA-S-68-394



(G) SINGULARITY LOCATIONS.

FIGURE 5.4-9.- CONCLUDED.

~~CONFIDENTIAL~~

~~CONFIDENTIAL~~

5.4-55

NASA-S-68-395

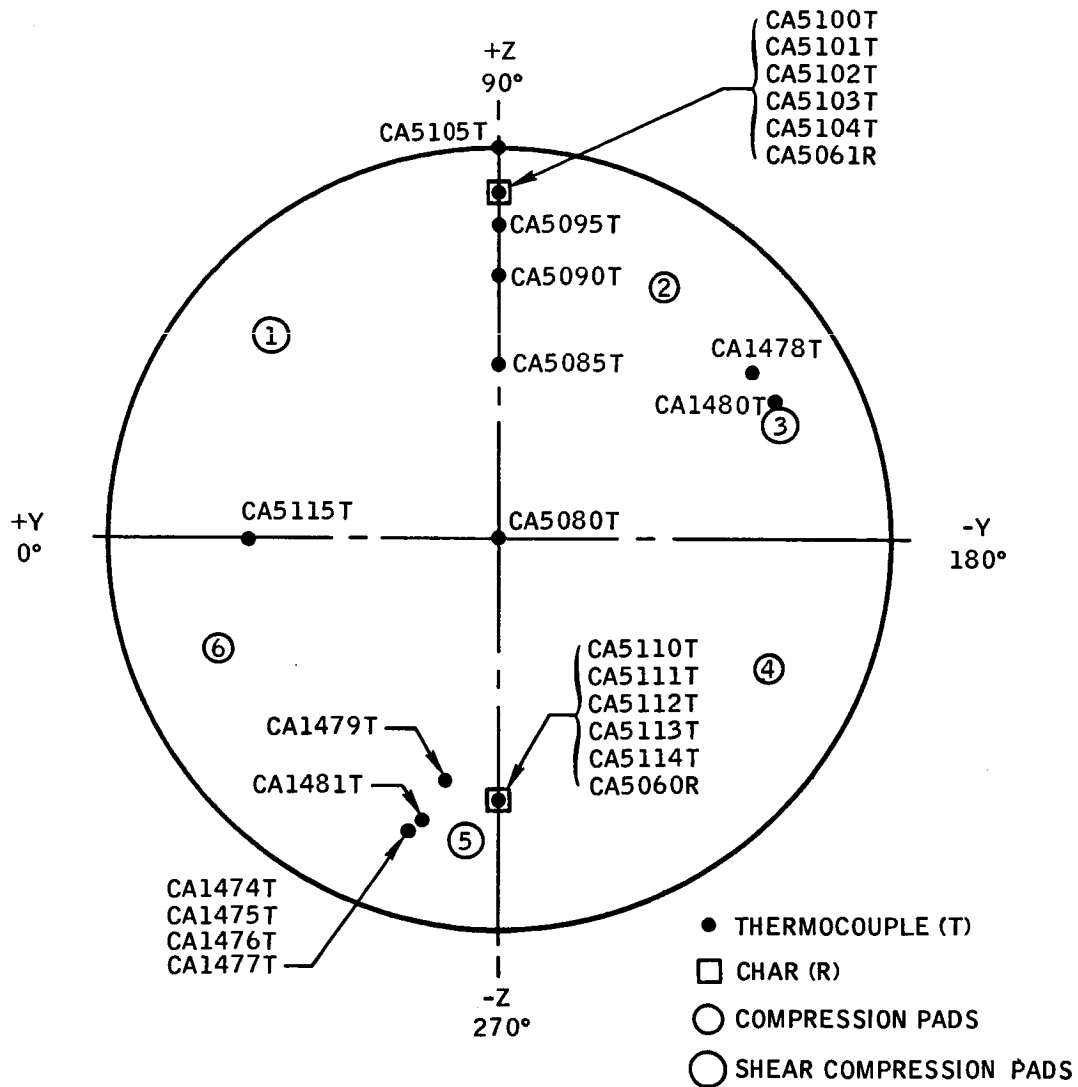


FIGURE 5.4-10.- AFT HEAT SHIELD ABLATOR TEMPERATURE AND CHAR MEASUREMENTS.

~~CONFIDENTIAL~~

~~CONFIDENTIAL~~

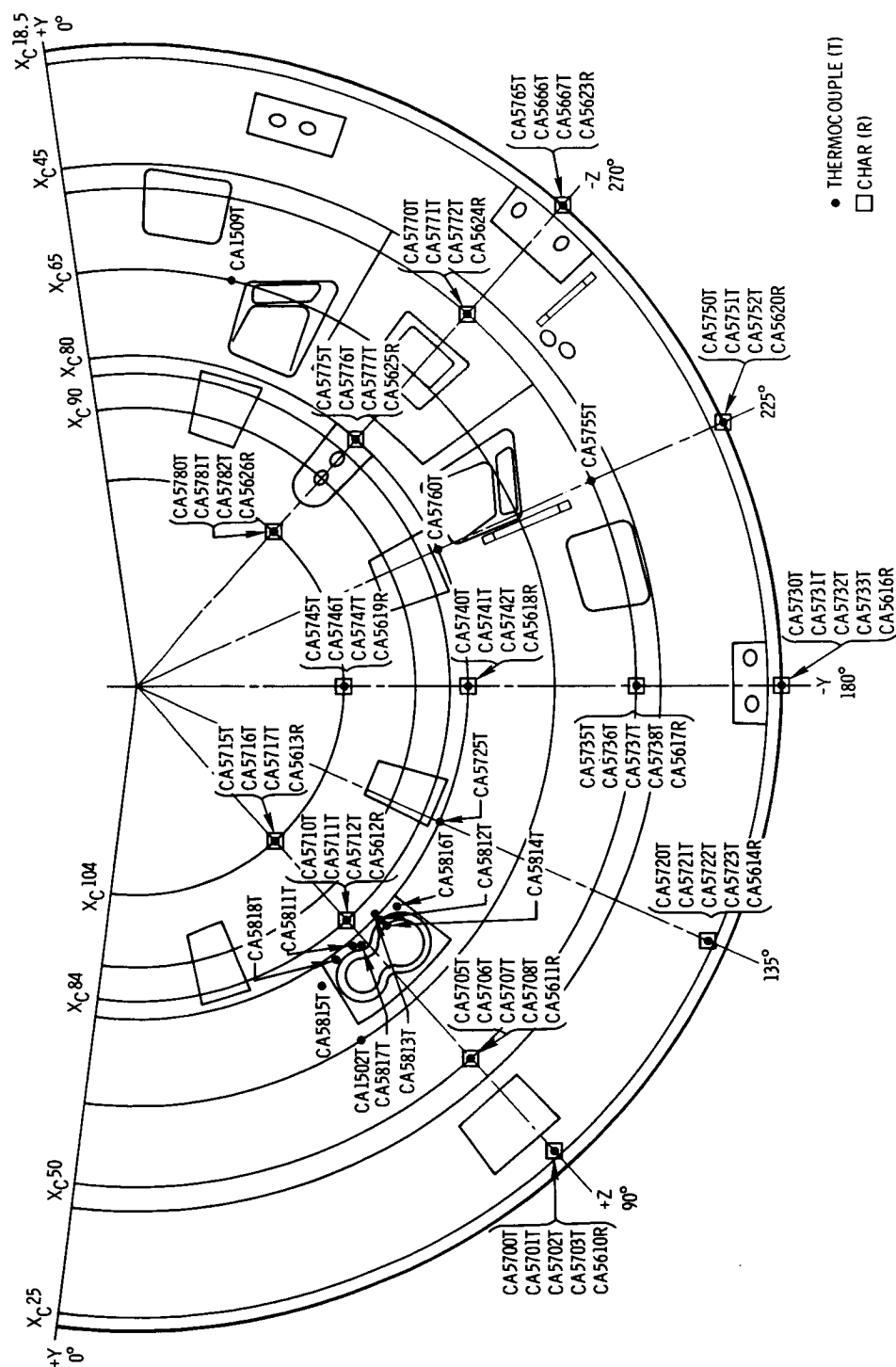


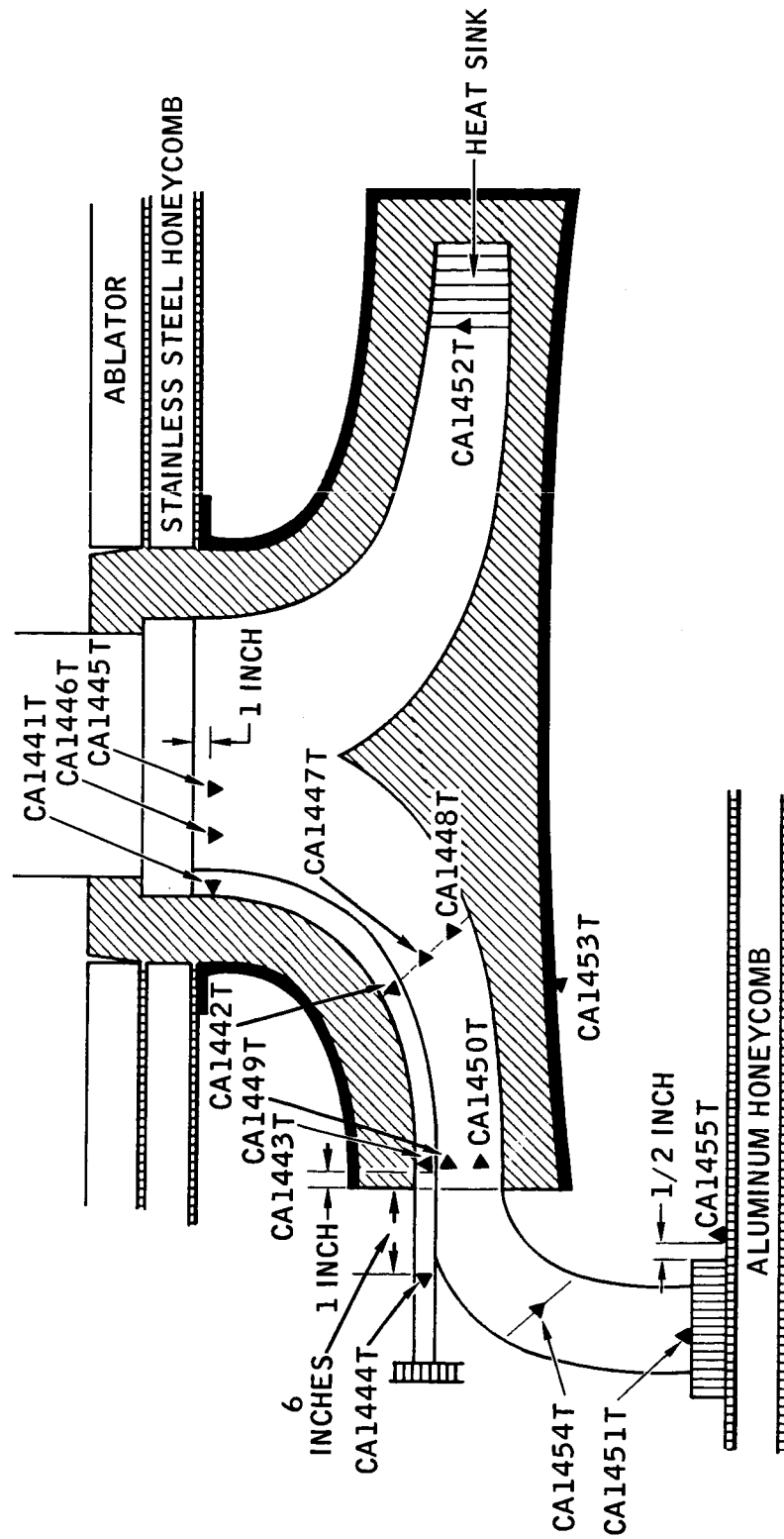
FIGURE 5.4-11. - CONICAL HEAT SHIELD ABLATOR AND ASTRO-SEXTANT AREA TEMPERATURE AND CHAR MEASUREMENTS.

~~CONFIDENTIAL~~



~~CONFIDENTIAL~~

5.4-57



(A) UMBILICAL.

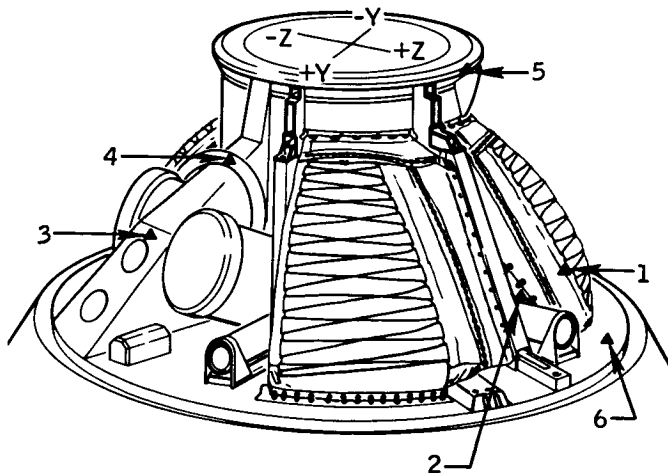
FIGURE 5.4-12.- MAJOR COMPONENT THERMODYNAMIC MEASUREMENT LOCATIONS.

~~CONFIDENTIAL~~

~~CONFIDENTIAL~~

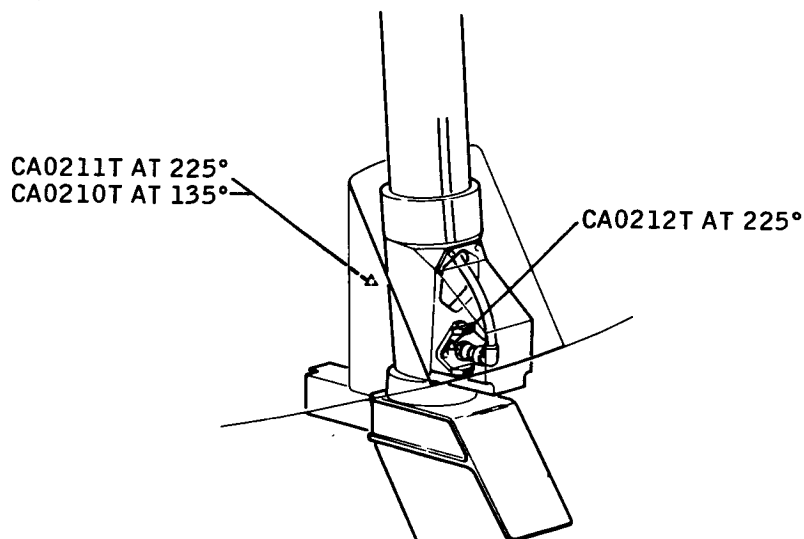
NASA-S-68-398

## LEGEND:



1. CA7762T, MAIN PARACHUTE  
6 INCHES ABOVE FORWARD  
DECK IN CENTER OF PARA-  
CHUTE CLOSEST TO +Z -AXIS
2. CA7760T, TOP OF PILOT  
MORTAR 3/4d FROM PLACE  
CLOSEST TO +Z -AXIS
3. CA7676T, UPPER SURFACE  
OF TOP RCS ENGINE MIDWAY
4. CA7761T, PARACHUTE HAR-  
NESS WHERE IT CROSSES  
OVER RCS ENGINE WEB SUP-  
PORT INSIDE DACRON WRAPPIN(C)
5. CA7674T, UPPER  
TUNNEL RING
6. CA7675T, FORWARD BULK-  
HEAD +Z -AXIS 1 INCH FROM  
EDGE

(B) PARACHUTE COMPARTMENT.



(C) LAUNCH ESCAPE SYSTEM TOWER WELL AND DISCONNECT.

FIGURE 5.4-12.- CONTINUED.

~~CONFIDENTIAL~~

~~CONFIDENTIAL~~

5.4-59

NASA-S-68-399

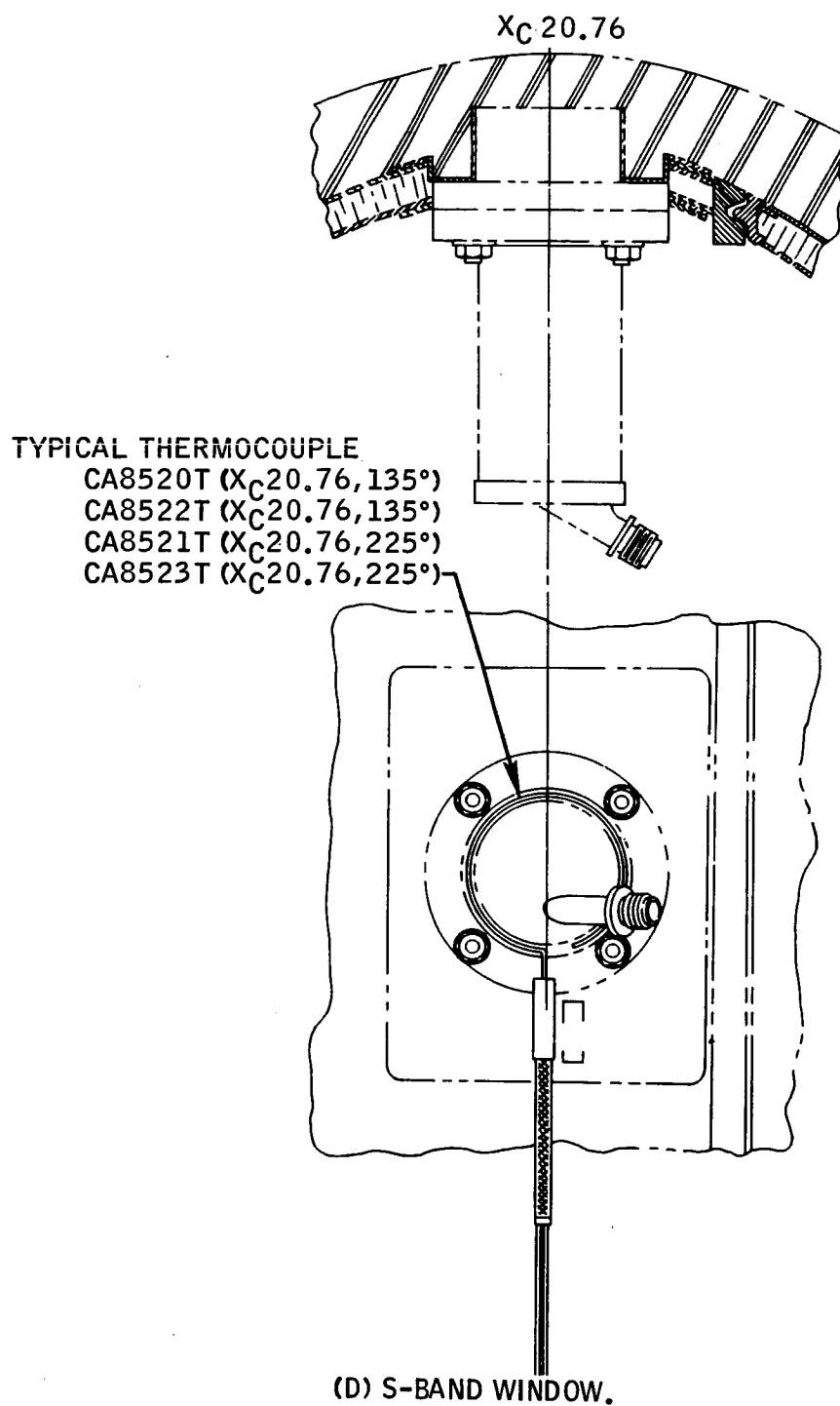
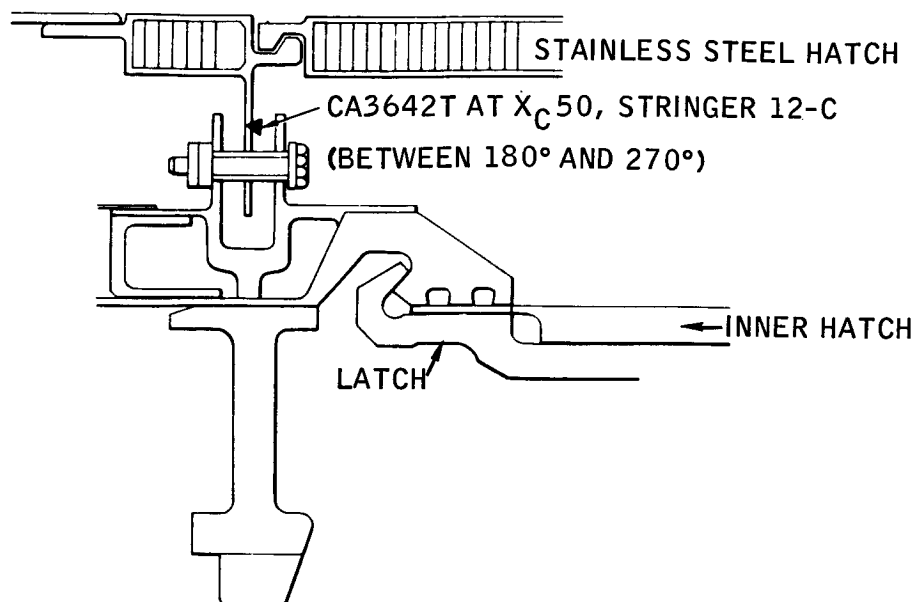


FIGURE 5.4-12.- CONTINUED.

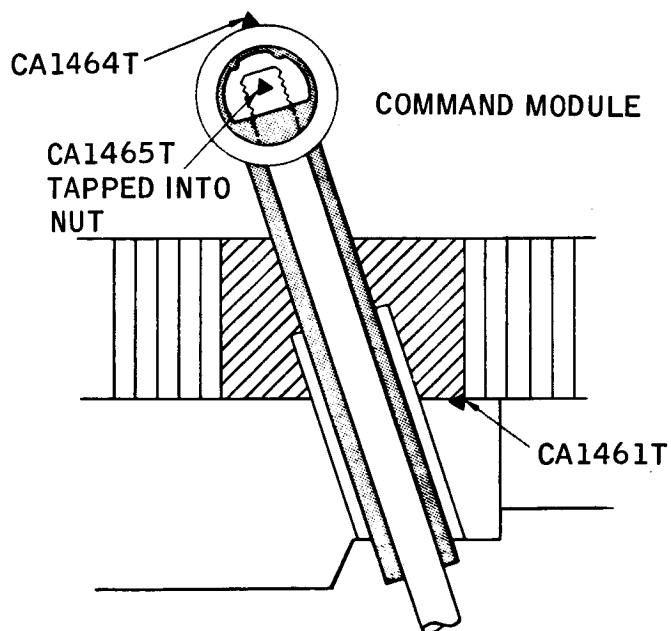
~~CONFIDENTIAL~~

~~CONFIDENTIAL~~

NASA-S-68-400

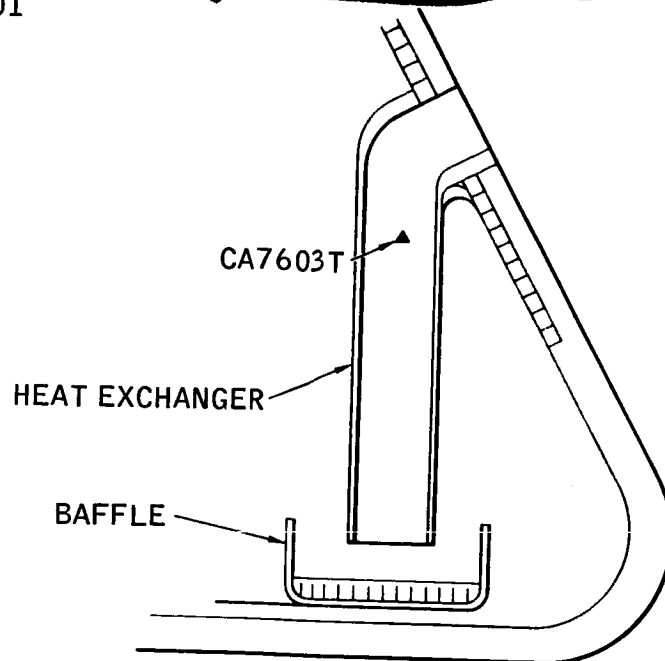


(E) CREW COMPARTMENT (HATCH STRINGER 12-C).

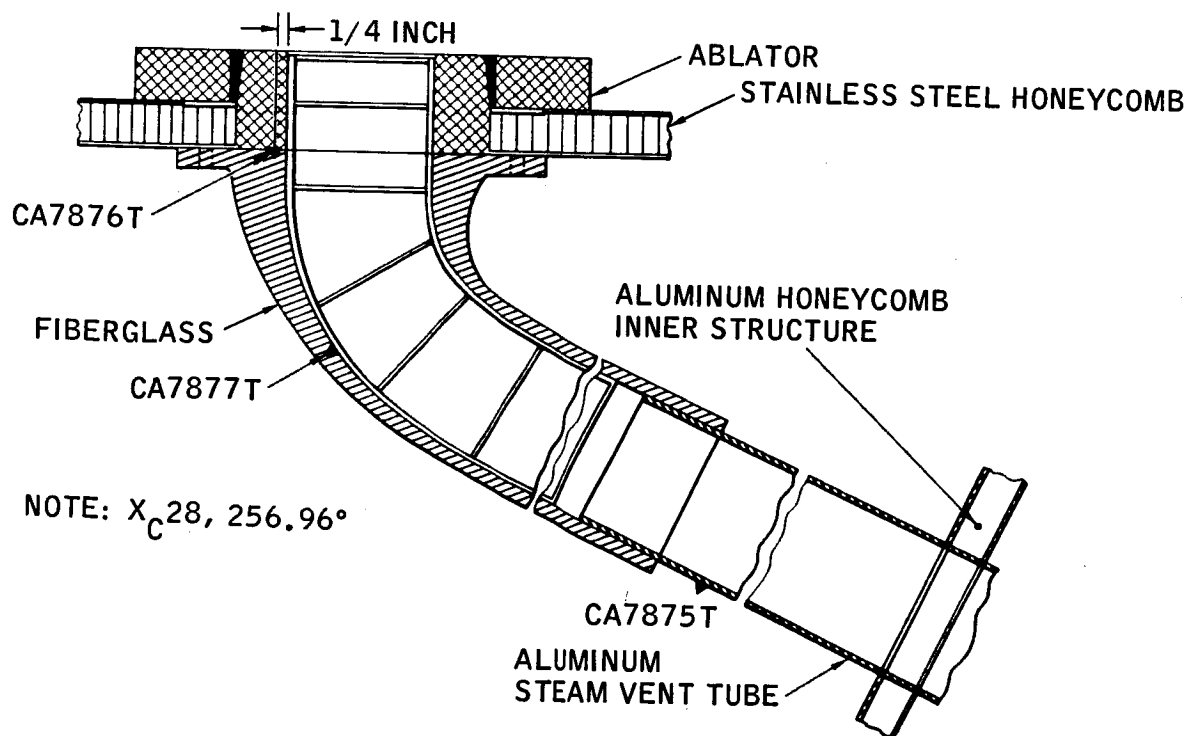
(F) AFT HEAT SHIELD (TENSION TIE 1).  
FIGURE 5.4-12.- CONTINUED.~~CONFIDENTIAL~~

~~CONFIDENTIAL~~

5.4-61



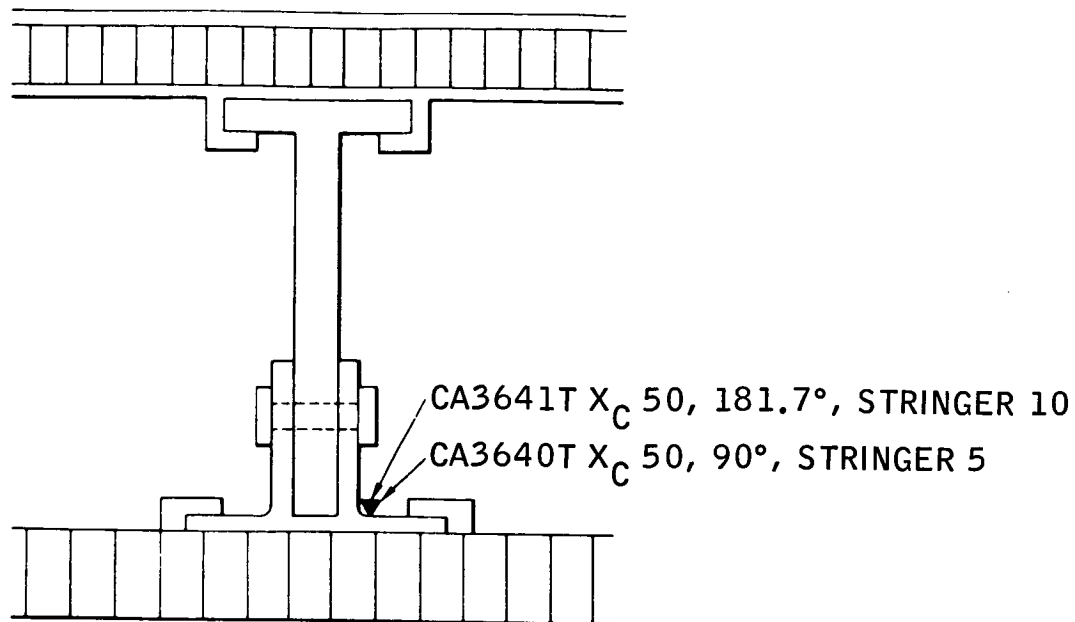
(G) COMMAND MODULE AIR VENT.



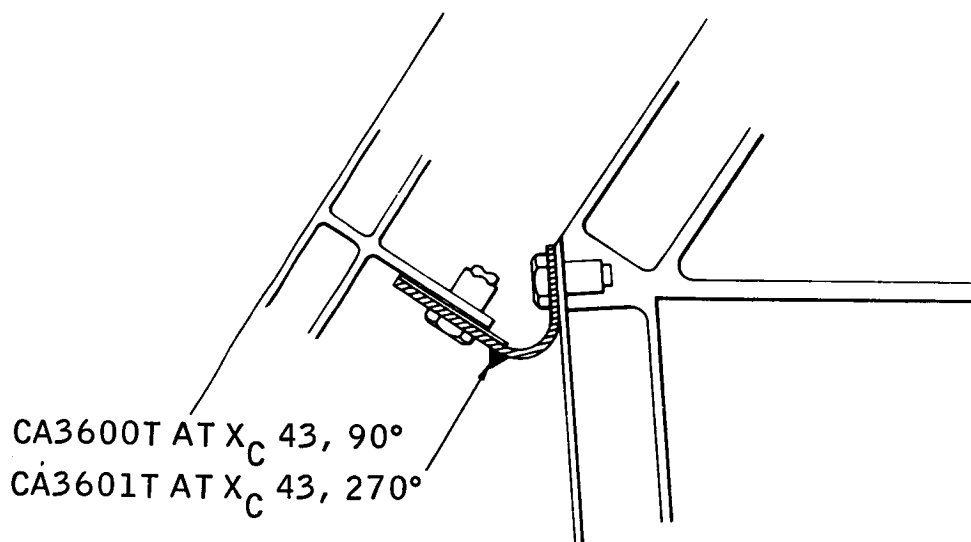
(H) STEAM VENT.

FIGURE 5.4-12.- CONTINUED.

~~CONFIDENTIAL~~

~~CONFIDENTIAL~~

(I) COMMAND MODULE STRINGER.



(J) SIDEWALL HEAT SHIELD ATTACHMENT.

FIGURE 5.4-12.- CONTINUED.

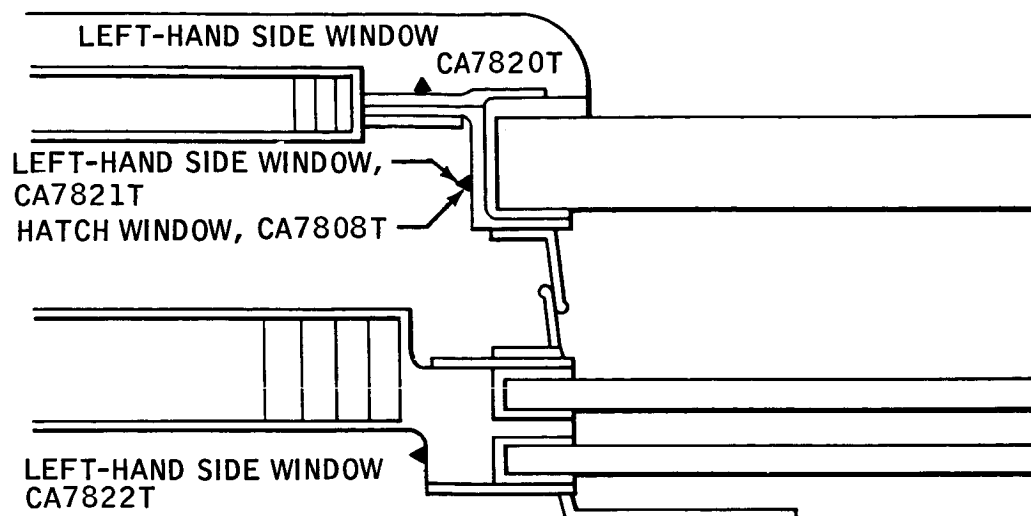
~~CONFIDENTIAL~~

~~CONFIDENTIAL~~

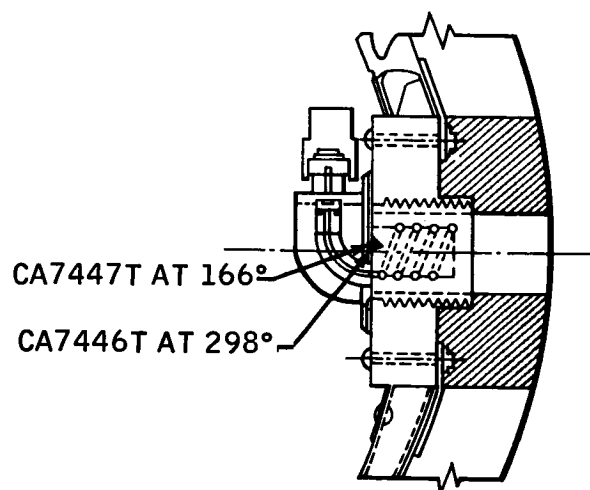
5.4-63

NASA-S-68-403

WINDOWS BETWEEN 180° AND 270°



(K) COMMAND MODULE WINDOW.



(L) C-BAND ANTENNA.

FIGURE 5.4-12.- CONCLUDED.

~~CONFIDENTIAL~~

5.4-64

~~CONFIDENTIAL~~

NASA-S-68-404

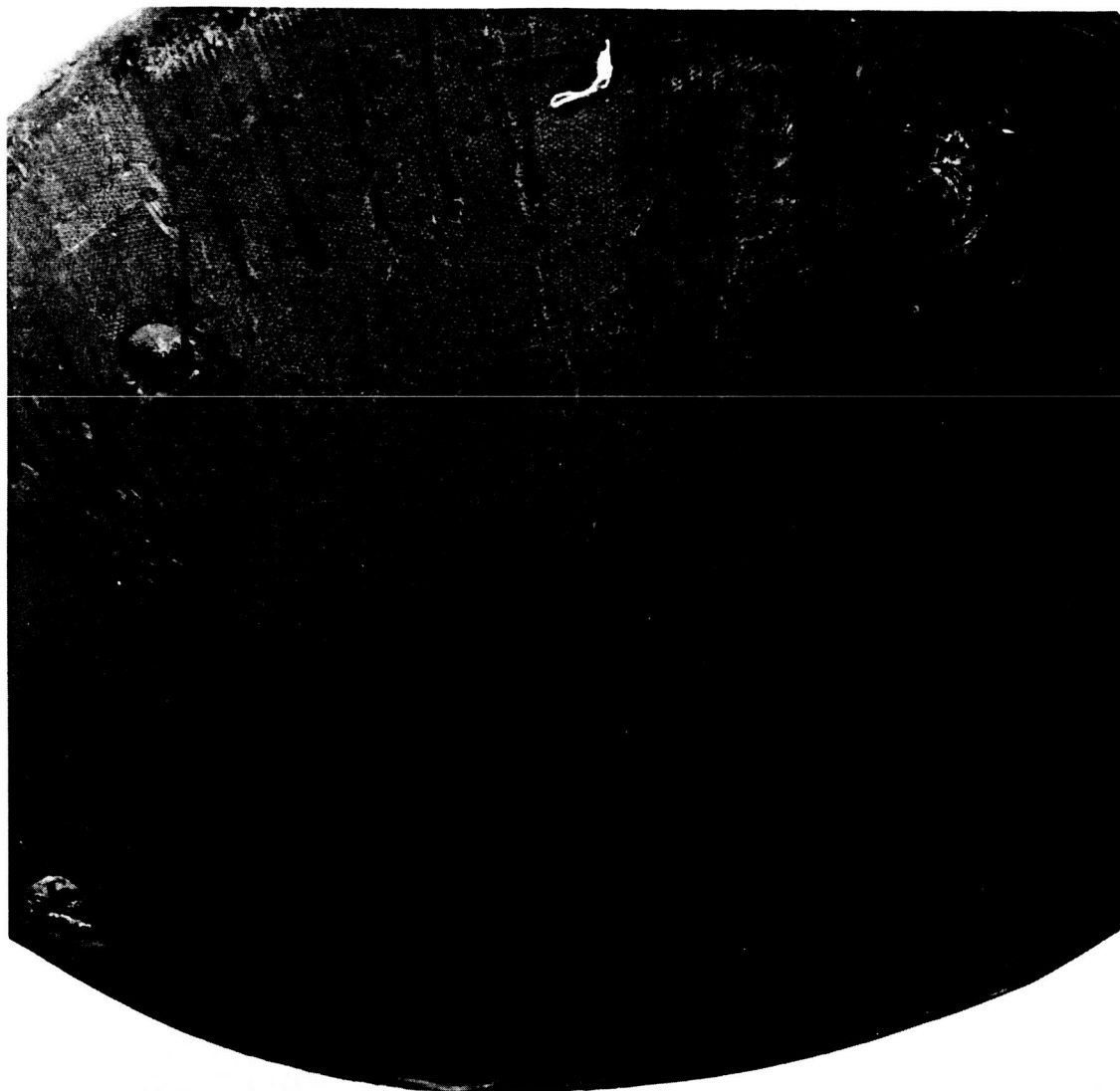


FIGURE 5.4-13.- POSTFLIGHT PHOTOGRAPH SHOWING CHAR CONDITION  
OF AFT HEAT SHIELD.

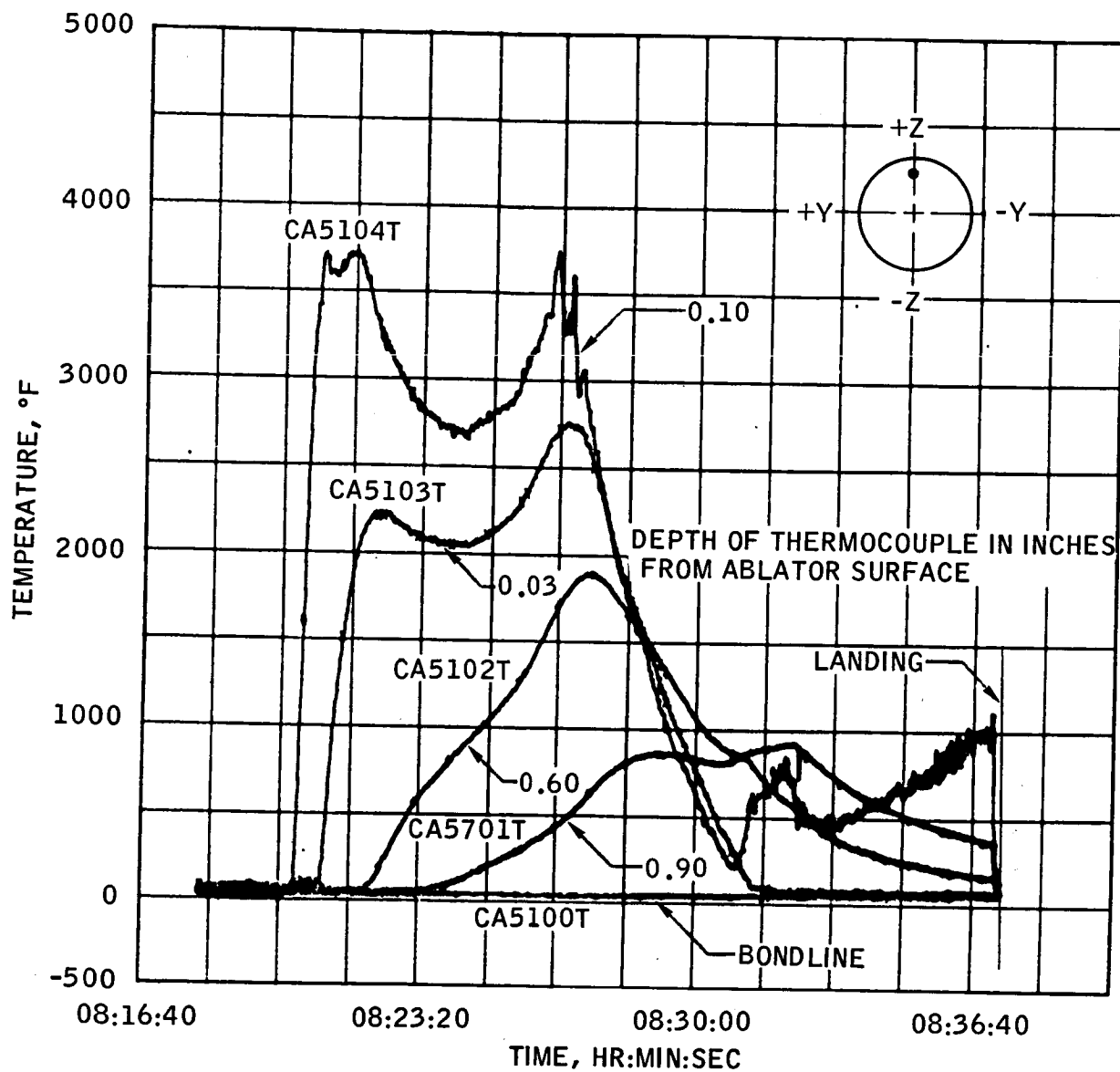
~~CONFIDENTIAL~~



~~CONFIDENTIAL~~

5.4-65

NASA-S-68-405



(A) STATION  $Z = +71.82$ ,  $Y = 0$ .

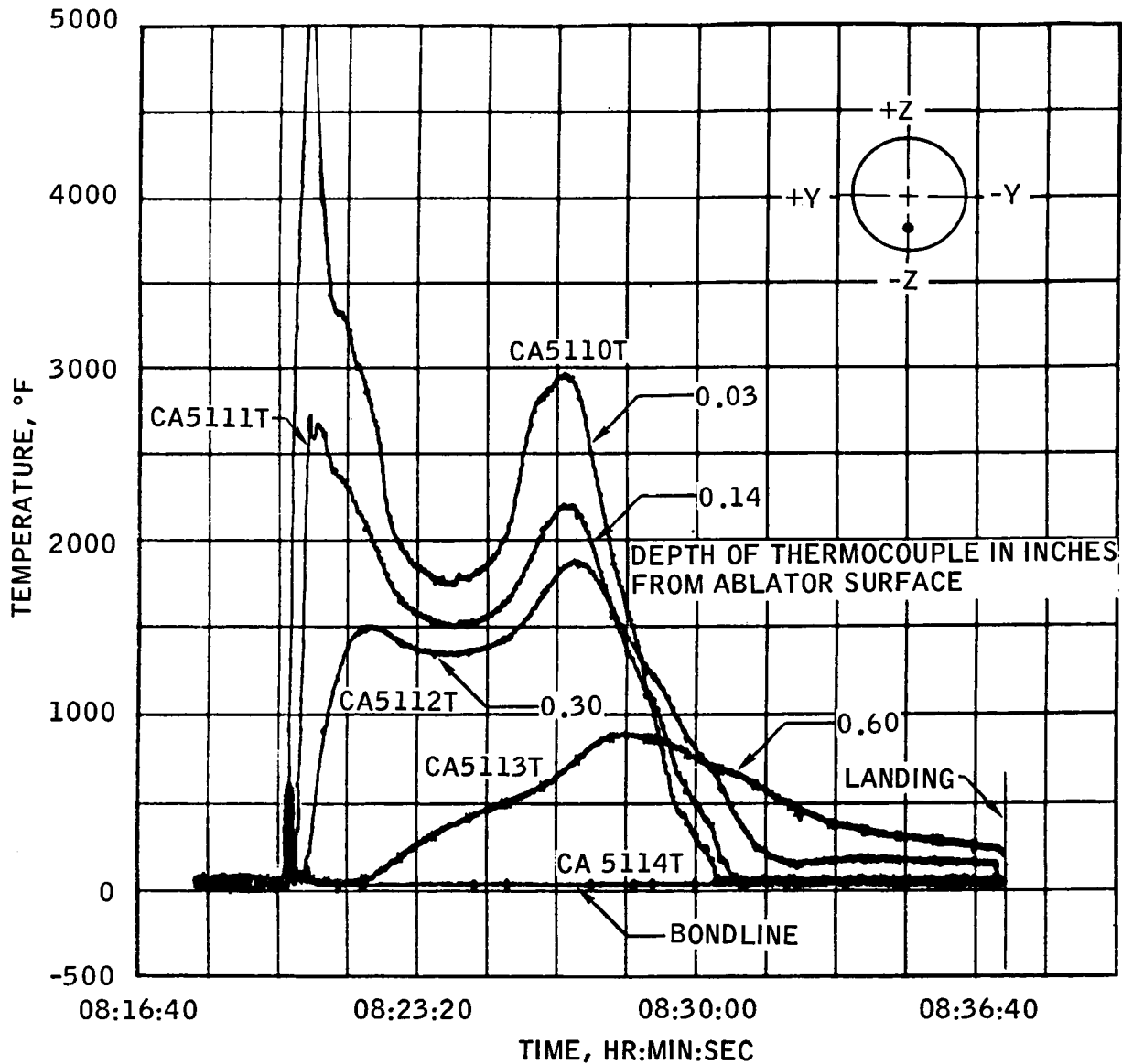
FIGURE 5.4-14.- AFT HEAT SHIELD TEMPERATURE MEASUREMENTS AT DEPTHS INDICATED.

~~CONFIDENTIAL~~

5.4-66

~~CONFIDENTIAL~~

NASA-S-68-406



(B) STATION Z= -50.0, Y= -1.99.

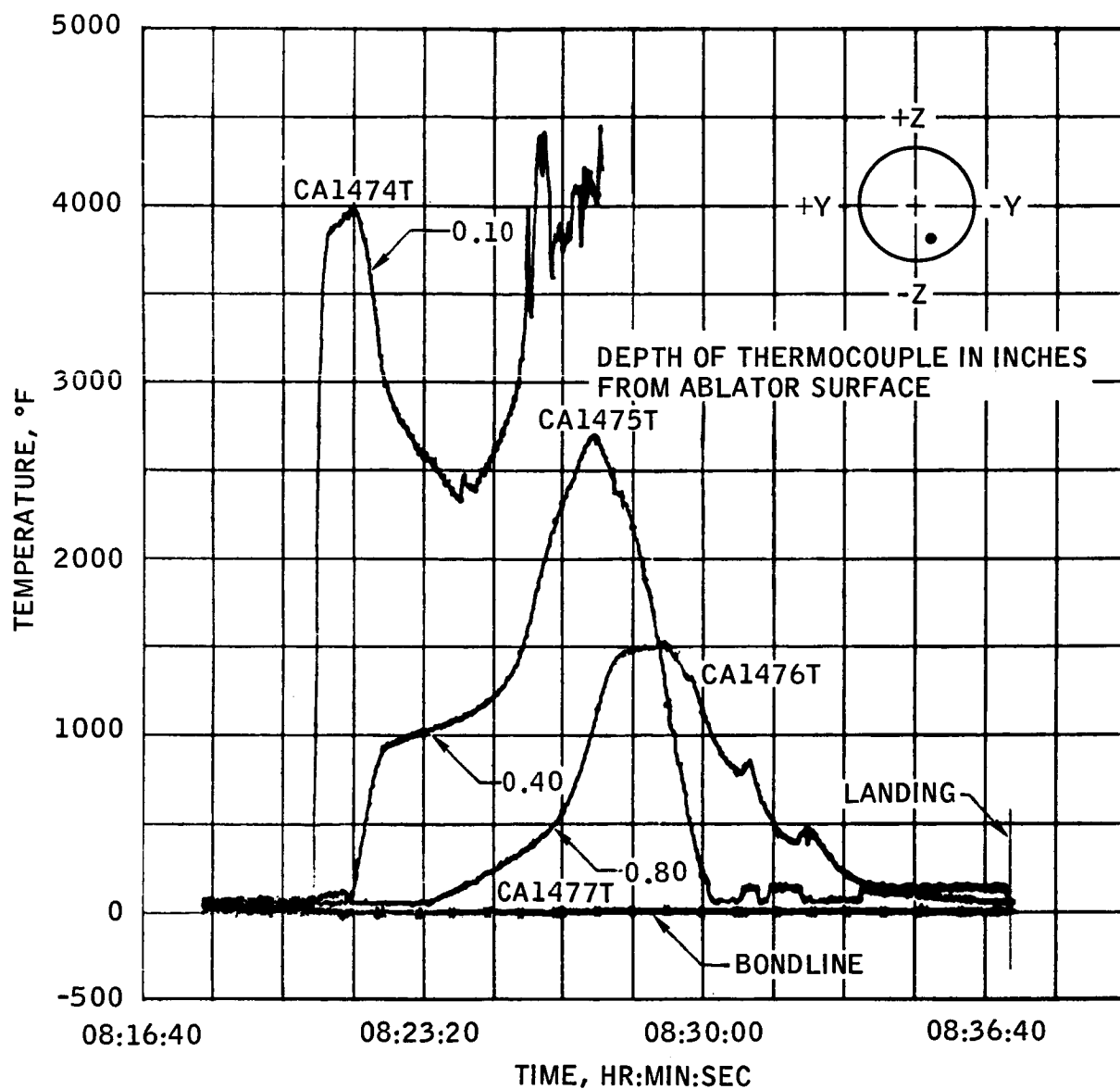
FIGURE 5.4-14.- CONTINUED.

~~CONFIDENTIAL~~

~~CONFIDENTIAL~~

5.4-67

NASA-S-68-407



(C) STATION Z= -64.85, Y= -14.68.

FIGURE 5.4-14.- CONCLUDED.

~~CONFIDENTIAL~~

~~CONFIDENTIAL~~

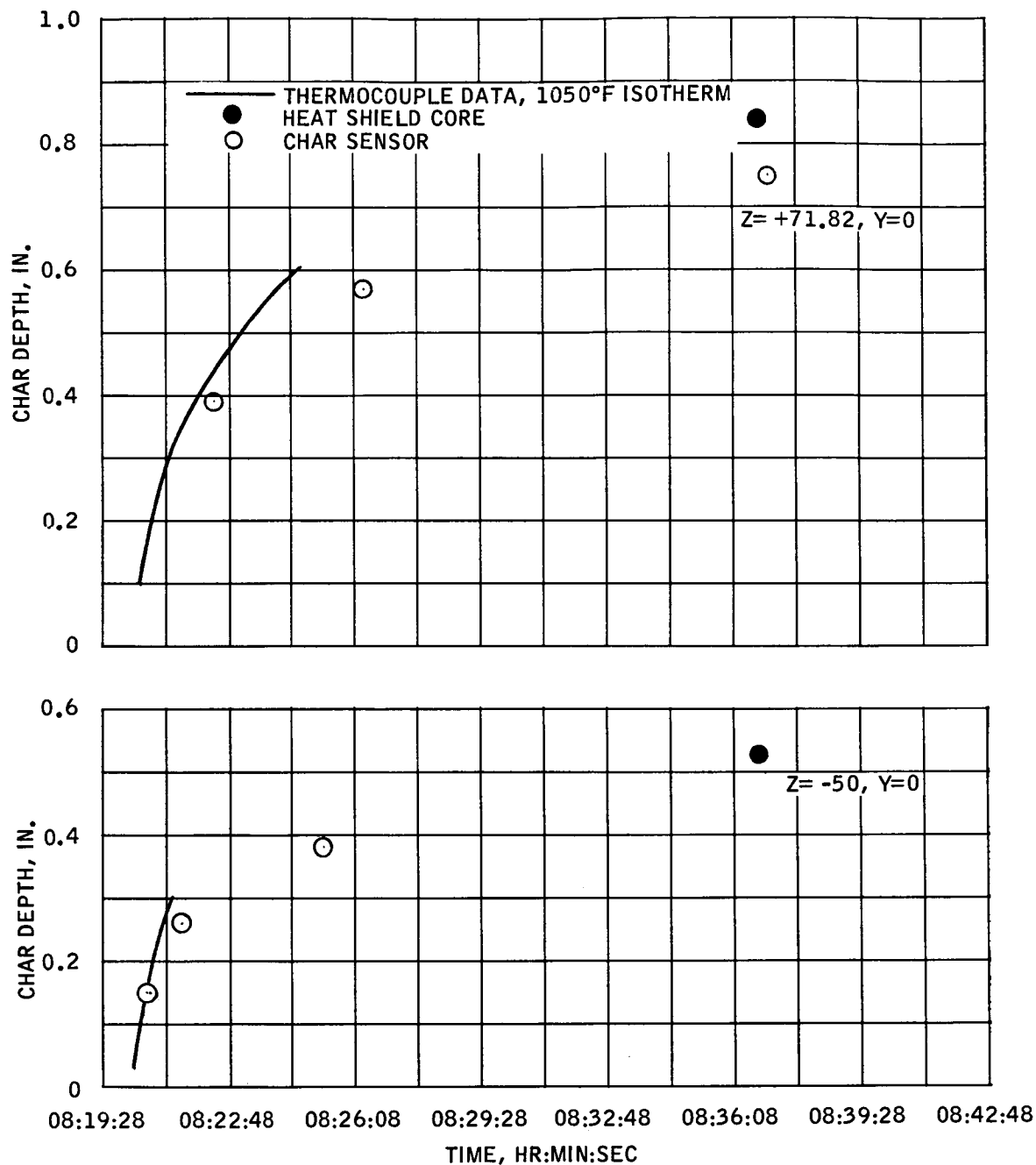


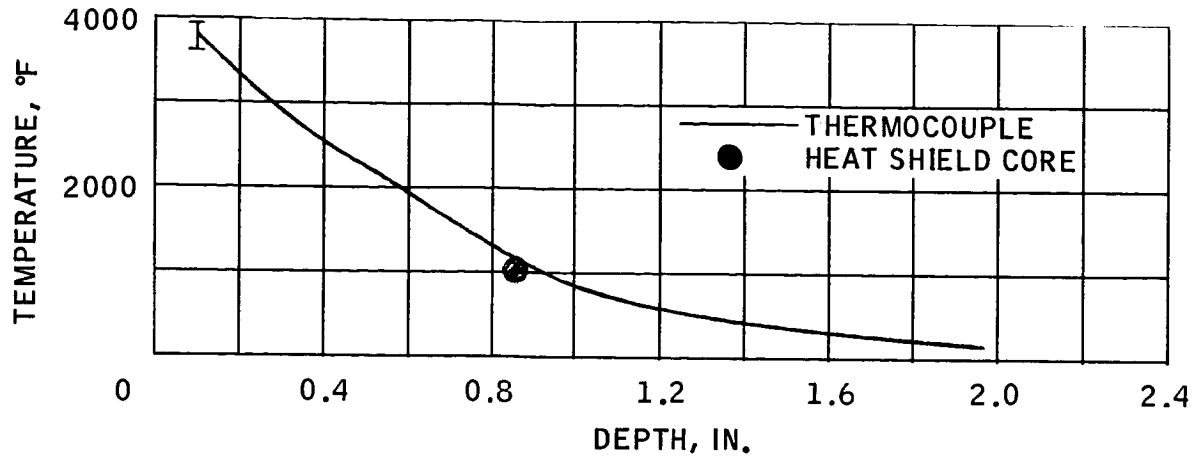
FIGURE 5.4-15.- AFT HEAT SHIELD 1050°F ISOTHERM COMPARISON  
WITH CHAR SENSOR AND CORE CHAR.

~~CONFIDENTIAL~~

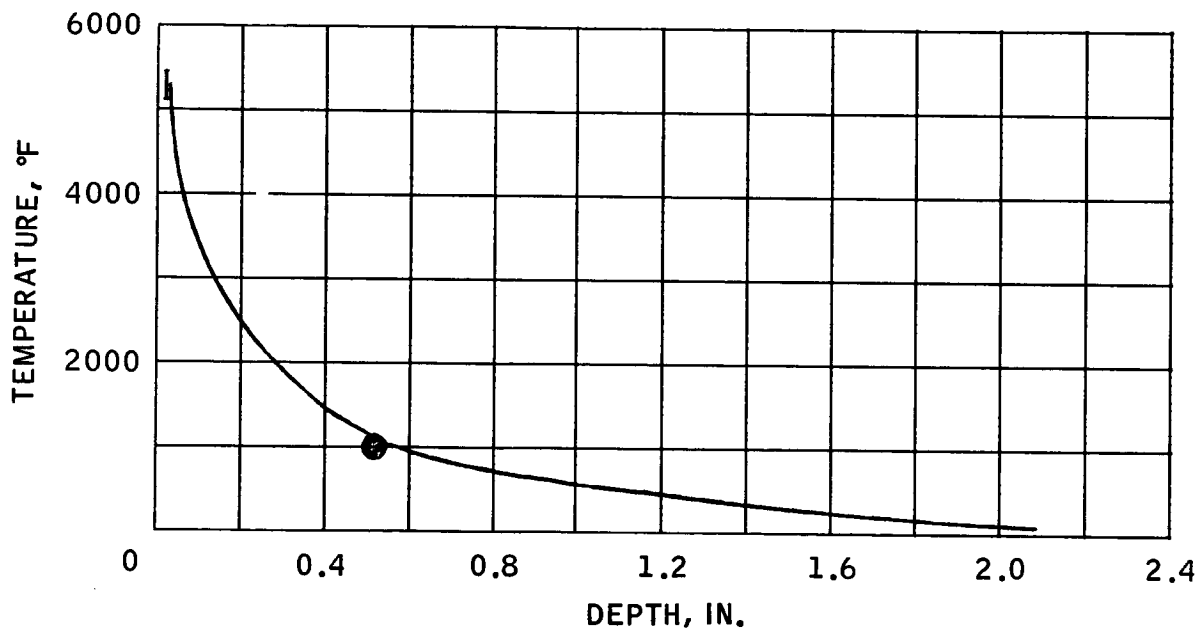
~~CONFIDENTIAL~~

5.4-69

NASA-S-68-409



(A)  $Y=0, Z=+71.82.$



(B)  $Y=0, Z=+50.$

FIGURE 5.4-16.- MAXIMUM TEMPERATURE MEASURED IN DEPTH AND COMPARISON OF CHAR INTERFACE WITH 1050°F ISOTHERM.

~~CONFIDENTIAL~~

~~CONFIDENTIAL~~

NASA-S-68-410



FIGURE 5.4-17.- POSTFLIGHT PHOTOGRAPH SHOWING DETAILS OF  
TYPICAL SHEAR COMPRESSION PAD, LOCATED AT  $\theta = 152^{\circ}45'$ .

~~CONFIDENTIAL~~

~~CONFIDENTIAL~~

5.4-71

NASA-S-68-411

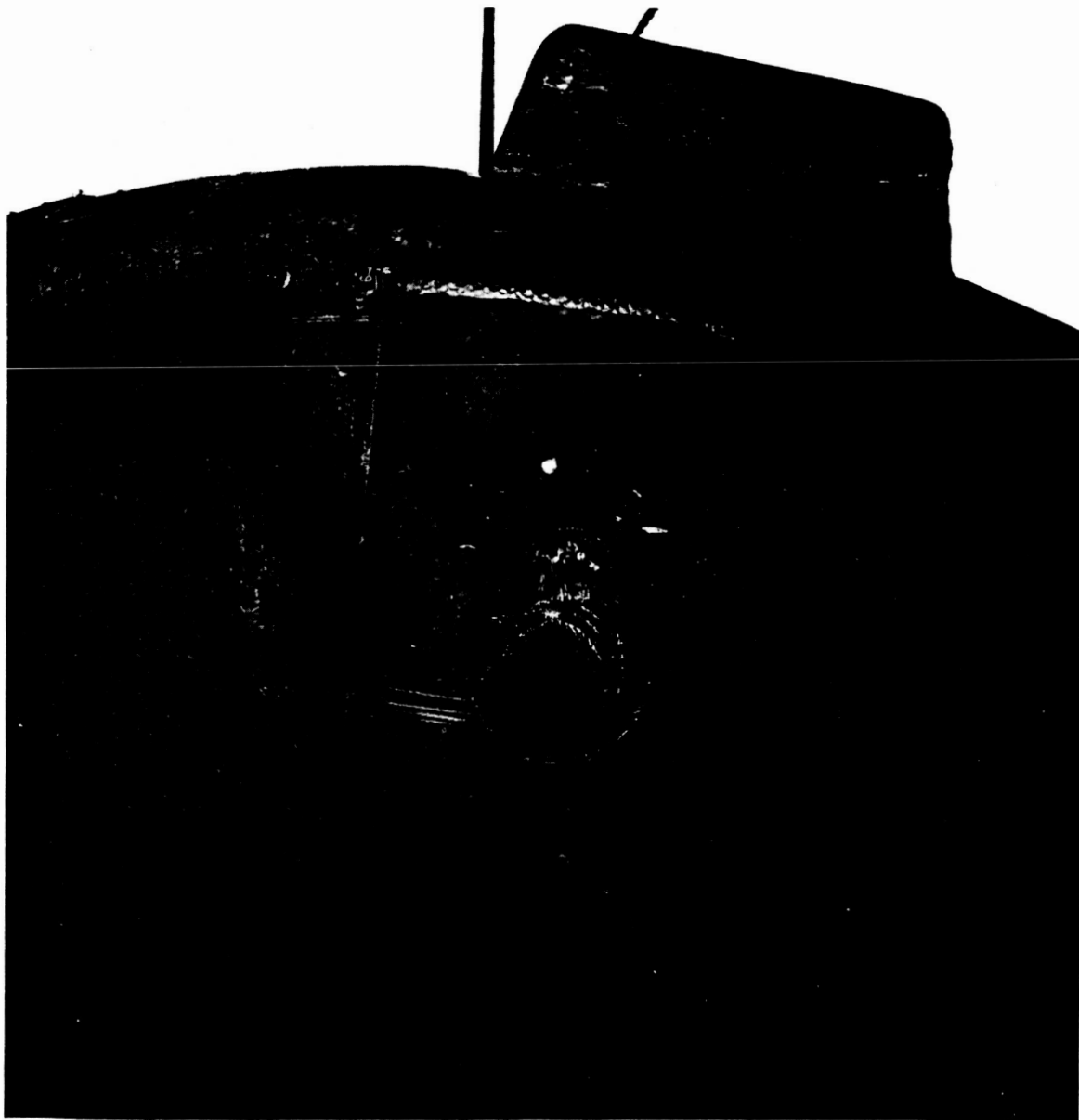


FIGURE 5.4-18.- POSTFLIGHT PHOTOGRAPH SHOWING CHAR  
CONDITION OF UMBILICAL RAMP.

~~CONFIDENTIAL~~

~~CONFIDENTIAL~~

NASA-S-68-412

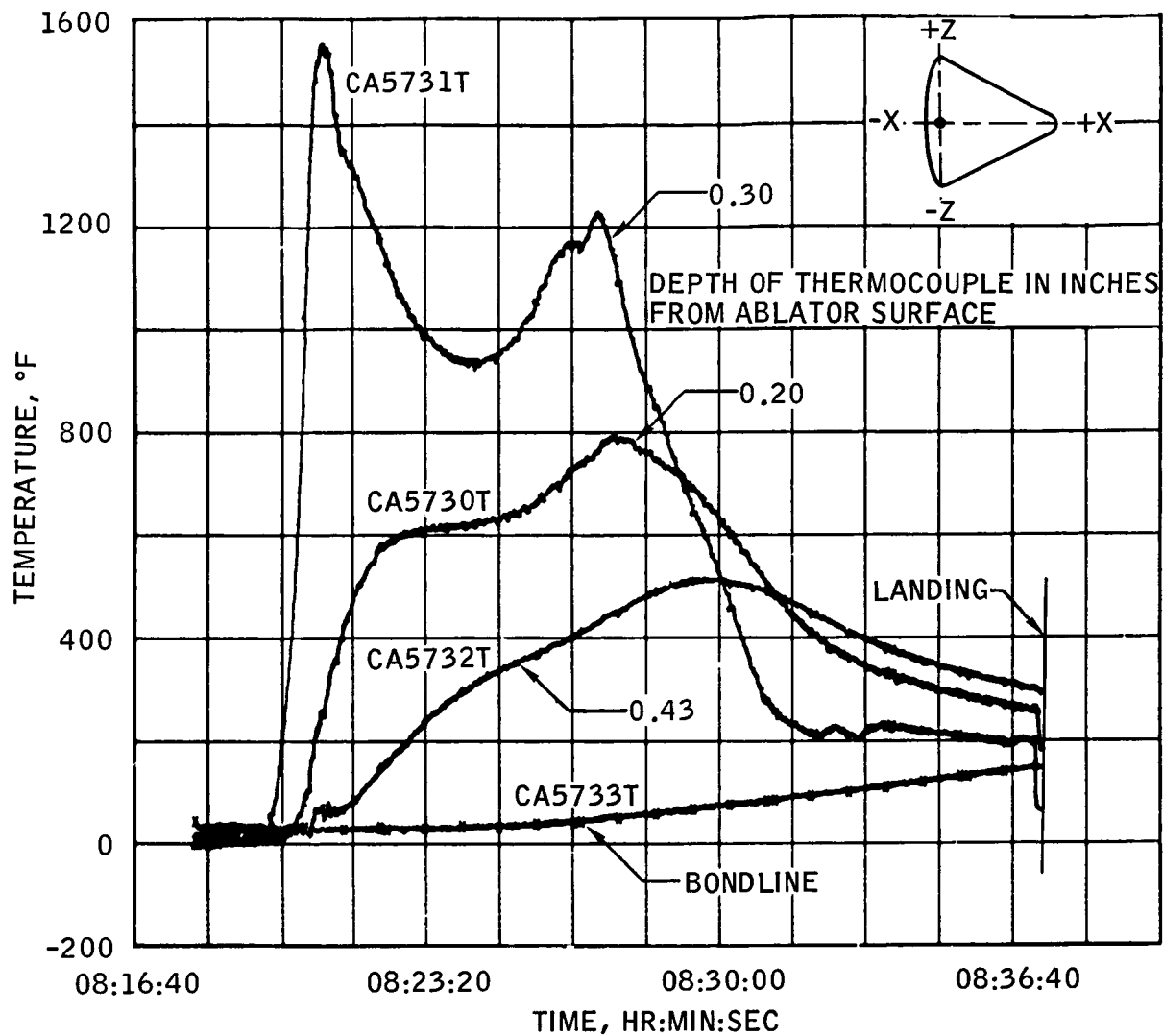
(A) STATION  $X_c = 18.5$ ,  $\theta = 180^\circ$ .

FIGURE 5.4-19.- TOROIDAL HEAT SHIELD TEMPERATURE MEASUREMENTS AT DEPTHS INDICATED.

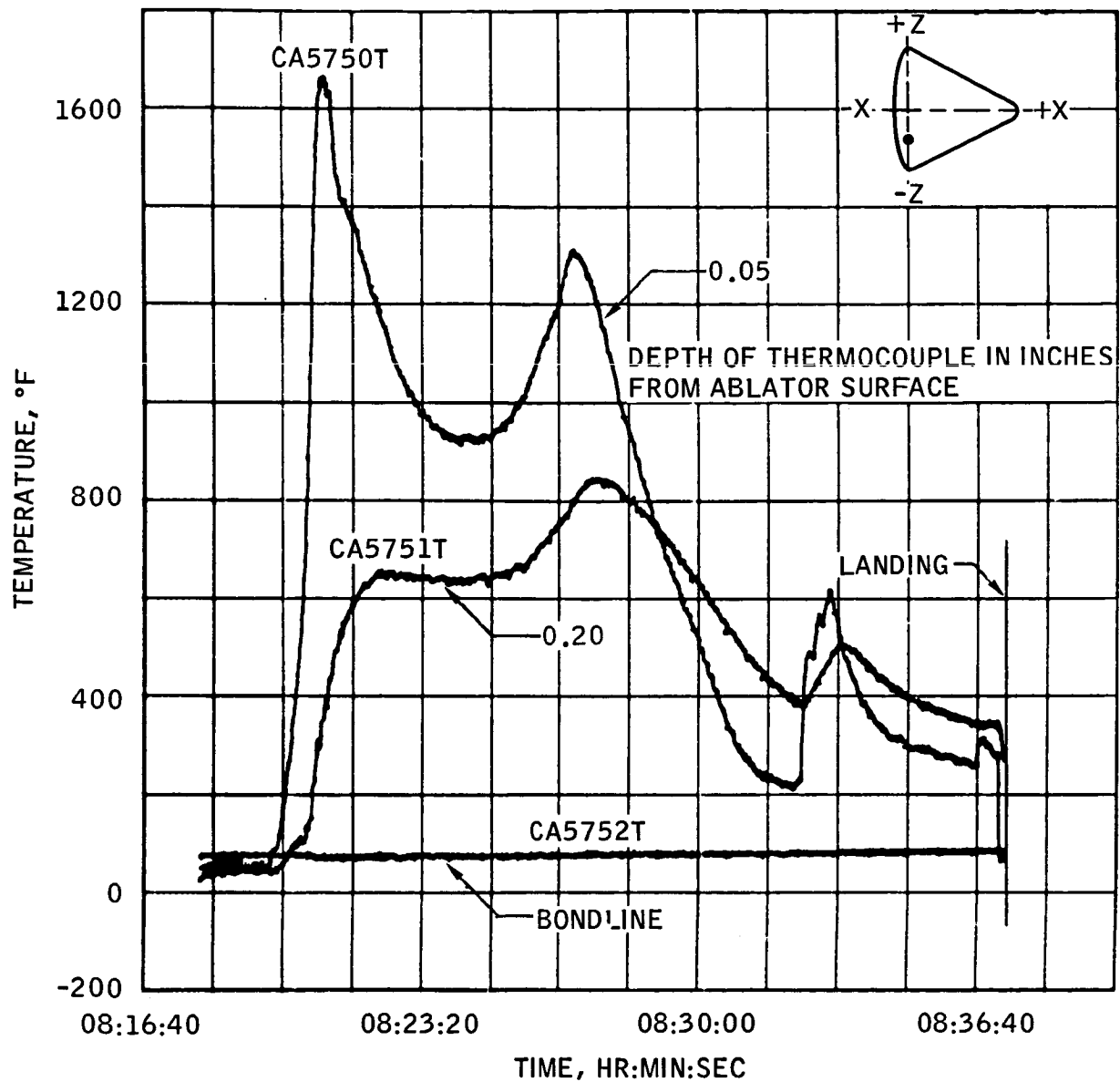
~~CONFIDENTIAL~~



~~CONFIDENTIAL~~

5.4-73

NASA-S-68-413



(B) STATION  $X_C = 18.5$ ,  $\theta = 225^\circ$ .

FIGURE 5.4-19.- CONTINUED.

~~CONFIDENTIAL~~

~~CONFIDENTIAL~~

NASA-S-68-414

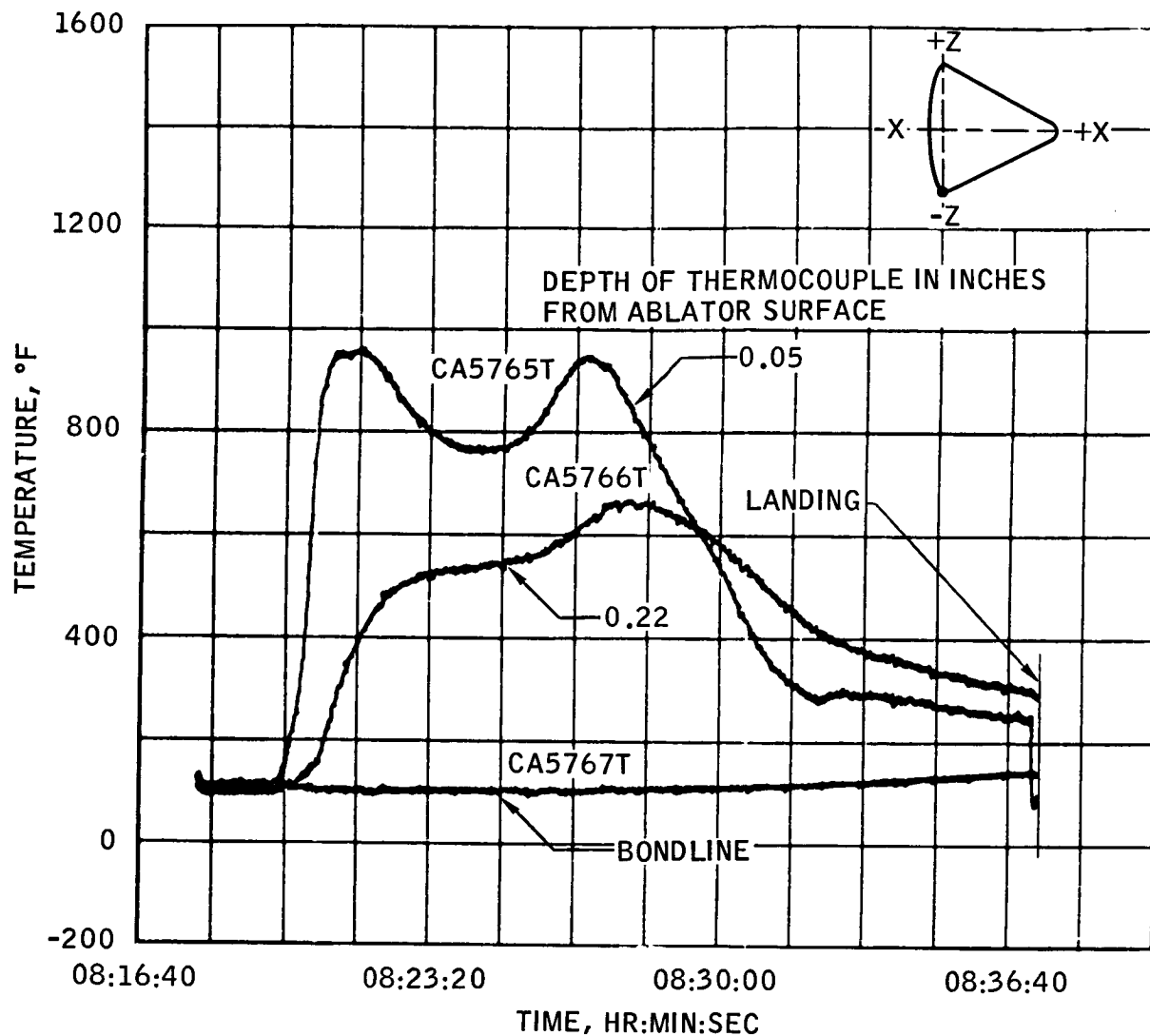
(C) STATION  $X_c = 18.5$ ,  $\theta = 270^\circ$ .

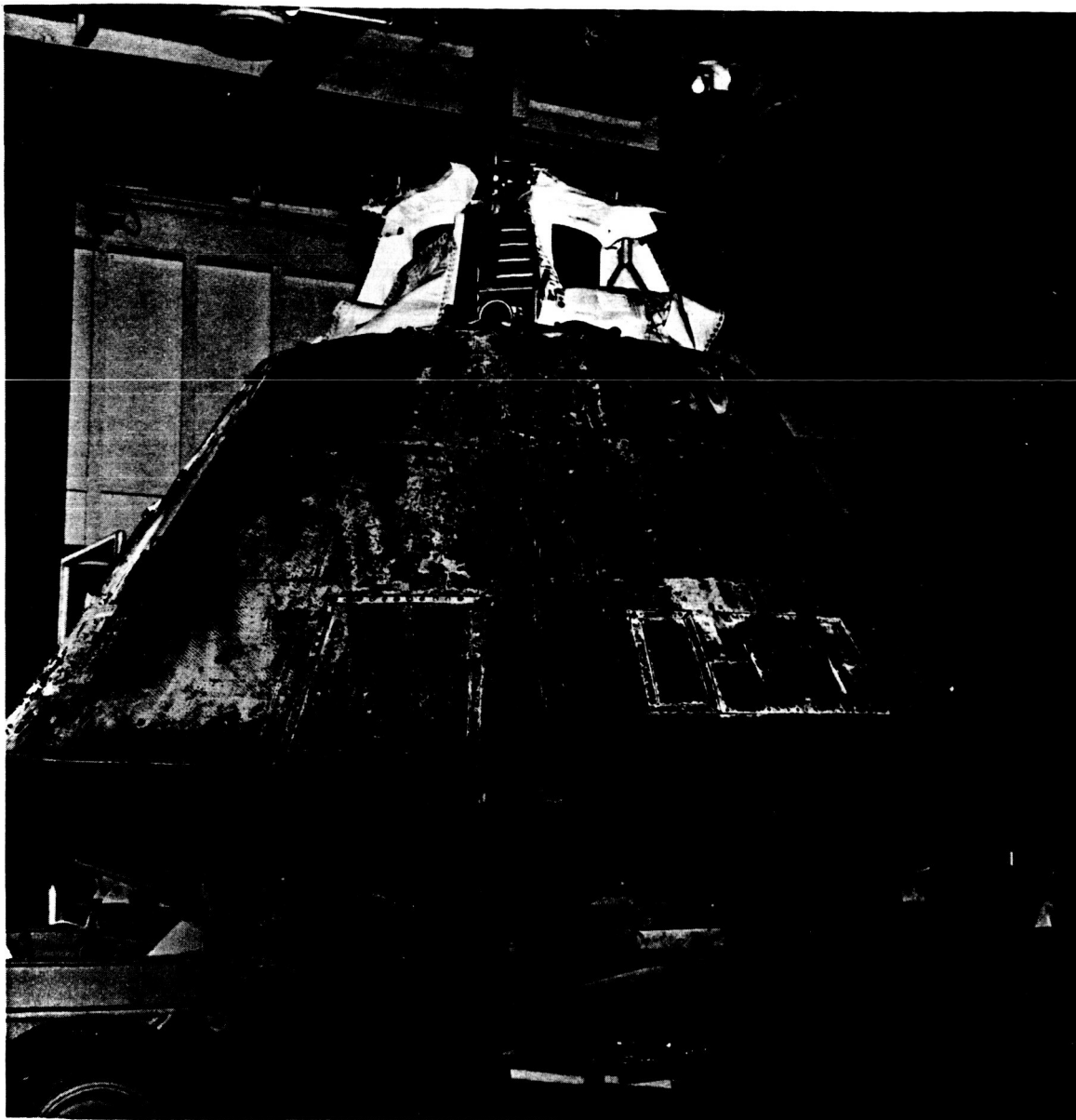
FIGURE 5.4-19.- CONTINUED.

~~CONFIDENTIAL~~

~~CONFIDENTIAL~~

5.4-75

NASA-S-68-415



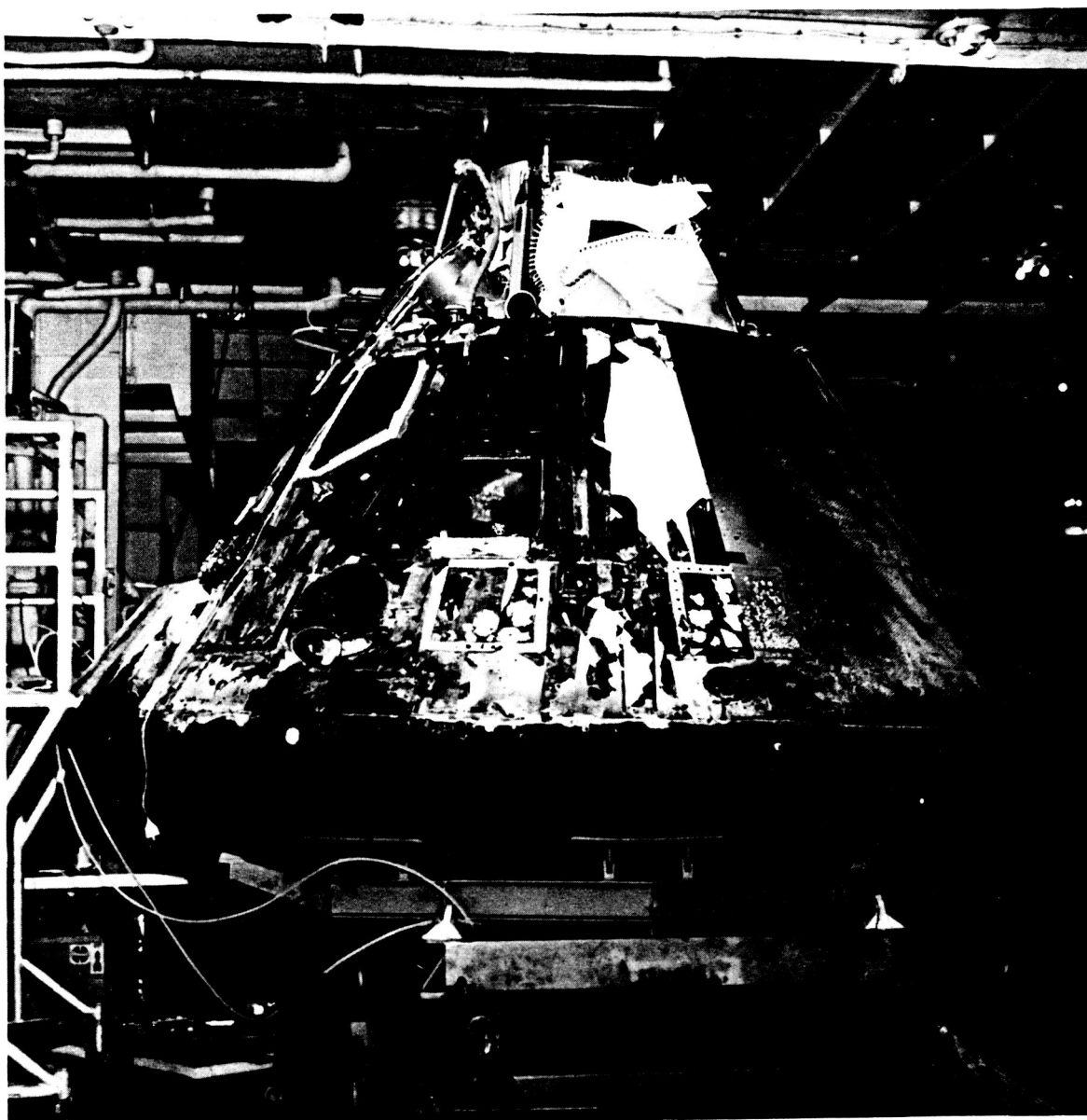
(A) +Z-AXIS TO +Y-AXIS.

FIGURE 5.4-20.- POSTFLIGHT PHOTOGRAPHS OF CONICAL HEAT SHIELD.

~~CONFIDENTIAL~~

~~CONFIDENTIAL~~

NASA-S-68-416



(B) +Y-AXIS TO -Z-AXIS.

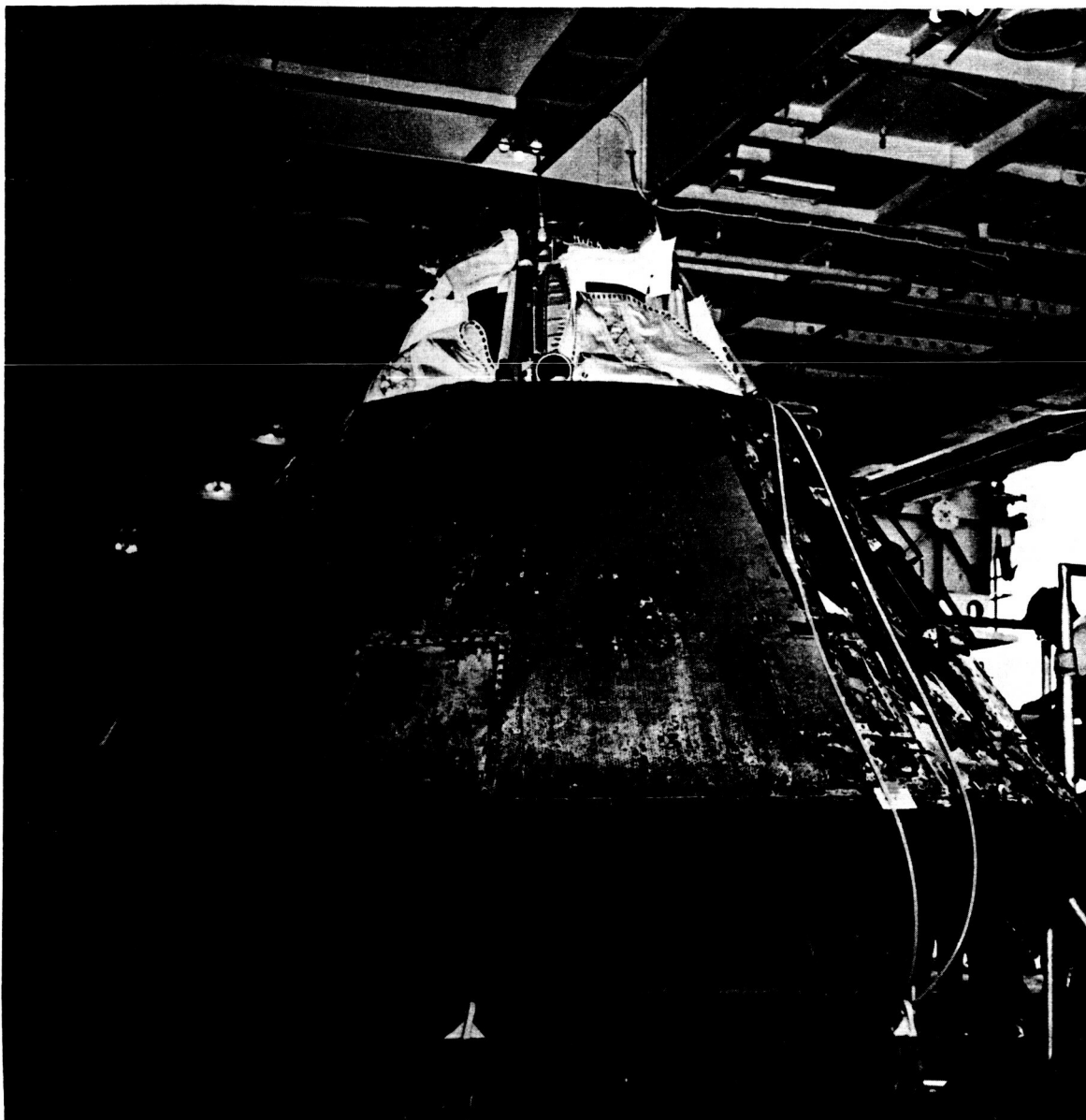
FIGURE 5.4-20.- CONTINUED.

~~CONFIDENTIAL~~

~~CONFIDENTIAL~~

5.4-77

NASA-S-68-417



(C) -Y-AXIS TO +Z-AXIS.

FIGURE 5.4-20.- CONTINUED.

~~CONFIDENTIAL~~

5.4-78

~~CONFIDENTIAL~~

NASA-S-68-418



(D) -Z LEE SIDE OF SPACECRAFT.

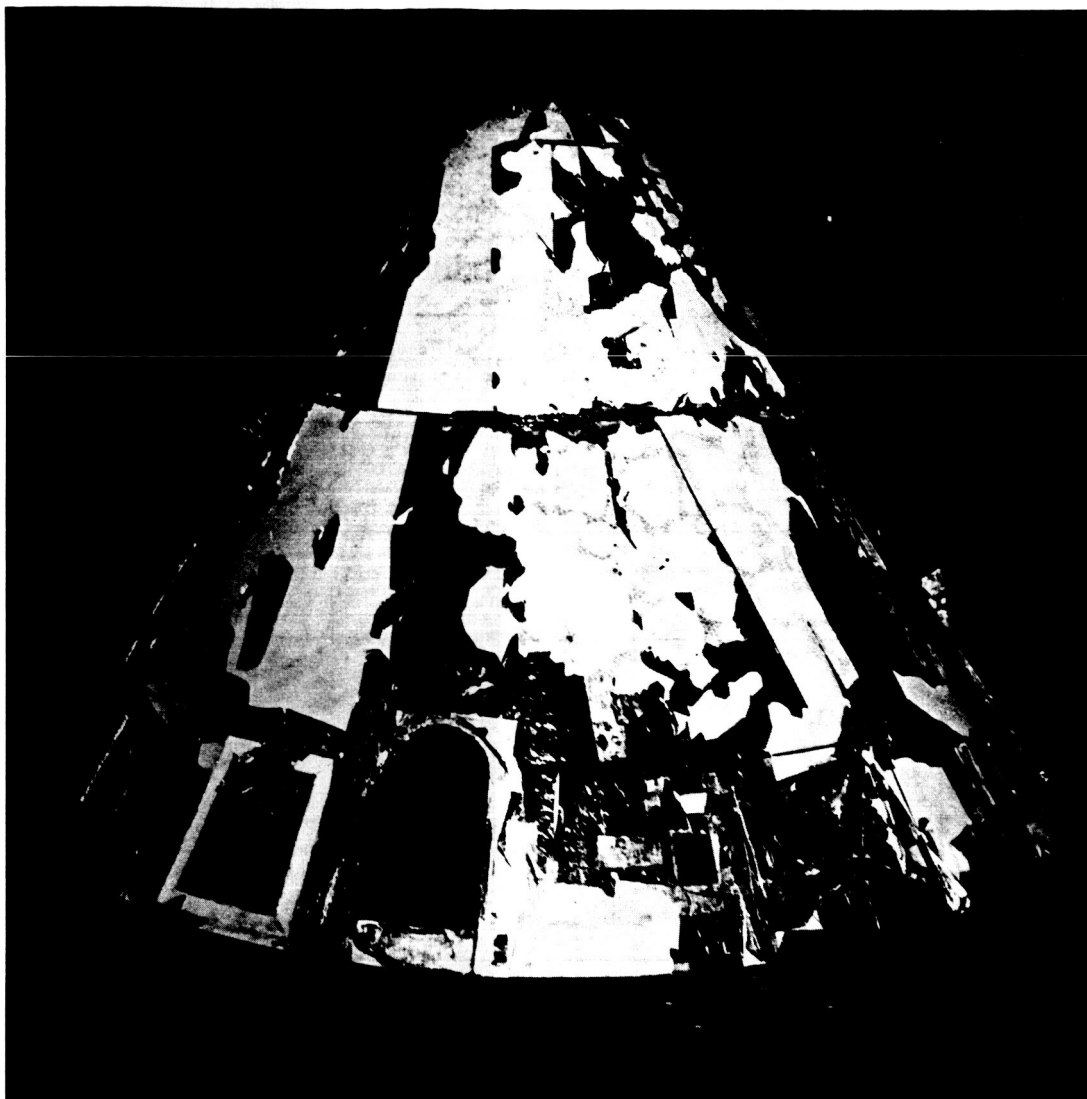
FIGURE 5.4-20.- CONTINUED.

~~CONFIDENTIAL~~

~~CONFIDENTIAL~~

5.4-79

NASA-S-68-419



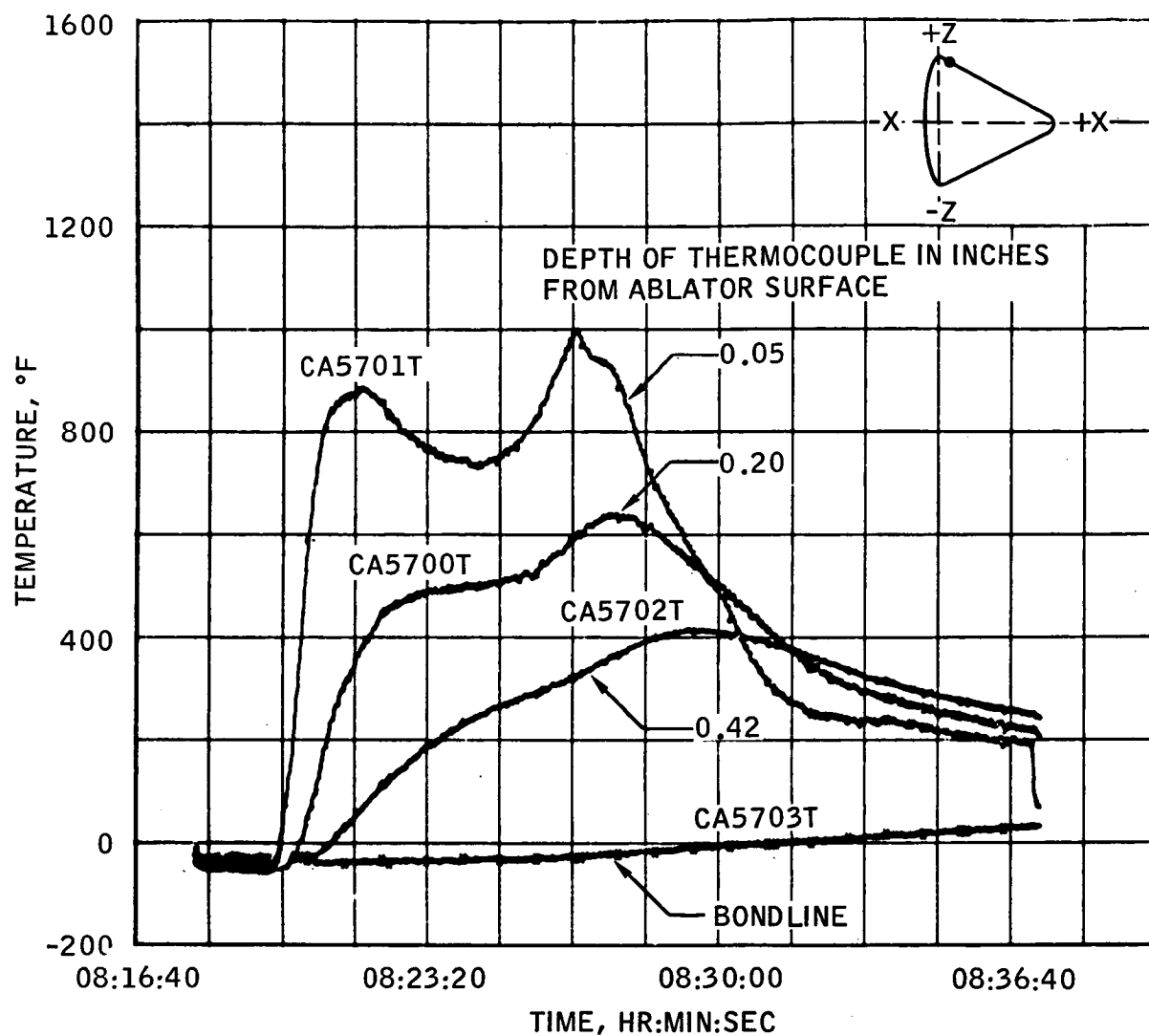
(E) FORWARD COMPARTMENT HEAT SHIELD.

FIGURE 5.4-20.- CONCLUDED.

~~CONFIDENTIAL~~

~~CONFIDENTIAL~~

NASA-S-68-420

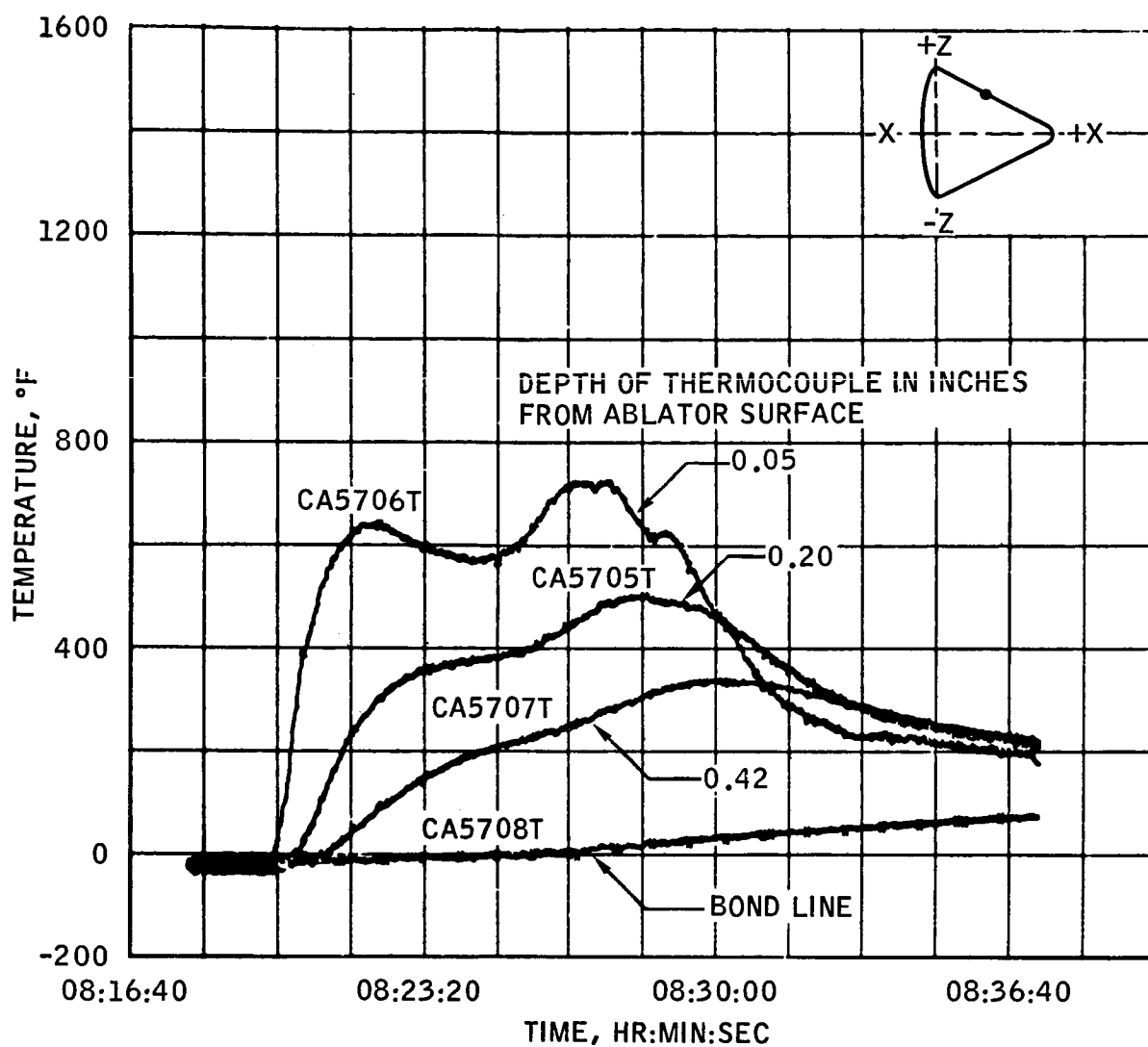
(A) STATION  $X_C = 26$ ,  $\theta = 90^\circ$ .FIGURE 5.4-21.- CONICAL HEAT SHIELD TEMPERATURE MEASUREMENTS  
AT DEPTHS INDICATED.~~CONFIDENTIAL~~



~~CONFIDENTIAL~~

5.4-81

NASA-S-68-421



(B) STATION  $X_c = 50$ ,  $\theta = 90^\circ$ .

FIGURE 5.4-21.- CONTINUED.

~~CONFIDENTIAL~~

~~CONFIDENTIAL~~

NASA-S-68-422

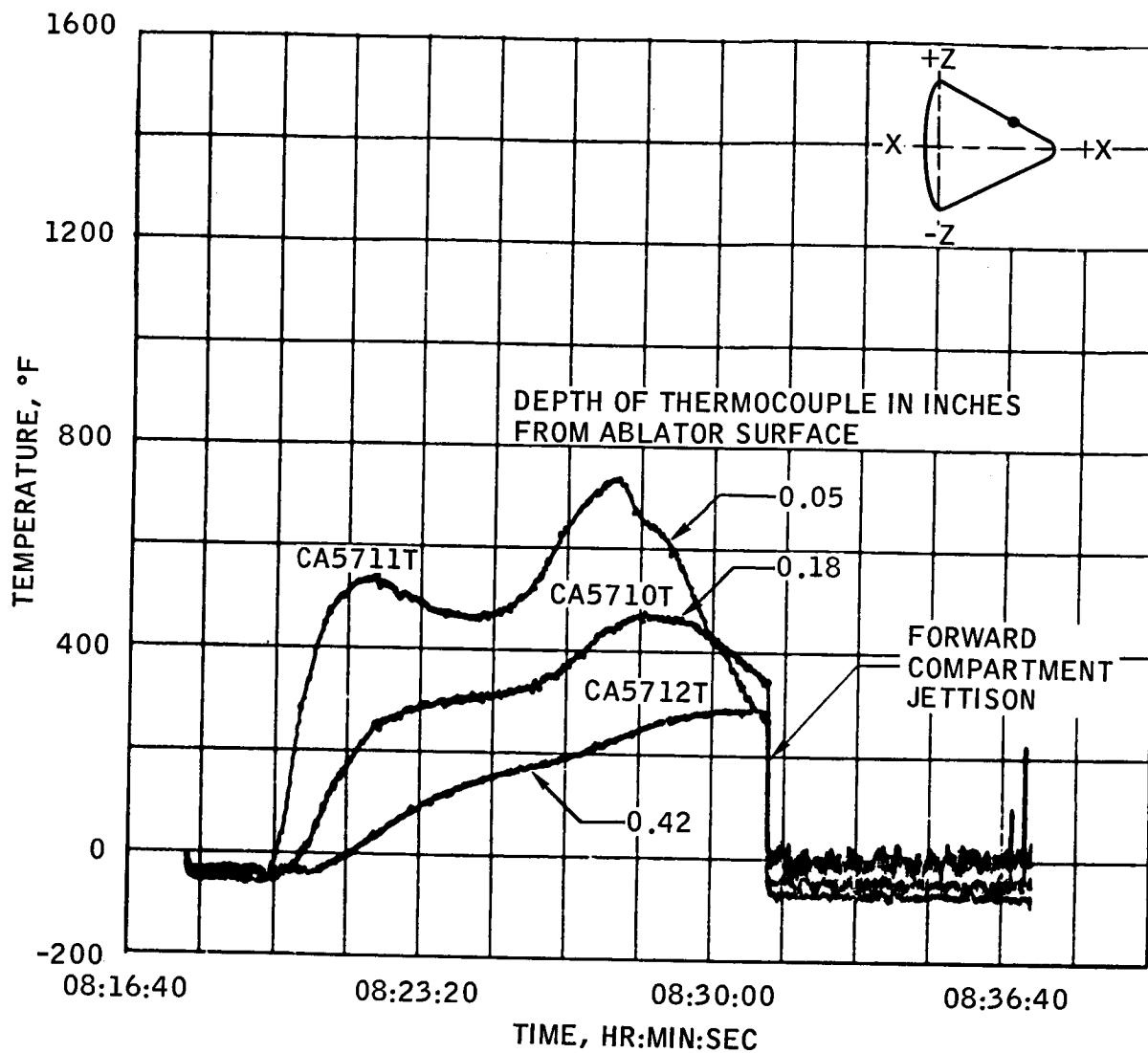
(C) STATION  $X_C = 84$ ,  $\theta = 90^\circ$ .

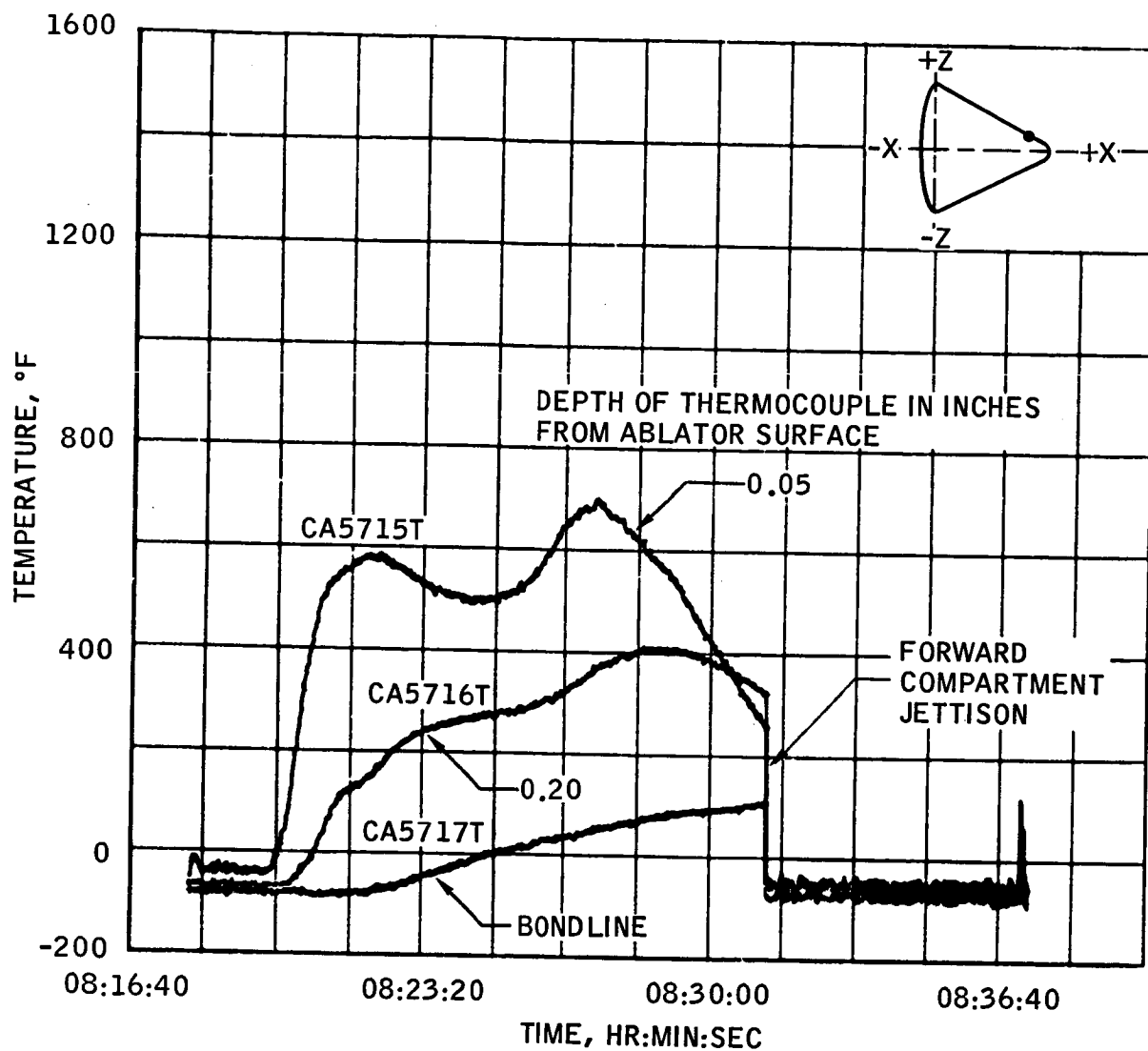
FIGURE 5.4-21.- CONTINUED.

~~CONFIDENTIAL~~

~~CONFIDENTIAL~~

5.4-83

NASA-S-68-423



Ø) STATION  $X_C = 104$ ,  $\theta = 90^\circ$ .

FIGURE 5.4-21.- CONCLUDED.

~~CONFIDENTIAL~~

~~CONFIDENTIAL~~

NASA-S-68-424

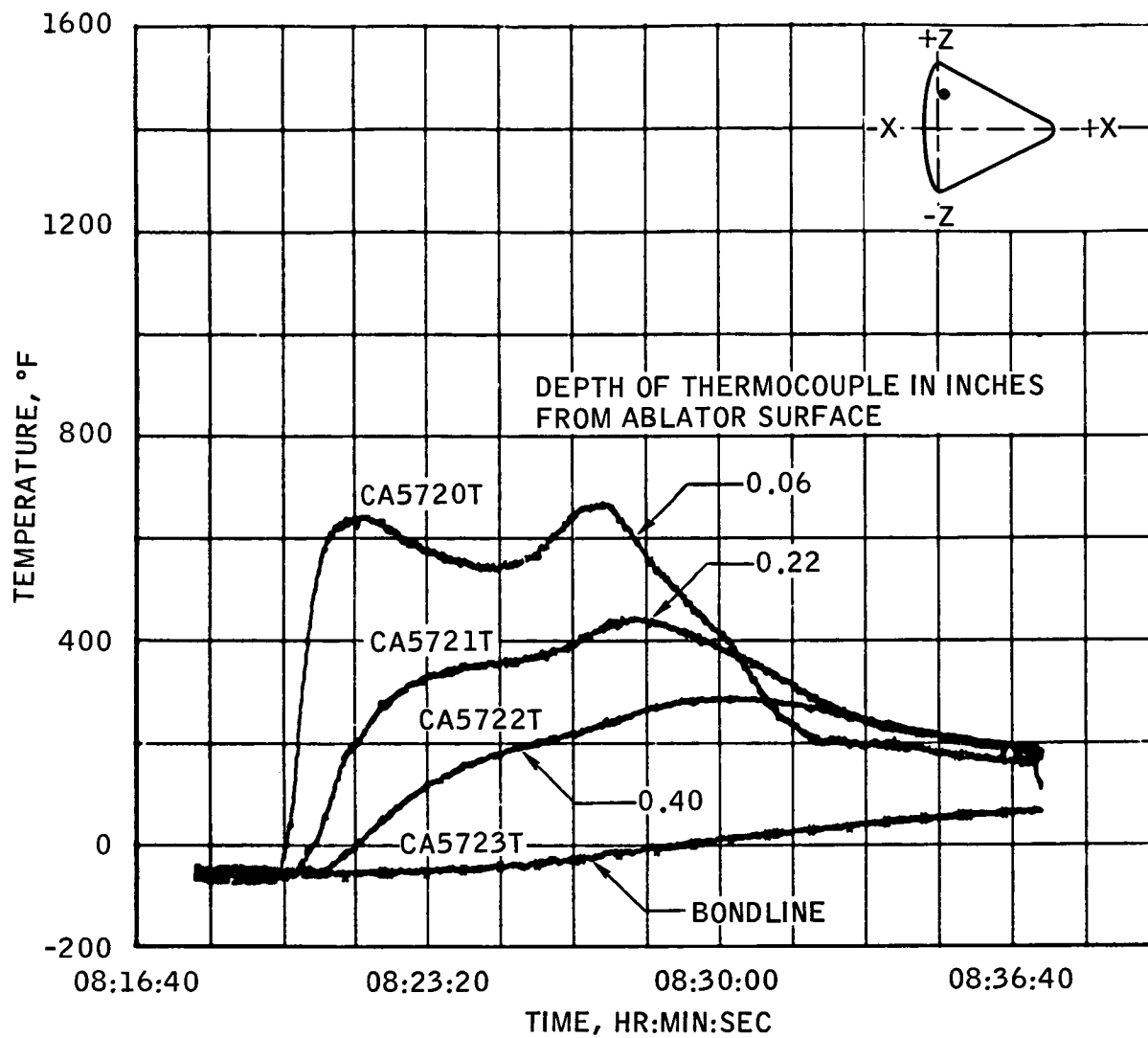
(E) STATION  $X_C = 26$ ,  $\theta = 135^\circ$ .

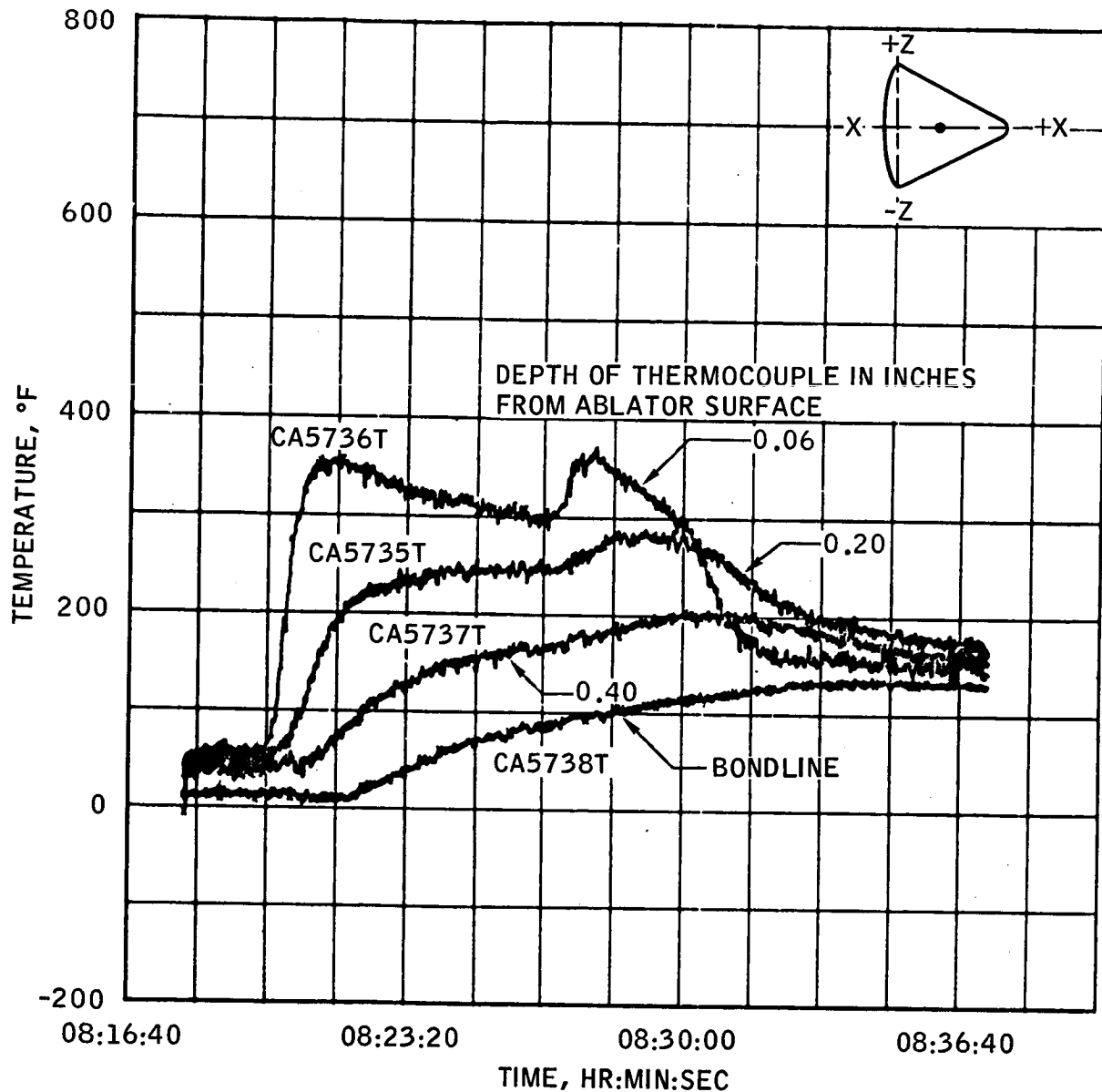
FIGURE 5.4-21.- CONTINUED.

~~CONFIDENTIAL~~

~~CONFIDENTIAL~~

5.4-85

NASA-S-68-425



(F) STATION  $X_C = 50$ ,  $\theta = 180^\circ$ .

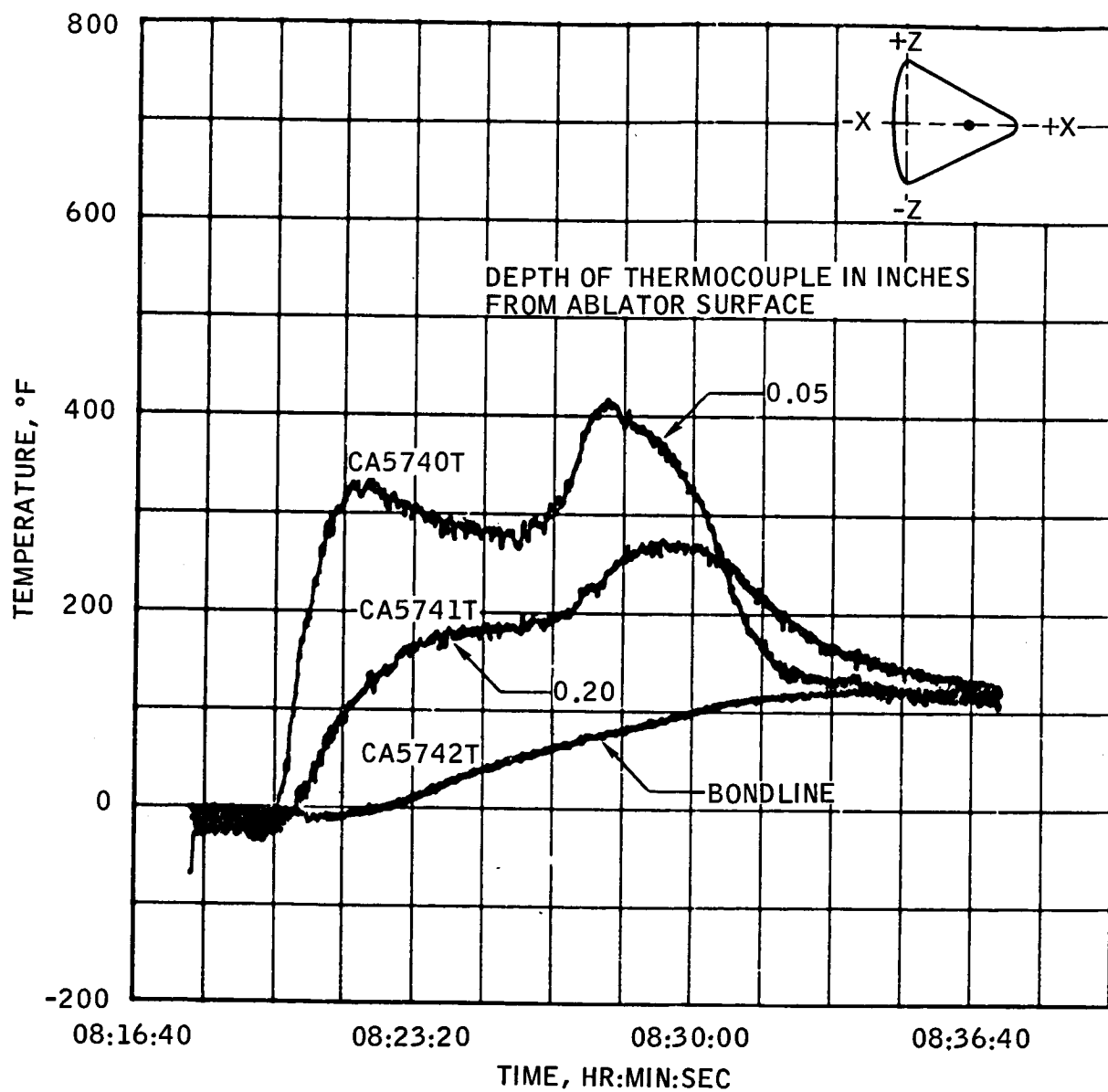
FIGURE 5.4-21.- CONTINUED.

~~CONFIDENTIAL~~

5.4-86

~~CONFIDENTIAL~~

NASA-S-68-426



(G) STATION  $X_C = 80$ ,  $\theta = 180^\circ$ .

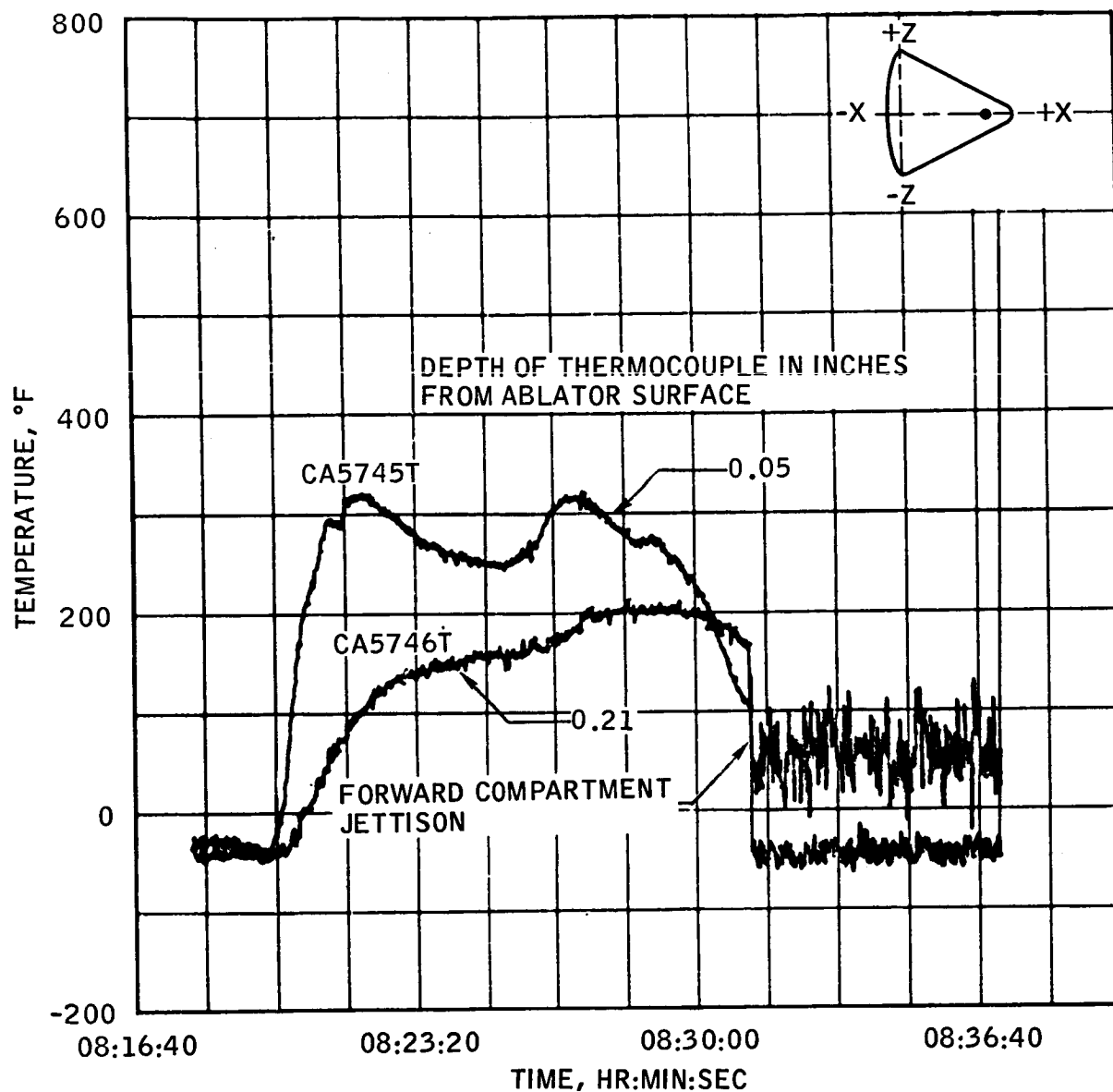
FIGURE 5.4-21.- CONTINUED.

~~CONFIDENTIAL~~

~~CONFIDENTIAL~~

5.4-87

NASA-S-68-427



(H) STATION  $X_C = 104$ ,  $\theta = 180^\circ$ .

FIGURE 5.4-21.- CONTINUED.

~~CONFIDENTIAL~~

~~CONFIDENTIAL~~

NASA-S-68-428

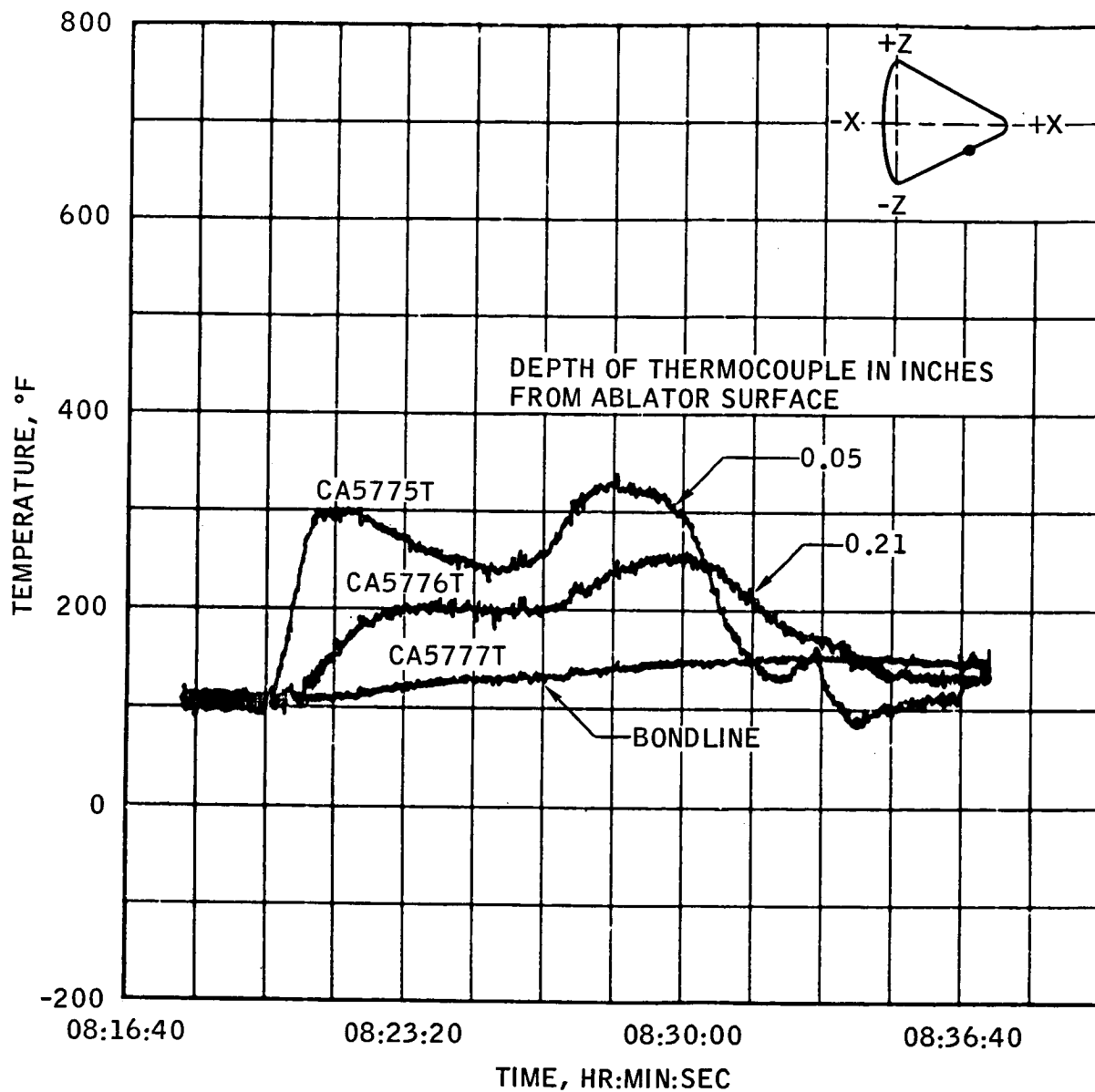
(I) STATION  $X_C = 80$ ,  $\theta = 270^\circ$ .

FIGURE 5.4-21.- CONTINUED.

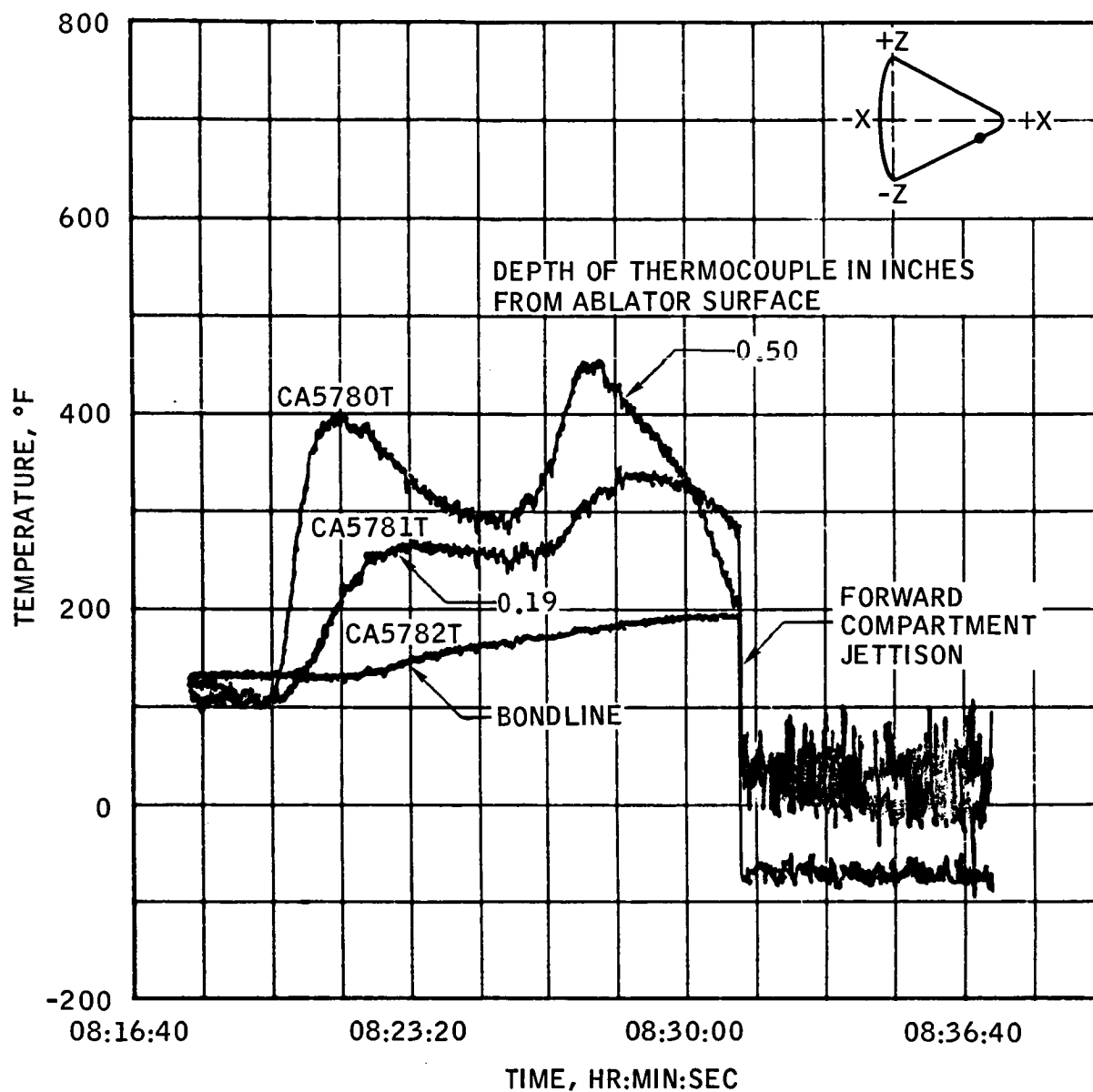
~~CONFIDENTIAL~~



~~CONFIDENTIAL~~

5.4-89

NASA-S-68-429



(J) STATION  $X_C = 104$ ,  $\theta = 270^\circ$ .

FIGURE 5.4-21.- CONCLUDED.

~~CONFIDENTIAL~~

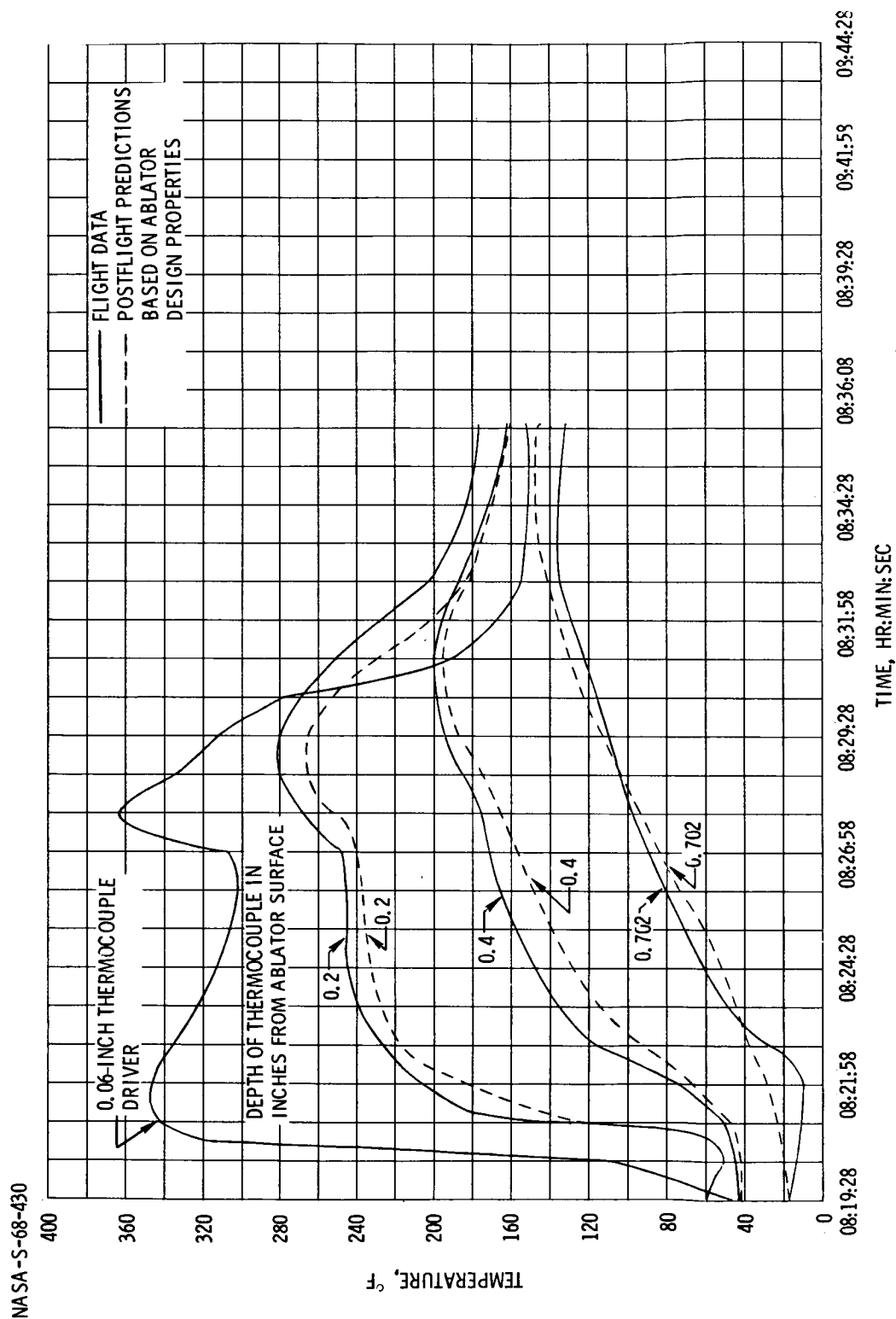
~~CONFIDENTIAL~~

FIGURE 5.4-22. - COMPARISON OF APOLLO 4 MEASURED AND PREDICTED HEAT SHIELD TEMPERATURE DATA AT  $X_C = 50$ ,  $\theta = 180^\circ$  USING 0.05-INCH THERMOCOUPLE DRIVER.

~~CONFIDENTIAL~~

~~CONFIDENTIAL~~

5.4-91

NASA-S-68-431

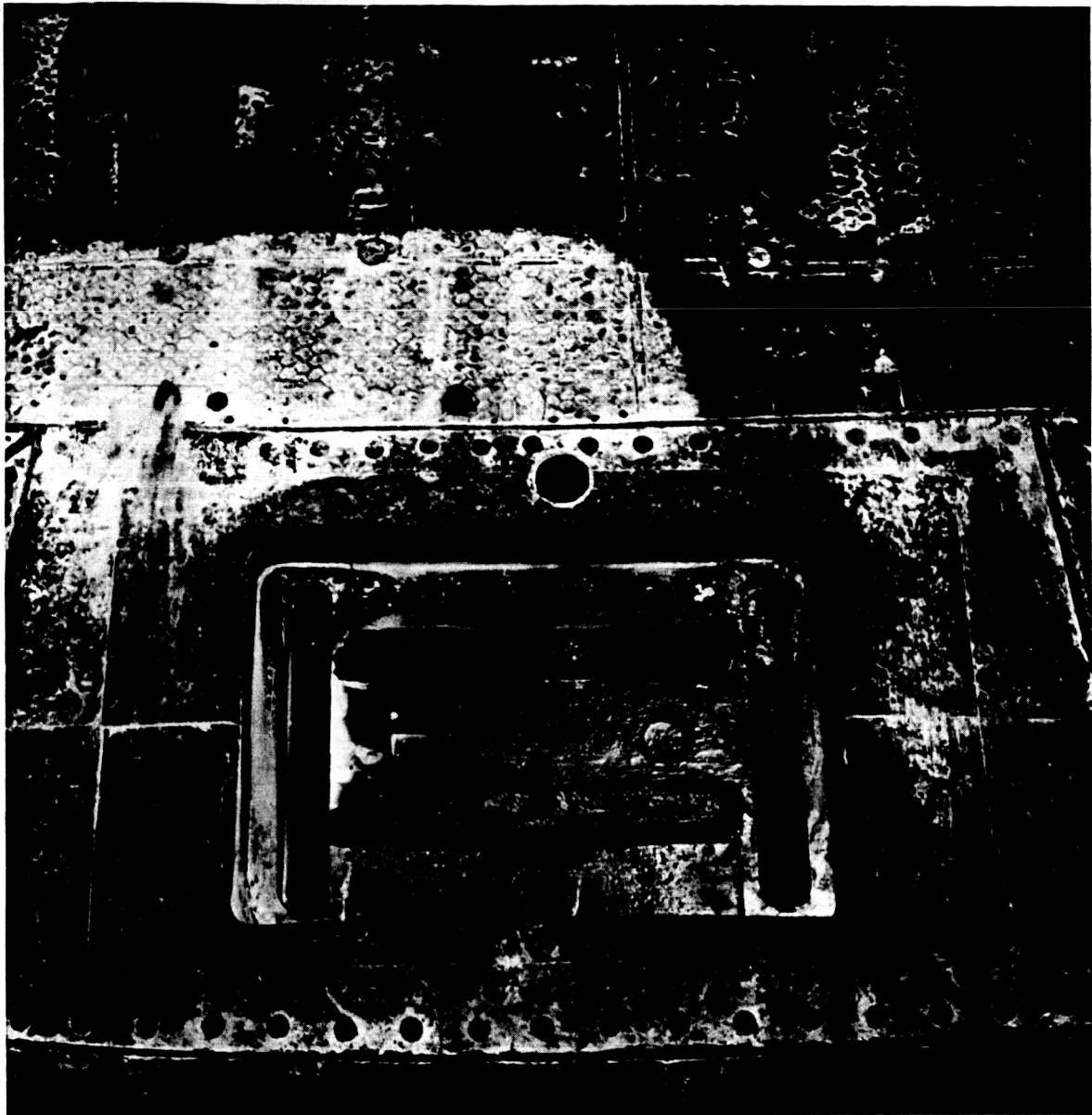


FIGURE 5.4-23.- SIMULATED WINDWARD UMBILICAL CAVITY,  
LOCATED AT  $\theta = 87^\circ$ .

~~CONFIDENTIAL~~

~~CONFIDENTIAL~~

NASA-S-68-432

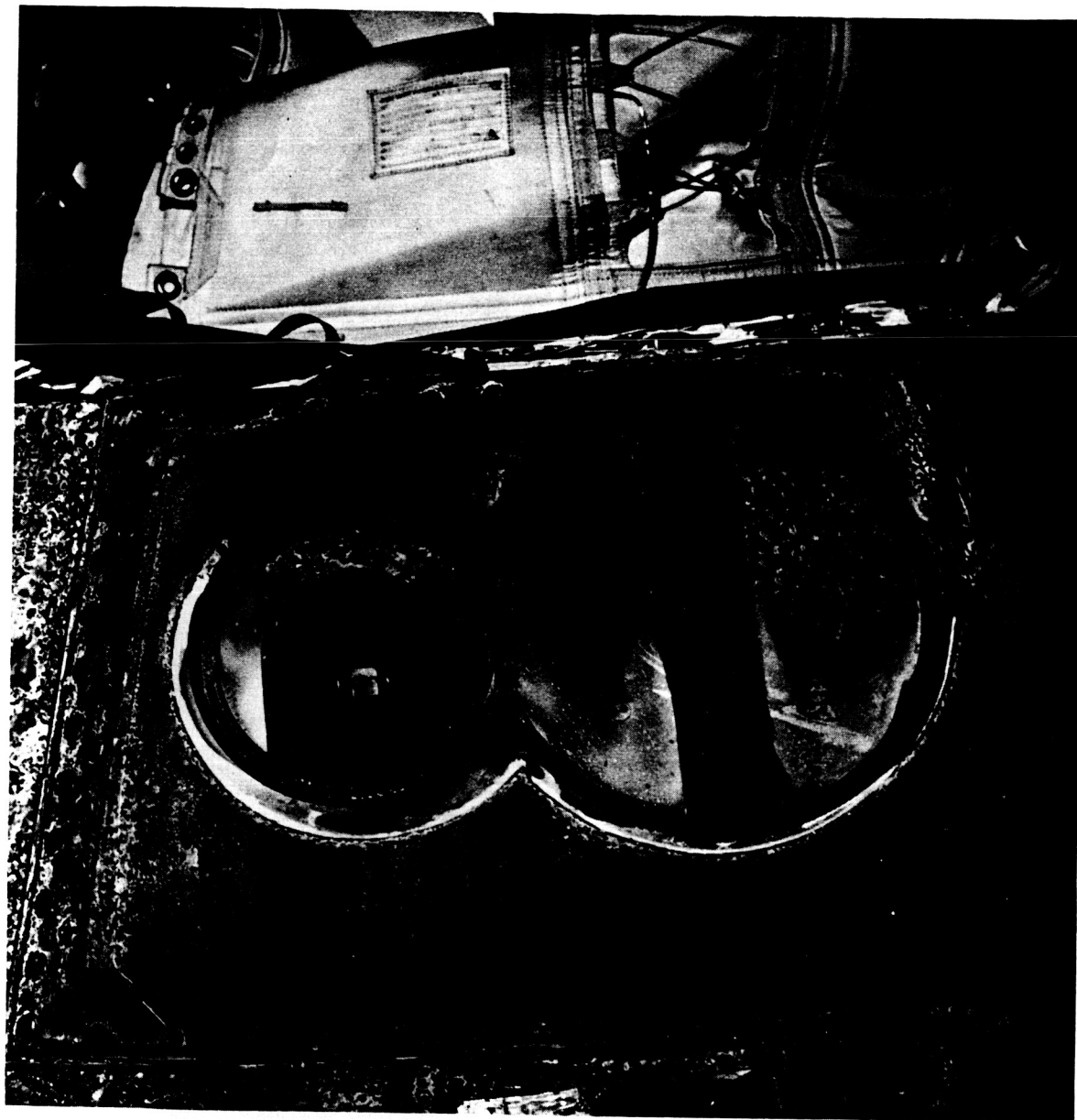


FIGURE 5.4-24.- CHARRED ASTRO-SEXTANT AREA

~~CONFIDENTIAL~~

~~CONFIDENTIAL~~

5.4-93

NASA-S-68-433

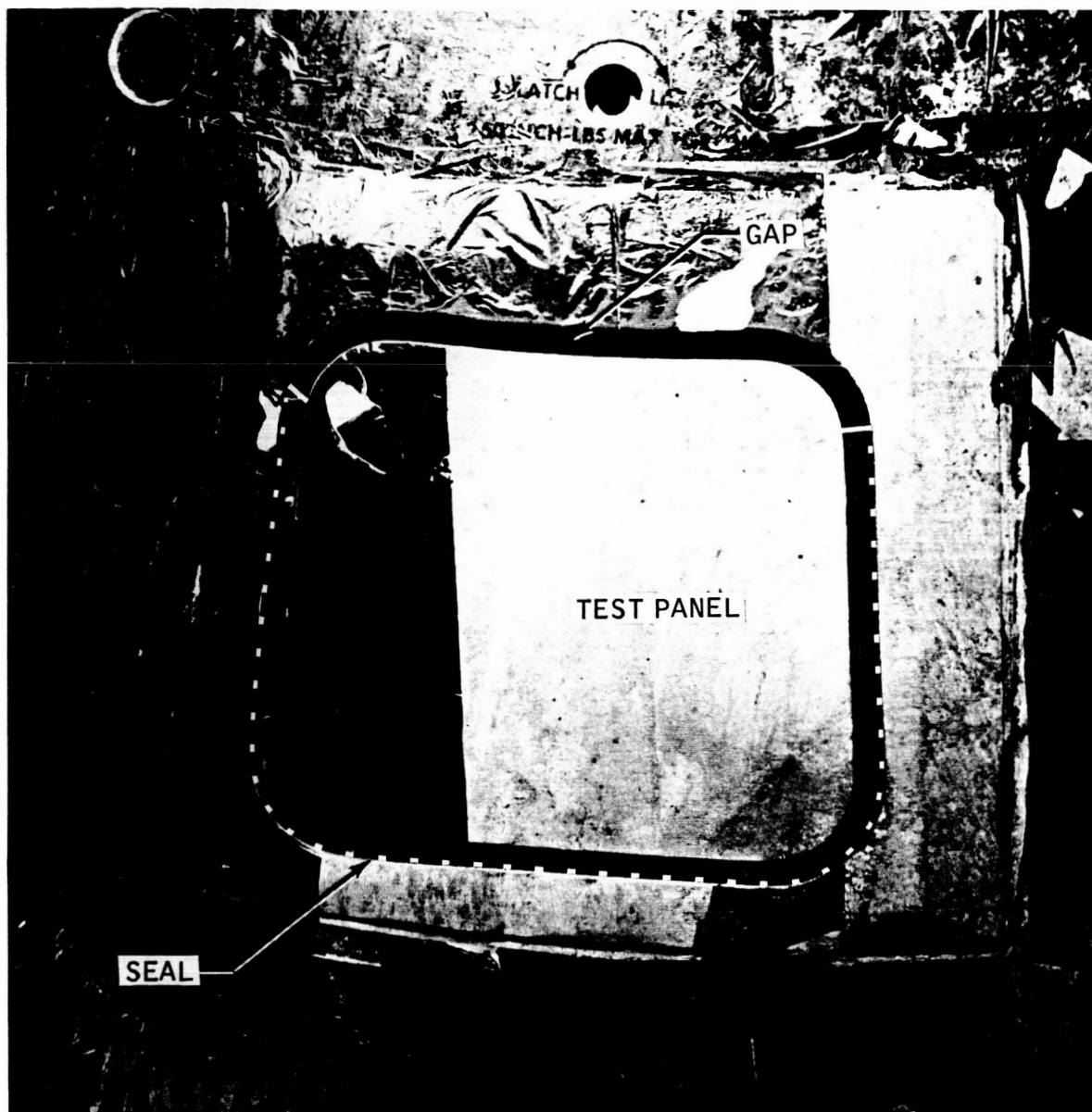


FIGURE 5.4-25.- UNIFIED SIDE HATCH TEST PANEL SHOWING GAP AND SEAL.

~~CONFIDENTIAL~~

~~CONFIDENTIAL~~

NASA-S-68-434

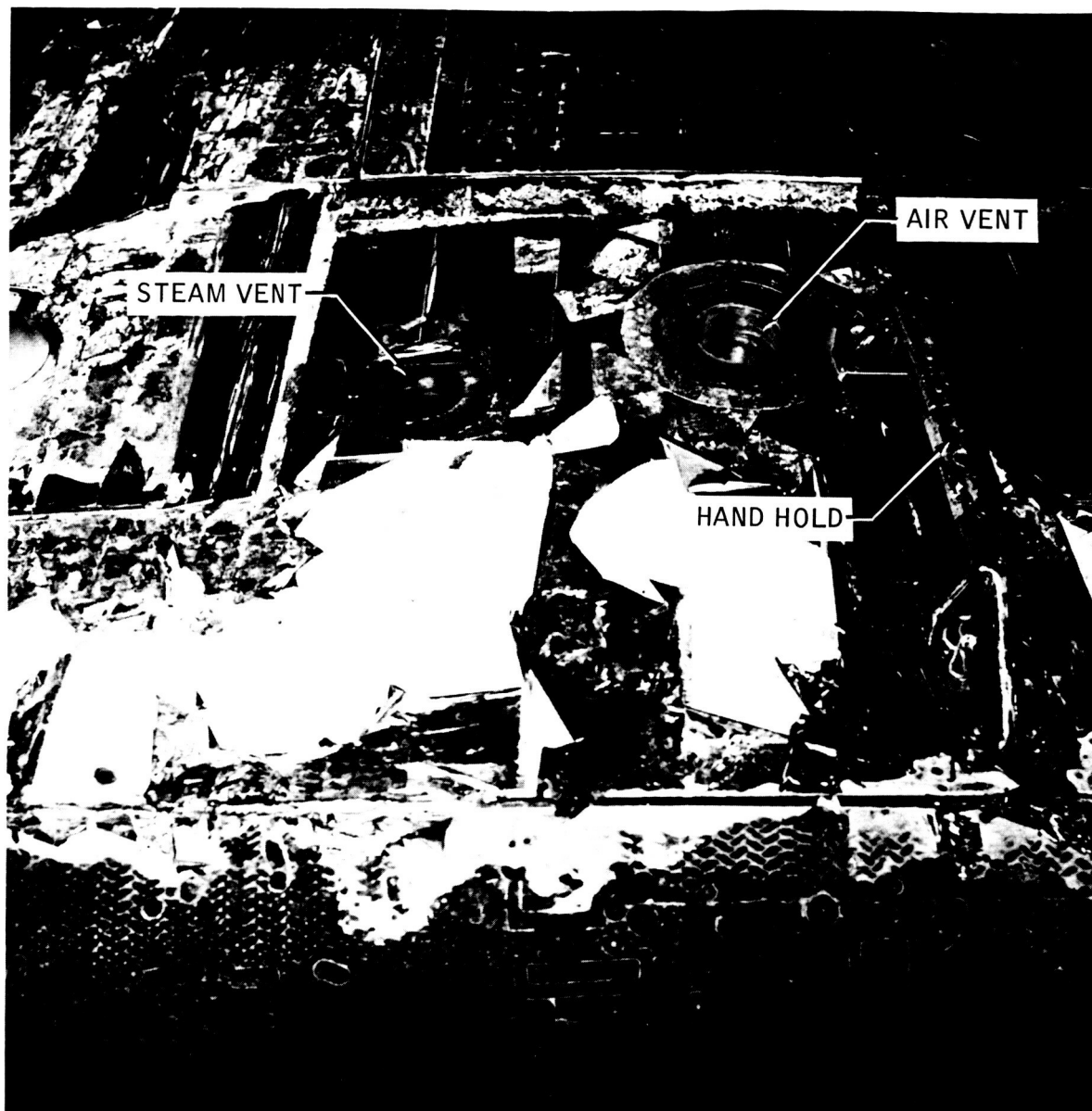


FIGURE 5.4-26.- STEAM VENT, AIR VENT, AND EVA HAND HOLD.

~~CONFIDENTIAL~~

~~CONFIDENTIAL~~

5.5-1

## 5.5 EARTH LANDING SUBSYSTEM (ELS)

The earth landing subsystem (ELS) functioned properly and successfully landed the spacecraft. One main parachute was recovered and returned for analysis. This was the first Apollo spacecraft parachute recovered to date.

This was the second flight test of a complete Block I ELS and was identical to the ELS configuration flown on Mission AS 202 (ref. 4). For Apollo 4 mission, operation of the ELS was controlled by a baro-switch and logic functions in the earth landing sequence controller. The functions of the controller were sequenced through two mutually redundant ELS controllers with crossover provided for all ELS events except main parachute harness disconnect.

### 5.5.1 Performance

As planned for the normal entry recovery mode, closure of the high-altitude baroswitches (at 08:31:16.6 and 12.21 in. Hg) initiated logic power to the master event sequence controller for forward heat shield jettison, and to the ELS controller systems A and B, to start the 2-second timer. Forward heat shield jettison occurred at 08:31:17.0, and drogue mortar fire was initiated at 08:31:18.6 after the normal 2-second time delay in the ELS controllers.

Drogue disconnect and pilot mortar fire were initiated simultaneously by closure of the low altitude baroswitches at 08:32:05.8 and 20.8 in. Hg. Spacecraft landing occurred at 08:37:09.2. The average rate of descent from 5000 feet to sea level was approximately 26.6 ft/sec. Pressure altitude is plotted against time from start of the ELS controller to landing in figure 5.5-1. This plot is generated from data recorded by the onboard barometric static pressure transducer, corrected to actual day.

The times of ELS event sequencing were determined by reference to pyrotechnic bus measurements. The ELS controller event times were not recorded by the onboard tape recorder (data storage equipment) as planned because of the loss of the 5-volt instrumentation power prior to activation of the ELS controller.

No visual or radar references were available to evaluate the deployment performance of the forward heat shield parachute, drogue parachutes, or pilot and main parachutes.

The forward heat shield, with deployed parachute attached, was found floating in the landing area. Inspection of the recovered forward heat

~~CONFIDENTIAL~~

~~CONFIDENTIAL~~

shield showed no evidence of the heat shield having recontacted the command module after jettison. The forward heat shield parachute was retrieved.

A qualitative judgment can be made of the CM/ELS dynamic performance by analyzing evidence of the amount of contact between components of the ELS and the CM upper deck structure. There was no evidence of contact of the drogue parachute steel cable risers with the airlock upper lip (fig. 5.5-2), which indicates that the CM was in a favorable aft heat shield-forward attitude at drogue parachute deployment. Minimal contact of the main parachute harness legs with the drogue mortar cans (fig. 5.5-2) and no evidence of other ELS component contact on the upper deck indicates a nominal main parachute deployment sequence.

#### 5.5.2 Postflight Test Activity

Postflight inspection of the one main parachute recovered revealed a number of unexplained burn holes in the canopy material. The data indicate no apparent adverse effects resulting from the holes. Investigations conducted to date lead to the conclusion that the burn holes were caused by ablating of the RCS engine nozzle ablaters after full deployment of the parachute.

Postflight inspection also disclosed damage in the area of the negative pitch engine mounting panel attach bolts. A check of the apex cover also showed damage in the same area. This condition is being investigated at the present time.

~~CONFIDENTIAL~~



~~CONFIDENTIAL~~

5.5-3

NASA-S-68-435

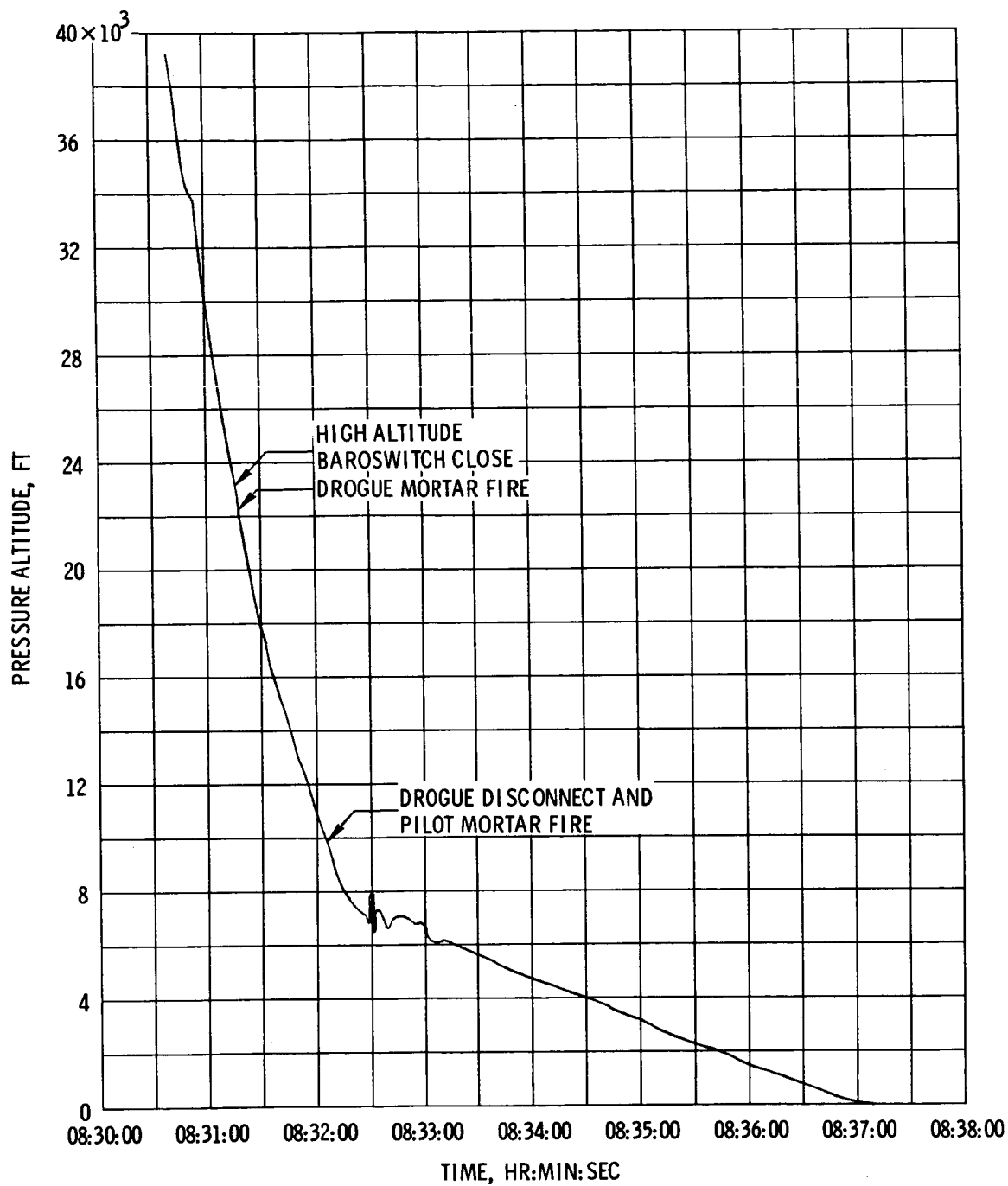
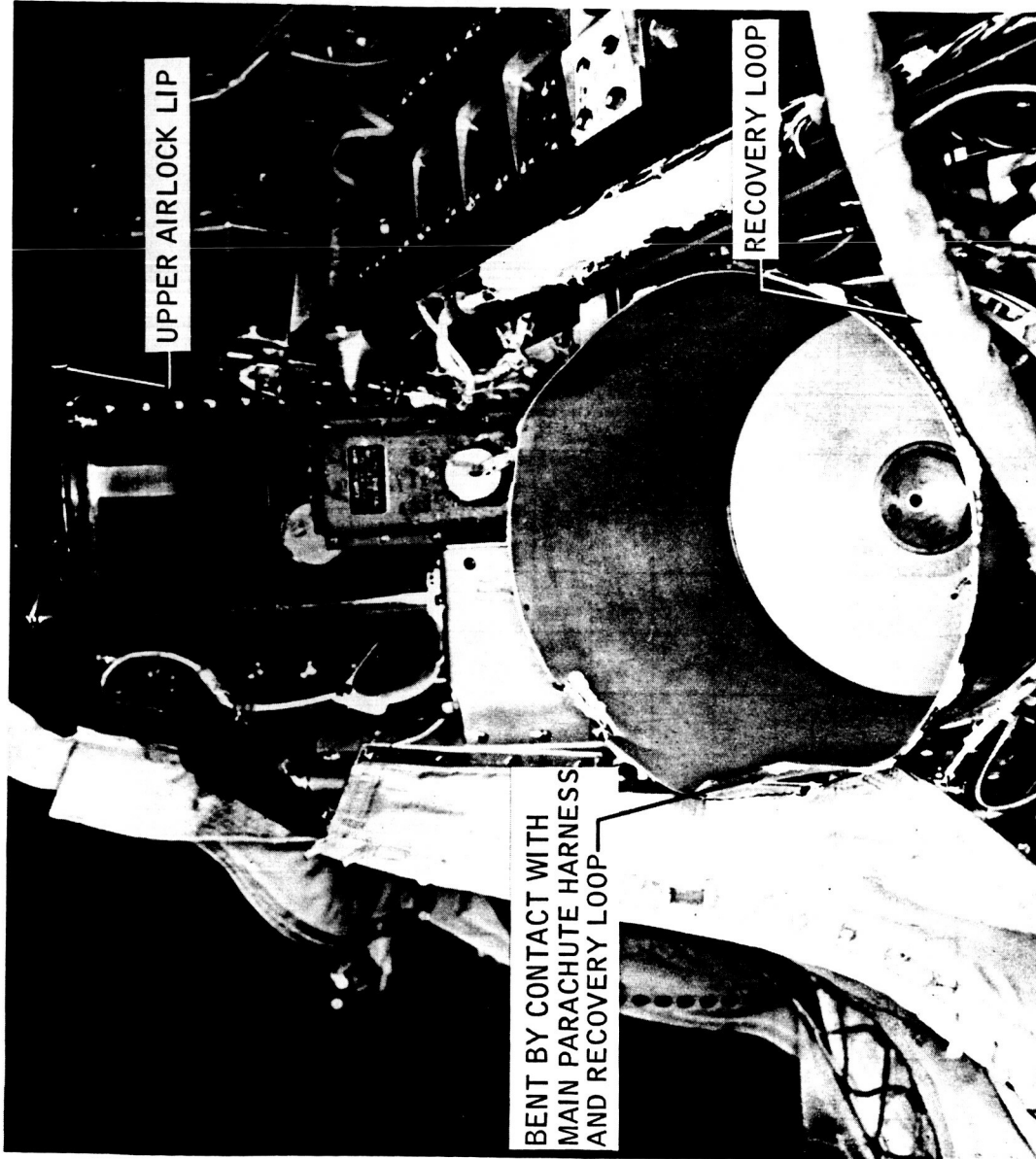


FIGURE 5.5-1. - PRESSURE ALTITUDE DURING DESCENT.

~~CONFIDENTIAL~~

~~CONFIDENTIAL~~

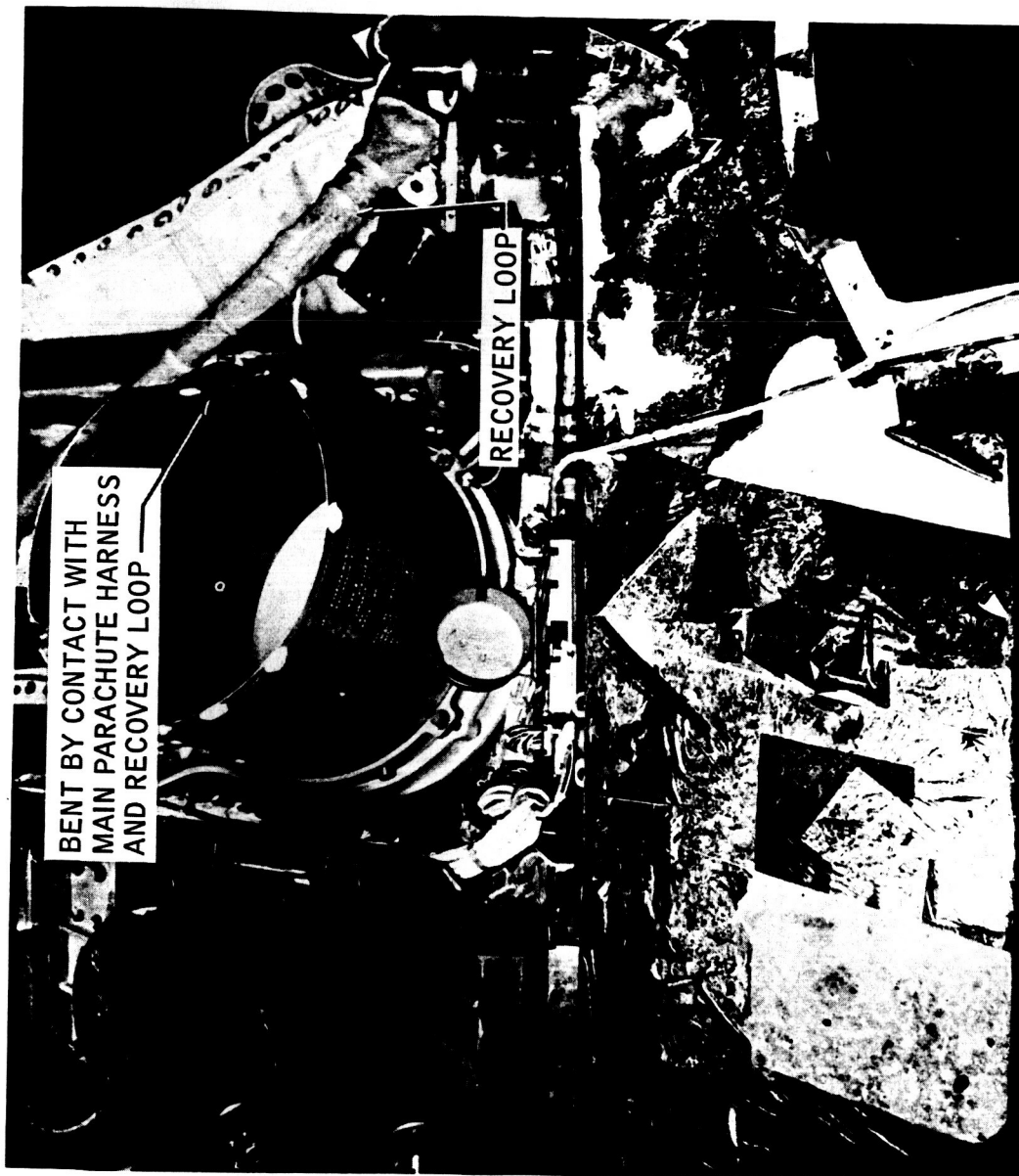
(A) DROGUE MORTAR CAN NO. 1.

FIGURE 5.5-2.- EARTH LANDING SUBSYSTEM UPPER DECK AFTER RECOVERY.

NASA-S-68-436

~~CONFIDENTIAL~~

NASA-S-68-437



(B) DROGUE MORTAR CAN NO. 2.

FIGURE 5.5-2.- CONCLUDED.

~~CONFIDENTIAL~~

5. 5- 5

~~CONFIDENTIAL~~

~~CONFIDENTIAL~~

THIS PAGE INTENTIONALLY LEFT BLANK

~~CONFIDENTIAL~~

~~CONFIDENTIAL~~

5.6-1

## 5.6 MECHANICAL SUBSYSTEMS

### 5.6.1 Summary

The mechanical subsystems flown on the Apollo 4 spacecraft included the canard subsystem, the uprighting subsystem, the deployment mechanisms for the recovery aids, and the latching mechanisms for the side ablative, side pressure, forward pressure, and boost protective cover hatches. All components performed satisfactorily. The canard and uprighting subsystems were not required to operate.

### 5.6.2 Performance

The deployment mechanisms for the postlanding recovery aids consisted of those used to deploy the vhf and hf antennas, the flashing light, and the sea-dye marker/swimmer umbilical. All of these mechanisms operated properly except as discussed in the following paragraph.

Postflight inspection of the antennas and flashing light revealed that they deployed satisfactorily and functioned as planned except for the vhf antenna deployment mechanism located adjacent to gusset no. 2. Although the mechanism deployed properly, the latch used to insure that the antenna remained in the erect position did not engage. However, the mechanism spring force was sufficient to maintain the antenna in the erect position because the antenna performed as required, was not damaged, and was in the erect position after landing of the CM. Signals were received from all antennas after deployment. The flashing light was observed to be operating satisfactorily during recovery operations (section 9.3), and the flash rate, during recovery operations, was 18 flashes per minute, which is within the specification requirement of 8 to 24 flashes a minute.

The deployment mechanism latch for the sea-dye canister was triggered by a lanyard that was pulled when the hf antenna was erected after landing. The canister was deployed overboard by redundant springs but remained attached to the CM by a cable which included the swimmer interphone umbilical. The dye canister was in the water for only 20 minutes before the swimmer placed it on top of the flotation collar. During this short period, the dye had dispersed to an estimated slick size of 15 000 sq. ft., and the recovery forces stated that the slick was sufficient. During recovery operations, the canister was overloaded and broke free from its lanyard (see section 9.3).

The side ablative hatch, the side pressure hatch, and the forward pressure hatch were securely retained in place by their respective latching mechanisms. The integrity of the spacecraft structure, pressure

~~CONFIDENTIAL~~

~~CONFIDENTIAL~~

seal, and heat shield ablator was successfully maintained. After spacecraft recovery, the latching mechanisms operated properly to release the hatches. The latching mechanism for the boost protective cover hatch retained that hatch in place during the launch phase.

~~CONFIDENTIAL~~

~~CONFIDENTIAL~~

5.7-1

## 5.7 ELECTRICAL POWER SUBSYSTEM

Operation of the electrical power distribution subsystem was nominal throughout the flight. All test objectives were met. All power switching occurred as planned and programmed.

The voltage measurements for main buses A and B ranged between 29.2 and 28.0 V dc from launch to CM/SM separation, except during the periods of highest current transients, which occurred during the start of the service propulsion subsystem gimbal motors. The main bus A dc voltage and total spacecraft currents during the peak-power period for the first SPS burn are shown in figure 5.7-1. The main bus voltages were stable at 27 V dc during the entry phase of the mission.

The ac bus voltages ranged between 113.8 and 117.0 V ac during the mission. The inverter temperature ranged from 111.8° F to 120.3° F for inverter no. 1, 88° F to 97° F for inverter no. 2, and 58° F to 58.8° F for inverter no. 3. Inverter no. 1 was carrying the highest load and consequently had the highest temperature; also, inverter no. 3 was not operating and the temperature was the same as that of the cabin.

Entry battery temperatures ranged from 72.3° F to 94.3° F for battery A and 70.5° F to 88° F for battery B. The auxiliary battery voltages ranged from 30.5 to 33.0 V. The pyrotechnic battery voltages from launch through CM/SM separation were 36.8 V or higher, except during pyrotechnics firings. After the apex cover was jettisoned and the drogue parachute deployment pyrotechnics had fired, the pyrotechnic battery recovered to only 35 V for battery B and 36 V for battery A, instead of open-circuit voltage of 37 V for each battery. A small current drain caused by a pyrotechnic initiator high resistance shorting after it was fired would keep the battery from returning to the open-circuit voltage.

The load sharing between the batteries and the fuel cells during SPS burns was as expected. The three entry batteries carried approximately 25 percent of the total load. The entry battery currents and voltages when the SPS gimbal motors were started are shown in figures 5.7-2 and 5.7-3, respectively. During the first few seconds, the postlanding battery did not share the load with batteries A and B. This was caused by the difference in energy discharge before the batteries were tied to the main buses during the SPS burn. Batteries A and B were discharged approximately 10 A-hr more than the postlanding battery. This greater discharge reduced the battery internal impedance and consequently gave a higher voltage under load. This, in turn, would back-bias the diodes which were in series with the postlanding battery during current stabilization.

~~CONFIDENTIAL~~

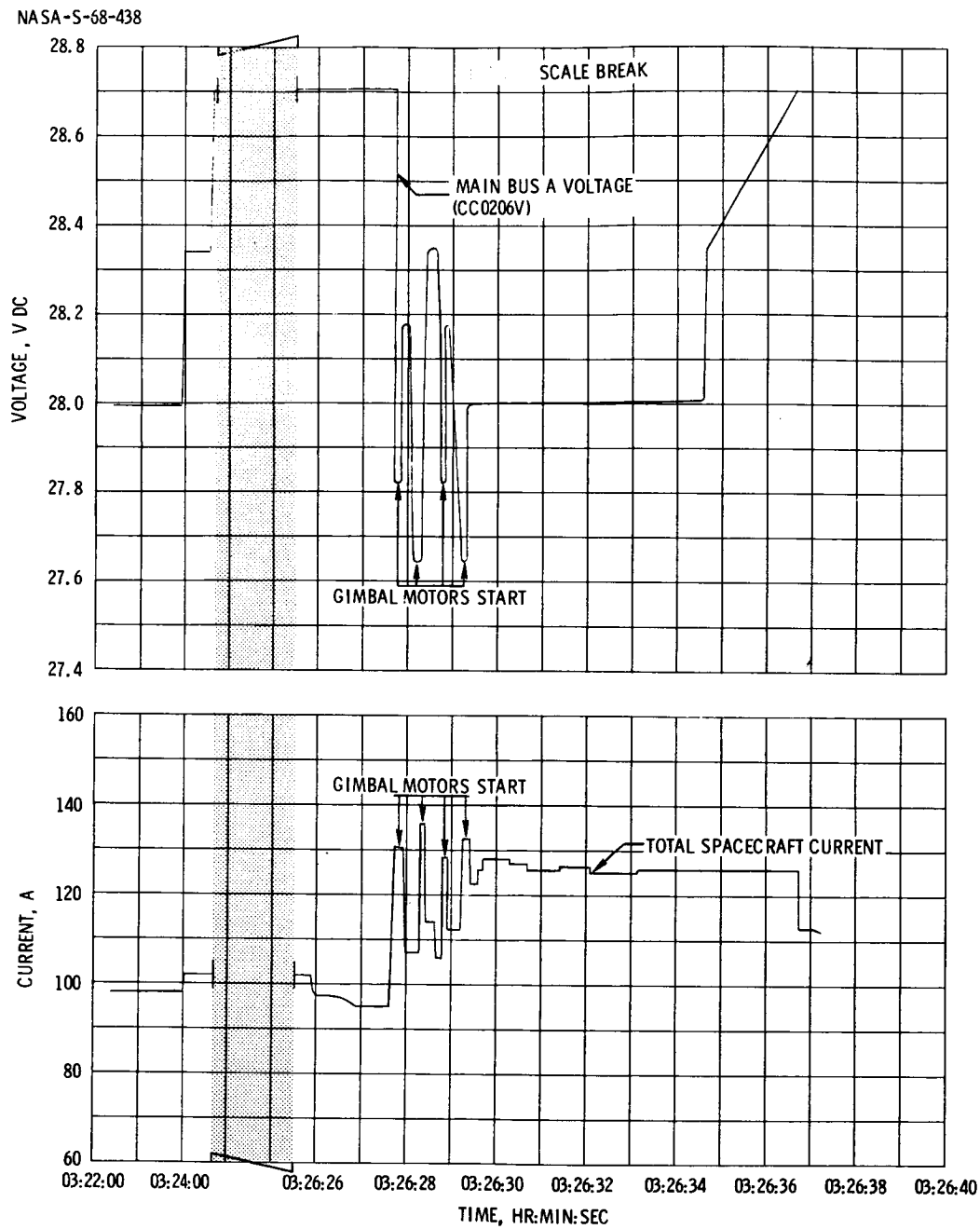
~~CONFIDENTIAL~~

FIGURE 5.7-1. - MAIN DC BUS A VOLTAGE AND TOTAL SPACECRAFT CURRENT DURING GIMBAL MOTORS START-UP.

~~CONFIDENTIAL~~



~~CONFIDENTIAL~~

5.7-3

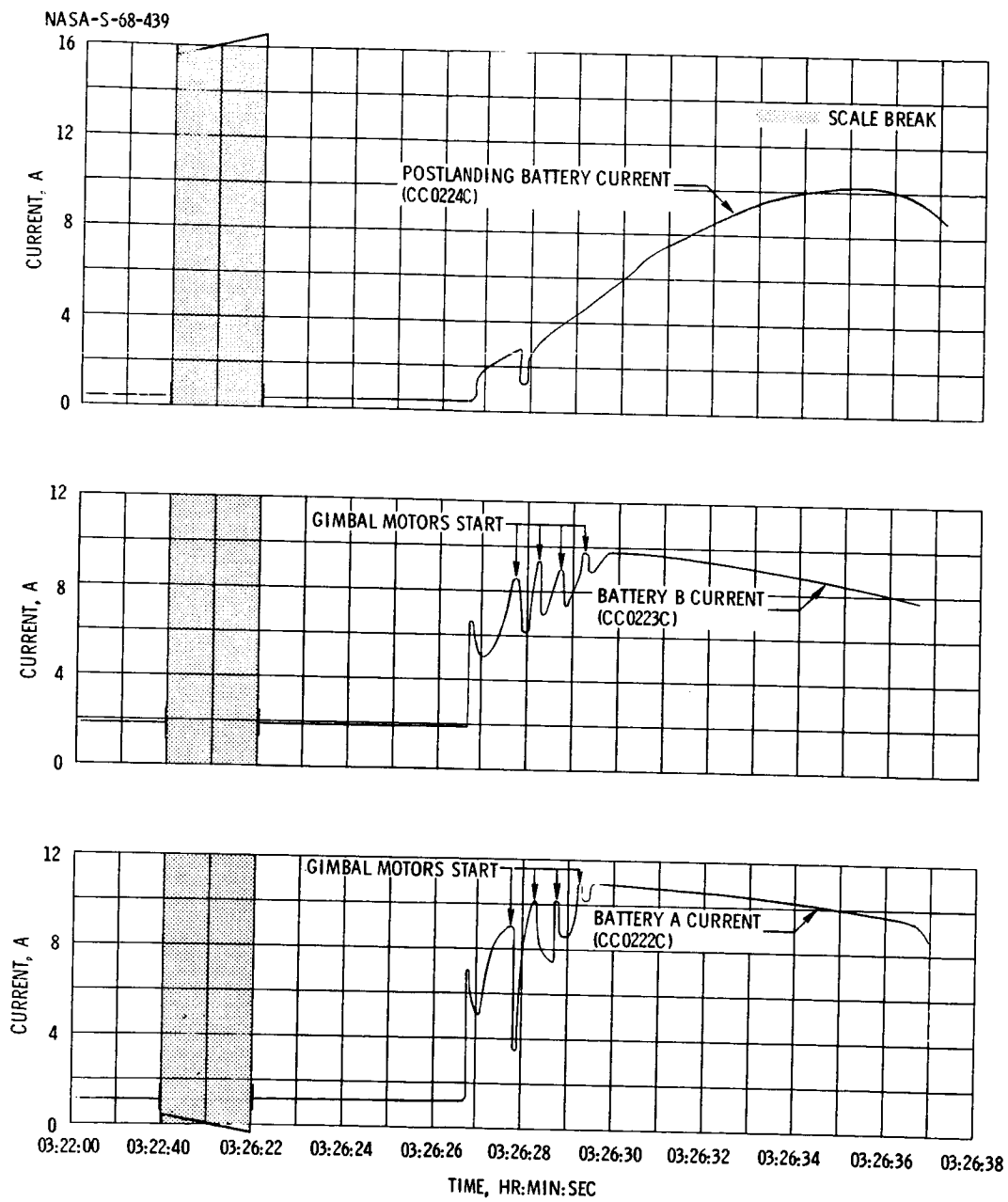


FIGURE 5.7-2. - ENTRY BATTERY CURRENTS DURING GIMBAL MOTORS START-UP.

~~CONFIDENTIAL~~

5.7-4

NASA-S-68-440

~~CONFIDENTIAL~~

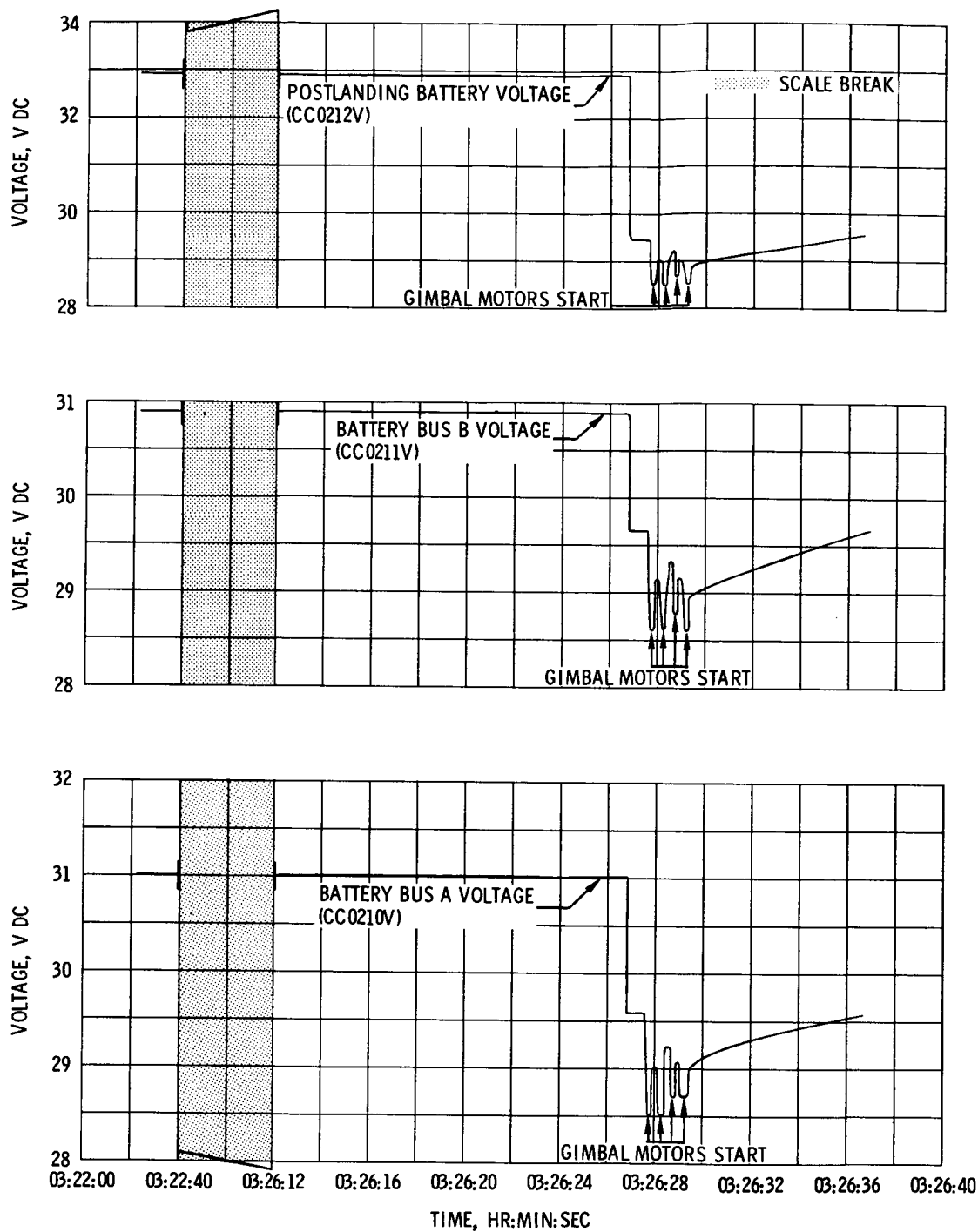


FIGURE 5.7-3. - ENTRY BATTERY VOLTAGES DURING GIMBAL MOTORS START-UP.

~~CONFIDENTIAL~~

~~CONFIDENTIAL~~

5.8-1

## 5.8 FUEL CELLS

### 5.8.1 Summary

The main dc power was satisfactorily supplied by three Block I fuel cell powerplants, augmented by three auxiliary batteries during peak electrical loads. All mission objectives were met. The objectives included extended zero-g operation of fuel cells, inflight fuel cell reactant purge, thermal control of fuel cells, and satisfactory system performance during launch environments, CSM/S-IVB separation, and service propulsion subsystem operation.

### 5.8.2 Prelaunch Operation

At T minus 37.5 hours the fuel cells were heated to operating temperature and placed on the spacecraft bus. Fuel cell no. 1 was placed on bus A, fuel cell no. 2 was placed on buses A and B, and fuel cell no. 3 was placed on bus B. Prior to launch the fuel cells were preheated to  $440 \pm 10^\circ \text{F}$  in order to increase fuel cell performance in the event of the loss of one fuel cell during the launch phase.

### 5.8.3 Performance

At launch the fuel cells were operating at approximately 35 A and 29.4 V and were delivering 1030 W each. The corresponding power delivered to the command module (CM) bus after line loss was 980 W per powerplant. After thermal stabilization at approximately 00:01:45, the fuel cells shared the load within 1 A. A typical load profile is shown in figure 5.8-1.

A comparison of indicated reactant consumption and water production with the calculated quantities for the flight is presented in table 5.8-I. The calculations were based on the following.

- a. The quantity of water produced and hydrogen consumed was calculated by converting the total mission ampere-hours to equivalent theoretical quantities.
- b. The quantity of hydrogen consumption indicated during the flight was converted to equivalent water produced.
- c. The net change was indicated by the potable tank quantity measuring instrumentation.

~~CONFIDENTIAL~~

~~CONFIDENTIAL~~

The difference between these methods of comparison was 2.4 pounds. All quantities agreed within the limits of optimum instrumentation accuracy and readability.

The fuel cell flowmeters agreed favorably with calculated consumption rates with the following two exceptions.

a. Fuel cell no. 2 hydrogen flowmeter showed an indication of zero shift. This shift was apparent during the countdown demonstration test, prelaunch, and during flight. Since this was not a mandatory flight measurement, there was no detrimental effect on the flight or on mission success. By correcting the flight data for the zero shift, the indicated flow rates agreed with calculated values within the limits of instrumentation accuracy.

b. Fuel cell no. 3 oxygen flowmeter failed at approximately 00:01:30. This transducer was a known problem during spacecraft check-out at the contractor's facility and at Kennedy Space Center. The system was checked for electrical short circuits prior to flight and none were indicated. A decision was made to use this flowmeter rather than replace the unit since it was noncritical. Replacement would have required a debrazing and rebrazing operation which could have contaminated the fuel cell system.

The capability to purge the three fuel cells subsequent to the cold-soak period at 07:30:00 was satisfactorily demonstrated. The oxygen flow increase indicated during the purge was 0.57 pound. This agrees with the specification value of approximately 0.55 lb/hr. The hydrogen flow indicated during the purge was 0.21 lb/hr, which corresponds to the maximum meter readout. The specification value is approximately 0.65 lb/hr. The inadequacy of the hydrogen flowmeter to monitor the purge flow rate was known and was accepted in order that the flowmeter would retain its accuracy in the normal operating range. An indication of purge flow is all the data required to confirm a hydrogen purge. The three purge cycles were for 2 minutes each and were spaced 3 minutes apart, making a total of 5 minutes for each fuel cell purge cycle.

The fuel cell condenser exit temperatures averaged between 157° F and 159° F as compared with specification values of 155° F to 165° F. During the flight of Spacecraft 011, fuel cell condenser exit temperatures increased to 200° F. These high condenser exit temperatures were caused by a reduced cooling capacity of the radiator coolant loops. Possible causes of unsatisfactory radiator coolant loop performance are as follows.

- a. Reduced glycol flow resulting from coolant pump filter plugging
- b. Incomplete coolant loop fill.

~~CONFIDENTIAL~~

~~CONFIDENTIAL~~

5.8-3

Fuel cell performance on the Apollo 4 mission verifies the elimination of this problem because of the incorporation of improved radiator fill techniques and increased coolant loop filter area (from 0.73 sq. in. to 6.60 sq. in.).

The fuel cell skin temperatures corresponded to predicted vacuum performance curves; a plot of random points is shown in figure 5.8-2.. A typical skin temperature profile is shown in figure 5.8-3.

All three fuel cell radiator outlet temperatures were within a range of 5° F throughout the flight, indicating normal radiator performance. The temperature was dependent on the environmental conditions. As the spacecraft passed into the shadow of the earth, the temperatures were at a minimum. As the spacecraft passed into the sunlight, the temperatures were at a maximum. Selected radiator return temperatures for fuel cell no. 3 are shown in figure 5.8-3 and are typical for all fuel cells.

~~CONFIDENTIAL~~

~~CONFIDENTIAL~~

TABLE 5.8-I.- SUMMARY OF FUEL CELL HYDROGEN  
CONSUMPTION AND WATER PRODUCTION

Condition	Hydrogen, lb	Potable water, lb
At lift-off minus 1 hour	25.8	6.1
At 08:00:00	23.5	24.3
	<hr/>	<hr/>
Indicated $\Delta$ change	2.3	18.2
Calculated $\Delta$ change <sup>a</sup>	2.05	18.35
Calculated $\Delta$ change <sup>b</sup>	-	20.60

<sup>a</sup>Hydrogen consumption calculated by total ampere-hours  $\times 2.57 \times 10^{-3}$ .

Water production calculated by total ampere-hours  $\times 2.297 \times 10^{-2}$ .

<sup>b</sup>Water production calculated by indicated hydrogen consumption  $\times 8.94$ .

~~CONFIDENTIAL~~

~~CONFIDENTIAL~~

5.8-5

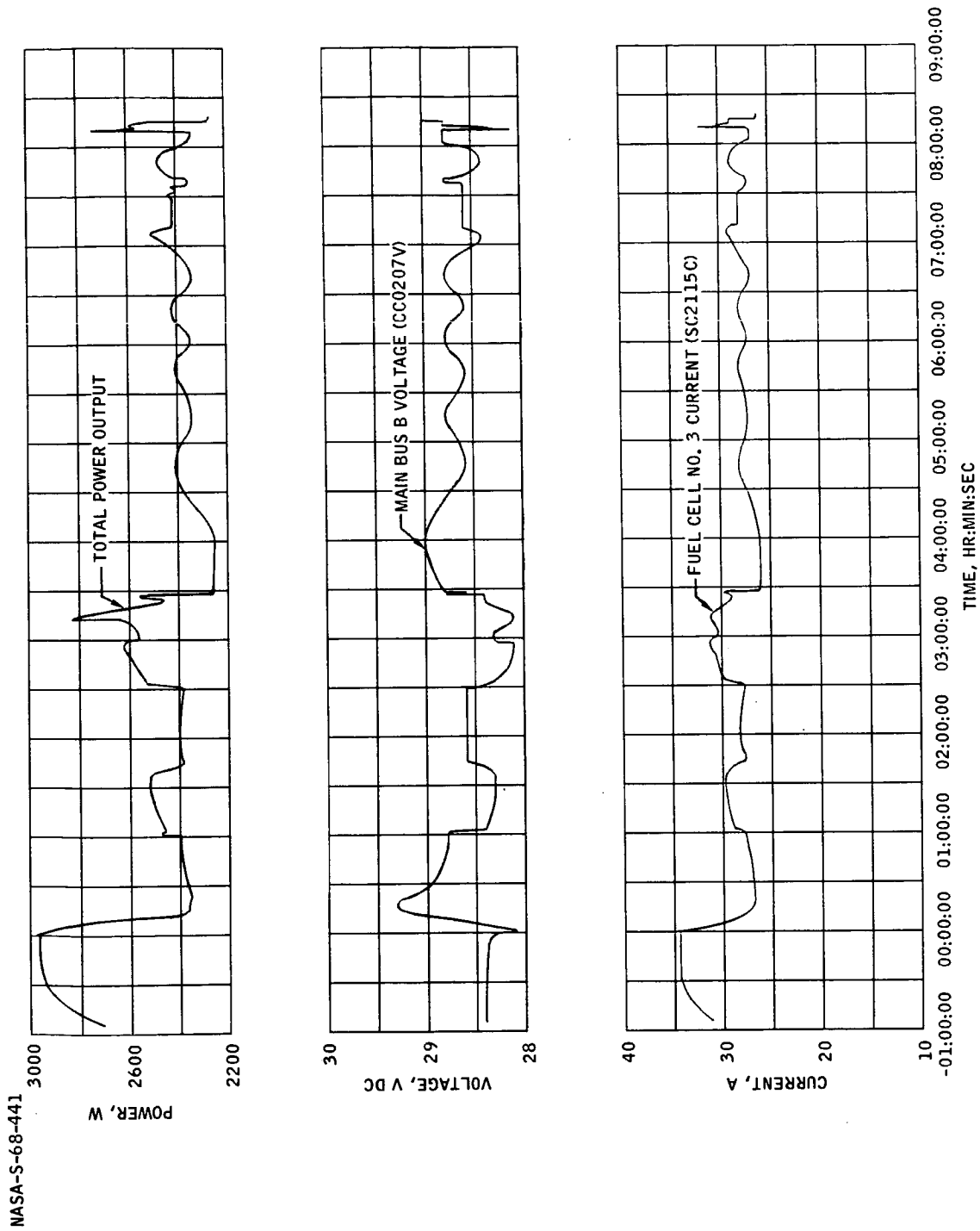


FIGURE 5.8-1.- LOAD PROFILE.

~~CONFIDENTIAL~~

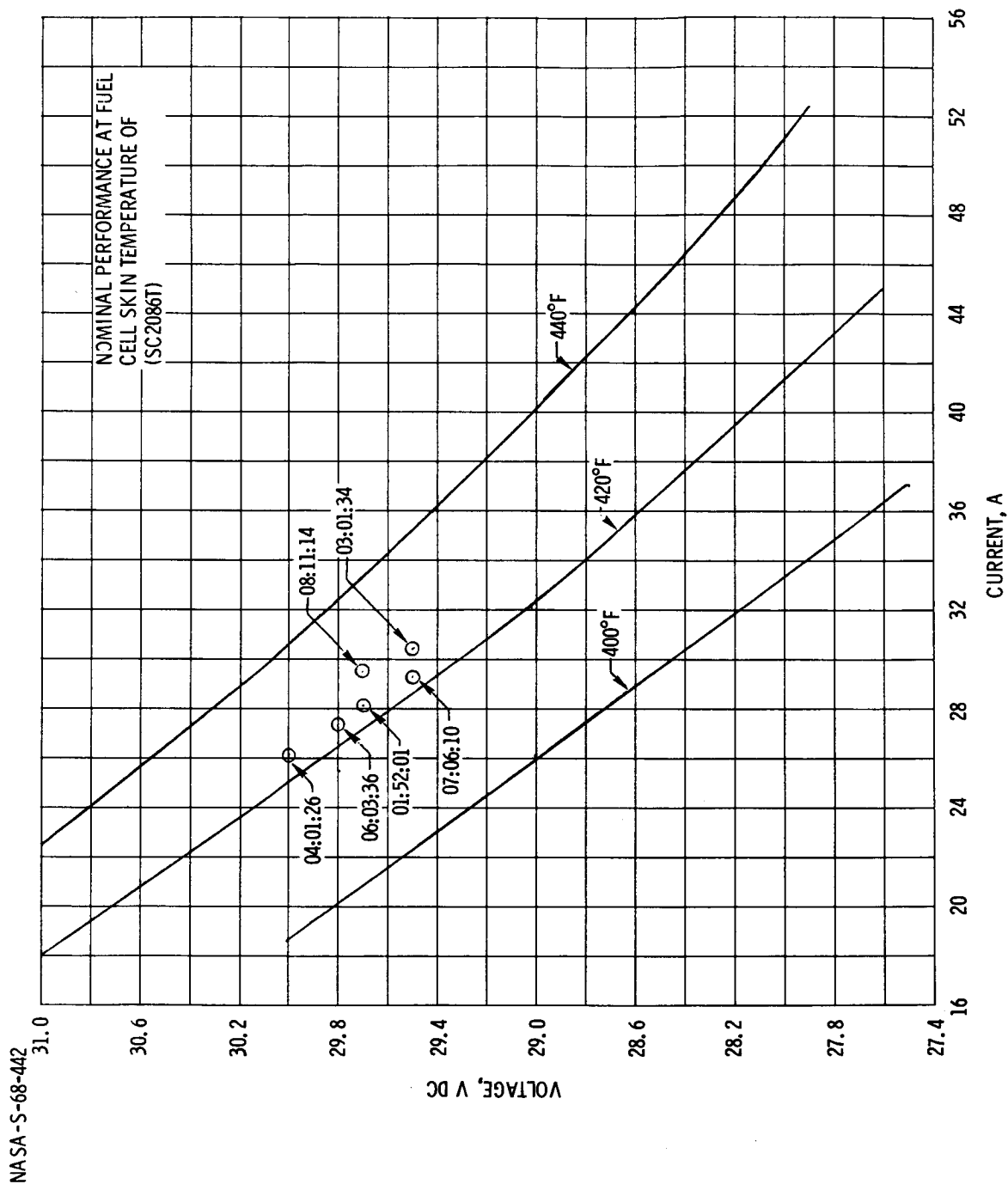
~~CONFIDENTIAL~~

FIGURE 5.8-2. - NOMINAL FUEL CELL PERFORMANCE COMPARED WITH ACTUAL FLIGHT DATA.

~~CONFIDENTIAL~~



~~CONFIDENTIAL~~

5.8-7

NASA-S-68-443

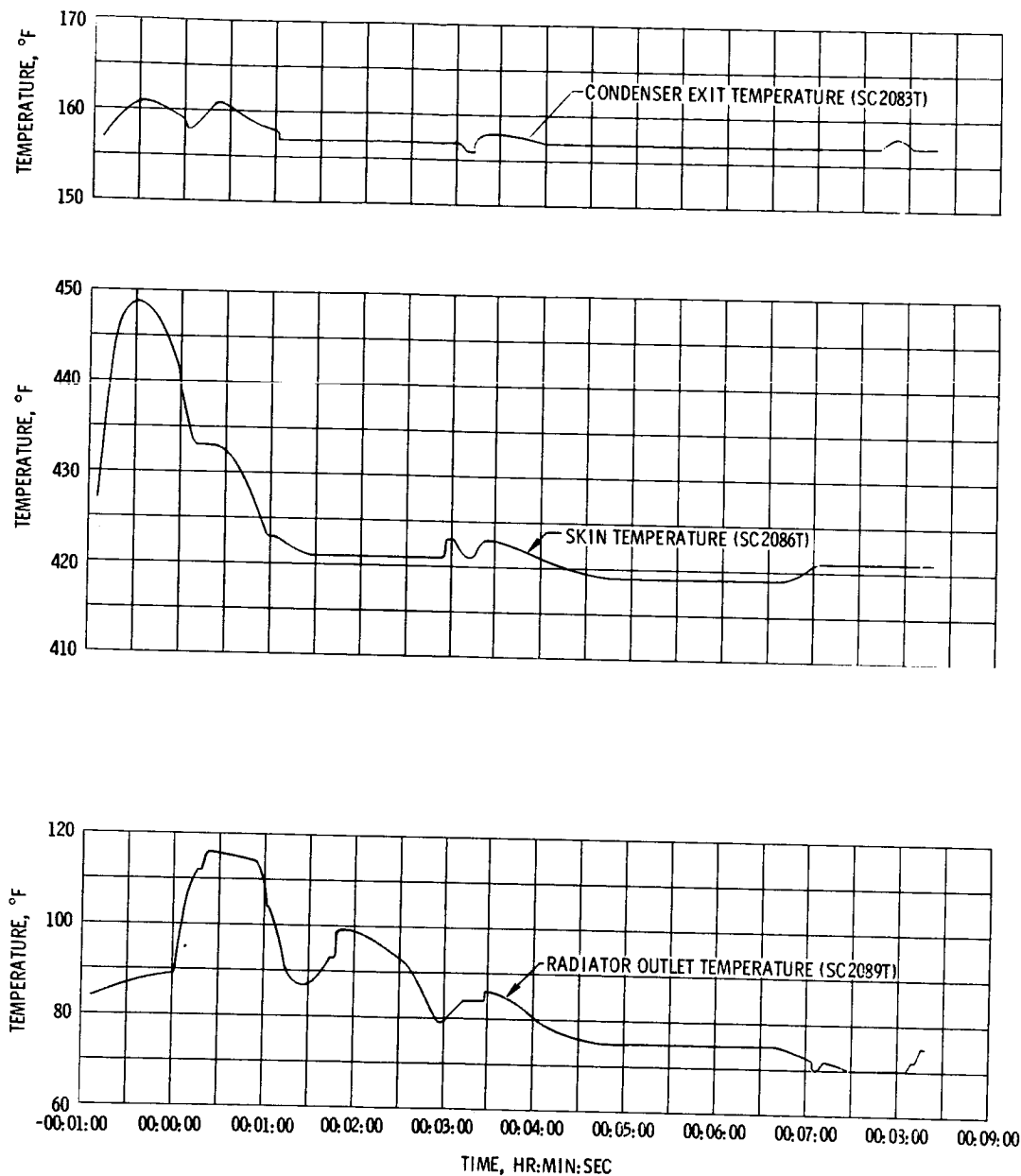


FIGURE 5.8-3. - FUEL CELL NO. 3 TEMPERATURES.

~~CONFIDENTIAL~~

~~CONFIDENTIAL~~

THIS PAGE INTENTIONALLY LEFT BLANK

~~CONFIDENTIAL~~

~~CONFIDENTIAL~~

5.9-1

## 5.9 SEQUENTIAL EVENTS CONTROL SUBSYSTEM

The sequential events control subsystem functioned satisfactorily throughout the flight, resulting in the related test objectives being met. See table 2.0-I for a list of significant flight events with planned and actual times. The master event sequence controller satisfactorily performed escape tower jettison, launch vehicle/spacecraft separation, command module/service module (CM/SM) separation, and apex cover jettison.

The SM jettison controller satisfactorily performed the function of separating the SM from the CM to preclude the possibility of recontact during entry.

The reaction control subsystem (RCS) controller satisfactorily performed CM fuel and oxidizer dumping, CM-RCS purge, and transfer of RCS jet logic from SM to CM at CM/SM separation.

The earth landing sequence controller, in conjunction with the pyrotechnic continuity verification box, performed drogue and main parachute deployment and disconnect. The baroswitches operated within specification tolerances (the 24 000-foot baroswitch operated at 23 200 feet and the 10 000-foot baroswitch operated at 9700 feet). See section 5.5 for details.

Loss of the 5-V instrumentation power supply reference voltage precluded telemetry event measurements of the following earth-landing sequencer functions: drogue parachute deployment, main parachute deployment, baroswitch lock-in, and main parachute disconnect. Confirmation of proper operation of each of these functions was obtained from other data and postflight tests.

~~CONFIDENTIAL~~

~~CONFIDENTIAL~~

THIS PAGE INTENTIONALLY LEFT BLANK

~~CONFIDENTIAL~~

~~CONFIDENTIAL~~

5.10-1

#### 5.10 PYROTECHNIC SUBSYSTEM

Review of flight data indicates that all pyrotechnic devices functioned as required for the Apollo 4 mission.

Two CM oxidizer dump valves and one helium dump valve, each of which contained a pressure cartridge, were not required to function during the Apollo 4 mission and were recovered as live ordnance.

Pyrotechnic battery voltages did not return to open circuit voltage levels after apex cover jettison and drogue parachute deployment. Some leakage current can be expected after pyrotechnic initiator firings, sufficient to keep the pyro batteries from returning to open circuit voltage levels.

~~CONFIDENTIAL~~

5.10-2

~~CONFIDENTIAL~~

THIS PAGE INTENTIONALLY LEFT BLANK

~~CONFIDENTIAL~~

~~CONFIDENTIAL~~

5.11-1

#### 5.11 LAUNCH ESCAPE SYSTEM

Observation of TV tape playbacks indicates that performance of the launch escape system (LES) was satisfactory and that the tower jettison motor fired as programmed to remove the LES, including the boost protective cover, from the command module. The preflight planned sequence was S-II ignition at 00:02:33.3 with LES separation occurring at 00:03:08.8, or 35.5 seconds later. The actual flight times were S-II ignition at 00:02:32.2 with LES separation occurring at 00:03:07.2, or 35.0 seconds after ignition.

~~CONFIDENTIAL~~

~~CONFIDENTIAL~~

THIS PAGE INTENTIONALLY LEFT BLANK

~~CONFIDENTIAL~~



~~CONFIDENTIAL~~

5.12-1

## 5.12 EMERGENCY DETECTION SUBSYSTEM

### 5.12.1 Summary

A primary objective of the Apollo 4 mission was evaluation of the emergency detection subsystem (EDS) in the open-loop mode with the automatic abort capability disabled. A constraint had been placed on the Apollo 6 mission until a successful evaluation could be made of the automatic abort capability in the open-loop configuration on the Apollo 4 mission. The system performance was nominal during the Apollo 4 mission, thus removing the constraint to the Apollo 6 mission.

### 5.12.2 Description

During the launch phase, the EDS receives indications of any emergency conditions from the launch vehicle, from spacecraft systems, and from the Q-ball differential pressure meter mounted at the apex of the launch escape tower.

In the closed-loop configuration, the normal mode for manned flight, the EDS can initiate automatic abort in the event of excessive vehicle angular rates, loss of thrust on two of the first stage engines, or interruption of the electrical interface between the command module (CM) and the launch vehicle instrument unit. In the open-loop configuration flown on Apollo 4, the abort circuit was opened in the spacecraft by leaving the automatic abort-enabling switch on the main display console in the OFF position at launch.

Crew displays of EDS parameters in the spacecraft were monitored only by telemetry. Those launch vehicle status displays which are redundant were monitored in the A-system only. The single output of the Q-ball (supplied by Marshall Space Flight Center) was displayed in the CM and was telemetered. As in earlier unmanned CM's, provisions for tower jettison and nonautomatic abort, which normally would be crew functions, were included in the mission control programmer.

### 5.12.3 Performance

No conditions approaching manual or automatic abort levels were encountered at any time during the launch phase. No automatic abort signals were generated by the launch vehicle. Redundant enabling commands were properly received from the launch vehicle at lift-off and were properly extinguished 5 seconds later.

~~CONFIDENTIAL~~

~~CONFIDENTIAL~~

Launch vehicle engine-status lights correctly extinguished as the S-IC stage engines successively reached normal thrust, and illuminated as the engines cut off prior to staging. Because of a special sequence used in the launch vehicle for the Apollo 4 mission, the momentary extinction that, in the manned missions, will indicate S-IC/S-II separation did not occur. The status lights correctly indicated S-II stage thrust on, cutoff, and separation, and S-IVB stage thrust on and cutoff. No indications of launch vehicle guidance failure or excessive rates were received. The S-II stage second plane separation light illuminated as expected during the S-II stage first plane separation sequence, and extinguished 30 seconds later at the second plane separation.

Because of low-velocity winds aloft, the output of the Q-ball (fig. 5.12-1) was lower than expected. The highest value occurred at 00:00:47 and was equivalent to 0.95 psid. The tentative abort limit for Saturn V - Apollo manned flights is 3.20 psid. Output of the Q-ball was essentially zero after 00:01:25. The Q-ball output indications received in the spacecraft have been confirmed by redundant measurements from the launch vehicle.

Spacecraft angular rate measurements, which drove the rate indicators in the flight director attitude indicator, are compared with the preliminary EDS abort limits for the S-IC (first) stage of powered flight in figure 5.15-2. The manual and automatic abort limits have been overlaid on a normal ascent phase plot of the guidance and navigation subsystem. Figures 5.12-2, 5.12-3, and 5.12-4 show the same measurements compared with the preliminary EDS abort limits for the S-II stage, S-IVB stage first burn, and S-IVB second burn, respectively. Both the manual and automatic abort limits are shown on the figures. The manual limits were of no effect in the Apollo 4 mission and are shown for information only. In a manned flight, violation of one of the manual limits, in conjunction with another cue, would require the crew to abort. The automatic limits are the rates at which the automatic abort circuit in the launch vehicle instrument unit would have generated an abort command. The measurements used in the automatic abort circuit are generated by rate gyros in the instrument unit. The spacecraft measurements are shown in this section for reference only. The measured rates are well within the preliminary abort limits throughout the launch vehicle powered flight phases.

The performance of the EDS is considered to have been satisfactory in all respects.

~~CONFIDENTIAL~~

~~CONFIDENTIAL~~

5.12-3

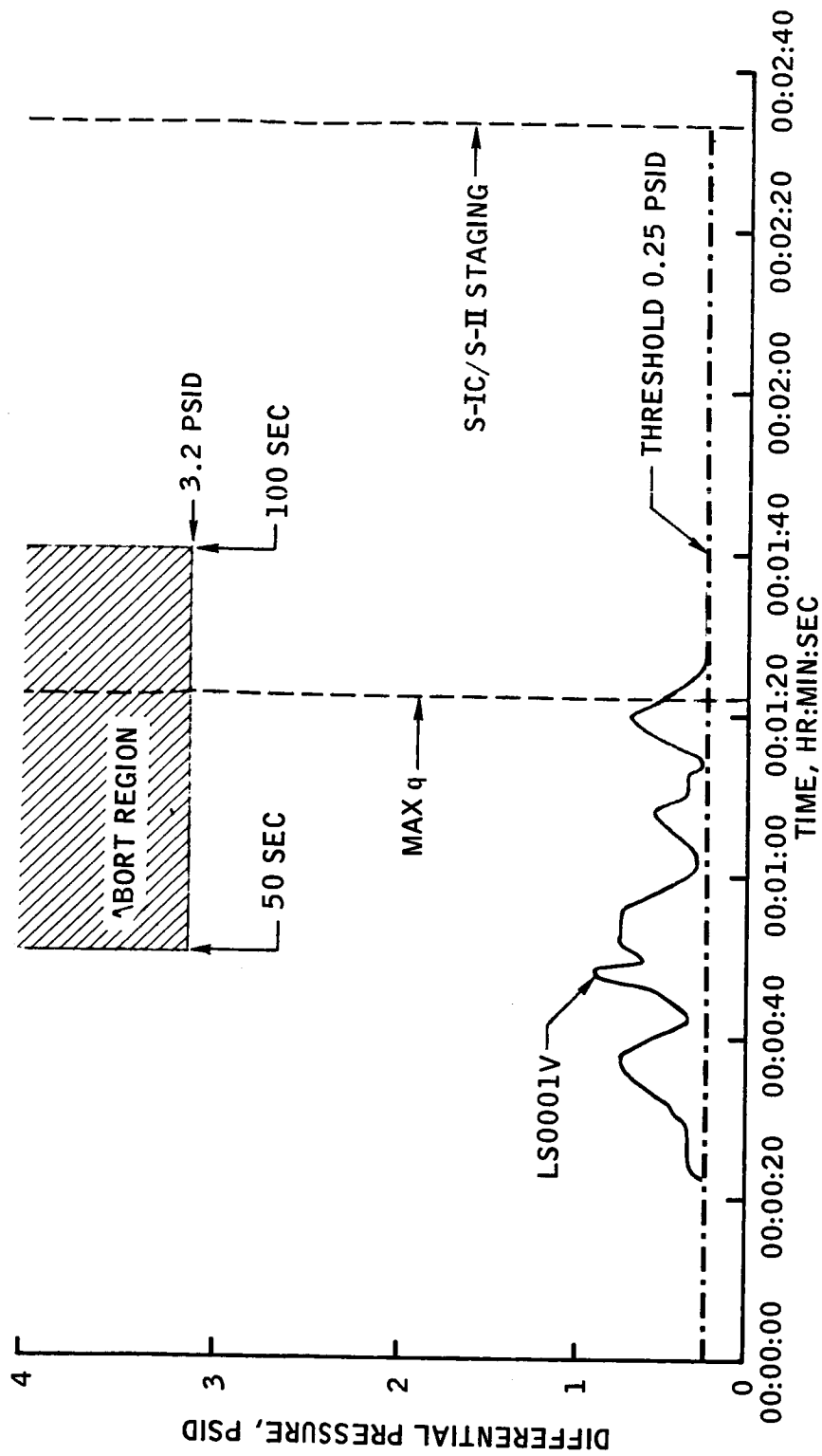


FIGURE 5.12-1.- EMERGENCY DETECTION SUBSYSTEM, ANGLE OF ATTACK PARAMETER ( $\Delta P$ ).

~~CONFIDENTIAL~~

~~CONFIDENTIAL~~

NASA-S-68-445

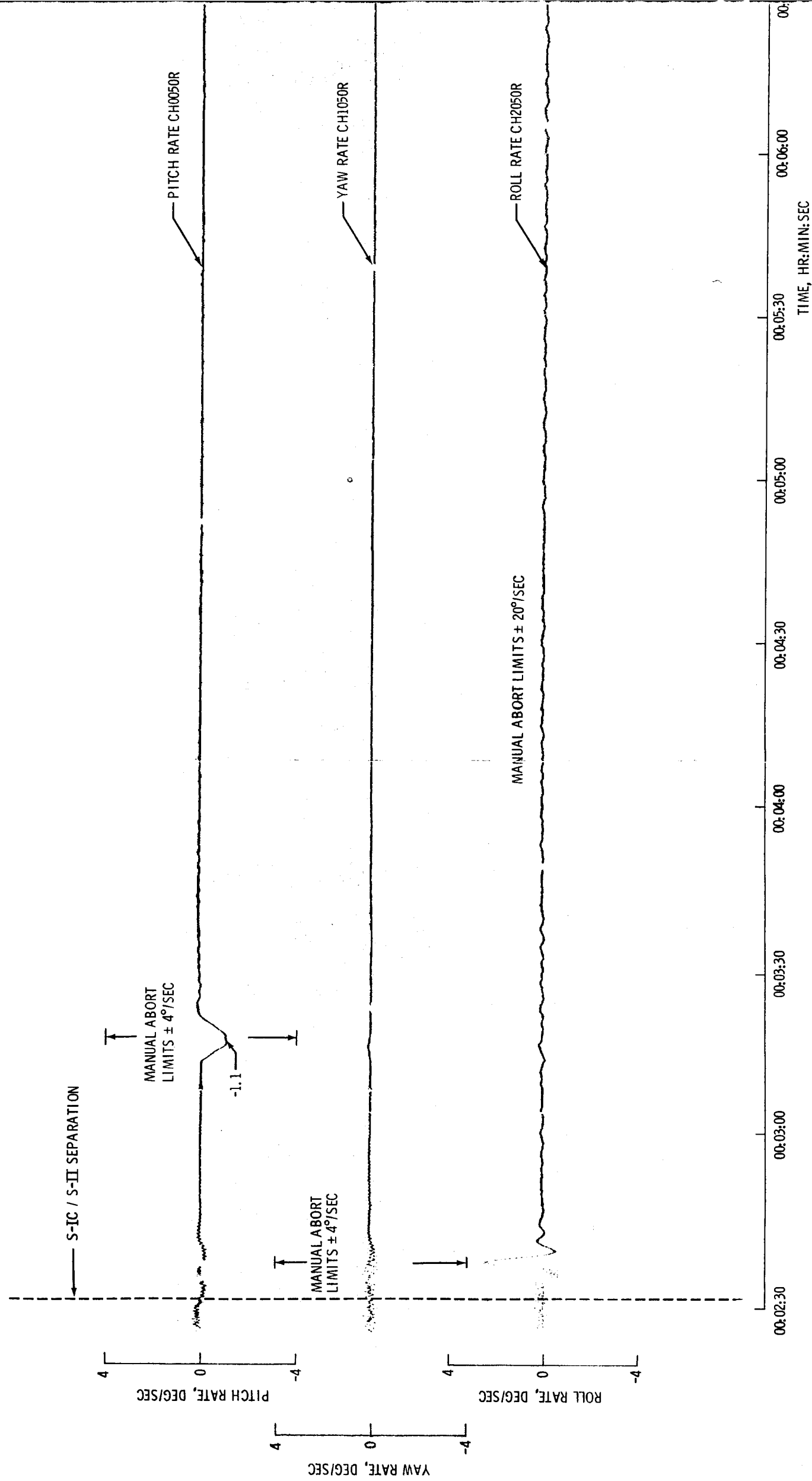
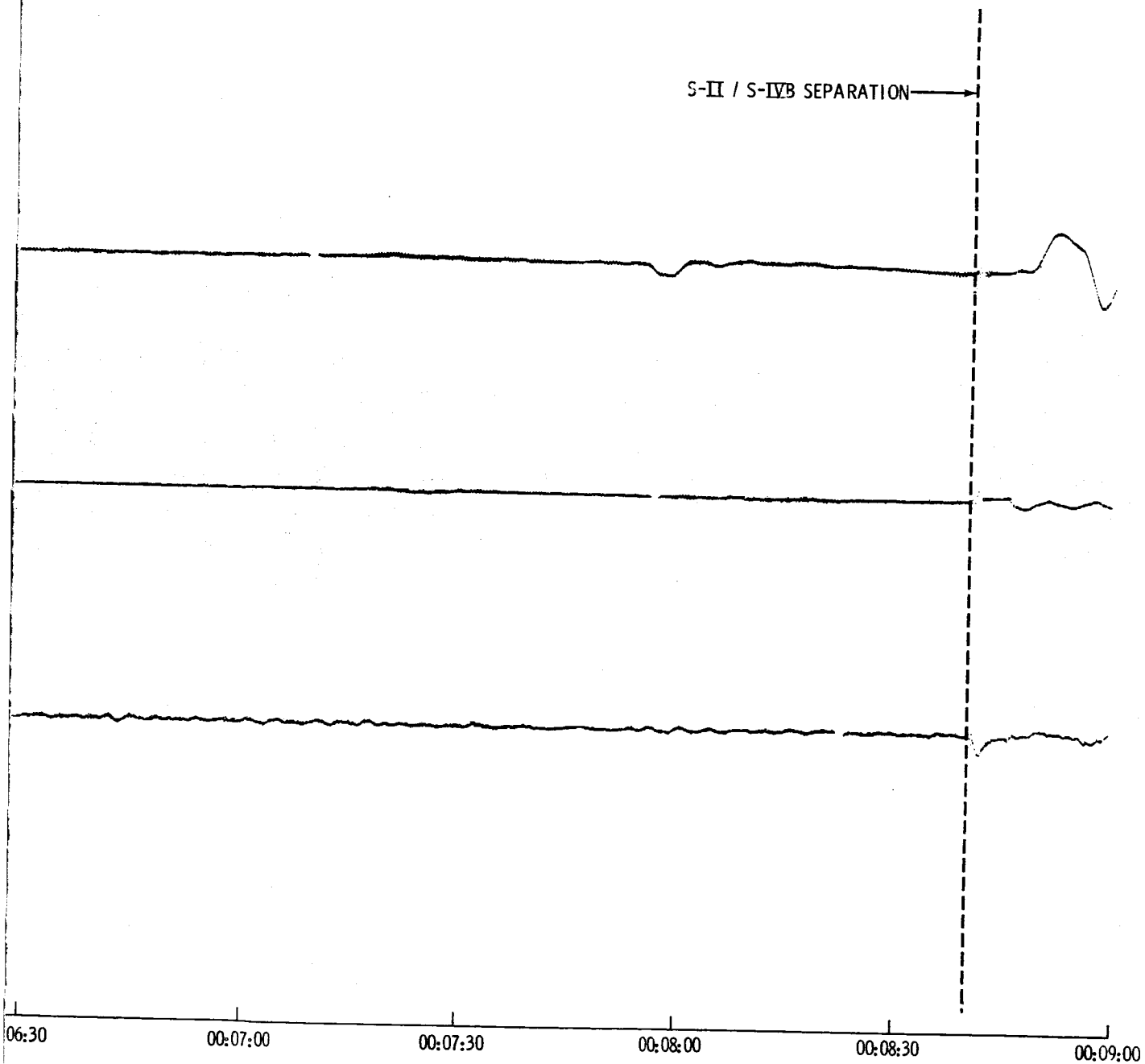


FIGURE 5.12-2. - ANGULAR RATES AND EMERGENCY DETECTION SYSTEM ABORT LIMITS DURING S-II STAGE BURN.

Fold-out #1

~~CONFIDENTIAL~~

S-II / S-IVB SEPARATION →



FOLD-OUT #2

~~CONFIDENTIAL~~

5.12-5

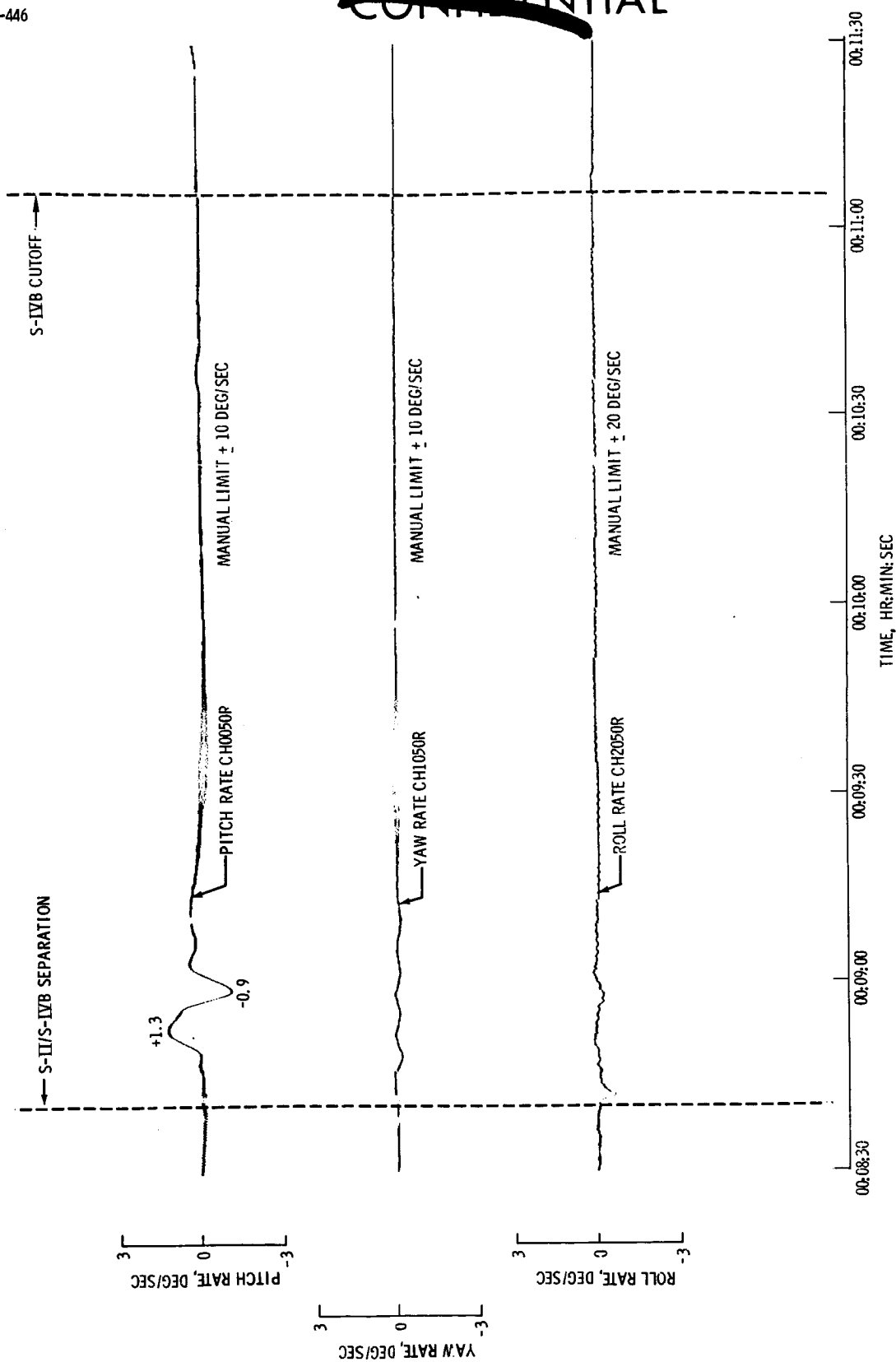


FIGURE 5.12-3. - ANGULAR RATES AND EMERGENCY DETECTION SYSTEM ABORT LIMITS DURING FIRST S-IVB STAGE BURN.

~~CONFIDENTIAL~~

~~CONFIDENTIAL~~

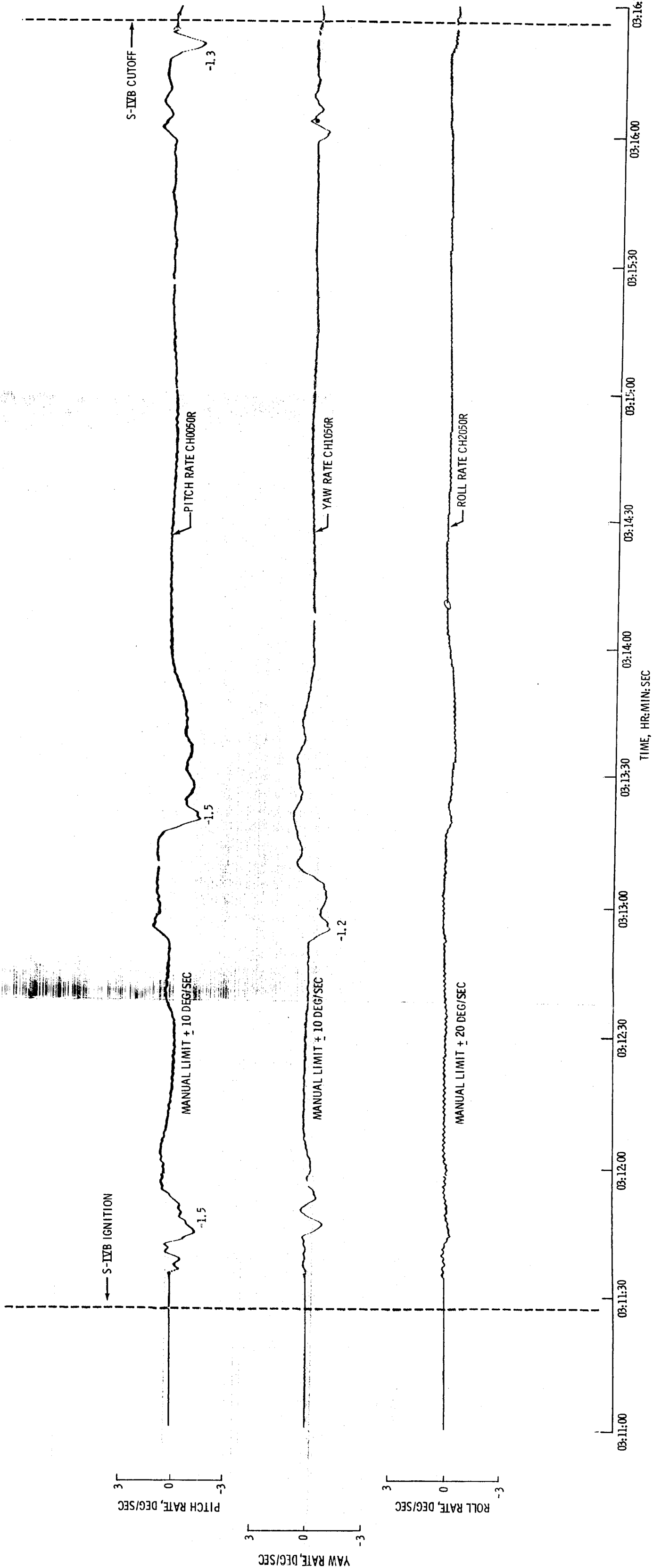


FIGURE 5.12-4.-ANGULAR RATES AND EMERGENCY DETECTION SYSTEM ABORT LIMITS DURING SECOND S-IVB STAGE BURN.

~~CONFIDENTIAL~~

~~CONFIDENTIAL~~

5.13-1

## 5.13 COMMUNICATIONS SYSTEM PERFORMANCE

The communications system was evaluated by analysis of the spacecraft communications subsystem as an entity and the spacecraft communications subsystem and Manned Space Flight Network (MSFN) communications equipment as an integrated system. A diagram of the communications capabilities during the Apollo 4 mission is presented in figure 5.13-1. For a description of the spacecraft communications subsystem refer to section 13.1. Apollo manned missions will utilize the unified S-band communications system for all data, voice, and tracking. Therefore, analysis of the unified S-band system performance has been emphasized.

The information in this section is based on preliminary evaluation of recorded data and premission predictions that were based on nominal trajectory and spacecraft attitudes. Updated information will be presented in a supplemental report that will include predicted performance based on the actual flight trajectory and spacecraft attitudes.

### 5.13.1 Summary

Analysis of the available data indicates that the objectives of the spacecraft and MSFN S-band communications and spacecraft vhf communications were successfully accomplished. The data required to verify successful completion of the objective for the Apollo range instrumentation aircraft communications have not been analyzed. Basic results of the analyses are summarized as follows.

Coverage during the launch and initial powered flight phase was approximately as predicted. Two-way S-band phase lock between the Merritt Island unified S-band station and the spacecraft was lost during the period of flame attenuation. The received carrier powers at Merritt Island and at the spacecraft were low during the period of booster shadowing. Signals received at the Grand Bahama Island unified S-band site were not significantly affected by launch events or shadowing.

Performance during the two near-earth parking orbits was excellent. The S-band signal levels and data channel performance during the coast ellipse portion of the flight were very satisfactory. Good S-band telemetry data were received at ranges exceeding 12 000 n. mi. The vhf system also provided good data to a range of at least 4000 n. mi. — *actual*

The communications system performed well during the high velocity return until CM/SM separation. At that time, three of four Guam S-band receivers lost lock abruptly. The signal was later received by Guam (intermittently), two Apollo/range instrumentation aircraft, and recovery units.

~~CONFIDENTIAL~~



~~CONFIDENTIAL~~

The cause of the abrupt loss of lock by three of the four Guam receivers is believed to be flame attenuation from the SM reaction control sub-system thrusters.

Delays were experienced in transferring commands to the spacecraft. Each desired command was eventually accepted by the spacecraft equipment, and the delay caused no adverse effects on the mission. Certain problems (including updata delays) were caused, directly or indirectly, by errors in ground operation procedures or techniques. In some cases, these problems were caused, or aggravated, by spacecraft antenna pattern nulls.

This was the first opportunity for the complete MSFN to acquire and track the Apollo S-band signals, and the overall performance exceeded expectations.

#### 5.13.2 Communications Subsystem Performance

Data obtained during the Apollo 4 mission indicated that the spacecraft communications subsystem performed within nominal limits. The communication subsystem provided the uplink command and downlink data capability for Spacecraft 017. The onboard subsystem was comprised of Block I communication equipment configured similarly to the Spacecraft 011 subsystem (AS 202 mission). The primary difference between Spacecraft 011 and Spacecraft 017 was in the antenna hardware configuration. Spacecraft 017 used four Block II S-band omnidirectional antennas flush mounted on the periphery of the aft heat shield and two Block II vhf/uhf scimitar antennas mounted on the service module. The S-band antennas were connected in diametrically opposing pairs. The pair located at  $\phi = 135$  degrees and  $\phi = 315$  degrees was used throughout the Apollo 4 mission.

Unified S-band equipment.- The unified S-band equipment provided pulse code modulation (PCM) telemetry and simulated voice (400-Hz tone) information from prelaunch until the unified S-band equipment was turned off after spacecraft landing. The unified S-band equipment also exercised the pseudo-random noise ranging system and updata link. Performance of the unified S-band equipment was within nominal limits throughout the mission.

Very high frequency/amplitude modulation.- The Block I vhf/AM transceiver was modulated with a 400-Hz tone to simulate downlink voice. The tone was processed through the center couch module of the audio center and was then used to amplitude-modulate the transmitter carrier. The

~~CONFIDENTIAL~~

~~CONFIDENTIAL~~

5.13-3

vhf/AM transmitter operated continuously from prelaunch until it was turned off at CM/SM separation. Available data indicate nominal performance of the transmitter.

An earlier question concerning the power output of the vhf/AM transmitter was resolved satisfactorily. It was established that the acceptance test measurement of 7.75 watts (nominal 5 watts) output was taken with no modulation on the transmitted carrier. This procedure is in accordance with specified methods. During the flight, the vhf/AM transmitter was continuously modulated at approximately 90 percent. It is calculated that the power output with 90 percent modulation would be 11.24 watts, which agrees very closely with the PCM-measured value of 11.3 watts. This agreement was also confirmed by postmission laboratory tests both at Downey, California, and the Manned Spacecraft Center using production models of the transceiver.

Very high frequency/frequency modulation.- The vhf/FM telemetry transmitter operated continuously from prelaunch until CM/SM separation to provide real-time high-bit-rate (51.2 kilobits) PCM data. No vhf/FM operational anomalies have been found.

Pulse code modulation telemetry.- Non-return-to-zero PCM telemetry data were obtained throughout the mission. Real-time data were received from S-band and vhf/FM transmitters. Recorded data were obtained from the data storage equipment. No anomaly has been found in the operation of the PCM equipment.

Premodulation processor.- The premodulation processor contained the subcarrier oscillators for downlink S-band voice and pulse code modulation data, the pulse code modulation data driver for the vhf/FM transmitter, and the 70-kHz updata link subcarrier discriminator. Therefore, any malfunction within the premodulation processor would have resulted in some form of degradation of the S-band or vhf/FM data. The received data demonstrated the nominal performance of the premodulation processor.

C-band transponder.- All data show that C-band operation was normal. Successful tracking by ground C-band radars was accomplished and no anomaly was indicated.

Updata link equipment.- The updata link provides a command channel to update the time accumulator in the central timing equipment, update the Apollo guidance computer, and control certain vehicle functions during the mission. The updata link can operate either in the uhf or S-band mode. The uhf mode was used until just before the second S-IVB stage burn when the operational mode was changed to S-band. There was no anomaly associated with the spacecraft updata link equipment.

~~CONFIDENTIAL~~

~~CONFIDENTIAL~~

Central timing equipment.- The central timing equipment performed without any anomaly and interfaced properly with the 1024-kHz input from the guidance and navigation subsystem. The parallel time-code was successfully received through the PCM telemetry subsystem.

Data storage equipment.- The data storage equipment operated in the record mode only and provided inflight recording of various spacecraft measurements, including the PCM bit stream. Satisfactory performance was demonstrated by the retrieval of good-quality data.

High frequency recovery equipment.- The hf transceiver was operated in the beacon continuous-wave mode, and operation was nominal. The 14-foot hf antenna deployed successfully and the transceiver was activated approximately 11 seconds after spacecraft landing. There was no reported operational anomaly.

Very high frequency recovery equipment.- The two vhf recovery antennas were erected during the main parachute deployment sequence. The vhf recovery beacon signal was routed to one antenna while the vhf survival transceiver beacon signal was routed to the other. Both vhf beacons functioned properly, and signals were received satisfactorily by the recovery forces.

### 5.13.3 Performance During Launch Phase

Unified S-band radio frequency system.- Performance of the unified S-band radio frequency system was analyzed and the results are presented in the following paragraphs.

Acquisition and handover: Two-way phase lock with the spacecraft was established by the operators at Merritt Island prior to launch and was maintained until 00:02:32. At that time, one of the two Merritt Island receivers supporting the spacecraft unified S-band equipment, and both of the Merritt Island receivers supporting the launch vehicle instrument unit transponder lost lock. Analysis of the received signal power levels at Merritt Island showed that the flame associated with S-IC/S-II stage separation and S-II stage ignition attenuated the FM telemetry signal received from the launch vehicle instrument unit approximately 42 dB. Tests at MSC have shown that the spacecraft S-band receiver automatic gain control response time is too slow to follow an abrupt change in carrier power of the above magnitude. Thus, the conditions required for phase lock were not maintained, and the loss of lock was caused by flame attenuation resulting from S-IC/S-II stage separation and S-II stage ignition.

~~CONFIDENTIAL~~

~~CONFIDENTIAL~~

5.13-5

Merritt Island receiver 1-2, which did not lose lock at separation, recovered from the flame attenuation and maintained downlink lock until 00:03:04. The other Merritt Island receiver (2-2) was in and out of lock from 00:02:32 to 00:04:54. Reacquisition of two-way lock was initiated at 00:03:17 and was completed at 00:03:21. The cause is unknown for the 45-second delay before reacquisition was initiated. Uplink transmission from Merritt Island ceased at 00:07:00 for handover to Bermuda.

Handover was completed by establishing two-way lock with Bermuda at 00:07:02. Uplink transmission from Bermuda ceased at 00:11:57 for handover to the Apollo tracking ship Vanguard. Handover was completed and two-way lock established between the spacecraft and the Vanguard at 00:12:19. Thus, the handovers from Merritt Island to Bermuda and from Bermuda to the Vanguard were accomplished with a loss of uplink lock for 20 and 22 seconds, respectively. If the acquisition of both spacecraft and ground receivers had been accomplished on the first sweep, minimum time for each of the handovers would have been 4 to 8 seconds.

The S-band site at Grand Bahama tracked the spacecraft with one-way (downlink) lock from 00:01:10 until the handover of uplink from Merritt Island to Bermuda. During this handover, Grand Bahama lost downlink lock. The Grand Bahama site was receiving the signal from the launch vehicle instrument unit (IU) transponder on receiver 1-1 and the signal from the CM/SM unified S-band equipment on receiver 2-1 during the launch phase. When communications with the IU transponder was handed over from Merritt Island to Bermuda, the IU transponder switched to its auxiliary oscillator; this is an automatic function expected during handover. This switching caused receiver 1-1 at Grand Bahama to lose lock and automatically programmed the spacecraft receiver (receiver 2-1) at Grand Bahama to the acquisition antenna. The received carrier power at Grand Bahama with receiver 2-1 on the acquisition antenna was not sufficient to allow reacquisition of the CM/SM signal prior to loss-of-signal. The 3-foot diameter acquisition antenna has a gain approximately 20 dB less than the main antenna.

Received carrier power: Time histories of the received uplink and downlink carrier power levels during the launch phase are presented in figures 5.13-2 and 5.13-3. The received downlink carrier power levels at Merritt Island, Grand Bahama and Bermuda are compared with predictions in figures 5.13-4, 5.13-5, and 5.13-6, respectively.

As shown in figure 5.13-4, the level of the carrier power received at Merritt Island was relatively high from launch to 00:03:04, except for the transient at 00:02:32. From 00:03:15 to loss-of-signal, the received carrier power at Merritt Island was approximately 25 dB lower

~~CONFIDENTIAL~~

~~CONFIDENTIAL~~

than premission predictions indicated it would be. Since the difference between predicted and measured carrier power levels from the IU transponder was approximately the same and the track was valid, the difference between measured and predicted carrier power levels has been attributed to launch vehicle shadowing effects. This attenuation was expected; however, computed degradation was not attempted in the predictions.

The signal received at Grand Bahama during the launch phase was extremely good (fig. 5.13-5). From 00:01:30 to 00:03:10, the received carrier power was greater than -80 dBm. The exact power could not be determined because of strip chart recorder pen limits. Flame attenuation caused the received carrier power to drop to -90 dBm at S-IC/S-II stage separation. The IU transponder switched to the auxiliary oscillator momentarily at 00:03:10 and Grand Bahama receiver 1-1 dropped lock. Thus, the spacecraft receiver (receiver 2-1) at Grand Bahama automatically switched to the acquisition antenna. The difference between predicted and measured downlink carrier power levels from 00:03:10 to 00:04:34, when receiver 2-1 was switched back to the 30-foot main antenna, is approximately the same as the difference in the gains of the acquisition and main antennas. Predicted and measured carrier power levels compare very favorably (within 2 to 3 dB) from 00:04:34 to loss-of-lock at 00:07:10.

As shown in figure 5.13-6, the signal received at Bermuda from 00:07:09 to loss-of-signal was equal to or greater than the predicted level most of the time.

Telemetry.-- The unified S-band and vhf telemetry channel performance was evaluated by computing the probability of a bit error from the measured frame synchronization word error rate. The relationship utilized in these computations is as follows.

$$BEP = 1 - (1 - WER)^{1/N}$$

where

BEP = probability of a bit error

WER = word error rate

N = number of bits in the word (26 for the frame synchronization word)

During the first 7 minutes after launch, the bit error probabilities for vhf and S-band telemetry received at Merritt Island were  $1 \times 10^{-6}$ , or better, for a total time of 4 minutes 50 seconds and 5 minutes

~~CONFIDENTIAL~~

~~CONFIDENTIAL~~

5.13-7

20 seconds, respectively. The S-band and vhf telemetry bit error probability degraded below  $1 \times 10^{-3}$  for total times of 30 seconds and 20 seconds, respectively, for the same time period. Separation of the S-IC/S-II stages and the S-II ignition degraded the bit error probabilities of the vhf and S-band telemetry data received at Merritt Island. Jettison of the launch escape system also increased the S-band telemetry bit error probability.

Bit error rate data are not present from the S-band telemetry at Grand Bahama. From 00:01:30 to 00:07:00, Grand Bahama S-band received carrier power was sufficient to maintain a bit error rate less than  $1 \times 10^{-6}$ . The vhf telemetry bit error rate at Grand Bahama was  $1 \times 10^{-6}$ , or better, from approximately 00:01:30 until 00:09:00 and was not affected by launch events.

Simulated voice communications.- Simulated voice signals (400-Hz tone) transmitted via the vhf and unified S-band downlinks were received and recorded by each MSFN site that supported the launch phase of the mission. The recorded data were evaluated by determining the signal-to-noise ratio as a function of time and extrapolating expected voice performance from the signal-to-noise ratios.

Evaluation of the data recorded at the Merritt Island S-band site during the launch phase shows that the S-band down-voice channel would have provided good communications for most of the first 5 minutes 30 seconds of the mission. The signal-to-noise ratio was degraded on three occasions; while the line of sight to the Merritt Island site was passing through the launch vehicle exhaust plume (00:02:00 to 00:02:21), at S-IC/S-II stage separation, and when the Merritt Island receiver 1-2 was out of lock. Extrapolation of expected voice performance from the signal-to-noise ratio measurements indicates the word intelligibility would have been approximately 90 percent except during the aforementioned periods of degraded signal-to-noise ratios; during these times the word intelligibility would have been approximately 80 percent. The S-band down-voice channel would not have provided good voice communications from 00:05:30 until handover to Bermuda at 00:07:00.

The vhf/AM down-voice link would have provided good launch coverage. The measured signal-to-noise ratios indicate that word intelligibility would have been over 90 percent during most of the first 9 minutes of the launch phase. The three periods of time when the intelligibility would not have been greater than 90 percent were from 00:02:00 to 00:02:24, from 00:03:03 to 00:03:06, and during S-IC/S-II stage separation and S-II stage ignition. The predicted word intelligibility during these periods is over 85 percent.

~~CONFIDENTIAL~~

~~CONFIDENTIAL~~

The average signal-to-noise ratio measured from the data recorded at the Grand Bahama S-band site was greater than 20 dB from acquisition of signal to loss-of-signal during the handover from Merritt Island to Bermuda. This average signal-to-noise ratio corresponds to a predicted downlink word intelligibility greater than 90 percent. Note that the signal-to-noise ratios at Grand Bahama were not affected by launch events and that the voice communications afforded by the Grand Bahama site coverage would have filled the aforementioned void between Merritt Island and Bermuda.

The configuration of the spacecraft unified S-band equipment is such that the baseband uplink modulation is turned around and remodulated on the downlink carrier when the ranging switch is in the RNG position. Prior to launch, the ranging switch was placed in the RNG position and it remained there throughout the mission. Thus, a 1-kHz tone (voice simulation) was transmitted by Merritt Island during the launch phase. This tone was recovered from a recording of the downlink signal received at Merritt Island and signal-to-noise ratios were measured.

The average signal-to-noise ratio was greater than 20 dB except for the periods of time from lift-off to 30 seconds, from 00:02:00 to 00:02:21, from 00:02:32 to 00:03:21, and from 00:05:30 to handover to Bermuda at 00:07:00. Note that the poor signal-to-noise ratios from 00:05:30 to 00:07:00 were caused by the weak downlink carrier levels rather than the level of uplink power. For the periods of time other than these delineated, the predicted word intelligibility of the turned-around tone was greater than 90 percent.

Uplink voice communications would have been difficult but not impossible during the time periods from lift-off to 00:00:30 and from 00:02:00 to 00:02:21.

#### 5.13.4 Performance During Near-Earth Parking Orbits

Analysis of the communications system performance during the near-earth phase of the Apollo 4 mission has been limited to a preliminary examination of the data for irregularities, and an evaluation of all facets of the coverage afforded by a typical station (in this case, Hawaii) during the second revolution. Thus, the following material is directed to the detected irregularities and the results of the evaluation of the Hawaii pass.

Unified S-band radio frequency system.— Results of the evaluation of the unified S-band radio frequency system performance during the near-earth parking orbits are as follows.

~~CONFIDENTIAL~~

~~CONFIDENTIAL~~

5.13-9

Acquisition and handover: Downlink phase lock with the S-band signal received at Hawaii was established at 02:51:05. Handover from the Apollo/range instrumentation aircraft (ARIA 3) to Hawaii was initiated at 02:52:01 and completed at 02:52:15 when two-way phase lock was established. Hawaii maintained two-way lock until 02:57:03. Loss-of-signal at this time was caused by the spacecraft passing over the horizon.

Received carrier power: Time histories of the uplink and downlink carrier powers during the Hawaii coverage of the second revolution are presented in figures 5.13-7 and 5.13-8, respectively. As shown in figure 5.13-8, the carrier power received at Hawaii agrees with predictions except during the time when look angles to the vehicle were within the antenna keyhole (mechanical limits which inhibit automatic tracking of the target). During the time the look angle to the spacecraft was within the keyhole, two-way lock was maintained by slaving the antenna to the C-band antenna. This keyhole loss was expected.

Received carrier powers at Merritt Island and Carnarvon during the first orbital pass over each site were lower than predicted. As expected, the downlink carrier power received at Carnarvon differed from predictions by approximately 30 dB while the look angle to the vehicle was in the antenna keyhole. The received carrier power corresponded to predictions during the remainder of the Carnarvon pass.

As shown in figure 5.13-9, the carrier power received at Merritt Island was approximately 20 dB lower than the predicted value from acquisition of the signal until 26 seconds prior to loss-of-signal. Since the difference between the predicted and measured carrier powers remained constant and corresponds to the expected difference between the gain of the antenna main beam and first side lobe, the antenna may have been tracking on a side lobe. This problem will be investigated further when antenna X-angle and Y-angle residuals for the near-earth mission phase become available.

Telemetry.— The S-band and vhf telemetry bit error probabilities for Hawaii during the second revolution are presented in figures 5.13-10 and 5.13-11. The predicted keyhole effect caused a 1 minute 25 seconds loss of S-band telemetry data, starting at approximately 02:52:00 (fig. 5.13-10). A bit error probability of  $1 \times 10^{-6}$ , or greater, was present in 96 percent of the S-band telemetry data (excluding keyhole losses). A bit error probability of  $1 \times 10^{-6}$  was present in 52.5 percent of the vhf telemetry data. The S-band telemetry system performed as predicted. The actual keyhole was longer than predicted.

~~CONFIDENTIAL~~



~~CONFIDENTIAL~~

The vhf telemetry system did not perform as well as predicted. The vhf bit error probability for Hawaii during the second revolution was predicted as  $1 \times 10^{-6}$  or better. The actual vhf telemetry bit error probability for Hawaii was higher than  $1 \times 10^{-6}$  but not worse than  $1.5 \times 10^{-4}$ . During the Hawaii pass the maximum elevation angle was 10 degrees. With an elevation angle of 10 degrees or less, multipath effects will degrade the vhf telemetry bit error probability because of the wide antenna beam width. Therefore, the degraded vhf telemetry performance is attributed to multipath losses (fig. 5.13-11).

Simulated voice communications.- Analysis of the 400-Hz tone received via the S-band link at Hawaii during the second revolution showed that the signal-to-noise ratio was greater than 15 dB except while the look angle was within the antenna keyhole. A signal-to-noise ratio of 15 dB indicates a predicted word intelligibility of approximately 90 percent. Little or no downlink voice communications would have been possible while the look angle was within the antenna keyhole.

The signal-to-noise ratio of the data received by the vhf/AM receiver at Hawaii was greater than 20 dB from 02:49:59 to 02:57:09. Signal-to-noise ratios of this magnitude indicate the word intelligibility would have been greater than 90 percent.

Simulated S-band up-voice tests were conducted at Hawaii during the second revolution. The results of these tests were inconclusive because the recovered tone was very noisy when the received uplink and downlink S-band carrier power level indicated a good quality tone would have been present. An examination of the recorded data showed that the modulation spectrum did not correspond to the modulation spectrum recovered from data recorded at other sites under similar conditions. Because the levels of the up-voice and up-data subcarriers were low (compared to the levels of the down-voice and telemetry subcarriers), incorrect modulation indices and/or non-linear wide band recorder operation are indicated.

Ultra high frequency.- The uhf up-data link supported the near-earth parking orbits within nominal limits, except during the Carnarvon coverage of the second revolution. A procedural guidance computer state vector update by uhf was attempted over Carnarvon. Seven commands were transmitted and not accepted by the spacecraft up-data receiver/decoder. The backup uhf transmitter was selected at 02:28:30, and subsequent commands were accepted by the spacecraft equipment. The reason for the nonacceptance by the up-data receiver/decoder of the signals from the primary transmitter has not been identified. Attempts are being made to determine if any transmitter, modulation, or data parameters were out of tolerance.

~~CONFIDENTIAL~~

~~CONFIDENTIAL~~

5.13-11

5.13.5 Performance During Translunar Injection and  
High Ellipse Phase.

Communication system performance from initiation of the third revolution to landing is presented in this section. Emphasis has been placed on the performance of the unified S-band system at the maximum slant ranges observed during the pass over Carnarvon and Ascension.

Unified S-band radio frequency subsystem.- The results of the analysis of the performance of the unified S-band frequency subsystem are as follows.

Acquisition and handover: Two-way phase lock between the Merritt Island S-band site and the spacecraft unified S-band equipment was established at 03:09:08 and maintained until handover to Bermuda. Handover was initiated at 03:14:01 and completed 10 seconds later. During the cold-soak attitude maneuver, the spacecraft receiver dropped lock at 03:18:25. The ground transmitter frequency sweep, which is required to regain spacecraft receiver lock, was initiated at 03:20:47. The reason for the delay of 2 minutes 22 seconds between the time two-way lock was lost and the time reacquisition was attempted is not known. The uplink modulation, which consisted of the pseudo-random range code and command subcarrier, was not removed prior to the initiation of transmitter frequency sweep. Indications of two-way lock were obtained at 03:20:57; however, the received carrier power at the spacecraft was extremely weak. Three attempts to transmit commands to the spacecraft between 03:21:10 and 03:22:29 were unsuccessful. Therefore, Bermuda was requested to handover to the Vanguard.

Examination of the two-way Doppler data (obtained from high speed tracking data transferred to the Mission Control Center-Houston from Bermuda) revealed that the spacecraft S-band receiver locked to a range code component rather than to the desired carrier. Handover from Bermuda to the Vanguard was completed at 03:23:12. Although scheduled for a passive track during this phase of the mission, the Vanguard was able to send the desired commands to the spacecraft. ←

Handover from Bermuda to Ascension was scheduled for 03:25:00. Therefore, Ascension personnel brought their S-band carrier up and initiated acquisition sweep of the transmitter frequency. The presence of two signals in the spacecraft unified S-band equipment caused it to lose lock. From 03:25:00 to 03:26:31, both Ascension and the Vanguard attempted to obtain two-way lock by sweeping their transmitter frequencies. Two-way lock was obtained by Ascension at 03:26:31 and the Vanguard transmitter was turned off at 03:26:50.

Ascension maintained two-way lock until 07:06:25. At that time, handover to Carnarvon was initiated. This handover was completed 12 seconds later.

~~CONFIDENTIAL~~

~~CONFIDENTIAL~~

The handover from Carnarvon to Guam was accomplished at 08:12:48 during the service propulsion subsystem second burn. Guam maintained two-way lock until CM/SM separation. At that time, Guam receivers 1-1, 2-1, and 1-2 suddenly lost lock. This loss of lock is attributed to severe flame attenuation as the four SM reaction control system thrusters ignited to effect separation.

Guam receiver 2-2 maintained lock. The received carrier power at the input to receiver 2-2 dropped from -85 dBm to -100 dBm at CM/SM separation, then recovered quickly to -85 dBm. Guam was configured such that S-band data were being patched from receivers 1-1 and 1-2 to the PCM decommutation system. Since both of these receivers lost lock, telemetry data also were lost. The configuration of dual MSFN S-band sites is such that only receivers 1-1 and 1-2 contain the angle error channels required to automatically track the vehicle. Thus, the automatic track capability was lost. The S-band antenna operator selected the program track mode at 08:18:04. In this mode of operation, the antenna pointing information is derived from predicted data contained in the site acquisition message. The acquisition message utilized by the Guam operators was not correct; therefore, the antenna boresight moved off the spacecraft and caused the spacecraft S-band receiver and Guam receiver 2-2 to lose lock at 08:18:08.5.

The Apollo/range instrumentation aircraft (ARIA 3) obtained two-way S-band lock at 08:30:04 and tracked the spacecraft to landing.

Received carrier power: A comparison of downlink carrier powers at Merritt Island, Bermuda, and the Vanguard showed that the measured signal levels compared very favorably with predictions. Uplink carrier powers during the same time period appeared nominal except during the time the unified S-band equipment was out-of-lock and locked to the range code component during the Bermuda pass. During the time the unified S-band equipment was locked to the range code component, the received power was approximately 27 dB weaker than it had been prior to loss of lock. This difference is approximately equal to the predicted difference in power between the range code component and the carrier.

Time histories of the received uplink and downlink carrier powers during the Ascension and Carnarvon coverage of the high ellipse are presented in figures 5.13-12 and 5.13-13, respectively. The received uplink power from 03:25:31 to 08:12:48 was at least 10 dB greater than the level required to maintain positive up-voice and updata circuit margins.

Plots of the received uplink and downlink carrier powers during Guam coverage are presented in figures 5.13-14 and 5.13-15. As shown

~~CONFIDENTIAL~~

~~CONFIDENTIAL~~

5.13-13

in figure 5.13-14, the received uplink power was greater than -71 dBm from handover to 08:18:04.5. The received carrier power at Guam receiver 1-1 varied between -123 dBm and -81 dBm. The peaks and nulls in this plot were caused by the look angle between the spacecraft and Guam being in the worst interferometer (heavily scalloped) region of the spacecraft antenna patterns.

The uplink carrier power received during communications with Apollo range instrumentation aircraft (ARIA 3) is presented in figure 5.13-16.

Telemetry.- The Ascension and Guam S-band telemetry bit error probabilities during the third revolution are presented in figures 5.13-17 and 5.13-18.

The Ascension S-band telemetry bit error probability was  $1 \times 10^{-6}$ , or better, 97 percent of the time as shown in figure 5.13-17. The received carrier power indicates that sufficient signal was available from 03:40:00 to 07:00:00 to maintain a bit error probability of  $1 \times 10^{-6}$  or better. Occasional errors were noted in the Ascension bit error data. The S-band telemetry system performed approximately as predicted.

The Guam S-band telemetry bit error probability, presented in figure 5.13-18, was affected by the predicted interferometer effect. Eighty-two percent of the S-band telemetry data had a bit error probability of  $1 \times 10^{-6}$  or better. Only 6 percent of the S-band telemetry data were not acceptable, that is, had a bit error probability worse than  $1 \times 10^{-3}$ .

The only irregularity noted during the third revolution for the Guam S-band telemetry was the abrupt cutoff at CM/SM separation.

Simulated voice communications.- Analysis of simulated voice communications during the third revolution was limited to the down-voice link. Signal-to-noise ratios were measured for a 45-minute period (including apogee) of Carnarvon coverage and the entire Guam coverage. Extrapolation of the signal-to-noise ratios to expected voice channel performance indicated the word intelligibility would have been equal to, or greater than, 90 percent for the times stated above, except for two brief periods of the Guam coverage. The two brief periods of degraded voice channel performance at Guam were caused by nulls in the spacecraft antenna patterns and occurred prior to handover from Carnarvon to Guam.

Unified S-band updata.- All updata transmissions during the third revolution, except those described below, were nominal in every respect.

~~CONFIDENTIAL~~

~~CONFIDENTIAL~~

The oxygen tank heater OFF real-time command (RTC-70) was transmitted from Bermuda and was not accepted by the spacecraft update receiver/decoder three times between 03:21:10 and 03:22:29. The non-acceptance can be attributed to the fact that the spacecraft unified S-band equipment was locked to a range code component rather than the S-band carrier (see table 5.13-I). As shown in table 5.13-I, RTC-70 was transmitted by the Vanguard at 03:24:01 and was accepted by the spacecraft.

Transmission of the guidance computer word VERB was attempted by the Vanguard before the unified S-band exciter operator could establish uplink phase lock and activate the command modulation. These words were not actually transmitted to the spacecraft. As indicated in table 5.13-I, all command transmissions after activation of command modulation were accepted by the spacecraft.

A procedural guidance computer update was initiated from Ascension at 05:24:17. The word VERB was transmitted, accepted by the update receiver/decoder, and transferred to the computer. At 05:24:27, the word SEVEN was transmitted and accepted by the update receiver/decoder. However, the KKK check, a redundancy check of the transmitted characters, by the computer failed and the data were rejected by the computer. This rejection necessitated a transmission of computer CLEAR and RESET commands. These commands were transmitted at 05:25:15 and 05:25:30, respectively, were accepted by the update receiver/decoder, and were transferred to the guidance computer. All subsequent guidance computer words transmitted from Ascension were accepted without reoccurrence of the KKK check failure. Postmission examination of the rejected SEVEN word showed that the correct bit structure was transmitted and was accepted by the update receiver/decoder. Thus, the KKK failure apparently occurred at the dormant interface between the receiver/decoder and the guidance computer 15-bit shift register.

Transmission of the direct thrust on command (RTC-11) subsequent to service propulsion subsystem engine ignition necessitated commanding the service propulsion subsystem engine off during the pass over Guam. Refer to section 9.1.5 for an explanation of transmission of RTC-11. The direct thrust off command (RTC-12) was executed from the Mission Control Center and was transmitted from Guam at 08:15:35.5. The direct thrust off command was a priority command, and was automatically retransmitted until the update receiver/decoder message acceptance signal was received at the Mission Control Center. Examination of the data recorded at Guam revealed that the command was retransmitted to the spacecraft three times. The time delays between transmissions were 251, 244, and 546 msec, respectively.

Each of the four transmissions was accepted by the update receiver/decoder as evidenced by four message acceptance signals in the reduced

~~CONFIDENTIAL~~

~~CONFIDENTIAL~~

5.13-15

telemetry data. Since the command validation was transmitted from Guam to the Mission Control Center-Houston (MCC-H) once per second and there were some propagation and MCC-H processing delays, the time delay between Guam and MCC-H was sufficient to account for three automatic retransmissions. The difference in time between first and last transmissions was 1.041 seconds.

At 08:15:53.8, the SPS ON/OFF reset command (RTC-13) was transmitted and accepted by the updata receiver/decoder. Evaluation of telemetry data verified that reset was accomplished with this transmission. Retransmission of the reset (RTC-13) was accomplished at 08:16:02.4, and this transmission was also accepted by the updata receiver/decoder. The second reset command (RTC-13) was transmitted because of a delay in receiving message acceptance of the first transmission at the Mission Control Center. Flight controllers in the Mission Control Center attempted to transmit the reset command (RTC-13) one time prior to the transmission at 08:15:53.8. This attempt was inhibited in the ground processing equipment, and the command was not transmitted to the spacecraft.

Unified S-band ranging system.- A preliminary analysis of the tracking data obtained using the S-band ranging system has been performed for the coast phase of the high ellipse. This analysis was performed by comparing the S-band observables with a best estimate trajectory computed from S-band and C-band radar data. The comparison of the S-band observables obtained at Ascension with the best estimate trajectory computed from S-band and C-band radar data resulted in the following conclusions.

The residuals between the S-band range rate (Doppler) and the computed best estimate varied from -0.08 Hz at 04:53:00 to +0.82 Hz at 06:36:00. The variation between observations was approximately 0.23 Hz. The Doppler residual of 0.82 Hz is approximately equivalent to a range residual of 0.17 ft/sec (assuming 6.5 cm/sec correlation per 1 Hz). A residual of 0.1 ft/sec is used for noise and bias errors in tracking/trajectory analysis.

The range residual varied from +30 meters at 03:29:00 to -80 meters at 05:11:00 to +110 meters at 07:04:00. A range residual of  $\pm 27.4$  meters is usually allotted for noise and bias errors in the range parameter.

The antenna Y-angle residuals varied from 0.0405 degree at 03:29:00 to -0.0096 degree at 07:04:00. These residuals are well within the 0.137-degree limit allowed in analysis for noise and bias errors.

~~CONFIDENTIAL~~

~~CONFIDENTIAL~~

The antenna X-angle residuals varied from +0.0429 degree at 03:29:00, to +0.0032 degree at 05:21:00, to +0.0285 degree at 07:05:00.

Residuals between S-band data points obtained from Carnarvon and the best estimate trajectory based on S-band and C-band radar data are as follows.

a. The Doppler residuals varied from -0.6 Hz at 07:08:00 to -1.1 Hz at 07:36:00.

b. The range residuals varied from +100 meters at 07:08:00 to +15 meters at 07:36:00.

c. The Y-angle residuals varied from -0.0050 degree at 07:08:00 to -0.099 degree at 07:36:00.

d. The X-angle residuals varied from -0.333 degree at 07:08:00 to -0.432 degree at 07:36:00.

The ranging information just discussed is preliminary. An analysis is being performed to improve the best estimate trajectory and to provide better interpretation of the available data. Based on the preliminary data, the performance of the S-band ranging system during the Apollo 4 mission appears to be very good.

~~CONFIDENTIAL~~

~~CONFIDENTIAL~~

5.13-17

TABLE 5.13-I.- COMMAND EVENTS - BERMUDA AND THE U.S.N.S. VANGUARD

Time from range zero, hr:min:sec	Event
03:18:25	Spacecraft unified S-band equipment lost lock
03:20:57	Bermuda acquired apparent two-way lock (evaluation showed unified S-band equipment was locked to range code component)
03:21:10	Bermuda transmitted spacecraft oxygen tank heaters off command (RTC 70) - Not accepted by spacecraft
	Bermuda transmitted spacecraft oxygen tank heaters off command (RTC 70) - Not accepted by spacecraft
03:22:29	Bermuda transmitted spacecraft oxygen tank heaters off command (RTC 70) - Not accepted by spacecraft
03:23:00	Bermuda requested to handover to the Vanguard
03:23:02	Vanguard attempted to transmit guidance computer word VERB - Command modulation not yet activated
03:23:09	Vanguard attempted to transmit guidance computer word VERB - Command modulation not yet activated
03:23:12	Vanguard established uplink lock
03:23:16	Vanguard attempted to transmit guidance computer word VERB - Command modulation not yet activated
03:23:26	Command modulation activated
03:23:30	Vanguard transmitted guidance computer word VERB - Accepted by spacecraft
03:23:35	Vanguard guidance computer word SEVEN - Accepted by spacecraft

~~CONFIDENTIAL~~



~~CONFIDENTIAL~~

TABLE 5.13-I.- COMMAND EVENTS - BERMUDA AND THE U.S.N.S. VANGUARD -

Concluded

Time from range zero, hr:min:sec	Event
03:23:38	Vanguard transmitted guidance computer word FIVE - Accepted by spacecraft
03:23:42	Vanguard transmitted guidance computer word ENTER - Accepted by spacecraft
03:24:01	Vanguard transmitted spacecraft oxygen tank heaters off command (RTC 70) - Accepted by spacecraft

~~CONFIDENTIAL~~

~~CONFIDENTIAL~~

5.13-19

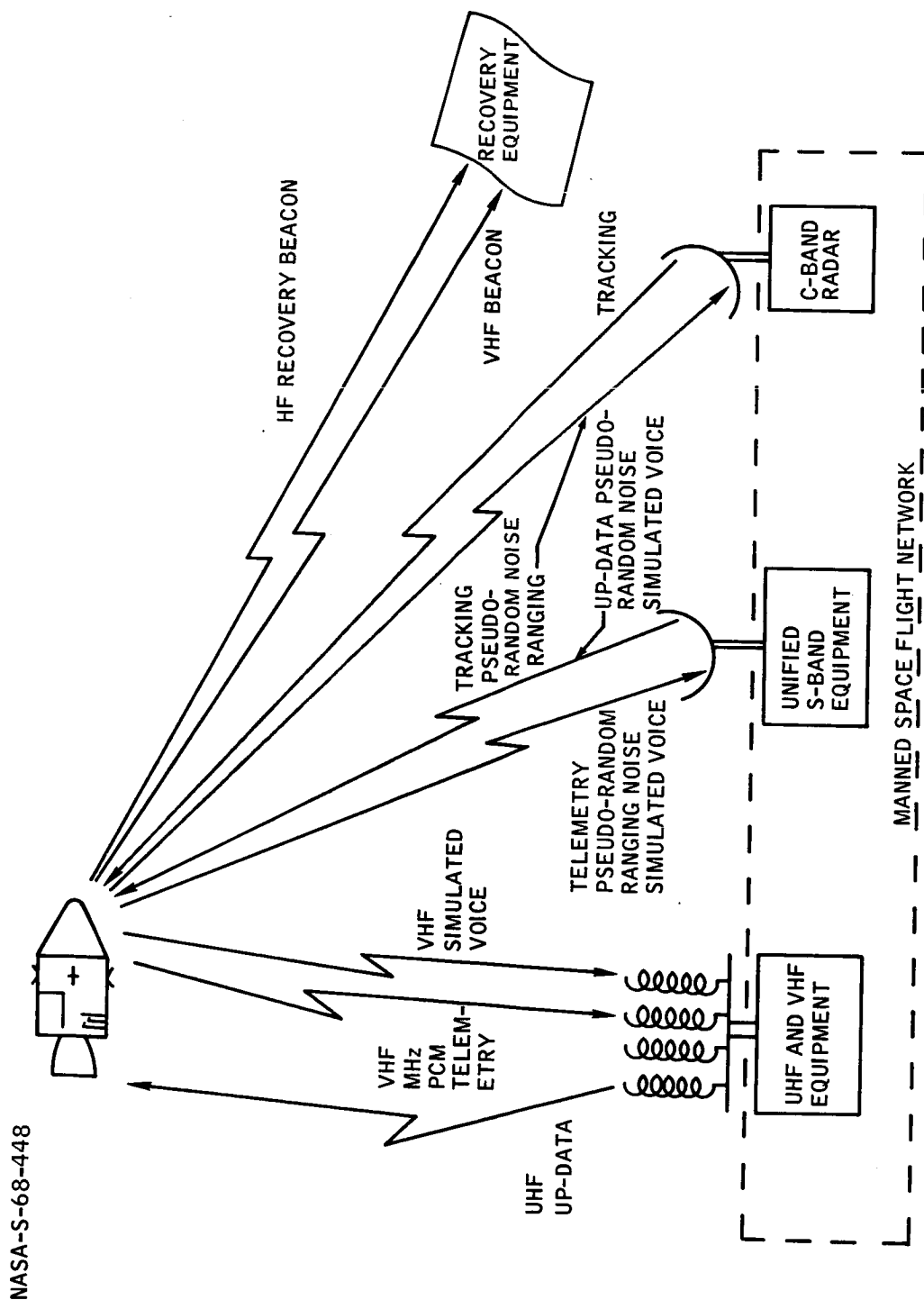


FIGURE 5.13-1.- APOLLO 4 COMMUNICATIONS CAPABILITIES.

~~CONFIDENTIAL~~

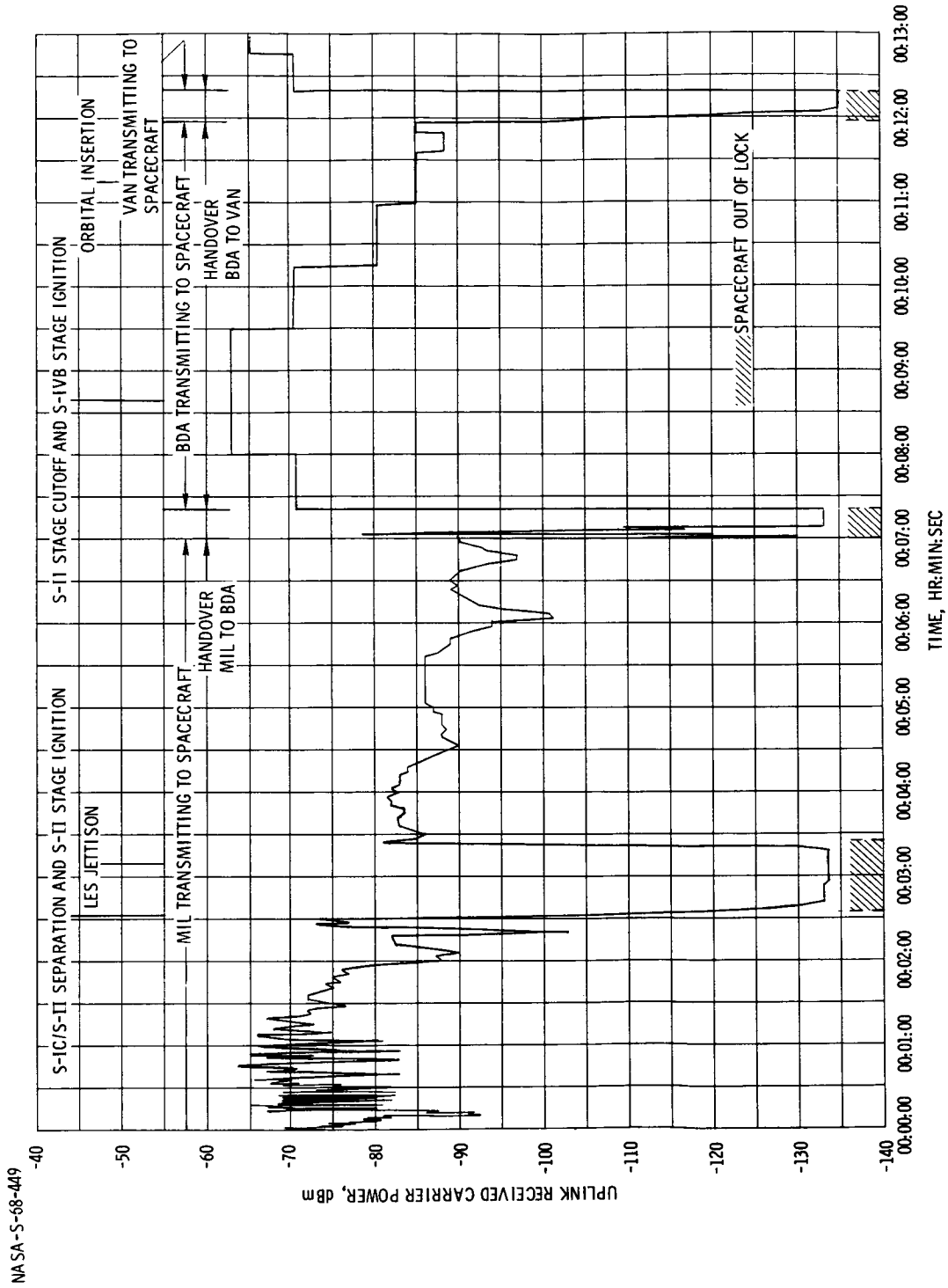
~~CONFIDENTIAL~~

FIGURE 5.13-2. - UPLINK RECEIVED CARRIER POWER AT SPACECRAFT, LAUNCH PHASE.

~~CONFIDENTIAL~~

~~CONFIDENTIAL~~

5.13-21

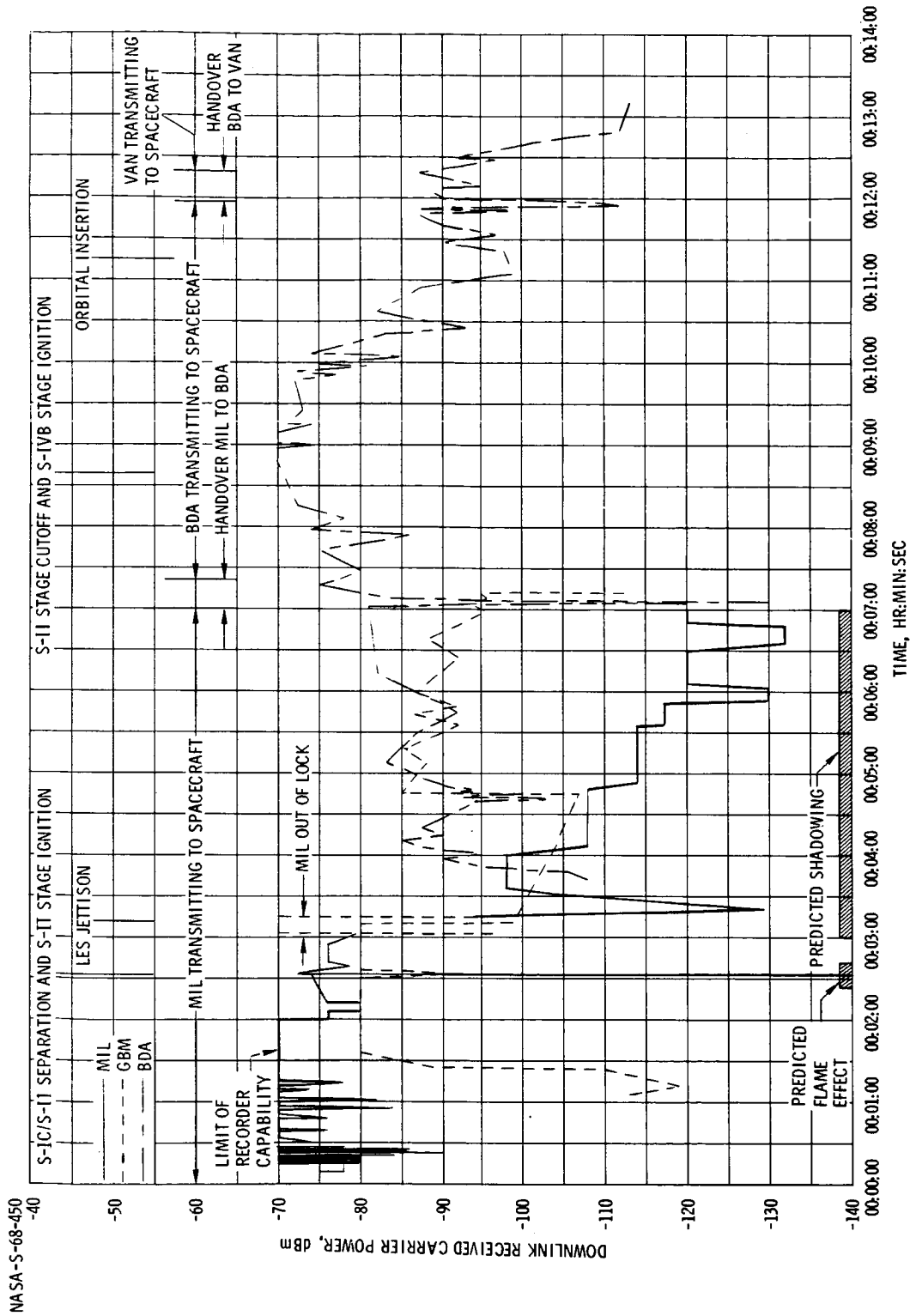


FIGURE 5.13-3. - DOWNLINK RECEIVED CARRIER POWER AT MANNED SPACE FLIGHT NETWORK SITES, LAUNCH PHASE.

~~CONFIDENTIAL~~

~~CONFIDENTIAL~~

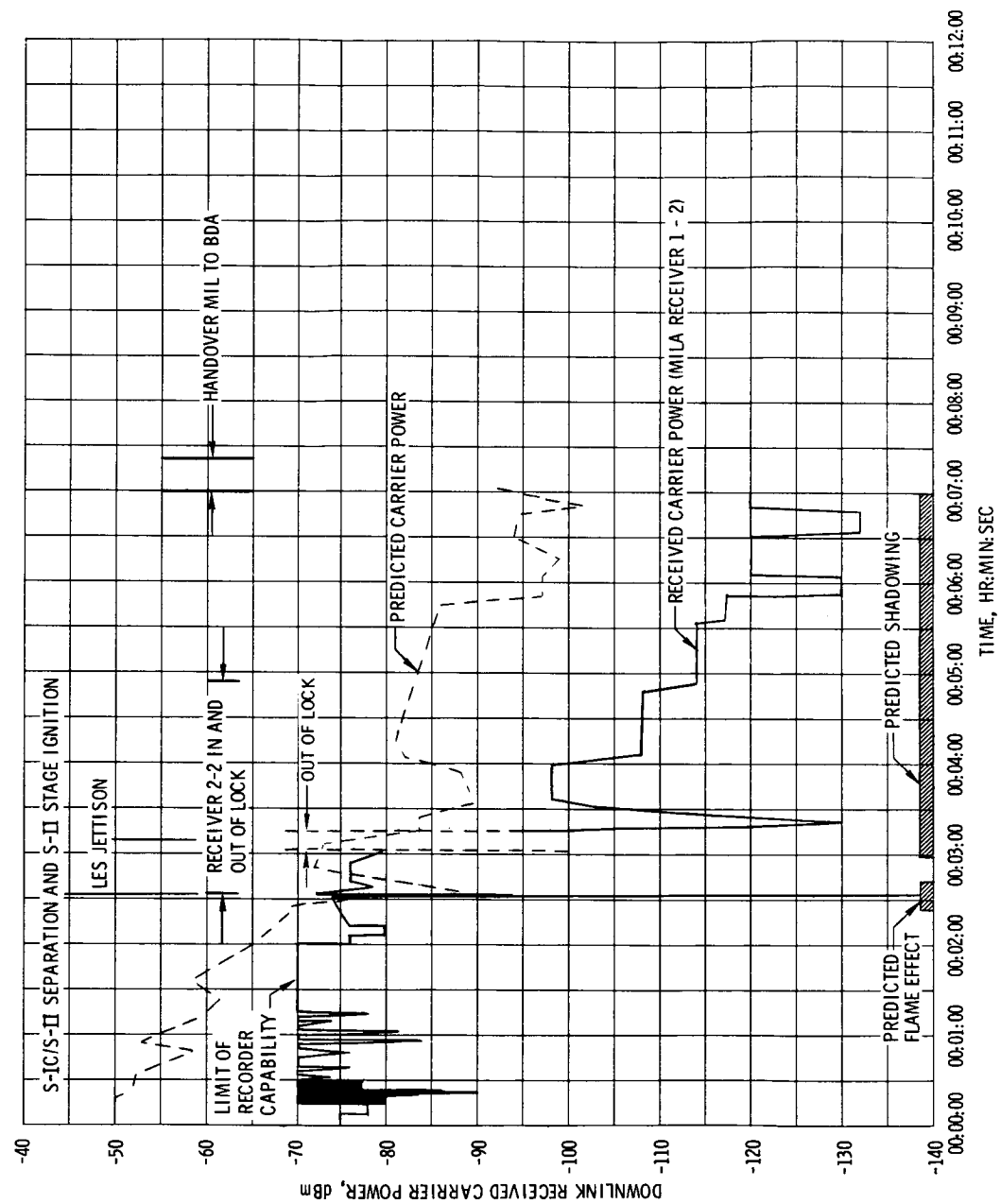


FIGURE 5.13-4. - DOWNLINK RECEIVED CARRIER POWER AT MIL, LAUNCH PHASE.

~~CONFIDENTIAL~~

~~CONFIDENTIAL~~

5.13-23

NASA-S-68-452

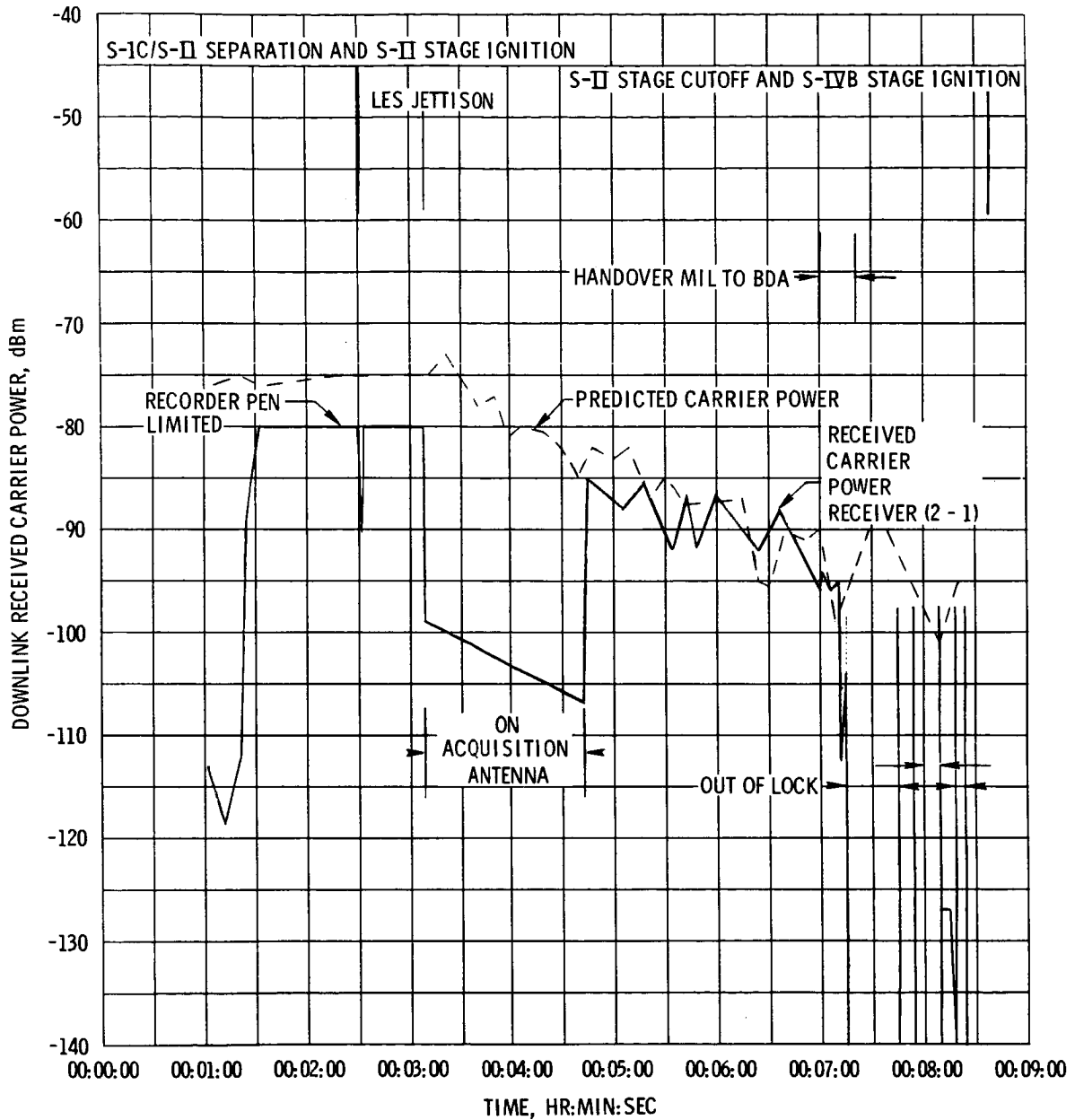


FIGURE 5.13-5. - DOWNLINK RECEIVED CARRIER POWER AT GBM, LAUNCH PHASE.

~~CONFIDENTIAL~~

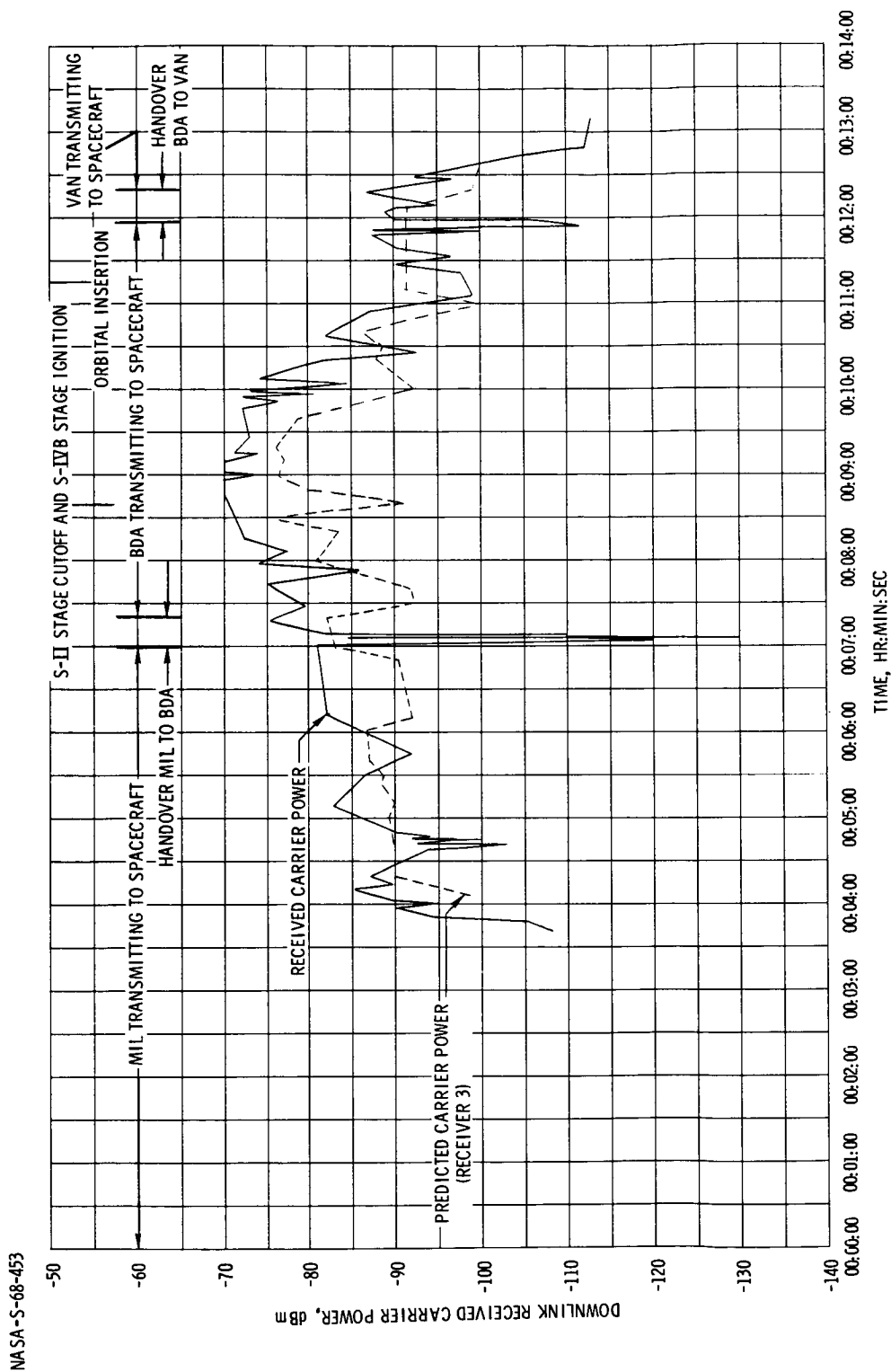
~~CONFIDENTIAL~~

FIGURE 5.13-6. - DOWNLINK RECEIVED CARRIER POWER AT BDA, LAUNCH PHASE.

~~CONFIDENTIAL~~

~~CONFIDENTIAL~~

5.13-25

NASA-S-68-454

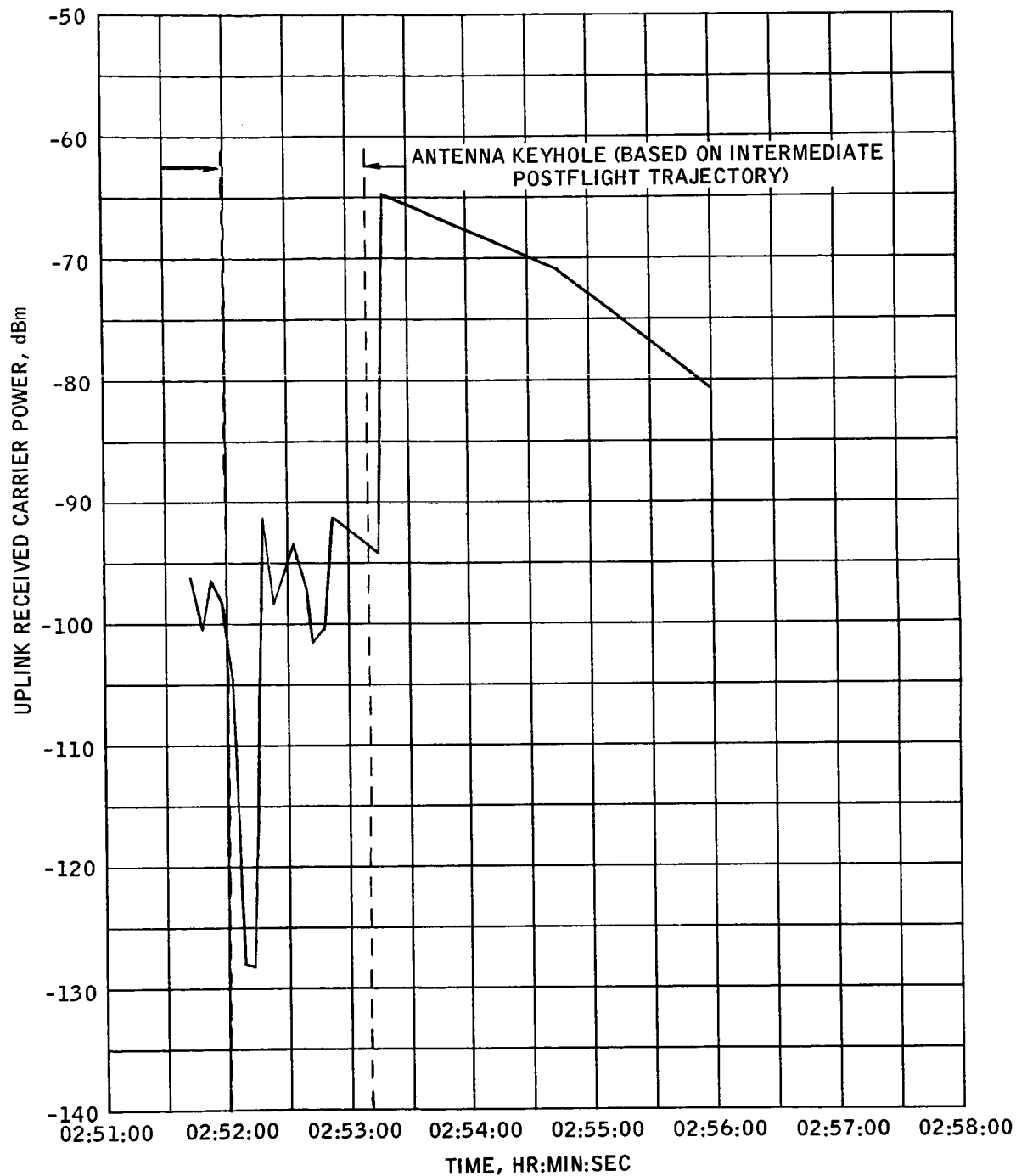


FIGURE 5.13-7.- UPLINK RECEIVED CARRIER POWER AT SPACECRAFT, HAWAII COVERAGE OF SECOND REVOLUTION.

~~CONFIDENTIAL~~



~~CONFIDENTIAL~~

NASA-S-68-455

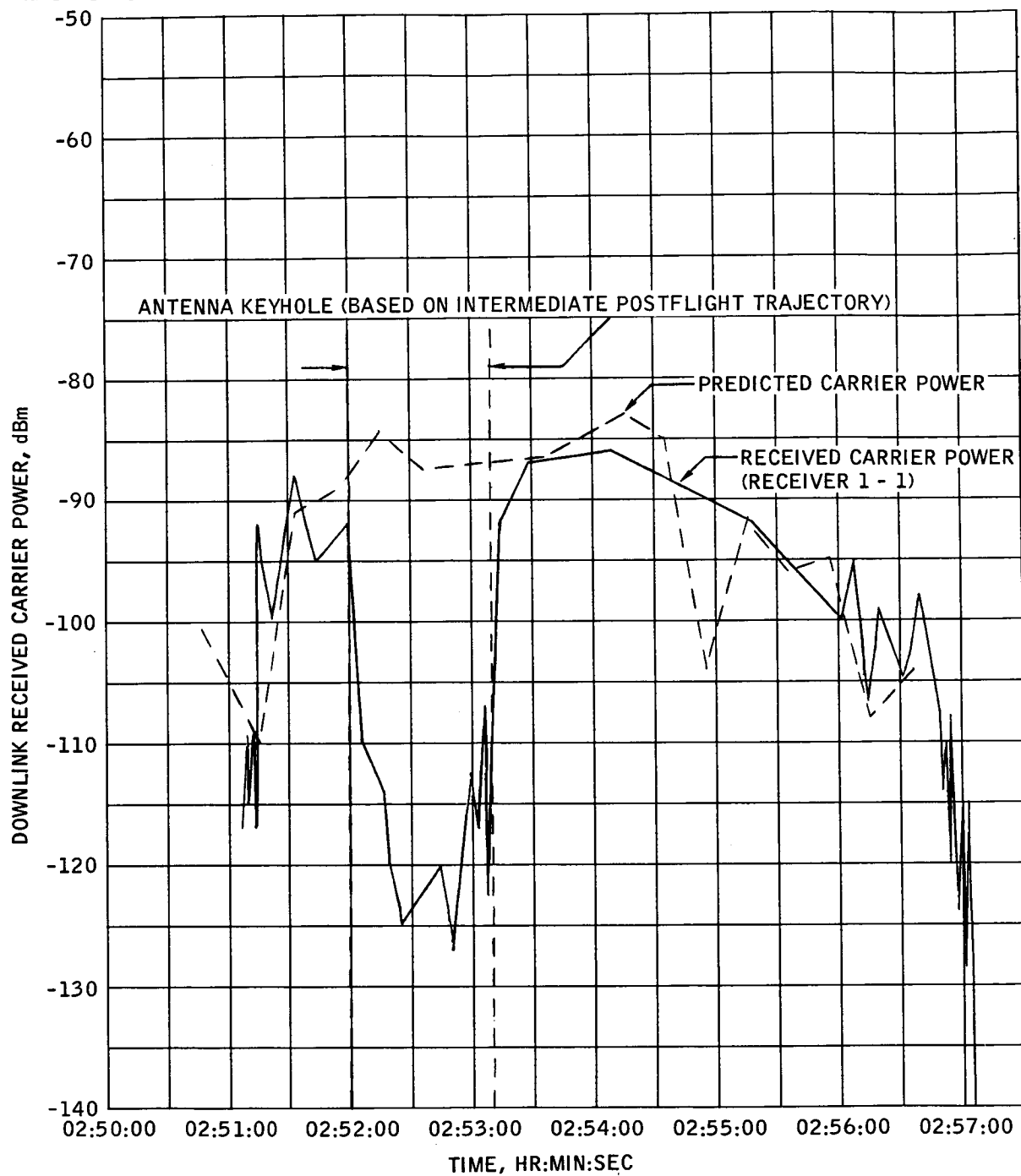


FIGURE 5.13-8.- DOWNLINK RECEIVED CARRIER POWER AT HAWAII, SECOND REVOLUTION.

~~CONFIDENTIAL~~

~~CONFIDENTIAL~~

5.13-27

NASA-S-68-456

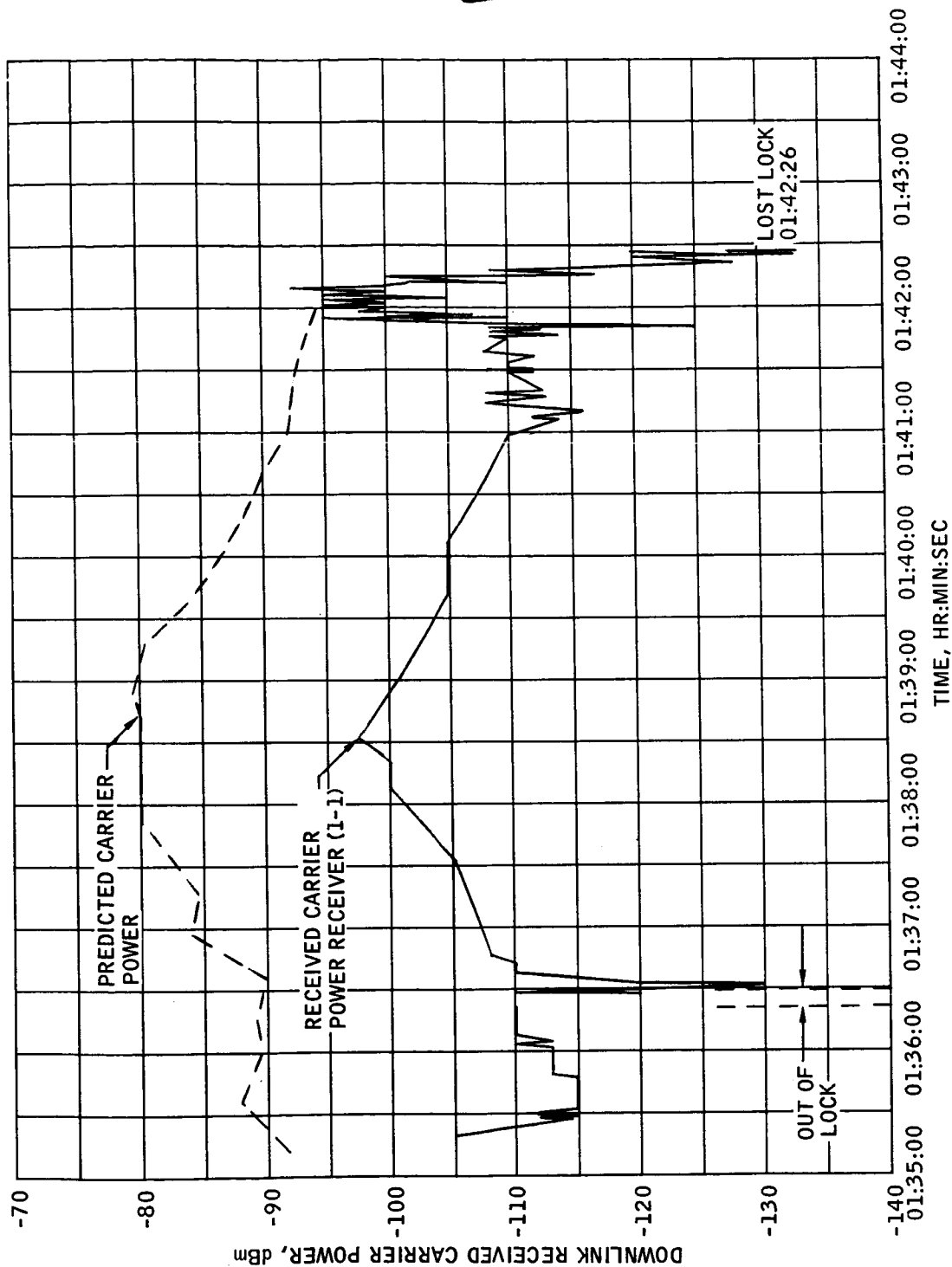


FIGURE 5.13-9.- DOWNLINK RECEIVED CARRIER POWER AT MIL FIRST AND SECOND REVOLUTION.

~~CONFIDENTIAL~~

5.13-28

NASA-S-68-457

~~CONFIDENTIAL~~

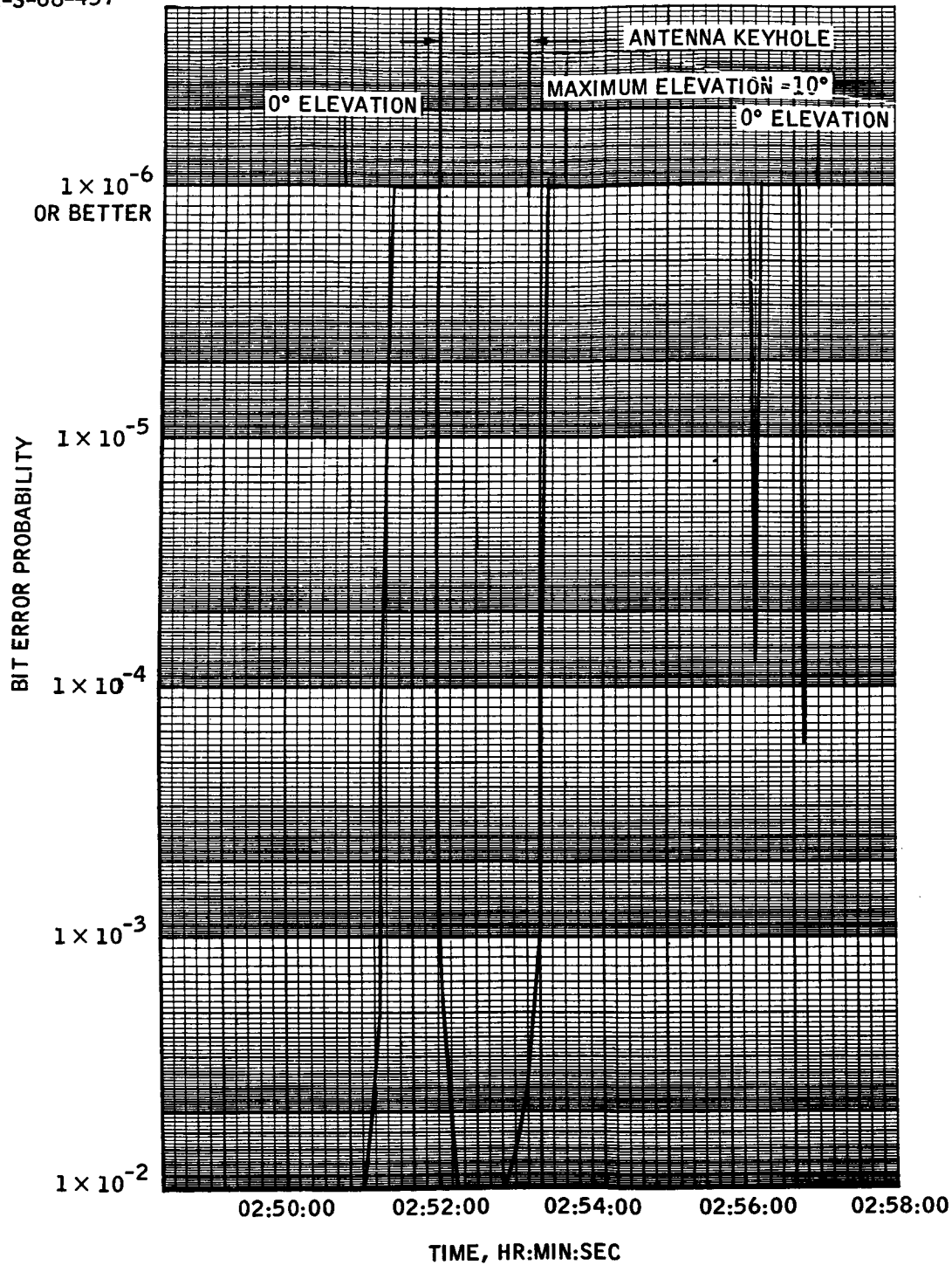


FIGURE 5.13-10.- UNIFIED S-BAND TELEMETRY BIT ERROR PROBABILITY, HAWAII COVERAGE OF SECOND REVOLUTION.

~~CONFIDENTIAL~~

~~CONFIDENTIAL~~

5.13-29

NASA-S-68-458

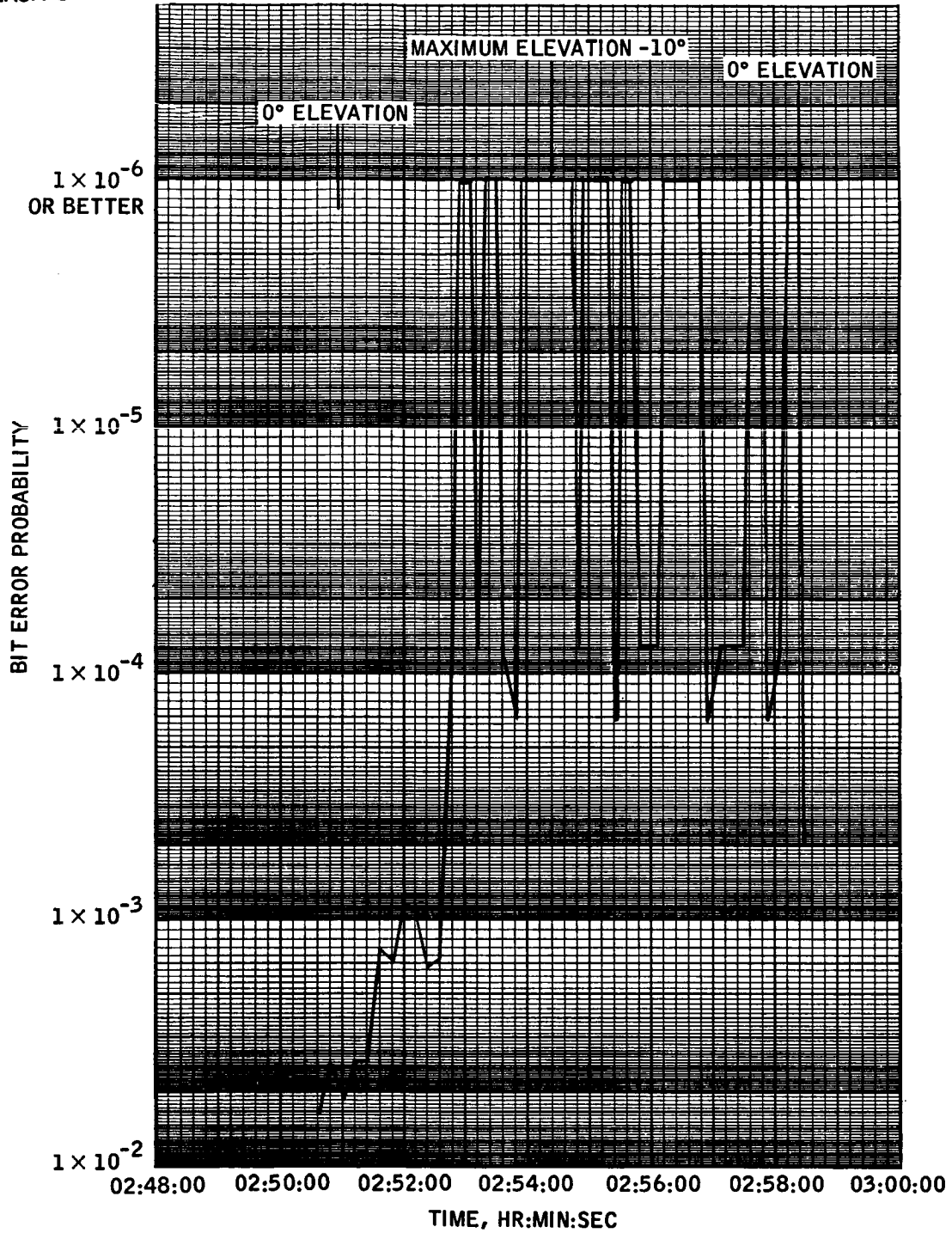


FIGURE 5.13-11.- VHF TELEMETRY BIT ERROR PROBABILITY,  
HAWAII COVERAGE OF SECOND REVOLUTION.

~~CONFIDENTIAL~~

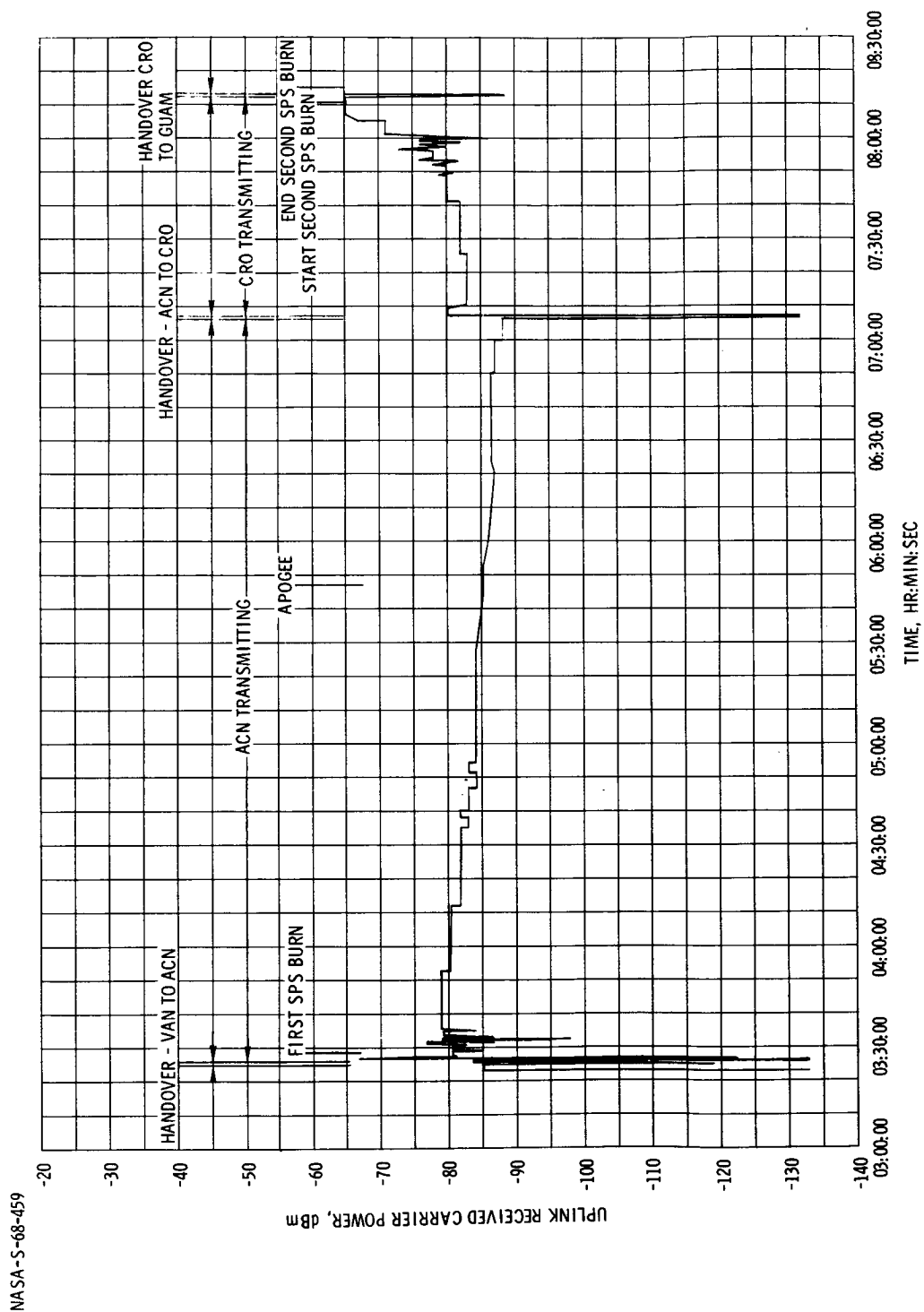
~~CONFIDENTIAL~~

FIGURE 5.13-12. - UPLINK RECEIVED CARRIER POWER AT SPACECRAFT, ACN AND CRO COVERAGE OF THIRD REVOLUTION.

~~CONFIDENTIAL~~

~~CONFIDENTIAL~~

5.13-31

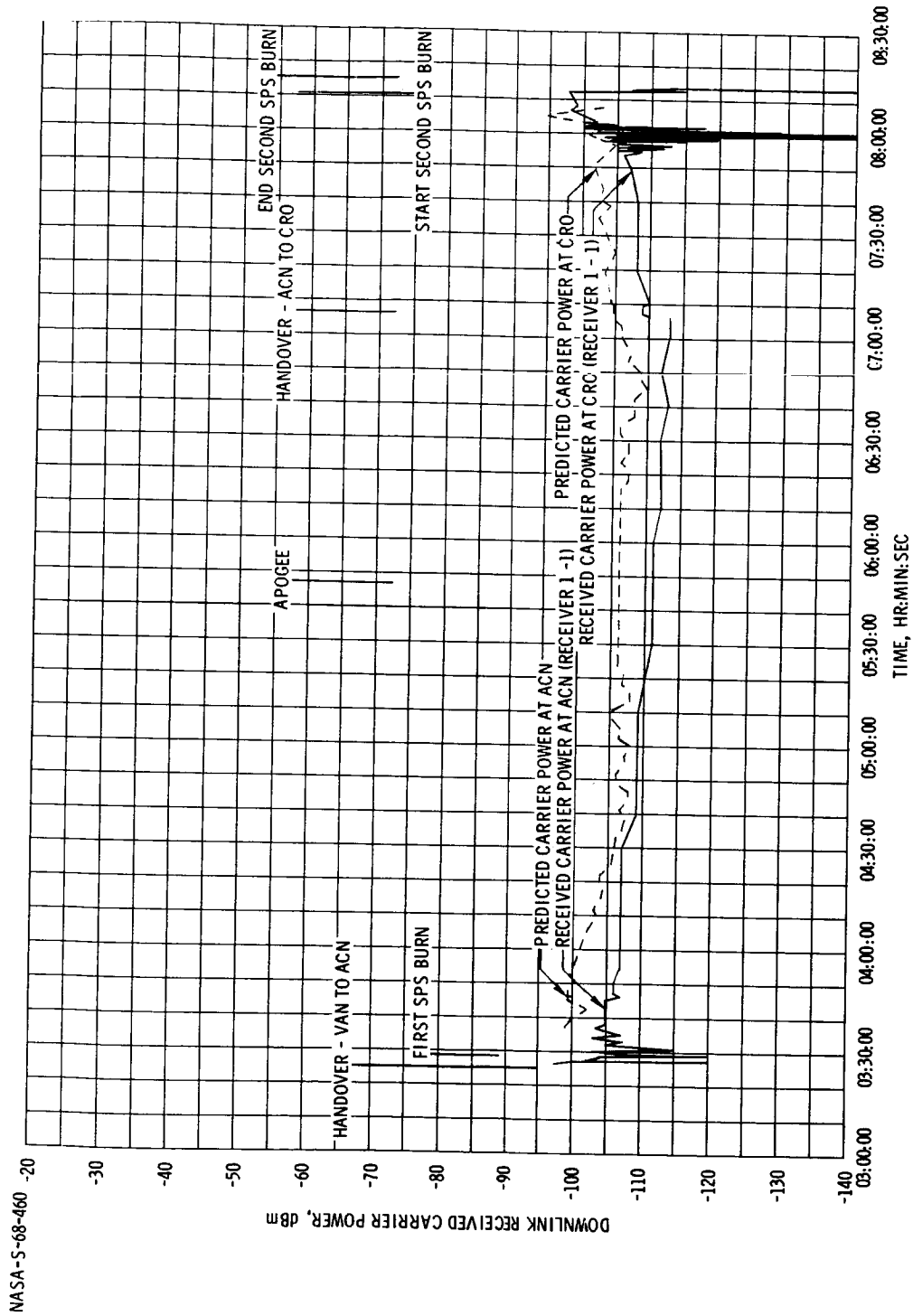


FIGURE 5.13-13. - DOWNLINK RECEIVED CARRIER POWER AT ACN AND CRO, THIRD REVOLUTION.

~~CONFIDENTIAL~~

5.13-32

~~CONFIDENTIAL~~

NASA-S-68-461

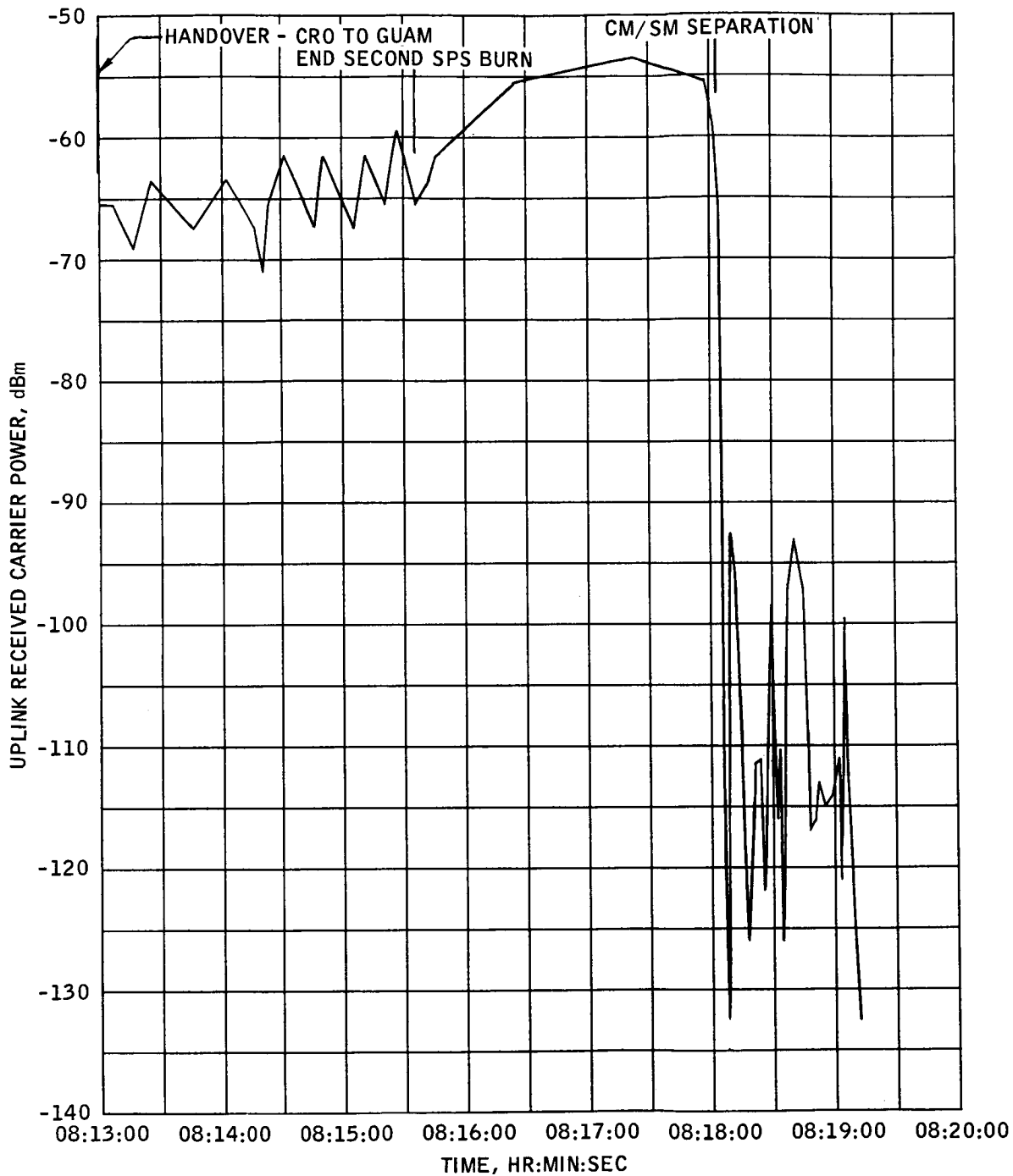


FIGURE 5.13-14.- UPLINK RECEIVED CARRIER POWER AT SPACECRAFT, GUAM COVERAGE OF THIRD REVOLUTION.

~~CONFIDENTIAL~~

~~CONFIDENTIAL~~

5.13-33

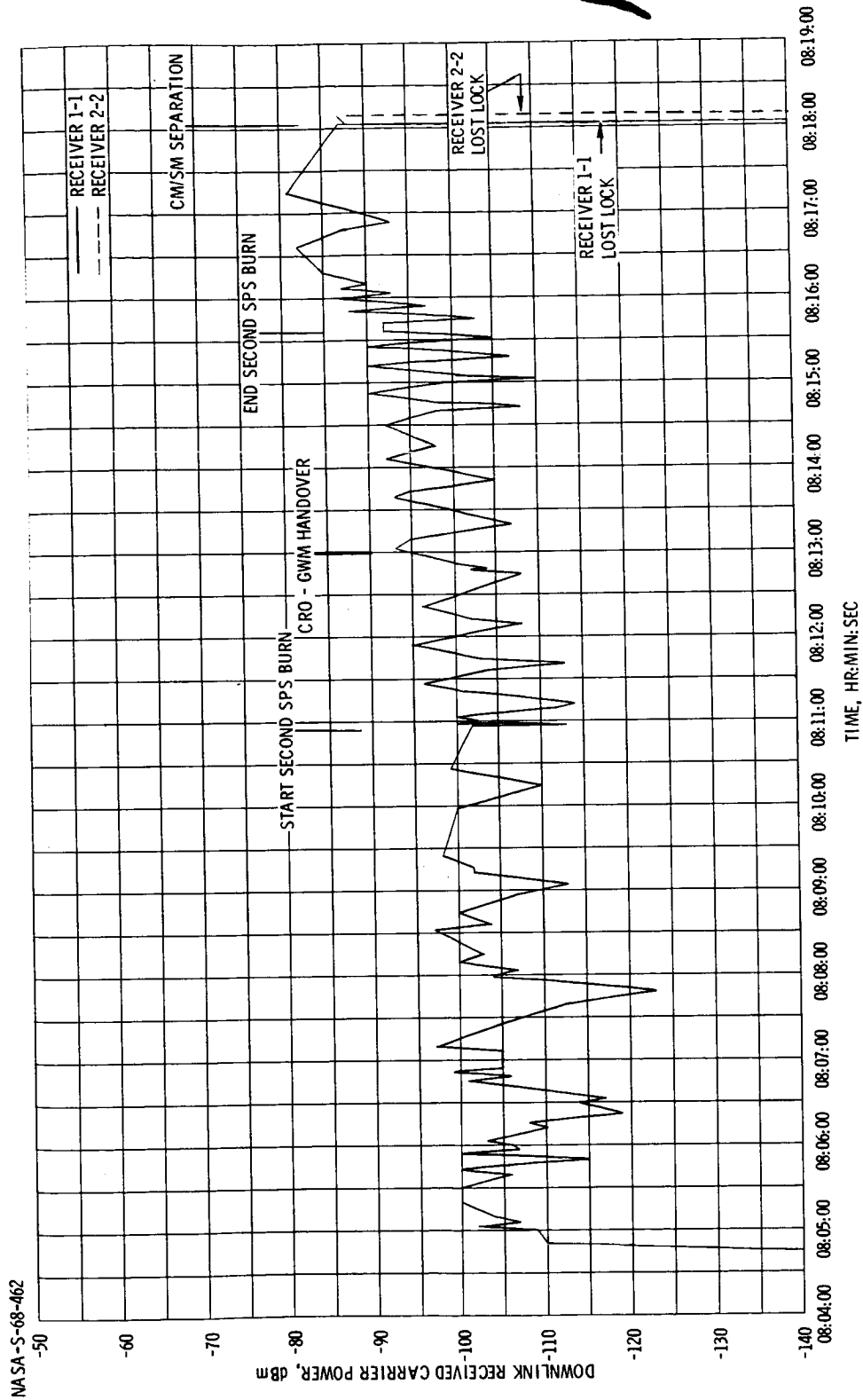


FIGURE 5.13-15. - DOWNLINK RECEIVED CARRIER POWER AT GUAM, THIRD REVOLUTION.

~~CONFIDENTIAL~~



~~CONFIDENTIAL~~

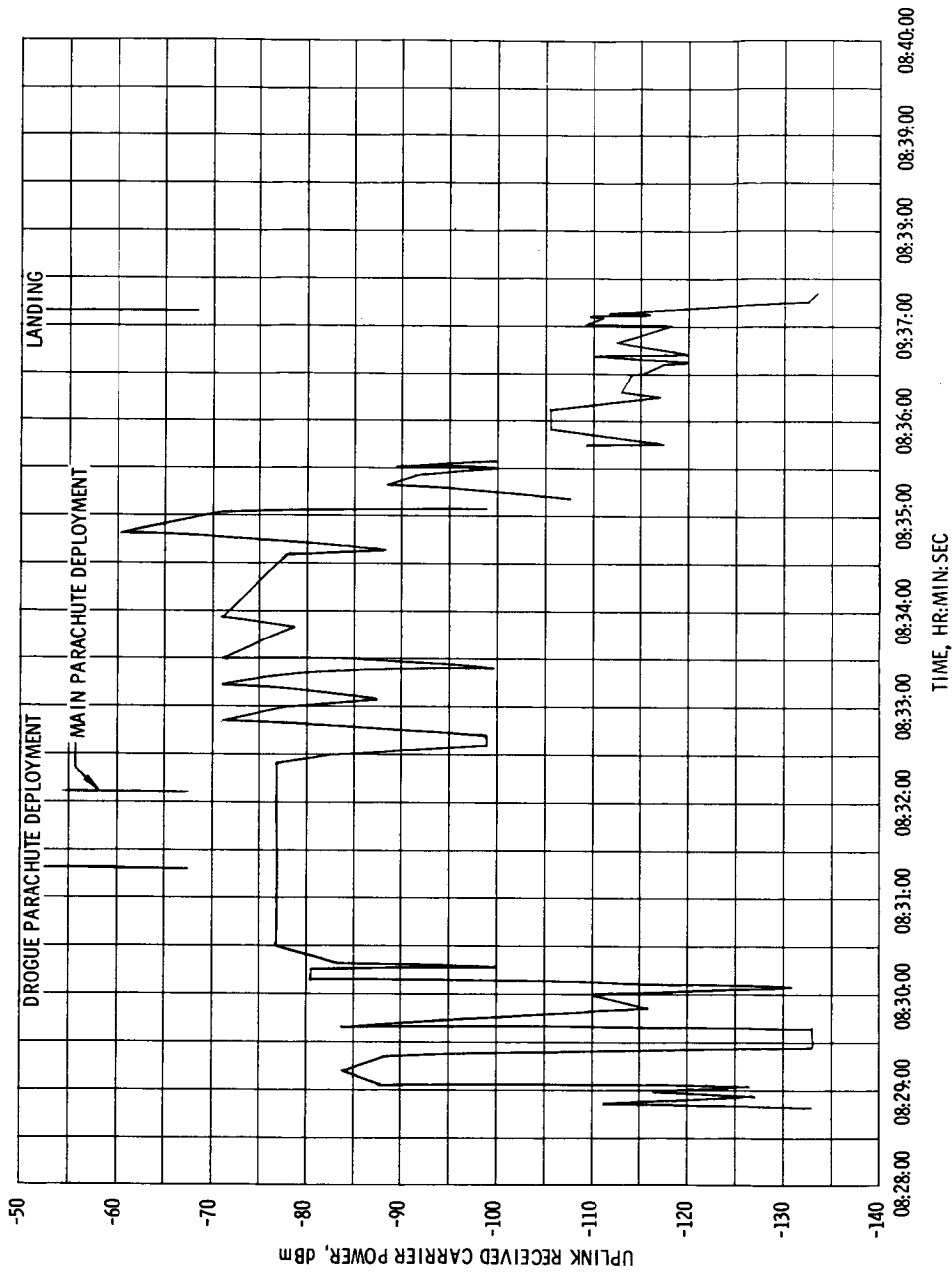


FIGURE 5.13-16. - UPLINK RECEIVED CARRIER POWER AT SPACECRAFT, ARIA 3 COVERAGE OF ENTRY.

~~CONFIDENTIAL~~

~~CONFIDENTIAL~~

5.13-35

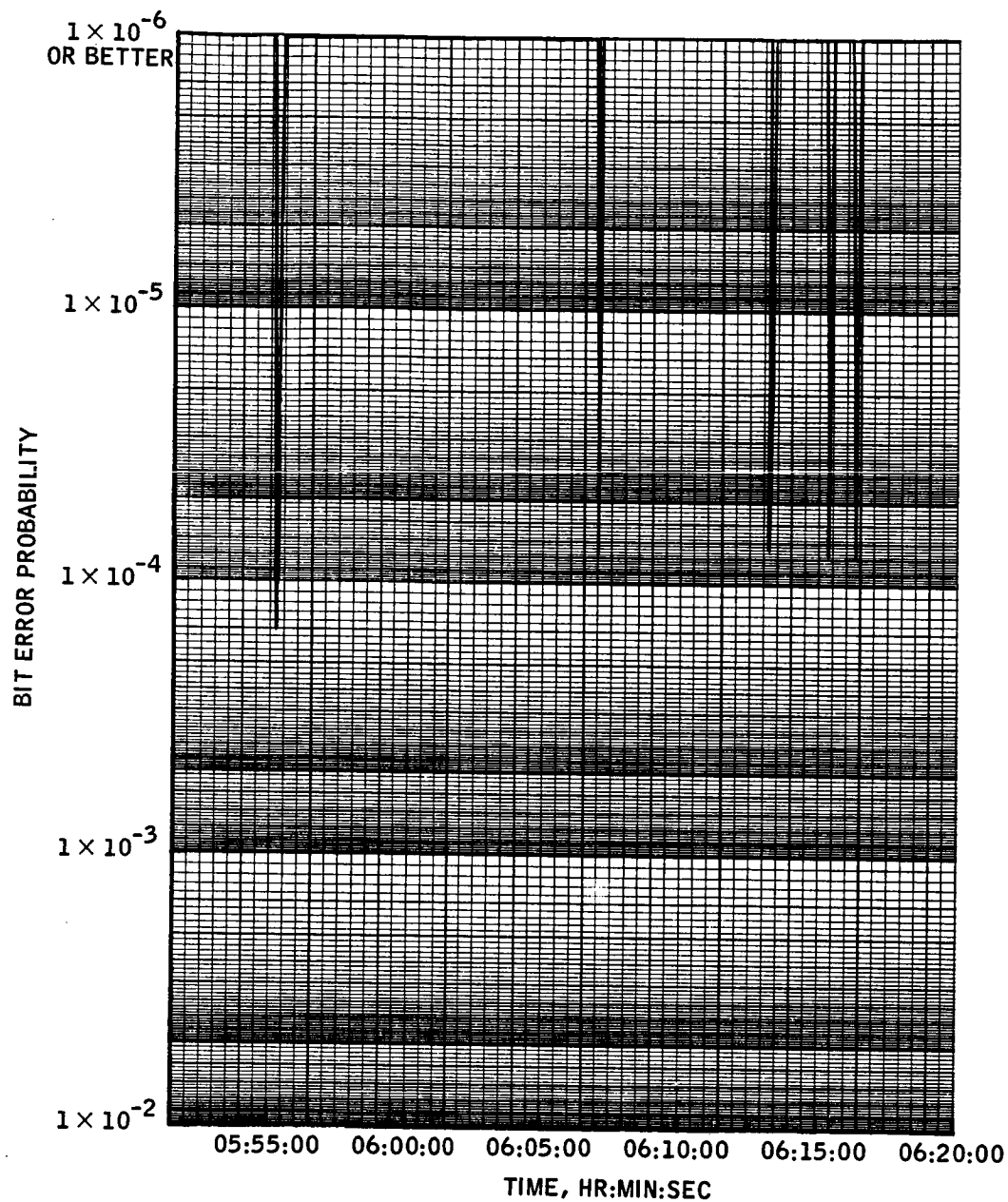


FIGURE 5.13-17.- UNIFIED S-BAND TELEMETRY BIT ERROR PROBABILITY, ASCENSION COVERAGE OF THIRD REVOLUTION.

~~CONFIDENTIAL~~

~~CONFIDENTIAL~~

NASA-S-68-465

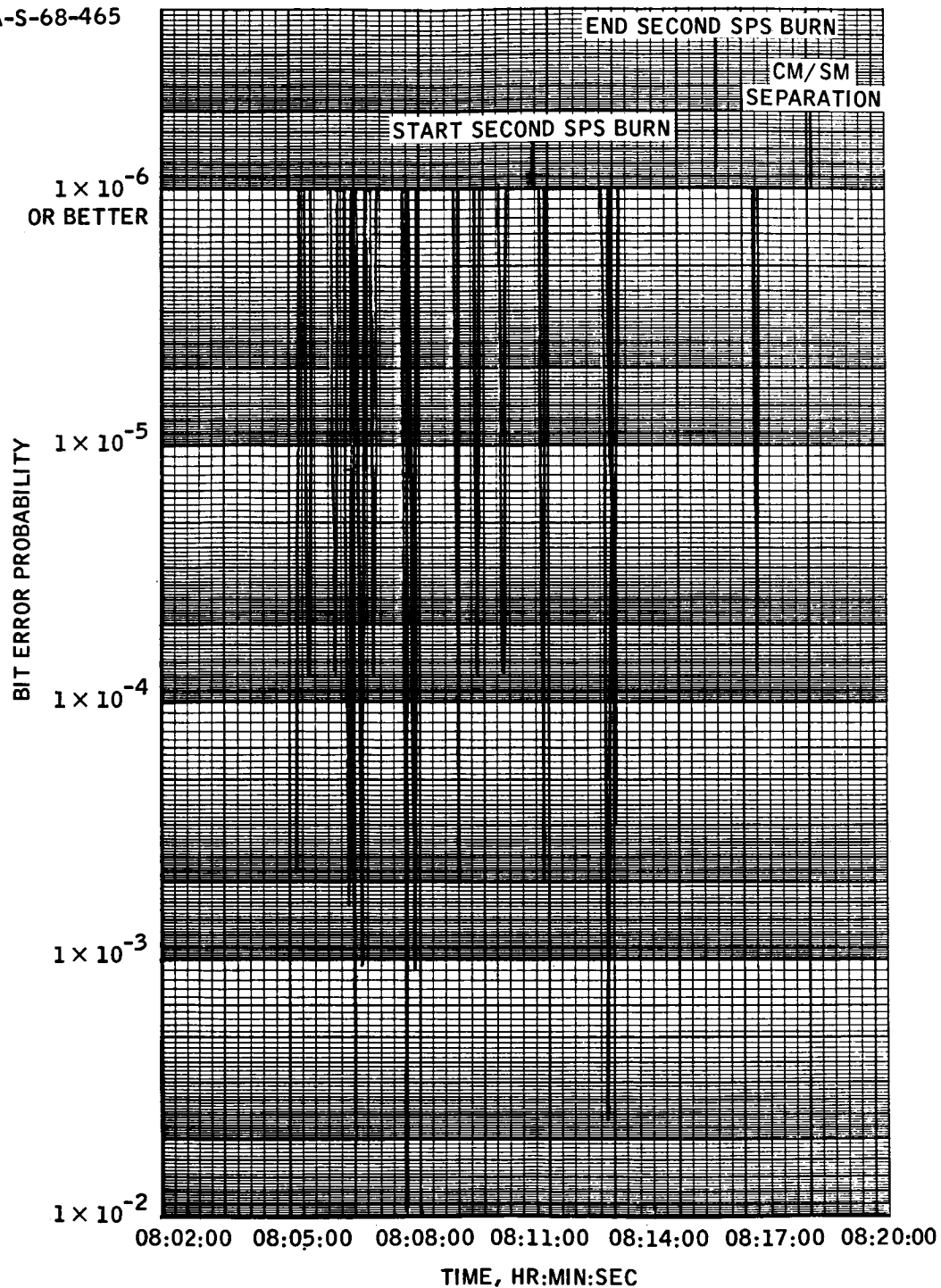


FIGURE 5.13-18.- UNIFIED S-BAND TELEMETRY BIT ERROR PROBABILITY,  
GUAM COVERAGE OF THIRD REVOLUTION.

~~CONFIDENTIAL~~

~~CONFIDENTIAL~~

5.14-1

#### 5.14 INSTRUMENTATION

The performance of the spacecraft instrumentation adequately supported both the flight control of the Apollo 4 mission and the postflight mission evaluation. Of the 810 measurements listed for the CSM-017 vehicle, only three measurements were not operational prior to the start of the automatic countdown sequence. A total of 807 measurements were transmitted from or recorded onboard the command module. These measurements consisted of 506 operational PCM and 301 flight qualification measurements. Of these 807, eight measurements failed to provide any mission data, three failed during the mission, three were probably measurement failures, 20 were questionable, and three were known to have calibration errors.

The eight measurements which did not provide any mission data were all of a sequential type as follows.

CE0001X	Drogue Deploy, Relay A
CE0002X	Drogue Deploy, Relay B
CE0003X	Main Parachute Deploy - Drogue Release A
CE0004X	Main Parachute Deploy - Drogue Release B
CE0007X	Baroswitch Lock-in, Relay A
CE0008X	Baroswitch Lock-in, Relay B
CE0321X	Main Parachute Disconnect, Relay A
CE0322X	Main Parachute Disconnect, Relay B

These measurements did not provide event data due to the failure of the 5-volt reference power supply for their signal conditioning equipment.

The following three measurements failed during the mission.

The electrical power subsystem measurement for the oxygen flow rate to fuel cell no. 3 (SC2144R) failed during the first revolution between 01:00:00 and 01:45:00. A fuse was blown in this measurement circuit twice previously; one time during factory checkout and the other time during pad testing. Replacement of the fuse in each instance appeared to eliminate the problem. Extensive testing could establish no cause for the power failures.

~~CONFIDENTIAL~~

~~CONFIDENTIAL~~

The CM reaction control subsystem temperature measurement for the system B clockwise engine oxygen valve (CR2206T) failed at 08:20:23 during entry. Postflight testing revealed a defective instrumentation signal conditioner.

The service propulsion subsystem (SPS) measurement for the engine nozzle outer skin temperature (SP0050T) did not provide correct data during the SPS burns. Measurement data indicated a constant ambient temperature rather than an increase in temperature during engine burn. The cause of the failure is unknown.

The following structure measurements exhibited data that indicated a probable failure when compared to related measurements.

CA5018R	Flux Aft Heat Shield Shear Pad No. 3 Calorimeter
CA5019R	Flux Aft Heat Shield Shear Pad No. 5 Calorimeter
CA5020R	Flux Aft Heat Shield Shear Pad No. 5 Calorimeter

Measurements CA5018R and CA5019R indicated that the initial temperatures were related to the second or third thermocouple wafer output levels. Measurements CA5020R indicated that the initial temperatures were related to the second thermocouple wafer output level. These data indicate that the instrumentation sequencer did not function or the ablator heat shield did not recede as anticipated. Postflight analysis of these measurements has been initiated to establish the cause of the measurement error.

The following 20 measurements were questionable.

The structural measurement for the CM/SM umbilical tube temperature, location 4 (CA1444T), exhibited intermittent and noisy data during entry. Postflight testing revealed an open circuit in an instrumentation zone box.

The structural measurement for the side heat shield temperature, location 3-B (CA5713T), exhibited noisy data throughout the mission. Postflight testing revealed the instrumentation thermocouple wiring insulation was frayed and caused erratic shorting of this instrumentation.

The environmental control subsystem (ECS) measurements of the cold plate differential pressures, branch 1 and 2 (CF0549P and CF0550P, respectively), were noisy. Noisy data were first exhibited after the first SPS burn. The noisy data indicated that the flow rate of the ECS water/glycol was experiencing considerable fluctuation. A postflight evaluation of the related glycol pump accumulator and pump outlet

~~CONFIDENTIAL~~

~~CONFIDENTIAL~~

5.14-3

pressure data indicated that the flow ratio was relatively constant. Further analysis has been initiated to establish the cause of the instrumentation error.

The structural measurements noted below exhibited data that indicated a wiring transposition had occurred.

CA5700T	Side Heat Shield, Location 1-A, Temperature
CA5701T	Side Heat Shield, Location 1-B, Temperature
CA5705T	Side Heat Shield, Location 2-A, Temperature
CA5706T	Side Heat Shield, Location 2-B, Temperature
CA5710T	Side Heat Shield, Location 3-A, Temperature
CA5711T	Side Heat Shield, Location 3-B, Temperature
CA5730T	Side Heat Shield, Location 7-A, Temperature
CA5731T	Side Heat Shield, Location 7-B, Temperature
CA5735T	Side Heat Shield, Location 8-A, Temperature
CA5736T	Side Heat Shield, Location 8-B, Temperature

These measurements are grouped in a thermocouple plug in the heat shield such that the thermocouple of location A is closer to the surface than the thermocouple of location B. Mission data indicated that those measurements in location B reached a higher temperature than those in location A. Postflight analysis confirmed that a wiring reversal occurred at the thermocouple plug assembly in each case.

The ECS measurement CF0484T water/glycol cold plate outlet temperature, branch no. 2, data did not agree with related cold plate temperatures. Postflight test analysis of the measurement instrumentation configuration and installation will be made to establish whether this measurement is influenced more by the cabin temperature than the water/glycol fluid temperature.

The environmental control subsystem measurement of the oxygen tank no. 1 temperature (SF0041T) contained approximately  $\pm 4$  percent of noise throughout the mission. This noise rendered the measurement questionable in the calculation of oxygen quantity using a pressure-volume-temperature computation technique. An instrument measurement circuit change will be incorporated in Block II spacecraft (CSM 103 and subsequent) to filter

~~CONFIDENTIAL~~

~~CONFIDENTIAL~~

out objectionable noise. This change will be applicable to all four oxygen and hydrogen tank temperature measurements.

The structural vibration measurements noted below exhibited a low signal-to-noise ratio.

CA2530D	Y-axis CM LEB Kick Ring Vibration
CA2531D	Z-axis CM LEB Kick Ring Vibration
CA2532D	X-axis CM LEB Honeycomb Bulkhead Vibration
CA2533D	Z-axis CM LEB Honeycomb Bulkhead Vibration

These measurements utilized transducers with instrumentation ranges which greatly exceeded the actual spacecraft vibration levels.

The following measurements were known to have calibration errors prior to the mission.

The ECS measurement for barometric static pressure reference (CE0035P) was suspected to be out of calibration at launch. This measurement was indicating ambient pressure of 14 psia. On-pad accuracy of this measurement is  $\pm 0.75$  psia. Postflight tests will provide actual calibration data on this measurement to enable a correct barometric pressure profile and relief crack pressures to be computed. (See section 5.19).

The ECS measurement of waste water tank quantity (CF0009Q) indicated an error of 12-percent quantity when empty during pad checkout. The instrumentation was recalibrated but again assumed a 12-percent error. Data were obtained from this measurement throughout the mission but were suspect because of the error noted. A postflight analysis has been initiated to establish the cause of this instrumentation error.

The SPS engine chamber pressure measurement (SP0661P) had an uncertainty of  $\pm 10$  percent. This measurement failed during pad checkout due to malfunctioning signal conditioning equipment. The instrumentation is of a matched sensor and signal conditioner pair. Replacement of the pressure sensor could not be made due to the transducer being inaccessible. A selected signal conditioner was installed to minimize calibration error. The measurement performed satisfactorily throughout the mission. The measurement uncertainty did not significantly affect mission evaluation of engine performance.

Both operational and development instrumentation hardware used on CSM 017 performed satisfactorily. The flight camera, as a part of the instrumentation system, also performed all mission requirements satisfactorily.

~~CONFIDENTIAL~~

~~CONFIDENTIAL~~

5.15-1

## 5.15 GUIDANCE AND CONTROL SUBSYSTEM

### 5.15.1 Summary

The guidance and control (G&C) subsystem included the guidance and navigation (G&N) subsystem, the stabilization and control subsystem (SCS), and the mission control programmer. Performance of these subsystems was equal to or better than preflight predictions throughout the mission. All G&C mission objectives were met. Analysis of navigation error propagation during ascent, the SPS burns, and entry indicates that inertial measurement unit (IMU) gyro drifts and accelerometer biases and scale factors remained within specification tolerances. All sequencing and computational operations performed by the Apollo guidance computer have been verified to have been correct. All attitude maneuvers were nominal. The cold-soak attitude was maintained properly throughout the coast phase although continuous venting from the environmental control system water boiler produced a disturbance torque which caused unsymmetrical limit cycles in the pitch and yaw axes. SCS attitude reference system performance was nominal. Thrust vector control during the two service propulsion subsystem (SPS) burns was nominal; however, larger than normal start transients were experienced during the first burn. These transients have been attributed to random propellant slosh from the no-ullage start. Guidance during both burns was satisfactory. The 215 ft/sec overburn experienced during the second SPS burn was caused by a ground override of the G&N cutoff command. Guidance commands issued by the G&N subsystem during entry have been verified correct in postflight simulations. Sequencing of the mission control programmer was satisfactory throughout the mission.

### 5.15.2 Integrated Subsystem Performance

Ascent/parking orbit phases.- The lift-off discrete from the launch vehicle was detected by the Apollo guidance computer at 00:00:00.54. Upon receipt of this signal the Apollo guidance computer released the IMU from gyrocompassing by issuing Guidance Reference Release (GRR) and began the boost monitor phase. During this phase the Apollo guidance computer was programmed to drive the Y-axis (pitch) coupling display unit in accordance with a preset polynomial normally matching that set in the launch vehicle guidance computer. The difference between the pitch angle from the coupling display unit and the corresponding IMU pitch angle is displayed on the flight director attitude indicator (FDAI) for use on manned flights and to the ground monitoring facilities to provide a measure of launch vehicle performance. On this mission a late change was made in the launch vehicle pitch profile for predicted November winds but the change was not reflected in the Apollo guidance computer

~~CONFIDENTIAL~~



~~CONFIDENTIAL~~

program. The predicted and actual error resulting from this change is reflected in figure 5.15-1. The coupling display unit values computed by the Apollo guidance computer have been verified as being correct. Therefore, the difference between the predicted and actual curves is attributed to initial misalignment of and flexure between the two IMU mounts. The pitch misalignment prior to lift-off was 1.28 degrees.

Figure 5.15-2 contains a time history of spacecraft body rates during launch vehicle first-stage operation. The oscillations noted were significantly larger than those on the AS 202 mission, and the oscillations continued until second-stage ignition.

At the time of launch escape tower jettison the G&N switched from boost monitor mode to tumble monitor mode, wherein a continuous check was made for body rates in excess of 5 deg/sec. This mode continued until CSM/S-IVB separation. No excessive rates were noted.

Table 5.15-I contains a comparison of state vectors computed by the spacecraft G&N subsystem, the S-IVB guidance system and from postflight trajectory data at significant points during this and other mission phases. The relative insignificance of the errors noted, although based on preliminary analysis, represents excellent G&N performance.

Separation of command and service module from S-IVB stage.- Separation of the CSM from the S-IVB began at 03:26:26.5. Sequencing operations during the separation and 10-second ullage maneuver were nominal and the total separation velocity was 1.9 ft/sec. Figure 5.15-3 contains a time history of major events during the separation maneuver and the first SPS burn. Figure 5.15-4 is a plot of the accumulated velocity as derived from two different data sources. The curve labeled RCS  $\Delta V$  was computed from reaction control subsystem (RCS) engine on/off times, nominal thrusts, and weight and balance data. A four-engine RCS direct ullage maneuver is assumed from 03:26:26.5 to 03:26:29.5. At 03:26:29.5 the RCS enable inhibit was removed by the master event sequence controller and the attitude control subsystem started correcting for a positive yaw disturbance torque. The curves labeled  $\Delta V_x$ ,  $\Delta V_y$ , and  $\Delta V_z$  are velocity components sensed by X-axis, Y-axis, and Z-axis IMU accelerometers, respectively. The resultant velocity change of 1.9 ft/sec agrees with the RCS  $\Delta V$  of 1.8 ft/sec within measurement tolerances.

Separation of the CSM/S-IVB was very clean with no evidence of re-contact. Rate disturbances caused by center-of-gravity offset were very small. The largest rate error during the direct ullage maneuver was a gradual buildup to +0.67 deg/sec in yaw; the pitch and roll errors were less than  $\pm 0.20$  deg/sec. As soon as the master event sequence controller enabled the SCS attitude control capability, pulsing of the negative yaw engines started to null the yaw rate error, and at the end of the

~~CONFIDENTIAL~~

~~CONFIDENTIAL~~

5.15-3

ullage maneuver all rate errors were less than  $\pm 0.10$  deg/sec. Spacecraft dynamics during the separation maneuver are shown in figure 5.15-5.

First service propulsion subsystem burn.- Figure 5.15-3 contains the sequence of events for the first SPS burn. All discretized and mode changes were nominal with the G&N in automatic control. Figure 5.15-5 shows spacecraft dynamics during the maneuver to the burn attitude. SCS response to G&N attitude commands was nominal in every respect. Figure 5.15-6 contains a time history of pertinent parameters telemetered during the burn. The initial transients experienced were somewhat large, approximately 0.8 and 0.9 degree in pitch and yaw attitude, respectively, but are attributed to random propellant slosh from the no-ullage start. This conclusion is corroborated by the fact that the engine gimbals stabilized close to the initial trim settings (see table 5.15-II) and that the approximate 0.5 Hz oscillations noted during the transient were close to those predicted for slosh modes. No unusual SPS shutdown transients were noted.

Guidance for the SPS velocity change maneuvers was based on a targeted orbital eccentricity and semilatus rectum. The velocity change was further constrained to be in-plane, that is, along the velocity vector at ignition. This latter constraint differed from the guidance law for the AS 202 mission in that desired landing point was not a targeted parameter. As in the AS 202 mission, cross product steering was used to generate control commands to the SPS gimbals. In cross product steering, the sensed thrust vector (adjusted for gravity and field force effects) is directed along the velocity-to-be-gained ( $V_g$ ) vector in a sense to reduce  $V_g$ . Figure 5.15-7 is a time history of velocity-to-be-gained for the first SPS burn. Also indicated are the values of  $V_g$  during the last 4 seconds of burn calculated postflight from Apollo guidance computer data; these values show the accuracy of the Apollo guidance computer SPS thrust model. The final errors in  $V_g$  were +0.05, +0.50, and +0.41 ft/sec in the X-axis, Y-axis, and Z-axis, respectively. The result of these errors was a miss of 66 642 feet (11.0 n. mi.) in the targeted apogee altitude (based on a conic propagation of the postburn state vector). Table 5.15-III synthesizes the target and achieved orbit from the first SPS burn. Both the semilatus rectum and the eccentricity exceeded the targeted values.

Coast phase.- Figure 5.15-8 contains a time history of spacecraft dynamic parameters during the maneuver to the cold soak attitude. Maximum maneuver rates of approximately -3.8, +3.0, and -6.1 deg/sec were obtained in pitch, yaw, and roll, respectively. Figure 5.15-9 contains typical limit cycles in each axis during the cold-soak attitude hold period. SCS performance, as calculated from switching levels and loop

~~CONFIDENTIAL~~

~~CONFIDENTIAL~~

gains, was nominal although a continuous disturbance torque (minus pitch and yaw) caused unsymmetrical limit cycles throughout the mission. The disturbance is attributed to continuous venting from the water boiler in the environmental control subsystem which normally expels steam at a rate and in the correct direction to cause the dynamic response noted.

Second service propulsion subsystem burn.- Figure 5.15-10 shows the maneuver to the second SPS burn attitude. Maximum maneuver rates of approximately 1.0, 3.0, and 6.5 deg/sec were noted in pitch, yaw, and roll, respectively. SCS response was again nominal. Figure 5.15-11 contains the sequence of events for the burn. Figure 5.15-12 contains a time history of dynamic parameters. As noted, the initial transients for the second SPS burn were much lower than for the first burn. Because the second burn was preceded by a normal RCS ullage maneuver, the low transients further substantiate the propellant slosh conclusion for the first burn. The gimbal trim and steady state values are included in table 5.15-II.

As shown in figure 5.15-11, normal control of the second SPS burn was inhibited by real-time commands. At 08:10:54.80 the burn was initiated automatically by the G&N as planned. This was followed by a direct thrust on command (RTC 11). Refer to section 9.1.5 for an explanation of transmission of RTC 11. The G&N continued to exercise normal thrust vector control, driving the velocity-to-be-gained ( $V_g$ ) toward zero (fig. 5.15-13). At approximately 08:15:22, the Apollo guidance computer detected that less than 4 seconds of thrust were required to achieve the targeted orbit, commanded constant attitude, and set the engine-off time at 08:15:25.68.

The presence of the direct thrust on command (RTC 11) inhibited the G&N engine cutoff command, however, and the burn continued at the cutoff attitude until approximately 08:15:36, when the direct thrust off command (RTC 12) was accepted by the ground command controller of the mission control programmer. As shown in figure 5.15-13, the delay in issuing engine cutoff resulted in an overburn of 215.6 ft/sec, as sensed by the G&N. This overburn resulted in a miss of the target entry orbit.

The actual entry orbit parameters and the intended target for the second SPS burn are shown in table 5.15-IV. The entry orbit achieved was hyperbolic as indicated by the eccentricity exceeding unity. The overburn also resulted in reducing the effective perigee of the orbit by more than 285 000 feet from the value of 20 990 612 defined by the target eccentricity and semilatus rectum.

Command module/service module separation.- The separation of the CM from the SM occurred at 08:18:02.6. There was a pitch-down disturbance torque applied to the CM at separation, causing rate errors of minus

~~CONFIDENTIAL~~

~~CONFIDENTIAL~~

5.15-5

4.5 deg/sec and minus 0.4 deg/sec in pitch and yaw, respectively, and attitude excursions of approximately minus 4 degrees in pitch at separation plus 3 seconds and approximately minus 4 degrees in yaw at separation plus 6 seconds. The disturbing force continued at a decreasing magnitude for about 10 seconds. The disturbance appeared to be external to the CM because during the 10 seconds that it was being applied, it transferred from the pitch axis to the yaw axis, then back to the pitch axis. One possible source of a disturbing force of this nature is impingement of the -X translation engines of the SM-RCS upon the CM heat shield while the SM is rolling and translating away from the CM.

Entry.- Figure 5.15-14 contains a time history of dynamic parameters during the entry phase. The pitch and yaw oscillations noted were comparable to those experienced during the AS 202 mission, with long periods of operation within the rate deadbands. Response of the SCS and the spacecraft to G&N roll commands was nominal throughout the mission.

The entry interface velocity and flight-path angle were 213 ft/sec higher and 0.203 degree shallower, respectively, than had been predicted. This was caused by the overburn previously described. The off-nominal conditions, however, did not adversely affect the performance of the guidance system in achieving the desired target. The planned velocity at the entry interface altitude was 36 333 ft/sec with a planned flight path angle of minus 7.13 degrees. The values calculated by the G&N were 36 559.1 ft/sec and minus 6.890 degrees, respectively. These entry parameters compare favorably with the interface conditions obtained from the Guam tracking data following the SPS burn. The Guam radar data indicated a velocity of 36 546 ft/sec and flight-path angle of minus 6.927 degrees.

The G&C subsystem operated properly throughout the entry phase. The sequence of events reconstructed from the onboard telemetry tape is depicted in figure 5.15-15.

The spacecraft reached the entry interface at 08:19:28.5 with the initial roll guidance program (P 63) in command. The G&N indicated a desired inertial range of 2084 n. mi. and a predicted cross range error of 7.9 n. mi. Approximately 27 seconds later (08:20:43), the CM had passed through the 0.05g level and the Apollo guidance computer transferred control to the hunttest guidance program (P 64).

The hunttest guidance phase was entered at a velocity of 33 060 ft/sec and at a desired inertial range of 1648 n. mi. In this phase the desired exit conditions to which the G&N would guide during the upcontrol phase were calculated. A hunttest solution was found (range to target minus predicted range to target (DIFF)  $\leq$  25 n. mi.) at 08:21:23, and the upcontrol guidance phase (P 65) was entered. The duration of the hunttest phase was 40 seconds. The value of DIFF at hunttest solution was 3.42 n. mi.; the desired inertial range was 1440 n. mi.

~~CONFIDENTIAL~~

~~CONFIDENTIAL~~

The minimum altitude indicated by the G&N during first entry was 165 040 ft and was reached at 08:20:45. Peak acceleration based on G&N data was 7.3g. The maximum altitude reached during the altitude skip was 235 991 feet, as indicated by the G&N at 08:24:11. The desired range at maximum altitude was 790 n. mi.

No skip phase was required to reach the desired target, so the G&N bypassed the Kepler guidance phase (P 66) and went directly from the upcontrol guidance phase to the final guidance phase (P 67) at 08:24:11. The G&N indicated the second acceleration peak of 4.25g at 08:27:11 at a velocity of 15 803 ft/sec. At this time, the G&N desired range was 205.7 n. mi. The G&N terminated guidance (relative velocity less than 1000 ft/sec) at 08:29:57. At drogue parachute deployment, the G&N indicated an overshoot of the desired target point of 2.2 n. mi.

In figure 5.15-16, the commanded bank angle (roll command) and the actual bank angles (CDUX) are presented as a function of time. Both curves were either taken directly or were derived from the onboard telemetry tape. Comparison of the two parameters indicates very good response of the spacecraft to the bank angle commands. Table 5.15-V is a comparison of the telemetered navigation data and guidance commands with a reconstructed set. The reconstructed set was developed by calculating the navigation and guidance commands directly from the accelerometer data on the telemetry tape. This comparison indicates that the G&N subsystem interpreted the accelerometer data correctly.

A summary of the touchdown data for this mission is shown in figure 5.15-17. The G&N subsystem indicated a touchdown resulting in an overshoot of 2.2 n. mi. The recovery forces estimated touchdown to be at longitude 172 degrees 32 minutes west and latitude 30 degrees 06.41 minutes north, resulting in an undershoot of 10 n. mi. There was no radar tracking during spacecraft entry; consequently, no absolute navigation accuracy can be obtained. However, a reconstructed trajectory has been produced by applying the IMU errors, listed in table 5.15-VI, to the accelerometer data. The corrected accelerometer data trajectory indicated a touchdown at longitude 172 degrees 29 minutes west and latitude 30 degrees 1 minute north for an undershoot of 5.2 n. mi. A comparison of the G&N navigation data with this reconstructed trajectory is contained in table 5.15-VII. This comparison shows that the G&N had a downrange navigation error of approximately 2.0 n. mi. at entry interface and that the error propagated throughout the entry to a downrange navigation error at drogue deploy of approximately 7.4 n. mi. This error is within the 1-sigma touchdown accuracy predicted before the mission.

~~CONFIDENTIAL~~

~~CONFIDENTIAL~~

5.15-7

### 5.15.3 Guidance and Navigation Subsystem Performance

Inertial subsystem.- The inertial subsystem consisted of the IMU and associated electronic components. Figure 5.15-18 contains the pre-flight test history of the IMU inertial components: the inertial rate integrating gyros and the pulsed integrating pendulous accelerometers. The data indicate excellent stability in all cases and are summarized in table 5.15-VIII. The compensation value of accelerometer bias, scale factor, and gyro acceleration drift along spin reference axis (ADSRA) loaded in the computer was the data mean obtained prior to the final calibration at T minus 40 hours. In an attempt to obtain a more accurate value for zero-g null bias drift (NBD), the g-sensitive component of the measured term (acceleration drift along the output axis) was extracted prior to computation of the mean for the X-gyro and Y-gyro. The Z-gyro g-sensitive component was not extracted due to its effect on gyro-compassing. Drift due to acceleration along the input axis (ADIA) cannot be measured explicitly after the system is installed in the spacecraft; therefore, preinstallation data were used for the compensation value. Rather large shifts in the differences between ADIA terms which can be measured in the spacecraft were noted in the final calibration; however, because of the low confidence in this test and the insensitivity of the mission to these coefficients, no change was made in the compensation value. No flight effects were noted.

During preflight testing, a malfunction was detected in the inertial subsystem emergency heater circuitry. Inertial instrument performance could have been affected if the primary heater circuit had also malfunctioned in flight. In this event the system would have automatically switched into the emergency mode. An overtemperature thermostat was also provided in the system as a backup control. However, the primary temperature mode functioned properly throughout the mission, no flight effects were observed, and all temperatures remained within specification tolerances. Postflight testing is underway to determine the cause of the malfunction.

A preliminary set of inflight IMU error coefficients has been derived based on comparisons of G&N and launch vehicle guidance system velocity computations during ascent and the second S-IVB burn, and on an entry trajectory point fit. The error sources represent deviations from the compensated value and are shown in table 5.15-VI. It should be emphasized that these error coefficients are preliminary and are subject to change upon receipt of final trajectory data.

Figure 5.15-19 contains the ascent velocity comparison with the launch vehicle and with velocities computed from quick-look data from the AZUSA tracking system. The poor quality of the tracking data is evident from the rapid divergence and noise shown. Also shown are the

~~CONFIDENTIAL~~

~~CONFIDENTIAL~~

corrections for gravity computation error and the resultant fit using the error sources previously described. The launch vehicle data were used as the reference; therefore, any errors accrued by the S-IVB platform are falsely attributed to the IMU. The launch vehicle errors are reported to be less than 1 meter/sec in each axis and are based on extrapolation of orbital tracking data back to insertion. This fact, coupled with the second SPS burn and entry fits, gives some confidence in the coefficients selected.

An initial error of approximately 2 ft/sec was noted in the X-axis (vertical) and was caused by the difference in time of guidance reference release for the two platforms. The X-axis error propagation shown (fig. 5.15-19) is characteristic of an accelerometer scale factor error. An error of 140 ppm provided a reasonably good fit to the difference curve.

The source of the Y-axis error (out of plane) appears to be predominantly an azimuth misalignment of approximately 300 arc seconds (1.45 mr) at lift-off. An azimuth misalignment during gyrocompassing can be caused by null bias drift of any gyro, by an input axis acceleration sensitive drift of the X-axis gyro, by internal misalignment, or by a number of other terms. However, the Y-axis gyro bias appears to be the most likely source because it would account for the errors noted at entry. The Z-axis error downrange is accounted for by a Z-axis accelerometer scale factor error of 123 ppm.

The accelerometer bias errors were computed during the high-attitude coast period. An uplink command was sent which caused the accumulated counts to be displayed for a period of over 40 minutes. Table 5.15-IX contains a comparison of the bias calculated during this period with that loaded preflight. It has been determined that the water boiler venting mentioned in section 5.15.2 had little or no effect on this calculation.

It should be reemphasized that the errors noted in the preceding paragraphs are preliminary and are subject to change when accurate tracking data become available. A supplementary report of G&N performance will be issued at that time. It should also be noted that the level of errors noted is representative of excellent IMU performance throughout the mission.

Computer subsystem.— The computer subsystem consisted of the Apollo guidance computer and two displays and keyboards (DSKY's).

The Apollo guidance computer performed all sequencing correctly during the mission. Table 5.15-X contains the major mode changes and the mission elapsed time at which they occurred as well as the nominal programmed time of occurrence. In figures 5.15-3 and 5.15-11, various

~~CONFIDENTIAL~~

~~CONFIDENTIAL~~

5.15-9

flagword indicators have been included in the CSM/S-IVB separation sequence, the first SPS burn sequence, and the second SPS burn sequence.

Three computer restarts were detected during the mission. Prior to CSM/S-IVB separation, in preparation for a possible backup separation command requirement, VERB 75 was sent via the uplink. The separation was nominal; therefore no backup was required and no ENTER for this VERB was sent. The Apollo guidance computer recognized the uplink condition at 03:23:31.355 (AGC Time = 12211.10) and set bit 4 (DSPLOCK) of the Apollo guidance computer downlink word STATE to the ON condition. (DSPLOCK is used to avoid conflicts between keyboard and subroutine calls.) The Apollo guidance computer continued normal computations until 03:26:26.614 (AGC Time = 12386.36) when the CSM/S-IVB separation (SIVBSMSEP) routine was entered. At this time the Apollo guidance computer recognized that the DSKY was in use by the uplink. The Apollo guidance computer then entered ENEMA in which many of the AGC computations were reinitialized, and the downlink list was recycled to word number 1. The normal computational flow was then reentered. The restart was a result of the uplink condition at the time of entry into the CSM/S-IVB separation (SIVBSMSEP) routine. The computer performed as it was intended with no resultant loss of guidance or navigation information.

Prior to spacecraft entry, two other scheduled restarts occurred; one at entrance into the CM/SM separation maneuver program (08:16:06) and the other at actual separation (08:18:02). The restart sequence was identical to that described previously.

Periodically during attitude maneuvers, fail indications from the coupling data units (CDUFAIL) were noted; however, this is a normal occurrence for this mechanization. The Apollo guidance computer periodically scans the IN2 register for a coupling data unit fail (Bit 10 = 1 for a CDU error output >1.2 milliradians for greater than  $5 \pm 2$  seconds.) If this condition is detected, the Apollo guidance computer will determine whether the IMU is or is not in the fine align mode. If the IMU is in the fine align mode, the CDUFAIL light (bit 6 of DSPTAB+11) will be turned on. If the IMU is not in the fine align mode the Apollo guidance computer determines this and considers the problem to be an external one; consequently, no output indication of a CDUFAIL is generated. However, bit 10 (CDUFAIL) of the IN2 register and the PCM analog bilevel word CG5002X (CDUFAIL) will indicate a failure. All CDUFAIL indications noted were in other than fine align mode and resulted from the inability of the coupling data units to respond to an input command rapidly enough to maintain the error signal below its required threshold.

The Apollo guidance computer received several blocks of data from the command link of the MSFN during the mission. Preplanned state vectors to update the onboard state vector were transmitted from the

~~CONFIDENTIAL~~



~~CONFIDENTIAL~~

Carnarvon and Ascension network stations prior to the first and second SPS burns, respectively. An unplanned request for an Apollo guidance control display of counts from the pulsed integrating pendulous accelerometers was sent from Ascension in order to obtain data in the Apollo guidance computer downlist for estimating changes in accelerometer bias. The previously mentioned commands sent in preparation for CSM/S-IVB separation were uplinked from the tracking ship Vanguard.

The state vector update from Carnarvon was initially rejected by the spacecraft communications subsystem, but after the ground transmitters were switched the update was accepted both by the communications subsystem and the Apollo guidance computer. The state vector update from Ascension was accepted by the communications subsystem but the second command was rejected by the Apollo guidance computer. A KKK check, a redundancy check of the transmitted characters, failed. Corrective uplink procedures, prearranged for this eventuality, were accomplished and the state vector update was completed without further incident. The Ascension-transmitted commands requesting an Apollo guidance computer display of accelerometer counts and the Vanguard commands were accepted by the communication subsystem and the Apollo guidance computer without any requirement for retransmission.

Optical subsystem.- The optical subsystem consisted of the sextant and the scanning telescope. On this mission, the optical subsystem was used for prelaunch alignment checks and to hold the optics in a preferred orientation for entry heating effects. Operation was normal throughout.

#### 5.15.4 Stabilization and Control Subsystem Performance

The stabilization and control system provided attitude and thrust vector control in response to G&N commands by actuation of the reaction control subsystem thrusters and SPS gimbal actuators. G&N attitude commands were summed by the SCS with internally generated rate errors to determine the command required. In addition, the SCS provided a backup source of spacecraft attitude information. Performance was nominal throughout.

Table 5.15-XI contains a comparison of selected control loop gains and deadbands computed from flight data with those observed preflight. All values were within tolerances imposed by data granularity. The psuedo-rate capability was mechanized for the first time on this mission. With this capability, RCS pulse width and duty cycle are modulated in response to the magnitude of the total error signal so as to provide minimum impulse limit cycle attitude control and thereby minimum fuel consumption. Because of the water boiler venting disturbance (section 5.15.2), the optimum limit cycle was not realized; however, the

~~CONFIDENTIAL~~

~~CONFIDENTIAL~~

5.15-11

data indicate that psuedo-rate performance was proper with a typical pulse width, after convergence, of approximately 18 msec.

The backup attitude reference system, mechanized by caging the body-mounted attitude gyros through the attitude gyro coupling unit, performed properly throughout the mission. The attitude gyro coupling unit was aligned to the G&N prior to lift-off and was realigned twice during the mission; once at the beginning and again at the end of the coast phase. Comparison of angles from the attitude gyro coupling unit with IMU gimbal angles during the coast phase indicates a maximum drift rate of approximately 5.6 deg/hr, a value well within specification tolerances. The maneuver rates experienced during entry exceeded the attitude gyro coupling unit torquing capability; however, the float displacements in the body-mounted attitude gyros were not large enough to reach the mechanical stops. Large drift rates caused by the off-null operation were noted. This condition is considered normal for the system as designed.

Prior to the mission, it was noted that the minus pitch axis thruster solenoid arc suppression circuitry contained in the SCS junction box was inoperative. This circuit is utilized to suppress inductive transients in the solenoid wiring which occur when the thrusters are turned off. Postflight testing disclosed that a crimped wire was the cause. No adverse effect was noted during the mission.

All SCS environmental data indicated normal operation throughout.

#### 5.15.5 Mission Control Programmer Performance

The mission control programmer supplied control function inputs to the following subsystems and controller.

- a. Environmental control subsystem
- b. Electrical power subsystem
- c. Stabilization and control subsystem
- d. Service propulsion subsystem
- e. Reaction control subsystem
- f. Earth landing subsystem
- g. Master event sequence controller

~~CONFIDENTIAL~~

~~CONFIDENTIAL~~

The mission control programmer was primarily a passive device, and no specific instrumentation was included for its analysis. Verification of continuity at the proper time was the only criterion considered during evaluation of this programmer. Proper performance was indicated throughout the mission.

~~CONFIDENTIAL~~

~~CONFIDENTIAL~~

5.15-13

TABLE 5.15-1.- STATE VECTOR COMPARISON

IMU axis	Insertion		Translunar injection (cutoff + 8 seconds)			First SPS burn (cutoff + 6 seconds)	
	Apollo guidance computer	S-IVB instrument unit	Apollo guidance computer	S-IVB instrument unit	Best estimate trajectory	Apollo guidance computer	Best estimate trajectory
X, ft	19 523 390	19 527 860	10 812 284	10 465 677	10 992 380	-6 504 166	-6 527 790
Y, ft	307 186	294 813	2 609	14 036	9 992	-2 298 513	-2 290 374
Z, ft	9 070 441	9 069 673	20 009 166	20 172 057	19 819 758	29 506 965	29 497 715
X, ft/sec	-10 785	-10 773	-22 284	-22 490	-22 201	-24 432	-24 403
Y, ft/sec	321	285	-3 458	-3 453	-3 451	-2 883	-2 877
Z, ft/sec	23 187	23 186	21 077	20 703	21 270	6 866	6 826
Time	00:11:15.6		03:16:34.3			03:28:28.6	

~~CONFIDENTIAL~~

IMU axis	Second update			400K feet	
	Apollo guidance computer	Update	Best estimate trajectory	Apollo guidance computer	Best estimate trajectory
X, ft	8 186 760	11 400 782	11 363 419	21 145 870	21 115 424
Y, ft	2 740 279	2 840 699	2 842 984	2 238 035	2 235 719
Z, ft	-34 632 183	-30 761 801	-30 792 221	-1 335 451	-1 369 568
X, ft/sec	15 675	15 020	15 034	-1 930	-1 850
Y, ft/sec	704	520	514	-2 175	-2 219
Z, ft/sec	16 304	18 714	18 692	36 431	36 537
Time	08:01:33.8			08:19:28.5	

~~CONFIDENTIAL~~

TABLE 5.15-II.- SERVICE PROPULSION SUBSYSTEM

## GIMBAL TRIM VALUES

SPS burns	Initial trim angle, deg		Steady state, deg	
	Pitch	Yaw	Pitch	Yaw
First	1.1	4.7	1.7	4.8
Second	1.5	5.7	1.8	4.8

~~CONFIDENTIAL~~

~~CONFIDENTIAL~~

5.15-15

TABLE 5.15-III.- COMPARISON OF ATTAINED ORBIT WITH TARGET

DURING FIRST SPS BURN

	Semilatus rectum, ft	Eccentricity	Perigee <sup>a</sup> , ft	Apogee <sup>a</sup> , ft
Apollo guidance computer at first SPS burn (cutoff + 6 sec- onds)	32 964 314	0.593895222	20 653 567	81 037 272
Target	32 928 189	0.593874991	<sup>b</sup> 20 670 552	<sup>b</sup> 81 103 914

<sup>a</sup>Derived from conic propagation.

<sup>b</sup>Derived from target parameters.

~~CONFIDENTIAL~~

~~CONFIDENTIAL~~

TABLE 5.15-IV.- COMPARISON OF ATTAINED ORBIT WITH TARGET  
DURING SECOND SPS BURN

	Semilatus rectum, ft	Eccentricity	Perigee <sup>a</sup> , ft	Apogee <sup>a</sup> , ft
Apollo guidance computer during second SPS burn (cutoff + 5 sec- onds)	42 396 644	1.021296725	20 705 338	$\infty$
Target	41 960 233	0.99909924	<sup>b</sup> 20 990 612	<sup>b</sup> 46 583 144 233

<sup>a</sup>Derived from conic propagation.

<sup>b</sup>Derived from target parameters.

~~CONFIDENTIAL~~

~~CONFIDENTIAL~~

5.15-17

TABLE 5.15-V.- APOLLO GUIDANCE COMPUTED ENTRY NAVIGATION AND GUIDANCE RECONSTRUCTION

	~400 000 ft altitude		Upcontrol phase		Second entry phase		Guidance termination	
Time	08:19:27		08:21:15		08:24:13		08:30:01	
Parameter	Apollo guidance computer	Recon-struction	Apollo guidance computer	Recon-struction	Apollo guidance computer	Recon-struction	Apollo guidance computer	Recon-struction
X, ft	21 149 896	21 149 883	20 844 100	20 844 149	20 065 127	20 065 679	17 957 537	17 958 501
Y, ft	2 242 638	2 242 631	2 021 033	2 021 046	1 704 516	1 704 702	1 302 408	1 304 412
Z, ft	-1 412 680	-1 412 704	2 548 144	2 548 161	6 454 067	6 454 126	10 850 714	10 850 732
X, ft/sec	-1 865	-1 866	-2 992	-2 991	-6 693	-6 688	-1 519	-1 511
Y, ft/sec	-2 168	-2 168	-1 145	-1 144	-2 341	-2 339	38.2	36.4
Z, ft/sec	36 427	36 426	26 764	26 765	21 386	21 385	1 660	1 660
Roll command, deg	-15.2	-15.2	41.8	30.1	0	0	82.0	84.3
Range-to-target, $\theta$ , n. mi.	2 093	2 093	1 432	1 431	773	772	2.3	2.2

~~CONFIDENTIAL~~



~~CONFIDENTIAL~~

TABLE 5.15-VI.- PRELIMINARY IMU ERROR COEFFICIENTS

Error source	One- $\sigma$ specification requirement	Flight data
Y-gyro bias, deg/hr	0.045	0.058
Azimuth misalignment, mr	3.5	1.45
X-accelerometer, scale factor, ppm	150	-140
Z-accelerometer, scale factor, ppm	150	123
X-accelerometer, bias cm/sec <sup>2</sup>	0.40	-0.09
Z-accelerometer, bias cm/sec <sup>2</sup>	0.40	-0.12

~~CONFIDENTIAL~~

~~CONFIDENTIAL~~

5.15-19

TABLE 5.15-VII.- APOLLO GUIDANCE COMPUTER ENTRY NAVIGATION ACCURACY

Parameter	~400 000 ft		Start upcontrol phase		Start second entry phase		Drogue deployment	
	Apollo guidance computer	Best estimate trajectory <sup>a</sup>	Apollo guidance computer	Best estimate trajectory	Apollo guidance computer	Best estimate trajectory	Apollo guidance computer	Best estimate trajectory
Time	08:19:25		08:21:13		08:24:11		08:31:19	
X, ft	21 153 564	21 160 597	20 849 983	20 863 735	20 078 464	20 081 583	17 868 115	17 831 485
Y, ft	2 246 968	2 243 329	2 023 308	2 015 926	1 709 190	1 695 385	1 297 035	1 283 841
Z, ft	-1 485 529	-1 496 174	2 494 439	2 476 138	6 411 261	6 235 357	10 949 049	10 880 681
X, ft/sec	-1 803	-1 743	-2 892	-2 887	-6 644	-6 691	-873	-1 057
Y, ft/sec	-2 162	-2 208	-1 131	-1 165	-2 334	-2 357	-95.8	-86.0
Z, ft/sec	36 423	36 423	26 941	26 984	21 421	21 381	1 124	968
Range-to-target, $\theta$ , n. mi.	2 105	2 103	1 441	1 444	783	786	-2.2	5.2

<sup>a</sup>Best estimate of trajectory is based on corrected accelerometer data trajectory.~~CONFIDENTIAL~~

~~CONFIDENTIAL~~

TABLE 5.15-VIII.- INERTIAL MEASUREMENT UNIT  
PREFLIGHT PERFORMANCE SUMMARY

Error source	X-axis			Y-axis			Z-axis		
	Flight load	Data mean	1 $\sigma$	Flight load	Data mean	1 $\sigma$	Flight load	Data mean	1 $\sigma$
<u>Accelerometer</u>									
Bias, cm/sec <sup>2</sup>	+0.41	+0.42	0.06	+0.21	+0.20	0.04	-0.28	-0.26	0.11
Scale factor, ppm	-421	-425	38	-202	-217	84	+139	+128	52
<u>Gyro</u>									
NBD <sup>a</sup> , meru <sup>b</sup>	+1.5	+1.0	2.6	-7.3	-6.5	0.7	-7.6	-7.8	1.1
ADSRA <sup>c</sup> , meru/g	-3.4	-3.5	0.8	+4.6	+4.9	0.9	-8.4	-8.0	1.3
ADIA <sup>d</sup> , meru/g	-3.4	-6.3	3.9	-0.5	-0.5	3.2	+20.8	+20.7	4.1

<sup>a</sup>NBD — null bias drift.

<sup>b</sup>meru — milli-earth rate unit.

<sup>c</sup>ADSRA — acceleration drift along spin reference axis.

<sup>d</sup>ADIA — acceleration drift along input axis.

~~CONFIDENTIAL~~

~~CONFIDENTIAL~~

5.15-21

TABLE 5.15-IX.- COMPARISON OF INFLIGHT ACCELEROMETER  
BIAS WITH PREFLIGHT COMPENSATION

Axis	Accelerometer bias, cm/sec <sup>2</sup>	
	Inflight	Preflight
X	0.32	0.41
Y	0.22	0.21
Z	-0.40	-0.28

~~CONFIDENTIAL~~

~~CONFIDENTIAL~~

TABLE 5.15-X.- APOLLO GUIDANCE COMPUTER MAJOR

## MODE TIMELINE

Major mode	Mode no.	Planned time	Actual time
Inertial reference	04	-00:00:06.000	00:00:01.341
First stage booster monitoring	11	00:00:00.000	00:00:03.341
S-IVB booster monitoring with tumble monitor on	14	00:03:04.000	00:03:09.342
State vector update	27	02:26:35.000	Not available
S-IVB booster monitoring with tumble monitor on	14	-	Not available
Prethrusting for first SPS burn	31	03:28:07.000	03:26:28.614
Thrusting during first SPS burn	41	03:29:47.000	03:28:08.614
Maneuver to cold soak attitude	21	03:30:23.000	03:28:34.614
Hold attitude during orbital integration	22	03:30:48.000	03:29:00.614
Hold attitude with state vector update allowed	24	-	03:32:16.615
State vector update	27	-	05:26:25.671
Hold attitude with state vector update allowed	24	-	05:30:38.670
Hold second SPS burn attitude and wait for $T_{FF}$ : $T_{FF}$ minutes	26	08:01:37.000	Not available
Prethrusting for second SPS burn	32	08:02:01.000	08:08:54.617

~~CONFIDENTIAL~~

~~CONFIDENTIAL~~

5.15-23

TABLE 5.15-X.- APOLLO GUIDANCE COMPUTER MAJOR

MODE TIMELINE - Concluded

Major mode	Mode no.	Planned time	Actual time
Thrusting during second SPS burn	42	08:15:10.000	08:10:55.614
Hold attitude	23	08:19:44.000	08:15:25.006
CM/SM separation maneuver	61	08:20:15	08:16:06.025
Pre-entry maneuver	62	08:22:15	08:18:06.280
Initiate entry steering	63	08:23:05	08:18:56.280
0.05g indication	64	08:23:35	08:19:56.280
Upcontrol phase	65	-	08:21:23.280
Final phase	67	-	08:24:11.280

~~CONFIDENTIAL~~

~~CONFIDENTIAL~~

TABLE 5.15-XI.- SCS PARAMETER COMPARISON

	G&N attitude control mode		G&N entry control mode	
	Prelaunch test value	Flight value	Prelaunch test value	Flight value
Rate loop "gain"	$\frac{V \text{ dc @ CHXX60}}{\text{deg/sec rate @ CHXX50}}$	$\frac{V \text{ dc @ CHXX60}}{\text{deg/sec rate @ CHXX50}}$	$\frac{V \text{ dc @ CHXX60}}{\text{deg/sec @ CHXX50}}$	$\frac{V \text{ dc @ CHXX60}}{\text{deg/sec @ CHXX50}}$
Pitch	9.50	9.50	1.015	1.05
Yaw	9.50	9.50	1.015	1.16
Roll	9.75	9.76	1.00	1.02
Attitude error loop "gain"	$\frac{V \text{ dc @ CHXX60}}{\text{deg attitude error command}}$	$\frac{V \text{ dc @ CHXX60}}{\text{deg attitude error command}}$	$\frac{V \text{ dc @ CHXX60}}{\text{deg attitude error command}}$	$\frac{V \text{ dc @ CHXX60}}{\text{deg attitude error command}}$
Pitch	8.0	8.7	1.638	data not available
Yaw	8.1	9.1	1.452	data not available
Roll	10.1	10.3	1.775	data not available
Attitude error deadband	deg attitude error	deg attitude error	deg attitude error	deg attitude error
Pitch	$\pm 0.25$	$\pm 0.23$	$\pm 5.5$	data not available
Yaw	$\pm 0.249$	$\pm 0.22$	$\pm 5.4$	data not available
Roll	$\pm 0.198$	$\pm 0.194$	$\pm 5.3$	$\pm 5.1$

## G&amp;N DELTA V MODE

	Prelaunch test value	Flight value
Thrust vector control rate gain	$\frac{\text{deg SPS gimbal}}{\text{deg/sec rate gyro}}$	$\frac{\text{deg SPS gimbal}}{\text{deg/sec rate gyro}}$
Pitch	.774	.786
Yaw	.702	.793
Thrust vector control attitude gain	$\frac{\text{deg SPS gimbal}}{\text{deg G\&N command}}$	$\frac{\text{deg SPS gimbal}}{\text{deg G\&N command}}$
Pitch	1.38	1.40
Yaw	1.40	1.50

~~CONFIDENTIAL~~

~~CONFIDENTIAL~~

5.15-25

NASA-S-68-466

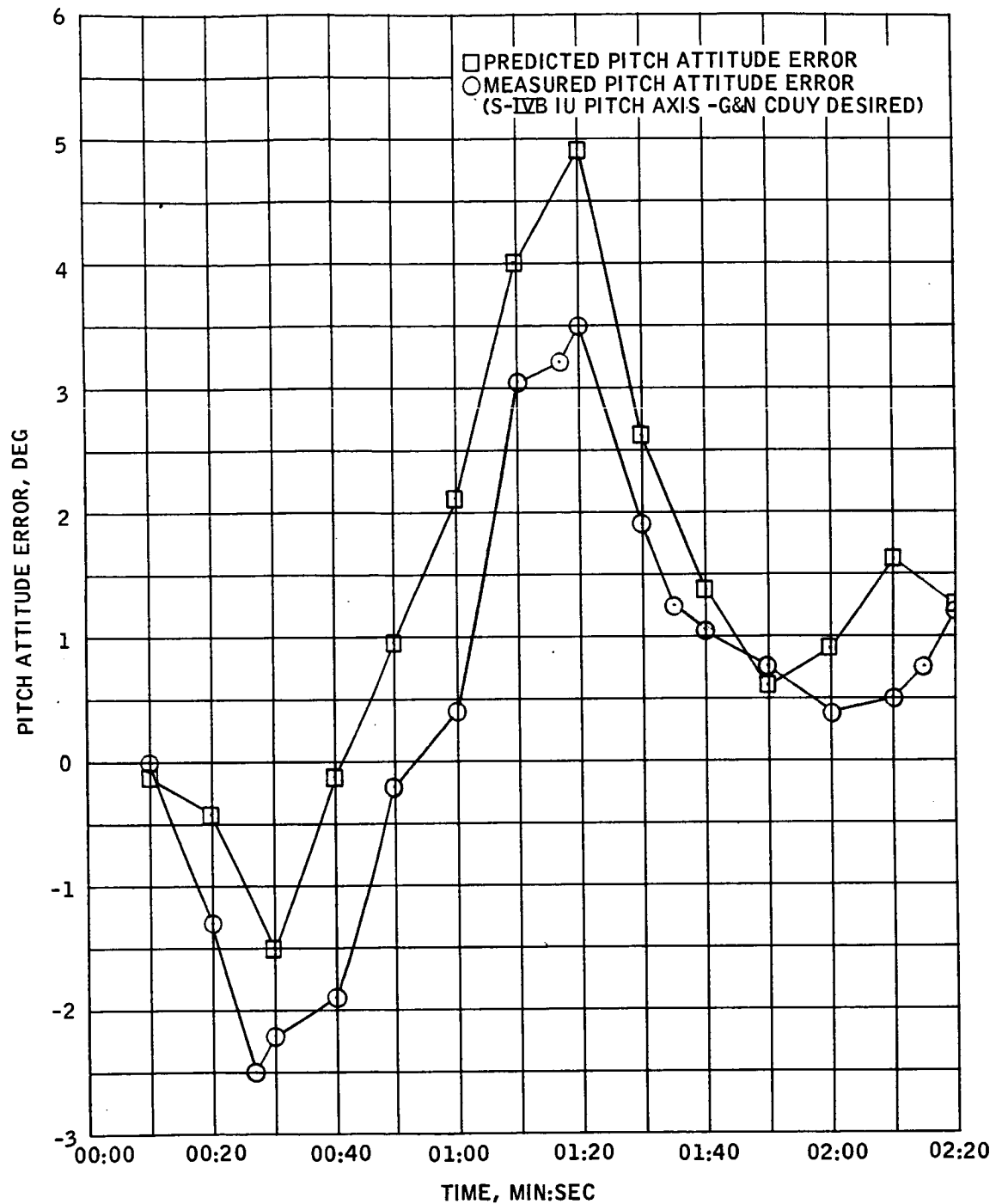


FIGURE 5.15-1.- BOOST MONITOR PHASE, PITCH ERROR.

~~CONFIDENTIAL~~



~~CONFIDENTIAL~~

NASA-S-68-467

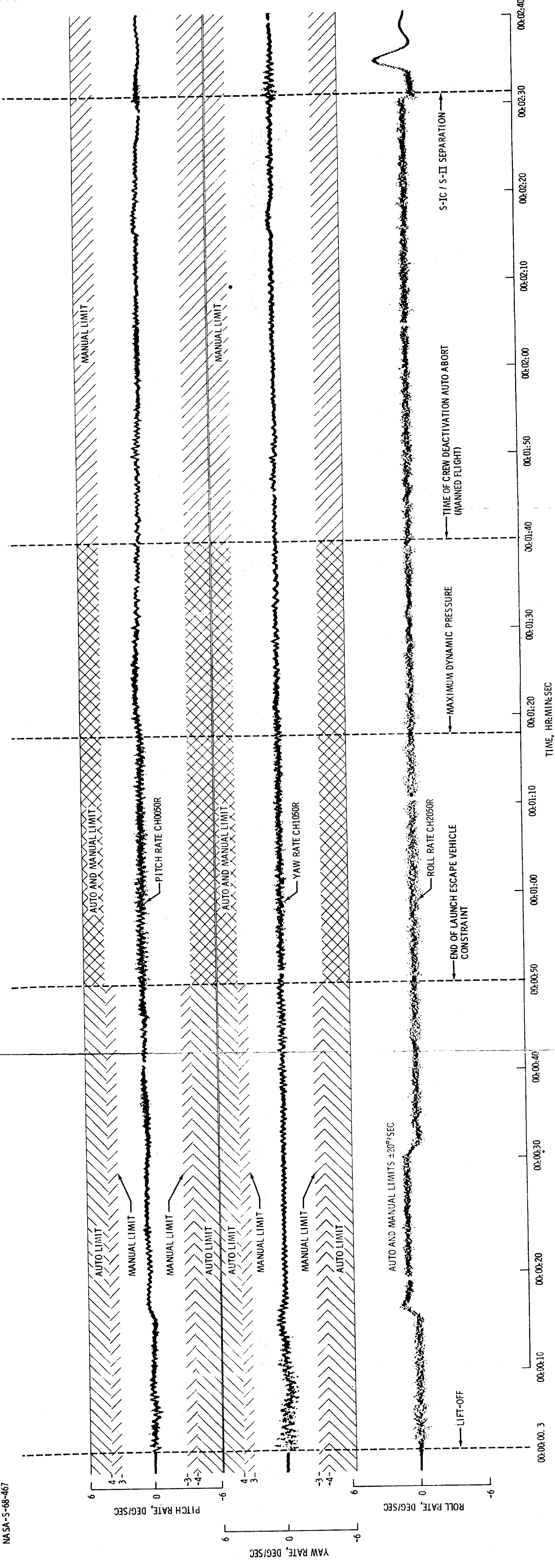


FIGURE 5.15-2. - SPACECRAFT DYNAMICS, ASCENT PHASE.

~~CONFIDENTIAL~~

~~CONFIDENTIAL~~

5.15-27

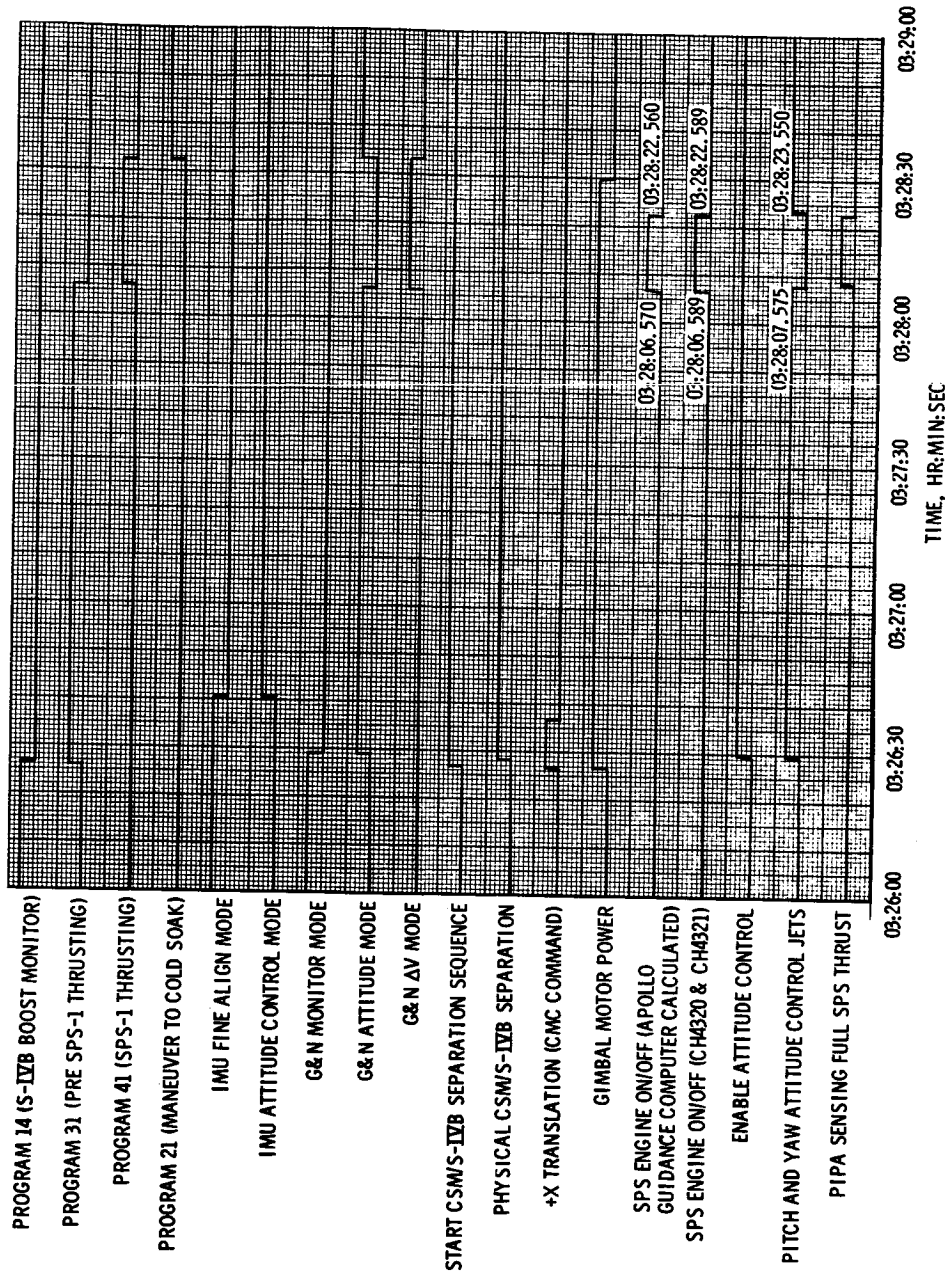


FIGURE 5.15-3. - S-IVB SEPARATION AND SERVICE PROPULSION  
SUBSYSTEM BURN NUMBER 1 SEQUENCE OF EVENTS.

~~CONFIDENTIAL~~

~~CONFIDENTIAL~~

NASA-S-68-469

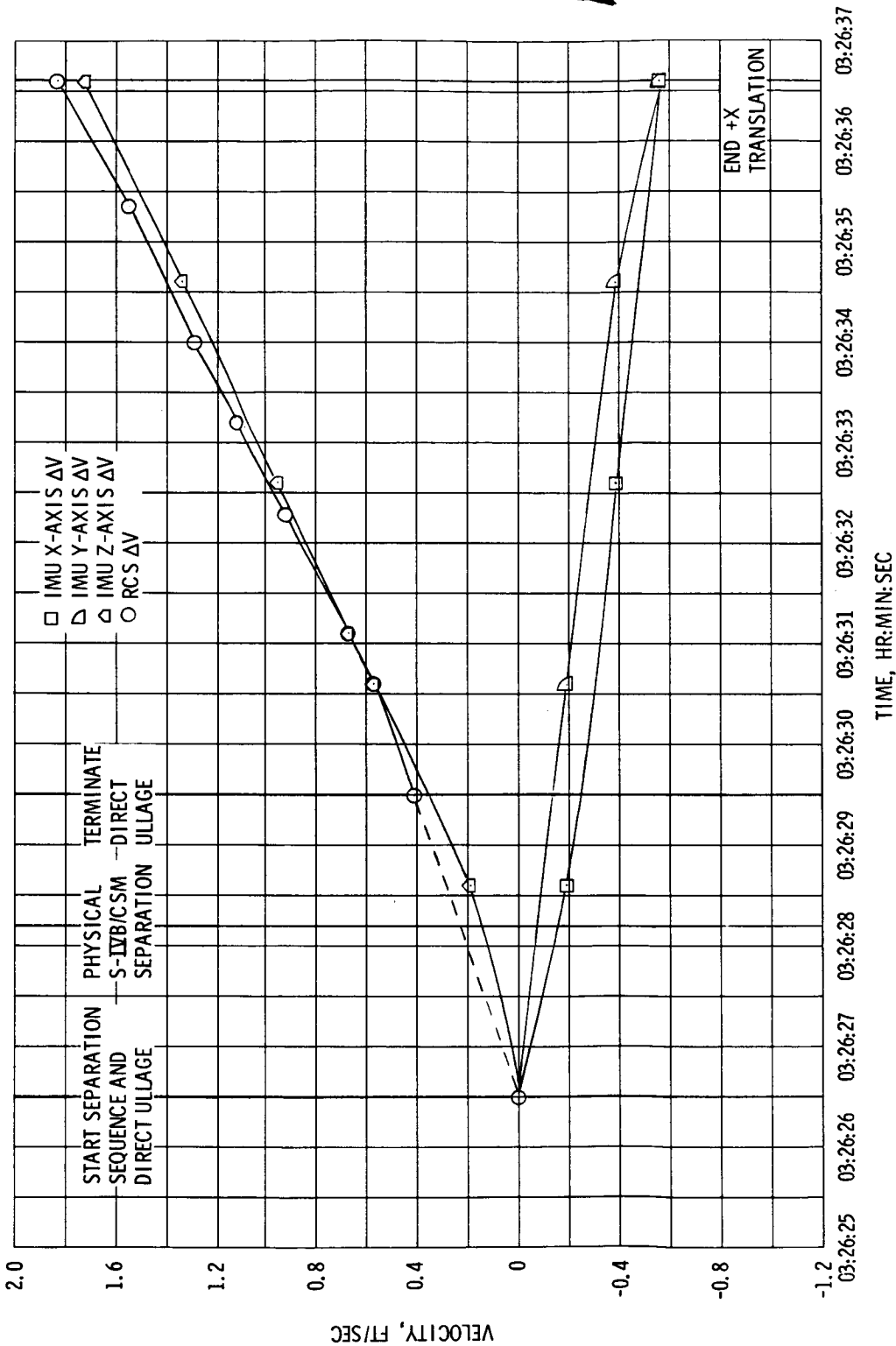


FIGURE 5.15-4. - VELOCITY ACCUMULATION, S-IVB/CSM SEPARATION.

~~CONFIDENTIAL~~

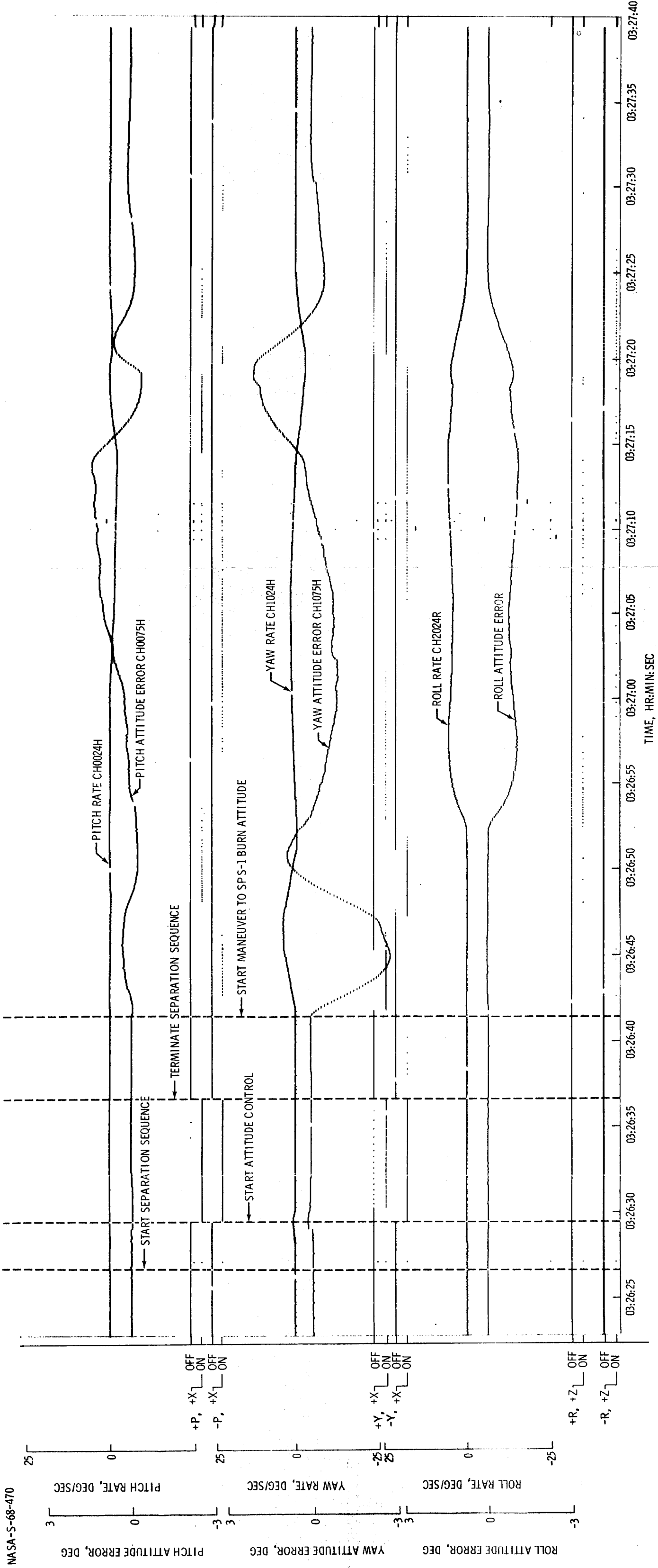


FIGURE 5.15-5. - SPACECRAFT DYNAMICS, S-IVB/CSM SEPARATION AND MANEUVER  
TO SERVICE PROPULSION SUBSYSTEM FIRST BURN ATTITUDE.

~~CONFIDENTIAL~~

NASA-S-68-471

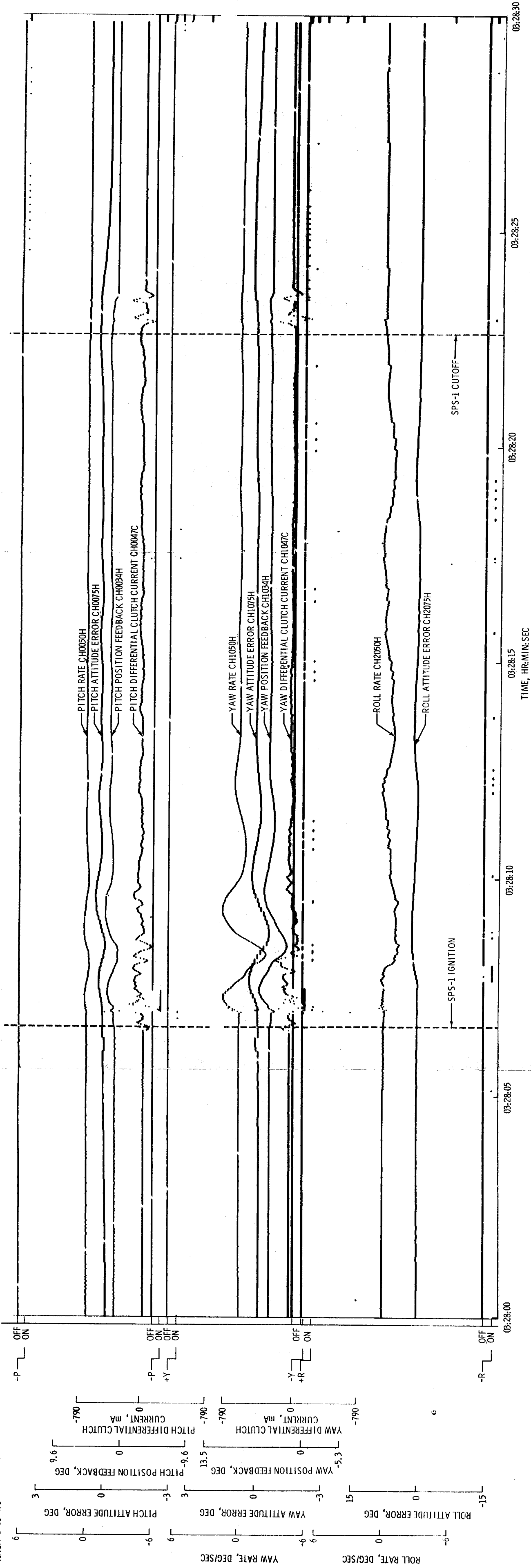


FIGURE 5.15-6.- SPACECRAFT DYNAMICS, SERVICE PROPULSION SUBSYSTEM FIRST BURN.

~~CONFIDENTIAL~~

~~CONFIDENTIAL~~

5.15-31

NASA-S-68-472

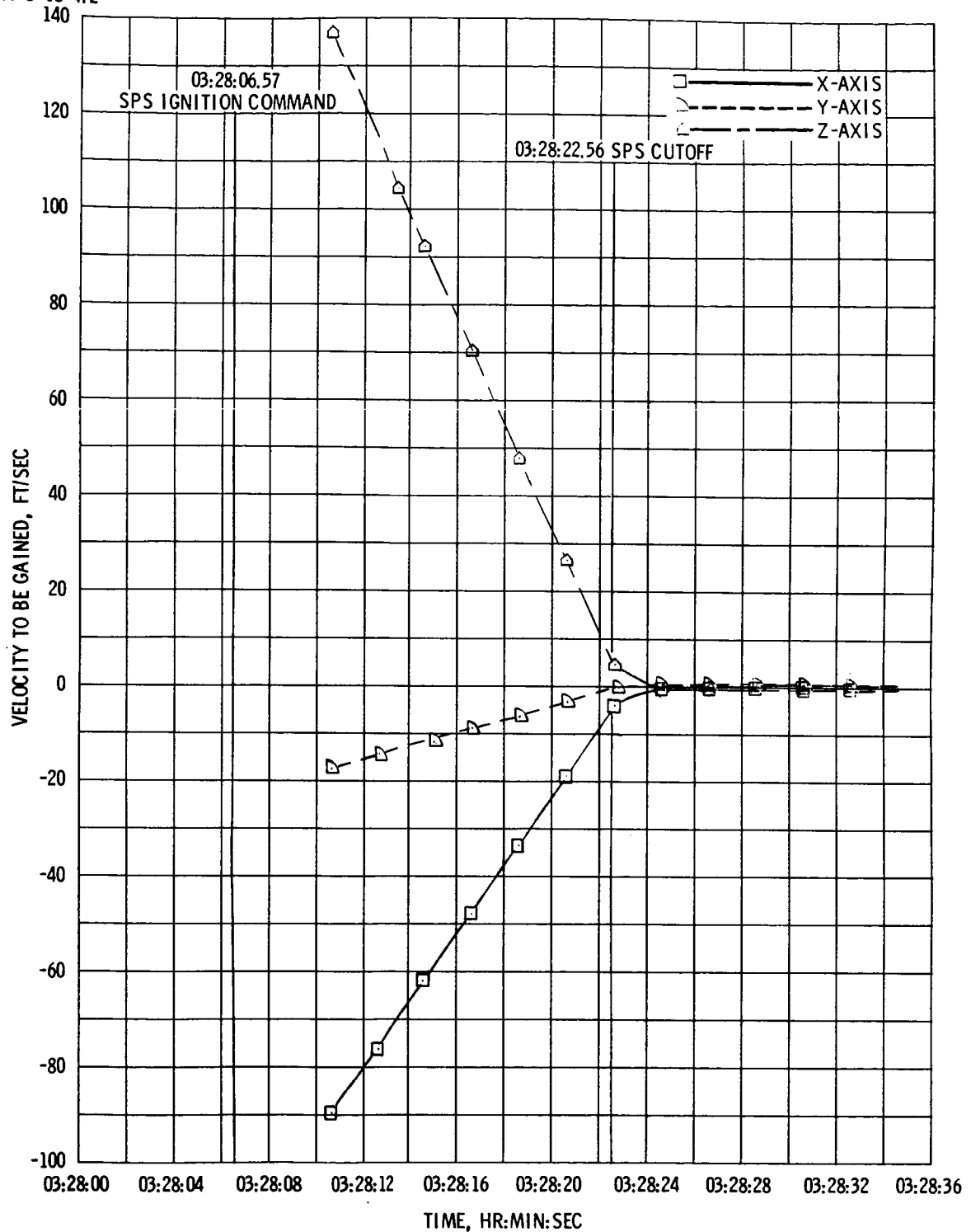


FIGURE 5.15-7. - VELOCITY TO BE GAINED ( $V_g$ ), SERVICE PROPULSION SUBSYSTEM FIRST BURN.

~~CONFIDENTIAL~~

~~CONFIDENTIAL~~

NASA-S-68-473

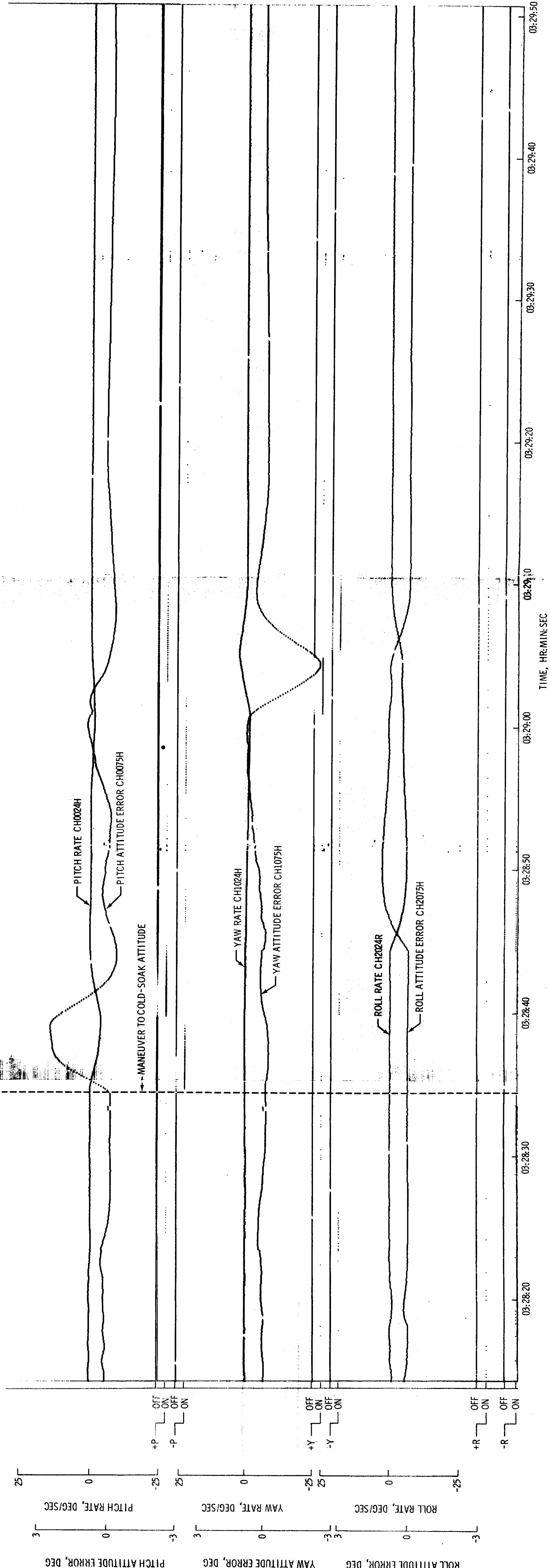


FIGURE 5.15-8.- SPACECRAFT DYNAMICS, MANEUVERS TO COLD-SOAK ATTITUDE.

~~CONFIDENTIAL~~

FIGURE 5.15-8.- SPACECRAFT DYNAMICS, MANEUVERS TO COLD-SOAK ATTITUDE.

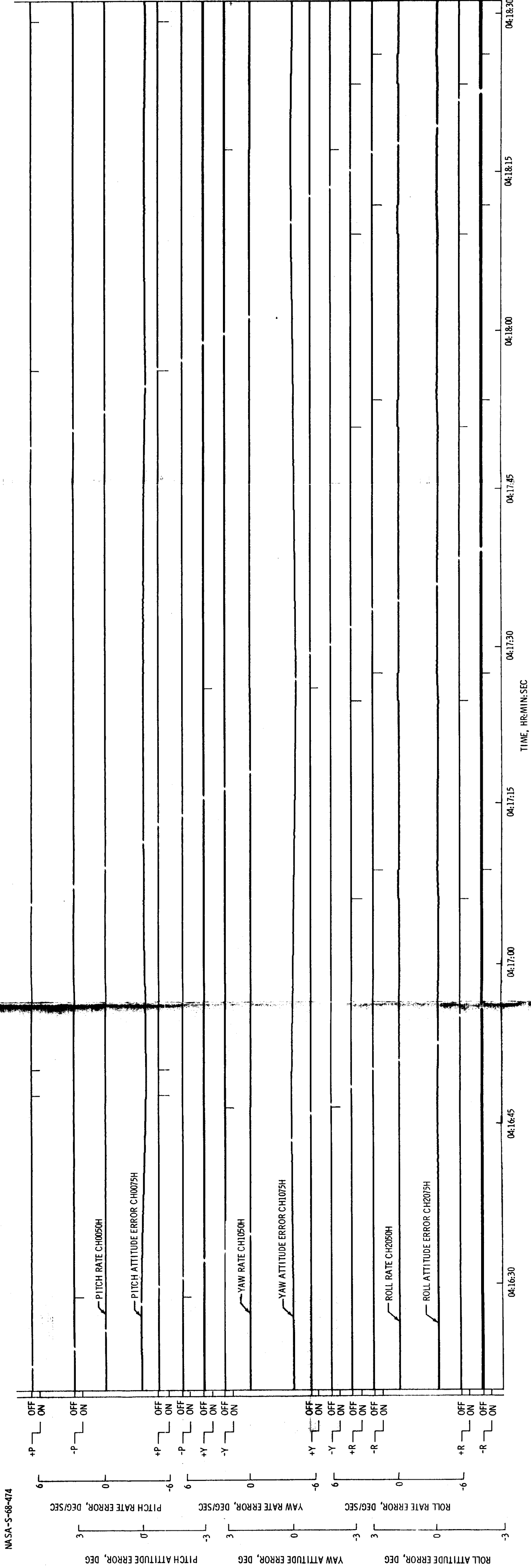


FIGURE 5.15-9. - SPACECRAFT DYNAMICS, TYPICAL COAST PHASE LIMIT CYCLE.



~~CONFIDENTIAL~~

NASA-S-68-475

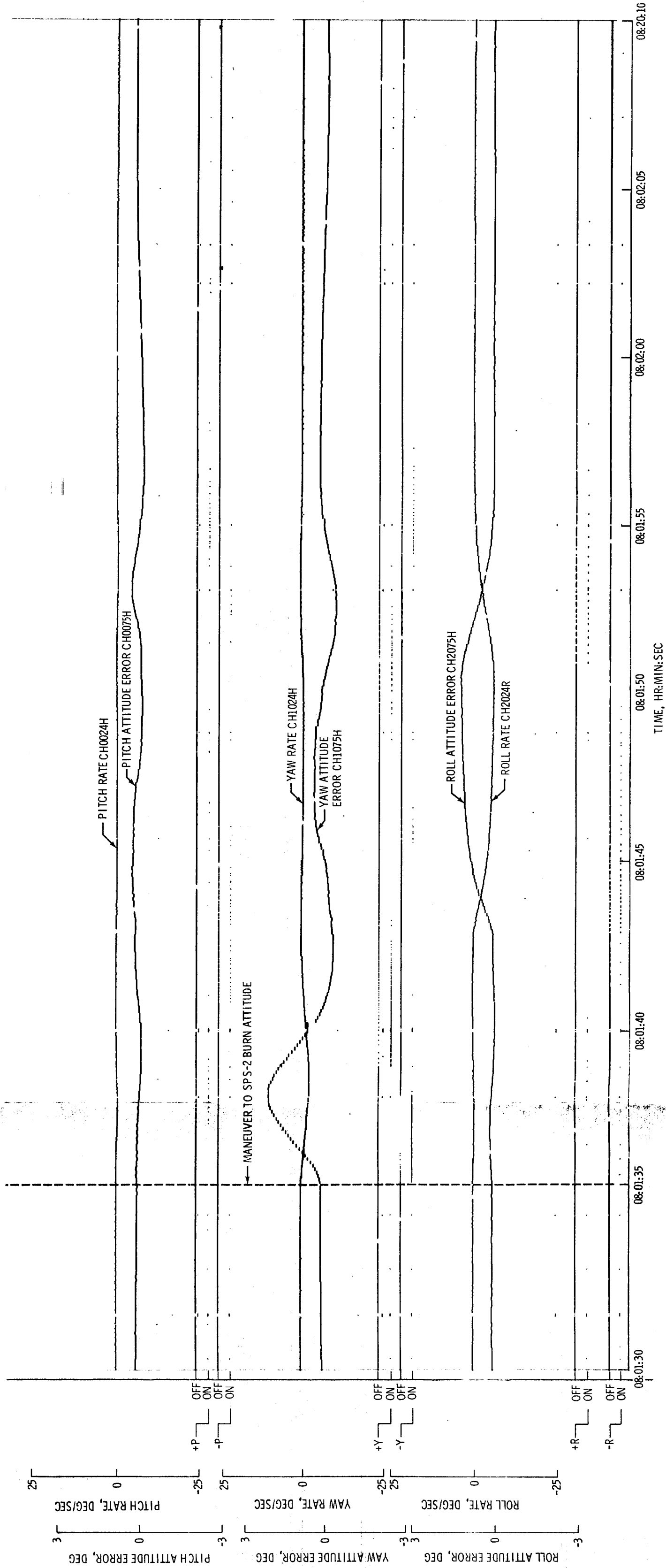


FIGURE 5.15-10. - SPACECRAFT DYNAMICS, MANEUVER TO SERVICE PROPULSION SUBSYSTEM SECOND BURN ATTITUDE.

~~CONFIDENTIAL~~

~~CONFIDENTIAL~~

5.15-35

NASA-S-68-476

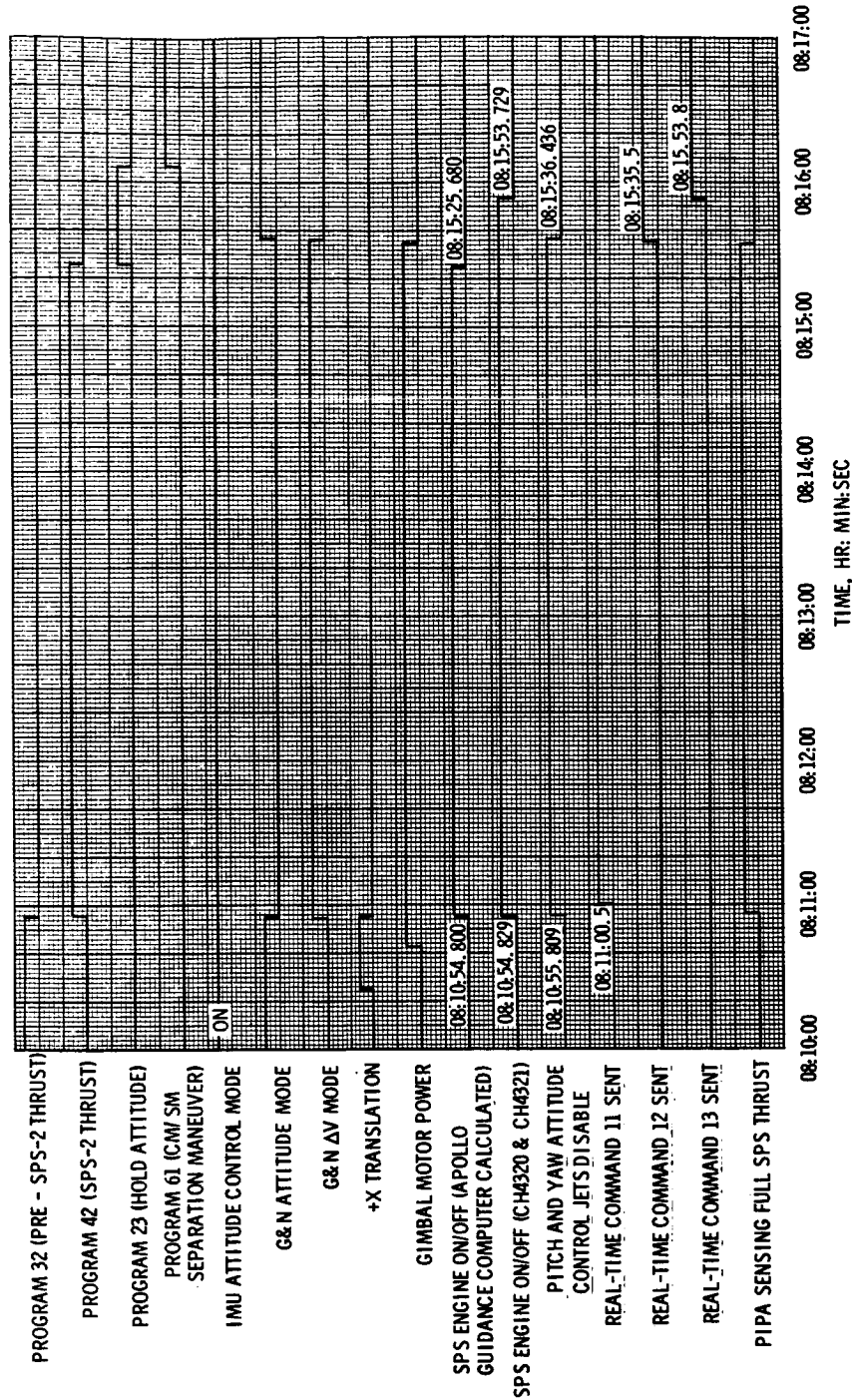


FIGURE 5.15-11. - SEQUENCE OF EVENTS FOR SERVICE PROPULSION SUBSYSTEM SECOND BURN.

~~CONFIDENTIAL~~

CONFIDENTIAL

5.15-36

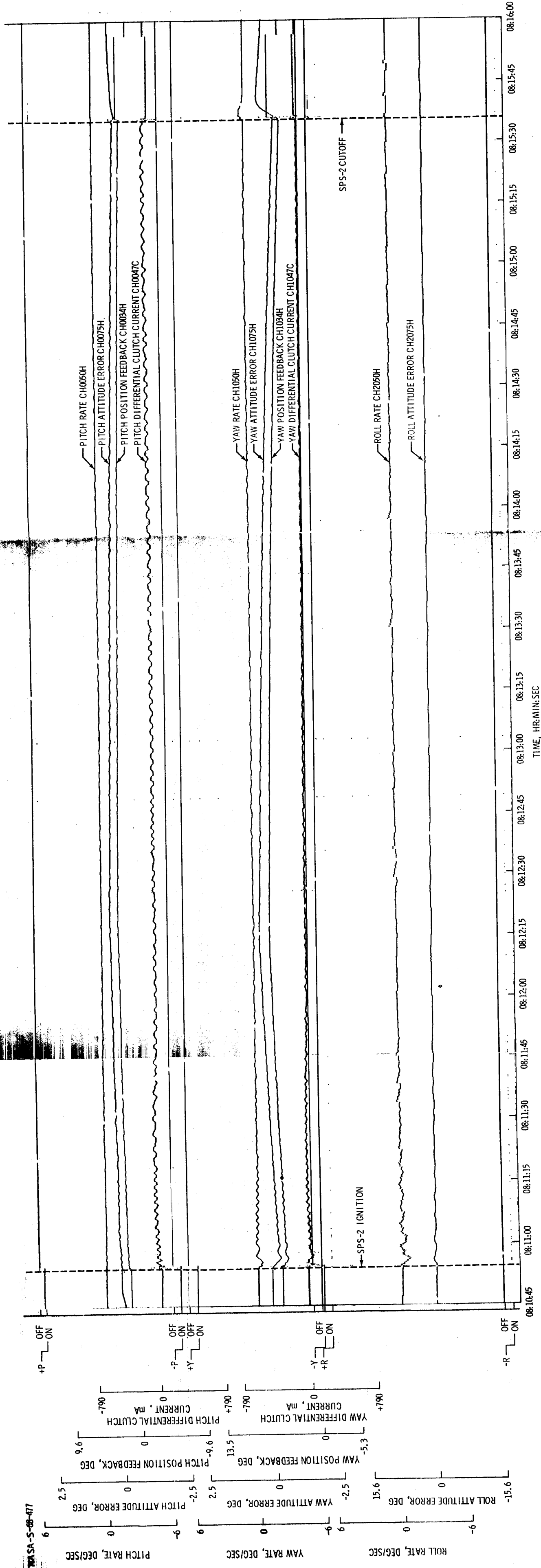


FIGURE 5.15-12. - SPACECRAFT DYNAMICS, SERVICE PROPULSION SUBSYSTEM SECOND BURN.

CONFIDENTIAL

~~CONFIDENTIAL~~

5.15-37

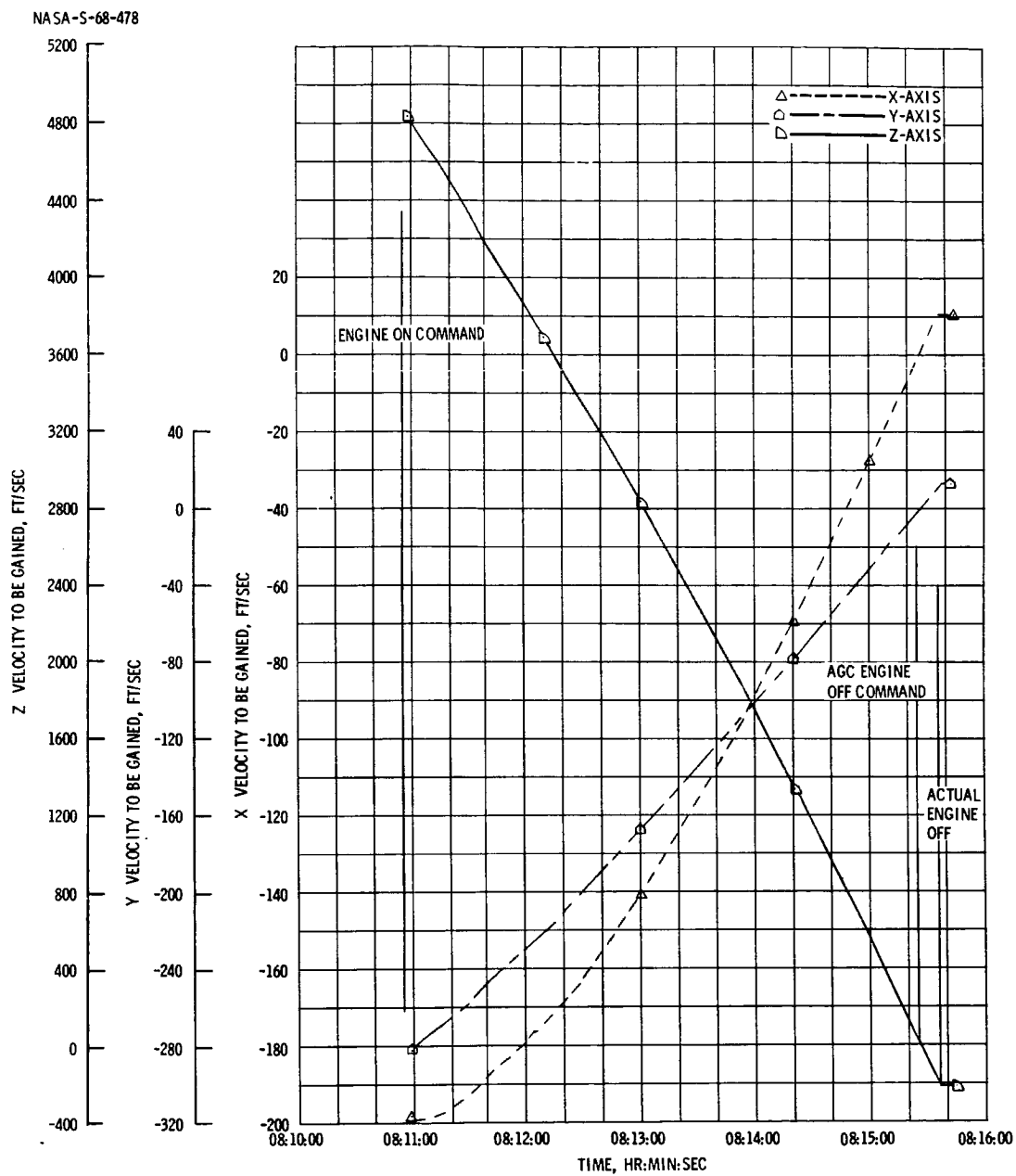
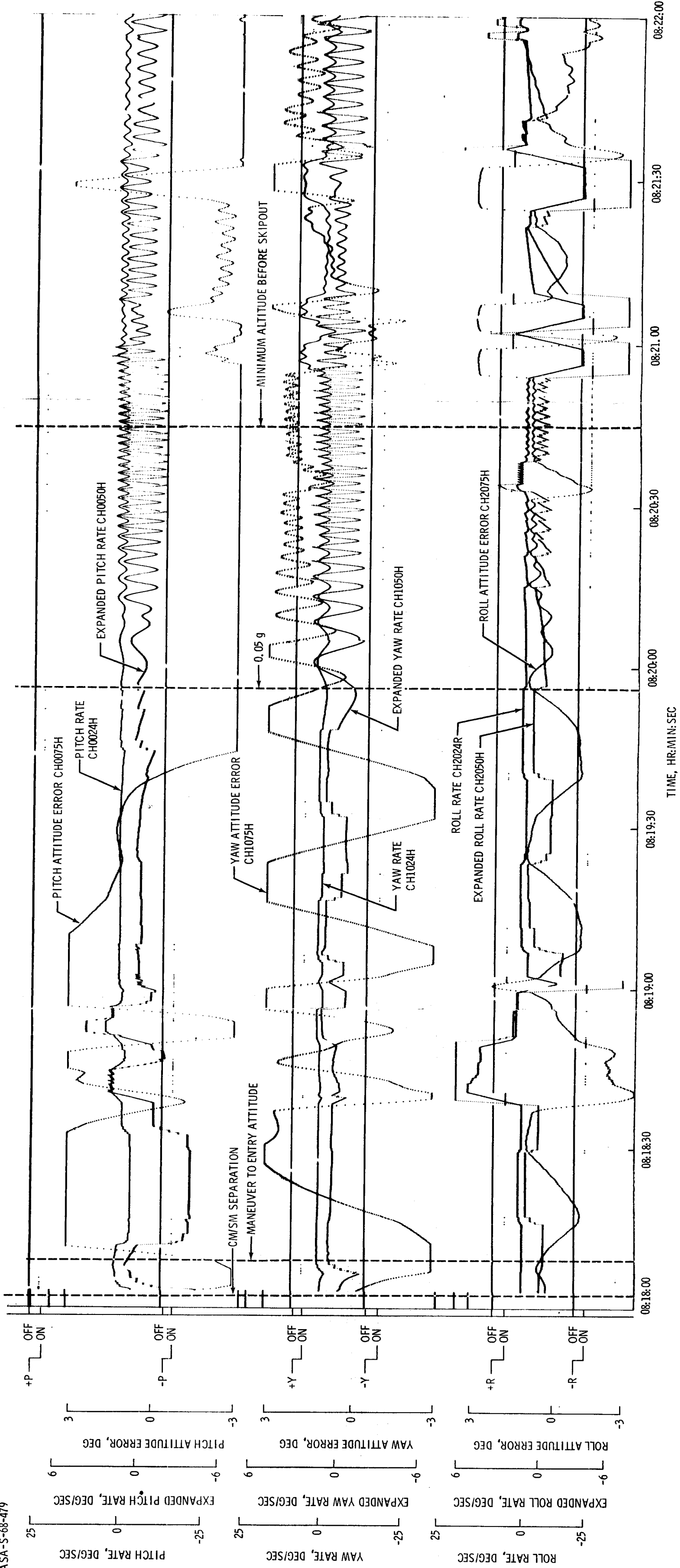


FIGURE 5.15-13. - VELOCITY TO BE GAINED ( $V_G$ ), SERVICE PROPULSION SUBSYSTEM SECOND BURN.

~~CONFIDENTIAL~~

~~CONFIDENTIAL~~



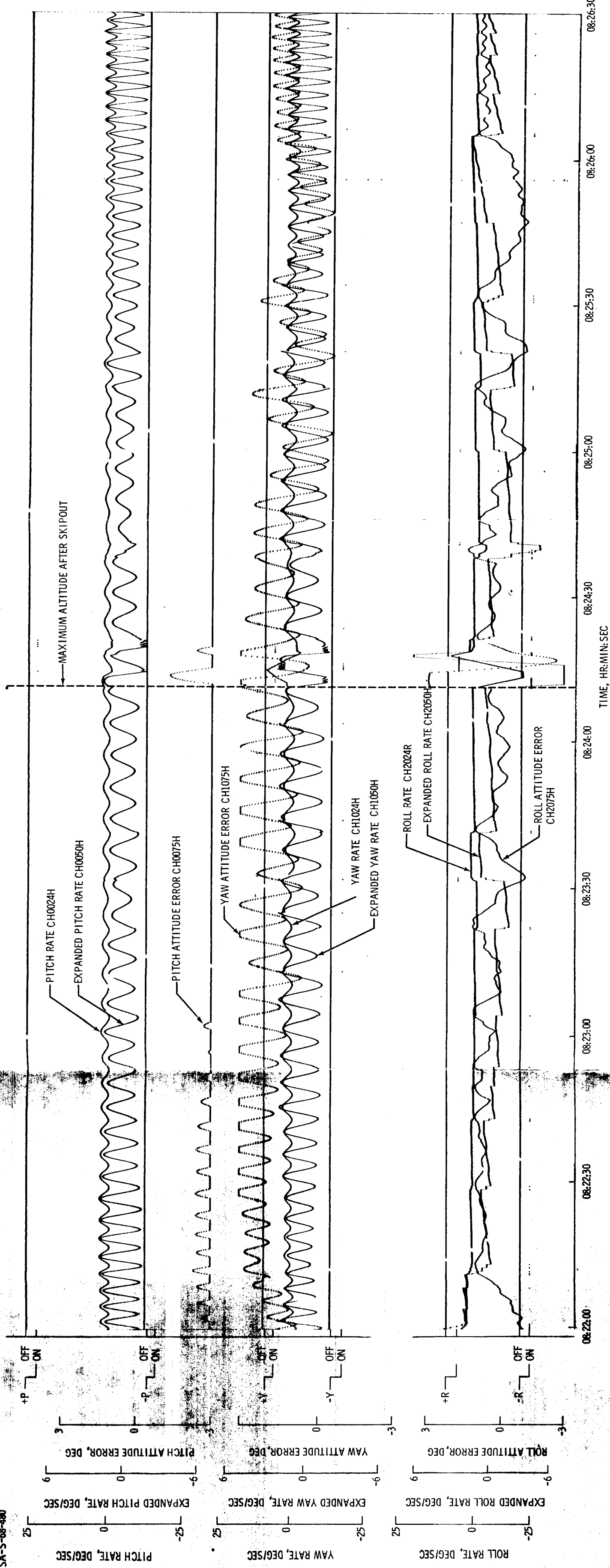
(A) 08:18:00 TO 08:22:00.  
FIGURE 5.15-14.- SPACECRAFT DYNAMICS, ENTRY.

~~CONFIDENTIAL~~

~~CONFIDENTIAL~~

5.15-39

NASA-S-68-480

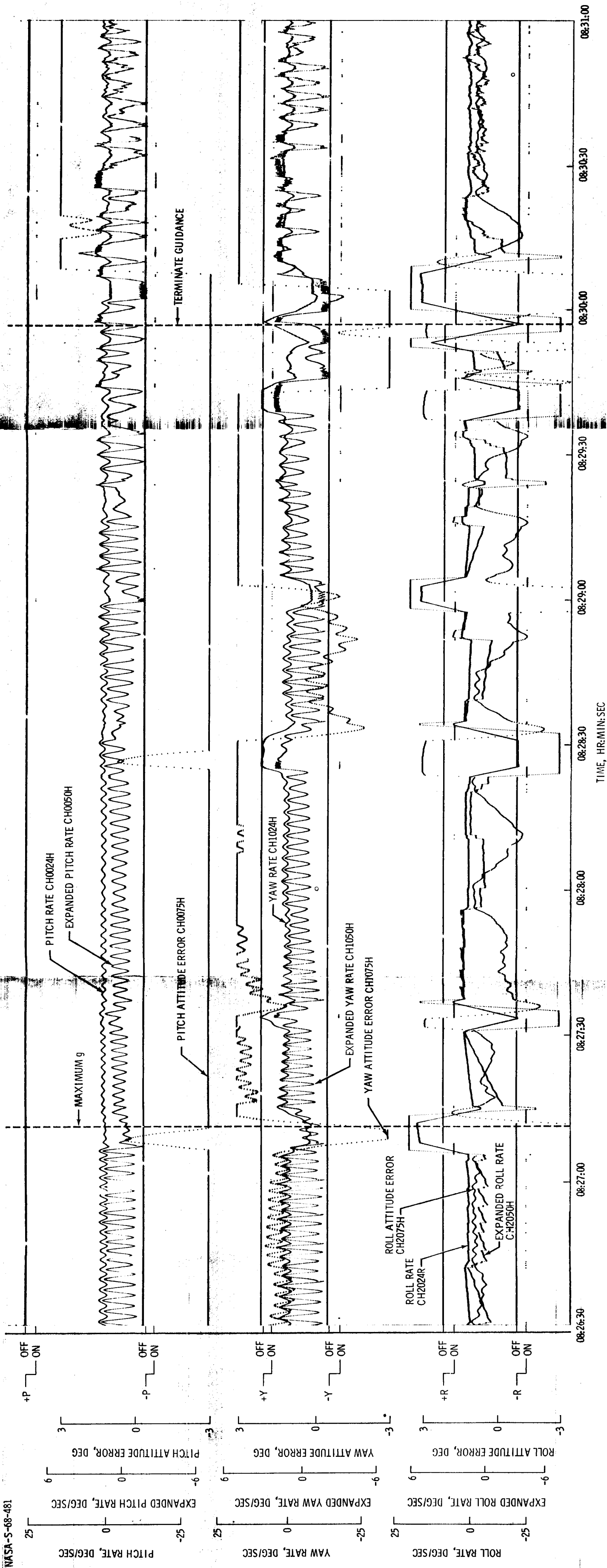


(B) 08:22:00 TO 08:26:30.

FIGURE 5.15-14. - CONTINUED.

~~CONFIDENTIAL~~

~~CONFIDENTIAL~~



(C) 08:26:30 TO 08:31:00.

FIGURE 5.15-14. - CONTINUED.

~~CONFIDENTIAL~~





~~CONFIDENTIAL~~

NASA-S-68-483

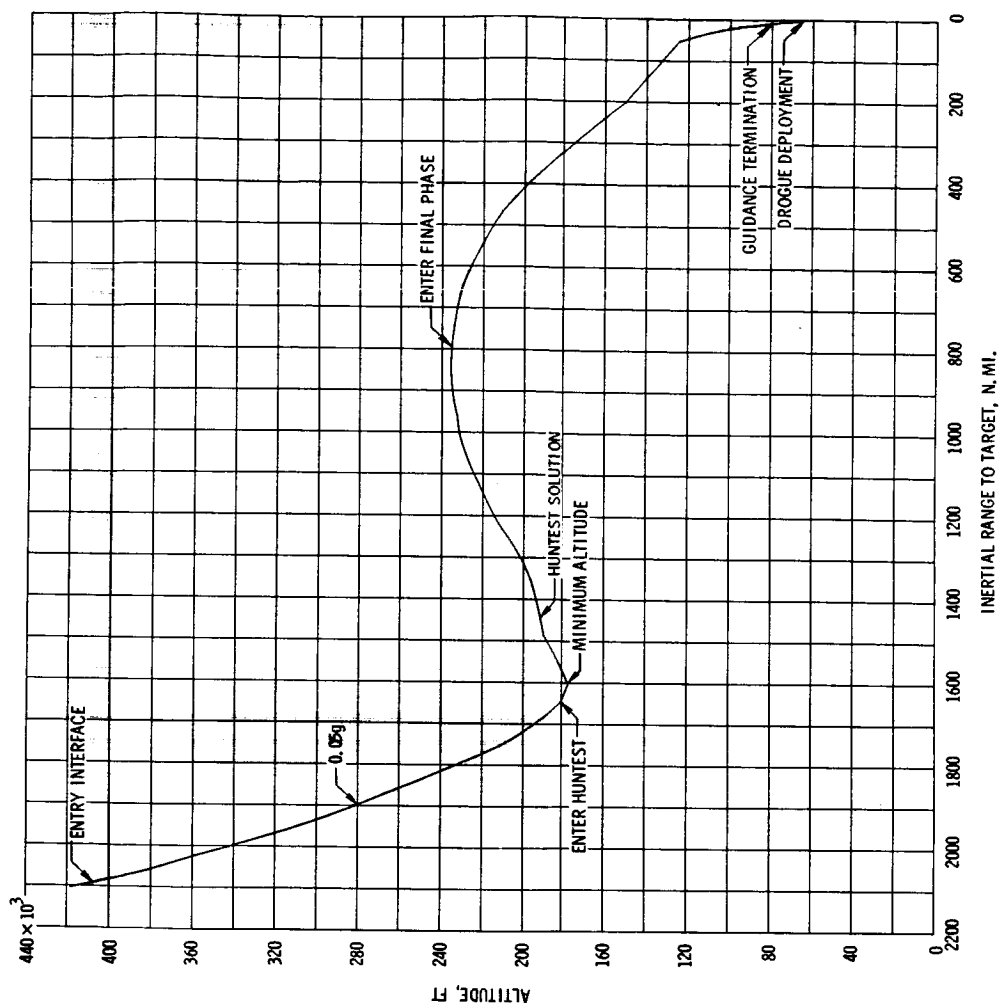


FIGURE 5.15-15. - ENTRY SEQUENCE PLOTTED AGAINST ALTITUDE AND RANGE.

~~CONFIDENTIAL~~

~~CONFIDENTIAL~~

5.15-43

NASA-S-68-484

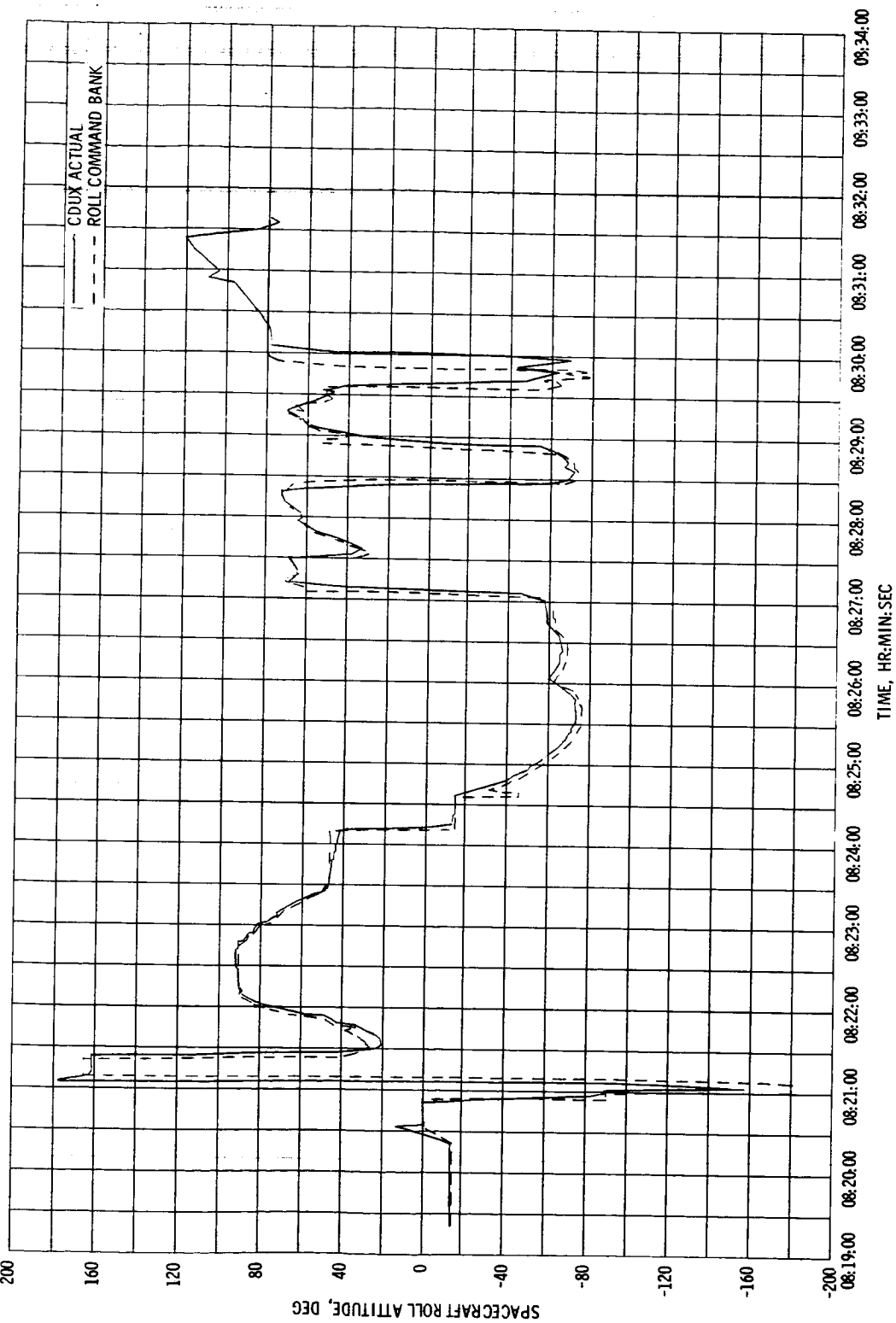


FIGURE 5.15-16. - ROLL COMMAND PLOTTED AGAINST ACTUAL ROLL (CDUX).

~~CONFIDENTIAL~~

~~CONFIDENTIAL~~

NASA-S-68-485

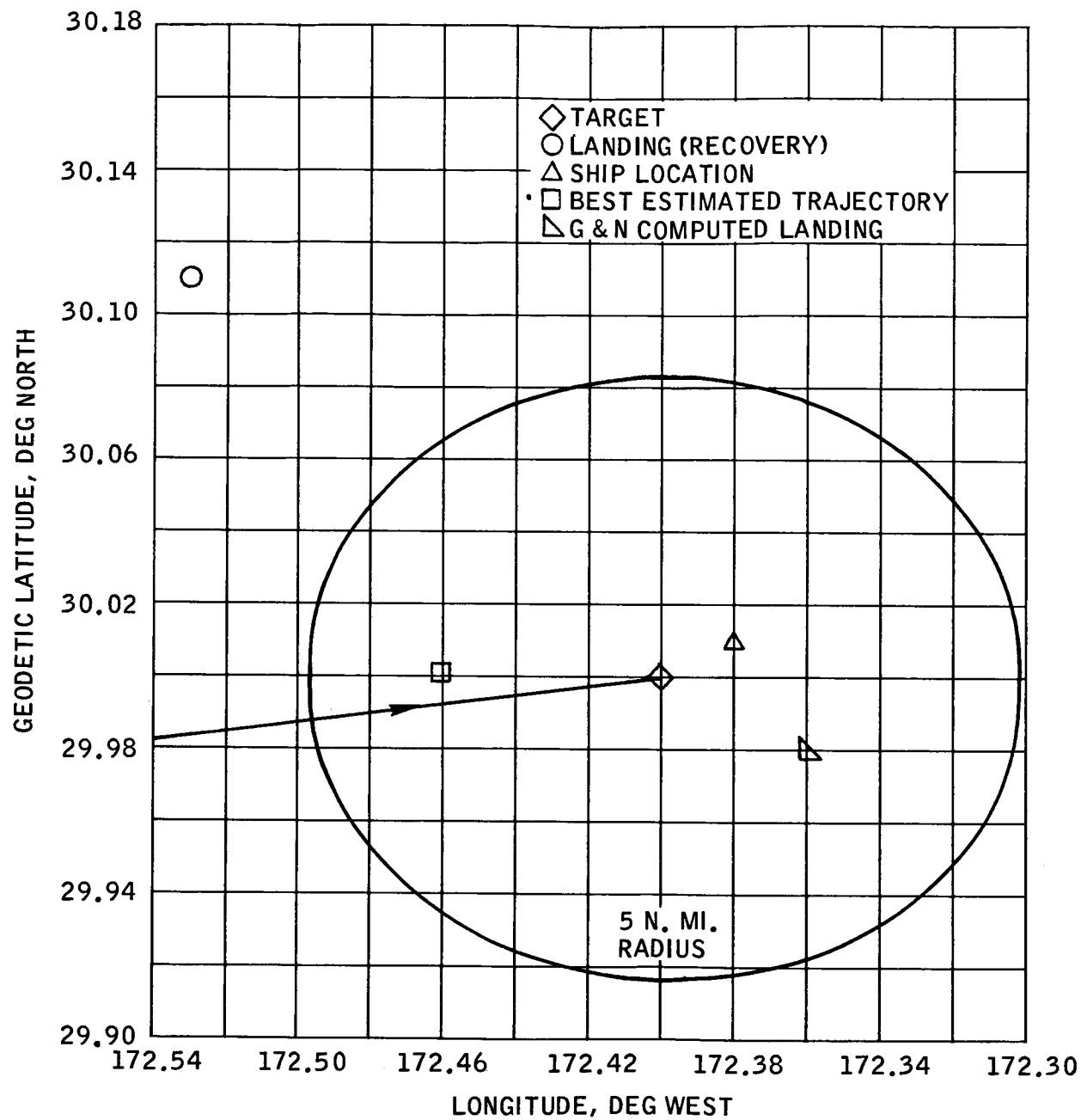


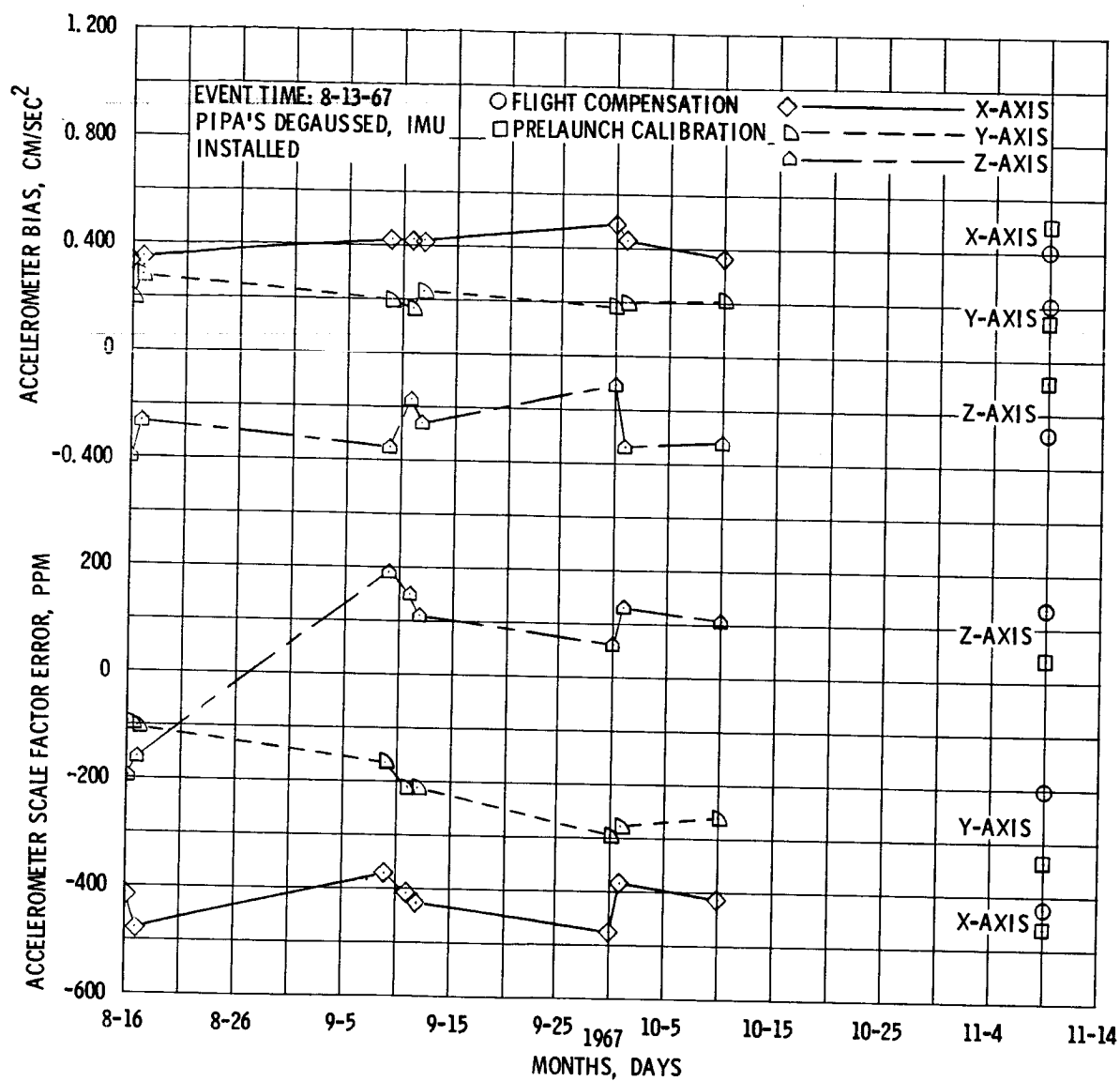
FIGURE 5.15-17.- LANDING POINT DATA.

~~CONFIDENTIAL~~

~~CONFIDENTIAL~~

5.15-45

NASA-S-68-486



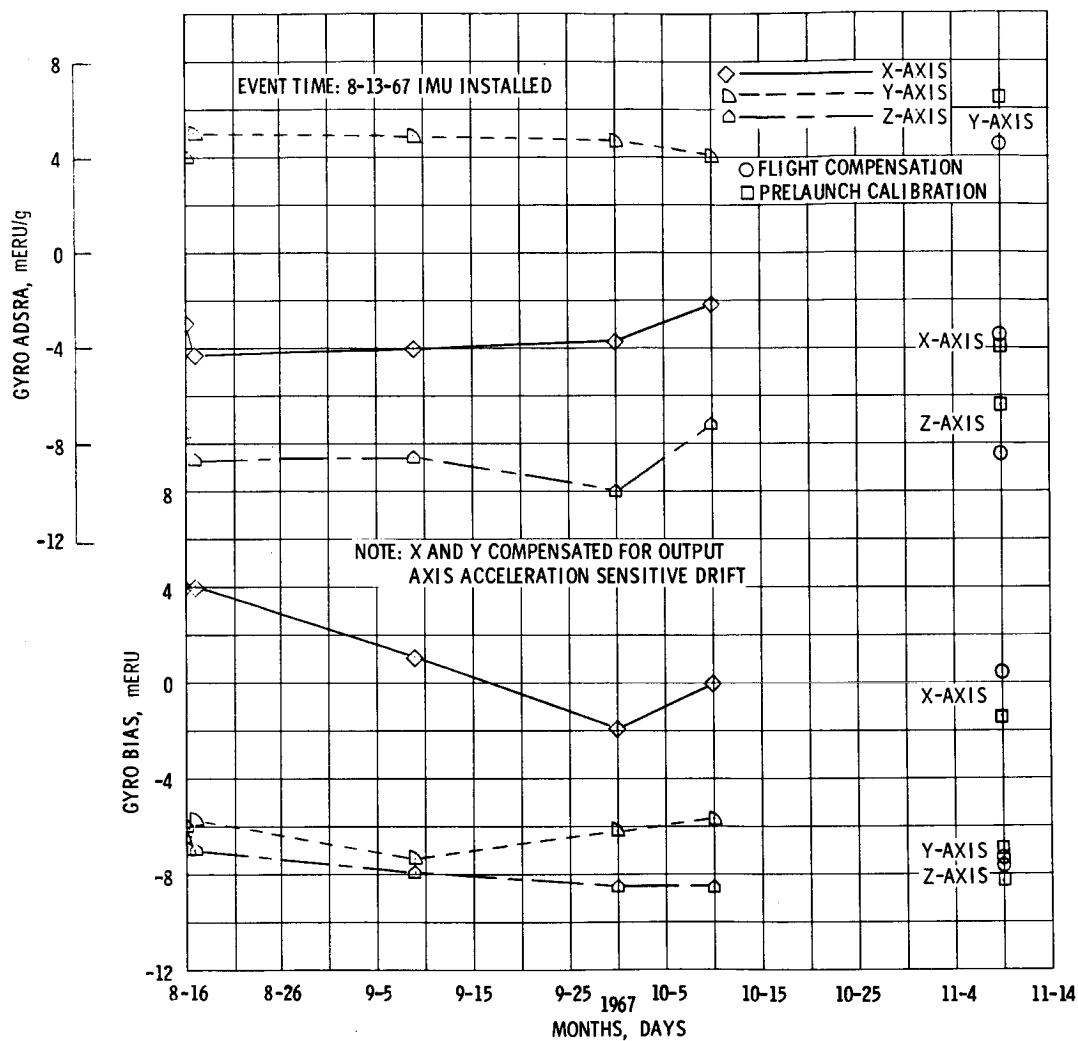
(A) X, Y, AND Z-AXIS ACCELEROMETER BIAS AND SCALE FACTOR ERROR COEFFICIENTS.

FIGURE 5. 15-18. - TIME HISTORIES OF GUIDANCE AND NAVIGATION SUBSYSTEM INERTIAL INSTRUMENT COEFFICIENTS ERRORS.

~~CONFIDENTIAL~~

~~CONFIDENTIAL~~

NASA-S-68-487



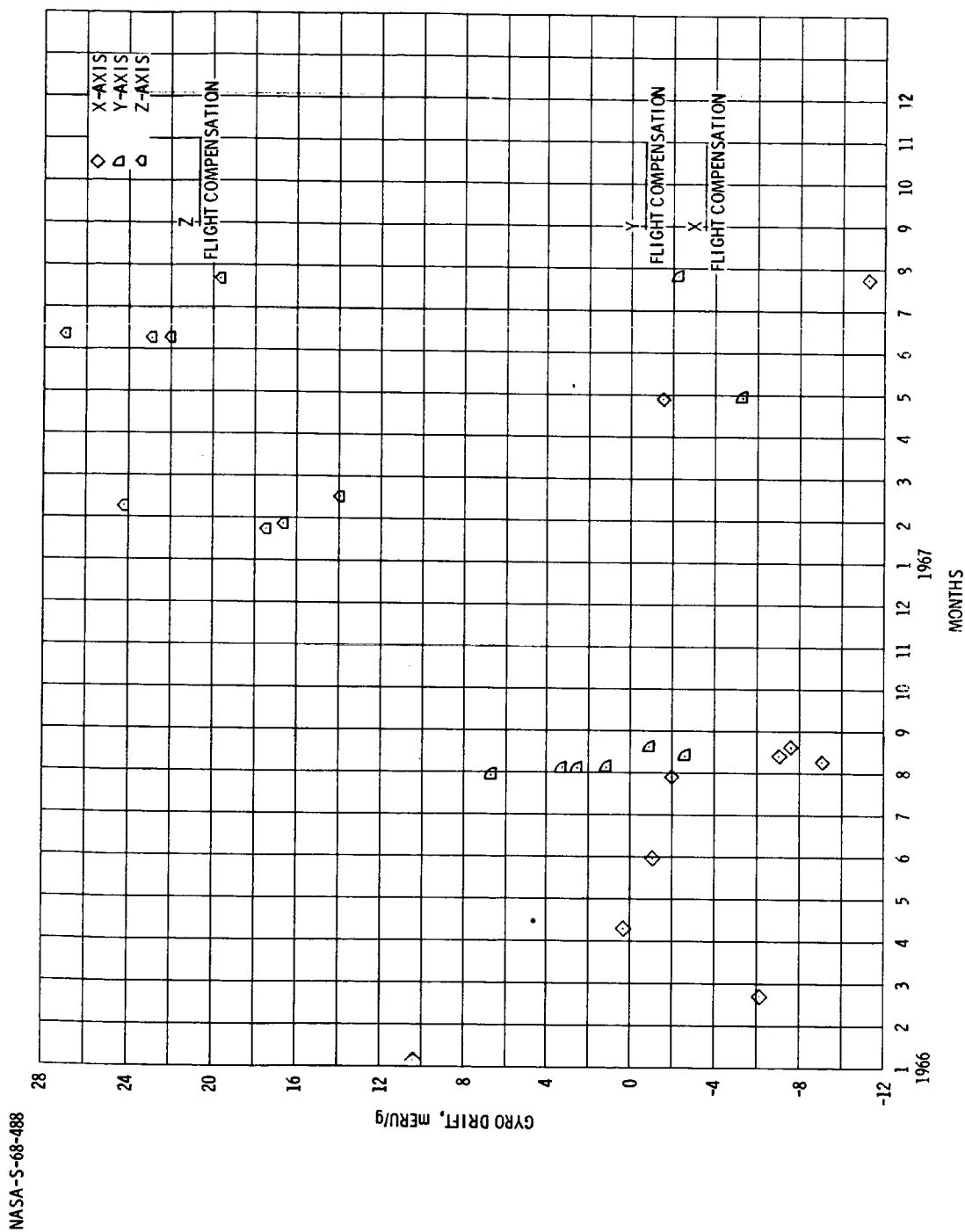
(B) X, Y, AND Z-AXIS GYRO ACCELERATION DRIFT SPIN REFERENCE AXIS (ADSRA) AND NULL BIAS DRIFT COEFFICIENTS (NDB).

FIGURE 5.15-18. - CONTINUED.

~~CONFIDENTIAL~~

~~CONFIDENTIAL~~

5.15-47



(C) X, Y, AND Z-AXIS GYRO ACCELERATION DRIFT INPUT AXIS (ADIA) COEFFICIENT.

FIGURE 5.15-18. - CONCLUDED.

~~CONFIDENTIAL~~

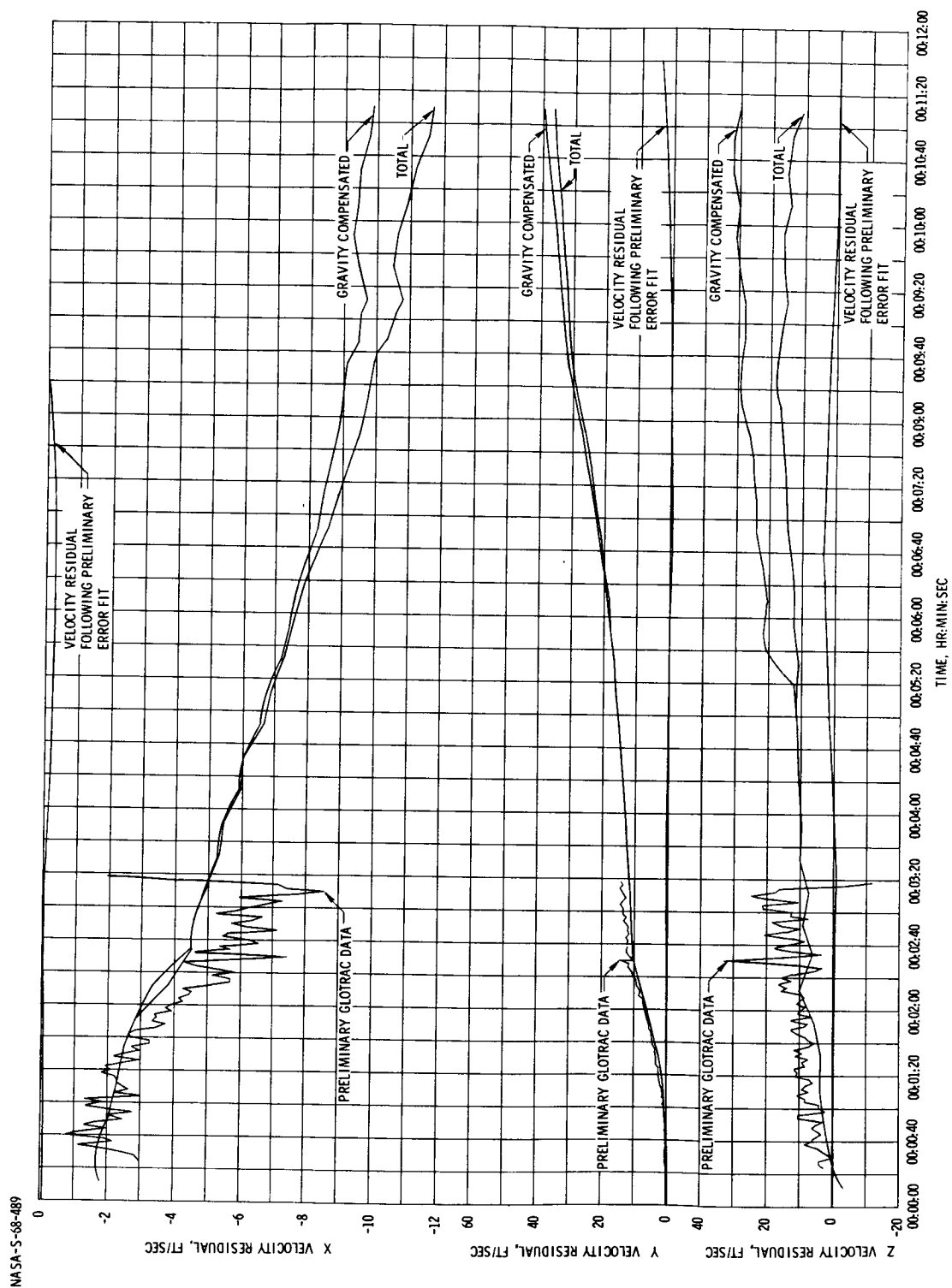
~~CONFIDENTIAL~~

FIGURE 5.15-19. - ASCENT VELOCITY RESIDUALS.

~~CONFIDENTIAL~~

~~CONFIDENTIAL~~

5.16-1

## 5.16 REACTION CONTROL SUBSYSTEM

The service module (SM) and command module (CM) reaction control subsystem (RCS) inflight performance was entirely within the nominal range throughout the mission. All maneuvers using the RCS thrusters were completed as planned. Satisfactory maneuver rates, accelerations, and translation velocity changes were attained. Propellant utilization was normal for both the CM-RCS and SM-RCS. The SM-RCS and CM-RCS are described in section 13.1.

The SM-RCS thermal control subsystem was flown for the first time on this mission and performed satisfactorily throughout the flight. The heaters on all four quads actuated satisfactorily in a repeatable manner. The quad package temperatures, as well as those of the engine injector heads which were instrumented, were maintained within acceptable limits through CM/SM separation.

The CM-RCS engines were maintained passively at acceptable temperatures from launch through subsystem activation. Maximum engine temperatures encountered from subsystem activation through landing were within design limits.

### 5.16.1 Service Module Reaction Control Subsystem

The SM-RCS configuration, except for the addition of a modified heavy duty engine-mounting structure, was almost identical to that of Spacecraft 011 (Apollo 202 mission). All of the SM-RCS components on Spacecraft 017 were certified Block I configuration units. No components were known to be malfunctioning or inoperative prior to lift-off.

Servicing and prelaunch activities.— The SM-RCS propellant servicing was accomplished between October 30, 1967, and November 2, 1967. Helium servicing was completed at 6:00 a.m. e.s.t., November 7, 1967. Most of the subsystem activation was accomplished during helium servicing because the helium isolation valves were opened and the propellant tank pad pressure was set at regulator lockup. The propellant isolation valves were opened at 6:42 a.m. e.s.t., November 9, 1967. Both the propellant and helium loads were within the loading specification tolerances. The propellant and helium loads are given in table 5.16-I.

The only anomaly associated with the SM-RCS was a prelaunch pressure decay in the quad A helium source pressure. Helium tank pressure data show that the helium pressures on quads B, C, and D remained within a  $\pm 2$ -bit count or an approximate  $\pm 40$  psi band from servicing to launch. The pressures at launch were within 20 psi of those at servicing. Quad A helium pressure data show a fairly uniform pressure decrease

~~CONFIDENTIAL~~



~~CONFIDENTIAL~~

from 4150 psia at servicing to 3910 psia at launch. The leak rate was approximately 5 psi per hour, or 26 scc per minute.

This pressure decrease, being continuous during the prelaunch period, indicated a leak. A decay rate of as much as 17 psi per hour and a minimum pressure of as low as 3440 psia were acceptable for an unmanned spacecraft at launch; hence, the actual leak caused no problems relative to the mission.

Service module reaction control subsystem performance.- Performance of the SM-RCS throughout the mission was nominal in every respect. All mission objectives were met and subsystem performance was verified to be satisfactory for subsequent missions. Spacecraft accelerations produced by the RCS were nominal for both attitude hold and maneuvering activities. All measured pressures and temperatures were also nominal, showing no unusual or unexplainable results.

Maneuvers: During the mission, the SM-RCS performed one direct ullage translation and two +X translations. The subsystem also oriented the spacecraft for the two service propulsion subsystem (SPS) burns, for the cold soak, and for the CM/SM separation. Additional functions included control of roll attitude and rate during the SPS burns, maintenance of attitude control during the extended cold-soak period and performance of the CM/SM separation -X translation and roll maneuver performed by the SM. The sequence of events is shown in table 5.16-II. Typical spacecraft accelerations in pitch, yaw, and roll produced by RCS firings during various phases of the mission are given in table 5.16-III. Because of the evaluation technique and instrumentation inaccuracies, the accelerations shown are estimated to be accurate only to within a few tenths of a degree per second squared. The velocity changes produced by the SM-RCS during the translation maneuvers are also shown in table 5.16-III. These velocities were taken from the guidance and navigation subsystem accelerometer data and are considered accurate to within a tolerance of +0.2 to -0.0 ft/sec.

Engine firing times and duty cycles: The average cumulative number of pulses and burn time for pitch, yaw, and roll activity during the mission are shown in figures 5.16-1 and 5.16-2, respectively. The number of seconds of firing time for each engine, the number of pulses, and the percent duty cycle for each engine for various maneuvers and phases of the mission are shown in table 5.16-IV. The quantity of propellant used per quad for these same phases is also shown. It can be seen that the total accumulated burn time, number of pulses, and duty cycle for any given engine were very low as expected for this mission. The maximum accumulated burn time on any one engine was 65.84 seconds. The maximum number of pulses on any one engine was 1324. The maximum duty cycle noted, other than during translation maneuvers, was 11.7 percent.

~~CONFIDENTIAL~~

~~CONFIDENTIAL~~

5.16-3

**Propellant consumption:** Propellant consumption by the SM-RCS, for the overall mission as well as for discrete maneuvers and other periods of the mission, was calculated, using two techniques, and compared with the preflight planned propellant budget.

One technique is called the pressure-volume-temperature (PVT) technique. The helium and propellant tank temperatures were not measured on Spacecraft 017 but were assumed to be equal and constant. The second technique involved summing the engine-on times (firing times) and establishing an average propellant flow rate for a discrete period from the realized duty cycles and predetermined flow rate data. The latter method is inherently more accurate than the PVT technique and is not sensitive to temperature; however, it requires continuous, high-rate telemetry. The expected and actual propellant consumption for quads A through D, and the total for all quads, is shown in figure 5.16-3.

When the actual helium temperature in a specific quad is less than the assumed temperature, the PVT technique indicates more propellant expended than is actually the case. The reverse holds true if the actual temperature is greater than the assumed. This can be noted particularly in the quad A (hot) and quad C (cold) PVT estimates. The temperature effect would be averaged out in the total expenditure of all four quads. Knowing the actual propellant consumed (such as from the on-time technique) and the helium pressure, an estimate of the temperature history may be made for each quad. Quad A helium temperature appeared to reach a maximum of 90° F; quad B appeared to warm very slowly and stayed near the prelaunch temperature of 75° F; quad C temperature appeared to drop to approximately 50° F; and quad D appeared to drop to near 50° F. The quad A helium leakage would not be expected to influence the PVT technique calculations because the 40 psi drop to be expected during the 8-hour flight would be equivalent only to approximately 3 pounds of propellant expended.

An analysis of figure 5.16-3 shows that 9 pounds less propellant than planned was required for the roll control and maneuver to the cold-soak attitude associated with the first SPS burn, and 15 pounds less for the orientation to the SPS second burn. Twenty-one pounds, or 38 percent, more propellant was required during the cold-soak attitude hold. This consumption and the high number of engine cycles previously noted as the maximum were probably because of correction of disturbances created by propulsive venting, as discussed in section 5.15. Propellant consumption for each maneuver is shown in table 5.16-IV along with the associated engine activity.

Thermal control.- The primary and secondary thermal control subsystems were both actuated at hatch closeout and remained active throughout the flight. The SM-RCS thermal control subsystem operated satisfactorily throughout the flight. The temperatures of the engine

~~CONFIDENTIAL~~

~~CONFIDENTIAL~~

mounting structures of each of the four quads, as well as the temperatures of the injector heads of the negative pitch engine (quad A) and the clockwise roll engine (quad C), were monitored from launch through CM/SM separation. All of these measurements (figs. 5.16-4 and 5.16-5) were within design limits throughout the flight.

This flight represented the first opportunity to evaluate launch heating effects on the SM-RCS quads with the heavy weight, four-legged engine mounting structure from a typical Saturn V lunar mission launch. Maximum launch temperatures of the four engine mounting structures and the two instrumented injector heads are shown in table 5.16-V. The injector head of the negative pitch engine on quad A reached its maximum temperature later than the other injector and mounts. This injector head was heated primarily by conduction from the warmer engine mounting structure. This engine was in the trailing position on the quad during launch and thus received minimum direct aerodynamic heat inputs.

The data in figure 5.16-6 and table 5.16-V indicate that for a lunar mission, the temperatures resulting from launch heating of the engine mounting structures will not reach the 190° F required for caution and warning light actuation.

The SM-RCS engines were inactive during the two-orbit phase of the mission prior to CSM/S-IVB separation. The performance of the thermal control subsystem during this period cannot be completely assessed because of gaps in the Manned Space Flight Network tracking coverage. However, the available data indicate that the thermal switches and heaters operated within the nominal requirements, and that the engine mounting structures and injector heads were maintained within the temperature range of 115° F to 140° F. Upper actuation temperatures (heaters OFF) of the quad A and quad C heater thermal switches were indicated to be 138° F and 134° F, respectively. A lower actuation temperature (heaters ON) of the quad C heater thermal switch was indicated to be 116° F. No data were available to indicate actuation temperatures for the quad B and quad D thermal switches during this period.

A summary of SM-RCS temperatures from CSM/S-IVB separation through CM/SM separation is shown in table 5.16-VI. As shown, the engine mounting structure and injector head temperatures reached maximum values of 143° F to 176° F after the maneuvers associated with CSM/S-IVB separation, the first SPS firing, and the orientation to the cold-soak attitude. The 176° F maximum soakback temperature of the negative pitch engine injector head of quad A resulted from the 10.1-second steady-state firing performed by this engine during CSM/S-IVB separation.

~~CONFIDENTIAL~~

~~CONFIDENTIAL~~

5.16-5

During the approximately 4.5-hour inertial cold-soak period, the spacecraft was oriented such that quad A experienced solar-soak conditions; quad C experienced cold-soak conditions; and quad B and quad D experienced side-sun conditions. A summary of the performance of the thermal control subsystem during the cold-soak period (03:29:00 to 08:01:00) is shown in table 5.16-VII.

Following the orientation to the cold-soak attitude, the quad A engine mounting structure slowly decreased in temperature to 131.5° F and then underwent a gradual temperature increase, reaching 138° F at the time of reorientation of the spacecraft for the second SPS burn. Because the thermal switch actuates the heaters ON at a temperature of  $120 \pm 5^\circ$  F, the quad A heaters were never actuated during the cold-soak period.

During the cold-soak period, the quad C heaters were actuated ON at 04:02:00 at an engine mounting structure temperature of approximately 116° F. The mounting structure temperature quickly increased to 128° F and then underwent a gradual decline, reaching 113° F at the time of reorientation of the spacecraft for the second SPS burn. Following their activation at 04:02:00, the quad C heaters remained on during the remainder of the cold-soak period.

During the cold-soak period, the quad B and quad D heaters underwent multiple cycles and maintained the engine mounting structures at satisfactory temperature levels. These data are summarized in tables 5.16-VI and 5.16-VII. The quad B engine mounting structure temperature is shown for a portion of the cold-soak period in figure 5.16-6. Typical thermal control subsystem operation is also shown on this figure.

The engine mounting structure and injector head temperatures increased as shown in figures 5.16-4 and 5.16-5 and table 5.16-VI as a result of the reorientation maneuver and the ullage firing for the second SPS burn. The injector head of the negative pitch engine of quad A reached a maximum value of 203.7° F after the 31-second steady-state ullage firing. Maximum soak-back temperatures were not obtained for the other parameters because of loss of data from the SM at CM/SM separation at 08:18:02.6.

With the exception of the periods during and immediately after the steady-state engine firings (CSM/S-IVB separation and ullage firing for the second SPS burn), the engine mounting structure temperatures and the injector head temperatures remained at about the same level. Although the available data are limited during the time from launch to S-IVB/CSM separation, while the SM-RCS engines were inactive, the data indicate that the injector heads remained within approximately

~~CONFIDENTIAL~~

~~CONFIDENTIAL~~

15° F of the engine mounting structures. During the cold-soak period, after the effects of the steady-state CSM/S-IVB separation firing had been dissipated, the temperatures of the engine mounting structure and injector head remained within 2° F to 3° F of one another.

Figure 5.16-7 shows the effect of the CSM/S-IVB separation firing on the injector head of the quad A negative pitch engine and on the engine mounting structure to which it was attached. The effect of engine-firing duty cycle on injector head temperature is also illustrated in figure 5.16-7. During the 10.1-second CSM/S-IVB separation and ullage firing, the injector head temperature increased rapidly. The steady-state firing was followed by 200 pulses of 20 msec average pulse width over a 2-minute period. The cooling effect of the short pulses during this period attenuated the rate of temperature rise of the injector head. The engine was then inactive for approximately 1 minute, during which time thermal soakback to the injector head from the combustion chamber was evident. At approximately 03:28:30, the engine fired continuously for 1.8 seconds and this was immediately followed by 124 pulses of 20-msec average pulse width over an approximate 1-minute period. The 1.8-second firing acted to cool the injector head as a result of the cooler propellants flowing through it. At approximately 03:29:00, the engine ceased firing and the thermal soakback to the injector from the combustion chamber elevated the injector head to a maximum temperature of 176° F.

#### 5.16.2 Command Module Reaction Control Subsystem

The CM-RCS configuration on Spacecraft 017 was identical to that of Spacecraft 011 (Apollo 202 mission). All CM-RCS components on the spacecraft were certified Block I configuration units. No components were known to be malfunctioning or inoperative prior to lift-off.

Servicing.- Propellant servicing of the CM-RCS was accomplished between October 30, 1967, and November 2, 1967. Helium servicing was completed November 7, 1967. Both the helium and the propellants were loaded to within the specification tolerances. Activation of the CM-RCS occurred at 08:18:01.5. The propellant and helium loads are given in table 5.16-I.

Performance.- Performance of the CM-RCS was entirely satisfactory from activation until subsystem purge. All mission objectives were met and performance was verified as satisfactory for subsequent missions. Accelerations in pitch, yaw, and roll were nominal throughout entry, as were the spacecraft attitudes. All measured subsystem pressures and temperatures were also nominal, showing no unusual or unexpected results.

~~CONFIDENTIAL~~

~~CONFIDENTIAL~~

5.16-7

Maneuvers: During entry, the CM-RCS performed a pitch maneuver and several roll maneuvers and provided attitude hold control. The sequence of CM-RCS events is shown in table 5.16-II. Spacecraft accelerations, produced with dual system control, are shown in table 5.16-III. Typical control cross-coupling effects, characteristic of the CM-RCS, are shown in table 5.16-VIII.

Subsystem pressures: Subsystem helium pressures from servicing through landing are shown in table 5.16-IX. The helium tank pressure and temperature during entry are shown in figures 5.16-8 and 5.16-9, respectively. The constant-pressure/temperature ratio prior to activation shows that the subsystem was not leaking. The helium source pressures both dropped 440 psi at activation. At the start of the propellant depletion burn, the subsystem A and B helium and propellant subsystems were interconnected. One regulator generally regulates at a slightly higher pressure than the others; hence, most of the helium required for the depletion burn comes from one source tank. This occurred as can be seen from the data in figure 5.16-8 and table 5.16-IX.

Eleven seconds after landing, spacecraft power was turned off which closed the engine valves. At that time, there was still 540 psia and 320 psia indicated source pressure in the A and B systems, respectively. This residual pressure is the result of the configuration of the propellant tanks and the helium purge systems. The configuration of the propellant tanks is such that when propellant has been expelled, regulated pressure forces the bladder around the tank standpipe, thus partially blocking the tank outlet holes. The purge system then attempts to dump regulated helium through the liquid side vent to the propellant side of the bladder and overboard through these same tank outlet holes. The net result is a slow purge. Hence, at engine-valve closure some pressure is trapped in the system. Both the propellant tanks and the purge system have been modified on the Block II systems to allow rapid purging.

Engine chamber pressure: Nominal engine chamber pressures were observed on all instrumented engines. Typical chamber pressure profiles for burn durations of 42.1, 0.14, and 0.050 seconds are shown in figure 5.16-10. The pressure rise and decay times and the pressure levels are normal for the two shorter pulses. The 42.1 second pulse is the propellant depletion burn. Burning is terminated and pressure decay occurs when one of the propellants is depleted. In this mission, as had been expected, the fuel was depleted first, and this left approximately 10.5 pounds of oxidizer to be expelled without burning. The effect of expelling this oxidizer into the hot engine was that some chamber pressure would be maintained and would extend the pressure decay time. This effect can be seen in figure 5.16-10.

~~CONFIDENTIAL~~

~~CONFIDENTIAL~~

Engine firing times and duty cycles: The average cumulative number of pulses and burn time for pitch, yaw, and roll activity during entry are shown in figures 5.16-11 and 5.16-12, respectively. The accumulated engine burn times, number of pulses, and duty cycles for each engine are given in table 5.16-X. The propellant consumed by each system is also shown. Maximum burn time on any one engine was 94.14 seconds, including the depletion burn. Excluding the 42.1-second depletion burn, the maximum burn time was 52.04 seconds. The maximum number of cycles on any one engine was 242. The average pulse widths per engine, not including the depletion burn, are also shown in table 5.16-X. The average pulse width for both systems was 0.188 seconds. The theoretical oxidizer-to-fuel ratio (O/F) corresponding to this average pulse width is 1.6 to 1.84; however, the propellant consumption, as calculated from the engine-on times, indicates the O/F ratio to be on the high side of this range.

Propellant consumption: CM-RCS propellant consumption for the mission was calculated using both the PVT technique and accumulated engine-firing times. For the PVT calculation, helium source and regulated pressure, and helium tank skin temperature were used as inputs. The total propellant used during the entire mission, including the fuel depletion burn, is shown in figure 5.16-13. The bias between the PVT and engine-on time calculations is caused by the uncertainties in initialization constants tending to produce a constant bias. The disparity between the propellant consumed by each system during the propellant depletion burn is attributed to interconnecting the systems for the burn. Propellant is depleted faster in one system than the other because of slight differences in the regulator settings. The propellant expended, and the associated engine activity, during various phases of the mission is shown in table 5.16-X. The propellant depletion burn was accomplished successfully, burning approximately 143.6 pounds of propellants.

Thermal control.- The CM-RCS was passively maintained within satisfactory temperature limits throughout the mission. The design of the subsystem was demonstrated to be adequate to withstand the combined thermal loads of engine firing and simulated lunar return entry after being subjected to an extended solar-soak period prior to entry. Typical temperatures encountered, during entry, by components of the CM-RCS engines as shown in figure 5.16-14. A summary of the thermal performance of the CM-RCS is given in table 5.16-XI.

The temperatures of the systems A and B helium tanks and of the oxidizer valves of six of the engines were monitored throughout the flight. Injector head temperatures and two engine outer wall temperatures were monitored during entry for each of four engines. Also, the temperature of the interface seal between the ablative thrust chamber

~~CONFIDENTIAL~~

~~CONFIDENTIAL~~

5.16-9

assembly and the ablative nozzle extension was monitored during entry for the two positive pitch engines as a means of detecting hot combustion gas leakage from the engines at this location.

Prior to the activation of the CM-RCS, the helium tank and oxidizer valve temperatures varied only slightly from the values measured at the time of launch.

From subsystem activation through landing, the helium tank temperatures decreased because of gas withdrawal effects, while all of the engine temperatures increased because of engine firing and aerodynamic entry thermal loads. All parameters remained well within design limits. No chamber/nozzle interface seal leakage was detected on either of the positive pitch engines.

Postflight examination.- Postflight examination of the CM-RCS revealed ruptured burst discs in the subsystem A oxidizer relief valve and in the subsystem B fuel relief valve. This was expected and has been characteristic on all previous missions and in the ground-based test program. It is caused by a pressure surge or regulator overshoot at subsystem pressurization. This problem has been eliminated on Block II systems by relocating the relief valves to provide more volume between the regulators and the relief valves. One other problem was noted during the postlanding subsystem deactivation procedures at Hawaii. A helium test port (TP 58) in subsystem A had an audible leak after the outer cap was removed. The test port has been removed for failure verification and analysis.

~~CONFIDENTIAL~~



~~CONFIDENTIAL~~

TABLE 5.16-I.- HELIUM AND PROPELLANT SERVICING

Subsystem	Helium, lb <sup>a</sup>	Fuel, MMH lb <sup>b</sup>	Oxidizer, N <sub>2</sub> O <sub>4</sub> lb <sup>b</sup>
CM-RCS			
System A	0.525	42.3	90.0
System B	0.525	42.5	90.8
SM-RCS			
Quad A	0.522	66.6	135.3
Quad B	0.525	66.7	135.4
Quad C	0.525	66.9	136.6
Quad D	0.522	67.0	134.9

<sup>a</sup> Helium servicing was completed at 6:00 a.m. e.s.t. on November 7, 1967.

<sup>b</sup> Propellant servicing was completed on November 2, 1967. Loads are based on pressure-volume-temperature (PVT) checks. Tolerances on the listed quantities are as follows.

Fuel        ±0.75 pound  
Oxidizer   ±1.0    pound

~~CONFIDENTIAL~~

~~CONFIDENTIAL~~

5.16-11

TABLE 5.16-II.- RCS SEQUENCE OF EVENTS

Event	Initiate, hr:min:sec	Complete, hr:min:sec
Lift-off		(12:00:01.3 G.m.t. November 9, 1967)
Begin parking orbit	00:11:05.6	
CSM/S-IVB separation		03:26:28.2
Direct ullage	03:26:26.5	03:26:29.5
+X translation	03:26:29.5	03:26:36.6
Maneuver to first SPS burn attitude	03:26:42.7	03:28:07.6
Inhibit pitch and yaw		03:28:07.6
First SPS burn (RCS roll control)	03:28:06.6	03:28:22.6
Pitch and yaw inhibit release		03:28:23.6
Maneuver to cold-soak attitude	03:28:34.6	03:29:45.9
Cold-soak attitude hold	03:29:45.9	08:01:30.4
Apogee		05:46:49.5
Maneuver to second SPS burn attitude	08:01:30.4	08:01:57.5
Second +X translation	08:10:24.9	08:10:55.8
Second SPS burn	08:10:54.8	08:15:35.4
Maneuver to CM/SM separation attitude	08:16:06.7	08:17:51
CM-RCS pressurize	08:18:01.5	
-X translation (SM)	08:18:02.5	

~~CONFIDENTIAL~~

~~CONFIDENTIAL~~

TABLE 5.16-II.- RCS SEQUENCE OF EVENTS - Concluded

Event	Initiate, hr:min:sec	Complete, hr:min:sec
+Roll maneuver (SM)	08:18:02.5	
CM/SM separation		08:18:02.6
CM-RCS control firings	08:18:02.6	08:31:16.6
Pitch to entry attitude	08:18:55.8	08:19:54.9
Main parachute deployment	08:32:05.8	
Propellant depletion burn	08:32:25.7	08:33:07.8
Helium purge	08:36:35.9	08:37:20.2
Landing		08:37:09.2

~~CONFIDENTIAL~~

~~CONFIDENTIAL~~

5.16-13

TABLE 5.16-III.- TYPICAL MANEUVER ACCELERATIONS AND TRANSLATION VELOCITY CHANGES

Event	Time, hr:min:sec		Accelerations, deg/sec <sup>2(a,b)</sup>						Translation ΔV	
			Pitch		Yaw		Roll			
	From	To	Plus	Minus	Plus	Minus	Plus	Minus	Burn time, sec	ΔV, ft/sec <sup>c</sup>
SERVICE MODULE <sup>d</sup>										
	3:26:26.5	3:26:29.5							3	
	3:26:29.5	3:26:36.6							7.1	1.9
	3:26:42.7	3:28:07.6	+0.7	-0.6	+1.1	-1.0			-	-
	3:28:34.6	3:29:45.9	+1.2	-1.3	+1.1	-0.9	+2.0	-2.0	-	-
	8:01:30.4	8:01:57.5				-1.1	+1.7	-	-	-
Second +X translation	8:10:24.9	8:10:55.8						30.9	6.1	
Maneuver to CM/SM separation attitude	8:16:06.7	8:17:51.0	+1.4	-1.2	+0.8	-0.7		-	-	-
COMMAND MODULE										
CM-RCS control	8:18:02.6	8:31:16.6	+10.6	-7.7	+10.6	-8.5	+7.9	-7.7	-	-

<sup>a</sup> Accelerations are estimated accurate only to within a few deg/sec<sup>2</sup>.

<sup>b</sup> Average angular acceleration during event which may include engine off-times.

<sup>c</sup> Taken from accelerometer data and considered accurate to within +0.2, -0.0 ft/sec.

<sup>d</sup> Maneuvers accomplished in pseudo-rate control mode.

~~CONFIDENTIAL~~

~~CONFIDENTIAL~~

TABLE 5.16-IV.- SERVICE MODULE REACTION CONTROL SUBSYSTEM PROPELLANT CONSUMPTION, ENGINE BURN TIMES,  
NUMBER OF PULSES, DUTY CYCLES, AND PRESSURE DROPS PER MANEUVER - Part 1

Event	Time, hr:min:sec		Propellants used, lb			
	From	To	Quad A	Quad B	Quad C	Quad D
Direct ullage	03:26:26.5	03:26:29.5	1.05	1.05	1.05	1.05
First +X translation	03:26:29.5	03:26:36.6	2.50	2.50	2.50	2.59
Maneuver to first SPS burn attitude	03:26:36.6	03:28:07.6	5.24	8.88	5.48	8.86
First SPS burn (roll control only)	03:28:07.6	03:28:23.6	0.30	0.34	0.30	0.34
Maneuver to cold-soak attitude	03:28:34.5	03:29:45.9	5.09	4.04	5.09	4.03
Minimum deadband attitude hold	03:29:45.9	08:01:30.4	19.13	18.88	19.22	18.82
Maneuver to second SPS burn attitude	08:01:30.4	08:01:52.5	1.71	3.47	1.71	3.46
Second +X translation	08:10:24.5	08:10:55.8	10.95	10.97	11.01	11.40
Second SPS burn	08:10:54.8	08:15:35.4	1.01	1.01	0.85	1.00
Maneuver to CM/SM separation attitude	08:15:36.0	08:17:51.0	6.26	5.73	6.27	5.78

~~CONFIDENTIAL~~

~~CONFIDENTIAL~~

5.16-15

TABLE 5.16-IV.- SERVICE MODULE REACTION CONTROL SUBSYSTEM PROPELLANT CONSUMPTION, ENGINE BURN TIMES,  
NUMBER OF PULSES, DUTY CYCLES, AND PRESSURE DROPS PER MANEUVER - Part 2

Event	Engine burn time, sec															
	Quad A				Quad B				Quad C				Quad D			
	-P	CCW	+P	CW	-Y	CCW	+Y	CW	-P	CCW	+P	CW	-Y	CCW	+Y	CW
Direct ullage	3.0	0	0	0	3.0	0	0	0	0	0	3.0	0	0	0	3.0	0
First +X translation	7.125	0	0	0	7.125	0	0	0	0.085	0	7.04	0	1.67	0	5.46	0
Maneuver to first SPS burn attitude	4.55	1.64	4.435	1.785	9.285	1.645	8.805	1.745	4.555	1.63	4.435	1.785	9.825	1.640	8.745	1.785
First SPS burn (roll control only)	0	0.935	0	0.875	0.535	0.030	0.945	0.915	0	0.920	0	0.875	0.020	0.94	0	0.875
Maneuver to cold- soak attitude	4.88	1.35	5.135	1.325	3.585	1.35	4.125	1.325	4.90	1.35	5.135	1.325	3.585	1.35	4.11	1.325
Minimum deadband attitude hold	0.405	17.255	6.105	18.210	2.800	17.090	3.125	18.580	0.435	17.150	6.085	18.600	2.775	17.080	2.815	18.790
Maneuver to second SPS burn attitude	0.730	1.295	0.745	1.225	2.99	1.295	3.2	1.23	0.73	1.295	0.745	1.225	2.99	1.295	3.17	1.225
Second +X trans- lation	30.845	0.105	0.050	0.225	30.565	0.105	0.385	0.225	0.460	0.105	30.455	0.225	6.605	0.100	24.350	0.225
Second SPS burn	0	1.495	0	0.935	0	1.50	0	0.930	0	1.245	0	0.765	0	1.475	0	0.935
Maneuver to CM/SM separation attitude	5.590	1.470	6.510	1.590	5.570	1.480	4.790	1.600	5.615	1.470	6.520	1.595	5.585	1.470	4.700	1.595

~~CONFIDENTIAL~~

~~CONFIDENTIAL~~

TABLE 5.16-IV.- SERVICE MODULE REACTION CONTROL SUBSYSTEM PROPELLANT CONSUMPTION, ENGINE BURN TIMES,  
NUMBER OF PULSES, DUTY CYCLES, AND PRESSURE DROPS PER MANEUVER - Part 3

Event	Number of pulses															
	Quad A				Quad B				Quad C				Quad D			
	-P	CCW	+P	CW	-Y	CCW	+Y	CW	-P	CCW	+P	CW	-Y	CCW	+Y	CW
Direct ullage	1	0	0	0	1	0	0	0	0	0	0	1	0	0	1	0
First +X translation	1	0	0	0	1	0	0	0	2	0	3	0	17	0	17	0
Maneuver to first SPS burn attitude	201	60	143	54	215	60	153	53	201	60	143	54	214	60	156	54
First SPS burn (roll control only)	0	22	0	17	2	22	1	18	0	23	0	17	1	22	0	17
Maneuver to cold-soak attitude	131	44	109	31	108	44	13	31	131	44	109	31	108	44	12	31
Minimum deadband attitude hold	21	995	347	892	158	981	161	889	23	984	349	893	157	981	160	891
Maneuver to second SPS burn attitude	38	53	37	26	49	54	88	26	38	54	37	26	49	54	88	26
Second +X translation	2	5	1	5	1	5	1	5	13	5	13	5	107	5	108	5
Second SPS burn	0	63	0	19	0	63	0	19	0	57	0	16	0	63	0	19
Maneuver to CM/SM separation attitude	206	54	165	52	252	54	157	52	205	55	164	52	252	55	159	88

~~CONFIDENTIAL~~

~~CONFIDENTIAL~~

5.16-17

TABLE 5.16-IV.- SERVICE MODULE REACTION CONTROL SUBSYSTEM PROPELLANT CONSUMPTION, ENGINE BURN TIMES,  
NUMBER OF PULSES, DUTY CYCLES, AND PRESSURE DROPS PER MANEUVER - Part 4

Event	Duty cycle, percent															
	Quad A				Quad B				Quad C				Quad D			
	-P	CCW	+P	CW	-Y	CCW	+Y	CW	-P	CCW	+P	CW	-Y	CCW	+Y	CW
Direct ullage	100	0	0	0	100	0	0	0	0	0	100	0	0	0	100	0
First +X translation	100	0	0	0	100	0	0	0	1.1	0	99.1	0	23.5	0	76.9	0
Maneuver to first SPS burn attitude	0.5	1.8	4.8	1.9	10.2	1.8	9.6	1.9	5.0	1.7	4.8	1.9	10.7	1.8	9.6	1.9
First SPS burn (roll control only)	0	5.8	0	5.4	3.3	0.1	5.9	5.7	0	5.7	0	5.4	0.1	5.8	0	5.4
Maneuver to cold-soak attitude	6.8	1.8	7.1	1.8	5.0	1.8	5.7	1.8	6.8	1.8	7.1	1.8	5.0	1.8	5.7	1.8
Minimum deadband attitude hold	<0.1	0.1	<0.1	0.1	<0.1	0.1	<0.1	0.1	<0.1	0.1	<0.1	0.1	<0.1	0.1	<0.1	0.1
Maneuver to second SPS burn attitude	2.6	4.7	2.7	4.5	11.0	4.7	11.8	4.5	2.6	4.7	2.7	4.5	11.0	4.7	11.7	4.5
Second +X translation	99.5	0.3	0.1	0.7	98.5	0.3	1.2	0.7	1.4	0.3	98.2	0.7	21.3	0.3	78.5	0.7
Second SPS burn	0	0.5	0	0.3	0	0.5	0	0.3	0	0.4	0	0.2	0	0.5	0	0.3
Maneuver to CM/SN separation attitude	4.1	1.0	4.8	1.1	4.1	1.0	3.5	1.1	4.1	1.0	4.8	1.1	4.1	1.0	3.4	1.1

~~CONFIDENTIAL~~



~~CONFIDENTIAL~~

TABLE 5.16-V.- SM-RCS LAUNCH HEATING SUMMARY

Parameter	Maximum temperature during launch, °F	Time of maximum temperature, hr:min:sec
Engine mounting structure, quad A	150	00:11:24
Engine mounting structure, quad B	143	00:11:00
Engine mounting structure, quad C	154	00:10:00
Engine mounting structure, quad D	145	00:11:12
Negative pitch engine injector head, quad A	<sup>a</sup> 132	<sup>a</sup> 00:20:00
Clockwise roll engine injector head, quad C	153	00:09:00

<sup>a</sup>Estimated values.~~CONFIDENTIAL~~

~~CONFIDENTIAL~~

5.16-19

TABLE 5.16-VI.- SUMMARY OF SM-RCS TEMPERATURES FROM CSM/S-IVB SEPARATION THROUGH CM/CI SEPARATION

Temperature at initiation of S-IVB separation, °F	Engine mounting structure, quad A	Engine mounting structure, quad B	Engine mounting structure, quad C	Engine mounting structure, quad D	Injector head negative pitch engine, quad A	Injector head clockwise roll engine, quad C
Maximum soak-back temperature after S-IVB separation maneuver firing, °F	123	139	128	124	124	129
Time of occurrence, hr:min:sec	03:39:00	03:37:00	03:37:00	03:39:00	03:31:00	03:32:00
Maximum temperature during cold-soak, °F	138	138	128	136	138	124
Preliminary limit, °F	229	229	229	229	350	350
Minimum temperature during cold-soak, °F	131.5	117.5	113	118	132	110
Preliminary limit, °F	113	113	113	113	88	88
Temperature at initiation of reorientation maneuver prior to second SPS burn, °F	138	125	113	135	138	110
Temperature at initiation of ullage firing for the second SPS burn, °F	142.5	135.5	124.5	131	144	127
Maximum soak-back, temperatures after ullage firing, °F	152.5	146.5	126	139	203.7	137
Time of occurrence, hr:min:sec	<sup>a</sup> 08:18:02.6	<sup>a</sup> 08:18:02.6	<sup>a</sup> 08:18:02.6	<sup>a</sup> 08:18:02.6	08:12:43	<sup>a</sup> 08:18:02.6

<sup>a</sup>CM-SM separation, with accompanying loss of SM-RCS data occurred at 08:18:02.6, prior to attainment of maximum soak-back temperature by these parameters.

~~CONFIDENTIAL~~

~~CONFIDENTIAL~~

TABLE 5.16-VII.- THERMAL CONTROL SUBSYSTEM PERFORMANCE SUMMARY  
DURING COLD-SOAK PERIOD (03:29:00 to 08:01:00)

	Quad A	Quad B	Quad C	Quad D
Number of actuations of heaters to ON	<sup>a</sup> 0	5	<sup>b</sup> 1	10
Number of actuations of heaters to OFF	0	5	0	10
Actuation temperature, heaters ON, °F	-	118 ±1	116 ±1	119 ±1
Actuation temperature, heaters OFF, °F	-	139 ±2	-	135 ±2
Heater cycle rate, minutes per cycle <sup>c</sup>	-	40 to 43	-	18 to 24
Heater duty cycle, percent <sup>d</sup>	0	18	<sup>b</sup> 38	45

<sup>a</sup>Quad A experienced solar soak during this period and never cooled sufficiently for the heater thermal switch to actuate the heaters ON.

<sup>b</sup>Quad C experienced cold soak during this period and after the heaters were actuated ON, the quad never warmed sufficiently for the thermal switch to actuate the heaters OFF.

<sup>c</sup>Time from actuation of the heater ON to the next actuation of the heater ON.

<sup>d</sup>The percentage of the time between 03:29:00 and 08:01:00 that the heater was ON.

~~CONFIDENTIAL~~

~~CONFIDENTIAL~~

5.16-21

TABLE 5.16-VIII.- TYPICAL CM-RCS CONTROL CROSS-COUPLING EFFECTS

Forcing maneuver	Time, hr:min:sec	Roll acceleration, deg/sec <sup>2</sup>	Cross coupling effects accelerations, <sup>a</sup> deg/sec <sup>2</sup>	
			Pitch	Yaw
Plus roll to lift vector up	08:18:38.0	7.5	1.7	-0.9
Minus roll to neutralize rates	08:18:48.9	-7.8	1.8	+0.8

<sup>a</sup>These accelerations are only typical values and are accurate to within only a few tenths of a deg/sec<sup>2</sup> (approximately ±0.3 to 0.4 deg/sec<sup>2</sup>).

~~CONFIDENTIAL~~

~~CONFIDENTIAL~~

TABLE 5.16-IX.- CM-RCS PRESSURE TRENDS

Event	Time, hr:min:sec	Helium source pressure, psia		Helium source temperature, °F		Pressure/absolute temperature ratio	
		Subsystem A	Subsystem B	Subsystem A	Subsystem B	Subsystem A	Subsystem B
Servicing		4260	4120	78	70	7.9	7.7
Lift-off	00:00:00.3	4220	4016	73	66	7.9	7.6
Begin parking orbit	00:11:05.6	4207	3995	74	65	7.9	7.6
CSM/S-IVB separation	03:26:28.2	4186	4015	72	66	7.9	7.6
Completion of maneuver to separation attitude	08:17:51	4165	3995	68	63	7.9	7.6
CM-RCS pressurize	08:18:01.5	3725	3554	68	65	7.0	6.8
Start pitch to entry attitude	08:18:55.8	3453	3302	63	58	6.6	6.4
Complete pitch to entry attitude	08:19:54.9	3411	3302	58	53	6.6	6.4
Start propellant depletion burn	08:32:27.7	2405	2210	36	32	4.8	4.5
Complete depletion burn	08:33:07.8	1316	866	24	23	2.7	1.8
Start helium purge	08:36:35.9	1127	468	19	19	2.4	1.0
Landing	08:37:09.2	729	342	14	19	1.5	0.7
Close engine valves	08:37:19.7	540	320	12	17	1.1	0.7

~~CONFIDENTIAL~~

~~CONFIDENTIAL~~

5.16-23

TABLE 5.16-X.- COMMAND MODULE REACTION CONTROL SUBSYSTEM PROPELLANT CONSUMPTION, ENGINE BURN TIMES,  
NUMBER OF PULSES, DUTY CYCLES, AND PRESSURE DROPS PER MANEUVER

	① CM-RCS control firings	② Pitch to entry attitude	③ Propellant depletion burn	①+②+③ Total for the mission
Time From, hr:min:sec To, hr:min:sec	08:18:02.6 08:31:16.6	08:18:55.8 08:19:54.9	08:32:25.7 08:33:07.8	
Propellant used, lb System A System B	45.18 45.18	2.14 2.14	71.78 71.78	116.96 116.96
Engine burn time, second System A +P -P +Y -Y +R -R System B +P -P +Y -Y +R -R	6.075 8.480 10.745 13.145 40.080 52.040 6.075 8.480 10.740 13.145 40.080 52.040	0.220 1.050 .315 .260 1.755 1.850 0.220 1.050 .315 .260 1.755 1.850	0 42.1 42.1 42.1 42.1 42.1 0 42.1 42.1 42.1 42.1 42.1	6.075 50.580 52.845 55.245 82.180 94.140 6.075 50.580 52.840 55.245 82.180 94.140
Number of pulses System A +P -P +Y -Y +R -R System B +P -P +Y -Y +R -R	69 88 89 138 70 241 69 88 89 138 70 241	4 15 6 5 9 5 4 15 6 5 9 5	0 1 1 1 1 1 0 1 1 1 1 1	69 89 90 139 71 242 69 80 90 139 71 242
Duty cycle, percent System A +P -P +Y -Y +R -R System B +P -P +Y -Y +R -R	0.7 1.0 1.3 1.6 5.0 6.5 0.7 1.0 1.3 1.6 5.0 6.5	0.3 1.7 0.5 0.4 2.9 3.1 0.3 1.7 0.5 0.4 2.9 3.1	0 100 100 100 100 100 0 100 100 100 100 100	3.0 25.6 26.8 28.0 41.7 47.8 3.0 25.6 26.8 28.0 41.7 47.8
Average pulse width, second System A +P -P +Y -Y +R -R System B +P -P +Y -Y +R -R	0.088 .096 .121 .096 .576 .216 0.088 .096 .121 .096 .576 .216	System A average pulse width was 0.188 second, corresponding to theoretical oxidizer/fuel ratio of 1.6 to 1.84  System B average pulse width was 0.188 second, corresponding to theoretical oxidizer/fuel ratio of 1.6 to 1.84		

~~CONFIDENTIAL~~

~~CONFIDENTIAL~~

TABLE 5.16-XI.- COMMAND MODULE REACTION CONTROL SUBSYSTEM THERMAL PERFORMANCE SUMMARY

Parameter	Engine	Sub-system	Lift-off	Completion of first SPS burn	Apogee	CM/SM separation	Initiation of depletion burn	Landing	Design limit
Helium Tank Temperature, °F	-	A	73.9	71.5	69.1	67.9 <sup>a</sup>	35.5	11.8	-
Helium Tank Temperature, °F	-	B	65.1	66.4	66.4	62.7 <sup>a</sup>	32.4	16.7	-
Oxidizer Valve Temperature, °F	-P	A	66.9	62.4	62.4	64.8 <sup>a</sup>	56.3	83.1	225 Max
Oxidizer Valve Temperature, °F	-Y	A	67.1	68.4	68.4	65.9 <sup>a</sup>	72.0	91.5	225 Max
Oxidizer Valve Temperature, °F	CCW	A	71.6	67.9	67.9	72.8 <sup>a</sup>	86.3	107.2	225 Max
Oxidizer Valve Temperature, °F	-P	B	64.3	60.7	60.7	63.1 <sup>a</sup>	61.9	86.1	225 Max
Oxidizer Valve Temperature, °F	+Y	B	74.9	71.2	67.6	66.3 <sup>a</sup>	74.9	88.5	225 Max
Oxidizer Valve Temperature, °F	CW	B	72.8	70.4	71.6	76.5 <sup>a</sup>	<sup>b</sup>	<sup>b</sup>	225 Max
Injector Head Temperature, °F	-Y	A	-	-	-	82 <sup>c</sup>	160	200	-10 Min
Injector Head Temperature, °F	CCW	A	-	-	-	90 <sup>c</sup>	289	320	-10 Min
Injector Head Temperature, °F	+Y	B	-	-	-	80 <sup>c</sup>	145	200	-10 Min
Injector Head Temperature, °F	CCW	B	-	-	-	90 <sup>c</sup>	281	295	-10 Min
Engine Outer Wall Temperature No. 1, °F	-Y	A	-	-	-	70 <sup>c</sup>	100	140	850 Max
Engine Outer Wall Temperature No. 2, °F	-Y	A	-	-	-	70 <sup>c</sup>	110	145	850 Max
Engine Outer Wall Temperature No. 1, °F	CCW	A	-	-	-	120 <sup>c</sup>	182	290	850 Max
Engine Outer Wall Temperature No. 2, °F	CCW	A	-	-	-	135 <sup>c</sup>	200	260	850 Max
Engine Outer Wall Temperature No. 1, °F	+Y	B	-	-	-	90 <sup>c</sup>	110	150	850 Max
Engine Outer Wall Temperature No. 2, °F	+Y	B	-	-	-	100 <sup>c</sup>	135	175	850 Max
Engine Outer Wall Temperature No. 1, °F	CCW	B	-	-	-	115 <sup>c</sup>	190	270	850 Max
Engine Outer Wall Temperature No. 2, °F	CCW	B	-	-	-	125 <sup>c</sup>	200	280	850 Max
Chamber/Nozzle Interface Temperature, °F	+P	A	-	-	-	142 <sup>c</sup>	163	195	-
Chamber/Nozzle Interface Temperature, °F	+P	B	-	-	-	128 <sup>c</sup>	148	177	-

<sup>a</sup>Values taken immediately prior to CM-RCS activation.<sup>b</sup>Data lost after 08:20:23.<sup>c</sup>Values taken immediately after CM-RCS activation.~~CONFIDENTIAL~~

~~CONFIDENTIAL~~

5.16-25

NASA-S-68-490

1400

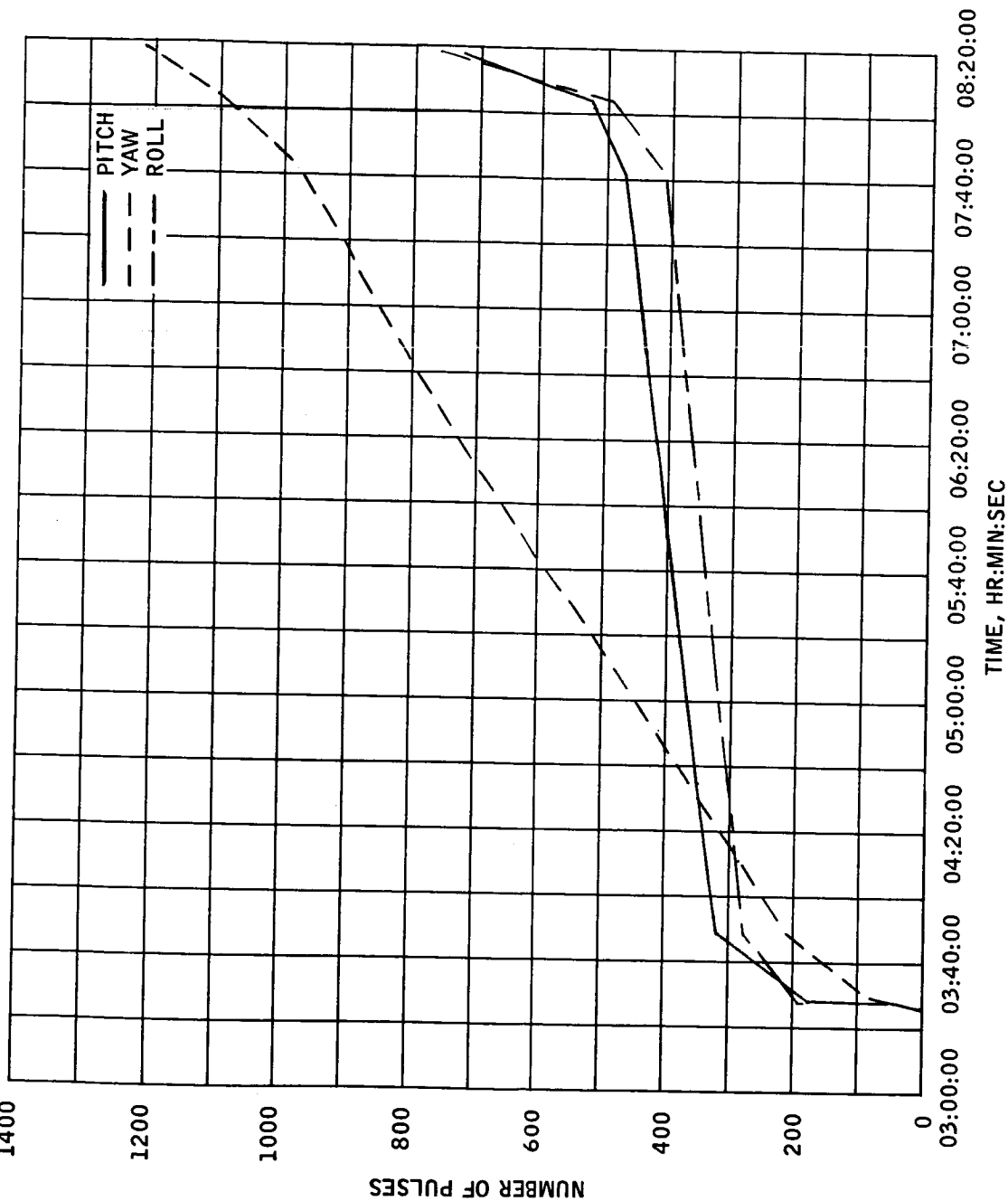


FIGURE 5.16-1.- AVERAGE NUMBER OF PULSES ACCUMULATED DURING SERVICE  
MODULE REACTION CONTROL SUBSYSTEM ACTIVITY.

~~CONFIDENTIAL~~



~~CONFIDENTIAL~~

NASA-S-68-491

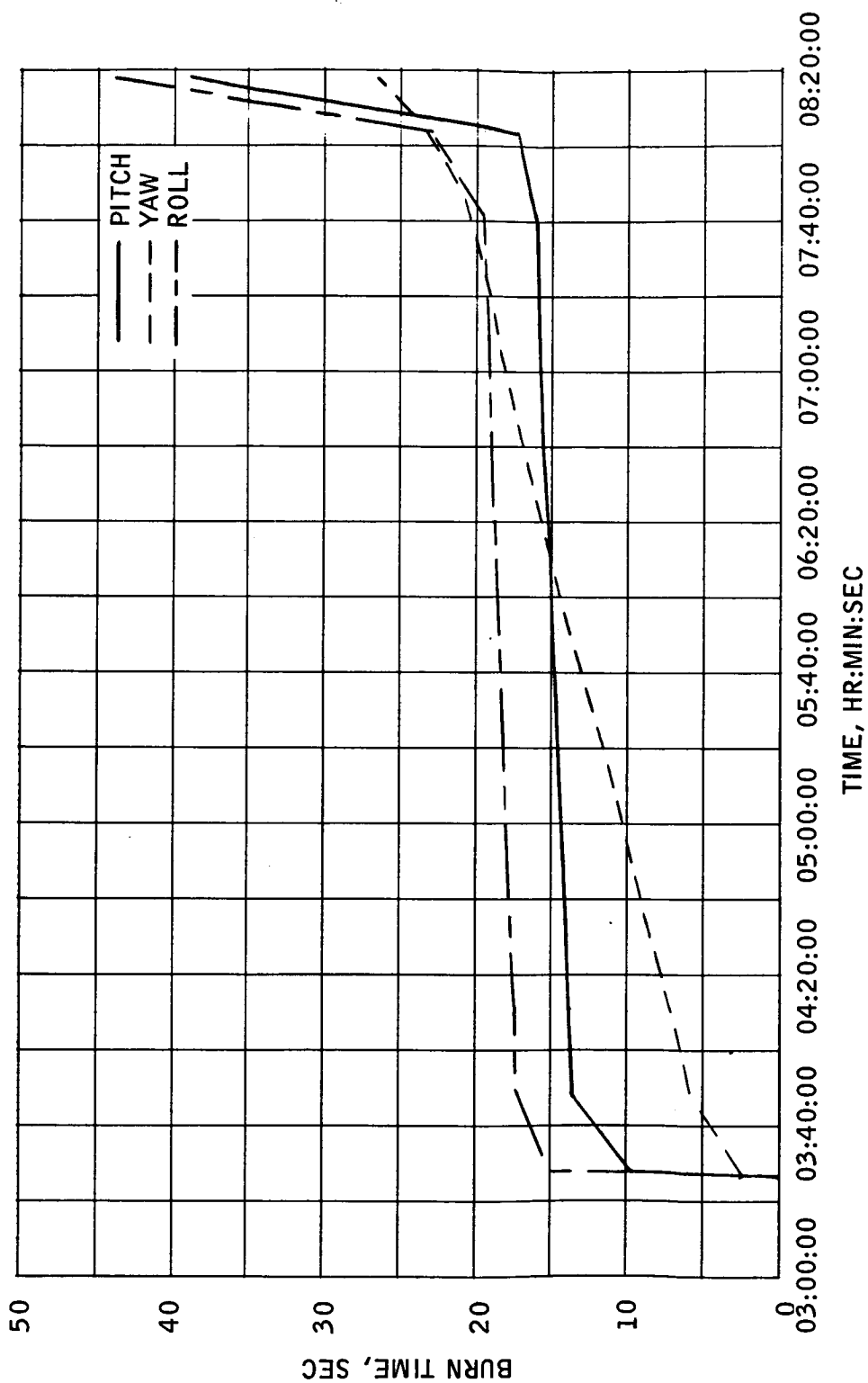
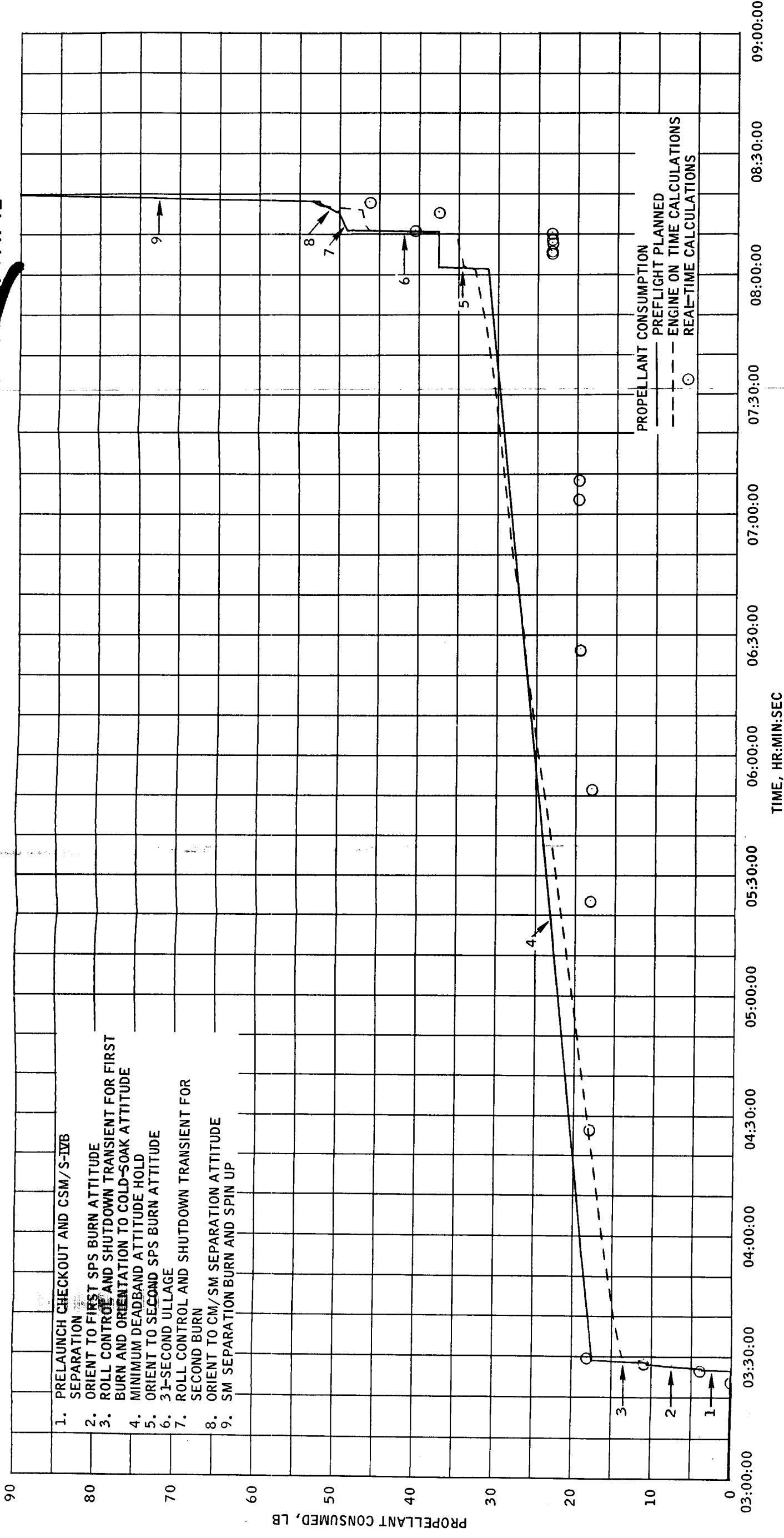


FIGURE 5.16-2.- AVERAGE BURN TIME ACCUMULATED DURING SERVICE MODULE REACTION CONTROL SUBSYSTEM ACTIVITY.

~~CONFIDENTIAL~~

~~CONFIDENTIAL~~

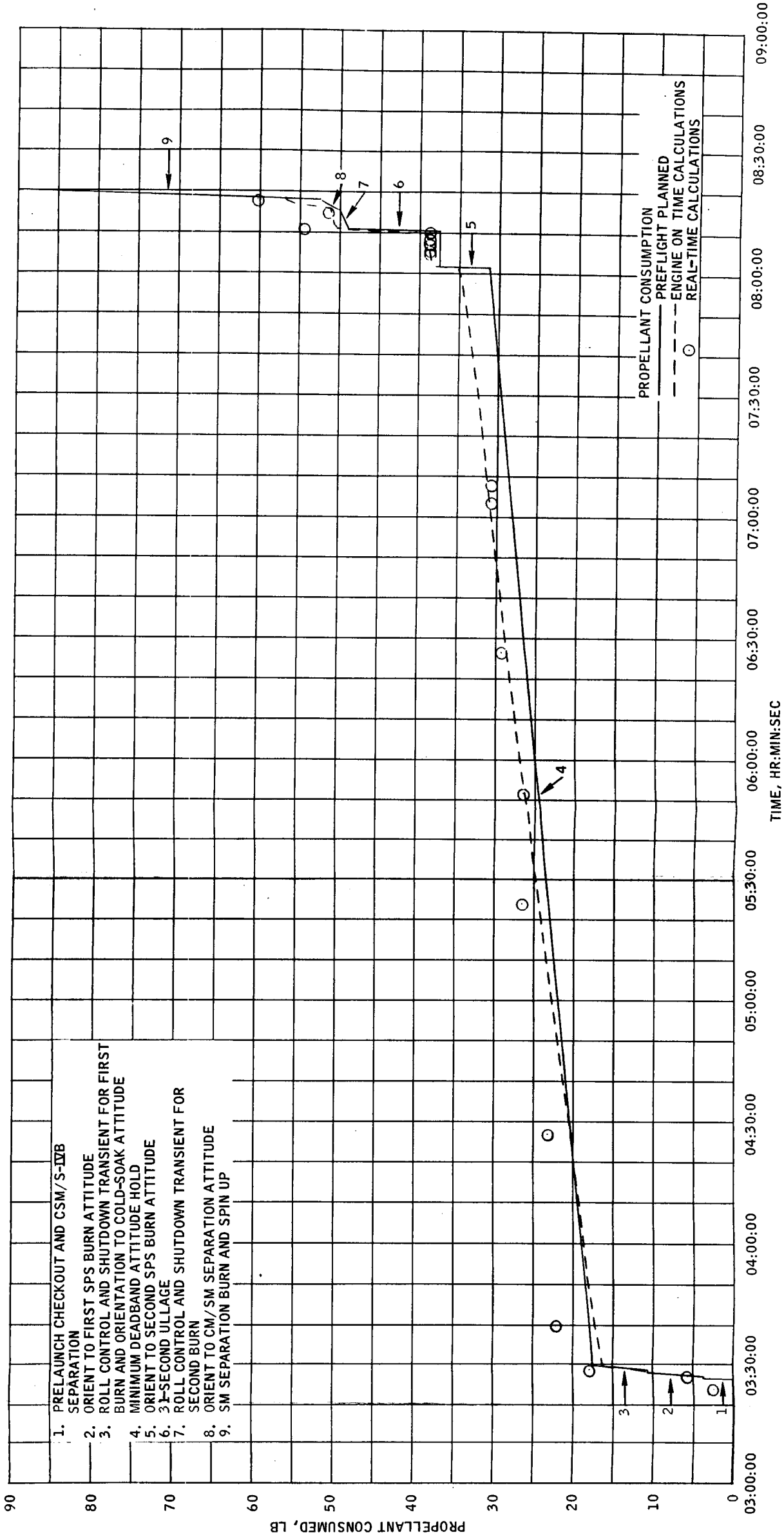
(A) QUAD A CONSUMPTION.

FIGURE 5.16-3.- SERVICE MODULE REACTION CONTROL SUBSYSTEM PROPELLANT CONSUMPTION.

~~CONFIDENTIAL~~

~~CONFIDENTIAL~~

NASA-S-68-493



(B) QUAD B CONSUMPTION.

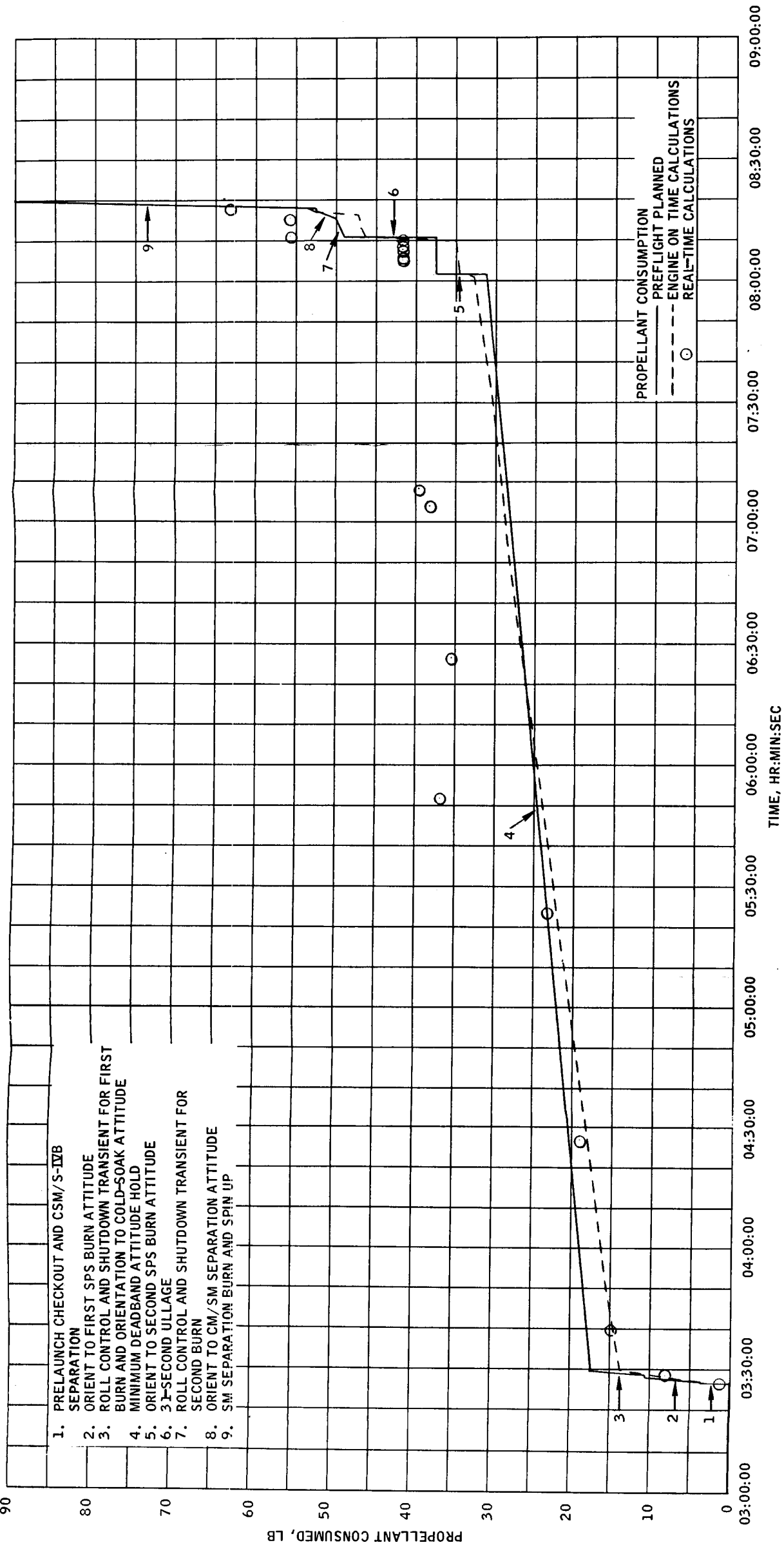
FIGURE 5.16-3.- CONTINUED.

~~CONFIDENTIAL~~

~~CONFIDENTIAL~~

5.16-29

NASA-S-68-494



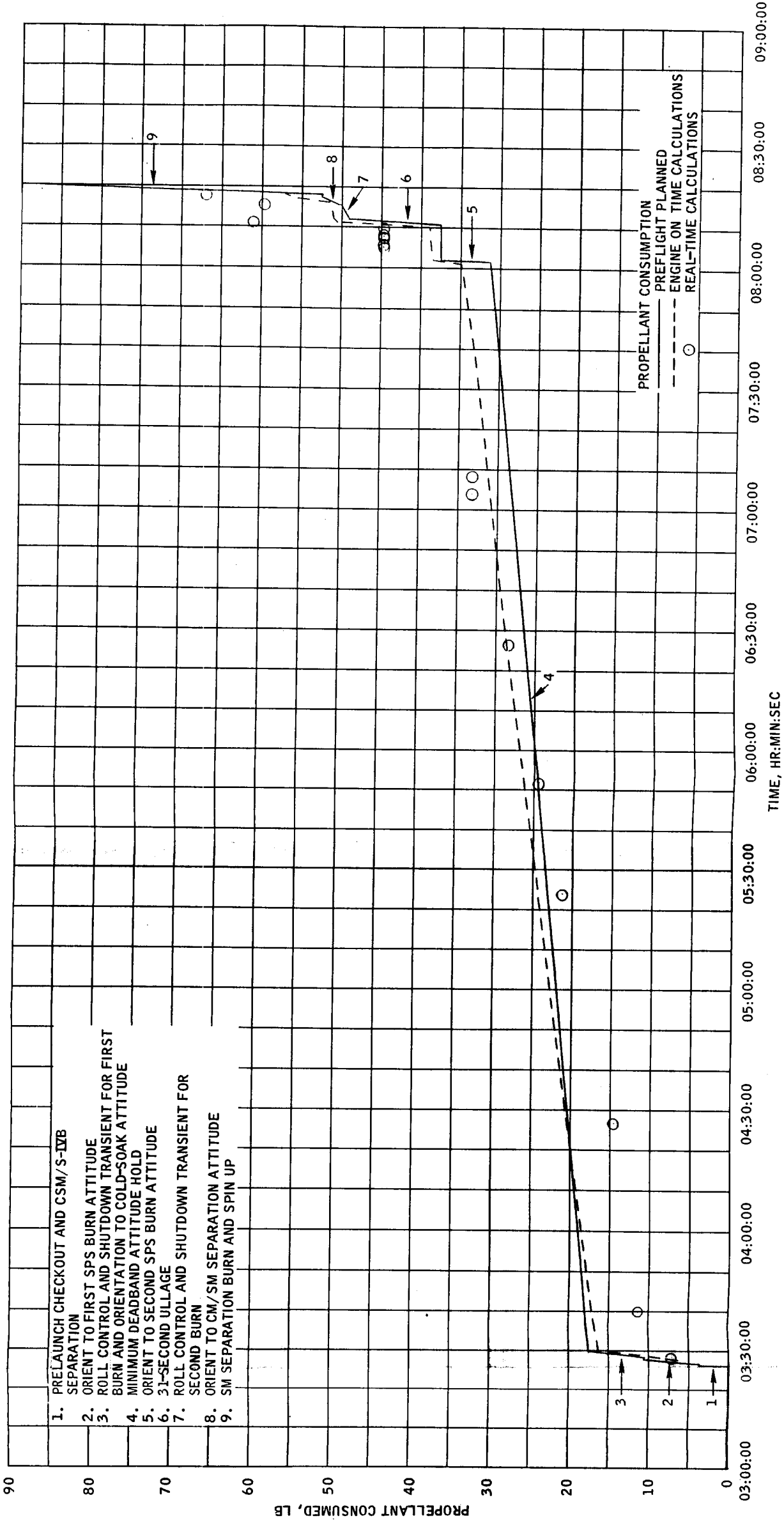
(C) QUAD C CONSUMPTION.

FIGURE 5.16-3.- CONTINUED.

~~CONFIDENTIAL~~

~~CONFIDENTIAL~~

NASA-S-68-495



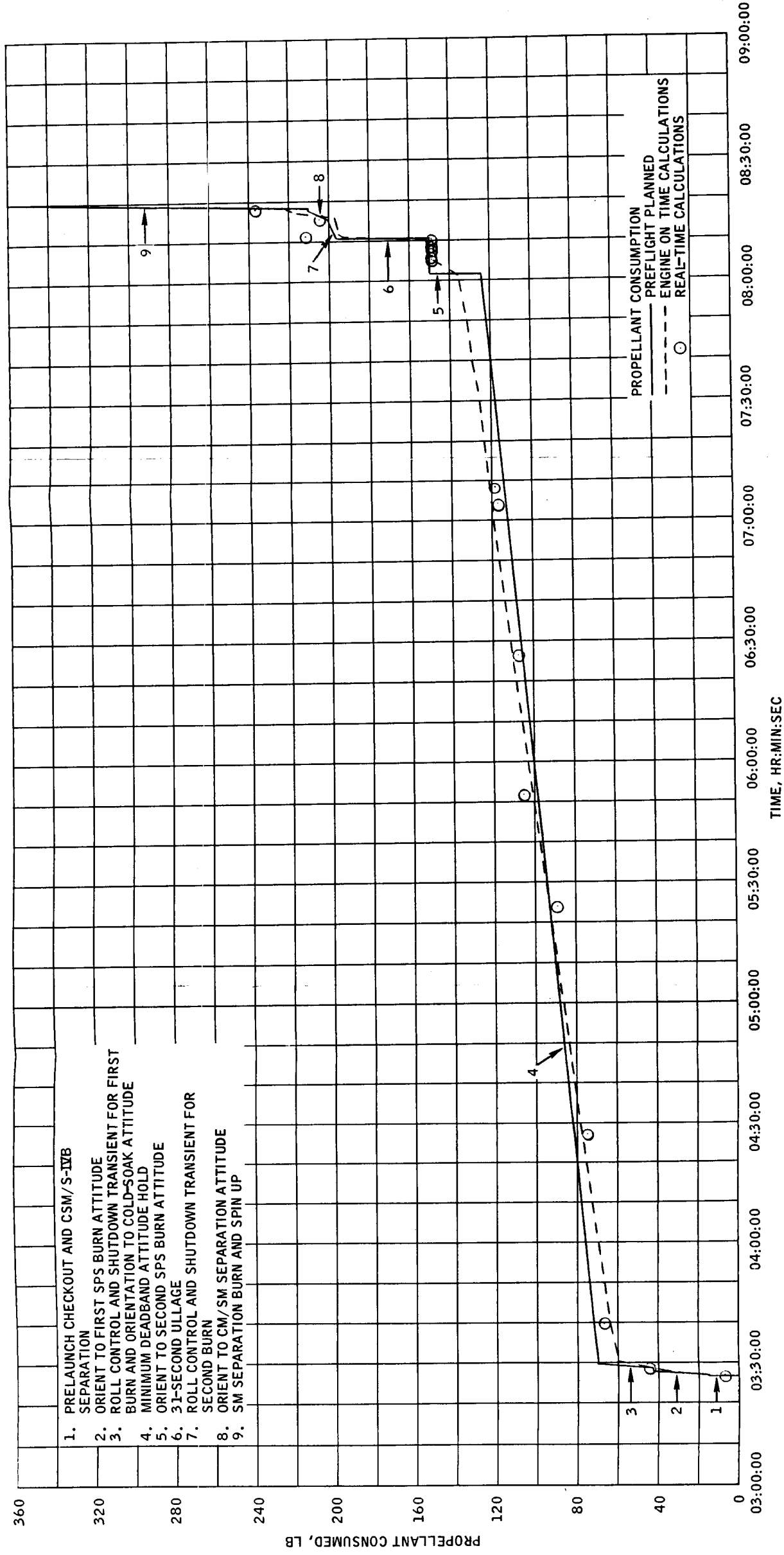
(D) QUAD D CONSUMPTION

FIGURE 5.16-3.- CONTINUED.

~~CONFIDENTIAL~~

~~CONFIDENTIAL~~

NASA-S-68-496



(E) TOTAL CONSUMPTION.

FIGURE 5.16-3.- CONCLUDED.

~~CONFIDENTIAL~~

~~CONFIDENTIAL~~

NASA-S-68-497

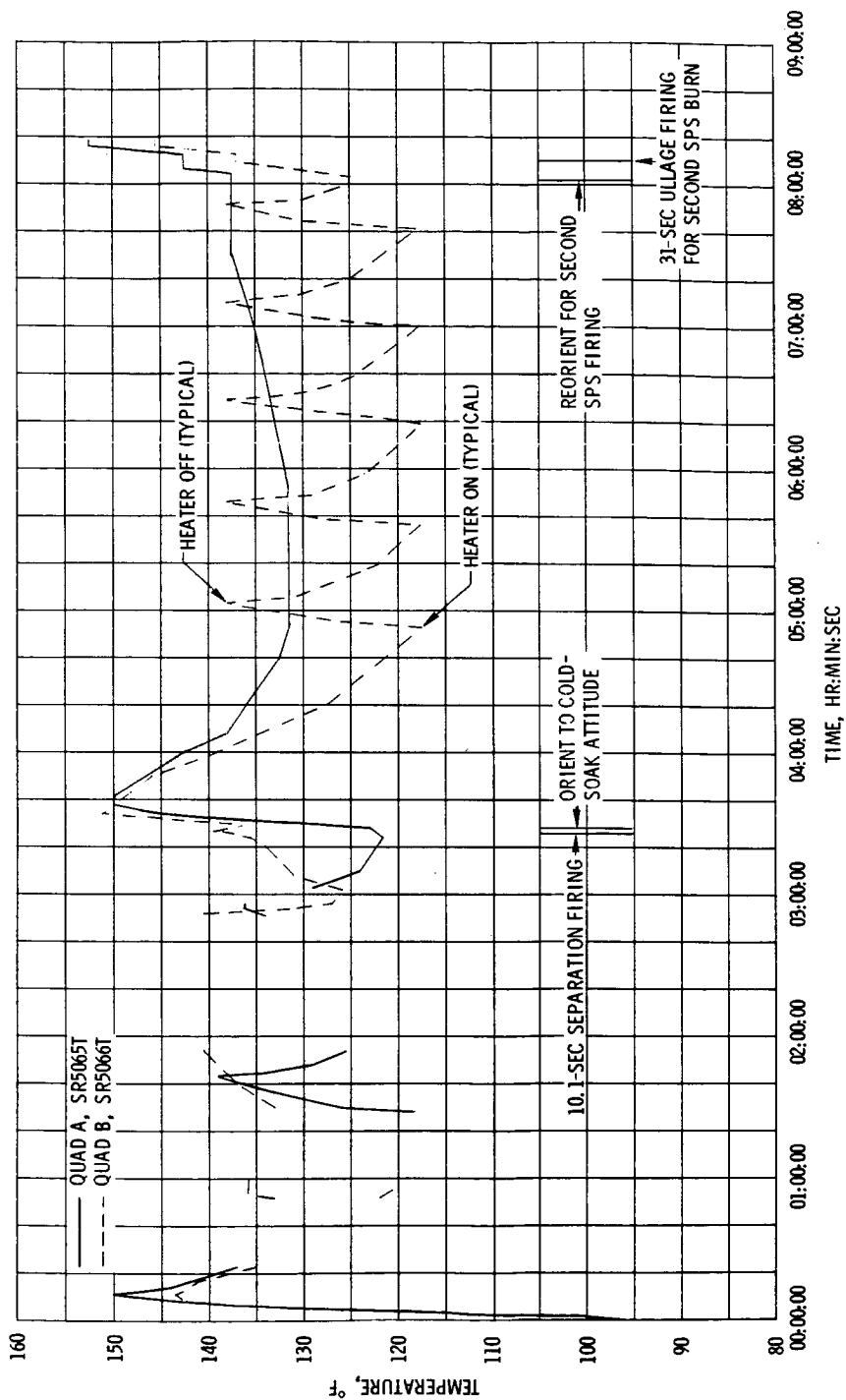
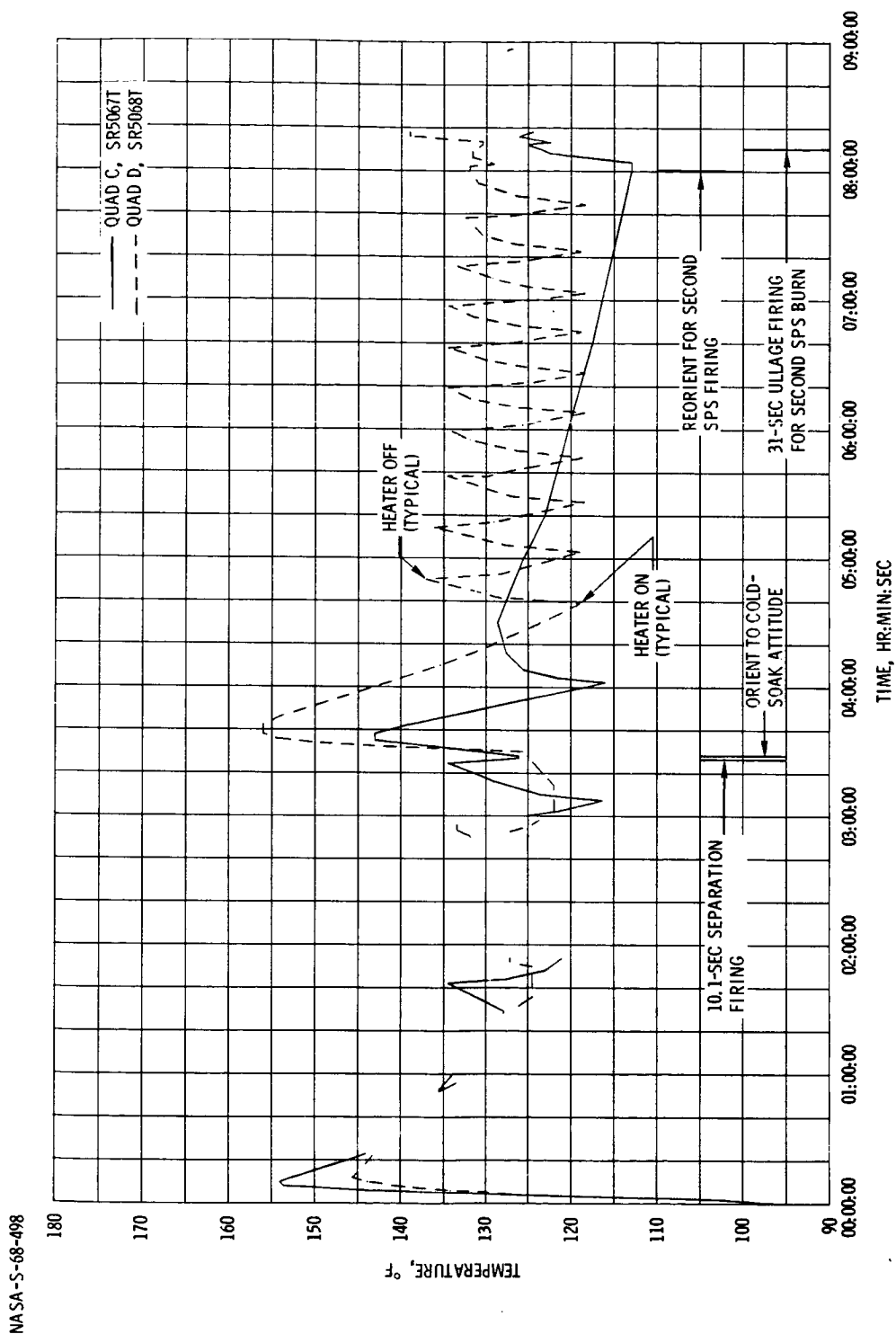


FIGURE 5.16-4. - SERVICE MODULE REACTION CONTROL SUBSYSTEM ENGINE MOUNTING STRUCTURE TEMPERATURES.  
(A) QUADS A AND B.

~~CONFIDENTIAL~~

~~CONFIDENTIAL~~

5.16-33



(B) QUADS C AND D.

FIGURE 5.16-4. - CONCLUDED.

~~CONFIDENTIAL~~



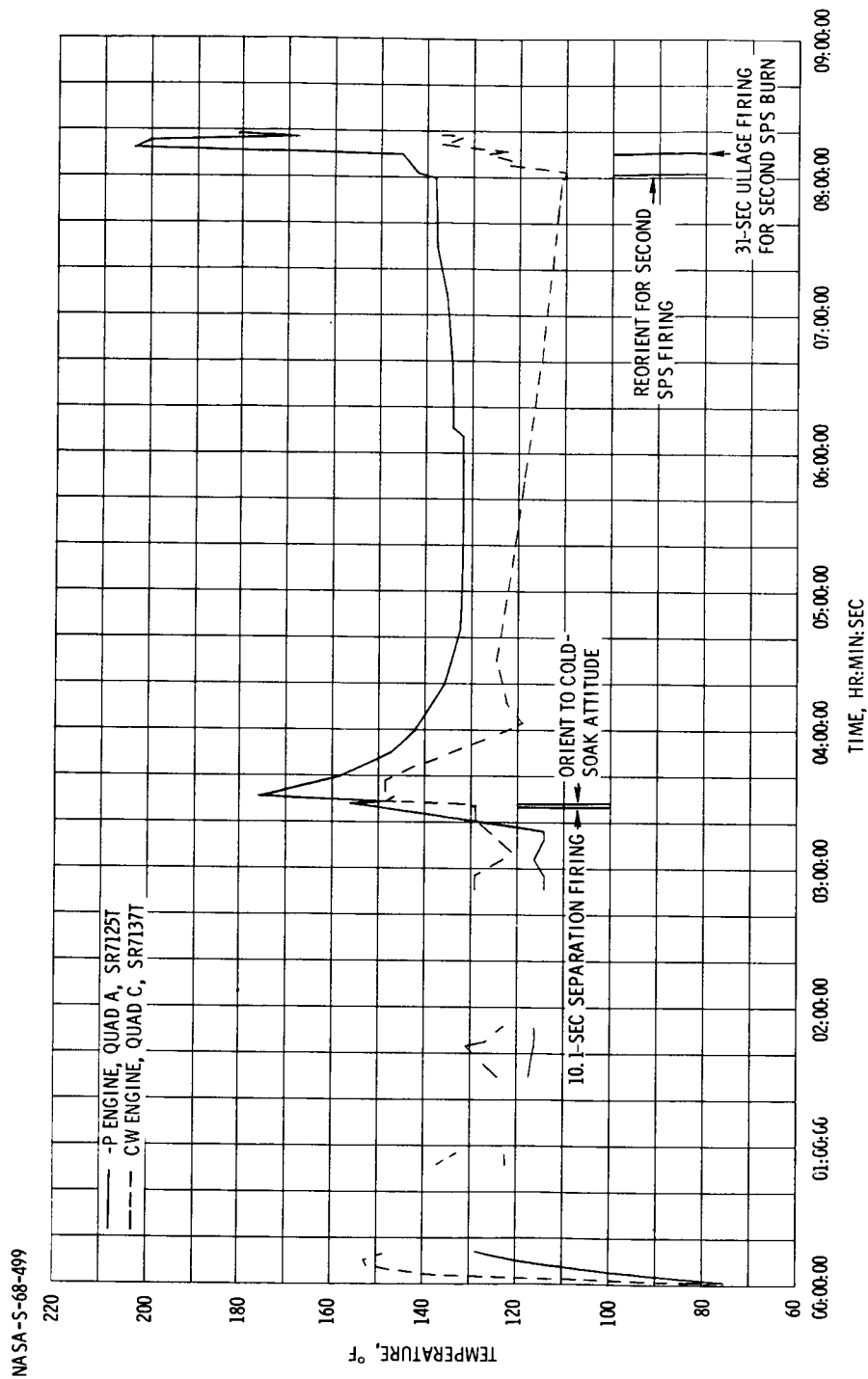
~~CONFIDENTIAL~~

FIGURE 5.16-5. - SERVICE MODULE REACTION CONTROL SUBSYSTEM ENGINE INJECTOR HEAD TEMPERATURES.

~~CONFIDENTIAL~~

~~CONFIDENTIAL~~

5.16-35

NASA-S-68-500

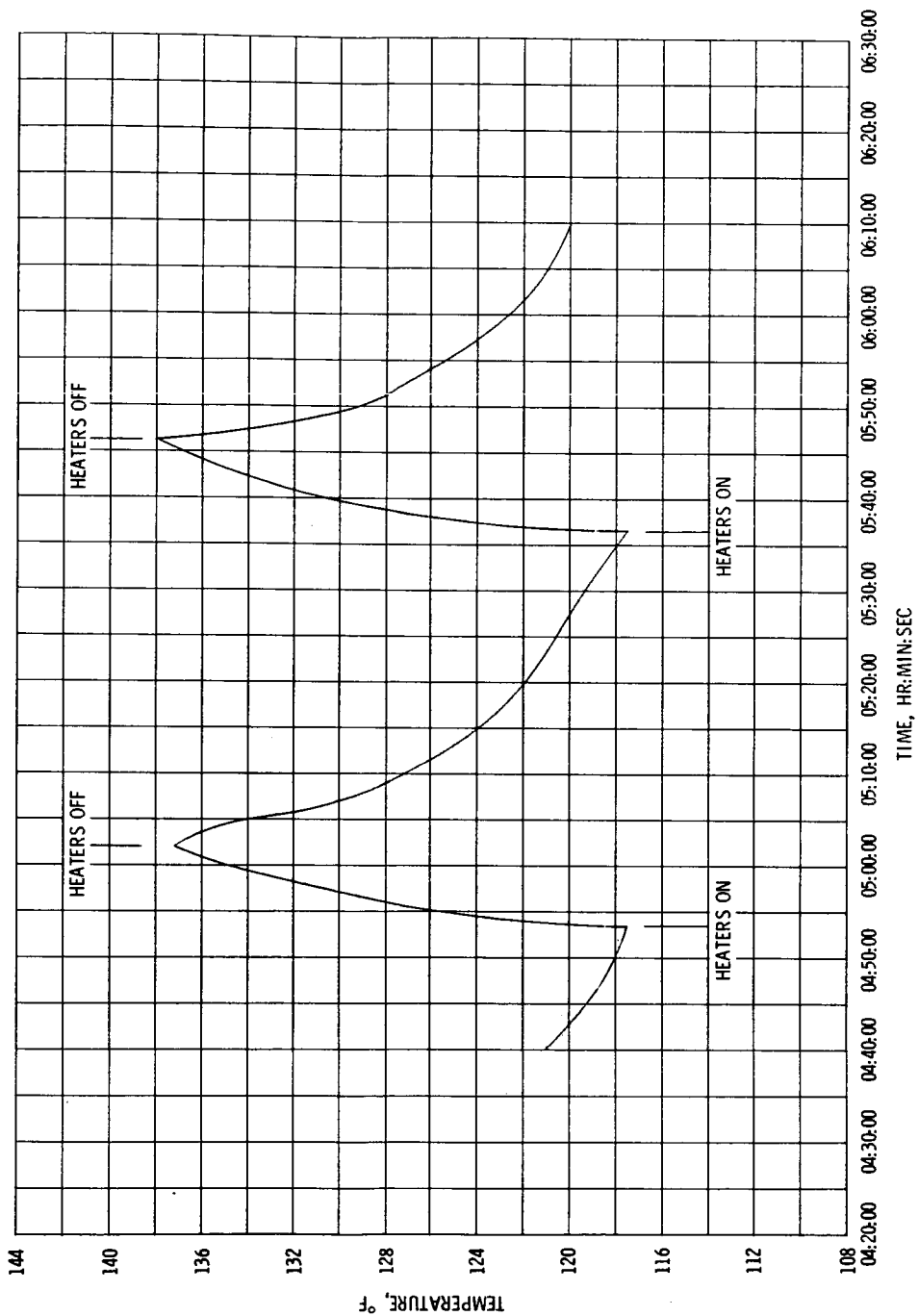


FIGURE 5.16-6. - QUAD B ENGINE MOUNTING STRUCTURE TEMPERATURE DURING PORTION OF THE COLD-SOAK PERIOD.

~~CONFIDENTIAL~~

~~CONFIDENTIAL~~

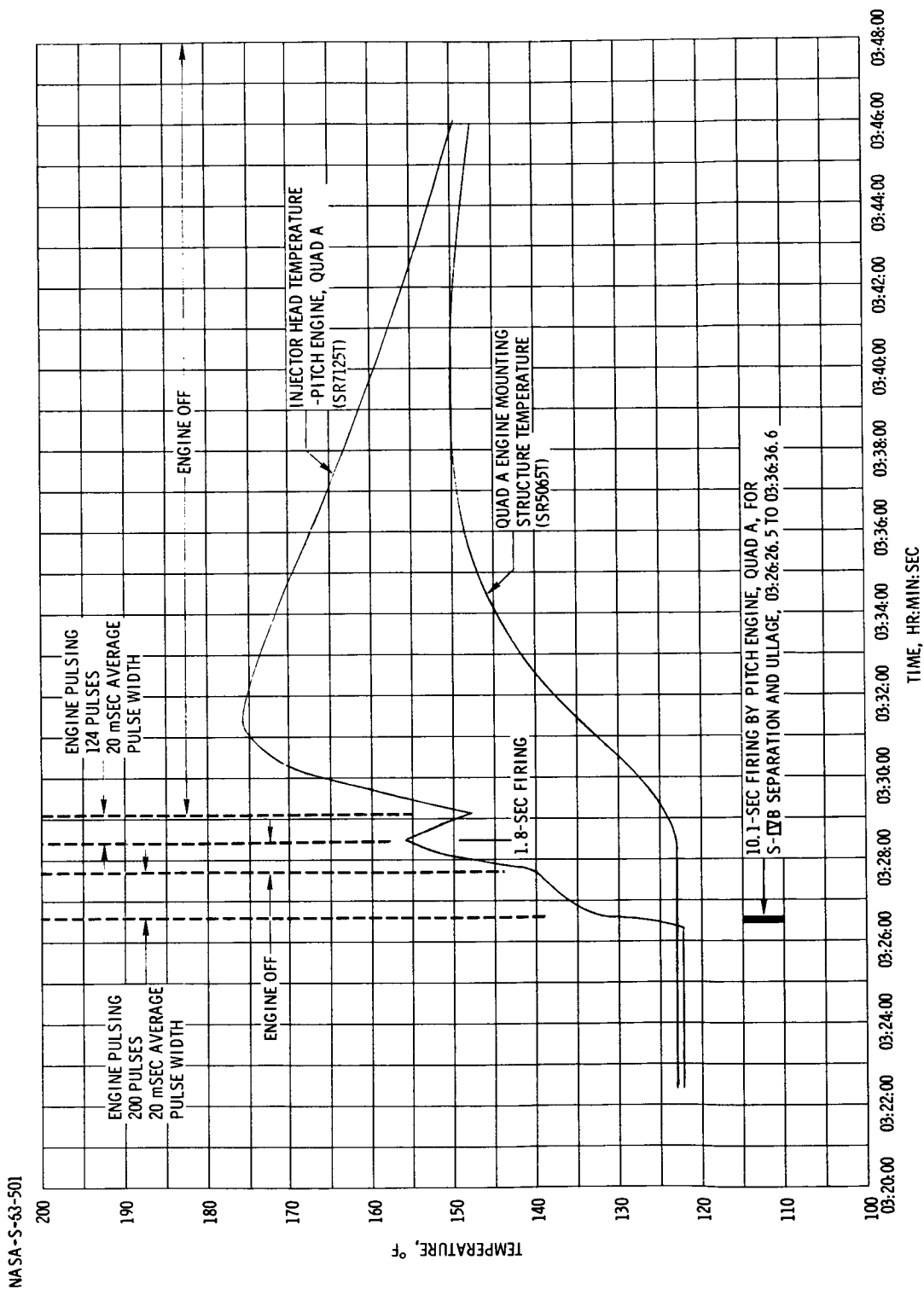


FIGURE 5.16-7. - EFFECT OF ENGINE FIRING ON INJECTOR HEAD AND ENGINE MOUNTING STRUCTURE TEMPERATURES.

~~CONFIDENTIAL~~

~~CONFIDENTIAL~~

5.16-37

NA SA-S-68-502

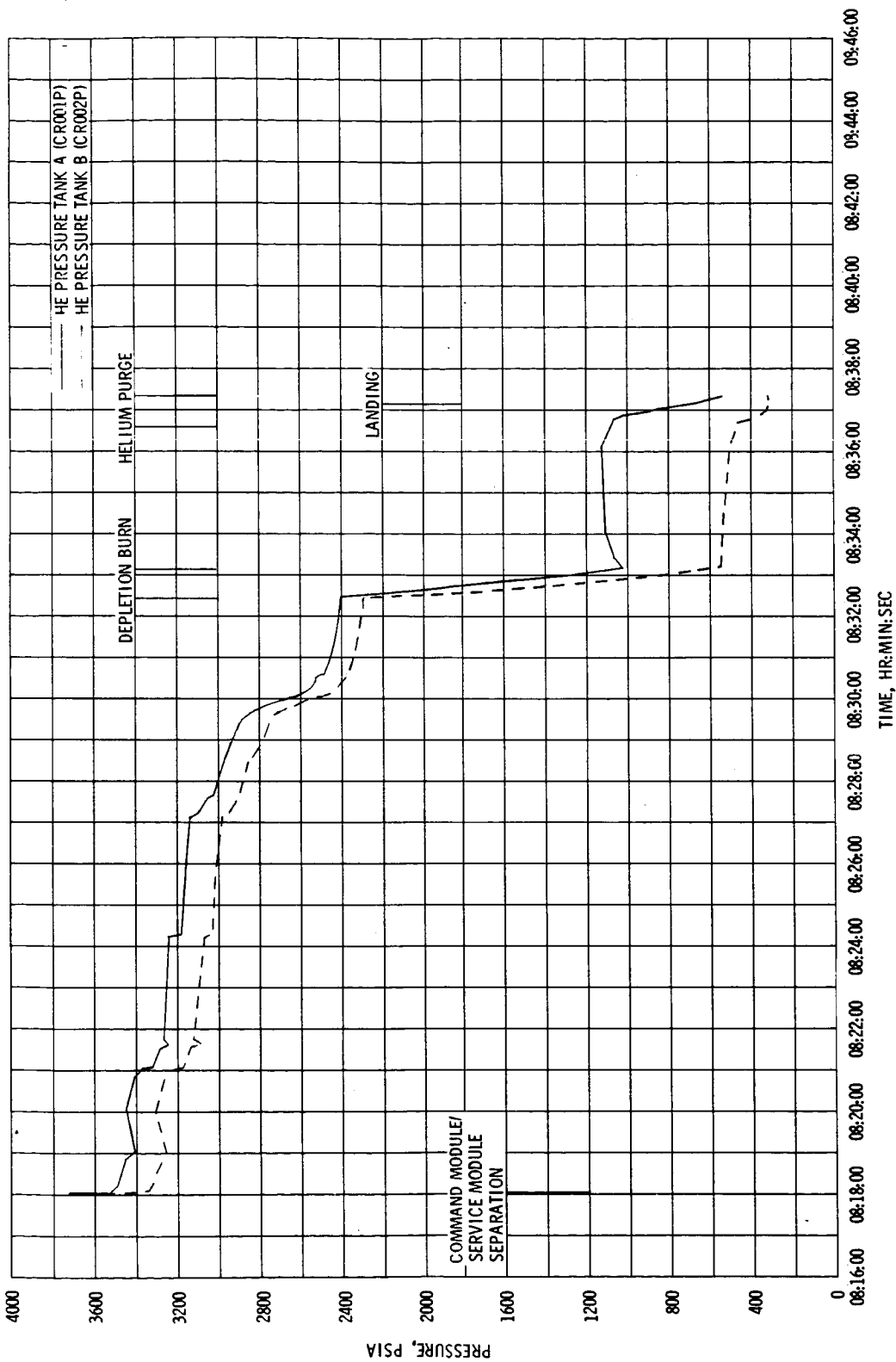


FIGURE 5.16-8. - COMMAND MODULE REACTION CONTROL SUBSYSTEM HELIUM TANK PRESSURES DURING ENTRY.

~~CONFIDENTIAL~~

~~CONFIDENTIAL~~

NA SA - S-68-503

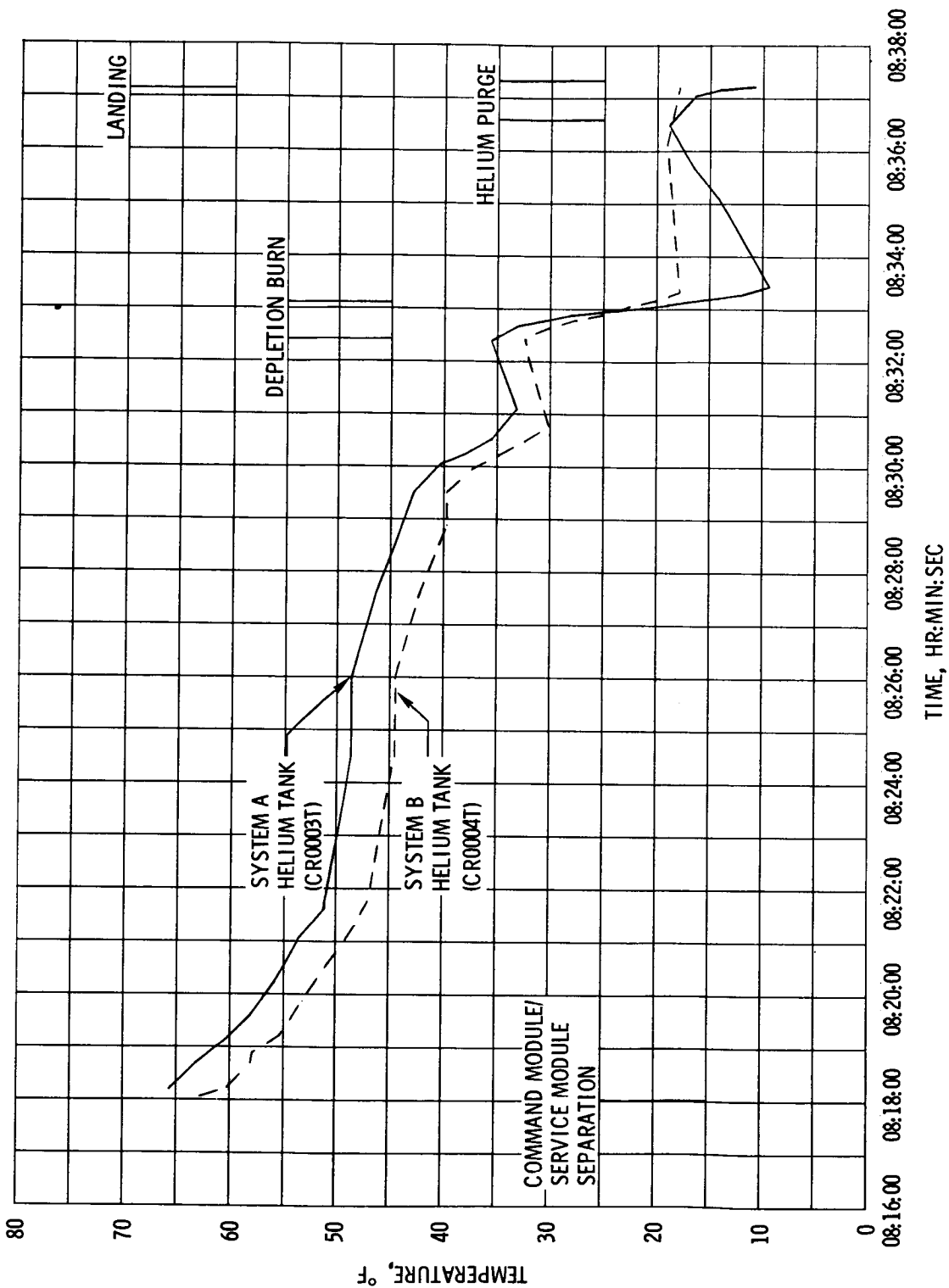


FIGURE 5.16-9. - COMMAND MODULE REACTION CONTROL SUBSYSTEM HELIUM TANK TEMPERATURES DURING ENTRY.

~~CONFIDENTIAL~~

~~CONFIDENTIAL~~

5.16-39

NASA-S-68-504

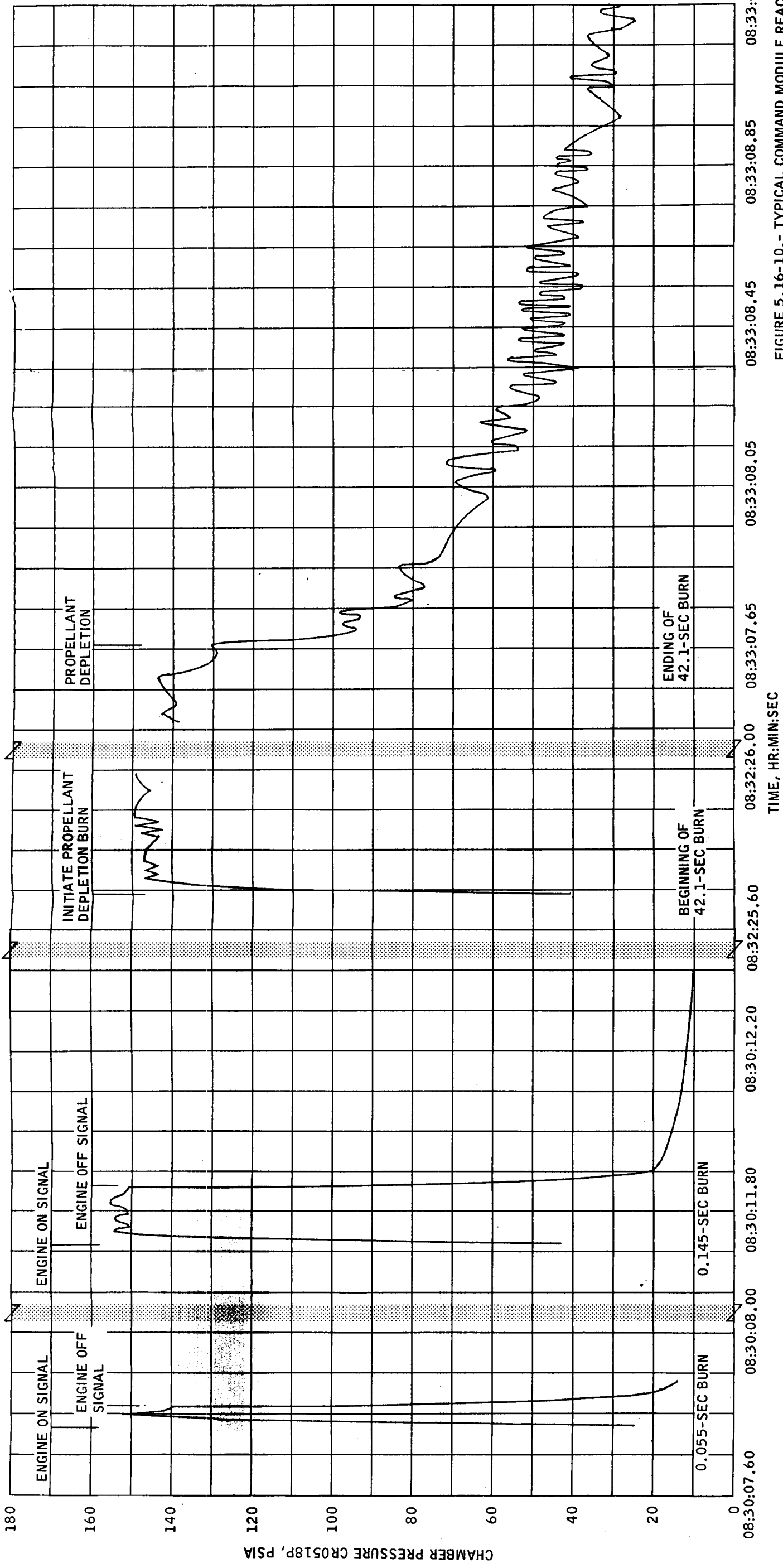


FIGURE 5.16-10.- TYPICAL COMMAND MODULE REACTION  
CONTROL SUBSYSTEM ENGINE CHAMBER PRESSURE  
FOR BURNS OF 0.005, 0.145 AND 42.1 SECONDS.

~~CONFIDENTIAL~~

~~CONFIDENTIAL~~

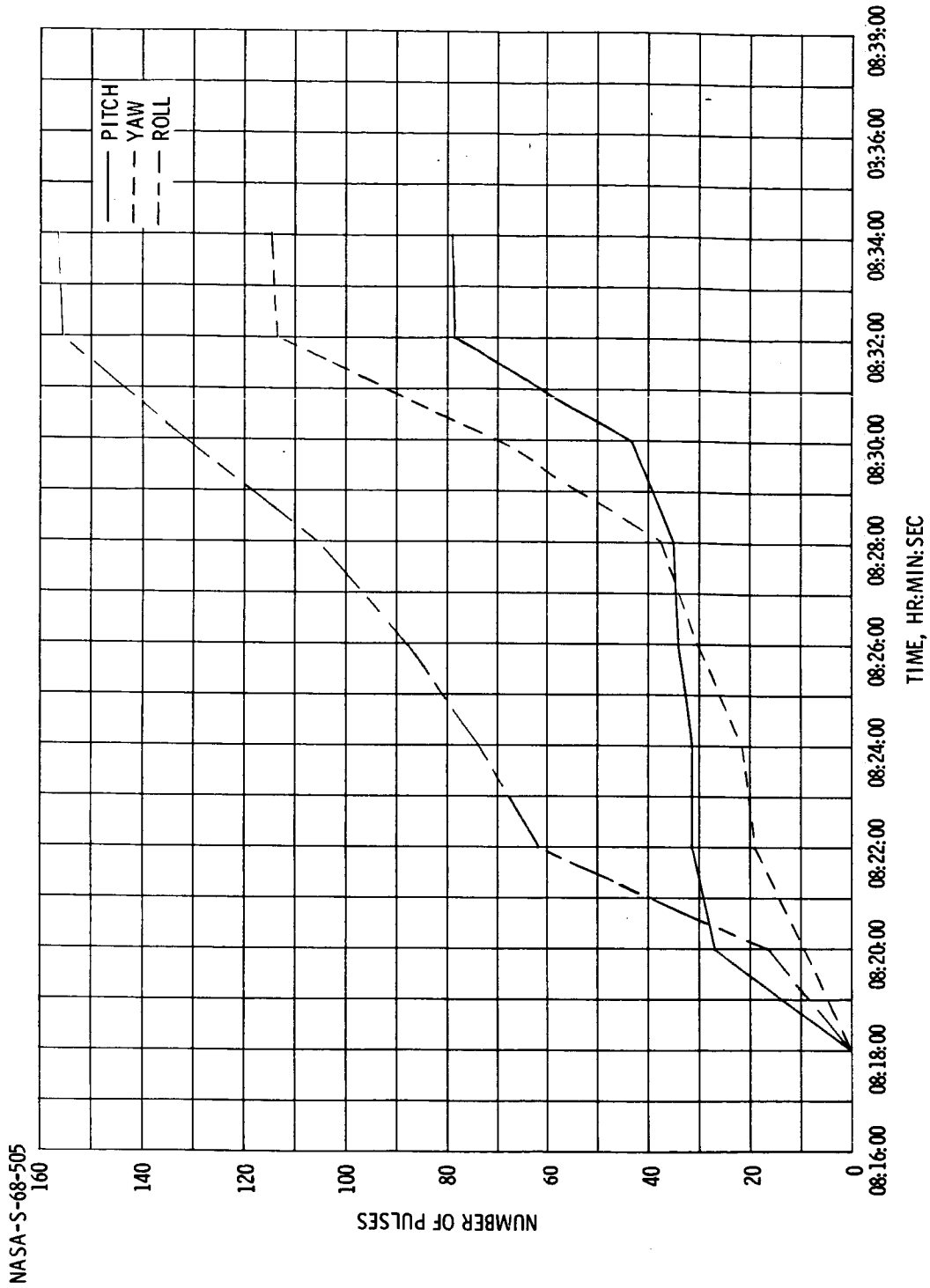


FIGURE 5.16-11.- AVERAGE NUMBER OF PULSES ACCUMULATED DURING COMMAND MODULE REACTION CONTROL SUBSYSTEM ACTIVITY.

~~CONFIDENTIAL~~

~~CONFIDENTIAL~~

5.16-41

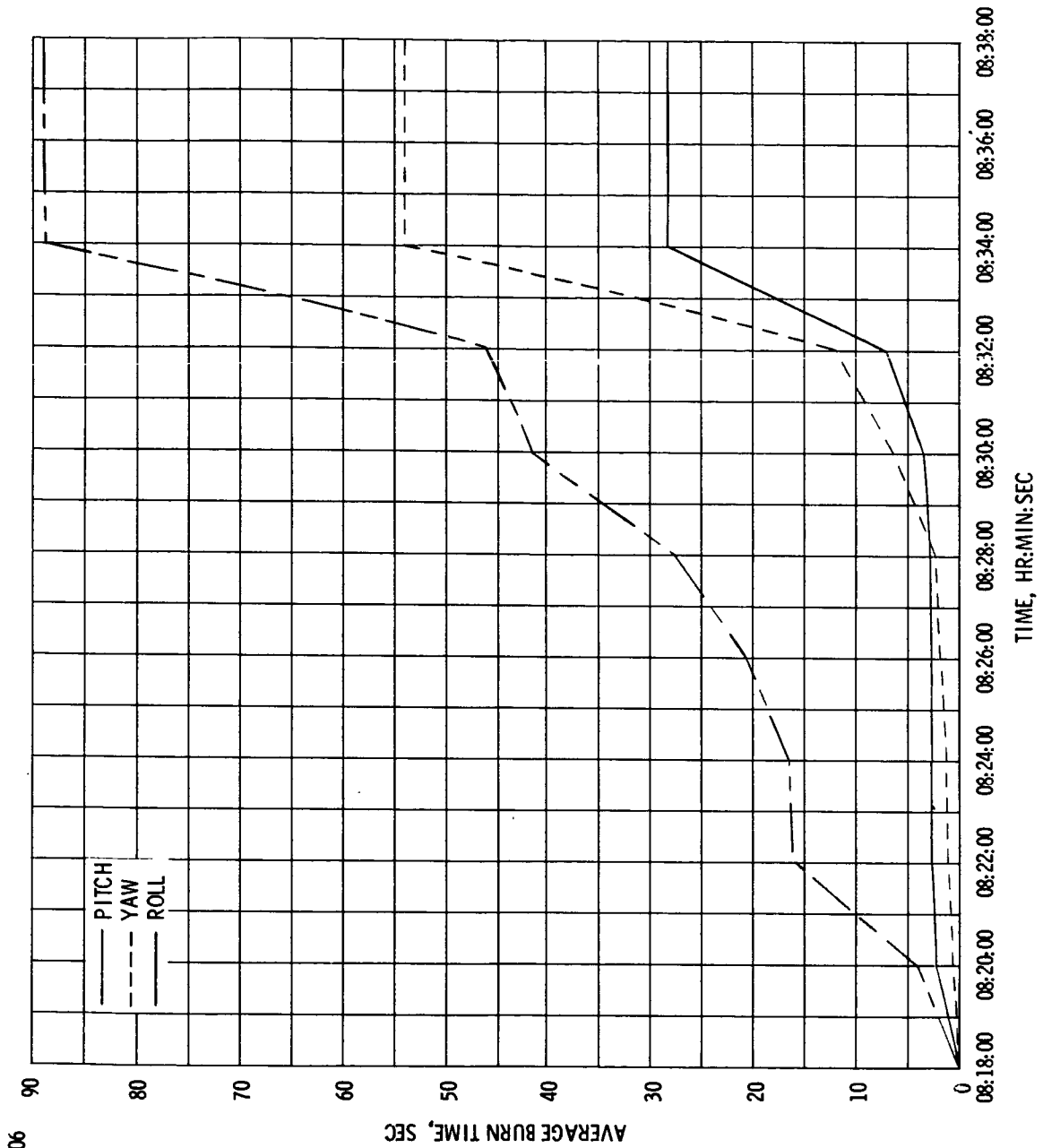


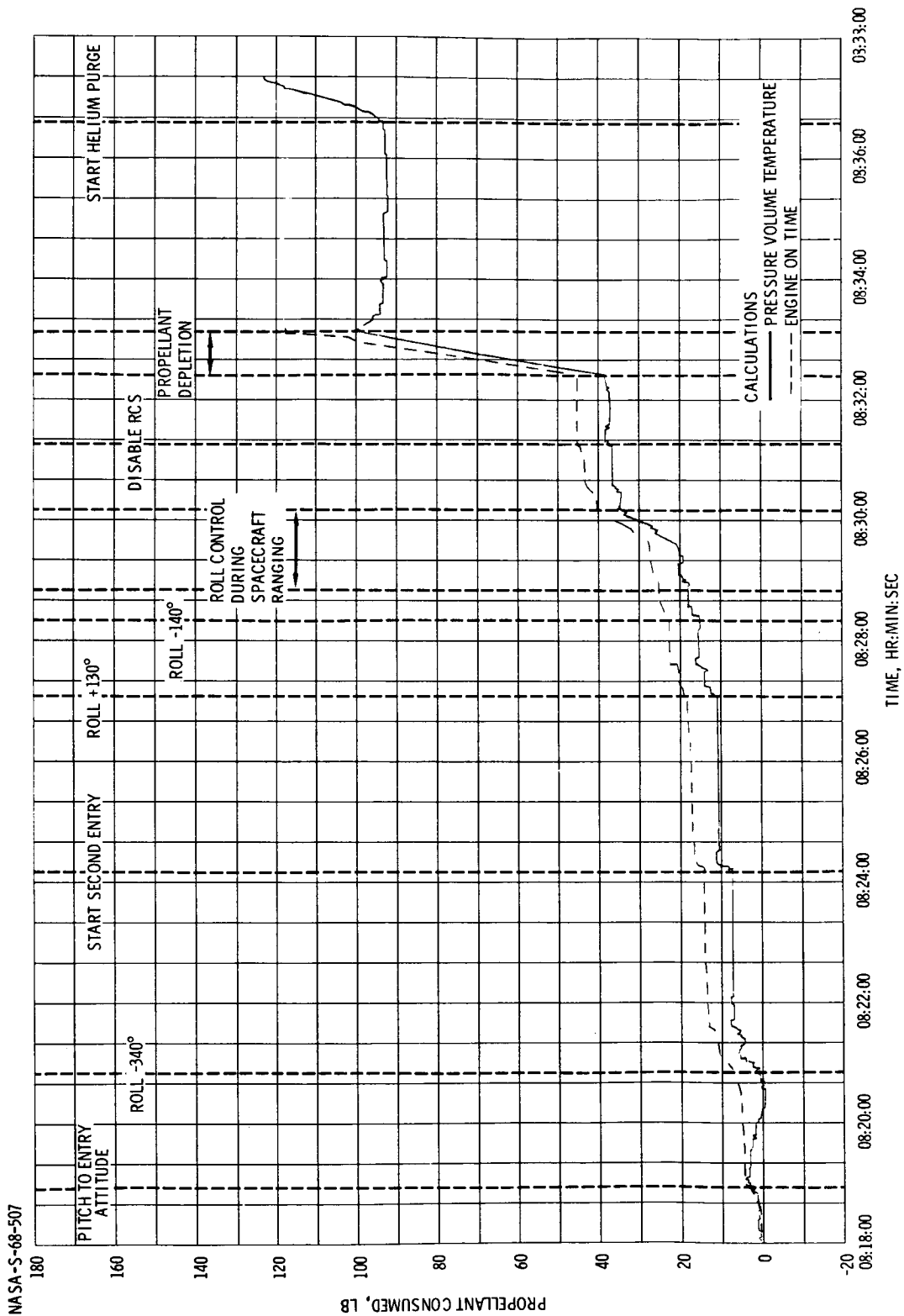
FIGURE 5.16-12. - AVERAGE BURN TIME ACCUMULATED DURING COMMAND MODULE REACTION CONTROL SUBSYSTEM ACTIVITY.

~~CONFIDENTIAL~~



5.16-42

~~CONFIDENTIAL~~



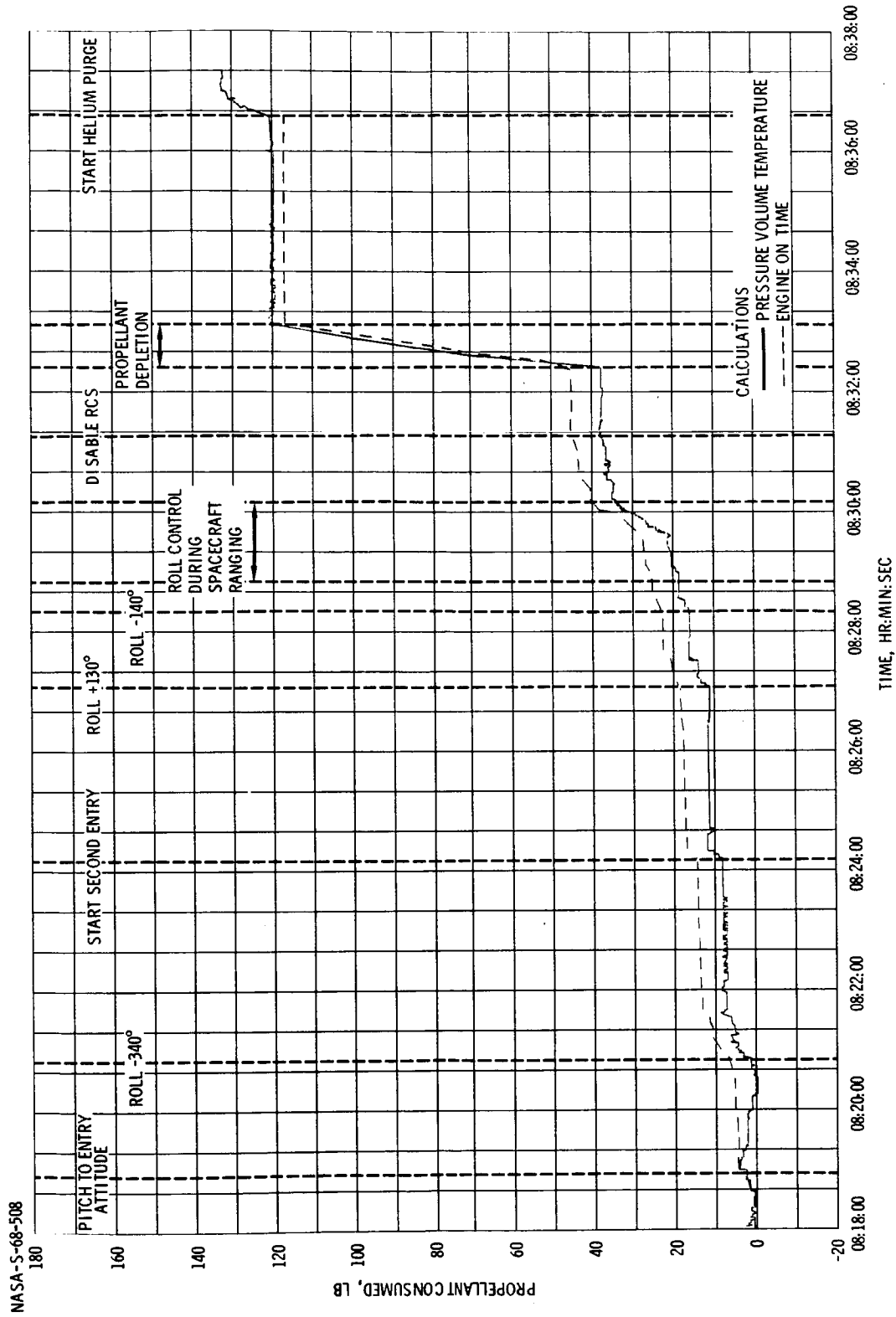
(A) SYSTEM A CONSUMPTION.

FIGURE 5.16-13.- COMMAND MODULE REACTION CONTROL SUBSYSTEM PROPELLANT CONSUMPTION.

~~CONFIDENTIAL~~

~~CONFIDENTIAL~~

5.16-43



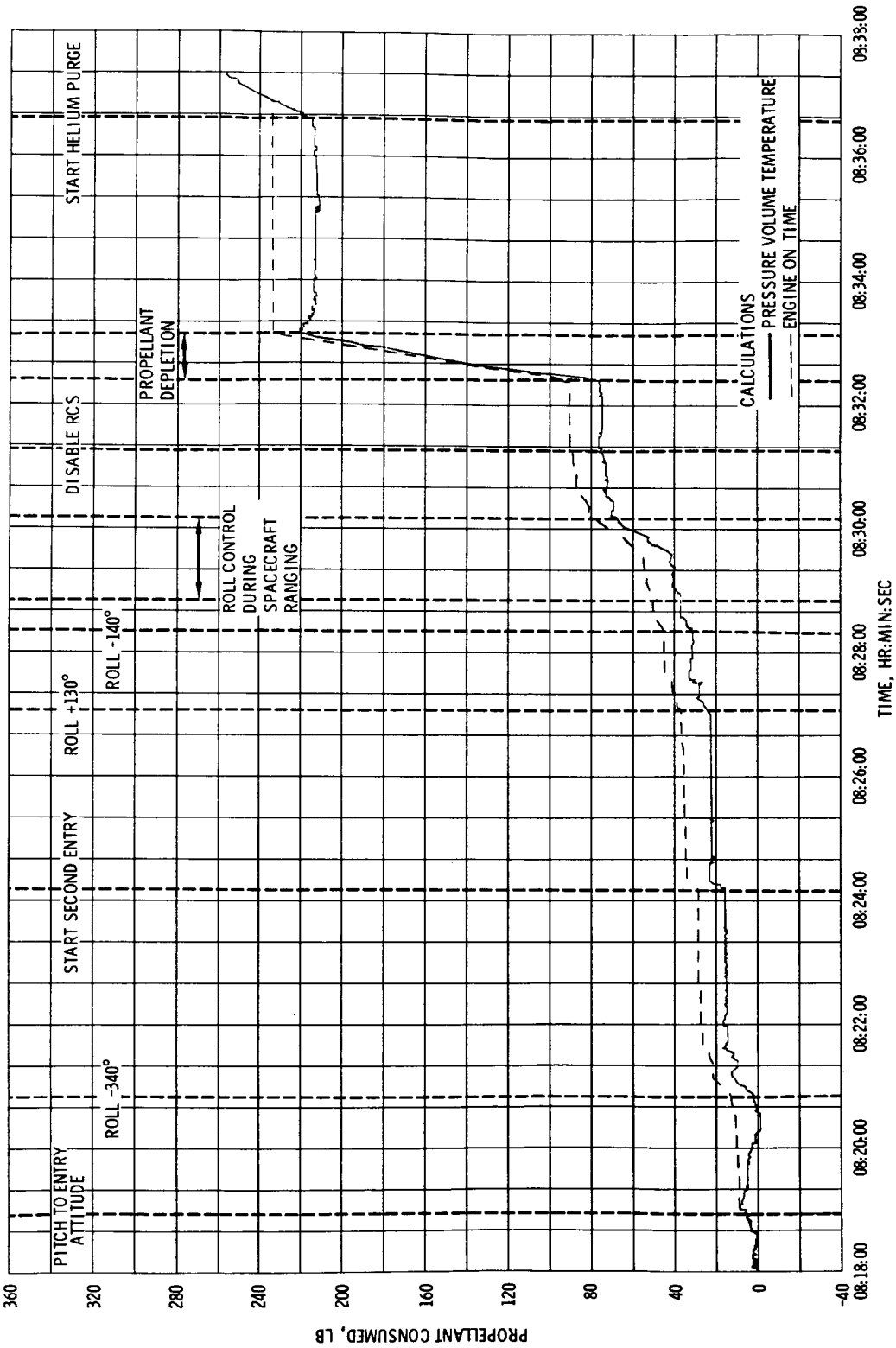
(B) SYSTEM B CONSUMPTION.

FIGURE 5.16-13. - CONTINUED.

~~CONFIDENTIAL~~

~~CONFIDENTIAL~~

NASA-S-68-509



(C) TOTAL COMMAND MODULE REACTION CONTROL SUBSYSTEM CONSUMPTION.

FIGURE 5.16-13, - CONCLUDED.

~~CONFIDENTIAL~~

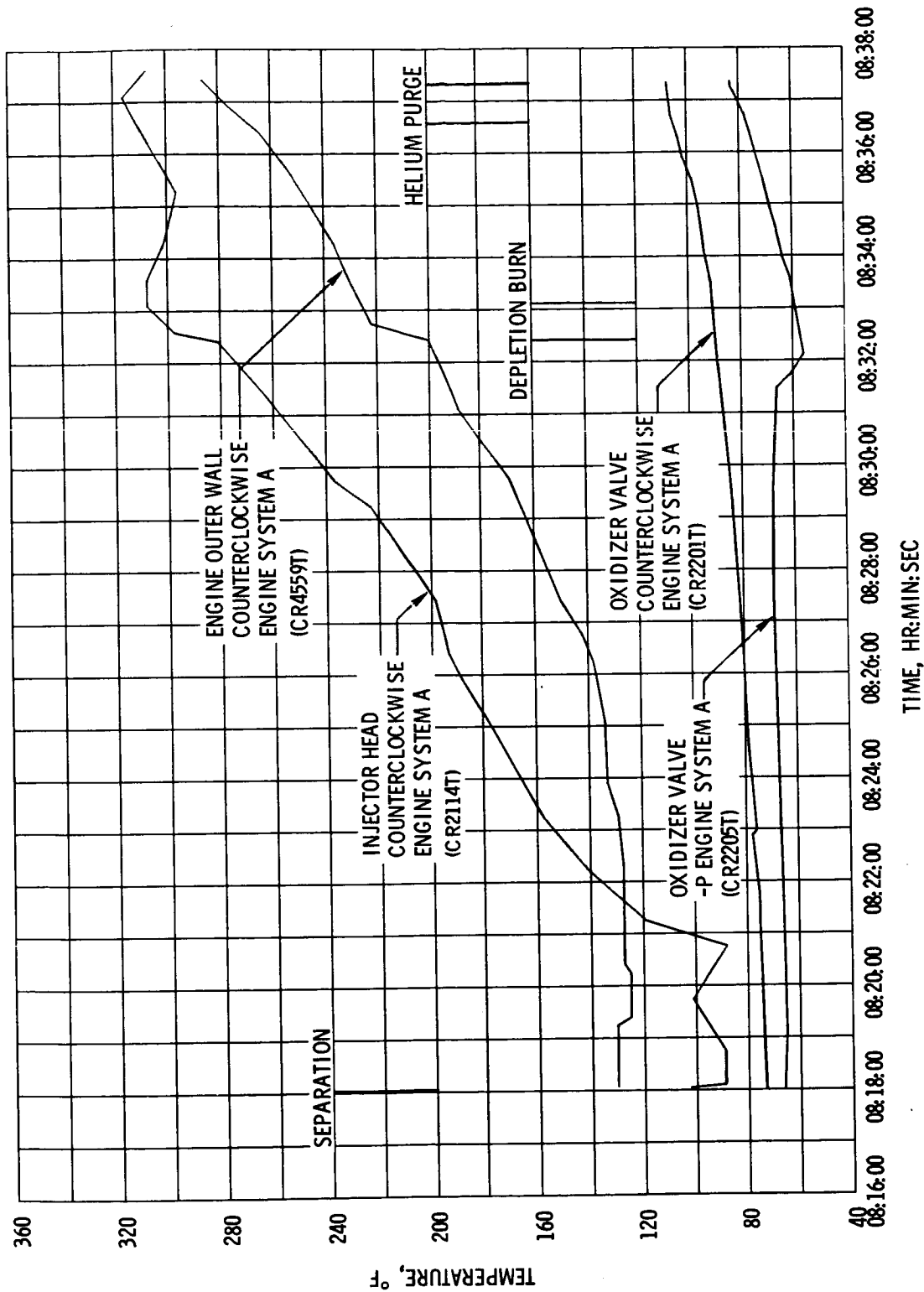


FIGURE 5.16-14. - TYPICAL COMMAND MODULE REACTION CONTROL SUBSYSTEM ENGINE COMPONENT TEMPERATURES DURING ENTRY.

5.16-46

~~CONFIDENTIAL~~

THIS PAGE INTENTIONALLY LEFT BLANK

~~CONFIDENTIAL~~

~~CONFIDENTIAL~~

5.17-1

## 5.17 SERVICE PROPULSION SUBSYSTEM

The primary SPS test objectives were to demonstrate a satisfactory no-ullage start and to determine subsystem performance during a long duration burn. The Apollo 4 mission plan called for two SPS burns; a short burn of approximately 15 seconds duration followed by a long burn of approximately 271 seconds duration. The no-ullage start was to be demonstrated on the first burn. These test objectives were satisfied.

The performance of the service propulsion subsystem (SPS) was analyzed and found to be within specification requirements and the expected tolerances. Engine flight performance, corrected to the standard inlet condition, resulted in a thrust of 21 483 pounds, a specific impulse of 311.6 seconds, and a propellant mixture ratio (O/F) of 2.008. These values are 0.08 percent lower, 0.42 percent lower, and 0.4 percent higher, respectively, than the acceptance test log results, but are well within the allowable variations.

### 5.17.1 Subsystem Description

The following are the major SPS hardware and flight configuration differences from the two previous missions (AS 201 and AS 202 missions) on which the SPS has been flown.

The propellant storage tanks were partially loaded. On previous flights, propellants were only in the sump tanks. The partial load in the storage tanks made possible the longest duration SPS flight burn to date (approximately 282 seconds). During this burn, the effects of storage tank depletion (propellant crossover) on SPS performance could be assessed for the first time.

Propellant retention screens were installed in the bottom of the propellant sump tanks, and these, in conjunction with the propellant retention reservoirs also located there, permitted the first demonstration of a SPS no-ullage start.

The flight combustion stability monitor was flown in the activated condition for the first time. However, the monitor was made inoperative during the second burn when the guidance and navigation mode of operation was overridden by the backup ground command.

The gauging system was in the primary mode during the flight and telemetered primary gauging data during each SPS burn. This was the first opportunity to obtain flight data from the primary gauging system in the propellant storage tanks.

~~CONFIDENTIAL~~

~~CONFIDENTIAL~~

## 5.17.2 Propellant Loading

The oxidizer storage tank was filled by overflowing the sump tank through the crossover line at a flow rate of approximately 60 gallons per minute. The trapped sump helium ullage gas was being entrained by the oxidizer that was being transferred and resulted in a sump ullage pressure decrease with a corresponding propellant level rise of about 3 inches above the standpipe in the sump tank. As a consequence, more oxidizer was loaded than planned. Based on the analysis of the storage tank primary gauging system, the sump tank propellant level was raised at pressurization approximately 6 inches above the standpipe. This level was above the maximum gaugeable level of the sump primary gauging probe. The oxidizer sump ullage volume was reduced from approximately 5.50 cu ft to approximately 3.46 cu ft.

The fuel storage tank servicing rate was reduced from 60 to 15 gal/min. This alleviated the helium entrainment problem on the fuel side. The resulting propellant loading was as follows.

	Oxidizer, lb		Fuel, lb	
	Planned	Actual	Planned	Actual
Storage tank <sup>a</sup>	-	4 643	-	2 278
Sump tank <sup>a</sup>	-	15 549	-	7 795
Total	20 077	20 192	10 022	10 073

<sup>a</sup>Includes gaugeable and nongaugeable quantities.

Eight oxidizer, nitrogen tetroxide ( $N_2O_4$ ), density samples at 39.2° F and three fuel, Aerozine (A-50), density samples at 77° F were measured. The mean density for  $N_2O_4$  was 1.4830 gm/ml (92.581 lbm/ft<sup>3</sup>) at 39.2° F. The mean density for A-50 was 0.90047 gm/ml (56.215 lbm/ft<sup>3</sup>) at 77° F.

## 5.17.3 Service Propulsion Subsystem Mission Description

After CSM/S-IVB separation, the CSM was reoriented from the cold soak attitude to the ignition attitude for the first SPS burn. SPS ignition for the first burn occurred at 03:28:06.6, following an attitude hold

~~CONFIDENTIAL~~

~~CONFIDENTIAL~~

5.17-3

phase of approximately 61 seconds. Since there were no propulsive events during the attitude-hold phase preceding the first SPS burn, the mission requirement of a no-ullage start was satisfied.

The first SPS burn lasted 16 seconds with cutoff by guidance and navigation command at 03:28:22.6. A service module reaction control subsystem ullage maneuver was initiated 30 seconds prior to second SPS ignition. The second burn ignition was initiated by guidance and navigation command at 08:10:54.8. Subsequently, a redundant direct thrust-on was commanded from the ground and disabled the SPS thrust ON/OFF command capability of the guidance and navigation subsystem. The SPS thrust ON ground command required that SPS thrust OFF be also commanded from the ground. The second SPS thrust OFF was initiated by ground command at 08:15:35.4. The burn duration was 10.1 seconds longer than planned, resulting in a velocity gain that was higher than planned.

#### 5.17.4 Steady-State Performance and Analysis

The major analysis effort for this report was concentrated on determining the subsystem performance during that period of the mission from storage tank depletion (or crossover) to cutoff of the second SPS burn.

The determination of the SPS performance during the portion of the second burn following crossover was accomplished by utilizing the Apollo propulsion flight analysis computer program. The program utilizes a weighted, least-squares technique in conjunction with all of the available data from the flight and from previous static tests, in addition to the physical laws which describe the behavior of the propulsion and propellant subsystems and their interaction with the spacecraft. The program embodies error models for the various flight and static test data used as inputs, and, by iteration methods, arrives at estimations of the subsystem performance history, initial propellant weights, and spacecraft weight which best reconcile the available data.

The program results presented in this report were based on simulations using data from the flight measurements listed in table 5.17-I. The initial estimate of the spacecraft weight without SPS propellants was the latest estimate as of November 30, 1967. The initial estimates of the propellant weights onboard at the beginning of the time period analyzed were extrapolated from the loaded weights discussed in the propellant loading section.

The questionable nature of the propellant utilization and gauging data as caused by data stabilization during the initial portion of the long burn, and the special problems associated with modeling subsystem performance during crossover precluded the possibility of a precise

~~CONFIDENTIAL~~



~~CONFIDENTIAL~~

determination of the performance prior to crossover. A more precise determination will be made upon completion of later detailed analysis. Propellant utilization and gauging data problems and the short burn time made inconclusive a detailed determination of performance during the first SPS burn for the same reasons.

The results of the analysis program simulation of the second burn from 105 to 275 seconds are contained in table 5.17-II. This 170-second portion of the burn occurred subsequent to propellant crossover. The values shown in table 5.17-II represent results at 79.2 seconds into the 170-second period, or at 08:13:59. These data are representative of the values throughout the portion of the burn analyzed. Thrust during the time period analyzed was between 21 381 and 21 414 pounds, specific impulse was between 311.2 and 311.4 seconds, and oxidizer/fuel (O/F) mixture ratio varied from 2.014 to 2.001.

The time histories of the measured chamber pressure (SP0661P) during both SPS burns is shown in figure 5.17-1. The chamber pressure calculated from the analysis program was 0.1 to 0.7 psi higher than the measured chamber pressure. This slight bias is well within the stated accuracy of 3 percent of full scale. Modifications made in the transducer mounting to correct problems associated with the thermal environment that appeared in the AS 202 mission data were satisfactory.

The program simulation also indicated that small biases of approximately +1.3 and +0.2 psi may have existed in the oxidizer and fuel inlet pressure measurements, respectively.

The simulation verified the initial estimate of the spacecraft weight, requiring only a 22-pound adjustment to the value used. The reported propellant loaded weights discussed in the propellant loading section were confirmed.

A strong indication of the accuracy of the analysis program simulation can be obtained by comparing the thrust acceleration calculated in the simulation to that derived from the Apollo guidance computer  $\Delta V$  data. The thrust acceleration during the portion of the burn analyzed, as derived from the Apollo guidance computer data, and the residual error between the Apollo guidance computer and program-calculated values are shown in figure 5.17-2. The residual error time history is shown to have nearly a zero mean and little, if any, discernible trend; this indicates that the simulation was valid.

The program-calculated performance parameters compared with their predicted values are shown in table 5.17-II. The calculated values of thrust, specific impulse, and engine mixture ratio were within 0.25 percent, 0.03 percent, and 0.90 percent, respectively, of their predicted

~~CONFIDENTIAL~~

~~CONFIDENTIAL~~

5.17-5

values. These differences are considered quite acceptable and well within the expected tolerances.

Although a detailed performance determination could not be accomplished for the short burn or the portion of the long burn prior to crossover, a review of the available data indicates performance and operation of the SPS during those portions of the mission were satisfactory. The chamber pressure histories (fig. 5.17-1) show no unexpected characteristics. The rise at crossover was predicted, although the magnitude of the increase indicated by the chamber pressure measurement (SP0661P) was slightly higher than predicted.

#### 5.17.5 Normalized Performance

Engine performance corrected to standard inlet conditions yielded a thrust of 21 483 pounds, a specific impulse of 311.6 seconds, and a propellant mixture ratio of 2.008. These values are 0.08 percent lower, 0.42 percent lower, and 0.40 percent higher, respectively, than reported in the acceptance test log. These differences are within the expected ranges. The operational trajectory was generated using the following data from the acceptance test log: constant steady-state thrust of 21 500 lb, specific impulse of 312.9 seconds, and a mixture ratio of 2.0. The standard inlet conditions performance values reported herein were calculated for the following conditions.

Oxidizer interface pressure	164 psia
Fuel interface pressure	170 psia
Oxidizer interface temperature	70° F
Fuel interface temperature	70° F
Oxidizer density	90.15 lbm/ft <sup>3</sup>
Fuel density	56.31 lbm/ft <sup>3</sup>
Thrust acceleration	1.0
Throat area (initial value)	121.66 sq in.

#### 5.17.6 Gauging Subsystem Analysis

The propellant utilization and gauging subsystem was operated in the primary mode. A bias in the propellant utilization and gauging subsystem

~~CONFIDENTIAL~~

~~CONFIDENTIAL~~

is normal because of a difference in liquid levels in the propellant sump tanks and inside the gauging system stillwell. The stillwell is a manometer which balances the pressure at the bottom of the stillwell with a fluid head. Under nonflow conditions, this fluid head is equivalent to the level of propellant in the tank. However, when the propellant is flowing, the fluid head in the stillwell is reduced by the dynamic head of the propellant flowing by the bottom of the stillwell through the zero-gravity retention reservoir. Data were not available for the gauging system for the first 6 to 10 seconds of the two burns; consequently, it was difficult to analyze the bias effect.

The first burn was a no-ullage start. As a result, there was slosh in the storage tanks for at least 4 seconds. The storage tank gauging system was very erratic for both fuel and oxidizer during the first burn and was apparently affected by the slosh. The flow-rate readings were approximately 25 percent high. During the second burn the storage tank gauging system appeared normal except both fuel and oxidizer systems indicated a bias of +100 pounds at the time of storage tank depletion.

After storage tank depletion, or crossover, the sump tank gauging probes indicated a lag in response. The gauging output was constant until approximately 4 seconds after crossover, which was indicated by engine inlet pressure increase. After the sump probes started to respond, an unusually high propellant flow rate was indicated for about 16 seconds for oxidizer and about 6 seconds for fuel. The values then stabilized and decreased linearly for the remainder of the burn. The observed characteristics are similar to the effects that would be anticipated from a time lag in either the liquid level in the stillwell or in the response of the capacitance system servo-activator. Similar characteristics of the gauging subsystem were observed during the AS 202 mission.

During sump tank depletion, but after stabilization, the gauging system results appeared normal. After accounting for the bias change with acceleration, the oxidizer flow rate derived from the gauging system agreed with the performance calculated flow rate within 0.5 percent and the fuel flow rate within 1.0 percent. Both gauging system values were lower than the calculated performance values.

#### 5.17.7 Pressurization Subsystems

Both SPS pressurization subsystems operated nominally throughout the mission. Helium bottle pressure and temperature data showed a constant, nominal helium expulsion during both SPS burns and there was no indication of helium leakage during the intermediate coast period. The propellant ball valve telemetered data indicated that both valve banks for the gaseous nitrogen subsystem operated nominally during the two SPS burns

~~CONFIDENTIAL~~

~~CONFIDENTIAL~~

5.17-7

and no pressure loss occurred from the gaseous nitrogen bottles during the coast period.

#### 5.17.8 Engine Transient Analysis

An analysis of the start and shutdown transients was performed to determine the transient impulse and time-variant performance characteristics during the mission and to ascertain the effectiveness of the no-ullage start. The results of this analysis, which encompassed the transient regimes for both SPS burns, are summarized in table 5.17-III. Engine acceptance test data, specification requirements, and previous spacecraft flight data were used to provide a better interpretation of the Apollo 4 flight test results and the applicability of these results to subsequent flight development missions and the lunar landing mission.

All transient specification criteria appeared to have been satisfied, except for the shutdown impulse repeatability and chamber pressure overshoot during start. The difference between the shutdown impulses from the two burns was approximately 1989 lb-sec. This exceeds the allowable tolerance for repeatability of 300 lb-sec. However, there is an uncertainty of  $\pm 0.1$  second on actual initiation of the shutdown signal for the second burn which results in an uncertainty of 2150 lb-sec impulse.

The chamber pressure overshoot during the first burn start transient was observed to be 49.5 percent above the nominal steady-state level. This overshoot is similar to those experienced during previous flights. The chamber pressure overshoot and valve response times denoted on these first three spacecraft development missions are shown in table 5.17-IV.

Analyses of the Apollo 4 first SPS start regimes indicate that the chamber pressure overshoot did not appear to be linked to the no-ullage start, but rather a function of the response times of the valve. Although the second start, which was preceded by an ullage maneuver, was characterized by a 15-percent lower overshoot, this reduction can be explained by the valves responding slower on the second burn. The magnitude of the overshoot is an inverse function of valve response time. The phenomenon of less rapid response on subsequent burns has been also noted on the AS 202 mission. A satisfactory explanation for this phenomenon is pending an evaluation of the environmental influences upon valve behavior. The valve used in the Apollo 4 mission had a faster response time than did valves used in previous missions and such could be the basis for an explanation of the characteristically higher overshoot obtained in this flight.

~~CONFIDENTIAL~~

~~CONFIDENTIAL~~

TABLE 5.17-I.- FLIGHT DATA USED IN THE ANALYSIS PROGRAM

Measurement no.	Description	Data range
SP0009P	Main Valve, Engine Oxidizer Inlet Pressure	0 to 300 psia
SP0010P	Main Valve, Engine Fuel Inlet Pressure	0 to 300 psia
SP0655Q	Oxidizer Tank no. 1 Primary Quantity	0 to 16 000 lb
SP0656Q	Oxidizer Tank no. 2 Primary Quantity	0 to 16 000 lb
SP0657Q	Fuel Tank no. 1 Primary Quantity	0 to 8000 lb
SP0658Q	Fuel Tank no. 2 Primary Quantity	0 to 8000 lb
SP0661P	Engine Chamber Pressure	0 to 150 psia
CG0001V	Computer Digital Data	40 bits

~~CONFIDENTIAL~~

CONFIDENTIAL

5.17-9

TABLE 5.17-II.- SERVICE PROPULSION SUBSYSTEM PERFORMANCE SUMMARY, APOLLO 4 MISSION

Mission description	VALUE						
	SPS FIRST BURN			SPS SECOND BURN <sup>a</sup>			
	Nominal	Measured	Actual <sup>b</sup>	Preflight <sup>c</sup> prediction	Measured	Actual <sup>d</sup>	Preflight prediction
SP 0003 - Oxidizer tank pressure, psia	Approximately 179	175	NA	179	176	181.5	179
SP 0006 - Fuel tank pressure, psia	Approximately 179	179	NA	179	175	184.2	179
SP 0009 - Oxidizer inlet pressure, psia	Approximately 154	153.5	NA	152	158.8	157.4	156
SP 0010 - Fuel inlet pressure, psia	Approximately 154	154.0	NA	155	158.6	158.4	158
SP 0661 - Engine chamber pressure, psia	Approximately 100	96.0	NA	98.2	101.0	101.2	99.9
Calculated performance parameters							
Oxidizer flow rate, lb/sec	Approximately 45.8	--	NA	44.56	--	45.86	45.57
Fuel flow rate, lb/sec	Approximately 22.9	--	NA	22.67	--	22.83	22.91
Propellant mixture ratio	2.00 (+1%)	--	NA	1.96	--	2.008	1.99
Vacuum specific impulse, sec	313 min	--	NA	311.7	--	311.4	311.5
Vacuum thrust, lb	21500 (+1%)	--	NA	20 958	--	21 388	21 334

<sup>a</sup>After propellant crossover.<sup>b</sup>Not available due to short burn duration.<sup>c</sup>MSC Internal note MSC-EP-R-67-33, AS-501 SPS Preflight Report, October 11, 1967.<sup>d</sup>Actual values from Apollo Propulsion Flight Analysis Computer Program.

CONFIDENTIAL

~~CONFIDENTIAL~~

TABLE 5.17-III.- SERVICE PROPUSSION SUBSYSTEM ENGINE TRANSIENT ANALYSIS SUMMARY

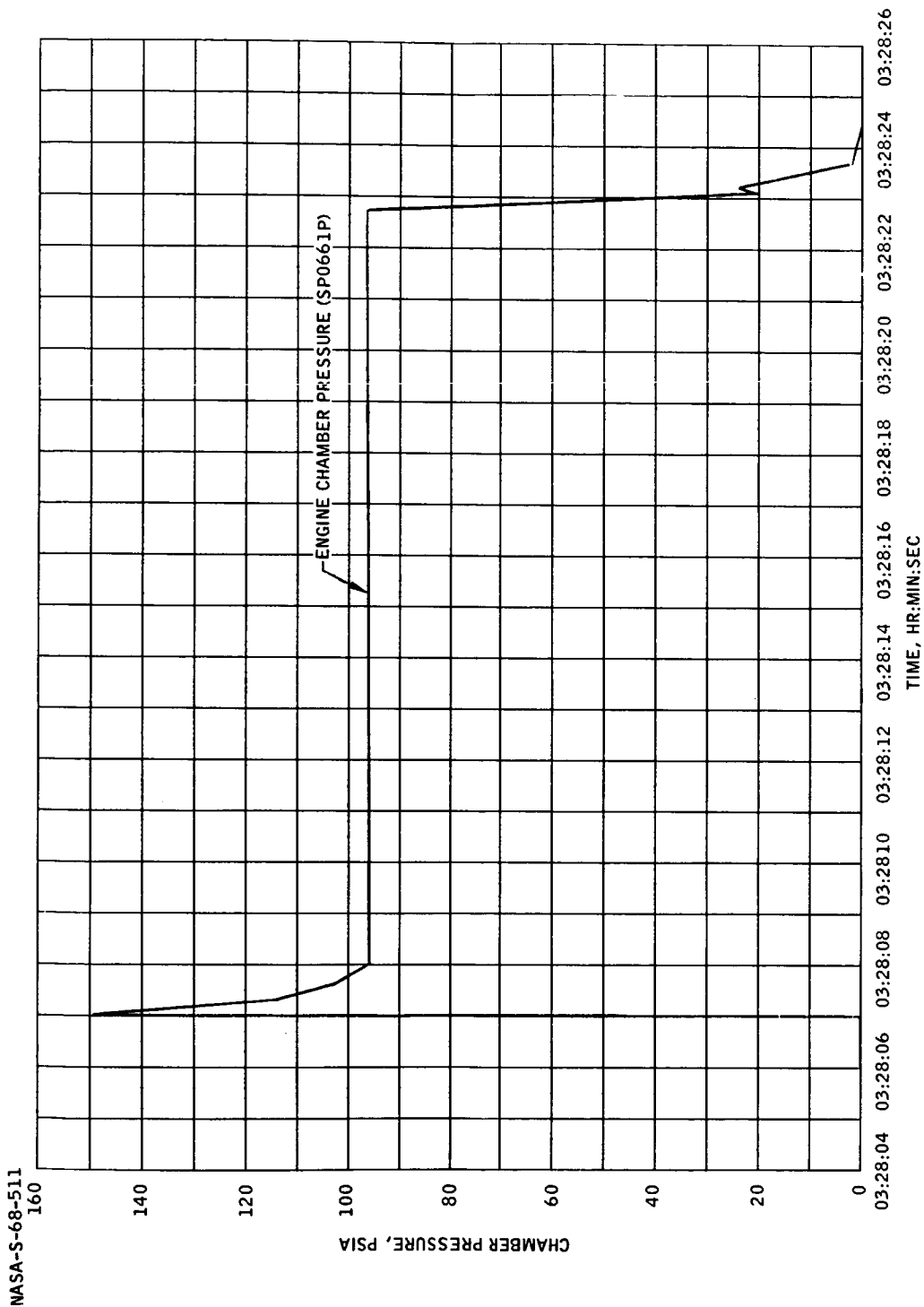
	Apollo 4 first burn	Apollo 4 second burn	Apollo 4 SPS engine 031 accept- ance test	AS-202 first burn	AS-202 fourth burn	Specification values
Start transient total vacuum impulse from engine start signal (FS-1) to 90 percent steady state thrust, lb <sub>f</sub> -sec	135.2	264.4	227	--	--	100 to 400
Time from engine start signal (FS-1) to 90 percent steady state thrust, sec	0.41	0.35	0.351	--	--	0.350 to 0.550
Engine run to run start repeatability, lb <sub>f</sub> -sec	+65	+65	--	--	--	+100
Shutdown transient total vacuum impulse from engine shutdown signal (FS-2) to 10 percent steady state thrust, lb <sub>f</sub> -sec	10 083.8	11 910.8	9450	--	--	8000 to 13 000
Time from engine shutdown signal (FS-2) to 10 percent steady state thrust, sec	0.82	0.89	0.751	--	--	0.650 to 0.900
Engine run to run shutdown repeatability, lb <sub>f</sub> -sec	a <sub>1</sub> 995	a <sub>1</sub> 995	--	--	--	+300
Shutdown transient total vacuum impulse from engine shutdown signal (FS-2) to zero percent thrust, lb <sub>f</sub> -sec	11 122.27	12 275.7	--	10 700	10 000	--
Time from engine shutdown signal (FS-2) to zero percent thrust, sec	1.79	1.50	--	--	--	--

<sup>a</sup>Indicated repeatability may have a significant error because of uncertainty in actual shutdown time of second burn.

~~CONFIDENTIAL~~

~~CONFIDENTIAL~~

5.17-11

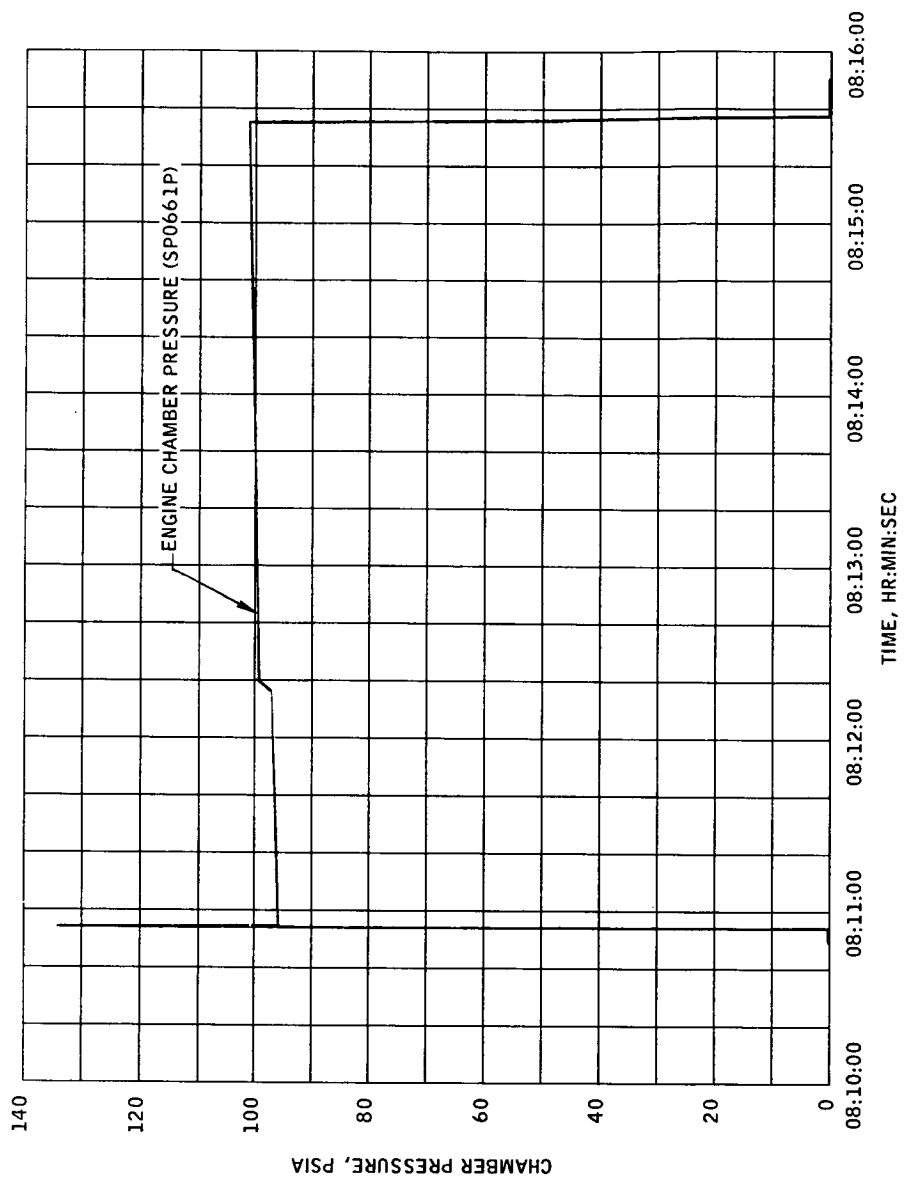


(A) FIRST BURN.

FIGURE 5.17-1.- SERVICE PROPULSION SUBSYSTEM CHAMBER PRESSURE DATA.

~~CONFIDENTIAL~~



~~CONFIDENTIAL~~

(B) SECOND BURN.

FIGURE 5.17-1.- CONCLUDED.

~~CONFIDENTIAL~~

~~CONFIDENTIAL~~

5.17-13

NASA-S-68-513

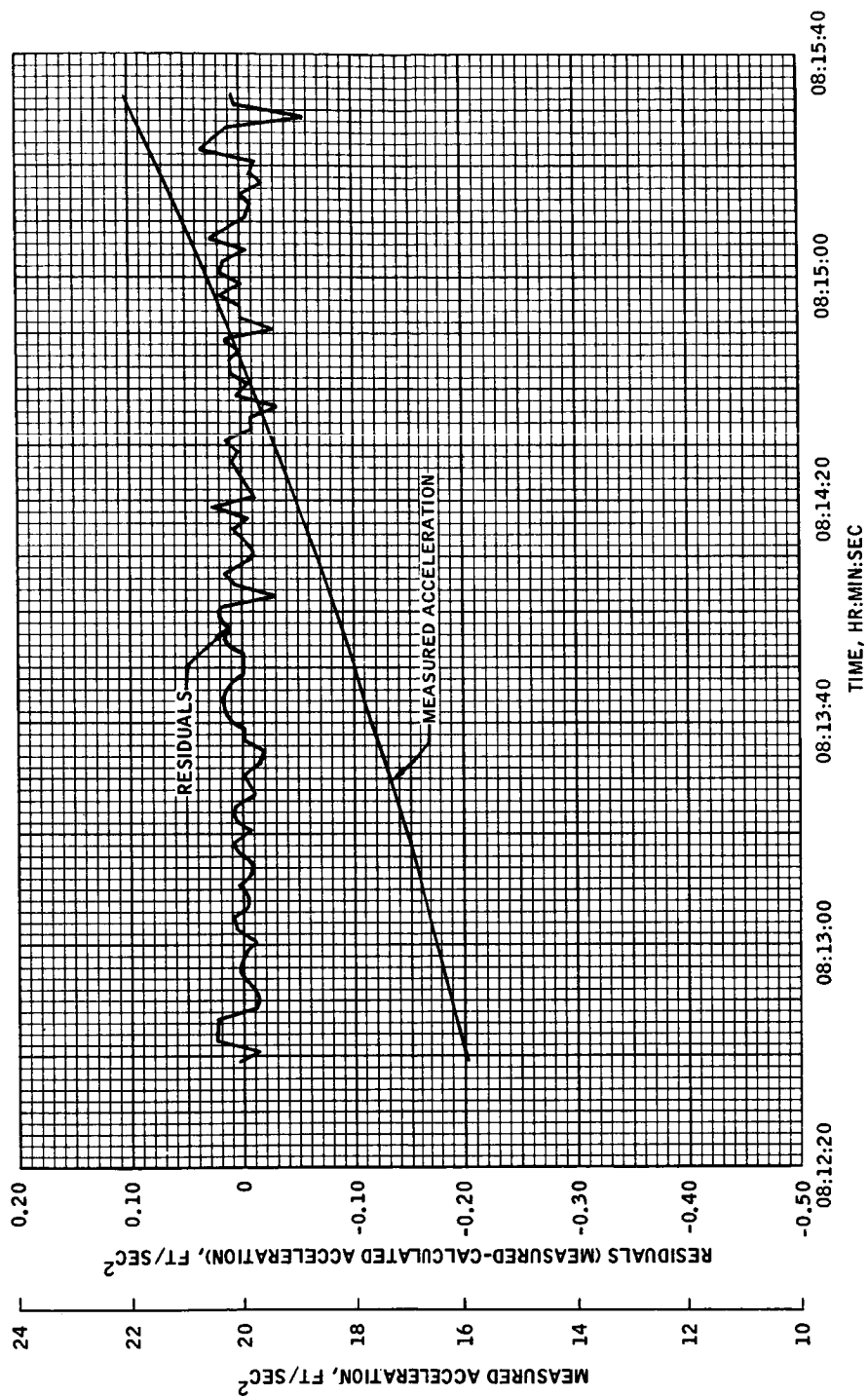


FIGURE 5.17-2.- SERVICE PROPUSSION SUBSYSTEM SECOND BURN ACCELERATION MATCH.

~~CONFIDENTIAL~~

5.17-14

~~CONFIDENTIAL~~

THIS PAGE INTENTIONALLY LEFT BLANK

~~CONFIDENTIAL~~

~~CONFIDENTIAL~~

5.18-1

## 5.18 CRYOGENIC SUBSYSTEM

### 5.18.1 Summary

The cryogenic storage subsystem successfully supplied gaseous reactants to the three fuel cell powerplants and gaseous oxygen to the environmental control subsystem. All flight objectives were met. These included extended zero-g operation of the cryogenic storage subsystem, equal depletion, pressure control, stratification control, and satisfactory system performance during the launch environment, CSM/S-IVB separation, and service propulsion subsystem operation.

### 5.18.2 Prelaunch Operations

Hydrogen tanks no. 1 and no. 2 were serviced to 27.7 and 28.0 pounds, respectively, at 35 hours prior to launch. Approximately 1 hour later, the hydrogen tanks were pressurized with 70° F gas and a rough quantity adjustment was made to 18.6 and 18.7 pounds, respectively. A fine quantity adjustment was not required for the hydrogen tanks because the rough adjustment provided the desired quantities. Both hydrogen tanks exhibited high pressures and excessive flow rate after servicing, resulting from the tanks not being chilled prior to servicing. The pressures increased sufficiently to cause both tanks to vent during the countdown. The flow rates dropped to a normal level approximately 24 hours after servicing, and the pressures started to show a downward trend when the fuel cells were placed on load. Approximately 30 hours prior to launch, oxygen tanks no. 1 and no. 2 were serviced to 320.9 and 323.0 pounds, respectively. Approximately 2 hours later, the oxygen tanks were pressurized with 70° F gas and fine quantity adjustments were made to 188.9 and 189.6 pounds, respectively.

Approximately 25 hours prior to launch, oxygen tank no. 2 experienced a pressure decay to 680 psia. Attempts to energize the heaters in oxygen tank no. 2 by switch positioning were unsuccessful. During additional heater circuit checkout procedures, the circuit breaker for oxygen tank no. 2 heaters was found to be open. The circuit breaker was closed just prior to cabin close-out. At cabin close-out, the heaters and fan controls for hydrogen tanks no. 1 and no. 2 and oxygen tank no. 1 were positioned in the AUTO mode. The oxygen tank no. 2 fan controls were in the AUTO mode and the heater control was placed in the OFF position. A decision was made to launch with oxygen tank no. 2 heater switch in the OFF position rather than oxygen tank no. 1 heater switch in the OFF position because of the difficulty experience with oxygen tank no. 2 heater control.

~~CONFIDENTIAL~~

~~CONFIDENTIAL~~

A real time command (RTC) was given through the MCP at T minus 9 hours 42 minutes to energize the heaters and fans in oxygen tank no. 2. An OFF command was sent 1 hour later. The pressure rose from 680 psia to 850 psia during the 1-hour period. Therefore, the previous difficulty experienced with tank no. 2 heaters is attributed to an inadvertent open circuit breaker.

At T minus 1 hour, the pressure in oxygen tank no. 2 had risen to 925 psia as a result of normal ambient  $O_2$  heating and it started to share the flow demand with oxygen tank no. 1. During the flight, control of this oxygen tank was performed through the mission control programmer (MCP). This action was taken for contingency planning to prevent overloading the electrical bus either by actuation of the oxygen tank heaters (370-watt load) during a service propulsion subsystem burn or by the loss of one fuel cell which would have resulted in the other two supporting all the electrical loads.

### 5.18.3 Performance

A plot of the general oxygen tank performance is presented in figure 5.18-1. Oxygen tank no. 1 performed within the specification limits throughout the prelaunch and flight phases of the mission. During flight, the oxygen tank no. 2 pressure-rise rate during RTC heater cycling was approximately the same as attained during prelaunch operations and was comparable to the rate exhibited by oxygen tank no. 1. It is concluded that the heaters for oxygen tank no. 2 functioned as designed and when activated by RTC provided the thermal energy required to maintain the tank at operating pressure.

After launch, both tanks performed normally until the first heater cycle at 02:00:00. At that time the fans came on automatically for oxygen tank no. 2, and the pressure dropped from 860 to 740 psia. This drop can be attributed to normal fluid thermal stratification which occurs in a cryogenic system during non-equilibrated periods especially in the prelaunch, gravity environment. During automatic operation, the normal heater and fan cycles will prevent this occurrence as shown by the oxygen tank no. 1 automatic heater and fan performance. The heaters and fans in oxygen tank no. 2 were energized by RTC at 02:31:21, and the heater and fans in oxygen tank no. 1 were energized by RTC at 02:34:14. The heaters and fans for both tanks were deenergized at 03:23:05. The pressures rose to nominal values and remained within operating limits for the remainder of the mission.

Tank temperature data were erratic throughout the flight for the following measurements:

- a. SF0041T - Oxygen tank 1 temperature

~~CONFIDENTIAL~~

~~CONFIDENTIAL~~

5.18-3

- b. SF0042T - Oxygen tank 2 temperature
- c. SF0043T - Hydrogen tank 1 temperature

The same symptoms were experienced during the countdown demonstration test. Subsequent testing revealed the presence of low-frequency noise on the signal-conditioner output signal. Capacitors will be included in Block II spacecraft (CSM 103 and subsequent) to filter out the noise interference.

Tank quantity depletion data agreed with the fuel cell reactant consumption data and with preflight predictions. A summary of the oxygen and hydrogen used from the cryogenic gas supply system (CGSS) during the flight to support both fuel cell and the environmental control subsystem (ECS) is shown in the following table:

	Hydrogen, lb		Oxygen, lb	
	Tank 1	Tank 2	Tank 1	Tank 2
Quantity at lift-off	12.5	12.7	156	181
Quantity at SM separation	11.7	11.8	146	173
Quantity used in flight	0.8	0.9	10	8

~~CONFIDENTIAL~~

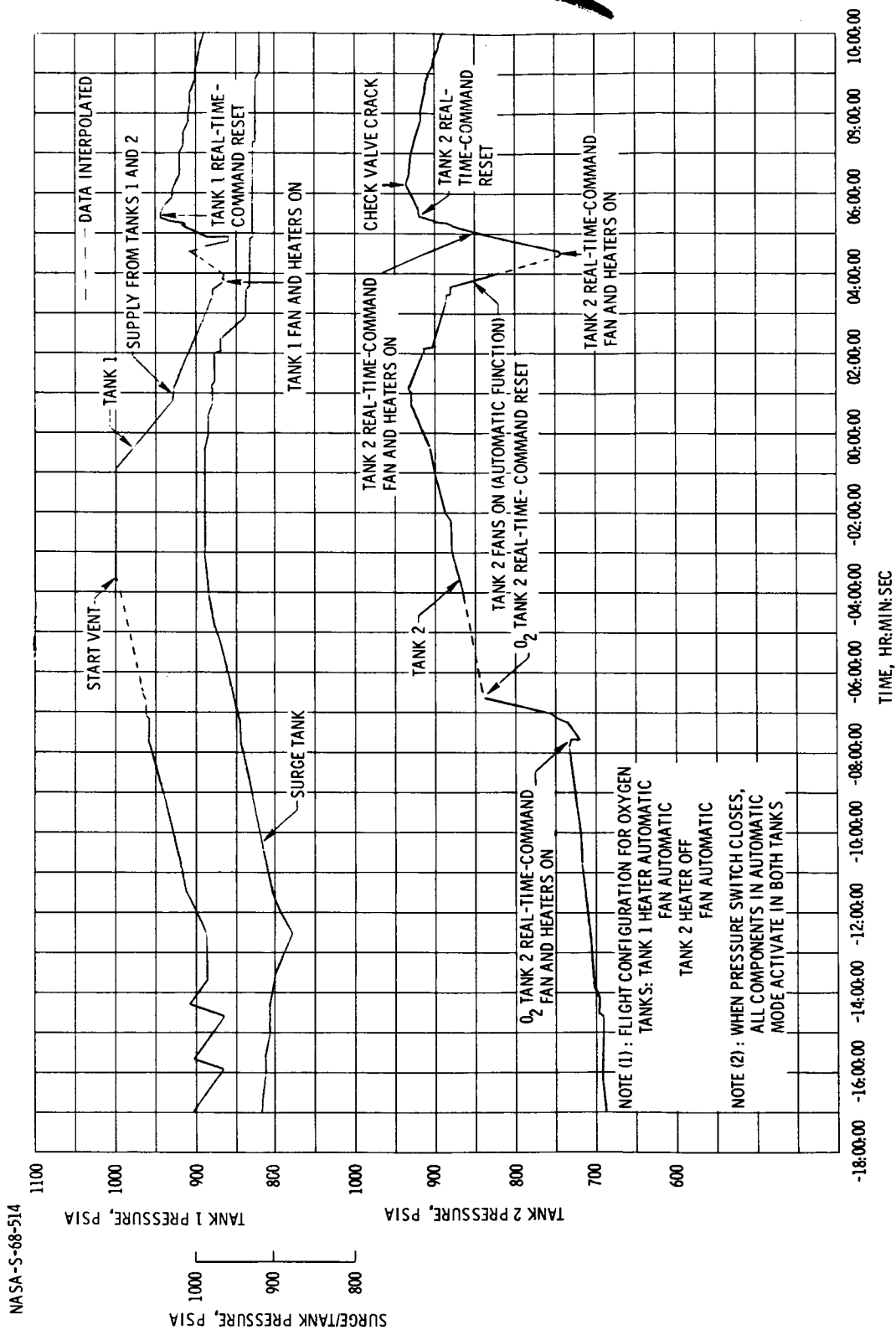
~~CONFIDENTIAL~~

FIGURE 5.18-1. - OXYGEN TANK PRESSURE AND EVENTS.

~~CONFIDENTIAL~~

~~CONFIDENTIAL~~

5.19-1

## 5.19 ENVIRONMENTAL CONTROL SUBSYSTEM

### 5.19.1 Launch Phase

Thermal control of the CM equipment was provided by circulating the heat transport fluid from the cabin heat exchanger and thermal coldplate network to the glycol evaporator. The mission control programmer (MCP) closed the motorized water-glycol isolation valve at lift-off minus 75 seconds, as planned, placing the water-glycol circuit on the internal circulation mode. The evaporator outlet temperature (CF0018T) was 39° F at lift-off minus 75 seconds and increased to a maximum of 52° F before active cooling commenced at approximately 00:01:44. Active cooling began at this time as the altitude was sufficient to initiate water boiling from the evaporator wicks which had been serviced with approximately 0.8 lb water prior to flight. The back pressure control valve was pre-set and fixed at an approximate 40-percent open position. Active cooling by water boiling occurred when the back pressure within the evaporator was less than 0.25 psia. The MCP sent an enabling signal to the evaporator water inflow control valve at the time of tower jettison, 00:03:07. This enable signal permitted automatic water control valve operation in response to electrical signals from the ECS temperature controller. The evaporator outlet temperature dropped to 38° F during the initial evaporator startup period, then stabilized at an average temperature of 41° F for the remainder of the mission. Water boiling in the glycol evaporator provided the only means of thermal control during the mission.

The cabin temperature was 61.5° F at lift-off and remained constant during early ascent. The expansion of the cabin gas dropped the temperature to 54.1° F during cabin pressure relief valve operation.

The cabin pressure relief valve began relieving cabin pressure at approximately 00:00:52 as expected, and functioned satisfactorily. Because of the absence of an aft compartment pressure profile, the actual relief or crack pressure cannot be established. The barometric static pressure reference (CE0035P) is representative of the aft compartment pressure, but cannot be utilized because the measurement was out of calibration at launch. Postflight testing of this measurement may provide a corrected barometric pressure profile, and the relief and crack pressures can then be computed. The cabin pressure stabilized at 5.8 psia after cabin pressure relief valve seal-off at 00:08:38. The cabin pressure remained between 5.8 and 5.6 psia for the entire mission, indicating a low cabin leakage rate. This value results in a computed cabin leakage rate of approximately 0.03 lb/hr, which is well within the specification maximum leakage rate of 0.20 lb/hr. The oxygen surge

~~CONFIDENTIAL~~



~~CONFIDENTIAL~~

tank dropped a total of 25 psi for the flight and no appreciable demand was indicated by the oxygen flowmeter through the mission; both of these facts confirm negligible cabin leakage. The cabin pressure regulator was not required to operate since the cabin pressure did not bleed down to the pressure regulator control range of 5.0 ( $\pm 0.2$ ) psia.

#### 5.19.2 Earth Orbital Phase

The glycol evaporator, the ECS temperature controller, and the entire water-glycol coolant circuit performed satisfactorily. A primary ECS mission objective was to verify operation of the heat rejection system throughout the mission. This objective was accomplished. The actual spacecraft heat load was calculated to be 5480 Btu/hr based on water usage data. This load was approximately 500 to 1000 Btu/hr lower than the predicted heat loads of 6000 to 6500 Btu/hr that had been used to set the inflight position of the glycol evaporator back pressure control valve. Subsequent to the pre-mission readiness review (PMRR), the predicted spacecraft heat load was revised to 5825 Btu/hr. This load is 345 Btu higher than the actual load of 5480 Btu/hr, and is satisfactory for heat load predictions. A variance of 10 to 15 percent between expected and actual heat loads is not unusual because of the uncertainties of the thermal storage capacity of the spacecraft structure and thermal cold-plate network. The average glycol evaporator inlet and outlet liquid temperatures for the mission were approximately 80° F and 41° F respectively. The actual heat load of 5480 Btu/hr resulted in lower-than-expected values for evaporator outlet glycol temperature and evaporator steam back pressure. It is desirable to maintain the steam back pressure above 0.10 psia as a margin to prevent freezing conditions (0.0886 psia) from occurring inside the evaporator; flight data indicated a back pressure of 0.09 psia for the mission. The average water-glycol flow rate produced by dual operation of the glycol pumps was approximately 190 lb/hr, based on a heat balance at the glycol evaporator. The pump discharge pressure and glycol accumulator quantity were utilized to obtain a comparative water-glycol flow rate from a pump characteristic curve. The flow rate obtained from the curve was approximately 175 lb/hr. The cabin temperature was approximately 60° F throughout the orbital phase of the mission.

The average glycol evaporator water usage rate during the mission was approximately 5.26 lb/hr, based upon the actual quantity of water drained from the waste water tank during postflight testing. The water usage rate was used to calculate the average mission heat load and water-glycol flow rate. A water usage rate of 5.60 lb/hr was expected, based on a predicted load of 5825 Btu/hr. Figure 13.1-18 shows a schematic of the water-glycol system.

~~CONFIDENTIAL~~

~~CONFIDENTIAL~~

5.19-3

The indicated waste water tank quantity for the mission is shown in figure 5.19-1. Telemetered measurement quantity data were reduced using a calibration curve estimated for the tank in a zero-g environment. Abrupt variations in the plotted quantities coincide with vehicle engine firings and indicate the acceleration sensitivity of the measurement. Due to this acceleration and known attitude sensitivity, the indicated quantity data subsequent to CM/SM separation are considered invalid and are not shown.

A calculated average water usage rate was determined from measured quantities of 57.37 pounds loaded during water servicing and 9.76 pounds drained during postflight testing at Downey, California. Deductions were made of an estimated 0.8 pound for prelaunch wetting of the evaporator wicks and 2.4 pounds for normal flow through the water valve after boiling had ceased and prior to valve shutoff. The net water usage of 44.4 pounds divided by the duration of active boiling equals an average water usage rate of 5.26 lb/hr. A tank quantity curve calculated from this average usage rate is shown in figure 5.19-1 and agrees with the indicated quantity, within acceptable tolerances, for the first three-fourths of the flight. The reason for the indicated low water-usage rate and deviation from the calculated average during the last fourth of the mission is not known. A postflight tank calibration is planned and additional study may be needed in predicting tank calibrations under zero-g conditions.

Readings from the potable water tank quantity transducer compared favorably with the corresponding average fuel cell water production rate during the mission (fig. 5.19-2). According to the fuel cell mission performance results, approximately 6.6 pounds of water was produced during the 3 hour period before lift-off and approximately 16 pounds was produced during the mission for a total fuel cell water production of 22.6 pounds.

### 5.19.3 Entry Phase

At CM/SM separation, the MCP closed the oxygen shutoff valve to isolate the CM oxygen supply system from the SM, and verified closure of the water-glycol shutoff valve as planned. Water boiling in the glycol evaporator provided cooling during entry until ambient pressure made water boiling ineffective. Subsequent cooling was supplied only by the glycol reservoir and system heat storage capacity. The evaporator outlet temperature (CF0018T) began increasing at 08:29:30 as ambient pressure increased and at 08:32:18 had reached 75.8° F, which is the upper limit of the measurement. The cabin pressure began increasing during descent, as the cabin pressure relief valve functioned normally. As stated previously,

~~CONFIDENTIAL~~

~~CONFIDENTIAL~~

the relief pressures for positive and negative cabin pressure relief cannot be computed until the barometric pressure profile is compensated for the calibration shift in the barometric static pressure reference (CE0035P) at launch. The cabin temperature increased to approximately 68° F during entry.

#### 5.19.4 Postrecovery Observations

Approximately 1 to 2 quarts of clear liquid were found in the cabin after spacecraft recovery. A chemical analysis of the liquid indicated that it was sea water and did not contain any water-glycol. The water probably entered the spacecraft through the cabin pressure relief valve. Salt water also was observed in the command modules from the Apollo 201 mission and Apollo 202 mission after recovery. The relief valve has a manually operated sealing feature which can be actuated during manned missions.

Vapor sensitive tapes for fuel, monomethylhydrazine (MMH), and oxidizer, nitrogen tetroxide ( $N_2O_4$ ), were installed in the CM to detect entry of any RCS fuel, oxidizer, or combustion products into the cabin through the cabin pressure relief valve during the RCS propellant depletion burn and excess  $N_2O_4$  dump period (fig. 13.1-19). The depletion burn and excess  $N_2O_4$  dump occurred during cabin pressurization while the CM was descending on the main parachutes. Cabin pressurization was performed by the cabin pressure relief valve, which allowed outside air to enter the cabin through the ECS steam duct. All  $N_2O_4$  tapes indicated some ingestion of  $N_2O_4$  into the crew compartment. Three of the tapes indicated a higher concentration than did the remaining tapes. Of these three, two were near the cabin pressure relief valve and the other was located on the MCP coldplate. These three tapes were reddish-pink in color and the remaining tapes were a light salmon-pink color, all of which verify ingestion of  $N_2O_4$ . This occurred because an excess of  $N_2O_4$  had been loaded and was dumped as raw oxidizer after depletion of the MMH.

The MMH tapes showed no evidence of fuel ingestion.

The tape supplier exposed  $N_2O_4$  tapes to a concentration of 1 ppm  $N_2O_4$  for 7 hours, which simulated the exposure time of the Apollo 4 mission tapes to cabin atmosphere prior to hatch removal. The resulting tape color indication was greater than or equal to the worst of the mission tapes, signifying that the highest concentration sensed during descent was less than 1 ppm. This is not considered unacceptable from a toxicological standpoint.

~~CONFIDENTIAL~~

~~CONFIDENTIAL~~

5.19-5

Prior to removal of the crew access hatch, two gas samples were taken of the cabin atmosphere while the spacecraft was onboard the recovery ship. Chemical analysis of the two gas samples indicated that 0.3 ppm of  $N_2O_4$  was present. There was no indication of MMH in the gas samples. The results of the gas samples confirm the vapor sensitive tape data and indicate that the  $N_2O_4$  concentration in the CM was 1 ppm or less.

The postlanding ventilation valves (PLV) were tested onboard the recovery ship to determine the flight environment effect on valve operation. The inlet valve operated normally at a minimum voltage of 25 V dc. The outlet valve opened after 1.23 seconds, indicating a minor sticking problem when compared to the average opening time of 0.72 to 0.82 second during subsequent postflight testing of these valves. The specification requirement is 1.5 seconds maximum to go from the full closed to the full open position. In addition, a limit switch is incorporated in each valve to prevent the valve motor from overheating if excessive torque is required to open the valve. Evidently, the opening torque was not sufficient to trip the limit switch even though the opening time was slightly longer than the average. Consequently, the minor sticking is not considered an anomaly. The valve operated normally at minimum voltage during the two subsequent actuations.

The potable water tank was drained during postflight testing at Downey, California. The drained quantity was measured to be 23.02 pounds, which is comparatively close to the total fuel cell production quantity. Two samples were taken from the potable water tank, after recovery, to test the hydrogen content of the fuel cell effluent water. The samples were collected in two 500 cc cylinders. Sample no. 1 contained approximately 249 cc of free gas prior to analysis, indicating leakage in the sample cylinder; sample no. 1 was disregarded. Sample no. 2 was analyzed and contained approximately 0.02 cc of free hydrogen. It should be noted that the hydrogen concentration is representative of that sample only; free hydrogen could have been trapped within the potable water tank and would not have been drawn off with the sample. The quantity measured would not cause any problems.

~~CONFIDENTIAL~~

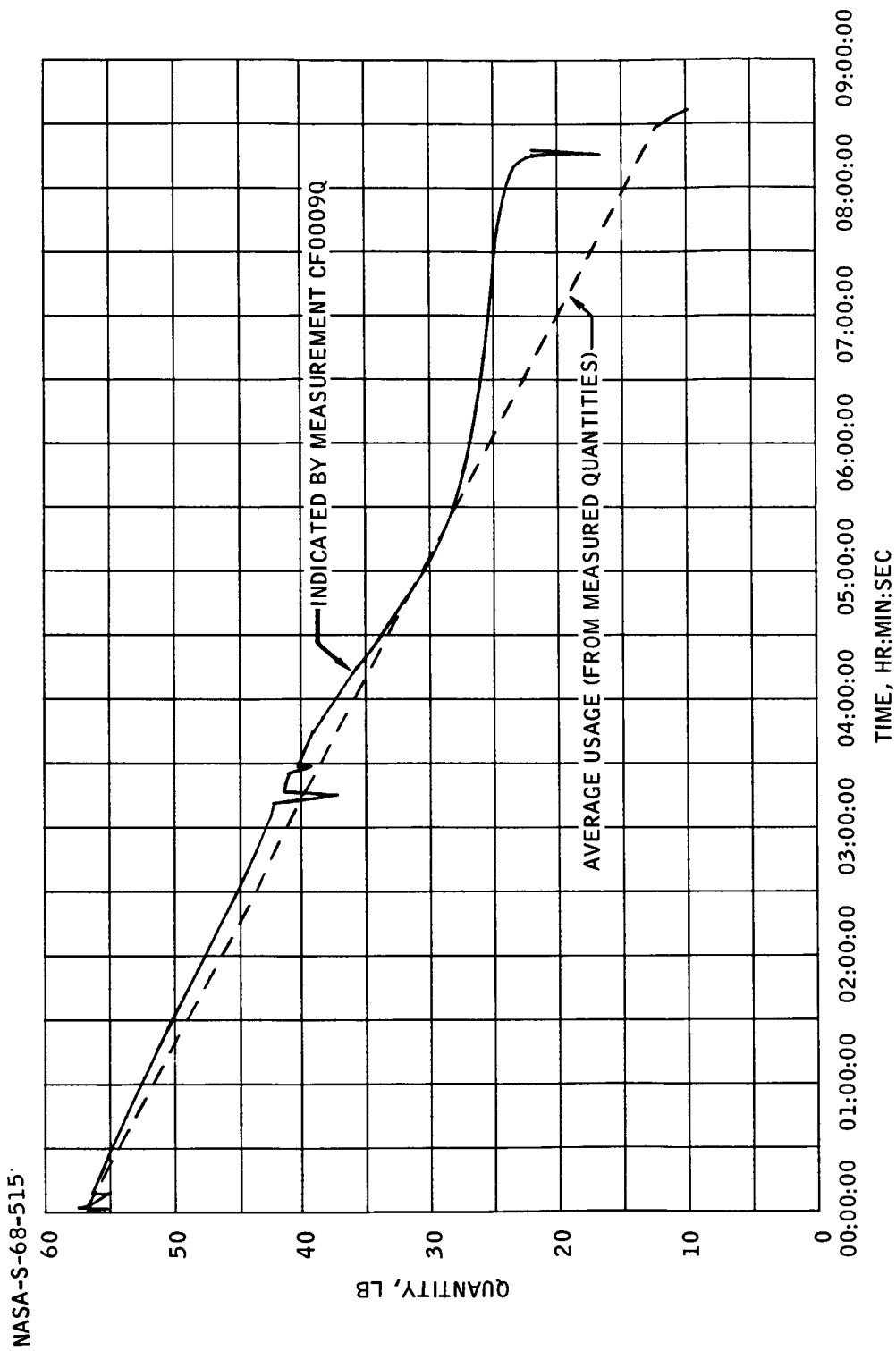
~~CONFIDENTIAL~~

FIGURE 5.19-1.- WASTE WATER TANK QUANTITY PLOTTED AGAINST TIME.

~~CONFIDENTIAL~~

~~CONFIDENTIAL~~

5.19-7

NASA-S-68-516

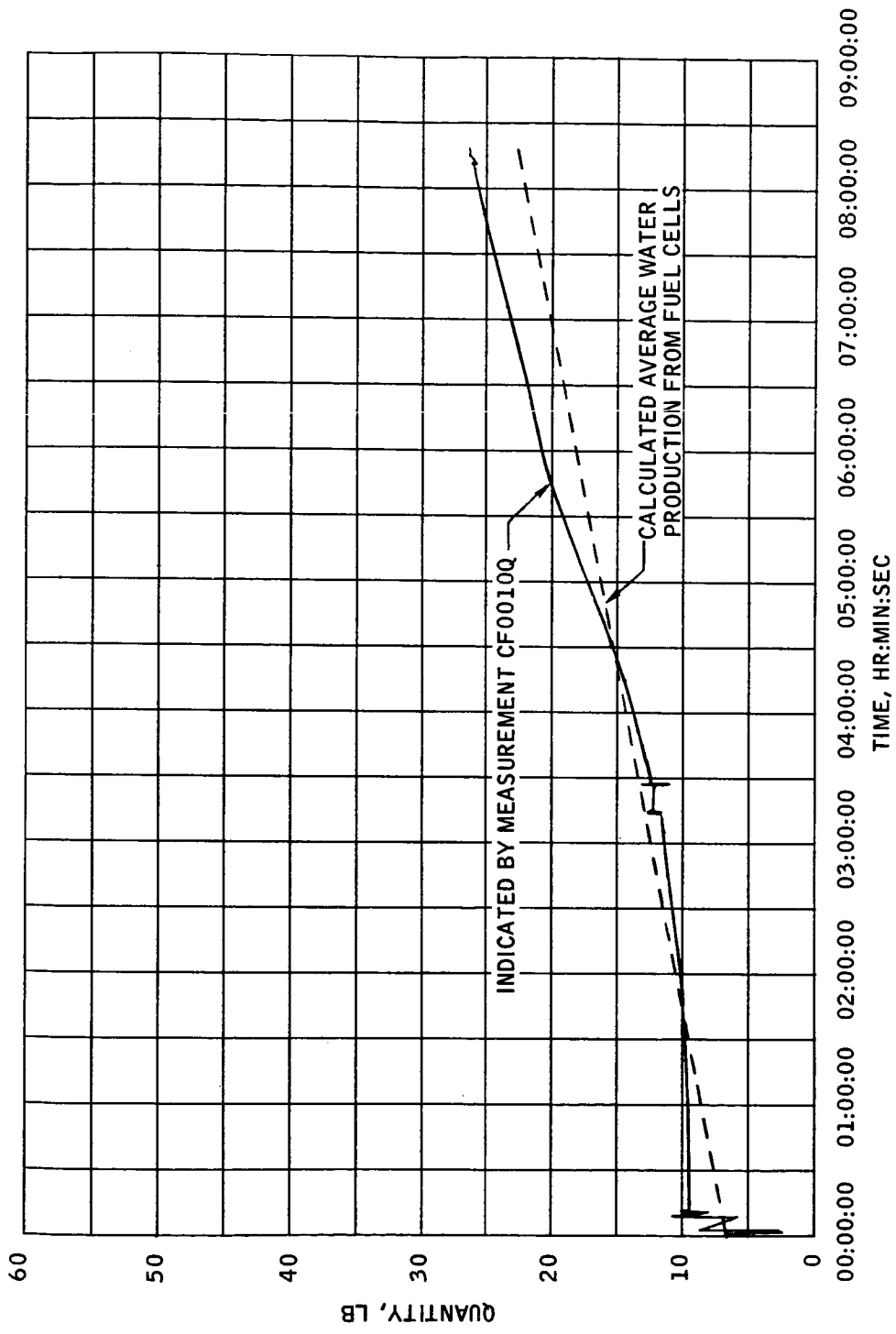


FIGURE 5.19-2.- POTABLE WATER TANK QUANTITY PLOTTED AGAINST TIME.

~~CONFIDENTIAL~~

5.19-8

~~CONFIDENTIAL~~

THIS PAGE INTENTIONALLY LEFT BLANK

~~CONFIDENTIAL~~

~~CONFIDENTIAL~~

5.20-1

## 5.20 CREW STATION PERFORMANCE

### 5.20.1 Crew Visibility

Summary.- All five of the command module windows had the same appearance postflight. Both the left and right rendezvous windows had a bluish discoloration. All of the windows had a uniform light gray film deposit. The deposit appeared more uniform than did the window film on the command modules flown on the AS 201 and AS 202 missions. After landing, a fog-like moisture condensation developed between the heat shield panel and the outer pressure cabin window assembly. This condensation was less extensive than it was on the command modules flown on the AS 201 and AS 202 missions. There was no evidence of moisture in the sealed space between the two panels of the pressure cabin window assembly.

A moderately dense gray film was deposited over the outer surface of each of the micrometeoroid windows. There was a random deposit of the thermal control coating spattered over the outer surface of the heat shield window. Through-the-window light transmission was reduced by the contamination, and visual acuity was reduced, but to a lesser degree than was experienced on the command module flown on the AS 201 mission, but to a greater degree than occurred on the command module flown on the AS 202 mission.

To establish the extent of visibility degradation as the result of window contamination, a grid-resolution photographic procedure was conducted on the spacecraft window system after the spacecraft had been returned to the contractor at Downey, California.

No preflight grid-resolution photographic procedures were conducted on the command module for the Apollo 4 mission. The numbers shown as preflight in table 5.20-I are typical and were derived from measurements of earlier spacecraft. Quality control of the four window panels and previous preflight examinations have indicated insignificant changes in resolution among various spacecraft window assemblies. Postflight grid-resolution photographic procedures were not conducted onboard the recovery ship. Past experience showed that resolution quality improves as a result of the fog-like condensation coalescing into water droplets. This is a postflight condition and would not have any impact on crew performance or safety.

Postflight inspection.- The first postflight inspection of the windows was conducted by the recovery team after the spacecraft had been secured onboard the aircraft carrier. The examination revealed light condensation of moisture between the heat shield window and the outer

~~CONFIDENTIAL~~



~~CONFIDENTIAL~~

window panel of the pressure cabin assembly of all windows except the right-side window. The right-side window had a heavy condensation of moisture.

There was evidence of a light to moderate contamination on all spacecraft windows. All windows had a light streaked water pattern randomly distributed over the viewing area. Water-run patterns were noted across the total window surface (figs. 5.20-1 and 5.20-2), but not to the extent noted on the command module on the AS 202 mission.

Examination of the spacecraft windows at the contractor facility at Downey, California, confirmed the report from the recovery team. There were water droplets present between the pressure cabin window outer surface and the heat shield window. These droplets were present on the left-side and right-side windows and the right rendezvous window. The condensation was the result of the higher temperature of the outer window (over 400° F), and its rapid cooling after landing in the water. The spacecraft was in the water approximately 2 hours and the space between the outer window and inner window assembly was vented to ambient conditions. The rapid cooling of the outer window and high moisture-laden air between the two window panes resulted in condensation on the window. Except for the right-side window, Spacecraft 017 had less water condensation between the heat shield window and pressure cabin window than did either Spacecraft 009 or 011.

There was evidence of some salt crystallization randomly located on the outer surface of the micrometeoroid windows. These crystallized areas were less in number and not as dense as noted on Spacecraft 009 and 011. The distribution of a light to moderate film was noted on all windows. The light gray film was more homogenous than was noted on previous Apollo flights. A major window contamination change from any previous flight was noted on the right side window. The contamination in the central area of the window had a flaky (peeled) appearance (fig. 5.20-3). The contaminant looked like it could be peeled off in a sheet. This was not the case for any window on Spacecraft 009 and 011. Considerable pressure had to be applied to remove the contaminant. The right and left rendezvous windows had a bluish discoloration of the right third area (fig. 5.20-4).

Spacecraft 017 was the first spacecraft utilizing micrometeoroid window panels. Close examination of the right-side and left-side windows revealed a general spattering on the heat shield window with very small particles of the aluminum thermal control coating. The material was probably forced through the 0.25-inch opening between the two windows during entry and was trapped and settled on the window surface. Close examination of the inner window assembly revealed no water or contamination. There was no definite evidence of the windows being deliberately

~~CONFIDENTIAL~~

~~CONFIDENTIAL~~

5.20-3

wiped or abraded, although the plastic covers used on the side windows did abrade extensively the contaminant on the right-side and left-side windows (fig. 5.20-3). However, the contamination did show evidence of being washed to some extent by the wavelapping action during the time the spacecraft was in the ocean.

Grid-resolution photography analysis.- The results of the resolution photography are shown in table 5.20-I. The right rendezvous window had the greatest reduction in resolution quality. The grid-resolution photography indicates a general loss in transmitted intensity, a moderate decrease in window resolution, and loss in through-the-window visual acuity. Subjective analysis of the window transmission and resolution characteristics indicate that with the light source (sunlight) to the rear at least 45 degrees, there would be a general reduction in visual acuity through the window. However, with the light source in front of the window, light-scatter transmission would be sufficient to destroy visual acuity, making out-the-window viewing very difficult (figs. 5.20-5 and 5.20-6).

#### 5.20.2 Crew Related Dynamics

Summary.- The vibration levels measured on the crew compartment forward bulkhead were assumed to represent the vibration environment to which crew members would be exposed. The predominant frequencies during these periods are lower than noted for Spacecraft 009 and Spacecraft 011 and are in the range of the natural resonant frequency of the upper torso. The vibration during these periods would not have jeopardized the physical well-being of the crew. Crew members would have experienced a general vibration of the body. Minor reduction of visual acuity in monitoring cabin displays would be experienced, resulting in greater concentration on critical displays by the crew.

Data.- Acceleration measurements (CA0001A and CA0007A) taken from the forward bulkhead of the crew compartment were used to determine the vibration environment. The Apollo 4 mission did not have lateral accelerometers located on the forward bulkhead; therefore, no data are available for analysis. Vibration environment was also recorded during the reentry phase.

The vibration levels during the launch phase were less than noted on Spacecraft 009 and Spacecraft 011. The resultant vibration reached 0.2g at ignition and maintained this level until lift-off, when the level increased to 0.6g, decreased to 0.2g within 2 seconds, and remained at this level until 00:00:58. At 00:00:58 the vibration level began increasing to 0.4g through max q and continued increasing to a maximum of 0.7g between 00:01:42 to 00:02:04. At 00:02:05 the vibration levels decreased until engine cutoff. The vibration amplitudes at inboard and outboard

~~CONFIDENTIAL~~

~~CONFIDENTIAL~~

engine cutoff appeared higher on Spacecraft 017 than on Spacecraft 009 and Spacecraft 011. Immediately following inboard engine cutoff, a 0.7g peak-to-peak longitudinal vibration developed and decreased to 0.3g in 2 seconds. At outer engine cutoff the vibration amplitude reached 1.3g, decreasing and stopping within 4 seconds (fig. 5.20-7 through 5.20-9).

Spectral analysis of the significant periods of vibration indicated that the majority of the energy was contributed by longitudinal components of 2.5, 4, 5, 8, and 16 Hz. The predominant frequency at lift-off was 4 Hz, at max q was 5 Hz, with a minor component at approximately 16 Hz. The vibration spectrum on Apollo 4 is the result of buffeting and wind shear and is not the typical sustained longitudinal sinusoidal oscillations (POGO) experienced on the early Gemini flights. Figure 5.20-7 shows a typical acceleration input to the CM X-axis. Analysis of the data shows random vibration superposed on a sine wave pattern. These sine waves correspond to major energy contributions (2.5, 4, 5, 8, and 16 Hz) from the launch vehicle bending modes and the effect of wind shear.

During entry, vibration amplitudes were 0.7g to 1.0g at 24 Hz. These amplitudes lasted for 2 seconds and occurred 15 seconds after maximum entry acceleration. Vibration amplitudes of the same magnitude occurred again 15 seconds before second maximum entry g-bias and again 20 seconds after second maximum acceleration.

Effects on crew.- None of the vibrations observed were of sufficient magnitude or duration to jeopardize the physiological well-being of the crew. At frequencies below 12 Hz, decrement in visual acuity is dependent upon the mechano-dynamic response of the human body that produces physiological stresses that impair body functions. The natural resonant frequency of the human upper torso is 3 to 4 Hz. The predominant 4 to 5 Hz experienced on the Apollo 4 mission is below the critical flicker rate of the eye. The crew would have been very aware of these vibrations as a total body vibratory motion. The 5 Hz vibration forms a trough between the vibration frequencies causing critical whole body motion and 6 Hz when the critical flicker rate of the eye becomes apparent.

### 5.20.3 Radiation Monitoring

There were three radiation monitoring instruments, an integrating radiation dosimeter (IRD) and two nuclear emulsion spectrometers (NES), onboard the Apollo 4 spacecraft. All three instruments were recovered successfully and returned to MSC in good condition.

The IRD measured a skin dose of 0.59 rads and a depth dose of 0.38 rads. Calculations were made prior to the Apollo 4 mission to provide an estimate of the degree of severity of the particle radiation

~~CONFIDENTIAL~~

~~CONFIDENTIAL~~

5.20-5

to be encountered during the mission. These estimates were 0.38 rads skin dose and 0.13 rads depth dose. The calculations were not made for the specific spacecraft, trajectory, dose point location, or dose point geometry which were involved in the measurement of radiation on Apollo 4. The premission calculations used the following inputs.

a. Trajectory: A segment of the nominal mission profile was used. The trajectory began with the second S-IVB ignition and terminated just before landing. This trajectory included the first SPS burn but did not take into account the second SPS burn.

b. Spacecraft: An analytical description of the Block I vehicle was used. This description was generated in 1963. An additional  $0.6 \text{ gm/cm}^2$  was added at MSC to reflect the additional thickness of the Block II heat shield as it was in mid 1966.

c. Dose point location: Both the premission calculations and the inflight measurements were made at the same approximate location in the spacecraft.

d. Dose point geometry: The dose points used in the premission calculations were located in a phantom (analytical description of a human torso). This provided much more shielding about the dose point than that of the dosimeter structure.

The inflight measurements are thought to be reasonable when one considers the differences between the calculations and measurements. Analysis is underway which will analytically reconstruct the inflight conditions of the measurement as nearly as possible. There is not expected to be any significant differences between the analytical results and the radiation dose measured on the Apollo 4 mission.

At the present, very little meaningful data are available from the NES's. The emulsions were found to be in good condition. No light leaks or mechanical abrasion marks were observed. The processing of the emulsions is proceeding in the normal fashion, with preliminary indications that a measurable radiation field was encountered. However, detailed information concerning the radiation spectrum will not be available until the lengthy tasks of processing and analyzing the emulsions have been completed.

In summary, the complete postflight analysis will provide quantitative information about the space radiation environment for the Apollo 4 mission. Additional qualitative dose rate information, which will be provided from the Van Allen Belt dosimeter to be flown on Spacecraft 020 (Apollo 6 mission), will be required before any conclusions can be made about the accuracy of the analytical dose calculations.

~~CONFIDENTIAL~~

~~CONFIDENTIAL~~

TABLE 5.20-I.- SPACECRAFT WINDOW RESOLUTION CHARACTERISTICS

Conditions	Resolution of each window, lines per mm				
	Camera system	Left rendezvous	Right rendezvous	Left side	Right side
Preflight, typical	56	40	40	50	50
Postflight, Downey	56	17	12	40	20

~~CONFIDENTIAL~~

~~CONFIDENTIAL~~

5.20-7

NASA-S-68-517

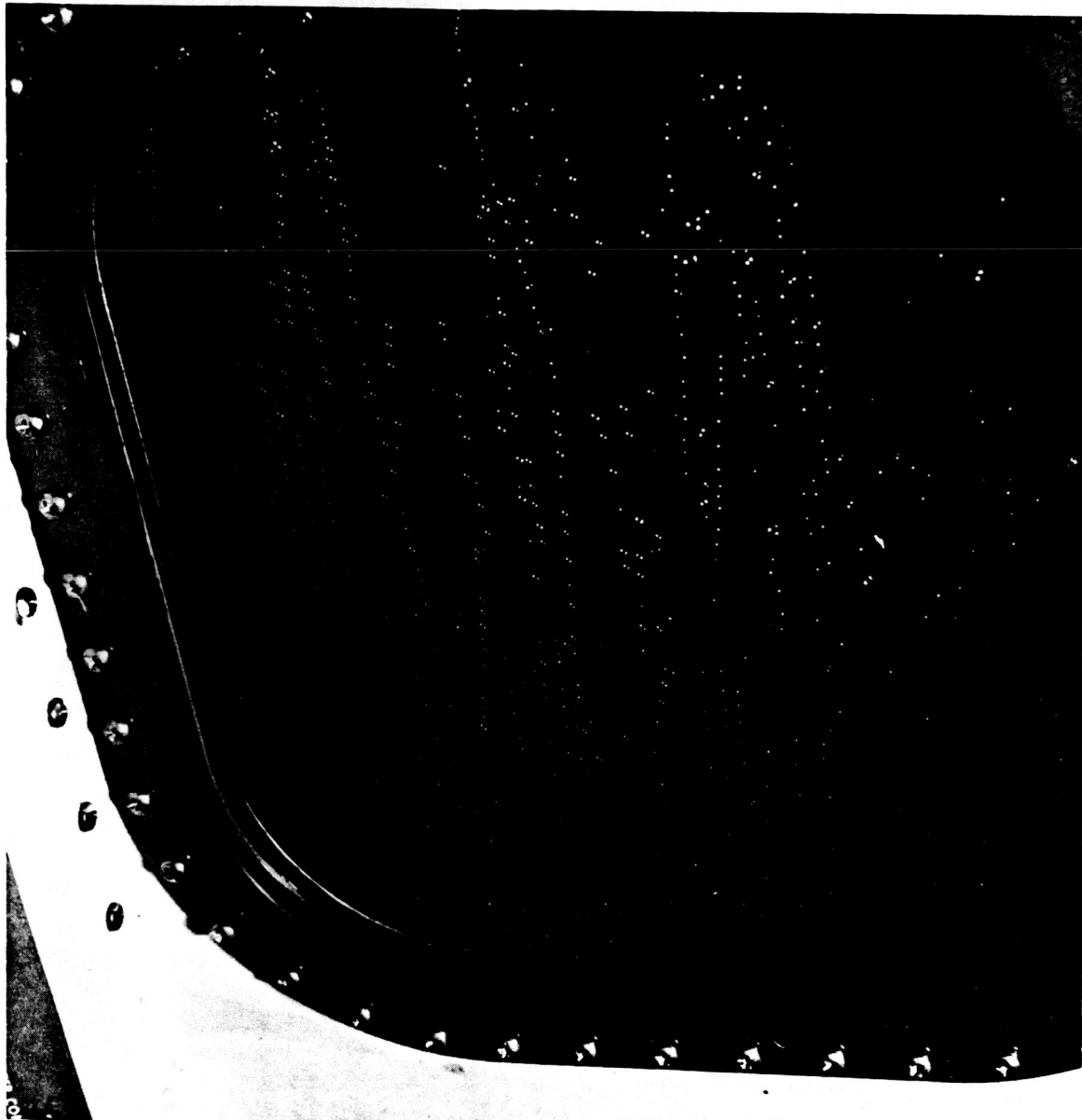


FIGURE 5.20-1.- POSTFLIGHT PHOTOGRAPH OF LEFT-SIDE WINDOW AFTER SPACECRAFT HAD BEEN SECURED ON RECOVERY SHIP.

~~CONFIDENTIAL~~

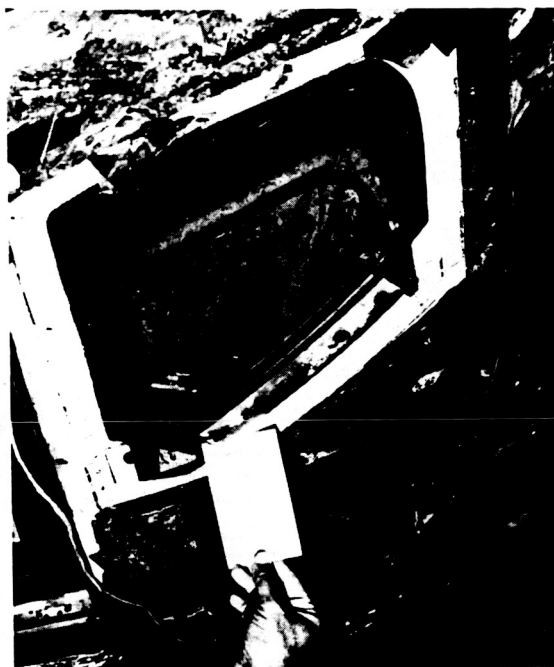
5.20-8

NASA-S-68-518

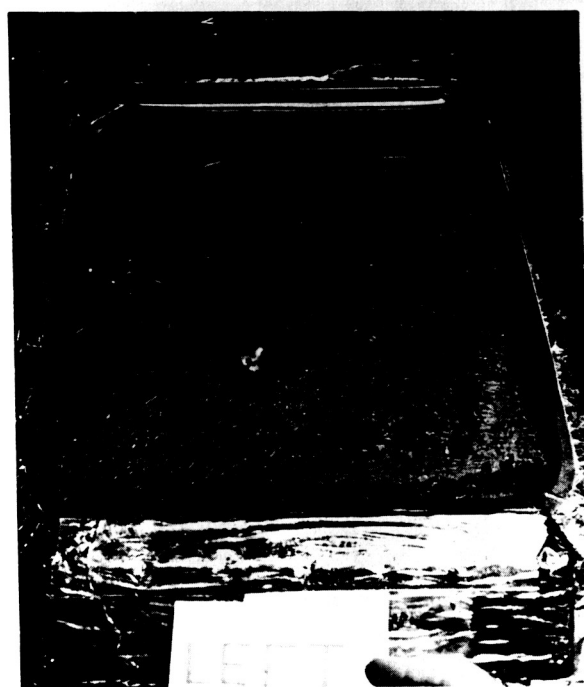
~~CONFIDENTIAL~~



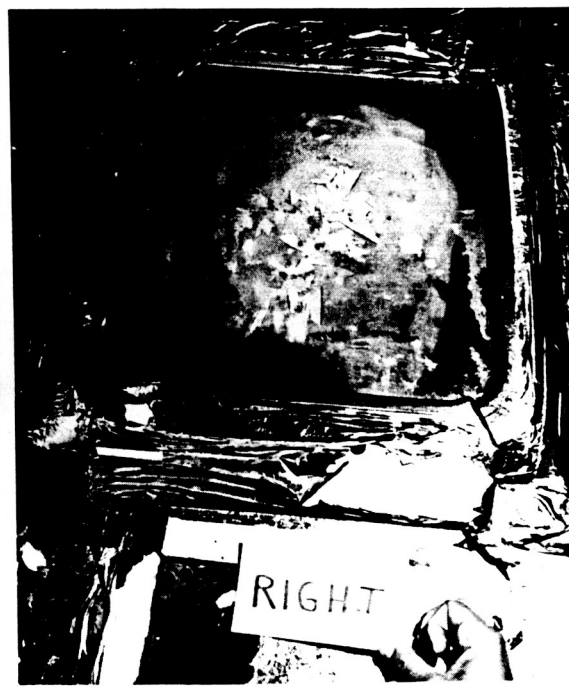
LEFT RENDEZVOUS



RIGHT RENDEZVOUS



LEFT SIDE



RIGHT SIDE

FIGURE 5.20-2. - SHIPBOARD PHOTOGRAPHS SHOWING POSTFLIGHT CONDITION OF SPACECRAFT 017 WINDOWS.

~~CONFIDENTIAL~~

~~CONFIDENTIAL~~

5.20-9

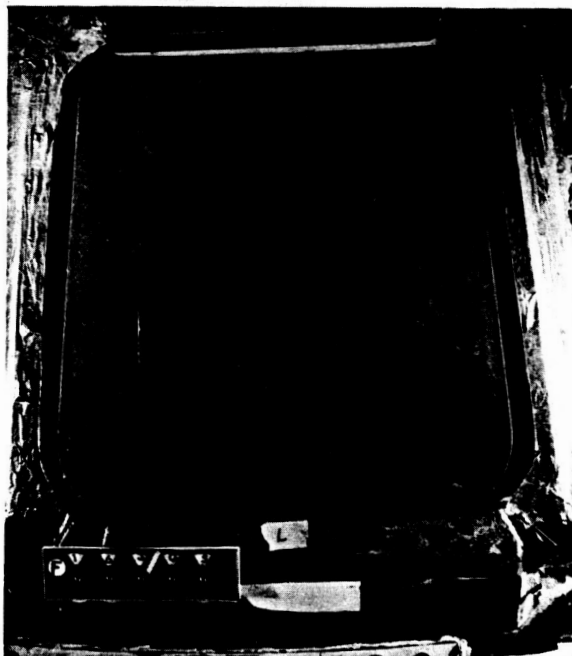
NASA-S-68-519



LEFT RENDEZVOUS



RIGHT RENDEZVOUS



LEFT SIDE



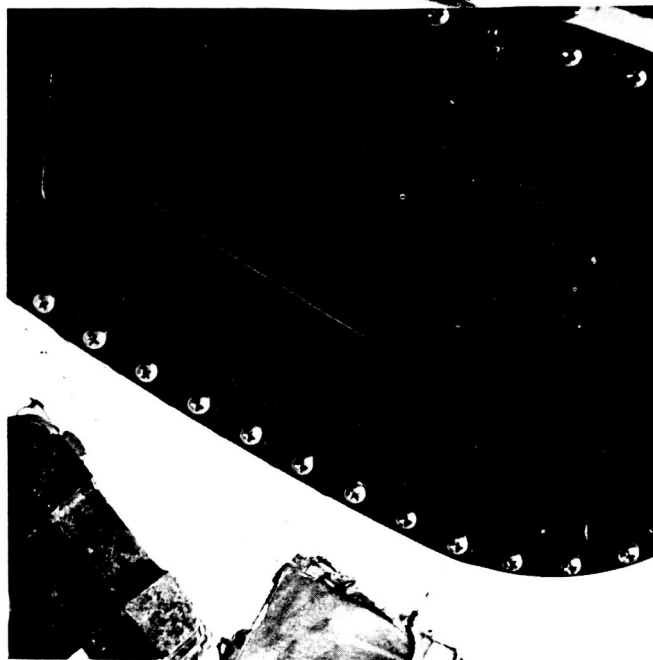
RIGHT SIDE

FIGURE 5.20-3. - POSTFLIGHT PHOTOGRAPHS OF SPACECRAFT WINDOWS TAKEN AFTER SPACECRAFT ARRIVED AT DOWNEY, CALIFORNIA.

~~CONFIDENTIAL~~



~~CONFIDENTIAL~~



LEFT RENDEZVOUS



RIGHT RENDEZVOUS

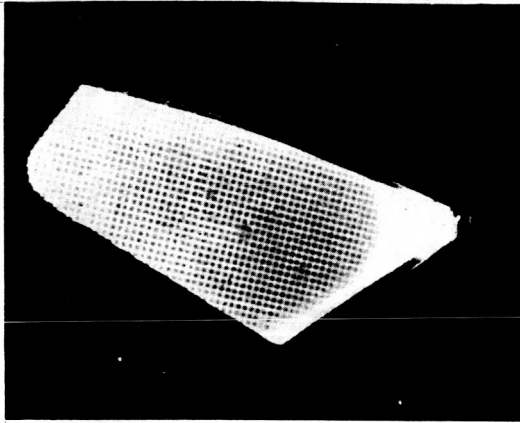
FIGURE 5.20-4. - POSTFLIGHT PHOTOGRAPHS OF SPACECRAFT WINDOWS SHOWING DISCOLORATION DUE TO CONTAMINATE.

~~CONFIDENTIAL~~

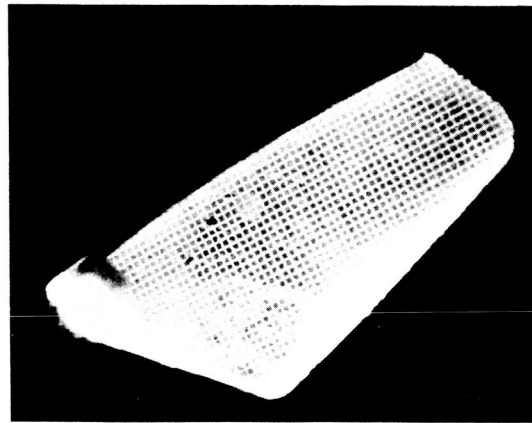
~~CONFIDENTIAL~~

5.20-11

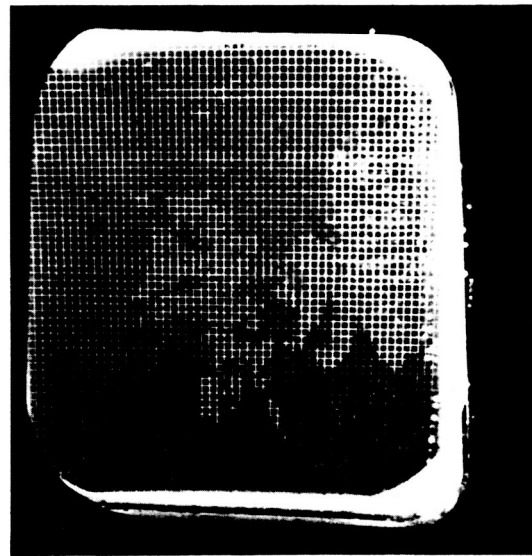
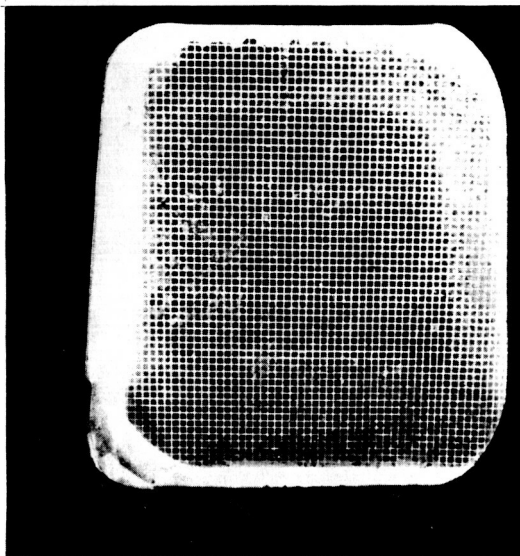
NASA-S-68-521



LEFT RENDEZVOUS



RIGHT RENDEZVOUS



~~CONFIDENTIAL~~

5-20-12

~~CONFIDENTIAL~~

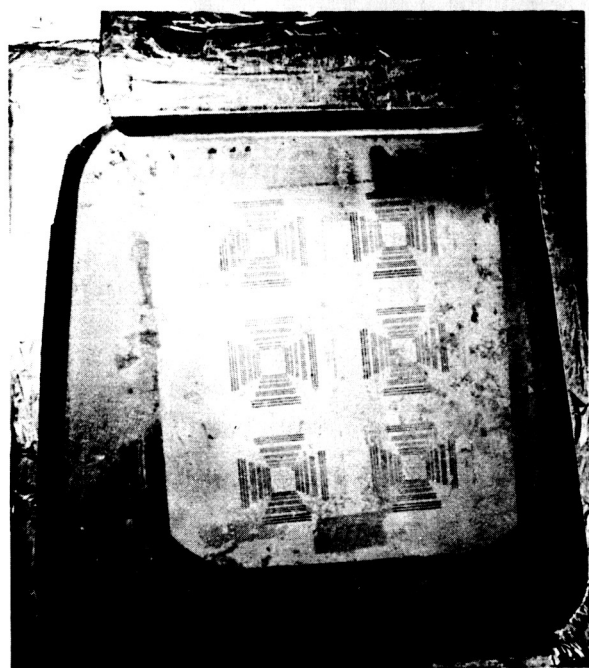
NASA-S-68-522



LEFT RENDEZVOUS



RIGHT RENDEZVOUS



LEFT SIDE



RIGHT SIDE

FIGURE 5. 20-6. - POSTFLIGHT RESOLUTION PHOTOGRAPHS TAKEN AFTER SPACECRAFT ARRIVED AT DOWNEY, CALIFORNIA.

~~CONFIDENTIAL~~

~~CONFIDENTIAL~~

5.20-13

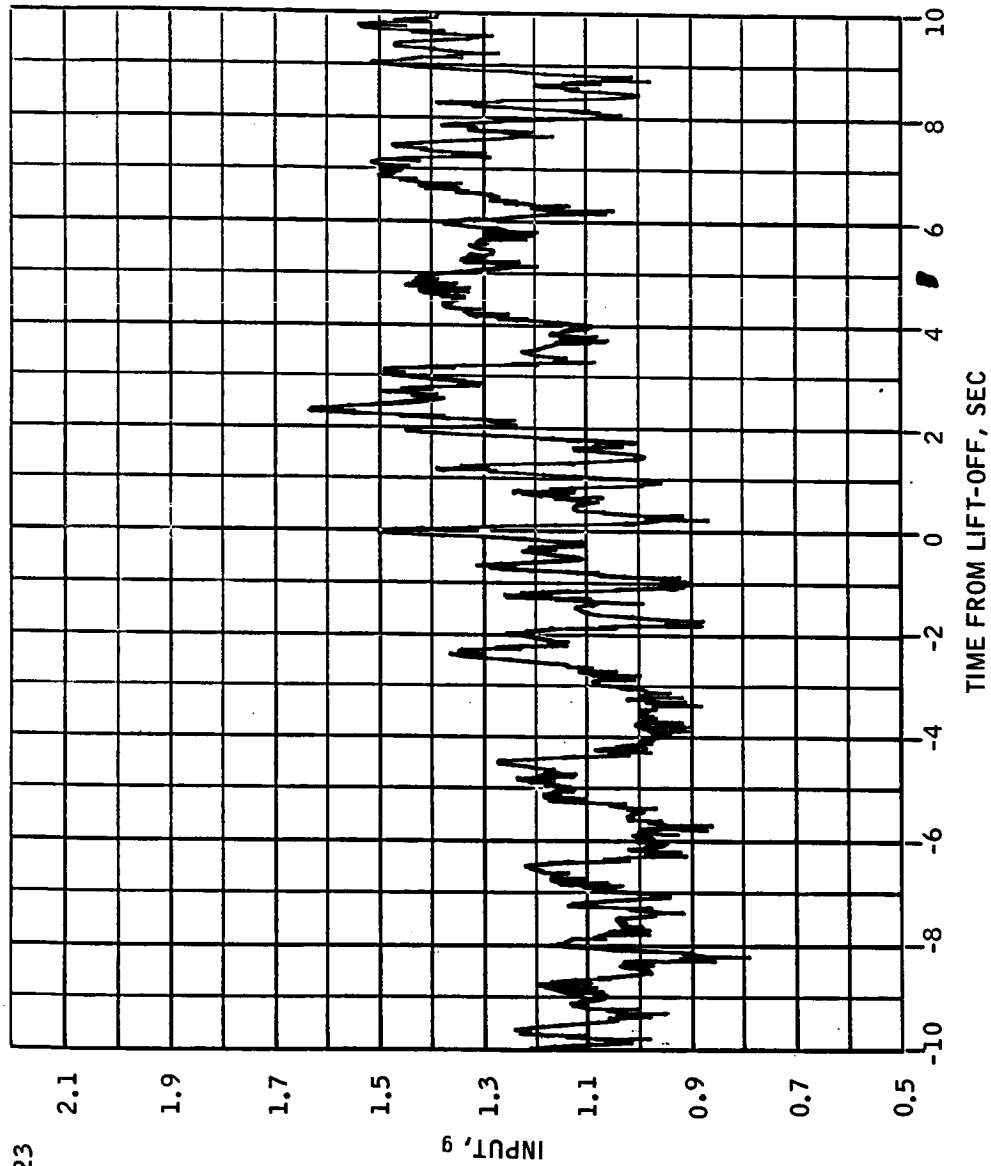


FIGURE 5.20-7.- ACCELERATION INPUT TO COMMAND MODULE X-AXIS  
AT LIFT-OFF, MEASUREMENT CA0001A.

~~CONFIDENTIAL~~

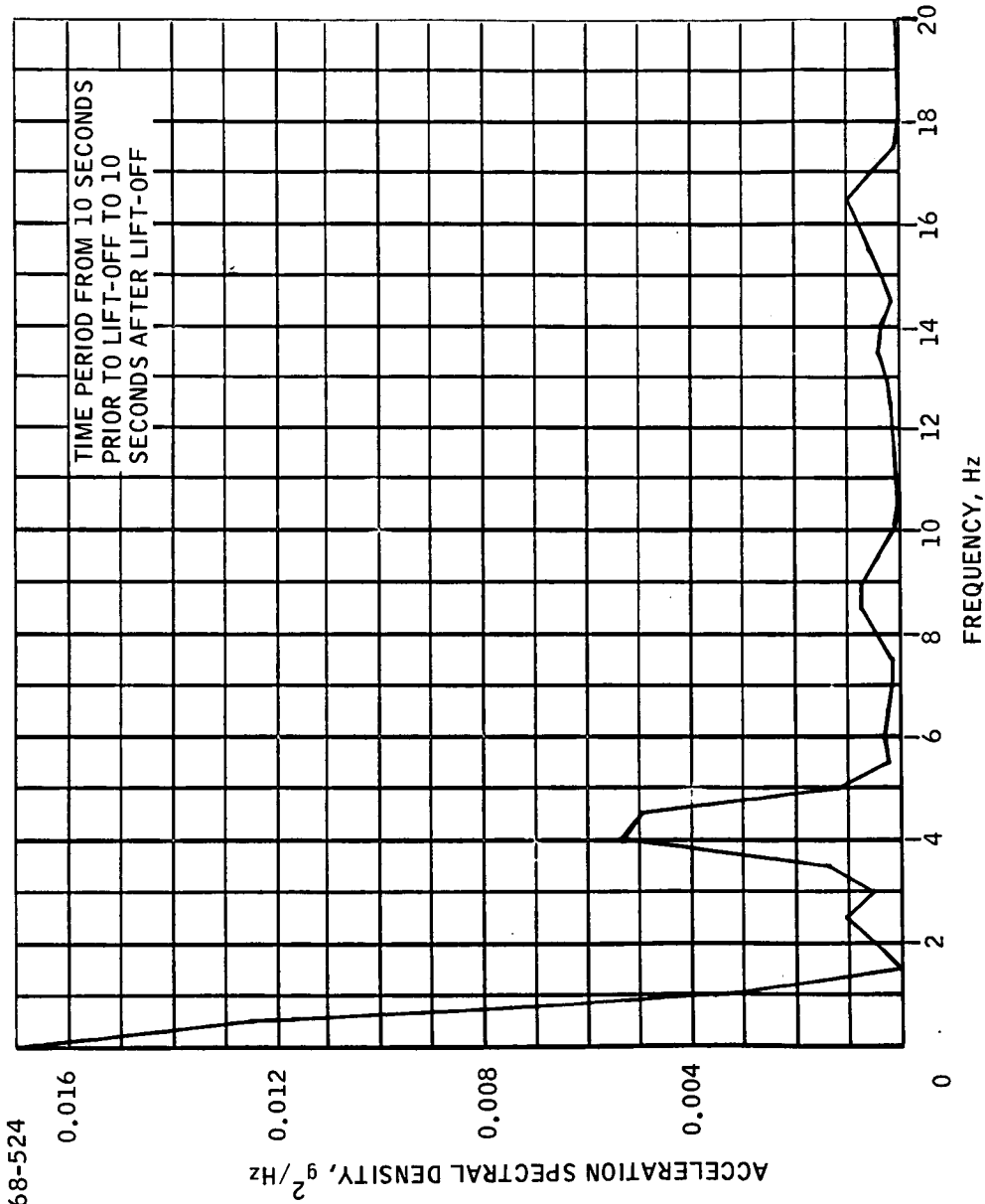
~~CONFIDENTIAL~~

FIGURE 5.20-8.- SPECTRAL DENSITY DERIVED FROM X-AXIS ACCELEROMETER  
AT TIME OF LIFT-OFF, MEASUREMENT CA0001A.

~~CONFIDENTIAL~~

~~CONFIDENTIAL~~

5.20-15

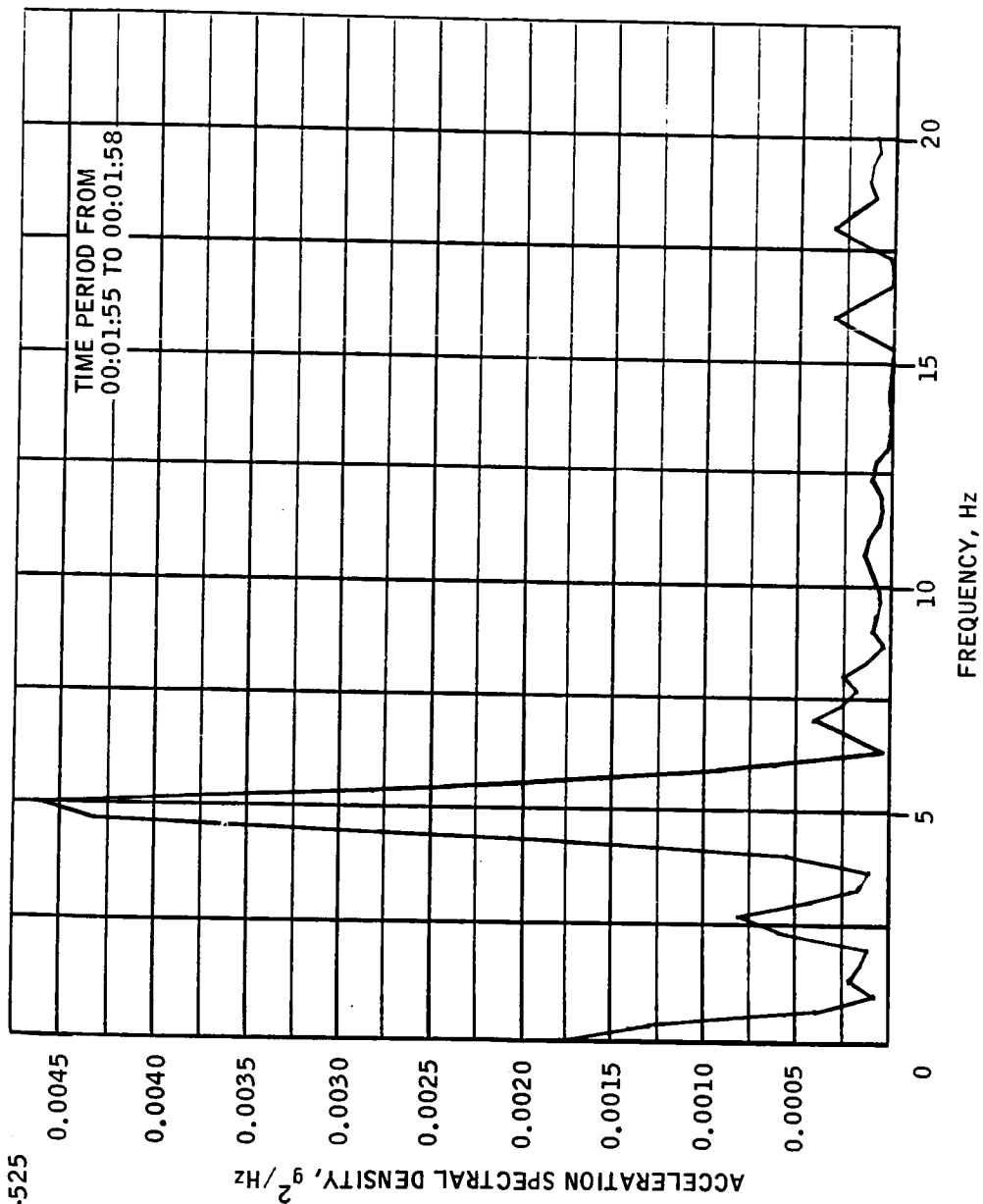


FIGURE 5.20-9.- SPECTRAL DENSITY DERIVED FROM X-AXIS ACCELEROMETER DURING PERIOD OF MAXIMUM RESPONSE, MEASUREMENT CA001A.

~~CONFIDENTIAL~~

~~CONFIDENTIAL~~

THIS PAGE INTENTIONALLY LEFT BLANK

~~CONFIDENTIAL~~

~~CONFIDENTIAL~~

6-1

## 6.0 LUNAR MODULE TEST ARTICLE

### 6.1 STRUCTURE

#### 6.1.1 Loads

The structural interaction loads between the simulated lunar module test article (LTA-10R) and the spacecraft lunar module adapter (SLA) were inferred to be less than design loads throughout the critical flight regions. A complete set of quantitative data were not obtained.

The design interaction loads between the SLA and the lunar module (LM) occur at lift-off, first-stage midboost (max  $q\alpha$ ), and end of first-stage boost (maximum longitudinal acceleration). Comparison of the LTA flight loads with these design conditions was to be based on data from strain gauges on the 16 outrigger struts and three linear accelerometers near the LTA center of gravity. Consequently, an error tolerance exists in the determination of the apex fitting loads since the loads at each apex are an algebraic summation of four large outrigger strut loads. In addition, analyses of the X-axis and Z-axis linear accelerometer data show that data from these instruments were invalid for the lift-off and max  $q\alpha$  portions of the mission (refer to LTA vibration section 6.1.2 and LTA instrumentation section 6.2).

Therefore, accurate apex loads for critical conditions could not be compared to the design loads. However, these loads were qualitatively assessed to be within design values.

The lower-than-design loads could be expected from the following factors.

#### a. Lift-off

1. Weight: 29 500 pounds actual vs 32 000 pounds design
2. Lower-than-design ground winds

#### b. Max $q\alpha$

1. Weight: 29 500 pounds actual vs 32 000 pounds design
2. Low angles of attack

~~CONFIDENTIAL~~



~~CONFIDENTIAL~~

## c. End of first-stage boost

1. Axial load: 4.2g actual vs 4.9g design.
2. Weight: 29 500 pounds actual vs 32 000 pounds design
3. SLA temperatures: 250° F average actual vs 400° F design

Throughout first-stage boost, a 5-Hz oscillation was evidenced in outrigger strut loads and reached maximum amplitudes after max q. For a detailed discussion of this oscillation, refer to section 6.1.2. Typical strut load oscillations are shown in figure 6.1-1. The effect of these oscillations on the apex loads is illustrated in figure 6.1-2.

## 6.1.2 Low Frequency Vibration

Low frequency oscillations of the LTA were predominant throughout most phases of lift-off and first-stage boost.

The X-axis and Z-axis accelerometers mounted on the LTA descent stage to measure low frequency linear accelerations of the LTA vehicle in the X and Z directions, respectively, and the Y-axis accelerometer mounted on the +Y LTA/SLA attach point to measure accelerations in the Y direction produced invalid data during lift-off and in the Mach 1 to maximum dynamic pressure region as discussed in section 6.2. A relocation of these accelerometers to more solid structure would be expected to produce valid low frequency data during lift-off and the maximum dynamic pressure region for the LTA-2R flight.

During lift-off, the primary frequencies of oscillation measured on the Y-axis descent stage and Y-axis attach point accelerometers were 4.5 and 12 Hz, corresponding to second longitudinal and first torsional modes of the launch vehicle (fig. 6.1-3). The peak values at lift-off are presented in table 6.1-I and are within design and low frequency vibration qualification criteria for the specific measurements. No assessment can be made of the overall LTA vehicle load value and vibration amplitude because of the invalid data during this time period.

During midboost the longitudinal oscillations described in section 5.1 were also present in the LTA as illustrated in figure 6.1-4. The peak values in table 6.1-I occurred at different times and exhibited the same beat period described in section 5.1. The oscillations were at a minimum at inboard engine cutoff and outboard engine cutoff and, therefore, did not exceed design loads for this flight. Low frequency vibration qualification criteria were not exceeded in amplitude, but the criteria for time and number of cycles at approximately 5 Hz were exceeded. The effect of the time and number of cycles having been exceeded is being investigated.

~~CONFIDENTIAL~~

~~CONFIDENTIAL~~

6-3

At first-stage inboard engine cutoff, major oscillations at 6.1 Hz occurred as shown in figure 6.1-5 and as tabulated in table 6.1-I. The cause of this oscillation is the same as that discussed in section 5.1. Longitudinal oscillations did not cause loads in excess of design loads but did exceed the low frequency vibration qualification criteria of 0.39g at 6.1 Hz.

At first-stage outboard engine cutoff, major longitudinal oscillations again occurred as shown in figure 6.1-6 and as tabulated in table 6.1-I. These oscillations did not cause loads in excess of design loads but substantially exceeded the low frequency vibrations qualification criteria of 0.48g at 6.8 Hz. The effect of this excessive vibration on the LTA structure is being investigated.

No significant low frequency oscillations of the LTA-10R were measured from second-stage ignition through insertion.

### 6.1.3 Vibro-Acoustics

The LTA-10R was instrumented with nine vibration measurements. Triaxial measurements having ranges of  $\pm 10.0g$  were made at the top of both the oxidizer and the fuel tanks. These instruments were capable of measuring accelerations down to a frequency of 5 Hz. Tank measurement locations on the LTA-10R vehicle were comparable to locations on the LTA-3 vehicle from which current tank vibration criteria were derived. LTA-10R descent engine vibrations were measured in the X, Y, and Z axes on the injector head with instruments ranged at  $\pm 30.0g$ . LM descent engine vibration qualification criteria were derived from measurements made during LTA-3 tests at locations similar to engine vibration measurements on LTA-10R.

Significant differences between LTA-10R and flight LM vehicles were:

- a. The LTA-10R tanks were spherical compared to short cylindrical midsection with spherical end domes for LM vehicles.
- b. The tank support structure on LTA-10R was longer than on LM production skirts.
- c. Tank plumbing was not installed on LTA-10R.
- d. LTA-10R tanks were maintained at 15 psia compared to an approximate 200 psia for LM vehicles.
- e. Thermal shielding was not installed on LTA-10R.

~~CONFIDENTIAL~~

~~CONFIDENTIAL~~

The above differences could affect the vibration response of the tank. All comparisons of LTA-10R data to LM qualification criteria given in the following discussions were made without any scaling to correct the flight data to design dynamic pressures, and factors of safety have not been applied to LTA-10R data.

Oxidizer tank vibrations.- The oxidizer tank vibration data show that the oxidizer tank accelerometers were overdriven during launch, transonic, and maximum dynamic pressure flight phases. The majority of the vibration energy during these phases was high frequency. Low frequency data were recovered by playback through low pass filters. The most significant vibration measured on the oxidizer tank was in the X-axis.

Acceleration spectral density analyses were conducted on the data using the same filter bandwidth (6 Hz) as was used in derivation of the tank vibration criteria. An examination of the oxidizer tank acceleration spectral density analyses, processed with a 6-Hz filter bandwidth showed narrow band peaks above the tank random vibration qualification criteria. Further analysis was then conducted with a filter bandwidth of 1 Hz and is shown in figure 6.1-7. The 200-Hz and 360-Hz oscillations have a very narrow half power point bandwidth and are similar to a discrete sinusoidal oscillation. Any comparison of the 200-Hz and 360-Hz peaks to the random vibration criteria would be of questionable value since the power spectral density of a sinusoidal oscillation is indeterminate. These peak oscillations have no structural significance for the tank support structure and are well above the fundamental mode of the tank.

The maximum measured values of low frequency acceleration on the oxidizer tank were 0.6g in the X-axis with a frequency of approximately 6 Hz during inboard engine cutoff and 1.0g at a frequency of approximately 6.0 Hz immediately prior to first-stage separation. The maximum measured value of lateral acceleration was 1.0g with a frequency of approximately 6.0 Hz in the Z direction immediately prior to first-stage separation.

Sinusoidal tests for LM tanks are specified as input levels, whereas the LTA-10R was instrumented so as to measure response of the top dome of the tank. All X-axis measurements on the LTA-10R measured approximately the same amplitudes and frequencies at corresponding times. This indicates there was no amplification of input levels to the tank; thus, measured X-axis amplitudes can be compared to sine input qualification criteria. Lateral accelerations showed that amplification of input accelerations did occur; therefore, they cannot be compared directly to the qualification criteria. The sinusoidal qualification criteria for all axes are specified as 0.23 inch double amplitude from 5 to 12.0 Hz

~~CONFIDENTIAL~~

~~CONFIDENTIAL~~

6-5

which is equivalent to 0.43g at 6 Hz. The X-axis amplitudes can be compared to the sinusoidal qualification criteria (0.43g at 6 Hz). The criteria were exceeded (0.6g at 6 Hz), during inboard engine cutoff and first-stage separation. It should be noted that the tanks were qualified for sinusoidal oscillations to the previously mentioned criteria and the resonant response of the tank during these tests would be expected to produce greater loads than were measured on LTA-10R. This is in the process of being verified.

In summary, oxidizer tank random vibrations on the LTA-10R did not exceed the applicable random vibration qualification criteria. LTA-10R oxidizer tank vibrations showed fairly discrete oscillations which approach the form of a sine wave at frequencies of 5 Hz, 260 Hz and 360 Hz. The high frequency oscillations at 200 Hz and 360 Hz may be considered representative of local motions in the area immediately adjacent to the point of measurement. The amplitude of these oscillations must be compared to actual qualification test response values before their significance can be established. Qualification test acceleration plots taken from qualification test report EDR 4944, dated 21 November 1966, are given in figure 6.1-8.

Fuel tank vibrations.- Fuel tank vibration measurements performed satisfactorily throughout the flight. Acceleration spectral density peaks from analysis of the fuel tank measurements were enveloped and compared to the criteria in figure 6.1-9. The LTA-10R data approach qualification criteria at 100 Hz. Peaks which occurred at 200 Hz and 360 Hz are discussed in the oxidizer tank section. Low frequency fuel tank oscillations were measured throughout the flight. The previous discussion of oxidizer tank low frequency vibrations can be applied to the fuel tank. A detailed comparison to tank response values measured during qualification tests is being made. Tank qualification test accelerations are given in figure 6.1-8.

Descent engine vibrations.- Descent engine vibration measurements performed satisfactorily throughout the periods of interest. A composite of acceleration spectral density at periods of maximum vibration is compared to the criteria in figure 6.1-10. The descent engine vibrations exceed the criteria at 40 Hz. A comparison of these data to actual qualification tests is being made.

Acoustic measurements.- The LTA-10R was instrumented with two microphones outboard of the +Z and -Z surfaces of the ascent stage. Data from these measurements show that the maximum sound pressure level (SPL) occurred at launch, as expected. Data at transonic and maximum dynamic pressure flight phases indicate that the sound pressure levels are at least 14 dB below those measured at lift-off. Analysis of the acoustic data at 85 to 87 seconds shows an overall SPL of 131 dB. The LTA-10R acoustic spectra at launch are compared to the LTA-3 acoustic spectra in

~~CONFIDENTIAL~~

~~CONFIDENTIAL~~

figure 6.1-11. The LTA-10R data agreement with LTA-3 data validates the acoustic spectrum used in the LTA-3 test, which provided many of the LM systems vibration qualification criteria. The LTA-10R vehicle was not equipped with thermal or micrometeoroid shielding; this shielding should reduce the acoustic noise acting on flight LM vehicles.

~~CONFIDENTIAL~~

CONFIDENTIAL

6-7

TABLE 6.1-1.- LUNAR MODULE LOW FREQUENCY VIBRATION  
DURING FIRST STAGE LAUNCH AND BOOST

	Launch release		Midboost		Inboard engine cutoff		Outboard engine cutoff	
	Frequency	Amplitude	Frequency	Amplitude	Frequency	Amplitude	Frequency	Amplitude
Lunar module x-axis	Invalid data		5.3 Hz	$\pm 0.2g$	6.1 Hz	$\pm 0.498g$	6.8 Hz	$\pm 1.13g$
Lunar module y-axis	12.0 Hz	$\pm 0.215g$	5.4 Hz	$\pm 0.08g$	6.1 Hz	$\pm 0.055g$	6.8 Hz	$\pm 0.062g$
Lunar module z-axis	Invalid data		5.4 Hz	$\pm 0.13g$	6.1 Hz	$\pm 0.083g$	6.8 Hz	$\pm 0.11g$
Lunar module apex attach point x-axis	4.5 Hz	$\pm 0.185g$	5.3 Hz	$\pm 0.15g$	6.1 Hz	$\pm 0.211g$	6.8 Hz	$\pm 0.555g$
Lunar module apex attach point y-axis	Invalid data		5.3 Hz	$\pm 0.071g$	NOTE: These are peak oscillatory values.			

CONFIDENTIAL

~~CONFIDENTIAL~~

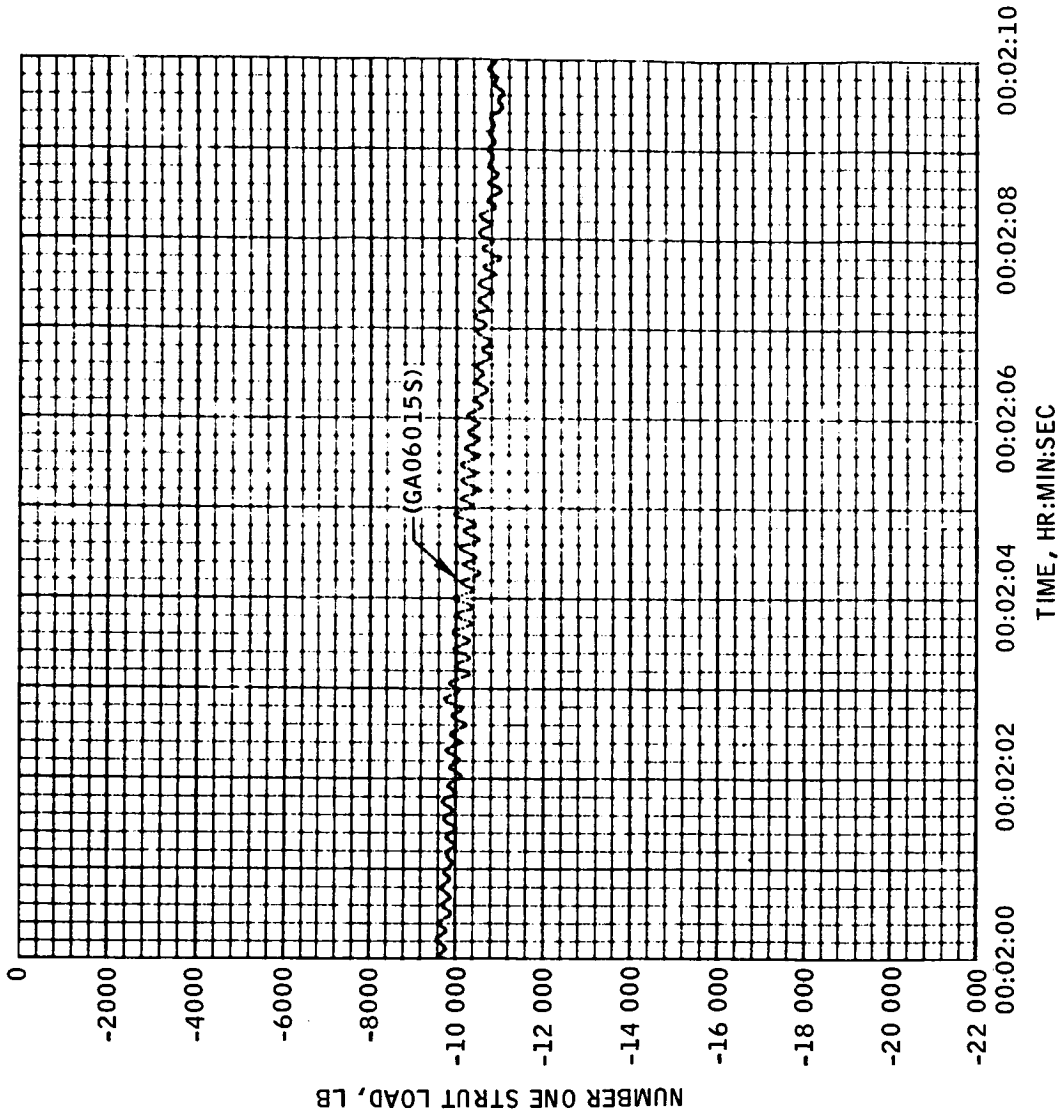


FIGURE 6.1-1.- +Z OUTRIGGER STRUT LOAD TYPICAL 5 Hz OSCILLATION.

~~CONFIDENTIAL~~

~~CONFIDENTIAL~~

6-9

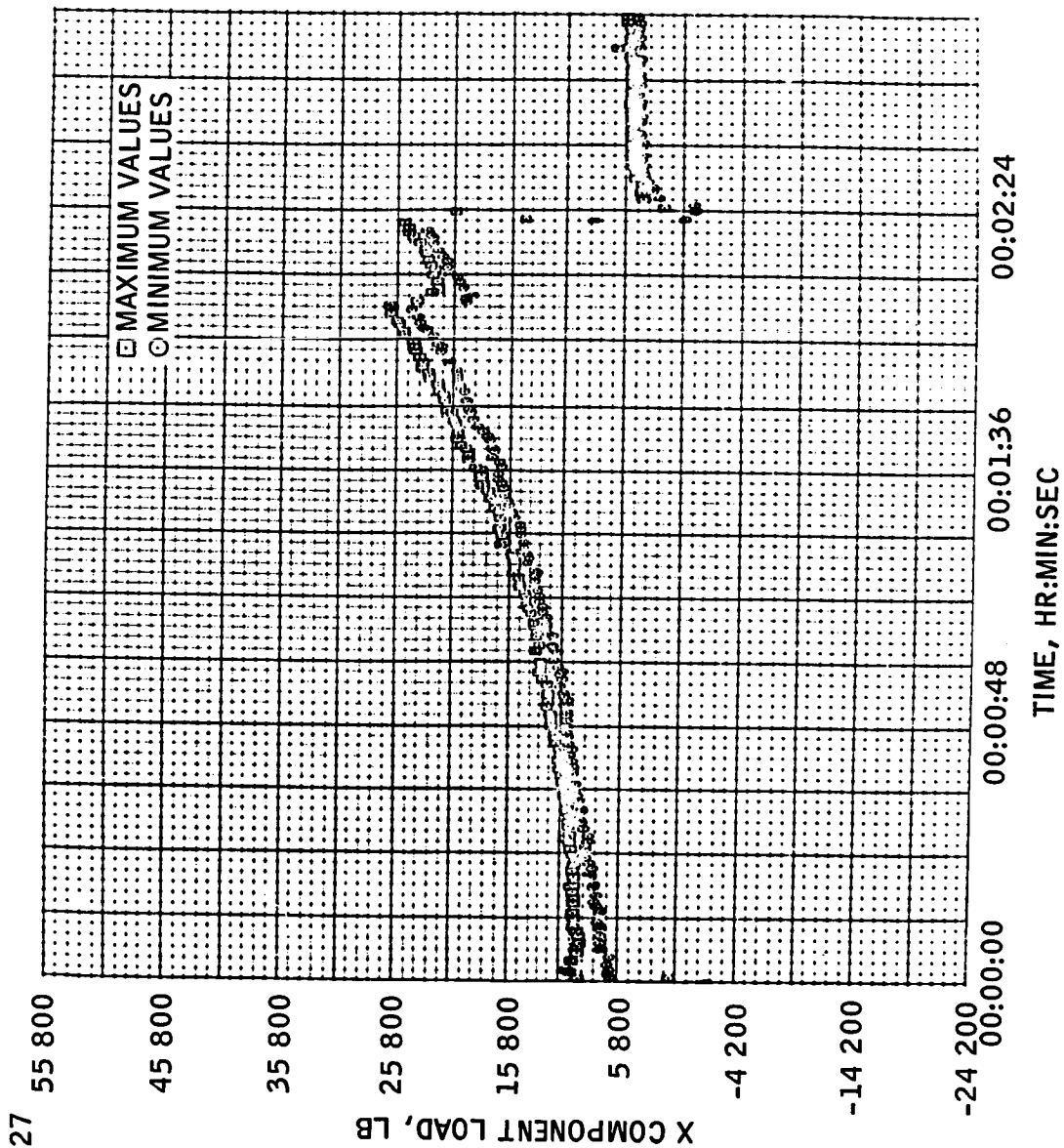


FIGURE 6.1-2.- EFFECT OF 5 Hz OSCILLATION ON +Z APEX  
X-COMPONENT OF LOAD.

~~CONFIDENTIAL~~



~~CONFIDENTIAL~~

NASA-S-68-528

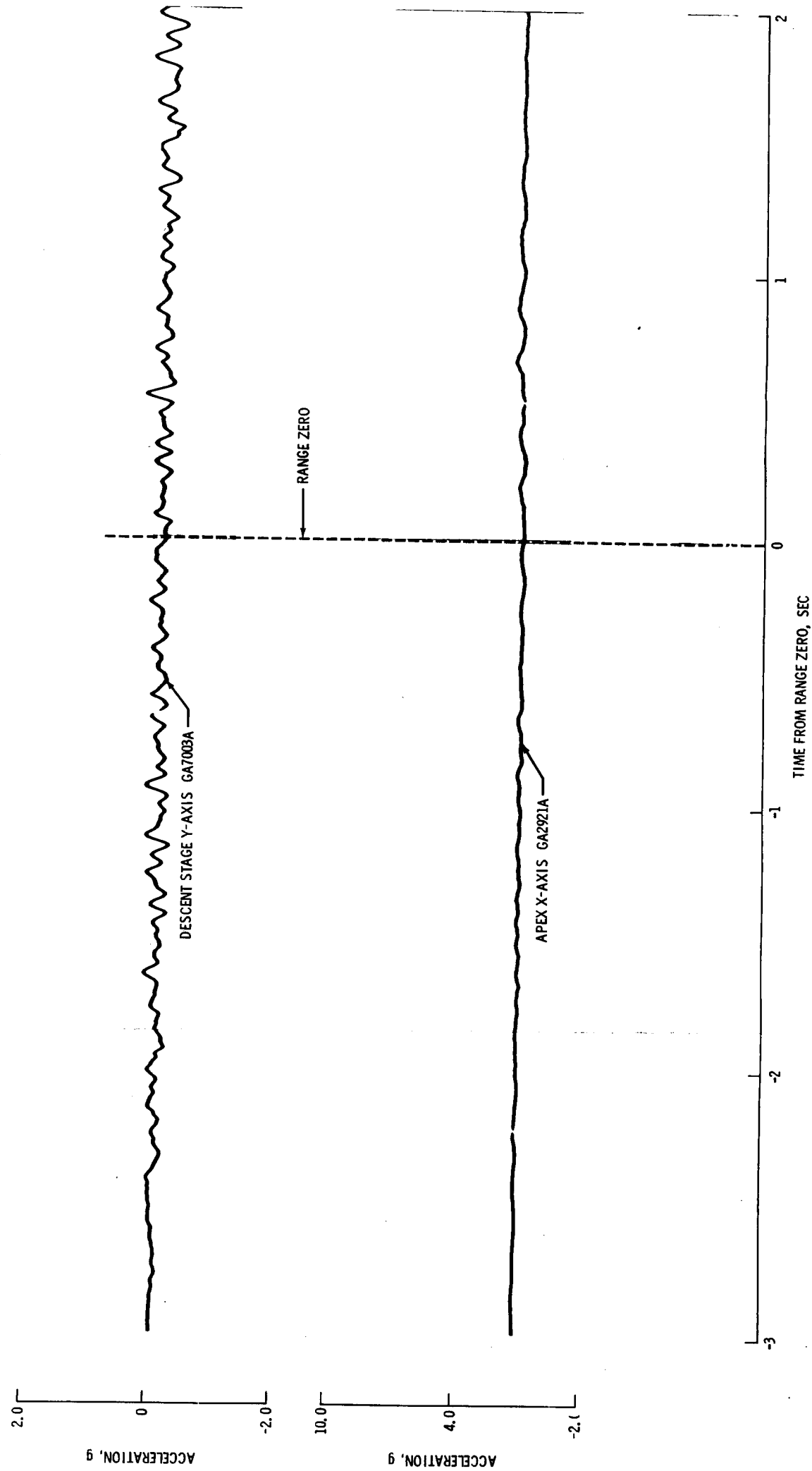


FIGURE 6.1-3. - LUNAR MODULE ACCELERATIONS AT LIFT-OFF.

~~CONFIDENTIAL~~

~~CONFIDENTIAL~~

6-11

NASA-S-68-529

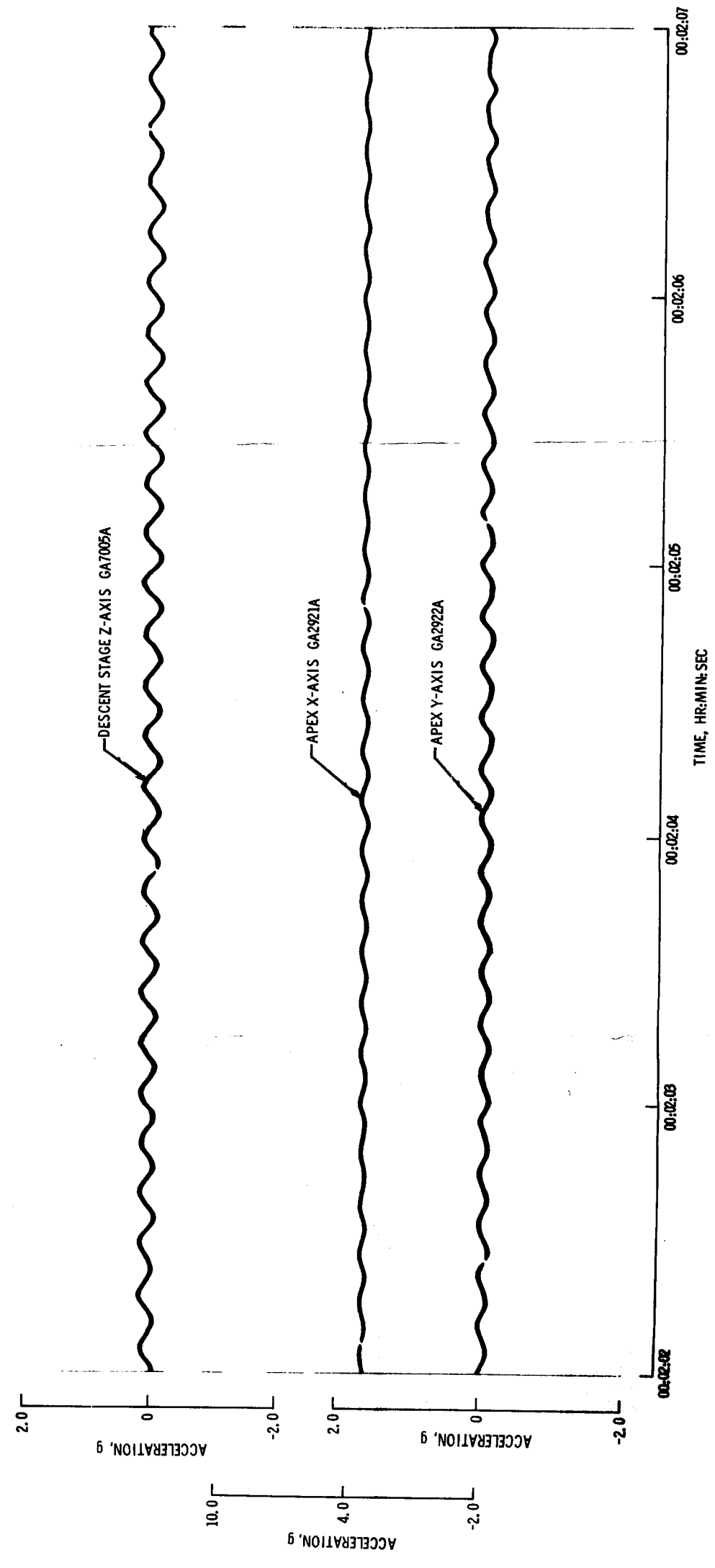


FIGURE 6.1-4. - LUNAR MODULE ACCELERATIONS DURING HIGH OSCILLATION PERIOD.

~~CONFIDENTIAL~~

~~CONFIDENTIAL~~

NASA-S-68-530

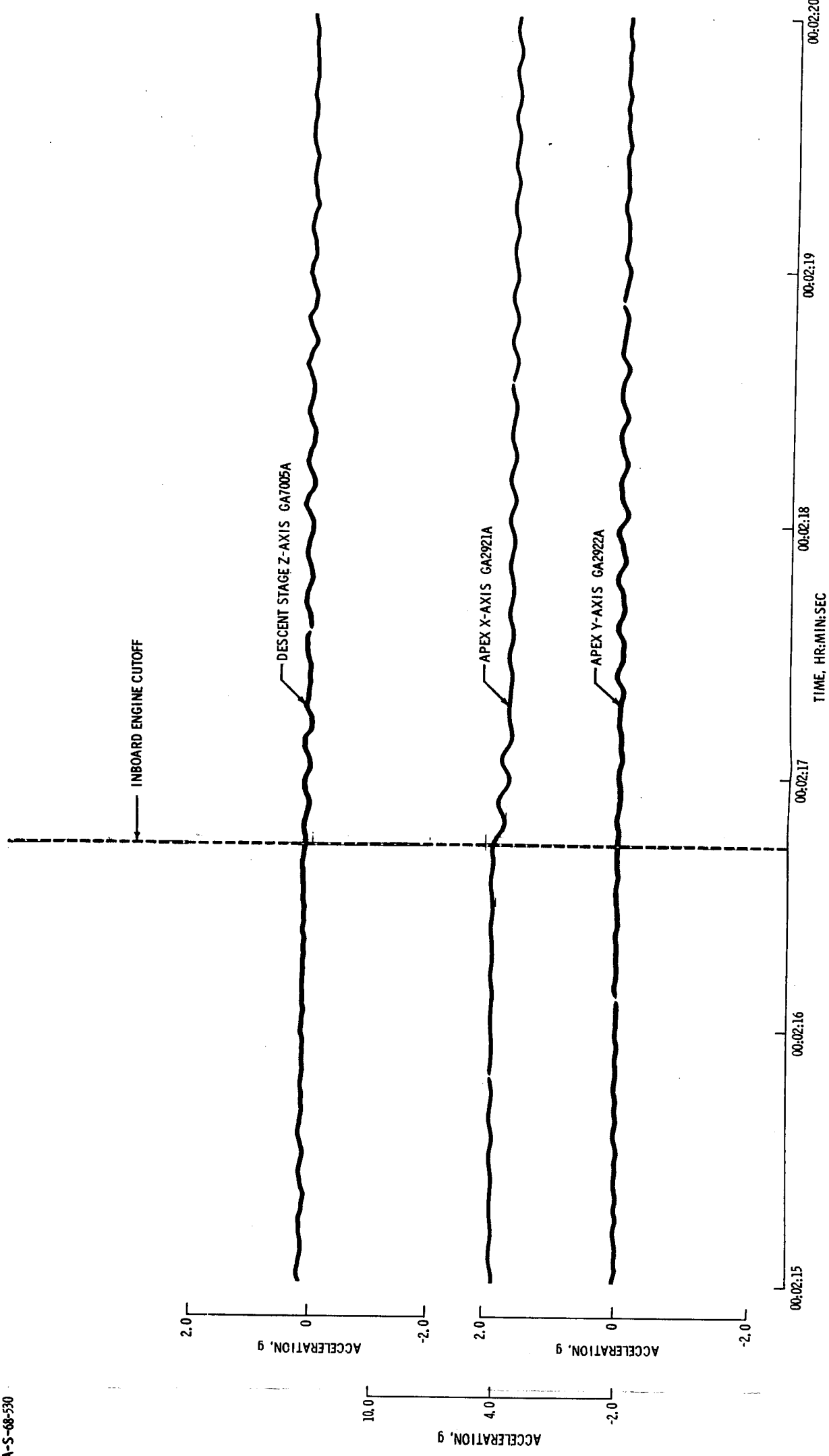


FIGURE 6.1-5. - LUNAR MODULE ACCELERATIONS DURING FIRST STAGE CENTER ENGINE CUTOFF.

~~CONFIDENTIAL~~

~~CONFIDENTIAL~~

6-13

NASA-S-68-531

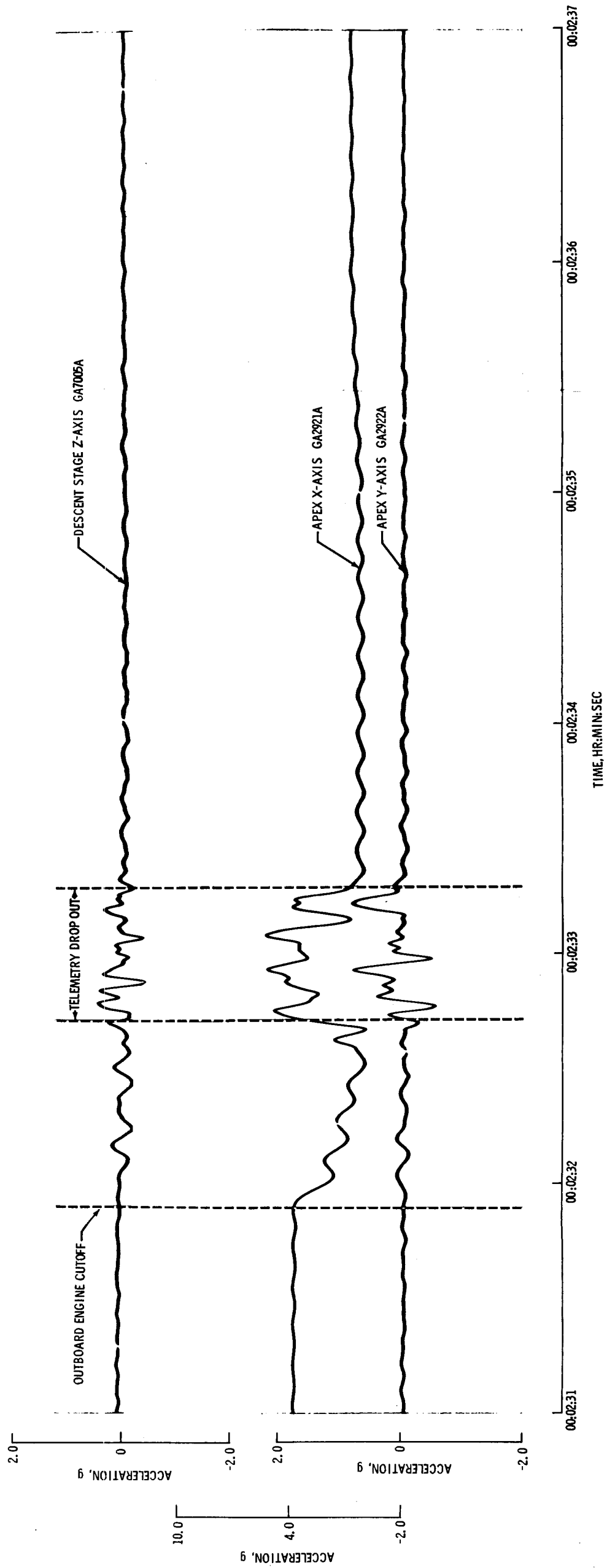


FIGURE 6.1-6. - LUNAR MODULE ACCELERATIONS DURING FIRST STAGE OUTBOARD ENGINE CUTOFF.

~~CONFIDENTIAL~~

~~CONFIDENTIAL~~

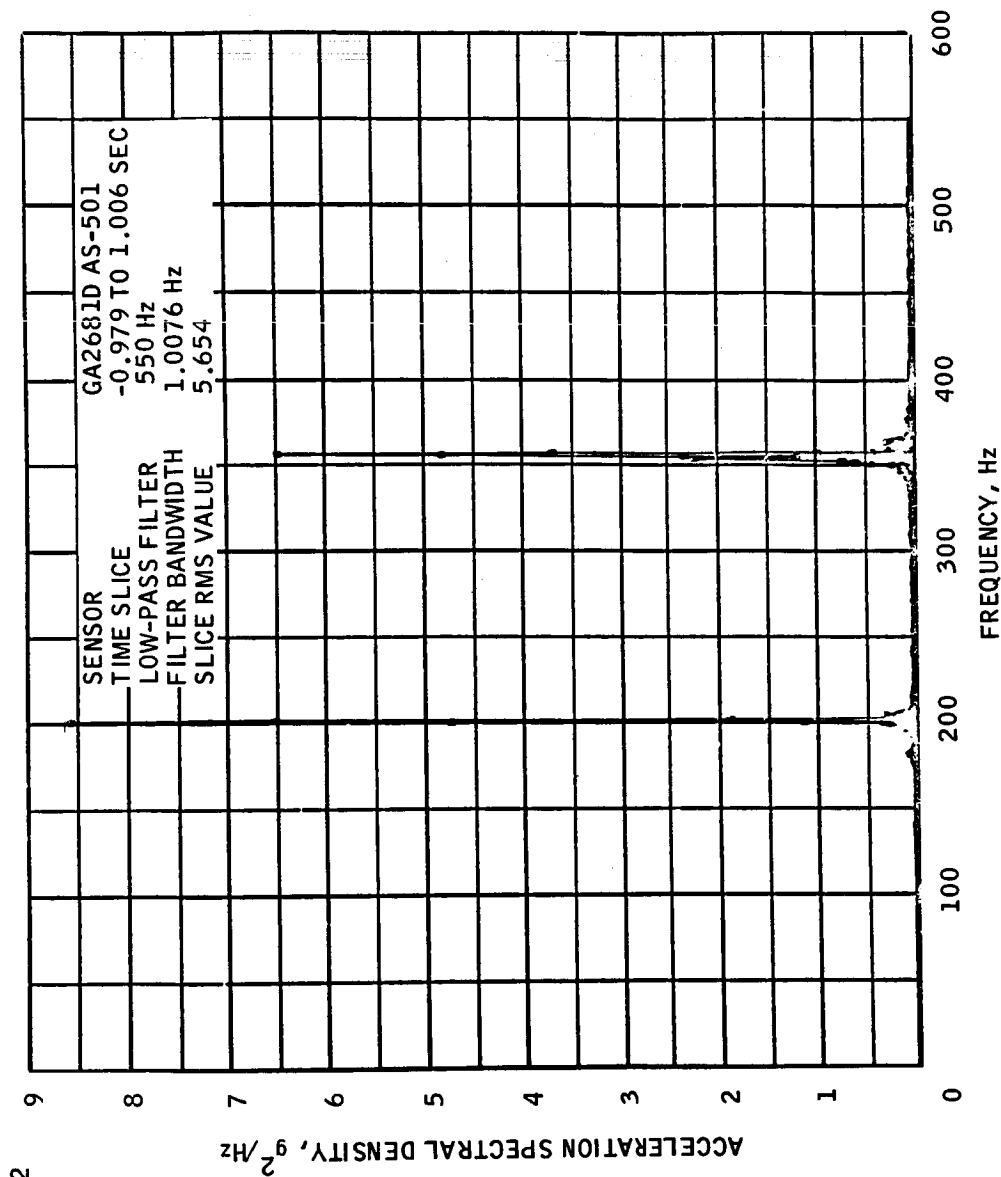


FIGURE 6.1-7.- ACCELERATION SPECTRAL DENSITY OF LTA-10R OXIDIZER TANK VIBRATION.

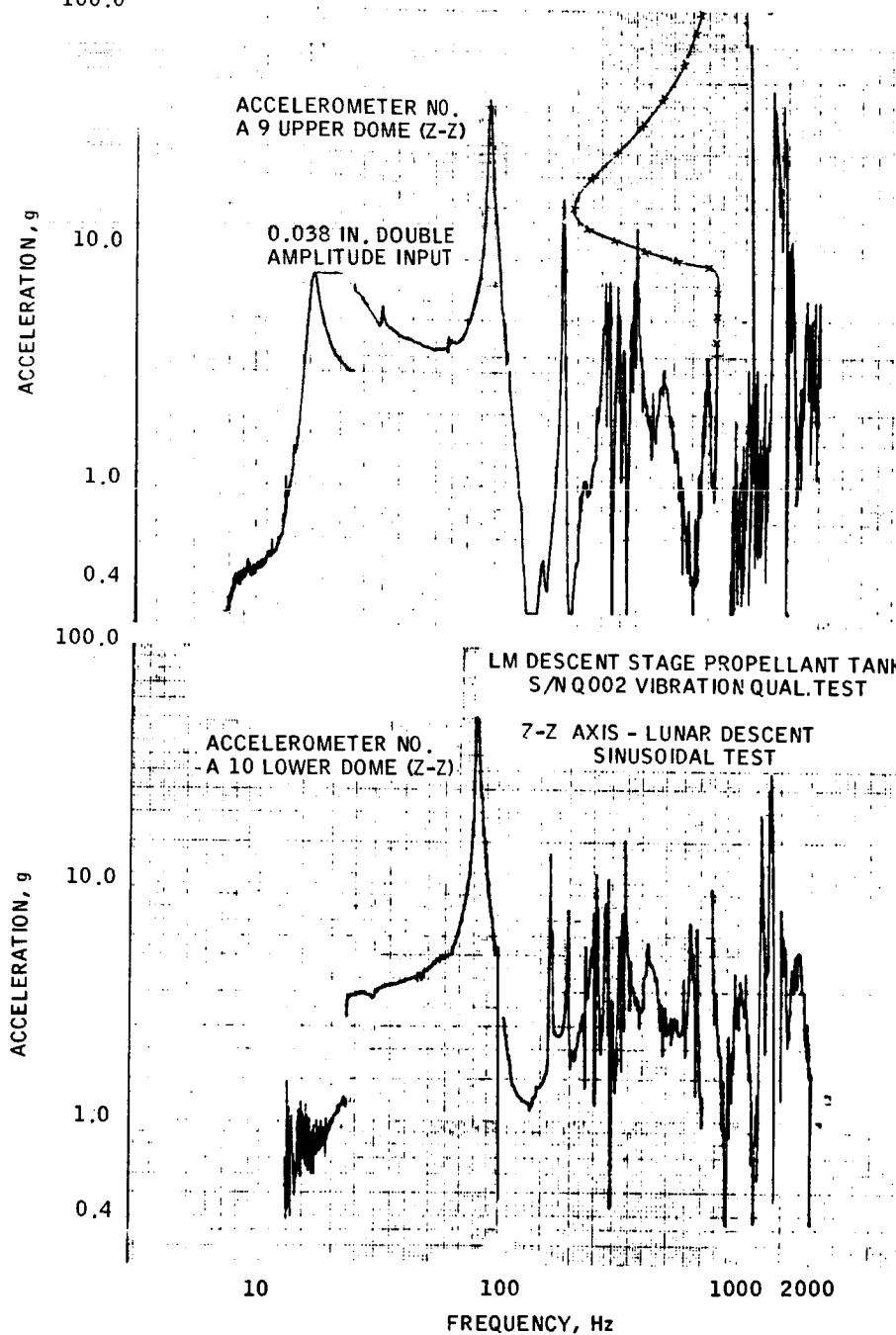
~~CONFIDENTIAL~~

~~CONFIDENTIAL~~

6-15

NASA-S-68-533

100.0



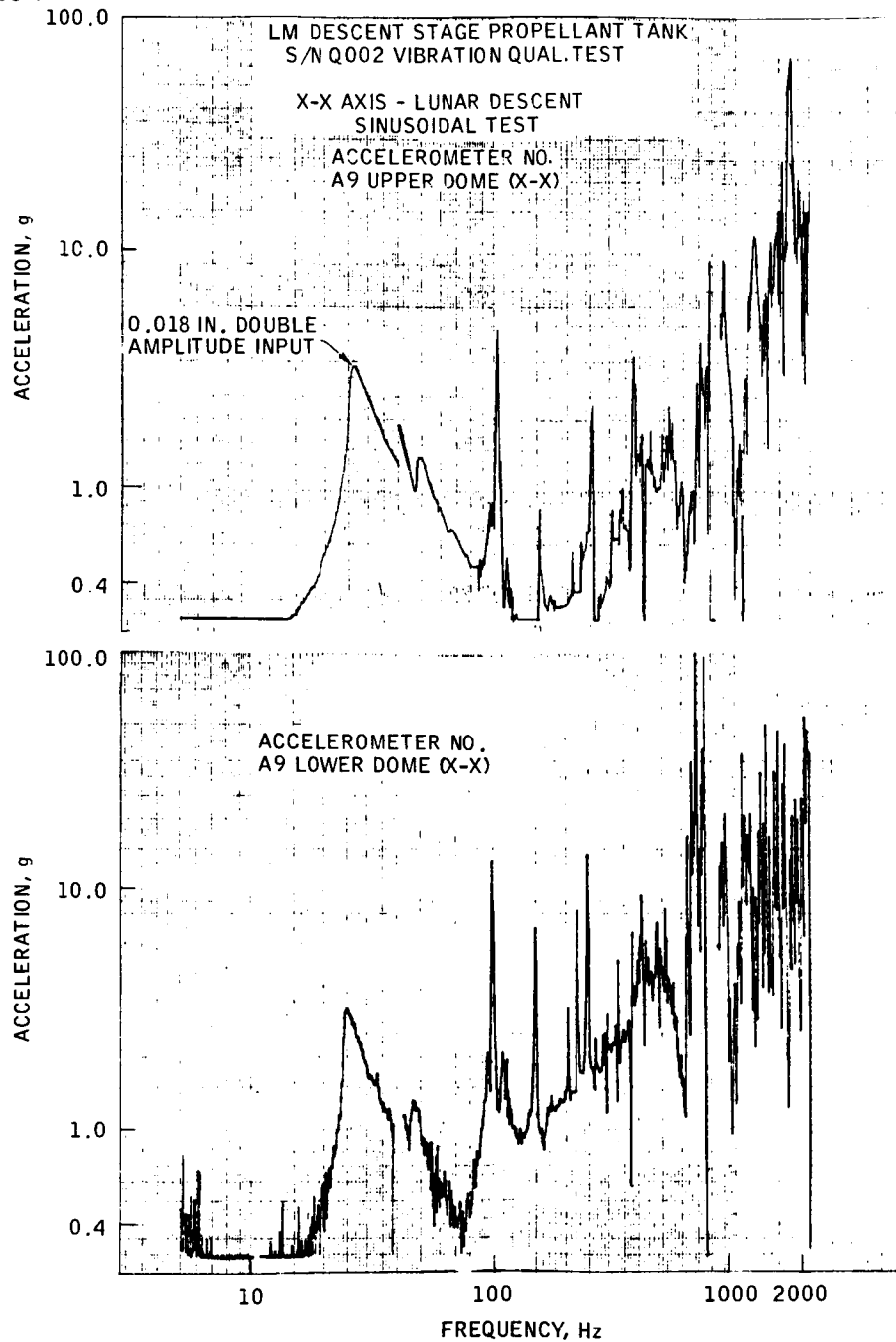
(A) RANDOM, TANK FULL.

FIGURE 6.1-8.- PROPELLANT TANK VIBRATION QUALIFICATION ACCELERATIONS.

~~CONFIDENTIAL~~

~~CONFIDENTIAL~~

NASA-S-68-534



(B) SINE, TANK FULL.

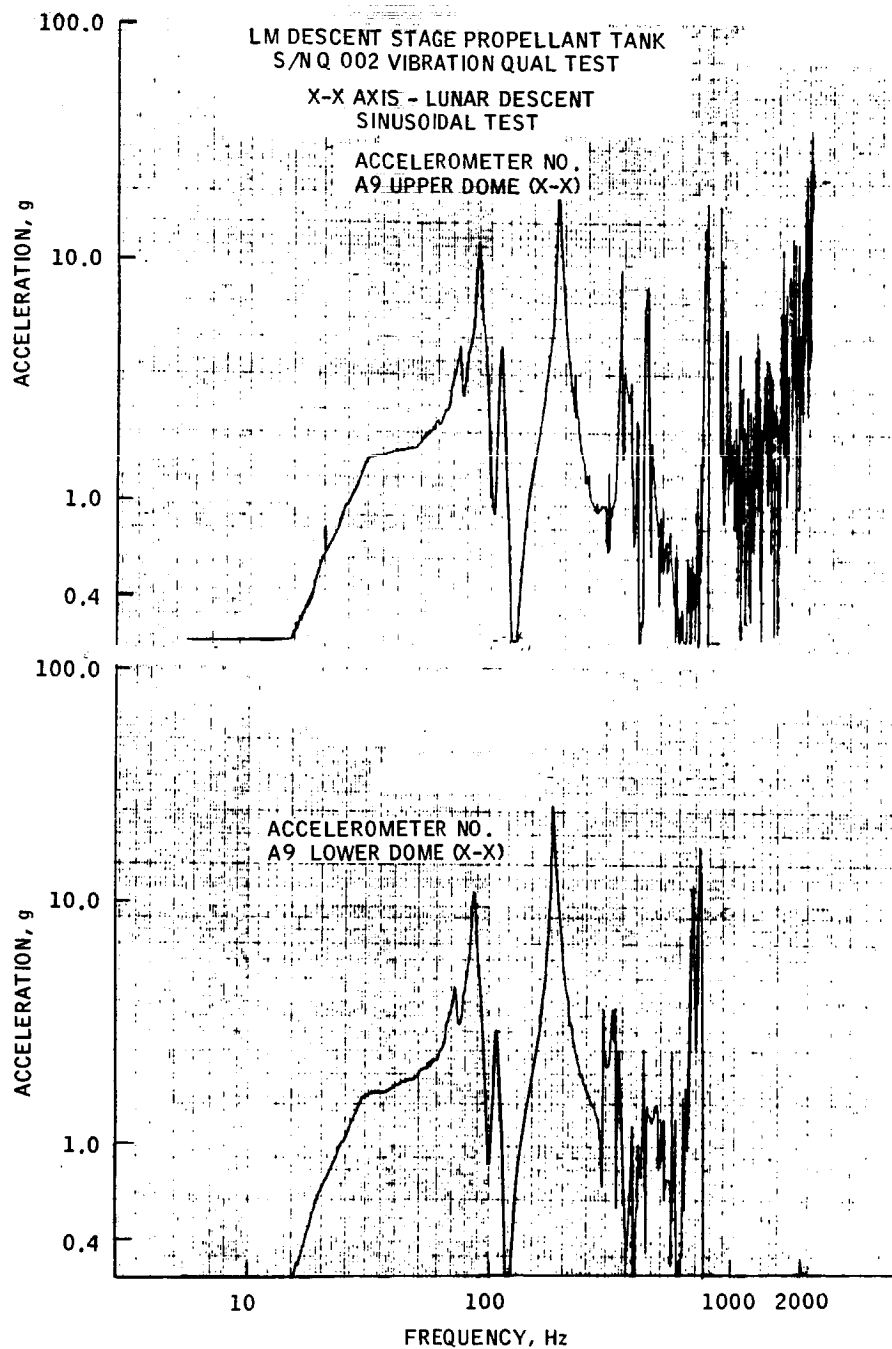
FIGURE 6.1-8.- CONTINUED.

~~CONFIDENTIAL~~

~~CONFIDENTIAL~~

6-17

NASA-S-68-535



(C) SINE, TANK EMPTY.

FIGURE 6.1-8.- CONCLUDED.

~~CONFIDENTIAL~~



~~CONFIDENTIAL~~

NASA-S-68-536

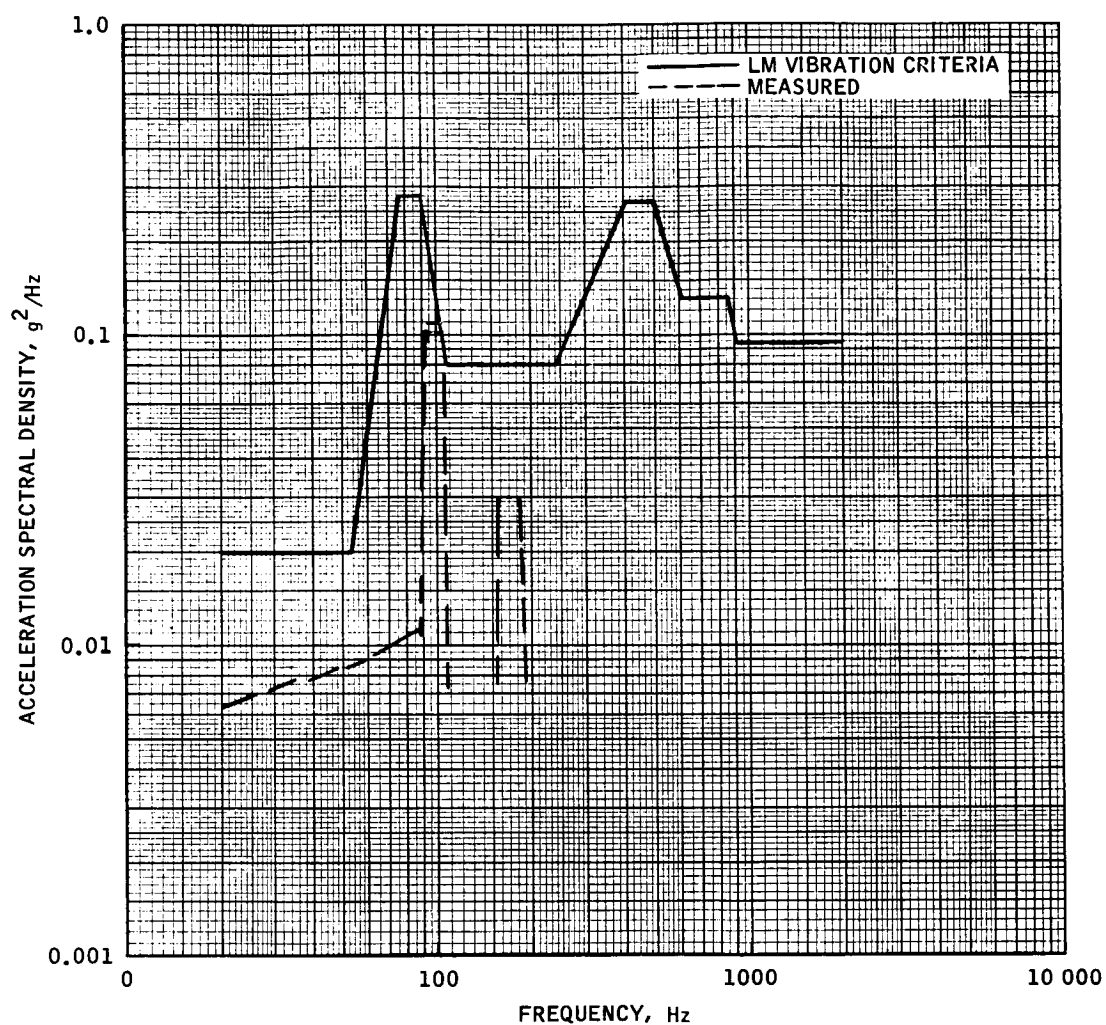


FIGURE 6.1-9.- COMPARISON OF LTA-10R FUEL TANK ACCELERATION SPECTRAL DENSITY TO QUALIFICATION CRITERIA.

~~CONFIDENTIAL~~

~~CONFIDENTIAL~~

6-19

NASA-S-68-537

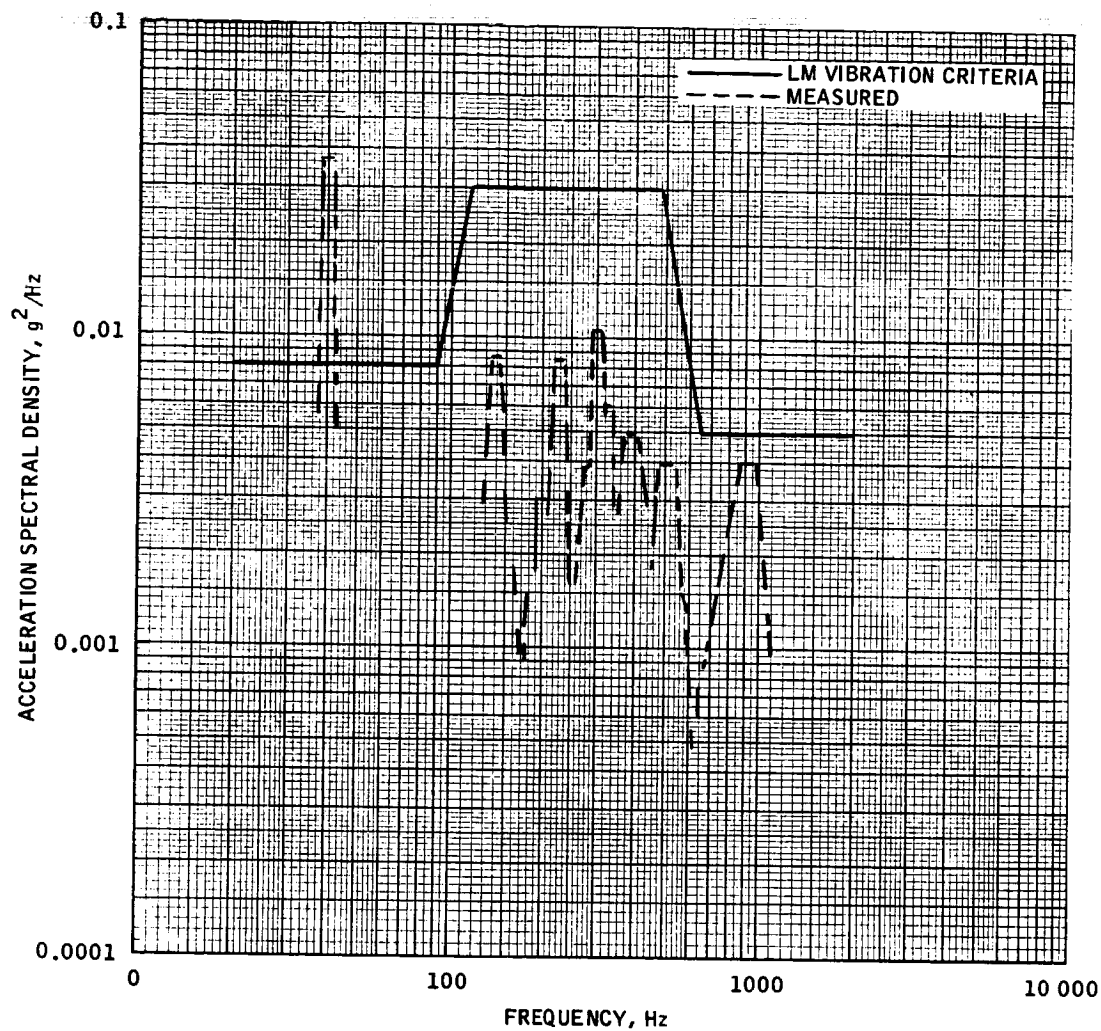


FIGURE 6.1-10.- COMPARISON OF LTA-10R DESCENT ENGINE ACCELERATION SPECTRAL DENSITY TO QUALIFICATION CRITERIA.

~~CONFIDENTIAL~~

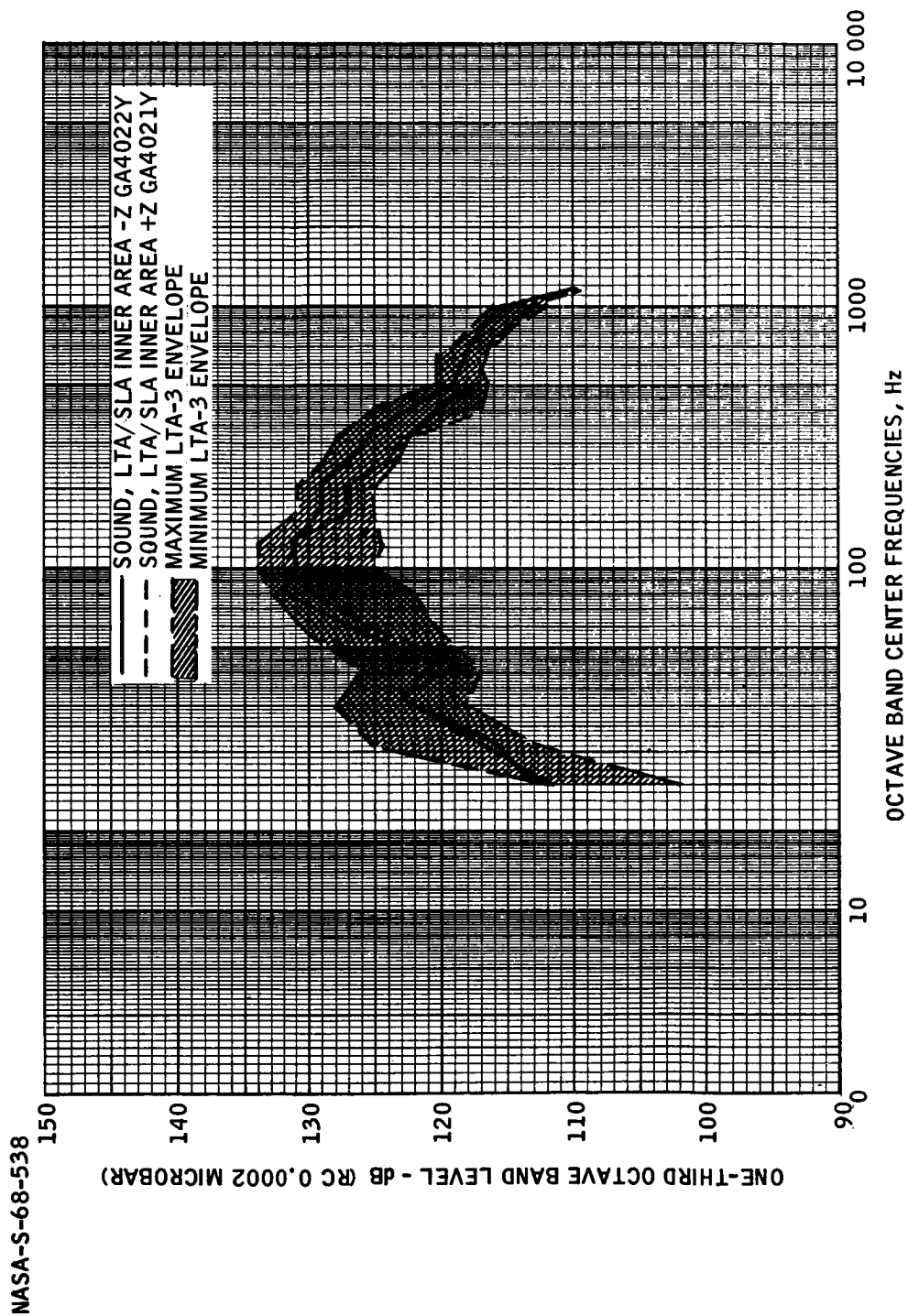
~~CONFIDENTIAL~~

FIGURE 6.1-11.- COMPARISON OF LTA-10R TO LTA-3 SOUND PRESSURE LEVELS SPECTRA AT LIFT-OFF.

~~CONFIDENTIAL~~

~~CONFIDENTIAL~~

6-21

## 6.2 INSTRUMENTATION

The two LTA-10R developmental flight instrumentation (DFI) FM telemetry links functioned during the launch phase of the mission, with two 1-second data losses occurring at S-II ignition (00:02:32.2) and again at S-IC interstage jettison (00:03:01.4).

A total of 38 measurements were instrumented, including strain gauge, accelerometer, thermal, and acoustical parameters. All channels operated normally except that three acceleration measurements operated erratically during the critical periods of boost phase. These measurements were the acceleration X-axis no. 1, descent stage, GA7001A, and the acceleration Z-axis, descent stage, GA7005A, both located in the descent engine cavity of LTA-10R; and vibration LTA-10R/SLA support fitting GA2922D, located on the +Y-axis apex joint fitting of the LTA-10R/SLA support structure. Erratic biased operation of the low frequency (below 14 Hz) acceleration component occurred in the high noise regions from T minus 3 to T plus 9 seconds and again in the max q region at 00:01:00 to 00:01:25. Postflight tests of a like accelerometer have produced similar biased results when the accelerometer was excited with a random vibration level of 7g rms superimposed on a 6-Hz sinusoidal vibration at 0.5g peak level.

It should be noted that all strain measurements (GA0601S through GA0616S) were not calibrated, prior to flight, by the application of known loads and the recording of known outputs. Calibrations used to reduce the strain data were analytically derived.

~~CONFIDENTIAL~~

~~CONFIDENTIAL~~

THIS PAGE INTENTIONALLY LEFT BLANK

~~CONFIDENTIAL~~

~~CONFIDENTIAL~~

7-1

7.0 FLIGHT CREW

(This section is not applicable.)

~~CONFIDENTIAL~~

~~CONFIDENTIAL~~

THIS PAGE INTENTIONALLY LEFT BLANK

~~CONFIDENTIAL~~

~~CONFIDENTIAL~~

8-1

8.0 BIOMEDICAL EVALUATION

(This section is not applicable.)

~~CONFIDENTIAL~~



~~CONFIDENTIAL~~

THIS PAGE INTENTIONALLY LEFT BLANK

~~CONFIDENTIAL~~

~~CONFIDENTIAL~~

9-1

## 9.0 MISSION SUPPORT

The Mission Support section of this report is based upon real-time observations and may not precisely agree with the refined data and information used in other sections of the report.

### 9.1 FLIGHT CONTROL

The Apollo 4 mission was controlled from the Mission Control Center-Houston (MCC-H) at the Manned Spacecraft Center, Houston, Texas.

#### 9.1.1 Prelaunch

Flight controllers began terminal countdown support at T minus 11 hours 40 minutes on November 8, 1967.

At T minus 11 hours, the following scheduled commands were successfully executed from MCC-H.

- a. C-BAND BEACON ON (RTC 75)
- b. VHF FM ON (RTC 77)
- c. ROLL RATE BACKUP (RTC 44)
- d. PITCH RATE BACKUP (RTC 45)
- e. YAW RATE BACKUP (RTC 46)
- f. CENTRAL TIMING EQUIPMENT UPDATE
- g. APOLLO GUIDANCE COMPUTER DISPLAY AND KEYBOARD CHECKOUT

One of the first problems the flight controllers encountered was with the spacecraft oxygen tanks. The pressure in the no. 2 tank was low at 687 psia, and the pressure in the no. 1 tank was at 907 psia. Both tanks should have had pressure readings in the normal operating range of 865 to 935 psia.

Initially, the trouble was believed to be with the pressure transducer in the no. 2 tank; however, the pressure trend for several hours indicated a gradual increase. A constant oxygen quantity readout verified tank integrity and the tank heaters, fans, and control circuitry became suspect.

~~CONFIDENTIAL~~

~~CONFIDENTIAL~~

At approximately T minus 9 hours 30 minutes, the spacecraft was closed out when the inner hatch was installed. Close observation had failed to disclose the real nature and cause of the anomalous pressure; however, the cryogenic tank heater switch positions were reversed prior to closeout. Also, the technicians at Kennedy Space Center reported that the circuit breaker for the heater control in the no. 2 oxygen tank was found to be open. (Refer to section 5.18 for an explanation of this problem.)

At T minus 8 hours 30 minutes, the countdown was held for approximately 2 hours to allow the launch vehicle count to catch up. During this hold period, the no. 2 oxygen tank heaters were commanded ON (RTC 65) by MCC-H to test the system. The heaters remained on for approximately 30 minutes for the test and, as a result of satisfactory operation, were left on for an additional 35 minutes to increase the tank pressure to an acceptable level.

The following launch vehicle prelaunch verification commands were successfully transmitted at T minus 4 hours and at T minus 1 hour 17 minutes.

- a. SECTOR DUMP
- b. SINGLE WORD DUMP

At T minus 42 minutes, the C-band radar at the Canary Island network station was reported inoperative and apparently could not be used for the mission.

At T minus 15 minutes, the central timing equipment was again updated and the propellant isolation valves for the four quads of the service module reaction control subsystem were opened.

At T minus 8 minutes 45 seconds, the spacecraft rate backup reset command (RTC 50) was sent and at T minus 1 minute 30 seconds, the body-mounted attitude gyros were observed to be driving the attitude gyro coupling unit. Also, the display and keyboard command (V75E) was sent to the Apollo guidance computer so that, if necessary, it would provide a backup to the lift-off discrete.

At T minus 2 minutes 50 seconds, after the launch vehicle automatic sequence had started, the telemetry computer at the Bermuda station faulted. The computer was recycled and at T minus 2 minutes the Bermuda station was ready to support the mission; no hold was called by MCC-H.

~~CONFIDENTIAL~~

~~CONFIDENTIAL~~

9-3

### 9.1.2 Launch Phase

The Apollo 4 lift-off occurred at 12:00:01.3 G.m.t. (only 1.3 seconds later than planned) on November 9, 1967.

S-IC flight. - Cutoff of the inboard and four outboard engines of the launch vehicle first stage (S-IC) occurred at the following times.

	<u>Planned</u>	<u>Actual</u>
Inboard engine cutoff	00:02:15.5	00:02:15.5
Outboard engines cutoff	00:02:31.9	00:02:30.8

No anomalies were noted during S-IC flight.

S-II flight. - Ignition and cutoff of the launch vehicle second stage (S-II) occurred at the following times.

	<u>Planned</u>	<u>Actual</u>
Ignition (start command)	00:02:33.3	00:02:32.2
Cutoff	00:08:36.3	00:08:39.8

After telemetry handover from the launch site to the Bermuda station, the S-IC stage engine no. 5 chamber pressure, which had been reading approximately 780 psia, dropped to approximately 160 psia. However, the THRUST OK measurement for the engine was nominal, the longitudinal acceleration was nominal, and an engine no. 5 chamber pressure readout received at KSC still indicated approximately 780 psia. Therefore, it was concluded that engine no. 5 was operating properly.

A difference of approximately 1.3 degrees from the expected roll attitude was observed and apparently was not removed during the S-II stage burn. However, the difference was reduced to zero during the S-IVB burn.

S-II stage second plane separation occurred at 00:03:01.4; the planned separation time was 00:03:02.6. The event was verified by two of three cues because the S-II recirculating battery voltage decayed slowly instead of going to approximately zero volts, which would have provided the third cue. The launch escape system was jettisoned at 00:03:07.2 (planned time was 00:03:08.8) with no anomalies.

At 00:04:30, a slight southerly trend (approximately 15 ft/sec) was indicated by the crossrange velocity from the Apollo guidance computer. The indication increased to approximately 50 ft/sec but was verified to

~~CONFIDENTIAL~~

~~CONFIDENTIAL~~

be from the Apollo guidance computer only and the error was corrected by the first navigation update to the computer.

A pitch-axis drift of 4 degrees in the attitude gyro coupling unit was observed at 00:08:30; most of the drift was attributable to readout error but some drift did exist.

S-II engine cutoff occurred approximately 4 seconds late and the propellant utilization shift occurred later than predicted. The cutoff conditions were observed to be a velocity of approximately 22 490 ft/sec and a flight path angle of 0.55 degree, or about 345 ft/sec low and 0.03 degree high, respectively.

S-IVB flight.- During the launch phase, ignition and cutoff of the launch vehicle third stage (S-IVB) occurred at the following times.

	<u>Planned</u>	<u>Actual</u>
Ignition (start command)	00:08:37.3	00:08:40.7
Cutoff	00:10:56.0	00:11:05.6

The slightly lofted flight path angle was corrected during the burn and the stage performed nominally. The later-than-planned cutoff time resulted from the low S-II velocity at engine cutoff.

Insertion was nominal with a cutoff velocity of 25 568 ft/sec, a flight path angle of 0.003 degree, and an altitude of 103.31 n. mi.

### 9.1.3 Earth Orbit - Revolution 1

Insertion into the planned 100 n. mi. circular orbit resulted in an actual orbit of 102.5 n. mi. by 99.3 n. mi. The S-IVB stage configured itself properly before engine cutoff for the two revolutions of coasting. Testing of the launch vehicle command and communications system was successfully conducted during the passes over Carnarvon and the continental United States.

The pitch axis drift in the spacecraft attitude gyro control unit was observed to have a true drift in zero-g of approximately 3 deg/hr, or about half the maximum permissible value. The drift presented no problem at this time. At approximately 01:28:00, during the Guaymas pass, the fuel cell no. 3 oxygen flow transducer failed.

~~CONFIDENTIAL~~

~~CONFIDENTIAL~~

9-5

#### 9.1.4 Earth Orbit - Revolution 2

The S-IVB stage pneumatic pressure decay rate increased to an indicated average of 4.0 psi/min. between 01:49:55 (Vanguard loss of signal) and 02:25:21 (Carnarvon acquisition of signal).

Carnarvon pass.- The first spacecraft navigation update was generated and loaded at the Carnarvon and Hawaii sites. Carnarvon successfully up-linked the navigational update to the spacecraft after having initial command problems resulting from an improperly aligned uhf transmitter. ← The problem was corrected by switching to another uhf transmitter. At 02:31:21, Carnarvon also commanded ON (RTC 65) the no. 2 tank heaters in the spacecraft oxygen system to increase the bottle pressure.

Hawaii pass.- At 02:54:14, MCC-H commanded ON (RTC 67) the oxygen tank no. 1 heaters. This action resulted in the heaters in both oxygen tanks being on in order to increase bottle pressure sufficiently to preclude heater cycling during the first firing of the service propulsion subsystem. Testing of the launch vehicle command and communications system was successfully performed during the pass.

At loss of signal at Hawaii (02:56:55), the S-IVB stage pneumatic pressure decay rate was observed to be approximately 15 psi/min. However, at that rate, the lifetime was approximately 2 hours and was satisfactory for restart of the S-IVB engine.

U. S. pass.- At Guaymas acquisition of signal (03:01:23), the S-IVB stage pneumatic pressure decay rate had increased to approximately 20 psi/min. This resulted in approximately a 1-hour lifetime and was satisfactory for restarting the S-IVB engine.

Subsequent to initiation of time base 6 at 03:06:00, an apparent problem with the continuous vent system was observed. The continuous vent line pressures were expected to decay to approximately 0 psi within 15 seconds after initiation of time base 6, but the pressure did not decay, indicating an apparent failure of the continuous vent valve to fully close. It was important for this system to be closed because the helium supply feed for liquid hydrogen tank repressurization was to be initiated at the same time that the vent system was closed. Mission rule command action was taken to close the valve. The proper command sequence was executed several times and proper vehicle command system response was received three times. However, the continuous vent line pressure still indicated pressure values greater than zero with a slow decay. The indication of bleed flow through the continuous vent system was apparently confirmed by the decay in the liquid hydrogen tank pressure after repressurization was terminated.

~~CONFIDENTIAL~~

~~CONFIDENTIAL~~

The final sequence of the mission rules command action (reopen the liquid hydrogen repress valve) was inadvertently omitted. Omission of the final step of the command sequence prevented the vehicle from taking advantage of the small remaining repressurization capability which could have improved a possibly marginal condition for the second S-IVB stage engine start. However, restart of the S-IVB stage engine was successfully accomplished.

Ten seconds prior to the second S-IVB stage ignition, the spacecraft updata link was automatically switched from the uhf command receiver to unified S-band.

#### 9.1.5 Translunar Injection - Revolution 3

Second S-IVB stage burn.- During the translunar injection, the ignition and cutoff of the second S-IVB stage burn occurred at the following times.

	<u>Planned</u>	<u>Actual</u>
Ignition (start command)	03:11:33.5	00:11:26.6
Cutoff	03:16:39.9	03:16:26.3

The S-IVB stage cutoff conditions resulted in an orbit of 9290 n. mi. by -43 n. mi. compared with the planned orbit of 9406 n. mi. by -49 n. mi.

Bermuda pass.- By the time of S-IVB stage cutoff, the pitch readout from the spacecraft attitude gyro coupling unit differed from the inertial measurement unit by approximately 20 degrees. Mission rule action required that when the difference exceeded 15 degrees, a command (RTC 47) could be transmitted to align the flight director attitude indicator (FDAI). The attitude to which the attitude gyro coupling unit would align differed considerably from the launch vehicle cold-soak attitude and commanding the FDAI to align would have created greater disparity in the readings. However, later in the flight, the Apollo guidance computer commanded FDAI into an align mode after the SPS firing had zeroed the drift in the attitude gyro coupling unit to within expected tolerances.

Controllers at MCC-H attempted to turn off both oxygen tank heaters, which had been on since the pass over the Hawaii station in revolution 2. The command (RTC 70) was transmitted three times unsuccessfully through the Bermuda station. The indications were that the Bermuda station did not have good two-way lock on the spacecraft unified S-band.

Vanguard pass.- Command was handed over to the Vanguard ship at approximately 03:23:00, and after an initial difficulty in maintaining

~~CONFIDENTIAL~~

~~CONFIDENTIAL~~

9-7

spacecraft unified S-band two-way lock, the station successfully uplinked the display and keyboard command (V75E) as a backup to the Apollo guidance computer separation discrete. The oxygen heaters OFF command (RTC 70) was transmitted with no difficulty at 03:24:05.

Ascension pass.- The Ascension station acquired the CSM/S-IVB at approximately 03:25:00. CSM/S-IVB separation occurred at 03:26:30 and the sequence was nominal.

First service propulsion subsystem burn.- Ignition and cutoff for the first SPS burn occurred at the following times.

	<u>Planned</u>	<u>Actual</u>
Ignition	03:28:20.1	03:28:06.6
Cutoff	03:28:35.1	03:28:22.6

The SPS performed satisfactorily during the firing, which resulted in an orbit of 9782 by -46 n. mi. compared with the planned orbit of 9903 by -41 n. mi. The Apollo guidance computer vectors taken after the burn agreed perfectly with the planned orbit. After SPS cutoff, the spacecraft maneuvered to the proper attitude for the extended heat shield cold-soak period.

Controllers at MCC-H performed extensive testing (through the Ascension station) of the launch vehicle communications and command system and all uplinked commands were accepted by the onboard system.

The second navigation update to the spacecraft was generated and loaded at the Ascension and Carnarvon stations. This navigation update was transmitted by MCC-H execution near spacecraft apogee. When the initializing keycode sequence (V76E) for the update was attempted, the VERB entered the Apollo guidance computer properly, but the keycode for the numeral 7 resulted in a KKK failure and an uplink block condition. The uplink block was corrected by transmitting the command sequence of all zeros/error/reset/clear; the navigation update was correctly entered in the computer at 05:24:27. The load was transmitted with AGC OVERRIDE OFF because the spacecraft was at the maximum slant range with the highest probability of errors.

Carnarvon pass.- After command was handed over to the Carnarvon station during revolution 3, the testing of the launch vehicle communications and command system continued, as planned, through the first 45 minutes of the pass. All commanding was successful. However, the navigation update A-command could not be verified until a sector dump command was transmitted.

~~CONFIDENTIAL~~



~~CONFIDENTIAL~~

Throughout the third revolution, the Carnarvon station experienced data oscillation problems with both the S-IVB and launch vehicle instrumentation unit telemetry. When instrumentation unit S-band telemetry was being processed, the analog data values would fluctuate as much as 20 PFS and as often as the ground computer update rate of once per second. The downlinked discretes, launch vehicle computer downlink (H60-603) data, and the synchronization patterns were all solid as the PCM ground station never broke lock. Many ground combinations were tried in attempting to circumvent the problem, but the results were the same for all attempted cases — oscillating telemetry analog parameters. One operation Carnarvon did not attempt was to interchange the ground S-band systems. Carnarvon used unified S-band system no. 2 for the duration of S-band reception. The PCM ground station operator could see the analog parameters oscillate as they passed through the decommutator; however, the discretes and the synchronization pattern were always solid. Data values were compared with MCC-H, which was receiving the instrumentation unit S-band data from the Ascension station; consequently, MCC-H was not displaying the oscillating analog parameters which were being viewed at Carnarvon. Later into the third revolution, at 07:02:00, when vhf data from the instrumentation unit was received at Carnarvon, the data oscillation problem still existed.

The spacecraft vhf antennas were procedurally switched in accordance with the flight plan. The -Z (upper) vhf antenna was used during most of the mission, but at 07:28:58 the system was commanded to go to the +Z antenna. An initial loss of vhf data was observed, as expected, but signal margins improved to normal levels.

As required by the flight plan, purge of each fuel cell was performed. The ground command sequence commenced at 07:29:49 and was completed at 07:40:58 but fuel cell no. 2 was purged for only 1 minute. Fuel cells 1 and 3 were each purged for the nominal 2 minutes. The shorter interval for fuel cell no. 2 was a result of improper time coordination with purge activity.

Second SPS burn.— Ignition and cutoff for the second SPS burn occurred at the following times.

	<u>Planned</u>	<u>Actual</u>
Ignition	08:10:56	08:10:54.8
Cutoff	08:15:26.9	08:15:35.2

The SPS solenoid drivers event lights illuminated at the predicted ignition time. However, there was no indication of the Apollo guidance

~~CONFIDENTIAL~~

~~CONFIDENTIAL~~

9-9

computer command to turn the engine on nor any rise in engine chamber pressure. In accordance with mission rule action, SPS ON command (RTC 11) was ground commanded approximately 6 seconds from the time the SPS solenoid drivers were indicated to have grounded (08:11:00); within 1 second the SPS ON command and a nominal rise in SPS chamber pressure were observed on the onsite displays.

Utilizing onsite telemetry computer special processing, it was determined that the SPS ON command from the Apollo guidance computer had preceded the ground commanded SPS ON (RTC 11) by approximately 6 seconds. No real explanation is evident as to why the Apollo guidance computer ON command and the chamber pressure data were not present for approximately 6 seconds.

The transmission of RTC 11 overrides the guidance and navigation subsystem's engine cutoff function. The transmission of RTC 12 is therefore required to cut off the SPS, followed by the transmission of RTC 13 to re-establish guidance and navigation subsystem control for entry.

Guam pass. - The second SPS burn was observed to perform nominally and the SPS OFF command (RTC 12) was transmitted from MCC-H at 08:15:32.4, followed by SPS ON/OFF reset command (RTC 13) at 08:16:02. The reset command was delayed while SPS OFF command (RTC 12) (a priority command) was still being transmitted.

SPS cutoff resulted in approximately 10 seconds of overspeed. The Apollo guidance computer commanded SPS shutdown at 08:15:25.1; the actual shutdown occurred at 08:15:35.2. The technique for shutting down the burn was to be based on the use of the Apollo guidance computer telemetry discrete (STEER FLAG). This discrete normally occurs 3 or 4 seconds prior to the Apollo guidance computer commanded cutoff and with average data delays would have allowed a slight overspeed of approximately 2 seconds.

The following timeline reflects the time delays making up the overspeed.

<u>Time</u>	<u>ΔT, sec</u>	<u>Event</u>
08:15:25.1	-	Apollo guidance computer SPS cutoff command observed from onboard time recording
08:15:29.6	4.5	Apollo guidance computer STEER FLAG observed at MCC-H (cue for SPS OFF (RTC 12) execute)

~~CONFIDENTIAL~~

~~CONFIDENTIAL~~

<u>Time</u>	<u>ΔT, sec</u>	<u>Event</u>
08:15:32.4	2.8	SPS OFF (RTC 12) received in command, communications, and telemetry system (CCATS)
08:15:35.2	2.8	SPS OFF message acceptance pulse received at Guam

---

(Total) 10.1 sec

SPS OFF was confirmed by MCC-H at 08:15:38.7. At cutoff, the second firing of the SPS had produced the following results.

<u>Entry interface</u>	<u>Planned</u>	<u>Guam</u>	<u>Apollo guidance computer</u>
Velocity, ft/sec	36 333	36 545	36 537
Flight-path angle, deg	-7.13	-6.94	-7.08

The Guam site experienced an abrupt loss of spacecraft unified S-band data apparently simultaneously with CM/SM separation. Separation was not monitored at MCC-H; however, onsite data indicated that separation occurred at 08:18:02.

#### 9.1.6 Entry

Spacecraft landing was predicted to occur at 08:36:54 in the planned target area at latitude 30 degrees North and longitude 172 degrees 24 minutes West. The predicted 7.7-g acceleration was lower than the nominal 8.6-g because of the shallower -6.94-degree flight-path angle.

~~CONFIDENTIAL~~

~~CONFIDENTIAL~~

9-11

## 9.2 NETWORK PERFORMANCE

General support from the NASA and Department of Defense network stations was excellent except as listed in the following paragraphs. The reported exceptions had little or no effect on the mission support activities.

### 9.2.1 Apollo/Range Instrumentation Aircraft

During the overlap of the first and second revolutions, the Apollo/range instrumentation aircraft (A/RIA No. 1) did not acquire the 400-Hz tone on the unified S-band subsystem.

During entry, the Apollo range/instrumented aircraft (A/RIA No. 4) did not receive a signal. This was caused by the spacecraft communications blackout period (during entry) coinciding with the expected times of acquisition and loss of signal.

### 9.2.2 Telemetry

During the first revolution, the instrument unit data received at the Canberra station (CNB) was reported by the flight controllers to be unusable. Recycling the onsite computer (624B) apparently did not correct the problem. Loss of signal (at 01:05:00) occurred before a definitive analysis could be made.

During the first revolution, personnel at the Guaymas station (GYM) inadvertently patched the spacecraft S-band receiver circuit to the S-IVB receiver circuit.

Prior to acquisition in the second revolution, the Bermuda station (BDA) switched from DECOMM 3 to DECOMM 4 because of a failed decommutator.

### 9.2.3 Tracking

The following problems were encountered with the network tracking stations.

At the Canary Island station (CYI), the C-band radar was inoperative because of a faulty elevation encoder prior to lift-off.

Flame attenuation caused data dropouts in the unified S-band subsystem at the Merritt Island Launch Area (MILA) station from 00:02:34 to

~~CONFIDENTIAL~~

~~CONFIDENTIAL~~

00:02:47, from 00:02:50 to 00:02:51, from 00:03:04 to 00:03:12, and from 00:03:15 to 00:03:27. The unified S-band subsystem at the Bermuda station also had data dropouts during the engine ignition period.

Equipment problems prior to lift-off prevented the Tananarive Capri radar from supporting the mission.

#### 9.2.4 Command

The following command problems occurred after lift-off.

At the Guaymas station at 00:25:00, a varying sense amplifier bias caused five command computer faults. A regulator (AIAI 303) was replaced, the program was reinitialized, and there was no loss of mission support. Also at Guaymas, at 01:26:00, the onsite command computer (642B) faulted while in acquisition with the spacecraft. However, the acquisition was handed over to the Texas station (Corpus Christi, Texas) at the normal time, and there was no mission effect.

At 01:28:00, a booster system engineer priority clear signal was sent after the Texas station had handed over to MILA. This signal should have been sent over the Texas station. The maintenance and operations controller could not obtain a normal priority clear from the computer address matrix and had to use skip key no. 3 to send a forced message acceptance pulse.

At 03:07:00, the booster system engineer received a ground reject indication for a command (special no. 1) over the Hawaii station (HAW). This is considered normal because the booster system engineer initiated the command before the two-way lock was established. Under this condition, the unified S-band technician had not made his manual selection for the subcarrier oscillator; consequently, the ground loop was not valid. At 00:03:12, the booster system engineer obtained two ground reject signals and one spacecraft reject signal. The ground rejects were caused by the same problem as previously described. The spacecraft reject was apparently caused by acquisition of a two-way lock in the middle of the command no. 1 uplink. This command was uplinked validly at the Texas station, but the booster systems engineer did not see the proper action take place onboard the S-IVB stage. Based on a quick look analysis, the ground instrumentation showed no apparent problem.

At 03:22:00, the electrical and communications controller received spacecraft reject signals when using the unified S-band carrier. The spacecraft downlink indicated inadequate signal strength. The Bermuda uplink was configured for a 2-kW output. Control was handed over to the

~~CONFIDENTIAL~~

~~CONFIDENTIAL~~

9-13

Vanguard tracking ship. The Vanguard was also configured for a 2-kW uplink, but the spacecraft downlink indicated that this signal strength and commands were successful. The problem at Bermuda was apparently caused by a side lobe lock in the unified S-band subsystem. The station was denied permission to drop the command subcarrier signal in order to sweep the exciter and reacquire.

#### 9.2.5 Goddard Space Flight Center Central Processors

At Goddard Space Flight Center at 04:25:00, the teletype output and console control functions of the on-line A-computer were lost. Recovery procedures were started immediately but the attempt at console initialization of the recovered program was not successful. The backup central processor also faulted at this time, precluding a computer switchover. A second recovery procedure was immediately started on the A-computer and was successful; however, the polynomial buffer terminal was hung. This buffer terminal was subsequently cleared and the system was operational at 04:32:00 after a loss of switching capability for 7 minutes. After the on-line system was determined to be functioning normally, a fresh load recovery was performed on the backup system. Both systems operated normally thereafter.

#### 9.2.6 Real Time Computer Complex

The real time computer complex (RTCC) at the Mission Control Center-Houston (MCC-H) performed satisfactorily during the mission. The following problems encountered with the RTCC operation caused little or no degradation of mission support.

At approximately 01:00:00, a programming problem affected the real-time display of the fuel cell parameters. This problem was in the processing of bilevel (828) low speed telemetry data. The same parameters were properly handled in rebroadcast messages, on telemetry log tape, and in the high speed telemetry formats.

At 02:03:00, the tracking controller reported that the acquisition vectors provided to the Department of Defense for the Cape Kennedy station (CNV) were improperly tagged. The station routing code for the program was GAMR instead of the current code of GCNV.

At 03:30:00, the RTCC was unable to provide a solution for the Apollo guidance computer data after cutoff of the first firing of the service propulsion subsystem (SPS). A subsequent examination indicated that the cutoff switch was closed 14 seconds after actual cutoff, and the two telemetry vectors received after cutoff showed the pulsed integrating

~~CONFIDENTIAL~~

~~CONFIDENTIAL~~

pendulous accelerometer time and the vector were actually recycled and, thus, were time tagged prior to the cutoff switch.

At 08:17:00, the RTCC was unable to compute solutions immediately after the second SPS firing. The problem was caused by both the telemetry and high speed radar vectors showing an orbit eccentricity greater than unity, thereby indicating a hyperbolic rather than an elliptic orbit.

During the spacecraft entry phase, a manual entry was made in the RTCC program to confirm the de-orbit SPS firing as 271 seconds. The program instead used 271.2 seconds.

~~CONFIDENTIAL~~

~~CONFIDENTIAL~~

9-15

### 9.3 RECOVERY OPERATIONS

Recovery plans and procedures were established for the Apollo 4 mission to assure rapid location and safe retrieval of the spacecraft following any conceivable landing situation. The recovery forces were also responsible for the location, retrieval, and return of the two camera capsules ejected from the S-II stage and any portion of the S-IC stage that might have been floating after impact.

#### 9.3.1 Recovery Force Deployment

Planned and contingency landing areas were defined in accordance with the termination-of-mission probabilities. Planned landing areas included the launch site, launch abort (continuous and discrete), secondary (mid-Pacific recovery zone), and the primary. All landing areas other than these were considered to be contingency landing areas.

Department of Defense forces provided recovery support in each of the various landing areas. The level of support provided was commensurate with the probability of a landing occurring within a particular area and with any special problems associated with such a landing. Table 9.3-I contains a summary of those forces committed to Apollo 4 recovery support. The planned landing areas, in which support forces were positioned for search and retrieval, were located and defined as follows.

The launch site landing area was that area in which a spacecraft landing would have occurred following an abort prior to launch or during the early part of powered flight. It included the area in the vicinity of Launch Complex 39A and extended seaward along the ground track for a distance of 41 n. mi.

The launch abort landing areas (fig. 9.3-1), continuous and discrete, were areas in which a spacecraft landing would have occurred following an abort after 100 seconds of flight but before insertion into orbit. The continuous launch abort landing area extended from the seaward extremity of the launch site area to 2350 n. mi. downrange and was bounded by lines 50 n. mi. either side of the ground track. The camera capsule and booster recovery area was located in the area near the U.S.S. Austin (see fig. 9.3-2). A detailed discussion of their recovery is contained in section 9.3.6.

The discrete launch abort landing area was bounded by an ellipse passing through the points 50 n. mi. uprange, 200 n. mi. downrange, and 50 n. mi. to either side of latitude 28 degrees 18 minutes North and longitude 19 degrees 30 minutes West.

~~CONFIDENTIAL~~



~~CONFIDENTIAL~~

The secondary landing areas were located within the mid-Pacific recovery zone (fig. 9.3-3). A landing in one of those areas could have occurred as the result of a failure/alternate mission, when the primary area could not be reached.

The primary landing area (fig. 9.3-4) contained the end-of-mission target point and was bounded by an ellipse passing through the points 75 n. mi. uprange, 100 n. mi. downrange, and 50 n. mi. to either side of latitude 30 degrees North and longitude 172 degrees 24 minutes West (end-of-mission target point.)

Provisions for recovery support in the event of a contingency landing consisted of fixed-wing search/rescue aircraft on alert at staging bases. The bases were located such that any point on the Apollo 4 ground track could be reached within 18 hours after notification of spacecraft landing. The bases were as follows.

Kindley AFB, Bermuda

Lajes AB, Azores

Plaisance Airport, Mauritius

Hickam AFB, Hawaii

Moron AB, Spain

Andersen AFB, Guam

#### 9.3.2 Spacecraft Location and Retrieval

All launch abort recovery forces were on station prior to launch, and all primary and secondary recovery forces were on station prior to the atmospheric entry of the spacecraft.

Two sonic booms heard aboard the primary recovery ship, U.S.S. Bennington, and radar vhf contact by aircraft in the area were the first indications that the landing would be near the nominal target point. Following the sonic booms, vhf electronic signals were received and visual contact was made by other recovery aircraft.

The separation of the apex cover, the deployment of the pilot parachutes and the main parachutes, and the landing of the spacecraft and apex cover were observed from recovery aircraft in the area.

~~CONFIDENTIAL~~

~~CONFIDENTIAL~~

9-17

A burnt-orange colored substance was observed emitting from the spacecraft while it was on the main parachutes and continued emitting until landing. It is assumed that this was the normal result of oxidizer ( $N_2O_4$ ) dumping.

The spacecraft landed at 2037 G.m.t. at latitude 30 degrees 06.4 minutes North and longitude 172 degrees 32 minutes West. The landing point was 10.3 n. mi. on a bearing of 309 degrees from true North from the predicted target point. The spacecraft was hoisted aboard the primary recovery ship at 2309 G.m.t. at the location of landing (see fig. 9.3-4).

Upon landing, the main parachutes separated from the spacecraft normally; however, one remained inflated while the other two sank and acted as sea anchors (fig. 9.3-5). The inflated one, with its pilot parachute, was cut free and recovered by swimmer personnel. The apex cover with its parachute was also recovered (fig. 9.3-6). The two drogue sabots were sighted. One sank during recovery efforts and the other sank before it could be reached.

Hoisting of the spacecraft aboard the recovery ship was hampered by sea swells of 8 feet and a wind speed of 20 knots.

A sequential listing of significant events that occurred during recovery is as follows.

<u>Time, G.m.t.</u>	<u>Event</u>
2032	Two sonic booms heard aboard the primary recovery ship.
	Pilot parachutes followed by main parachutes, observed from recovery aircraft.
	Aircraft established radar contact with spacecraft.
2033	Aircraft established vhf contact with spacecraft.
2037:10	Spacecraft landing observed by recovery aircraft.
2037:20	Apex cover landing observed by recovery aircraft.
2047	Swimmers deployed.

~~CONFIDENTIAL~~

9-18

~~CONFIDENTIAL~~

<u>Time, G.m.t.</u>	<u>Event</u>
2057	Collar inflated.
2133	Recovery ship at spacecraft.
2309	Spacecraft aboard recovery ship.

### 9.3.3 Recovery Force Electronic Reception

The Unified S-band transmitter was tracked by HC-130H search/rescue aircraft, equipped with AN-ARD-17 tracker equipment and at an altitude of 25 000 feet, during spacecraft orbit and entry. A summary of the data obtained is shown in the following table.

<u>Aircraft</u>	<u>Acquisition of signal, G.m.t.</u>	<u>Loss of signal, G.m.t.</u>	<u>Revolution</u>	<u>Location</u>	<u>Remarks</u>
Kindley Rescue (backup)	1207:30	1209:20	1	At Kindley	On Ground
Kindley Rescue 2	-	-	1	33°35'N 52°20'W	No signal
Lajes Rescue 1	1219:02	1221:20	1	29°15'N 19°10'W	Weak signal
Kindley Rescue 2	-	-	2	29°00'N 57°00'W	No signal
Lajes Rescue 1	-	-	2	23°44'N 22°11'W	No signal
Hawaii Rescue 4	1450:46	1455:04	2	15°10'N 162°00'W	
Hawaii Rescue 3	1450:46	1453:24	2	13°46'N 164°10'W	
Kindley Rescue 2	-	-	3	24°40'N 61°00'W	No signal

~~CONFIDENTIAL~~

~~CONFIDENTIAL~~

9-19

<u>Aircraft</u>	<u>Acquisition of signal, G.m.t.</u>	<u>Loss of signal, G.m.t.</u>	<u>Revolution</u>	<u>Location</u>	<u>Remarks</u>
Lajes Rescue 1	-	-	3	28°25'N 24°00'W	No signal
Hawaii Rescue 1	2023:16	2024:14	entry	28°40'N 166°50'E	
Hawaii Rescue 4	2027:26 2029:26	2028:36 2029:46	entry	31°05'N 177°50'E	
Hawaii Rescue 5	2030:24 2031:26	2030:34 2031:34	entry	28°21'N 175°51'W	
Hawaii Rescue 2	-	-	entry	25°45'N 170°25'E	No signal
Hawaii Rescue 3	-	-	entry	26°40'N 174°25'E	No signal
Hawaii Rescue 6	-	-	entry	32°29'N 168°49'W	No signal

VHF recovery beacons. - Signals from both spacecraft recovery beacons were received by the recovery aircraft listed as follows.

<u>Aircraft (type)</u>	<u>Initial time of contact, G.m.t.</u>	<u>Initial reception range, n. mi.</u>	<u>Type receiver</u>	<u>Aircraft position</u>
Hawaii Rescue 5 (HC-130H)	2032:28	205	AN/ARD-17	See fig. 9.3-3
Hawaii Rescue 6 (HC-130H)	2033:00	243	AN/ARD-17	See fig. 9.3-3
Photo 1 (SH-3A)	2033	11	ARA-25	Over recovery ship
Relay 1A (E-1B)	2033	11	ARA-25	Over recovery ship

~~CONFIDENTIAL~~

~~CONFIDENTIAL~~

<u>Aircraft (type)</u>	<u>Initial time of contact, G.m.t.</u>	<u>Initial reception range, n. mi.</u>	<u>Type receiver</u>	<u>Aircraft position</u>
Air Boss 1 (SH-3A)	2034	30	ARA-25	50 n. mi. uprange of recovery ship
Recovery 1 (SH-3A)	2034	1	SARAH	See fig. 9.3-4
Recovery 3 (SH-3A)	2034	11	SARAH	See fig. 9.3-4
Relay 1 (SH-3A)	2034	11	ARA-25	Over recovery ship
Air Boss 2 (E-1B)	2035	55	ARA-25	50 n. mi. down- range of recovery ship
Recovery 2 (SH-3A)	2037	40	SARAH	See fig. 9.3-4

HF transceiver.— There were no reports of beacon reception by recovery forces; however, 14 hf/df stations reported reception. The spacecraft position calculated from these data was within 40 n. mi. of the actual location.

#### 9.3.4 Spacecraft Postrecovery Inspection

The postrecovery procedures were conducted in accordance with the Apollo Recovery Operations Manual, the Post Retrieval Procedures Manual, their revisions and special procedures received after the mission. The following is a summary of observations made during recovery and post-recovery activities (see figures 9.3-6 through 9.3-10).

- a. The spacecraft did not submerge at landing and floated apex up at all times; uprighting bags were not deployed.
- b. The hf antenna was deployed normally.
- c. The flashing light was erected properly and was operating at a rate of 18 flashes per minute.

~~CONFIDENTIAL~~

~~CONFIDENTIAL~~

9-21

d. The fluorescein sea dye marker was deployed and diffused normally. Personnel onboard the recovery aircraft reported dye pattern as being approximately 50 by 300 feet in size and appearing very thin.

The sea dye canister was intact before installation of the flotation collar. After recovery it was noticed that it had separated from the swimmer interphone connection and had been lost. The separation and loss probably occurred because of stresses between the spacecraft and the flotation collar during retrieval.

e. The vhf antennas were both deployed and operating; however, the antenna on the -Y +Z gusset did not lock into position.

f. The main parachute disconnects operated properly.

g. The drogue parachute disconnects operated properly. Silicone remained on one side of the blade.

h. The apex cover was cracked at the pitch motor opening while being towed during recovery operations.

i. The outer lip of both drogue mortar cans were bent, apparently some bending occurred during parachute descent and some during recovery operations.

j. One swimmer reported that he thought he saw occasional "steam-like" wisps of white smoke or spray, which seemed to come from the -Z +Y roll engines, during collar installation.

k. A small quantity (1 to 2 quarts) of clear liquid was found inside the spacecraft. A sample of the liquid was taken and returned to NASA-MSC for analysis where it was found to be sea water.

l. Both the thrust chamber and the burned ablator in the vicinity of the roll engines indicated that the roll engines had functioned. The yaw and pitch engines showed somewhat less evidence of functioning.

m. Holder no. 5 for the vapor sensitive tapes could not be found.

n. The rendezvous window micrometeoroid panels (fig. 9.3-9) had light-to-medium water-streaked film on their exteriors. Moisture was noted between the micrometeoroid panels and the heat shield window panes.

~~CONFIDENTIAL~~

~~CONFIDENTIAL~~

o. The side window micrometeoroid panels (fig. 9.3-10) had medium-to-heavy film on their exteriors. Heavy condensation appeared to be between the heat shield and pressure vessel window panes.

p. The postlanding ventilation valves operated normally at a minimum of 25 V dc.

#### 9.3.5 Spacecraft Deactivation

The spacecraft arrived at Pearl Harbor, Hawaii, on November 11, 1967, onboard the U.S.S. Bennington. At Pearl Harbor, the landing safing team safed the unexpended pyrotechnics (command module reaction control subsystem oxidizer and helium-dump pyrotechnics) by replacing the initiator plugs with safing caps. The team verified that the remaining pyrotechnics were safe for reaction control subsystem (RCS) deactivation as well as for spacecraft transportation back to the mainland. The RCS deactivation procedures were performed in accordance with reference 5. The conditions noted during deactivation of the RCS are listed as follows.

a. High residual helium pressures were found in the oxidizer and fuel systems.

b. System B fuel helium relief valve (TP 13) was found to be ruptured; a cap was placed over the valve to prevent further leakage.

c. A fuel system helium check valve (TP 58) was found to be leaking.

d. Only residual quantities of propellants were found in the RCS.

Deactivation was successfully completed on the evening of November 13, 1967. The spacecraft was transported by a C-133B aircraft to Long Beach, California, and was returned to the contractor's facility for testing and analysis on the evening of November 15, 1967.

#### 9.3.6 S-IC and Camera Capsule Recovery

In addition to covering a launch abort, the U.S.S. Austin and associated forces were responsible for recovery of the two camera capsules ejected from the S-II stage and for any portion of the S-IC stage that might have been floating after impact.

~~CONFIDENTIAL~~

~~CONFIDENTIAL~~

9-23

Three helicopters, one for photographic and two for recovery purposes, were launched from the U.S.S. Austin. Kindley Rescue I sent time and bearing information on the booster by tracking its telemetry beacon.

A fixed-wing radar aircraft, an EC-121, provided multiple-target skin-tracking information.

A third fixed-wing aircraft, an RA-3B, was positioned to provide photographic data, however; none were obtained. Photographic coverage from the U.S.S. Austin, with special equipment (intermediate focal length optical tracker, IFLOT), was prevented by cloud cover.

Based on data from the radar aircraft, loss of the telemetry signal, and visual observation of booster debris by the RA-3B, booster breakup occurred at approximately 1206 G.m.t.

Both camera capsules were recovered (fig. 9.3-11); however, the antenna on the no. 1 capsule (coded A) did not erect. All other recovery aids on both capsules operated properly.

Capsule no. 2 was recovered at 1230 G.m.t., on a bearing of 254 degrees from true north and 7.6 n. mi. from the predicted impact point of latitude 30 degrees 23 minutes North and longitude 73 degrees 5 minutes West.

Capsule no. 1 was recovered at 1245 G.m.t., on a bearing of 262 degrees from true north and 11.8 n. mi. from the predicted impact point of latitude 30 degrees 23 minutes North and longitude 73 degrees 6 minutes West.

The capsules were taken from the U.S.S. Austin by a helicopter at 1425 G.m.t., November 9, 1967, and were flown to Patrick AFB, Florida, for transfer to Marshall Space Flight Center, Huntsville, Alabama.

Three pieces, identified as S-IC/S-II interstage ullage rocket motor fairings, were recovered at 1500 G.m.t. Two of the pieces were whole fairings and the other piece was only a part of a fairing (fig. 9.3-12).

The only material recovered from the S-IC stage were several small pieces identified as fuel tank insulation material.

The launch vehicle pieces were returned to Norfolk, Virginia, aboard the U.S.S. Austin, and then shipped to Marshall Space Flight Center, Huntsville, Alabama.

~~CONFIDENTIAL~~



~~CONFIDENTIAL~~

TABLE 9.3-I.- RECOVERY SUPPORT

Landing area	Maximum access/ retrieval time, hr		Type and quantity of support vehicles	Description of support
	Aircraft	Ship		
Launch site	1/4		LCU (1)	Landing craft utility (landing craft with spacecraft retrieval capabilities)
			CH-3C (2)	Helicopters with 3-man swim teams
			K-501 (2)	Fire suppression kits with 2 firemen
			LVTR (2)	Landing vehicle tracked retriever (tracked amphibious vehicles with spacecraft re- trieval capabilities)
Launch abort continuous	4	22	LPD (1)	Landing platform dock (helicopter carrier) U.S.S. Austin
			SH-3A (3)	Helicopters, two with 2-man swim teams and one photographic (camera and booster recovery)
			EC-121 (1)	Fixed-wing radar air- craft (camera and booster recovery)
			RA-3B (1)	Fixed-wing photographic aircraft (camera and booster recovery)

~~CONFIDENTIAL~~

~~CONFIDENTIAL~~

9-25

TABLE 9.3-I.- RECOVERY SUPPORT - Continued

Landing area	Maximum access/ retrieval time, hr		Type and quantity of support vehicles	Description of support
	Aircraft	Ship		
Discrete	2	15	HC-130H (2)	Fixed-wing search/ rescue aircraft with 3-man swim teams
			DD (1)	Destroyer, U.S.S. J. P. Kennedy
			LST (1)	Landing ship tank (large landing craft) U.S.S. York County
			AO (1)	Oiler, U.S.S. Sabine
Secondary	3	27	HC-130H (1)	Fixed-wing search/ rescue aircraft with 3-man swim team
			DD (1)	Destroyer, U.S.S. Carpenter
Primary	2	5	HC-130H (6)	Fixed-wing search/ rescue aircraft, with 3-man swim teams
			CVS (1)	Aircraft carrier, U.S.S. Bennington
			SH-3A (6)	Helicopters, three re- covery with 3-man swim teams, one photographic, one for air traffic con- trol, one for commu- nications relay.

~~CONFIDENTIAL~~

~~CONFIDENTIAL~~

TABLE 9.3-I.- RECOVERY SUPPORT - Concluded

Landing area	Maximum access/ retrieval time, hr		Type and quantity of support vehicles	Description of support
	Aircraft	Ship		
Contingency	18	-	E-1B (4)	Fixed-wing aircraft, one for air traffic control and one backup, two for communications relay backup
			HC-130H (10)	Fixed-wing search/ rescue aircraft with 3-man swim teams. (Includes 3 from launch abort areas and 2 from secondary area.)

Total:	Fixed-wing aircraft	20
	Helicopters	11
	Ships	7

~~CONFIDENTIAL~~

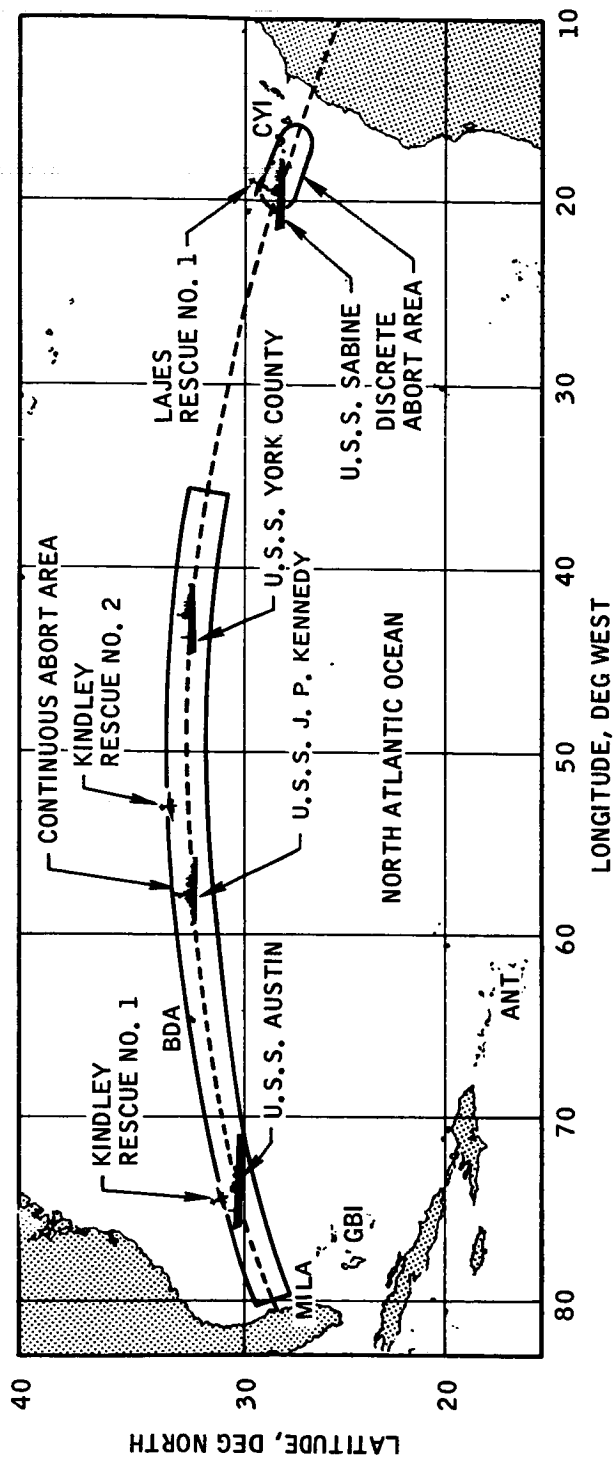


FIGURE 9.3-1.- APOLLO 4 LAUNCH ABORT AREAS AND RECOVERY FORCE STRUCTURE.

~~CONFIDENTIAL~~

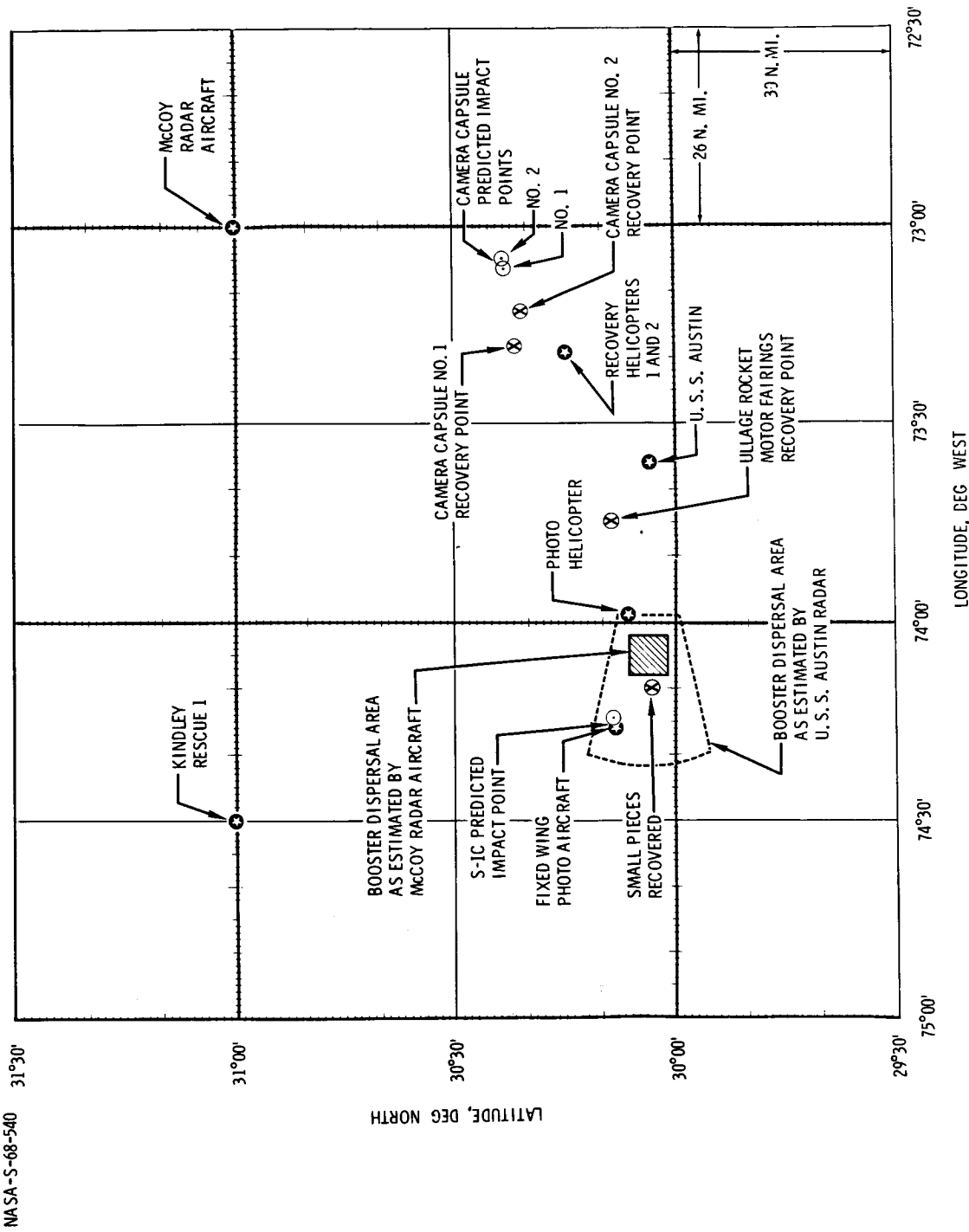


FIGURE 9.3-2. - BOOSTER AND CAMERA CAPSULE RECOVERY.

~~CONFIDENTIAL~~

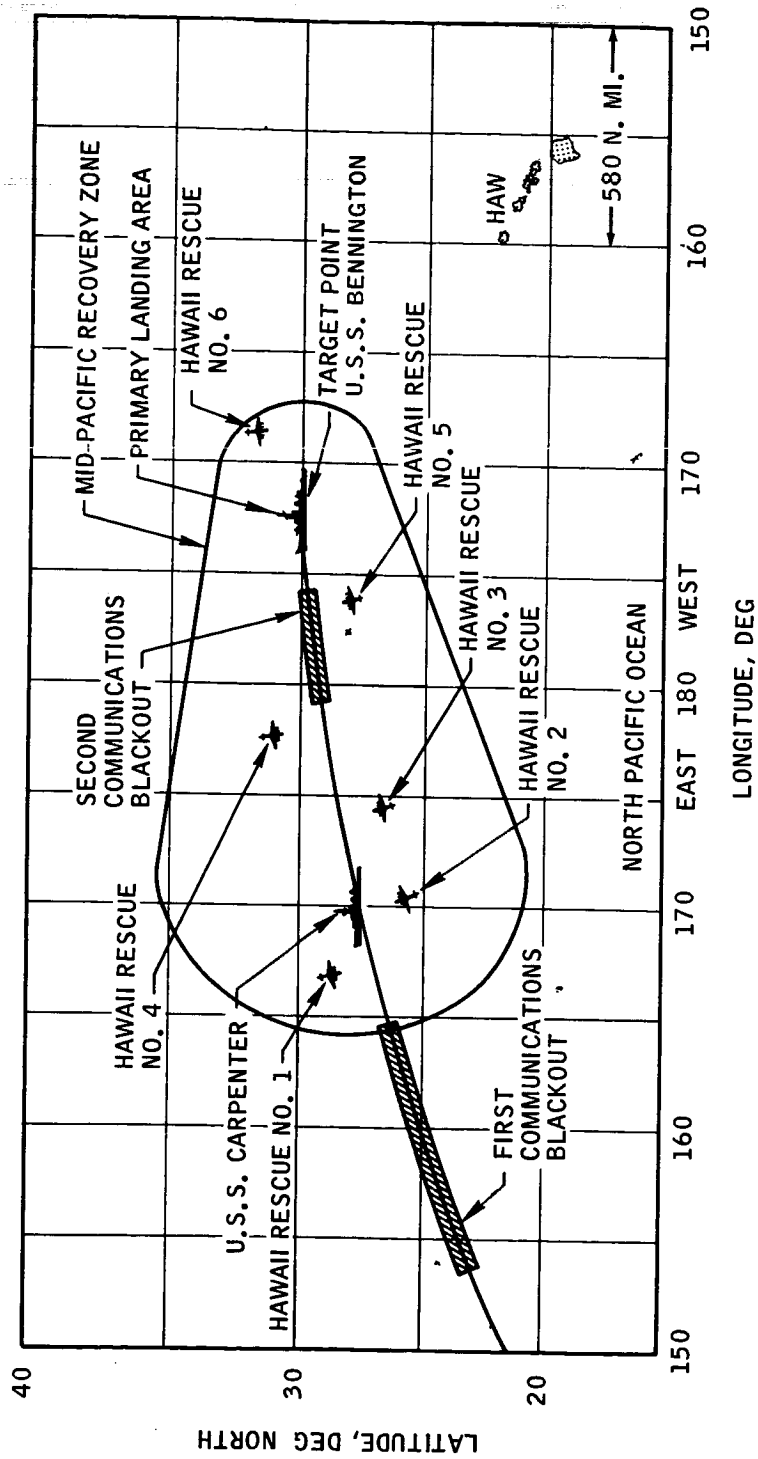


FIGURE 9.3-3.- MID-PACIFIC RECOVERY ZONE AND FORCE DEPLOYMENT.

~~CONFIDENTIAL~~

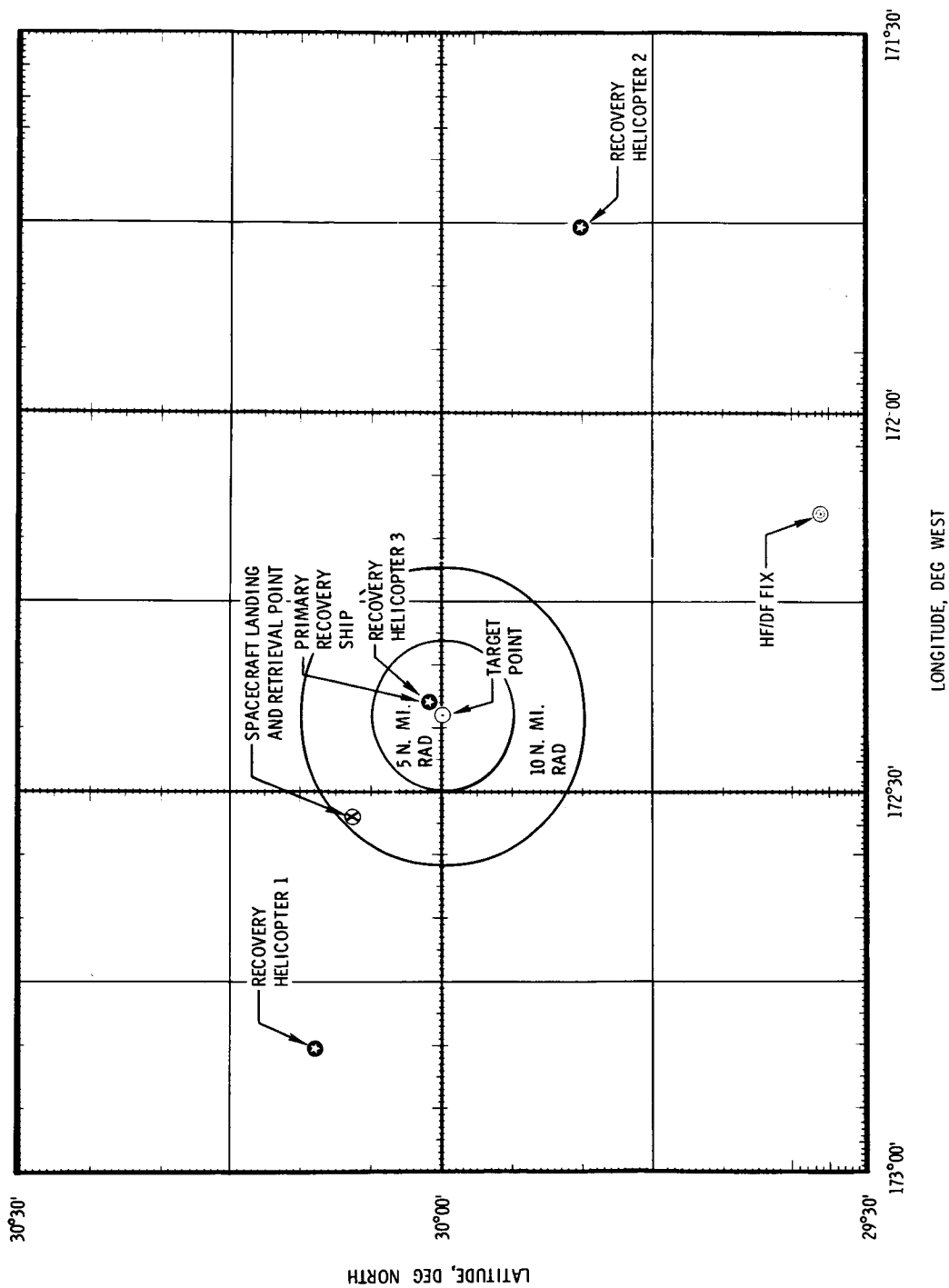


FIGURE 9.3-4. - PRIMARY RECOVERY AREA AND FORCE DEPLOYMENT.

~~CONFIDENTIAL~~

NASA-S-68-543

~~CONFIDENTIAL~~

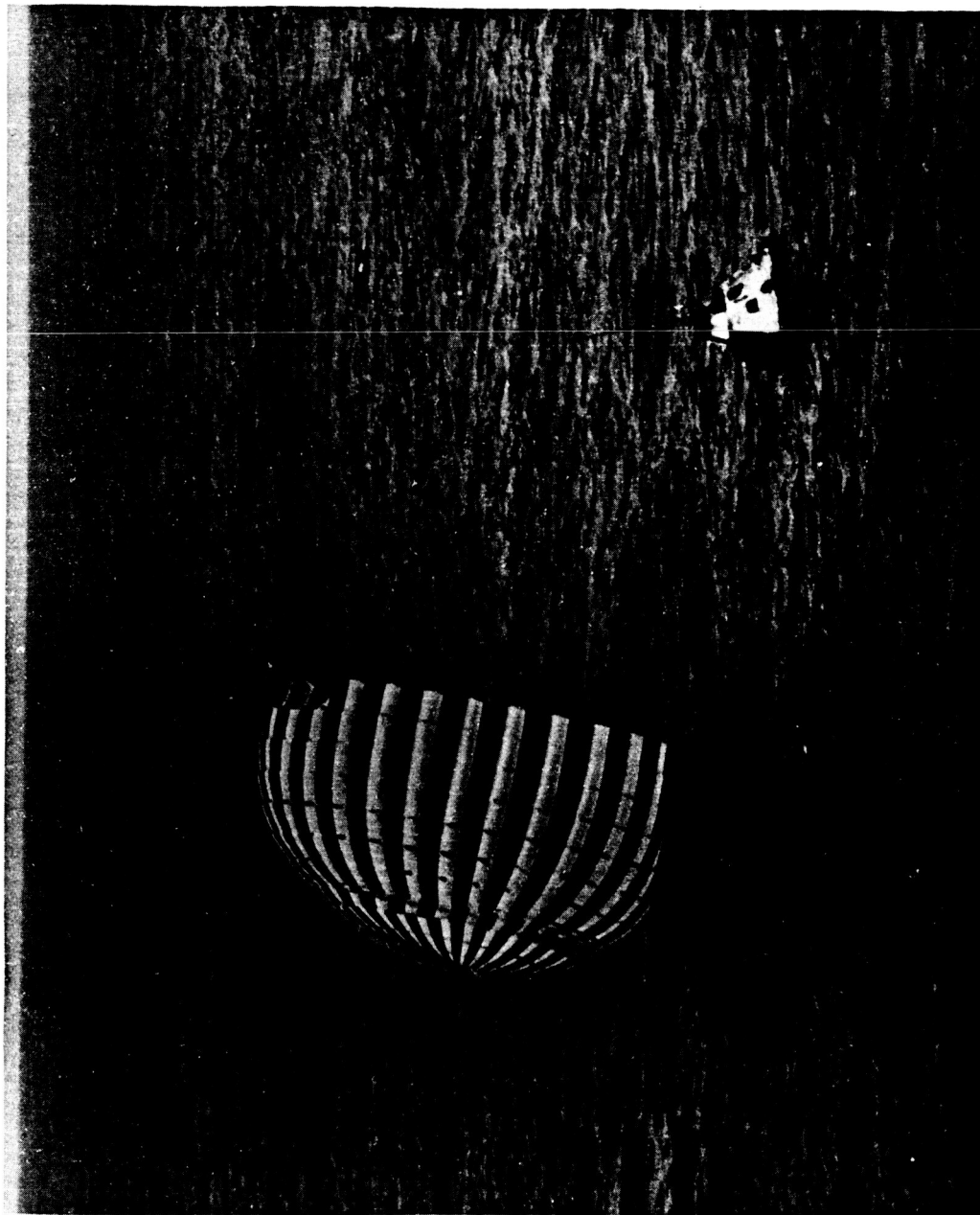


FIGURE 9.3-5. - SPACECRAFT AND PARACHUTE.

~~CONFIDENTIAL~~



~~CONFIDENTIAL~~

NASA-S-68-544



FIGURE 9.3-6.- FORWARD HEAT SHIELD.

~~CONFIDENTIAL~~

~~CONFIDENTIAL~~

9-33

NASA-S-68-545



FIGURE 9.3-7.- SPACECRAFT IN FLOTATION COLLAR.

~~CONFIDENTIAL~~

~~CONFIDENTIAL~~

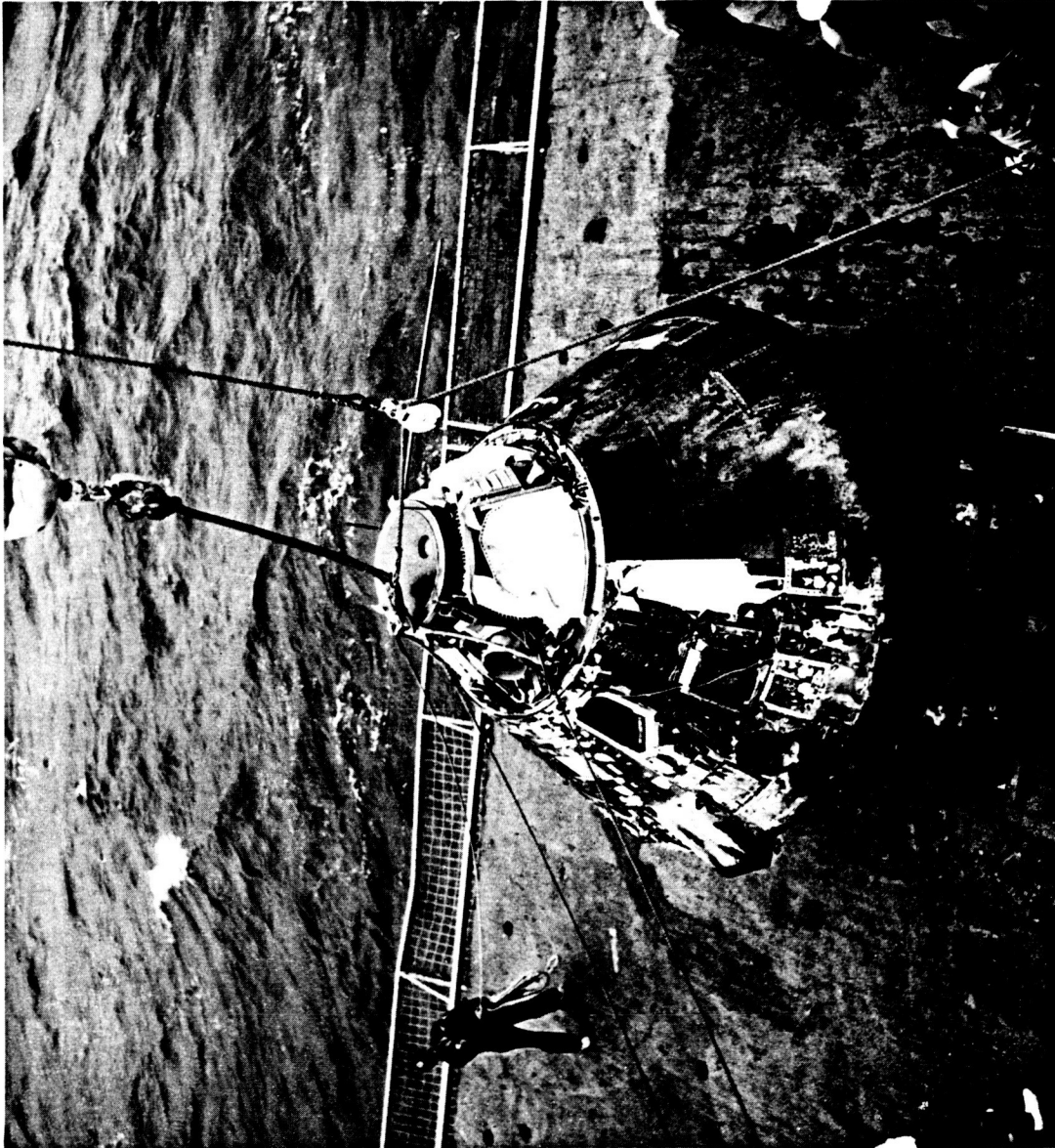


FIGURE 9.3-8.- SPACECRAFT AFTER RECOVERY.

NASA-S-68-546

~~CONFIDENTIAL~~

~~CONFIDENTIAL~~

9-35

NASA-S-68-547

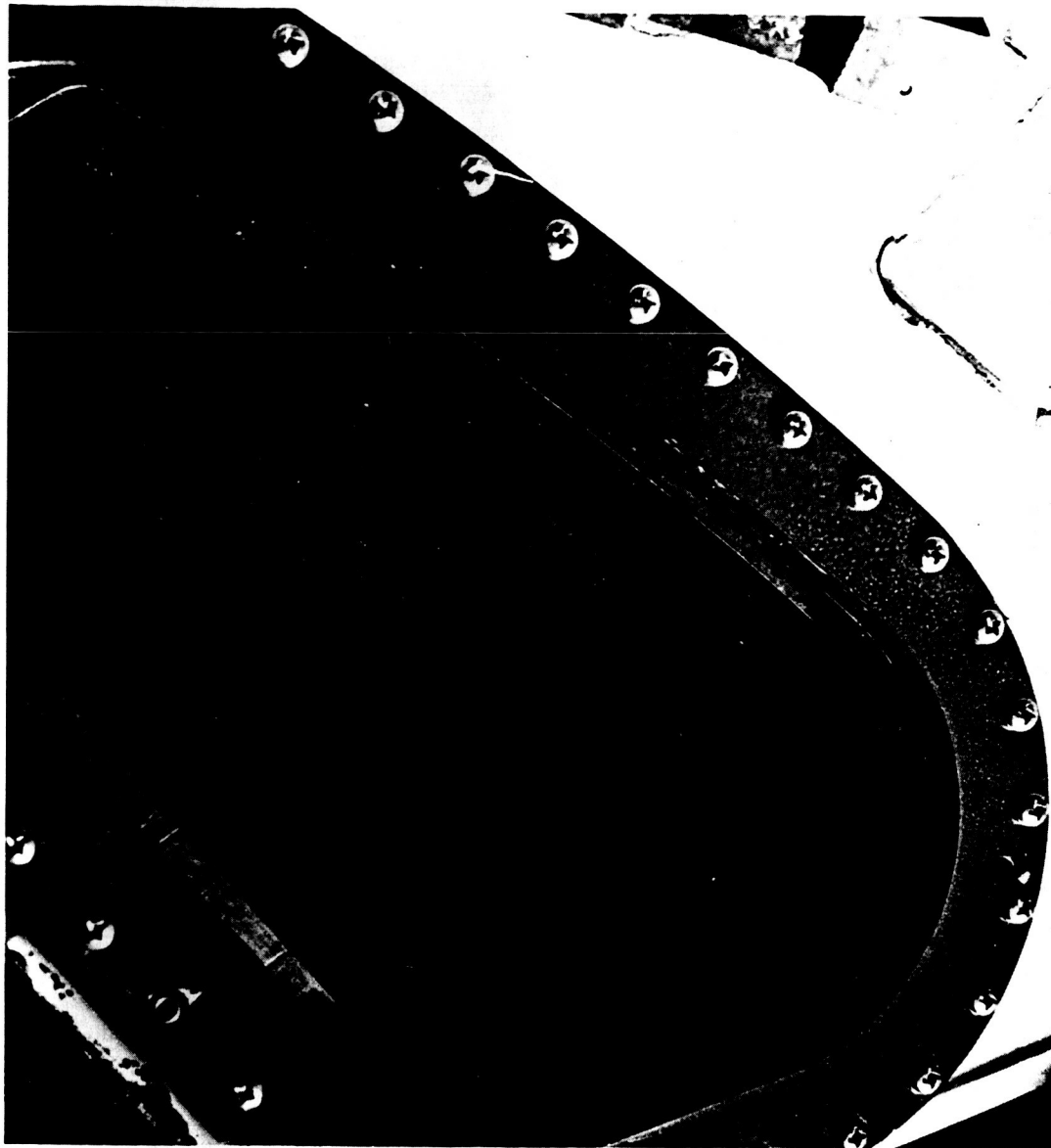


FIGURE 9.3-9.- LEFT RENDEZVOUS WINDOW (INSIDE VIEW).

~~CONFIDENTIAL~~

~~CONFIDENTIAL~~

NASA-S-68-548

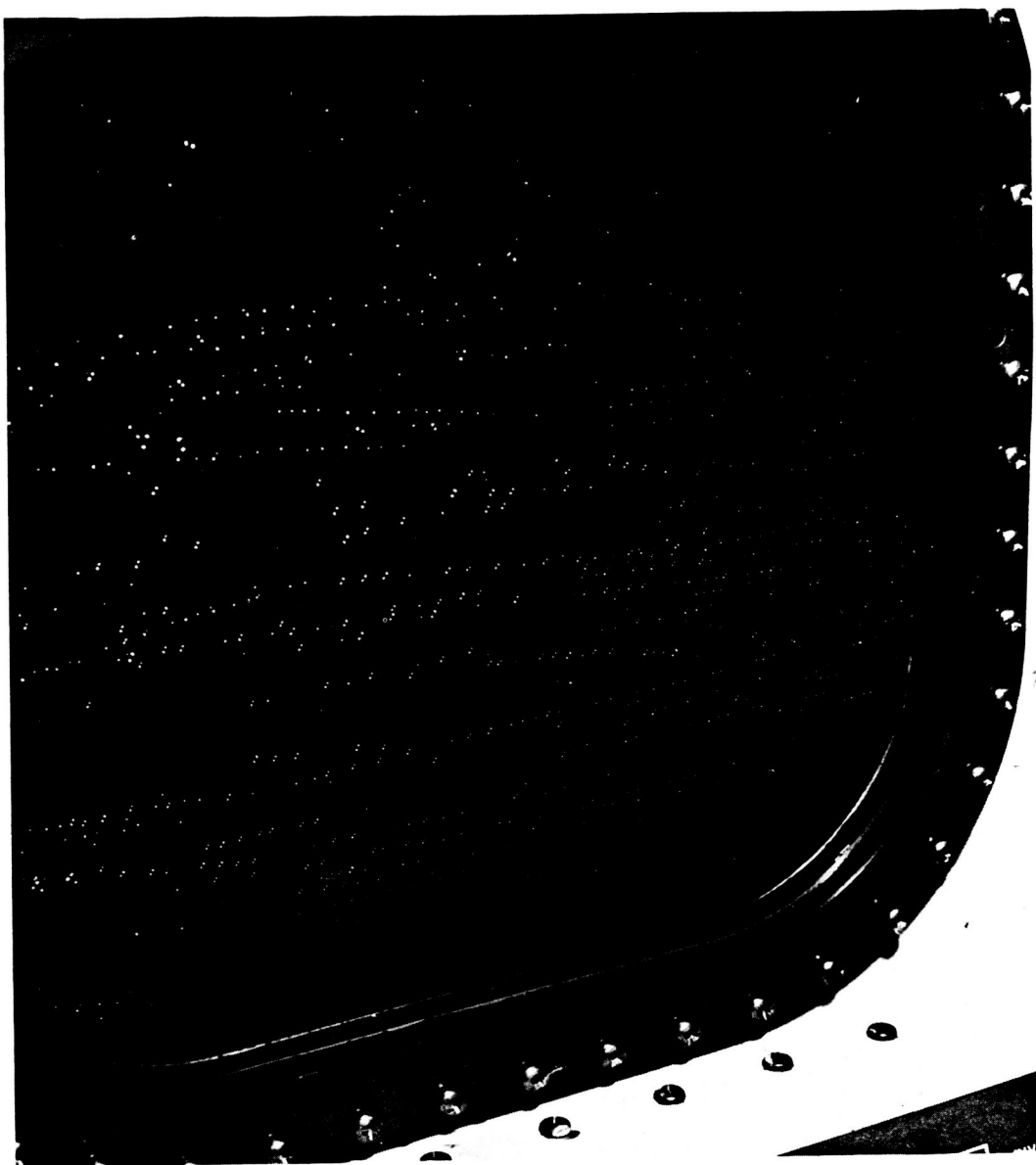


FIGURE 9.3-10.- RIGHT SIDE WINDOW (INSIDE VIEW).

~~CONFIDENTIAL~~

~~CONFIDENTIAL~~

9-37

NASA-S-68-549



FIGURE 9.3-11.- CAMERA CAPSULES.

~~CONFIDENTIAL~~

~~CONFIDENTIAL~~

FIGURE 9.3-12.- S-IC/S-II INTERSTAGE ULLAGE ROCKET MOTOR FAIRINGS.

NASA-S-68-550

~~CONFIDENTIAL~~

~~CONFIDENTIAL~~

10-1

10.0 EXPERIMENTS

(This section is not applicable.)

~~CONFIDENTIAL~~



10-2

~~CONFIDENTIAL~~

THIS PAGE INTENTIONALLY LEFT BLANK

~~CONFIDENTIAL~~

~~CONFIDENTIAL~~

U 11-1

## 11.0 CONCLUSIONS

The following conclusions were obtained from an evaluation of the data and postflight examinations and tests.

1. Performance of spacecraft subsystems was near-perfect. There was no evidence of any functional anomalies that affected the mission.
2. Performance of the emergency detection subsystem, operating in an open-loop mode, was as expected. No conditions approaching manual or automatic abort levels were encountered at any time during the launch phase.
3. Postflight inspection of the recovered command module indicated that the Block II thermal protection subsystem withstood the lunar entry environment satisfactorily.
4. Sufficient data were obtained to permit a thorough evaluation of the performance of the Block II thermal protection subsystem. Data from this mission served as a basis for updating the prediction method for calculating heat loads and heating rates.
5. The thermal performance of a gap and seal configuration simulating the unified crew hatch design was verified as being satisfactory.
6. Spacecraft strain gauge data indicated that no structural failures occurred during the mission. Structural loading was well within the capability of the spacecraft.
7. Vibration data measured in the command module indicated that qualification vibration levels were not exceeded.
8. Sufficient data were obtained to enable determination of the thermal response of the spacecraft and to determine the adequacy of the thermal analysis prediction techniques. Block II thermal control coating degradation was caused by the launch escape tower solid propellant jettison motor.
9. Satisfactory start and operation of the service propulsion subsystem was demonstrated in a zero-g environment with no reaction control subsystem ullage maneuvers.
10. Quantitative data were not obtained to confirm structural interaction loads at lift-off between the lunar module test article and the spacecraft lunar module adapter. This situation resulted from instrumentation inadequacies.

~~CONFIDENTIAL~~

~~CONFIDENTIAL~~

11. The lunar module test article acoustic spectra are in close agreement with those used during the LTA-3 qualification tests. This validates the lunar module subsystems qualification vibration criteria.

12. Design and procedural changes to the fuel cell water/glycol coolant loop eliminated the higher than nominal condenser exit temperatures that were experienced on Mission AS 202 (Spacecraft 011).

13. Design and procedural changes to the environmental control subsystem glycol evaporator and associated controls alleviated the slow response at initial startup of the evaporator and eliminated freezing and consequent obstruction of the steam duct due to excess water in the evaporator that were experienced on Mission AS 202 (Spacecraft 011).

14. The flight derived lift-to-drag ratio data were in good agreement with the predicted values in both the hypersonic flight regime and the region from entry interface to the start of the final entry phase. These data confirmed the changes made in the analysis techniques utilized in predictions of command module aerodynamics and precluded the repeat of the landing error experienced on Mission AS 202 (Spacecraft 011).

15. This was the first opportunity for the complete Manned Space Flight Network to acquire and track the Apollo S-band signals, and the overall performance exceeded expectations.

~~CONFIDENTIAL~~

~~CONFIDENTIAL~~

12-1

## 12.0 ANOMALY SUMMARY

Anomalies associated with the Apollo 4 mission are categorized as follows:

- a. Mission Anomalies
- b. Countdown Anomalies
- c. Test and Checkout Anomalies

Mission anomalies are defined as any difficulties that were disclosed after the time of lift-off.

Countdown anomalies are defined as any difficulties that were disclosed between the time of start of the precount to the time of lift-off.

Test and checkout anomalies are defined as any difficulties associated with the command module that occurred prior to start of the precount, for which a decision was made to fly as is, and which can be researched during postflight testing.

Difficulties associated with individual measurements are not classified as anomalies. All instrumentation difficulties are discussed in the instrumentation sections of this report. One exception is a failure of some portion of the instrumentation subsystem which results in loss of a group of measurements. This exception would be classified as an anomaly, as is the 5-volt reference problem.

None of the anomalies in any of the three categories affected the mission or mission objectives. The anomalies resolution process is still in work and final results will be provided in a supplement to this report.

### 12.1 MISSION ANOMALIES

#### 1. Loss of Instrumentation 5-Volt Reference

Statement — An instrumentation 5-volt power supply malfunctioned shortly after CM/SM separation, resulting in a loss of 8 sequence measurements associated with the earth landing sequential system.

Discussion — A similar anomaly occurred during Mission AS 202 (Spacecraft 011). Both anomalies resulted from the improper use of an oversized fuse in a CM/SM separation monitor instrumentation circuit.

~~CONFIDENTIAL~~

~~CONFIDENTIAL~~

During Apollo Mission AS 202 this anomaly was caused by an engineering error. The wrong size fuse was called out on engineering drawings. During the Apollo 4 mission this anomaly was caused by a workmanship and quality error incurred during the working of a change to correct the engineering error. In trying to relocate the measurement wiring to a proper size spare fuse, a wrong measurement wire was relocated. There was no effect on the mission as a result of this anomaly. There are alternate ways of recovering the information that was to have been provided by the 8 measurements.

Conclusion — This anomaly resulted from a workmanship and quality deficiency. The wrong wire was cut and wired to a spare fuse.

Corrective Action — All fuse box wiring will be checked on subsequent spacecraft to assure that it complies with released drawings.

## 2. Holes in Aft Heat Shield

Statement — Inspection of the Apollo 4 command module after the mission revealed three 0.25-inch holes in the aft heat shield ablator, but not extending to the ablator stainless steel interface.

Discussion — Block I aft heat shields were contoured after the initial buildup was completed. To contour the ablator, holes were drilled, wooden dowels were inserted, and the surface was hand sanded to the level of the dowels. All wooden dowels were then to be removed and the holes filled. A manufacturing and quality deficiency allowed three dowels to remain in the aft heat shield at the time of delivery. There was no adverse effect on the mission as a result of this anomaly. There is no evidence of any deep char on the heat shield at the three hole locations.

Conclusion — The three holes resulted from a manufacturing and quality deficiency that allowed three wooden dowels to remain in the aft heat shield at the time of delivery.

Corrective Action — The Spacecraft 020 heat shield was inspected on December 3, 1967, and no wooden dowels were found. For Block II aft heat shields the procedure is different in that final X-rays are taken after all open holes have been filled (as contrasted to final X-rays taken before all open holes are filled on Block I). All of the X-rays and manufacturing and quality records for Block II heat shields are being re-evaluated to assure absolute integrity of the aft heat shields. Another set of X-rays will be taken as the last step prior to painting for aft heat shields not yet delivered (effective on Spacecraft 108).

~~CONFIDENTIAL~~

~~CONFIDENTIAL~~

12-3

3. Failure of First Real Time Command 13 Execution To Be Transmitted to Spacecraft

Statement — Real time command (RTC) 13 was sent by the Mission Control Center-Houston (MCC-H) at the termination of the second SPS burn, in order to reset the RTC 11 (Thrust ON) and RTC 12 (Thrust OFF) commands. The first time this command was executed, it failed to be transmitted by MCC-H.

Discussion — Real time command 13 was first executed prior to the MCC-H receipt of the verification pulse indicating that RTC 12 had been accepted by the spacecraft. Normal ground system operation precluded transmission of the RTC 13 command while the RTC 12 (a unique priority command) still controlled the command program.

Conclusion — There is no indication of anomalous operation of either the spacecraft or the Manned Space Flight Network command system.

Corrective Action — None required.

4. Pyrotechnic Battery Voltages Did Not Return To Open Circuit Level

Statement — The pyrotechnic battery voltages did not return to the open circuit voltage level after apex cover jettison and drogue parachute deployment.

Discussion — The pyrotechnic battery voltage will normally return to the open circuit voltage level after a pyrotechnic firing if the pyrotechnic initiator is open circuited after the bridgewire burns out. The current drain after a pyrotechnic initiator fires is the result of the conductive explosive residue that remains within the initiator. This produces varying degrees of leakage current after firing.

Conclusion — This anomaly resulted from the leakage current of the pyrotechnic initiators after firing. Some leakage current can be expected after pyrotechnic firings.

Corrective Action — None required. All pyrotechnic initiator circuits are protected by fuse-resistors. Also, the voltage is removed from all pyrotechnic circuits after firing, except for the earth landing functions which begin occurring at 25 000 feet during entry. This insures that the current drain after firing is a minimum amount on the battery.

5. One of the Two VHF Antennas Erected But Failed to Lock in the Up Position Upon Landing

~~CONFIDENTIAL~~

~~CONFIDENTIAL~~

Statement — Inspection of the Apollo 4 command module upper deck after the mission revealed that one of two vhf recovery antennas failed to lock in the erect position.

Discussion — After recovery, the antenna was restowed and manually released and the latching mechanism engaged properly. The exact reason for the antenna being unlocked cannot be ascertained but could have been excessive friction at the pivot pin and ramp, wind loads or inertial loads against the spring force, or even by forces from a riser contact or at water landing.

Conclusion — The gusset no. 4 vhf antenna did not latch in place because the basic deployment spring force was marginal for latching the erected antenna when exposed to the actual flight dynamics.

Corrective Action — None required. Spacecraft 020 will fly with the same antenna design as on Spacecraft 017 since the antennas are installed and the forward heat shield has been put in place. However, even if the antennas do not latch, there is no reason to believe that the antennas will not function properly. The Block II deployment spring has two times the force of the Block I spring.

#### 6. Loss of S-Band Downlink at Guam

Statement — The Guam network station reported the loss of S-band downlink prior to confirming command module/service module separation at approximately 08:18:02. The station failed to reacquire before the spacecraft passed over the horizon.

#### 7. S-Band Difficulties at Bermuda

Statement — During coverage of the third revolution by the Bermuda (BDA) network station, the spacecraft S-band receiver lost lock. Also, the spacecraft did not accept the oxygen tank heaters and fans OFF real-time command (RTC 70) during three attempts from BDA, after BDA reacquired spacecraft receiver lock.

#### 8. Late SPS Shutdown During Second Burn

Statement — The second burn of the service propulsion subsystem (SPS) lasted approximately 10.1 seconds longer than planned.

#### 9. Initial State Vector Update Commands Transmitted by Carnarvon Were Not Accepted by the Spacecraft

Statement — A procedural guidance computer state vector via uhf was attempted at 02:28:10 over Carnarvon. Seven commands were transmitted.

~~CONFIDENTIAL~~

~~CONFIDENTIAL~~

12-5

They were not accepted by the spacecraft updata receiver/decoder. The backup uhf transmitter was selected at 02:28:30, and subsequent commands were accepted by the spacecraft equipment.

10. Actual Spacecraft Heat Load Lower Than Predicted, Resulting in a Low Glycol Evaporator Outlet Temperature

Statement — The actual spacecraft heat load was calculated to be 5480 Btu/hr based on water usage data. This load was approximately 500 to 1000 Btu/hr lower than the predicted heat loads of 6000 to 6500 Btu/hr that had been used to set the inflight position of the glycol evaporator back pressure control valve.

11. Interface Between Apex Cover and RCS Engines

Statement — The command module reaction control subsystem negative pitch engine panel and the panel-to-structure mounting bolts were found to be damaged during postflight inspection.

12. Holes in Recovered Main Parachute

Statement — Inspection of the recovered main parachute revealed a multitude of small burn holes and debris in the canopy.

~~CONFIDENTIAL~~



~~CONFIDENTIAL~~

## 12.2 COUNTDOWN ANOMALIES

## 1. RCS Quad A Helium Tank Pressure Decay

Statement — Quad A helium pressure data exhibited a pressure decrease from 4150 psia at servicing to 3910 psia at launch. The leak rate was approximately 5 psi per hour, or 26 scc per minute.

## 2. Cryogenic Servicing Problem

Statement — Both hydrogen tanks in the spacecraft cryogenic subsystem experienced excessive flow for several hours after servicing and pressurizing.

## 3. Oxygen Tank Number 2 Pressure Decay

Statement — Shortly after servicing and pressurizing the oxygen number 2 tank, the pressure decayed from the normal operating range and remained low for essentially 12 hours. The pressure decayed again during the early portion of the flight. In both cases the pressure was increased to the normal operating range by remote activation of the heaters and fans in the tank.

~~CONFIDENTIAL~~

~~CONFIDENTIAL~~

12-7

### 12.3 TEST AND CHECKOUT ANOMALIES

#### 1. Stabilization and Control Subsystem Junction Box Malfunction

Statement — A stabilization and control subsystem junction-box negative-pitch direct-control coil arc suppression circuit malfunctioned during the Flight Readiness Test.

#### 2. IMU Heater Problem in Emergency Mode

Statement — A malfunction was detected in the inertial subsystem emergency heater circuitry during the Countdown Demonstration Test.

~~CONFIDENTIAL~~

~~CONFIDENTIAL~~

## 12.4 POSTFLIGHT TESTING

The Apollo 4 command module was received at the spacecraft contractor's facility, Downey, California, on November 15, 1967. Postflight testing in support of the subsystem analyses and the resolution of anomalies is being conducted at the spacecraft contractor's facility, at the component vendors' facilities, and at the Manned Spacecraft Center. The testing is described in the following paragraphs and is still in progress at the time of publication of this report.

## 12.4.1 Heat Protection Subsystem

Cores were cut from selected areas of the aft and crew compartment heat shields for evaluation of entry effects. The core samples were sectioned and the ablator char and surface recession were analyzed. The astro-sextant passive thermal protection subsystem and the unified hatch test specimen were disassembled and inspected. Inspection of the aft heat shield revealed the presence of three 1/4-inch holes through the ablator; these holes were later determined to have been used during manufacture of the heat shield. Torque readings taken during removal of the 59 attachment bolts from the aft heat shield ranged from 20 to 580 in-lb; the installation torque had been 180 in-lb. Extreme variance in removal torques has existed on previously flown spacecraft.

## 12.4.2 Earth Landing Subsystem

The recovered main parachute was inspected, revealing a multitude of small burn holes and debris in the canopy. Much of the debris appeared to have come from the deck of the recovery ship.

## 12.4.3 Mechanical Subsystems

At recovery, it was found that one of the two vhf antennas on the upper deck did not lock when deployed. However, the antenna did lock when actuated by a member of the recovery team. Corrosion of the mechanism while in transit to Downey, California, prevented any meaningful post-flight testing.

## 12.4.4 Electrical Power Subsystems

Spacecraft batteries were load tested and found to be in good condition. The heater switch for the fuel cell oxygen tank no. 2 was checked for a reported preflight anomaly and was found to function properly. Trouble-shooting of the 5-volt instrumentation reference power supply

~~CONFIDENTIAL~~

~~CONFIDENTIAL~~

12-9

that failed during entry revealed incorrect wiring of the associated fuse box (C28A5), wherein the required preflight changeover from a 3-amp to a 1/4-amp fuse was not accomplished. Tests of the master event sequence controllers, earth landing sequence controllers, pyrotechnic continuity verification box, and reaction control subsystem (RCS) controllers verified that redundancy was still present. Inspection of the stabilization and control subsystem J-box (C29A1), which was suspected to have caused the preflight arc suppression problem, revealed that a wire was crimped between a mounting bolt and the case, resulting in an electrical short that caused an open diode.

#### 12.4.5 Environmental Control Subsystem

A leak check of the water/glycol subsystem was performed, and no leakage was found. A flow test of the water/glycol loop for the inertial measurement unit was conducted, and the flow and temperature data verified the flight data. The flow and temperature sensors were removed for laboratory recalibration. No evidence of RCS oxidizer ( $N_2O_4$ ) or fuel (MMH) solid deposits could be found in the spacecraft; slight ingestion (0.3 ppm  $N_2O_4$ ) of RCS contaminants had been indicated by onboard contamination-sensitive tapes and by the gas sample taken at recovery. As a result of preflight problems, the potable and waste water tanks quantity indicating systems, temperature controller, and oxygen pressure regulator were removed from the CM for analysis.

#### 12.4.6 Communications

The vhf updata receiver/decoder will be tested to determine the effect of over-deviation of the carrier on command acceptance. The power output of the S-band power amplifier is to be checked for deterioration.

#### 12.4.7 Pyrotechnics

The expended pyrotechnic initiators were removed from the CM and returned to MSC for electrical checks. These checks showed that the current leakage was sufficient to produce the voltage drop observed on the pyrotechnic busses prior to landing.

#### 12.4.8 Instrumentation

Heat shield calorimeters and pressure sensors, with the associated signal conditioning equipment, were removed from the CM for recalibration.

~~CONFIDENTIAL~~

~~CONFIDENTIAL~~

The polarity of two sway brace accelerometers (CK0036A and CK0037A) was in doubt but, after testing, was found to be correct. Recalibration of the cabin temperature sensor (CF0002T) was performed in the CM and was found to be satisfactory. The commutator loading of several heat shield temperature measurements was found to be incorrect, as had been indicated by the flight data. Two heat shield temperature measurements which had produced intermittent flight data were continuity checked with one (CA5713T) being found good and the other (CA1444T) open in the zone box. An RCS engine valve temperature measurement (CR2206T) which failed during entry, was tested and found to have an intermittent signal conditioner. The barometric pressure sensor (CE0035P), cabin pressure sensor (CF0001P), and glycol evaporator back pressure sensor (CF0034P) were removed from the spacecraft for recalibration.

#### 12.4.9 Guidance and Control Subsystems

The guidance and navigation (G&N) subsystem and the mission control programmer (MCP) were removed and returned to the respective vendors for testing and possible reuse. The MCP was subjected to redundancy testing and functioned properly. The G&N inertial measurement unit is to be analyzed for a preflight problem associated with the emergency heater control circuit.

#### 12.4.10 Reaction Control Subsystem

Two RCS +Y engines and two RCS clockwise roll engines were returned to the vendor for evaluation. RCS test port 58, which leaked during decontamination at Hawaii, was removed and returned to the vendor for failure analysis.

Anomaly testing was conducted in accordance with approved Apollo Spacecraft Hardware Utilization Requests (ASHUR's). A listing of the anomaly test ASHUR's is shown in table 12.4-I.

~~CONFIDENTIAL~~

~~CONFIDENTIAL~~

12-11

TABLE 12.4-I.- ASHUR's FOR POSTFLIGHT

ANOMALY TESTING

ASHUR No.	Subsystem	Purpose
017003	Instrumentation	To troubleshoot the 5-volt reference anomaly observed during entry
017005	SCS	To investigate the loss of arc suppression on CM RCS A and B pitch engine valves during the flight readiness test
017006	G&N	To perform a failure analysis on the loss of IMU emergency heater control experienced during the count-down demonstration test
017007	ECS	To investigate preflight calibration shifts in the waste and potable water tank quantity measurements
017016	ECS	To inspect CM interior components for evidence of RCS contamination entering the cabin during entry
017018	ECS	To resolve discrepancies concerning flow and temperature measurements in the IMU water/glycol coolant loop experienced during flight
017020	Instrumentation	To determine the cause of failure of the RCS B system clockwise engine oxidizer valve temperature measurement during entry
017021	ECS	To recalibrate the cabin temperature sensor for which questionable flight data were reported

~~CONFIDENTIAL~~

~~CONFIDENTIAL~~

TABLE 12.4-I.- ASHUR's FOR POSTFLIGHT

## ANOMALY TESTING - Continued

ASHUR No.	Subsystem	Purpose
017022	Instrumentation	To conduct continuity checks of the side heat shield temperature and SM/CM umbilical tube temperature measurements which produced intermittent flight data
017023	Instrumentation	To determine the aft heat shield surface recession and char thickness at selected calorimeter locations, since the flight data indicated less than the required recession for the instruments to function properly
017024	Instrumentation	To determine actual commutator loading of heat shield temperature measurements, which flight data indicated were reversed
017027	ECS	To recalibrate the cabin pressure transducer, for which the flight data were noisy
017028	ECS	To recalibrate the glycol evaporator back pressure sensor for verification of low readings during the flight
017030	Pyrotechnics	To determine if the pyrotechnics devices caused the observed current drain on the pyrotechnic batteries during the earth landing sequence
017036	EPS	To check the continuity of the fuel cell oxygen tank no. 2 heater switch as a possible cause of a preflight heater problem

~~CONFIDENTIAL~~

~~CONFIDENTIAL~~

12-13

TABLE 12.4-I.- ASHUR's FOR POSTFLIGHT

ANOMALY TESTING - Concluded

ASHUR No.	Subsystem	Purpose
017038	ELS	To recalibrate the barometric pressure sensor, for which flight data and calculated altitudes for drogue and pilot parachute deployments disagree
017040	Communications	To determine effect of over-deviation of the vhf updata carrier on command acceptance by the receiver decoder, as a result of non-acceptance of the initial state vector transmitted by Carnarvon
017041	Communications	To measure the power output of the S-band power amplifier for evaluation of deterioration indicated by the flight data
017042	Sequencers	To investigate open fuse-resistors and failed diodes uncovered during the postflight functional test of the master event sequence controllers
017501	Instrumentation	To verify the polarity of two sway brace accelerometers, for which flight data indicated reversals

~~CONFIDENTIAL~~



~~CONFIDENTIAL~~

THIS PAGE INTENTIONALLY LEFT BLANK

~~CONFIDENTIAL~~

~~CONFIDENTIAL~~

13-1

### 13.0 VEHICLE AND SYSTEMS DESCRIPTION

The space vehicle (fig. 13.0-1) for the Apollo 4 mission consisted of an Apollo spacecraft (Spacecraft 017), a lunar module test article (LTA-10R), and a Saturn V launch vehicle (AS 501). The combined space vehicle was approximately 363 feet long and weighed approximately 6 220 700 pounds before first-stage engine ignition.

The spacecraft consisted of a command and service module (CSM), a launch escape system, and a spacecraft lunar module adapter. The spacecraft is described in section 13.1 of this report. The lunar module test article is described in section 13.2. The launch vehicle consisted of three propulsion stages (S-IC, S-II, and S-IVB) and an instrument unit. The launch vehicle is described in section 13.3. Section 13.4 contains the weight and balance data for the CSM.

~~CONFIDENTIAL~~

~~CONFIDENTIAL~~

NASA-S-68-551

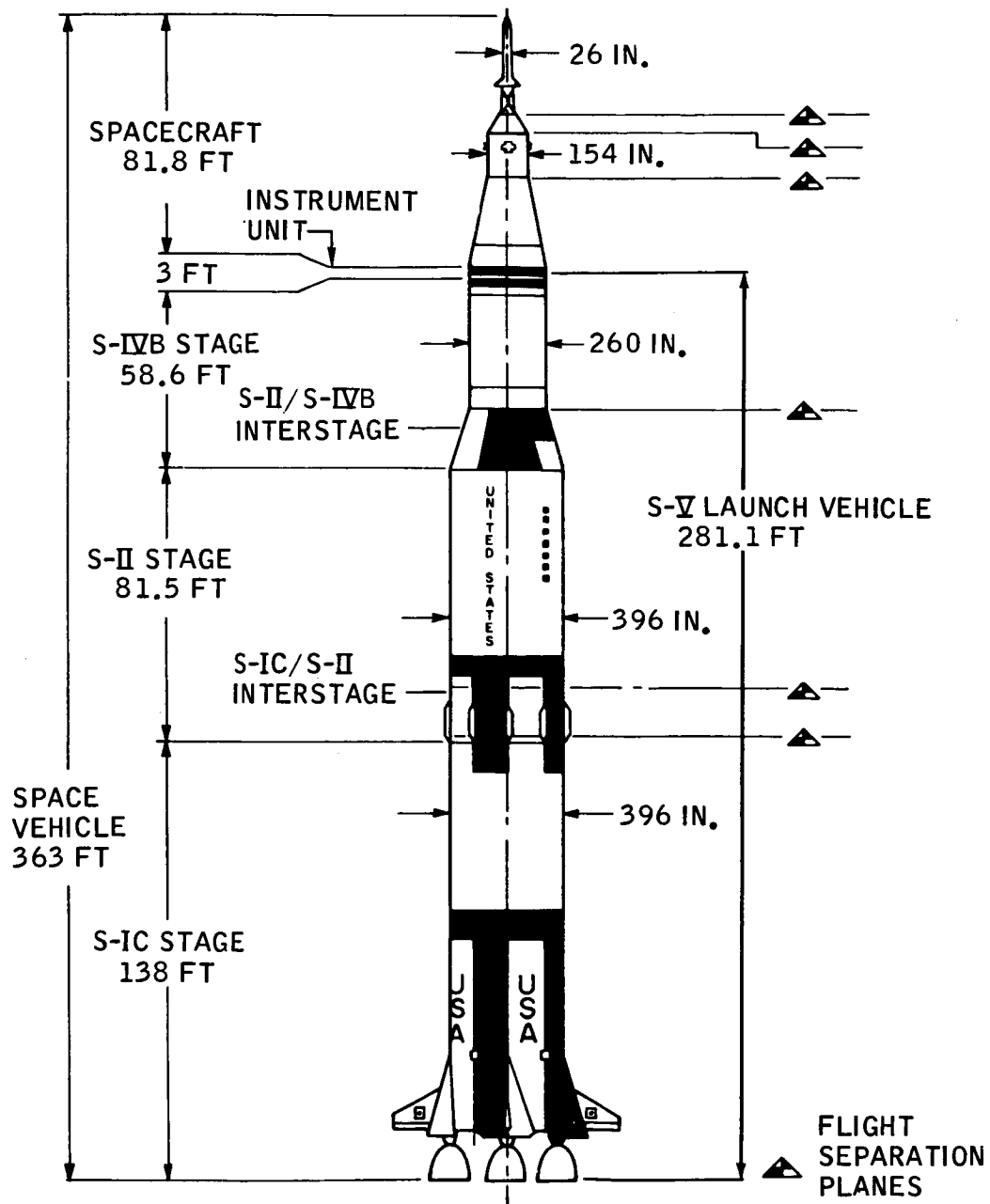


FIGURE 13.0-1.- APOLLO SPACE VEHICLE.

~~CONFIDENTIAL~~

~~CONFIDENTIAL~~

13-3

### 13.1 COMMAND AND SERVICE MODULE

The Apollo 4 spacecraft included a launch escape system (LES), a command module (CM), a service module (SM), and a spacecraft lunar module adapter (SLA) (fig. 13.1-1). The structure and major subsystems were of the same general configuration as previous Apollo spacecraft. The LES was approximately 398 inches long, the CM was approximately 133.5 inches long, the SM structure was approximately 162 inches long, and the SLA was approximately 302 inches long.

#### 13.1.1 Structures

The structural configurations of the LES, CM, SM, and SLA are described in the following paragraphs.

Launch escape system.- The LES was the forward-most part of the vehicle and consisted of an integral nose cone Q-ball, three rocket motors (escape, pitch, and tower jettison), a canard assembly, a structural skirt, a titanium-tube tower, and a boost protective cover. The boost protective cover was made of laminated fiberglass and Teflon. It was attached to the tower and was removed when the LES was jettisoned.

Command module.- The CM was a conically shaped structure and consisted of an inner pressure vessel (crew compartment) and an outer heat-shield structure. The inner structure was built of aluminum honeycomb panels and aluminum longerons to provide a pressure-tight crew compartment. The outer heat-shield structure was a stainless-steel honeycomb structure impregnated with an ablative material that provided a thermal barrier. The ablator thickness was a Block II design thickness. The heat shield was composed of three separate sections: the forward heat shield, the crew-compartment heat shield, and the aft heat shield. The space between the forward heat shield and the crew compartment contained the earth landing subsystem and related recovery aids. The space between the bottom of the crew compartment, the crew compartment heat shield, and the aft heat shield contained most of the CM reaction control subsystem.

The Apollo 4 CM configuration included a simulated Block II CM/SM umbilical panel and two Block II extravehicular activity (EVA) handrails. The new unified hatch was not installed for this mission; however, the Block I hatch had an instrumented test panel in place of the window in the outer hatch. The CM also contained a platform that carried the mission control programmer in place of the crew couches.

The command module window installation was a Block II configuration and consisted of one hatch window, two side windows, and two rendezvous

~~CONFIDENTIAL~~

~~CONFIDENTIAL~~

windows. Each window assembly consisted of four panels: two inner panels, each 0.20-inch thick with a 0.175-inch space between them, installed in the pressure cabin structure; one heat shield panel, 0.70-inch thick, installed in the heat shield structure, approximately 1 inch from the inner window assembly; and one micrometeoroid panel 0.35-inch thick that was placed over the heat shield window and was interfaced with the heat shield mold line. The space between the heat shield and the micrometeoroid window was approximately 0.5 inch. The space between the two panels installed in the pressure cabin structure was evacuated, refilled with dry nitrogen to 7.5 psia, and was sealed. The two inner panels were aluminum silicate. The heat shield and micrometeoroid windows were amorphous fused silica optical grade quartz. All windows had outer surface coatings (fig. 13.1-2).

Service module.— The SM was a cylindrical aluminum honeycomb shell with fore and aft aluminum honeycomb bulkheads. The interior was divided into sectors by six aluminum radial beams. Each radial beam had a triangular truss between the CM and SM, with pads at the apex to support the CM. Three pads were for compression loads and the other three pads were for shear and compression loads. Tension ties also were present on the same trusses that had shear-compression pads.

The SM housed a service propulsion subsystem (SPS), that included four propellant tanks, two helium pressurization tanks, and an engine; and also housed three fuel cells and two hydrogen and two oxygen storage vessels. The outer panels of bays 2, 3, 5, and 6 contained the four modular packages (quads) of the SM-RCS.

Spacecraft lunar module adapter.— The SLA structure was an aluminum honeycomb truncated conical shell. The aft section had four attachment points for the lunar module test article (LTA-10R). The forward section was separated into four panels by a mild detonation fuse explosive train at CSM/S-IVB separation. Thrusters rotated each panel about an aft hinge line to the open position where each was retained by a cable retention system. The SLA remained attached to the S-IVB stage after CSM/S-IVB separation.

#### 13.1.2 Earth Landing System

The purpose of the earth landing system (ELS) was to orient and decelerate the CM to an attitude and velocity safe for landing. The ELS consisted of two sequence controllers (subsystems A and B for redundancy), a forward heat shield parachute, two drogue parachutes, three pilot parachutes, three main parachutes, and associated devices such as mortars, reefing-line cutters, and parachute disconnects.

~~CONFIDENTIAL~~

~~CONFIDENTIAL~~

13-5

The ELS sequencers contained the required logic and provided the initiating functions for sequencing the various ELS events, which are outlined as follows.

- a. Forward heat shield parachute deployment and forward heat shield separation
- b. Drogue parachute mortar fire
- c. Drogue parachute disconnect and pilot parachute mortar fire
- d. Main parachute disconnect.

The ELS configuration was composed of four 7.2-foot nominal diameter ring-slot parachutes, (three pilot parachutes and one forward heat shield parachute); two 13.7-foot nominal diameter conical ribbon drogue parachutes; and three 83.5-foot nominal diameter ringsail main parachutes. The one forward heat shield parachute, two drogue parachutes, and three pilot parachutes were deployed by mortars. The three main parachutes were deployed from their packed configuration by the pilot parachutes. Reefing lines and cutters were incorporated in the drogue and main parachutes to maintain these parachutes in a partially inflated state for a predetermined time, and upon activation, to release the parachutes so that they could open fully.

The drogue and main parachutes were attached to the CM forward deck and were released from the CM, when required, by pyrotechnic cutting devices.

### 13.1.3 Mechanical Subsystem

Mechanical items included the canard assembly, the uprighting subsystem, impact attenuation subsystem, recovery aids and their associated deployment mechanisms, and the latching mechanisms for the side heat shield, side crew compartment, forward crew compartment, and boost protective cover (BPC) hatches.

Canard assembly.- The canard assembly was an integral part of the launch escape system and would have been used only in the event of a launch escape abort. This assembly consisted to two aerodynamic surfaces that would have been pyrotechnically deployed and locked in the deployed position. The canards would be used to position and stabilize the abort vehicle configuration in the aft-heat-shield forward position.

Uprighting subsystem.- The uprighting subsystem consisted essentially of three inflatable bags stowed in canisters on the CM upper deck. The

~~CONFIDENTIAL~~

~~CONFIDENTIAL~~

purpose of the subsystem was to achieve and maintain a CM apex-up (Stable I) flotation attitude after landing. If the CM had landed in the apex-down (Stable II) position, or subsequently turned over to that position, the three bags would have been simultaneously inflated by two electrically operated compressors. This uprighting operation would have been initiated by the mission control programmer (MCP).

Impact attenuation subsystem.- The purpose of the impact attenuation subsystem was to reduce the impact shock at CM landing. The external energy absorption was provided by the heat shield and inner structures and by the crushable ribs in the aft compartment. The normal crew couches inside the CM were replaced by the MCP platform. The four X-X axes platform struts contained solid spacers, and the two Y-Y and the two Z-Z axes struts contained normal crushable cores for absorption of energy directed along these axes.

Recovery aids.- Recovery aids consisted of one hf and two vhf antennas, a flashing light, and a sea-dye-marker/swimmer-umbilical, all located on the CM upper deck.

The two vhf antennas and the flashing light were each deployed by spring-operated mechanisms. Each mechanism was released by an 8-second time-delay pyrotechnic cutting device activated by lanyards attached to the main parachute riser. The flashing light had an independent power supply sufficient for approximately 24 hours of operating time. The hf recovery antenna was deployed on command by the MCP 11 seconds after the CM achieved the Stable I position after landing.

The sea-dye canister was designed to deploy overboard by springs and remain attached to the CM by a cable which included the swimmer interphone umbilical. The deployment mechanism latch was triggered by a lanyard that was pulled when the hf antenna was erected.

Hatch latching mechanism.- The hatch latching mechanisms for the side heat shield hatch, the side crew compartment hatch, the forward pressure hatch, and the boost protective cover hatch operated as follows.

Side heat shield hatch-latching mechanism: The side heat shield hatch was located on the -Z side of the outer structure of the CM conical surface. The hatch latches must retain the hatch in place to maintain the integrity of the structure and heat shield ablator. The hatch utilized mechanical engagement on all four sides. The hatch latch release mechanism consisted of a gear sector and pinion drive, bellcranks, linkages, and 22 toggle latches.

Side crew compartment hatch-latching mechanism: The side crew compartment hatch was located on the -Z side of the CM with cabin pressure

~~CONFIDENTIAL~~

~~CONFIDENTIAL~~

13-7

causing the "hard" seal against the CM inner structure. The hatch was held in place by machined-edge members on three sides and a latch/release mechanism on the remaining side. The mechanism consisted of a rack and pinion drive and six toggle latches.

Forward pressure hatch-latching mechanism: The forward pressure hatch was located at the top of the tunnel on the upper deck of the CM. The hatch-latching mechanism locked the hatch in position to maintain the structural and pressure-seal integrity of the pressure vessel throughout the mission. The hatch had a pressure seal seated by means of a breech-lock configuration. A bolt-type locking mechanism retained the hatch against rotation and disengagement.

Boost protective cover hatch-latching mechanism: The boost protective cover hatch-latching mechanism hardware consisted of a drive mechanism and inter-connecting linkages to actuate the knife-type latches located around the four sides of the hatch.

#### 13.1.4 Electrical Power Subsystem

The electrical power subsystem (EPS) supplied, controlled, and distributed all electrical power in the spacecraft from lift-off through recovery. It consisted of three fuel cell powerplants, a cryogenic gas storage subsystem, several batteries, three inverters, and power distribution harnesses.

Fuel cells.- The prime electrical power units were Bacon-type, chemical fuel cell powerplants, each rated to produce up to 1.42 kW at  $29 \pm 2$  volts dc. The powerplants were located in sector IV of the SM. A fuel cell powerplant flow diagram is shown in figure 13.1-3. The powerplant consisted of a power conversion section, a reactant control assembly, a waste heat and water removal assembly, and instrumentation. The conversion section was housed in an insulated and pressurized tank. The accessory section rested on top of the power section and support cone, and consisted of a nitrogen pressurization assembly, three regulators, motor-driven pumps, a secondary (glycol) coolant loop, components of the primary (hydrogen) regenerative loop, and the necessary plumbing. The 31 cells, approximately 1 volt each, were stacked in series inside the pressure jacket and held together by torsion tie rods. Oxygen and hydrogen were distributed through individual lines, feeding from the intake manifolds, to each of the cells. Regulators reduced the gas supply pressure to the required operating pressure of 53 psia for nitrogen, 64 psia for oxygen, and 61.5 psia for hydrogen.

The major differences between the fuel cell subsystem installed in Spacecraft 017 and the normal Block I configuration were as follows.

~~CONFIDENTIAL~~



~~CONFIDENTIAL~~

a. A 4 W heater was added to the hydrogen vent annulus as a result of Spacecraft 008 thermal vacuum testing. This heater will be included on all Block II spacecraft.

b. A Block II retrofit water/glycol coolant pump was installed on each fuel cell as a result of a problem with the coolant loop on Spacecraft 011 (AS 202 mission).

c. A mission control programmer was included on this vehicle to perform certain control functions normally accomplished by the flight crew.

d. A cork coating was applied to the EPS radiator to minimize boost heating during the launch phase. The cork coating varied in thickness from 0.017 to 0.075 inch.

Cryogenic subsystem.- The cryogenic storage subsystem provided gaseous hydrogen to the fuel cells and gaseous oxygen to the environmental control subsystem and fuel cells. The fluids were stored in four Dewar vessels located in sector 1 of the SM, two for oxygen and two for hydrogen. Pressure in the subsystem was maintained by heaters and uniform density was maintained by circulating fans. Oxygen was delivered to the fuel cell regulators at  $900 \pm 35$  psia and hydrogen at  $245 \pm 15$  psia. A fuel cell/cryogenics interface flow schematic is shown in figure 13.1-4.

Batteries.- The A, B, and C batteries, rated at 40 ampere-hours each, were used to supplement the fuel cells during the SPS burn peak power loads and, in addition, were the prime sources of power after separation of the CM from the SM. The two batteries which provided power for pyrotechnic ignition and two batteries which powered the SM jettison controller were rated at 0.75 ampere-hour each. These seven batteries comprised the normal complement of a manned spacecraft. Three additional auxiliary batteries provided power for the MCP.

Power conversion.- Primary dc power was converted into ac power by three solid-state inverters. Each inverter provided 115-volt, 400 Hz, 3-phase, ac power and was capable of carrying all of the spacecraft ac power load. Two inverters were active, one to power each of the two ac buses. The third inverter would have been automatically placed in use if either of the other two had failed.

Automatic switching functions.- The switching functions which would be performed by the crew during manned flights were performed by the MCP.

Power distribution.- A simplified schematic of the electrical power distribution is presented in figure 13.1-5.

~~CONFIDENTIAL~~

~~CONFIDENTIAL~~

13-9

### 13.1.5 Sequential Events Control Subsystem

The primary purpose of the sequential events control subsystem was to control the sequential operation of crew safety-related functions during the ascent and entry portions of the mission or in the event of an abort, and to perform the normal separation functions.

Sequential events controllers.- The sequential events control subsystem consisted of redundant controllers or functions which provided automatic, semiautomatic, and manual control for initiation or termination of functional events during various phases of the mission. These controllers included the master event sequence controller, the earth-landing sequence controller, the reaction control subsystem controller, the service module jettison controller, and the pyrotechnic continuity verification box. Each of the controllers consisted of relays, timers, and other components to control subsystems operation and automatic timing of events. A block diagram of the functions of the sequential events control subsystem is shown in figure 13.1-6.

Mission control programmer.- The mission control programmer (MCP) consisted of a spacecraft command controller, a ground command controller, and an attitude and deceleration sensor. The purpose of the MCP was to provide a logical sequencing of the spacecraft functions that are normally accomplished by the flight crew.

The spacecraft command controller provided the normal mission functions, using stimuli from the ground support equipment prior to launch, from the S-IVB stage during boost and orbit, and from the guidance and navigation (G&N) subsystem and the earth-landing sequence controller during the independent spacecraft portion of the flight. The spacecraft command controller also contained inverter protection circuitry against overvoltage, undervoltage, and overload on either ac bus. It also contained circuitry to select stabilization and control subsystem modes in case of a G&N subsystem failure.

The ground command controller provided the capability of 48 real-time backup ground commanded functions to be initiated, if required.

The attitude and deceleration sensor sensed the deceleration resulting from entry into the atmosphere, sensed the impact resulting from command module landing, and sensed flotation attitude after landing. The resulting switch closures provided the spacecraft command controller with additional stimuli for sequencing of postlanding functions.

~~CONFIDENTIAL~~

~~CONFIDENTIAL~~

### 13.1.6 Pyrotechnic Devices

Many functions on the spacecraft were initiated or accomplished by pyrotechnic devices. Most of these devices were actuated electrically by means of a hot-wire electrical initiator. These functions included solid propellant motor ignition in the LES, three spacecraft separation functions, deployment, disreefing and release of parachutes; CM-RCS propellant interconnect and dump valves; and antenna deployment.

The pyrotechnic devices were of the same type as those used on the AS 202 mission except for the SLA debris catcher and the single bridgewire Apollo standard initiators.

The function of the SLA debris catcher was to prevent all shrapnel and debris produced by the mild detonating fuse from traveling inboard when the splice plates were severed. The debris catchers were installed at the SLA separation planes. The configurations used for Spacecraft 011 and 017 are shown in figure 13.1-7.

The function of the single bridgewire Apollo standard initiator was the same as that of the dual bridgewire Apollo standard initiator used to initiate all pyrotechnic devices used on the Apollo spacecraft. The single bridgewire initiator was used to initiate the SLA separation subsystem, CM/SM separation subsystem, circuit interrupters, RCS pressurization valves, and the LES pyrotechnic devices. The dual bridgewire initiator was used to initiate the ELS pyrotechnic devices.

### 13.1.7 Emergency Detection Subsystem

The emergency detection subsystem (EDS) was an electrical sensing subsystem provided in the Apollo Space Vehicle to detect emergency conditions associated with launch vehicle powered flight. The Apollo 4 mission was the first test of the EDS in conjunction with the Saturn V launch vehicle. Space vehicle angular rates, launch vehicle guidance platform failure, engine thrust, stage separation, and vehicle angle of attack were sensed by the EDS and signals transmitted to instruments in the crew station. These displays normally would provide the necessary information for determining the necessity for abort action, from lift-off through CSM/S-IVB separation. Also included in the subsystem were provisions for initiation of an automatic abort during early S-IC burn in the event of extremely time critical emergencies; however, the system was flown open-loop and no automatic abort capability existed. Concurrent with manual abort initiation, the active engines of the launch vehicle would have been shut down to insure safe separation of the spacecraft from the launch vehicle. However, to avoid the possibility of the launch vehicle falling back into the launch complex area, launch vehicle

~~CONFIDENTIAL~~

~~CONFIDENTIAL~~

13-11

engine shutdown would have been inhibited for a predetermined period following lift-off.

#### 13.1.8 Communications Subsystem

The communications subsystem (fig. 13.1-8) included equipment for simulated voice transmission, for acquisition, processing, recording, and transmission of telemetry data, for reception of uplink data and commands; for ranging and tracking; and for aiding postlanding recovery operations. The primary functions of the equipment are listed below.

Simulated voice transmission.- Inflight voice communications were simulated by transmission of a 400-Hz tone by the S-band equipment and the vhf-AM transceiver.

Telemetry transmission.- Data acquired from the various spacecraft subsystems were processed and transmitted as pulse-code-modulated signals by the S-band transmitter and by the vhf-FM transmitter. Before launch, the pulse-code-modulated data were transmitted by hardline through the SM umbilical to the launch control center.

Update link.- Real-time commands to the spacecraft equipment and update information for the G&N subsystem were received by the update link and by the S-band equipment.

Tracking and ranging.- Tracking assistance was provided by the C-band transponder. Ranging and Doppler tracking were provided by the S-band equipment.

Recovery aids.- Recovery-aid signals were transmitted by the vhf recovery beacon, the vhf survival beacon, and the hf transceiver.

Antennas.- The vhf-AM, vhf-FM, and update-link signals were transmitted and received by two scimitar antennas located on the SM. Four C-band antennas were flush-mounted, 90-degrees apart, on the periphery of the CM. Four S-band antennas were flush-mounted, 90 degrees apart, on the lower periphery of the CM.

One hf and two vhf antennas were mounted on the upper deck of the CM and were deployed during the recovery and postlanding sequence.

#### 13.1.9 Instrumentation Subsystem

The instrumentation subsystem consisted of operational instrumentation, flight qualification instrumentation, the data group equipment,

~~CONFIDENTIAL~~

~~CONFIDENTIAL~~

a camera assembly installation, two integrating radiation dosimeters, and two nuclear emulsion spectrometers.

Operational instrumentation includes those parameters needed for prelaunch and inflight real-time performance and management of the spacecraft. This instrumentation consisted of the transducers and matching components used to measure temperatures, pressures, currents, voltages, frequencies, quantities, flow rates, events, attitudes, and attitude rates which were converted to a modulation wavetrain and transmitted to the Manned Space Flight Network for real-time display and ground-based magnetic tape recording.

The flight qualification instrumentation included the measurements used to acquire postflight data for performance analysis of the CM heat shield during entry, to provide additional data for specific mission objectives, and to obtain supplemental data for evaluating the performance of various subsystems. The types of measurements included pressure, temperature, acceleration, vibration, strain, and heat flux. This portion of the subsystem included transducers, signal conditioners, power supplies, current limiters, zone boxes, a five-point calibrator, a modulation package, and commutators.

Additionally, the instrumentation subsystem included the data group equipment, consisting of two onboard tape recorders (the data storage equipment and flight qualification recorder), the central timing equipment, and the signal conditioning equipment. During the first-stage (S-IC) launch phase as well as the entry phase of the mission, pulse-code-modulated data were recorded on the data storage equipment. The heat shield data and most of the remaining flight qualification data were commutated and recorded redundantly on the data storage equipment and on the flight qualification recorder. Certain critical structural measurements were recorded directly on the flight qualification recorder to provide continuous, rather than commutated, data. The central timing equipment provided timing signals to several spacecraft subsystems. The signal conditioning equipment accepted signals from various sensors and normalized these to a 0 to 5 V dc range suitable for telemetry. It also provided reference voltages to instrumentation and other subsystems.

The camera installation consisted of a 70-millimeter camera, a control box, a battery pack, a g-switch, and interconnecting wire harness. The camera was installed inside the crew compartment viewing out the left-hand side window. This installation was completely electrically self-contained, and required only mechanical interfaces with the spacecraft.

The two integrating radiation dosimeters were installed to measure the integrated skin and depth radiation dose within the CM. Each unit was battery powered, utilized an ionization chamber as the sensing element, and contained a digital register readout to indicate radiation dose.

~~CONFIDENTIAL~~

~~CONFIDENTIAL~~

13-13

Two emulsion spectrometers were installed, one at the CM crew compartment interior wall and the other near the center of the crew compartment, to determine the radiation shielding effectiveness of the CM through a defined solid angle of entry within the spectrometers. Each spectrometer consisted of an aluminum housing with tungsten inserts and a light-sensitive emulsion package. Data received from the emulsions will yield the radiation spectrum encountered.

#### 13.1.10 Guidance and Control

Guidance and navigation subsystem.- The guidance and navigation (G&N) subsystem consisted of three major subdivisions.

- a. The inertial subsystem was used to measure changes in velocity or position.
- b. The optical subsystem was used to verify G&N prelaunch alignment.
- c. The computer subsystem generated velocity and position control signals.

The G&N equipment consisted of a navigation base, an inertial measurement unit (IMU), an optical unit assembly, a power and servo assembly, an Apollo guidance computer, and display and control (D&C) panels. The computer display and keyboard (DSKY), coupling display units, and associated displays and controls were mounted on the D&C panel. Figure 13.1-9 is a functional schematic of the subsystem and its interfaces.

The inertial subsystem consisted of the IMU, three coupling data units, portions of the power and servo assembly, and portions of the lower D&C panel. The inertial subsystem was used for spacecraft guidance and control, and performed three major functions, which are as follows.

1. Measurement of spacecraft attitude with respect to inertial frame
2. Assistance in generating steering commands
3. Measurement of spacecraft velocity changes.

To accomplish these functions, the IMU provided an inertial reference consisting of a stable member gimballed in three degrees of freedom and stabilized by three inertial rate integrating gyros and associated servos. Prior to launch, the stable member was aligned in azimuth by means of a

~~CONFIDENTIAL~~

~~CONFIDENTIAL~~

gyrocompassing routine and was aligned to the local vertical by pulsed integrating pendulous accelerometers (PIPA's), which sensed gravity reaction force. Resolvers, mounted on the gimbal axes, acted as angular-sensing devices and measured the attitude of the spacecraft with respect to the stable member. These angular measurements (gimbal angles) were compared with the desired spacecraft attitude as calculated by the Apollo guidance computer and displayed on the coupling data units. Differences between the gimbal angles and the coupling display unit angles caused attitude error signals to be generated and sent to the stabilization and control subsystem, which drove the RCS engines during coast phases and controlled the thrust vector during SPS thrust phases to control spacecraft attitude. Acceleration of the spacecraft was sensed by the three PIPA's mounted orthogonally on the stable member. The resultant signals from the accelerometer loops were supplied to the Apollo guidance computer, which then calculated velocity and updated the state vector. The inertial subsystem modes of operation were controlled by the Apollo guidance computer.

The optical subsystem consisted of the optical unit assembly, two coupling data units, and portions of the power and servo assembly and D&C panel. The optical subsystem, used to verify the alignment of the IMU prior to launch, contained a sextant and a scanning telescope. Because of a previously encountered drift problem with this block of optical subsystems, a modification was made to the servo loop. This insured that the optics shaft axes would not drift in flight, thus allowing the astrosextant door modification to be evaluated.

The computer subsystem, which consisted of the Apollo guidance computer and portions of the D&C panel, was used to perform data handling and computations. The Apollo guidance computer was a general purpose digital computer employing a core-rope memory, parallel operation, and a built-in self-check capability. Programs were stored in the computer until selected for use. The computer subsystem performed three major functions, given as follows.

- a. Calculation of the steering signals and SPS engine discretizes necessary to keep the spacecraft on the required trajectory
- b. Positioning of the stable member in the IMU to a coordinate system defined by precise optical measurements made prior to launch
- c. Conduct of limited malfunction isolation by monitoring the level and rate of subsystem signals.

A bent pin on the main DSKY was detected during spacecraft checkout. This pin was subsequently clipped, disabling the main DSKY display lights. No flight effects resulted from this change.

~~CONFIDENTIAL~~

~~CONFIDENTIAL~~

13-15

Stabilization and control subsystem.- The stabilization and control subsystem (SCS) was integrated with the SPS, RCS, and G&N subsystems into a closed-loop spacecraft control unit. The SCS model K, Block I configuration was divided into three major functional assemblies which provided redundancy and backup capability to the G&N subsystem.

The attitude reference assembly provided a backup total attitude readout. The attitude control assembly processed all sensor inputs and provided rate damping to control spacecraft attitude with the RCS. The thrust vector control assembly processed guidance commands and provided rate damping and gimbal trim to control the SPS engine thrust vector. The SCS was modified to allow switching functions normally provided by the crew to be initiated by the MCP.

The three major assemblies consisted of the following units:

- a. Rate gyro assembly
- b. Attitude gyro/accelerometer assembly
- c. Pitch, roll, yaw, and auxiliary electronic assemblies
- d. Control assemblies
- e. Display/attitude gyro accelerometer electronic control assembly
- f. Attitude set/gimbal position indicator

A functional schematic of the SCS and its interfaces is shown in figure 13.1-10.

#### 13.1.11 Reaction Control Subsystem

The reaction control subsystem (RCS) consisted of two independent subsystems designated as the SM-RCS and the CM-RCS. After CSM/S-IVB separation, the SM-RCS controlled spacecraft rotation in all three axes. It was also used to perform minor translations, including CSM/S-IVB separation, SPS ullage, and CM/SM separation maneuvers. After CM/SM separation, the CM-RCS controlled command module rotation in all three axes.

The engine locations are shown graphically in figures 13.1-11 and 13.1-12 for the SM-RCS and CM-RCS, respectively. Propellant feed systems for the SM-RCS and CM-RCS are shown schematically in figures 13.1-13 and 13.1-14, respectively.

~~CONFIDENTIAL~~



~~CONFIDENTIAL~~

Service module reaction control subsystem.- The SM-RCS consisted of four individual, functionally identical packages (quads) located 90 degrees apart around the forward section of the SM periphery and offset from the Y- and Z-axes by 7 degrees 15 minutes. Each quad was mounted on its panel so that the reaction engines were on the outer surface and the remaining components were inside the SM. The quads were functionally interchangeable. The engine combustion chambers were canted approximately 10 degrees away from the panel structure, and the two roll engines on each quad were offset-mounted to accommodate plumbing to the engine. Each quad incorporated a pressure-fed, positive-expulsion, pulse-modulated, bipropellant system to produce the reaction thrust required to perform the SM-RCS control functions. An active SM-RCS thermal control subsystem was added on Spacecraft 017 (fig. 13.1-11). This subsystem consisted of two heater units and associated thermal switches, bonded to the engine mounting housing on each quad. Each heater unit contained two 36-W heating elements. Two of the elements were connected to a primary thermal switch set to open at 129° F and close at 120° F. The other two elements were connected to a secondary thermal switch set to open at 104° F and close at 70° F. RCS propellants for both the CM and SM engines consisted of the oxidizer (nitrogen tetroxide,  $N_2O_4$ ) and the fuel (monomethylhydrazine, MMH). The propellant transferring agent was pressurized helium gas. The reaction engines had the capability of being either pulse-fired to produce short thrust impulses, or continuously fired to produce a steady-state thrust level. Each engine included electrically operated fuel and oxidizer valves with automatic coils operated by signals from the stabilization and control subsystem and with direct coils operated by direct command. Direct commands can be provided from a hand controller by the crew, but were provided by the mission control programmer on this mission.

Command module reaction control subsystem.- The CM-RCS was comprised of two independent subsystems, designated A and B. Each subsystem consisted of an oxidizer and fuel propellant tank and distribution assembly, a helium pressurization assembly, electrically operated engine propellant valves, and six engine assemblies. All 12 engine nozzles were ported through the CM surface on the -Z side. The propellant and pressurizing tanks were located in the aft compartment on the +Z side. Either system had the capability of providing the impulse necessary to perform the required entry maneuvers and stabilization. The subsystems were activated and pressurized just prior to CM/SM separation. After entry, the systems were interconnected by pyrotechnic devices, and the remaining propellants were burned. The subsystem was purged with helium prior to CM handling.

~~CONFIDENTIAL~~

~~CONFIDENTIAL~~

13-17

### 13.1.12 Service Propulsion Subsystem

The service propulsion subsystem (SPS) consisted of four primary subassemblies: engine; propellant storage and feed; pressurization; and propellant quantity gauging subassemblies. A functional flow diagram is shown in figure 13.1-15.

Engine subassembly.- The engine subassembly produced a nominal thrust of 21 500 pounds, operating at a nominal mixture ratio of 2.0. The propellants were earth-storable and were hypergolic. The fuel was a 50/50 (by weight) blend of unsymmetrical dimethylhydrazine (UDMH) and anhydrous hydrazine ( $N_2H_2$ ). The oxidizer was nitrogen tetroxide ( $N_2O_4$ ). The engine bipropellant shutoff valve was pneumatically actuated by gaseous nitrogen. The combustion chamber was ablatively cooled. Bolted to the chamber was a nozzle extension composed of two columbium sections which started at the combustion chamber and extended to an area ratio of 40:1 and a titanium section from there to the exit (62.5:1). Nozzle extension cooling was accomplished by radiant heat transfer into space.

Propellant storage and feed.- Fuel and oxidizer were each contained in a set of two cylindrical tanks connected in series. The downstream (sump) tanks were directly connected to the upstream storage tanks by crossover lines and standpipes. Each sump tank outlet contained propellant retention screens and a reservoir to retain propellant over the feed line inlet during near zero-g conditions and to reduce the propellant settling time requirements. Thrust from the service module reaction control subsystem engines normally provided additional propellant settling.

Pressurization subassembly.- The helium pressurization supply was contained in two spherical pressure vessels at an initial nominal pressure of 4000 psia and at ambient temperature. Two solenoid valves isolated the helium from the fuel and oxidizer tanks during SPS engine non-thrusting periods. Two dual-stage regulators, arranged in parallel, were located downstream of the solenoid valves and provided pressure-regulated helium to the fuel and oxidizer tanks. Two sets of check valve assemblies, arranged in series-parallel configurations, prevented fuel or oxidizer from entering the pressurization subassembly. Pressure relief valves prevented overpressure in the propellant tanks. Heat exchangers were used in the helium lines to condition the helium to a temperature approximating that of the propellant in the tanks.

Propellant gauging subassembly.- Propellant quantity was measured by two separate sensing devices. The primary device used the capacitance of the propellant to gauge the propellant level in the tank and the secondary device measured quantity by point-sensors. These measurement devices were accurate during one-g or thrusting periods only, that is, when there was sufficient acceleration to force the propellants to the

~~CONFIDENTIAL~~

~~CONFIDENTIAL~~

rear ends of the tanks. During manned missions, the measurements in the propellant utilization gauging subsystem, will be used in conjunction with a propellant utilization valve in the oxidizer supply line to provide flight crew control of the minor oxidizer/fuel ratio adjustments which may be necessary to obtain simultaneous propellant depletion. The propellant utilization gauging subsystem was installed in the spacecraft and the primary device outputs were telemetered. The propellant utilization valve was inoperable.

#### 13.1.13 Environmental Control Subsystem

The purpose of the environmental control subsystem (ECS) was to provide heat rejection from the crew compartment electrical/electronic equipment and to control crew compartment pressure.

This subsystem was basically a partial Block I subsystem consisting of the water/glycol coolant circuit, water circuit, oxygen circuit, and the cabin cooling/recirculation elements (fig. 13.1-16). The pressure suit circuit, the associated pressure suit circuit distribution ducting and controls, the waste management circuit, and the postlanding ventilation blower and its associated wiring were not installed. The Block I ECS space radiators were installed on the SM but were not serviced with water/glycol and were inoperative on this mission. The coolant circuit evaporator and temperature controller were Block II components. The glycol coolant circuit is shown schematically in figure 13.1-17.

A solution of water/glycol (37.5 percent water/62.5 percent glycol) was serviced in the coolant circuit. This coolant circuit included the evaporator, the pump assembly, the reservoir, the coldplate network and associated interconnecting plumbing and valving, and the cabin heat exchanger. The total heat load absorbed by the water/glycol coolant was rejected by water evaporation in the coolant circuit evaporator.

Water was supplied to the coolant circuit evaporator from the water circuit. The water circuit obtained its main water supply (after pre-launch servicing) from the fuel cells as a byproduct of a chemical reaction in the production of electrical energy. The water circuit consisted of the potable and waste water tanks, the associated check valves, the relief valves, the shutoff valves, and the flow control valve and interconnecting plumbing.

Cabin pressure was controlled by the cabin pressure relief valve. The cabin pressure relief valve provided positive pressure relief during spacecraft ascent and negative pressure relief during spacecraft descent. The cabin pressure relief valve operated on a differential pressure principle, ceasing to relieve cabin pressure at a nominal value of 6.0 psid, referenced to atmospheric ambient pressure.

~~CONFIDENTIAL~~

~~CONFIDENTIAL~~

13-19

The oxygen surge tank and cryogenic oxygen storage vessels supplied oxygen through the high-pressure oxygen regulator assembly to the cabin pressure regulator and also to the tank pressure regulator for pressurization of the positive expulsion bladders in the potable water tank, waste water tank, and coolant circuit reservoir.

Fifteen pairs of vapor sensitive tapes were installed at various points in the CM cabin to detect ingestion of any CM-RCS fuel, oxidizer, or combustion products into the cabin through the cabin pressure relief valve during the cabin pressurization period after entry. The locations of these tapes are shown in figure 13.1-18.

The crew compartment was purged and pressurized with an approximate 90 percent nitrogen atmosphere prior to launch.

~~CONFIDENTIAL~~

~~CONFIDENTIAL~~

NASA-S-68-552

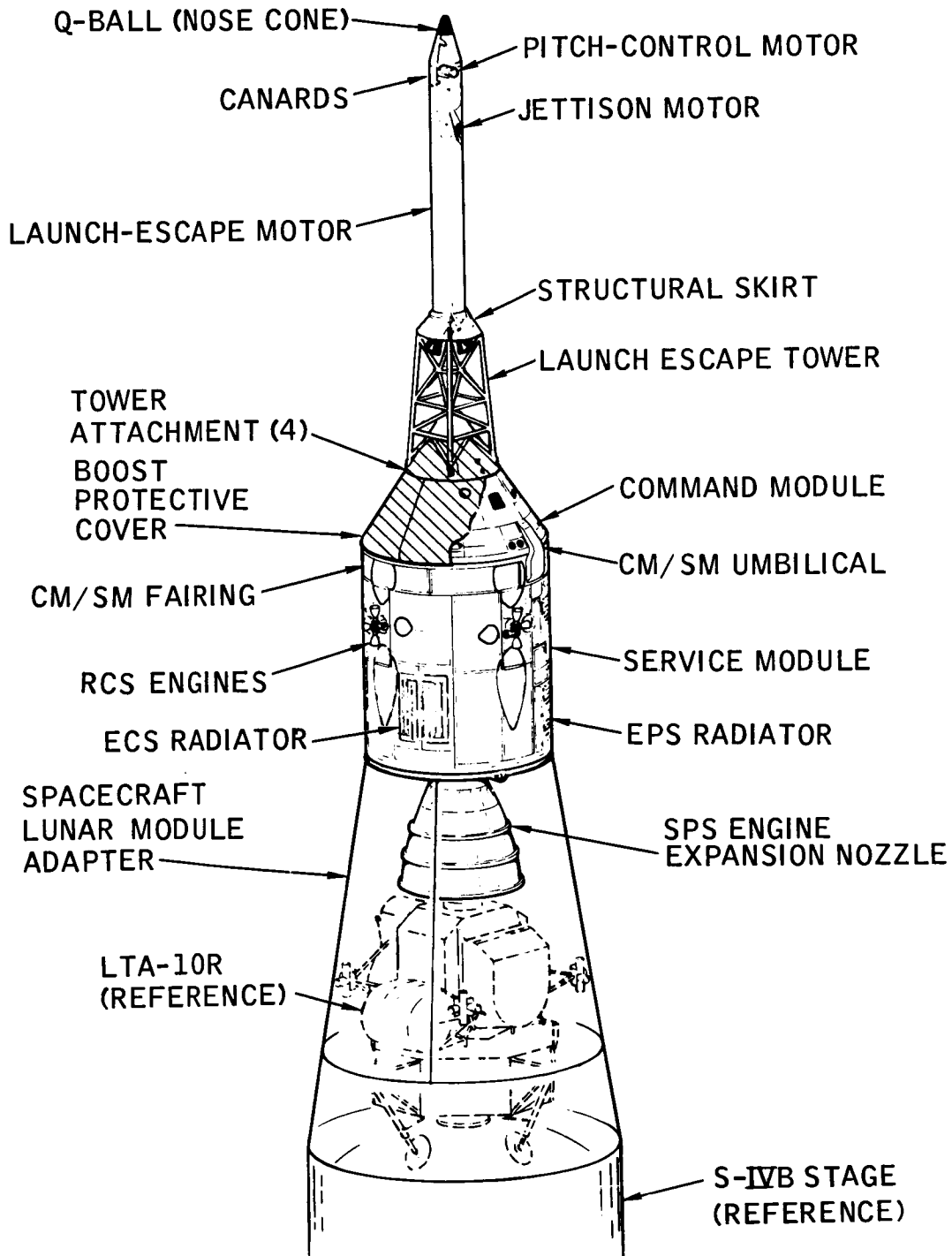


FIGURE 13.1-1.- SPACECRAFT 017.

~~CONFIDENTIAL~~

~~CONFIDENTIAL~~

13-21

NASA-S-68-553

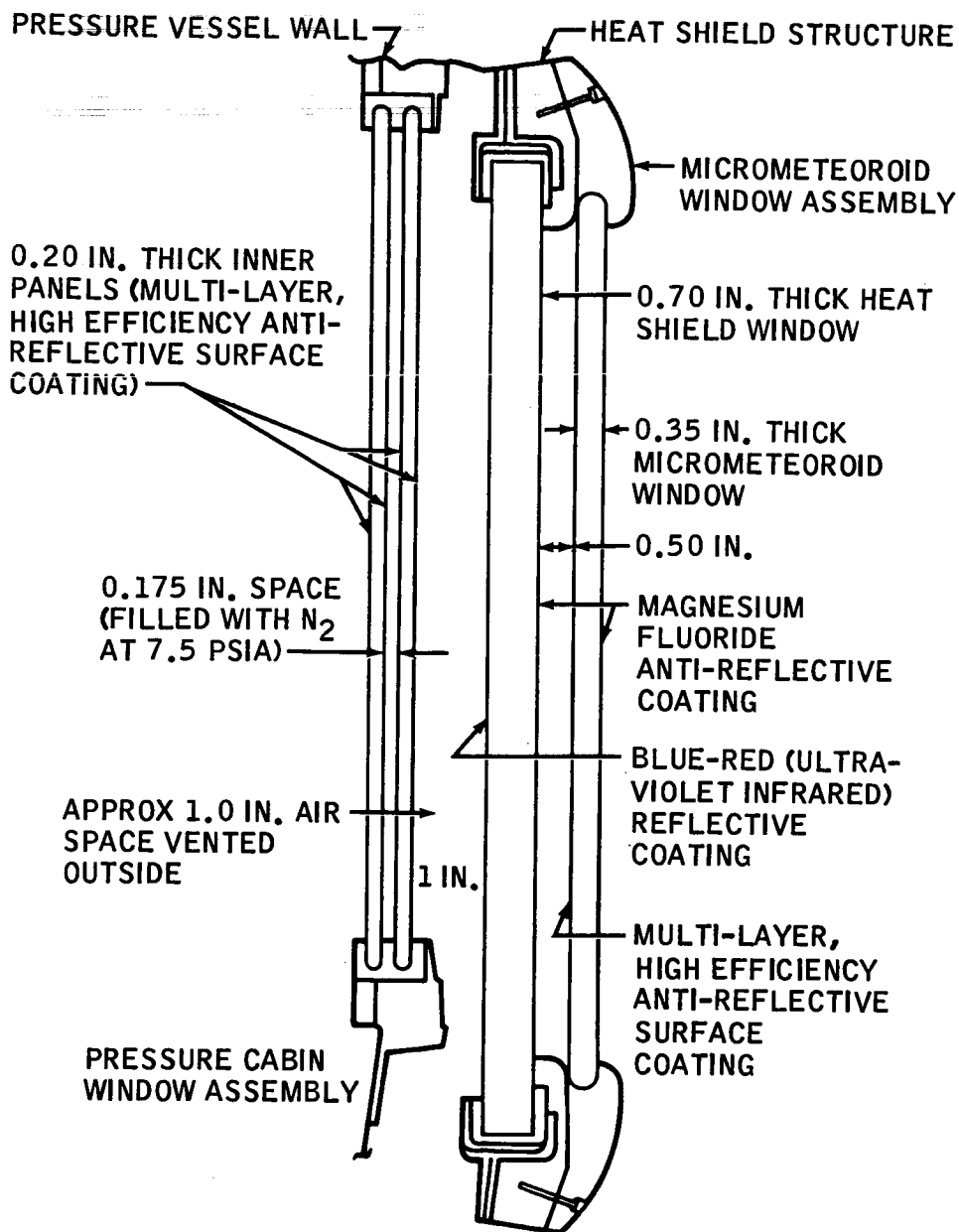


FIGURE 13.1-2.- COMMAND MODULE WINDOW ASSEMBLY.

~~CONFIDENTIAL~~

CONFIDENTIAL

NASA-S-68-554

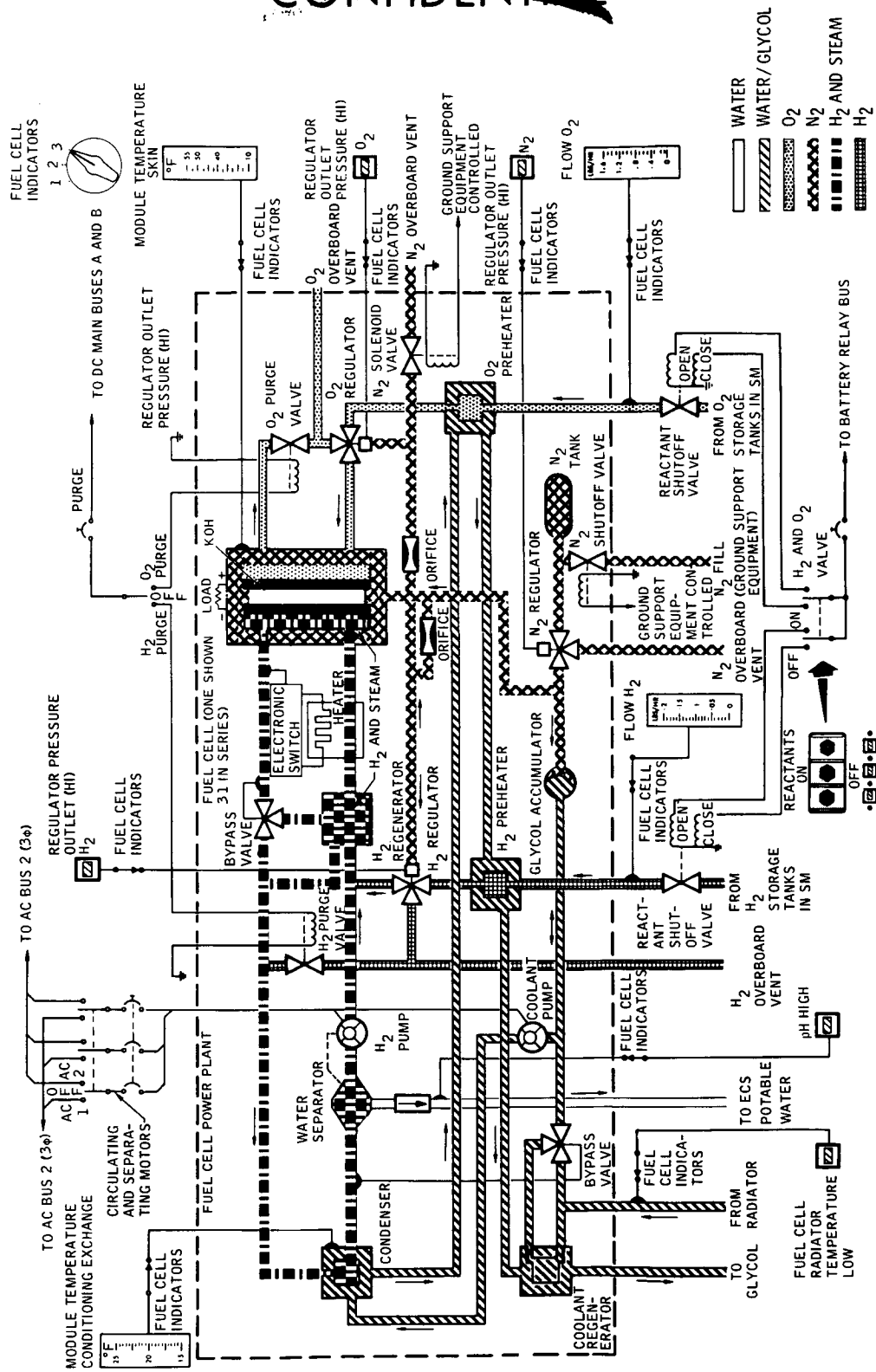
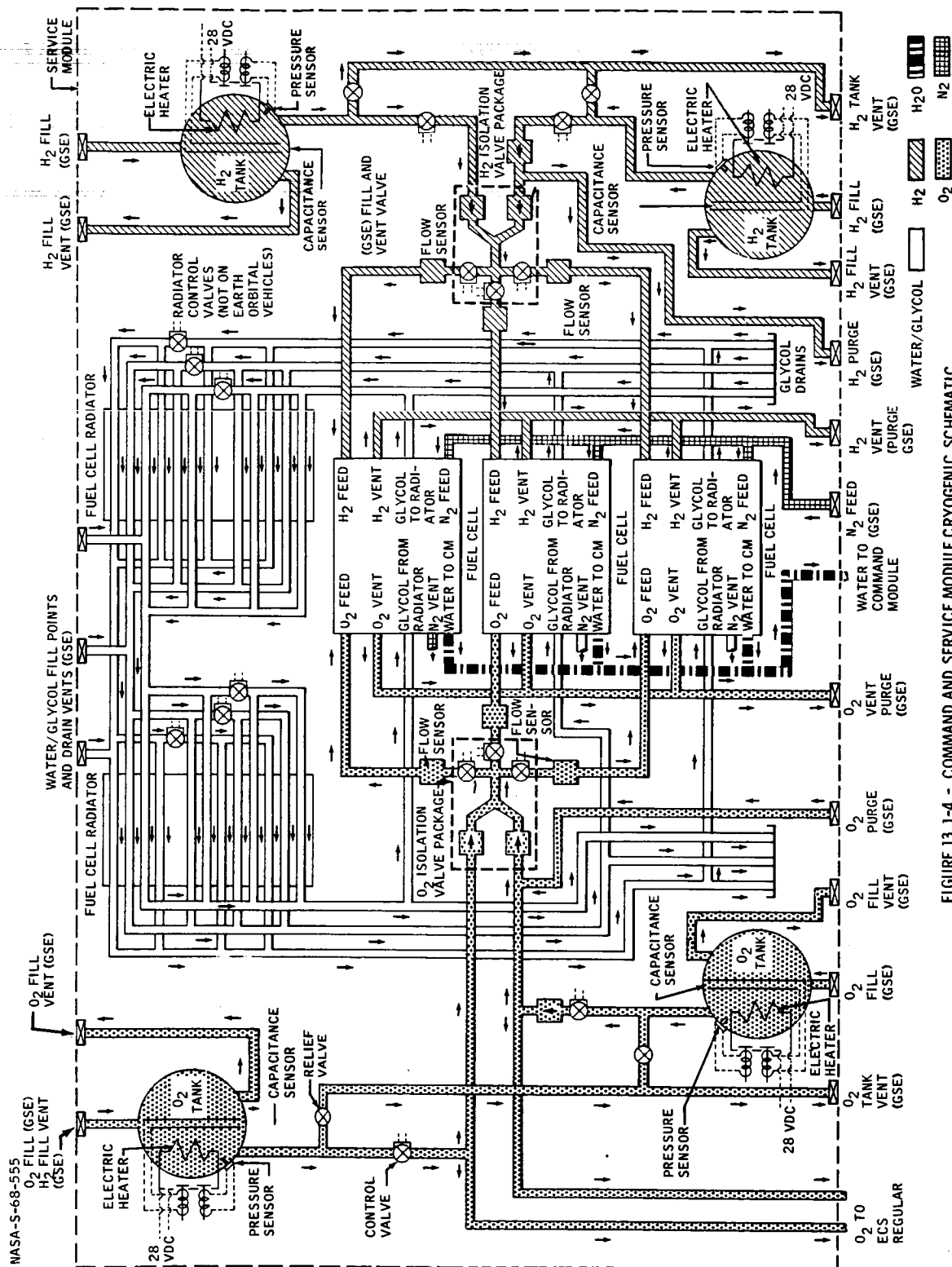


FIGURE 13.1-3. - FUEL CELL POWER PLANT FLOW DIAGRAM.

~~CONFIDENTIAL~~

FIGURE 13.1-4.- COMMAND AND SERVICE MODULE CRYOGENIC SCHEMATIC.





~~CONFIDENTIAL~~

NASA-S-68-556

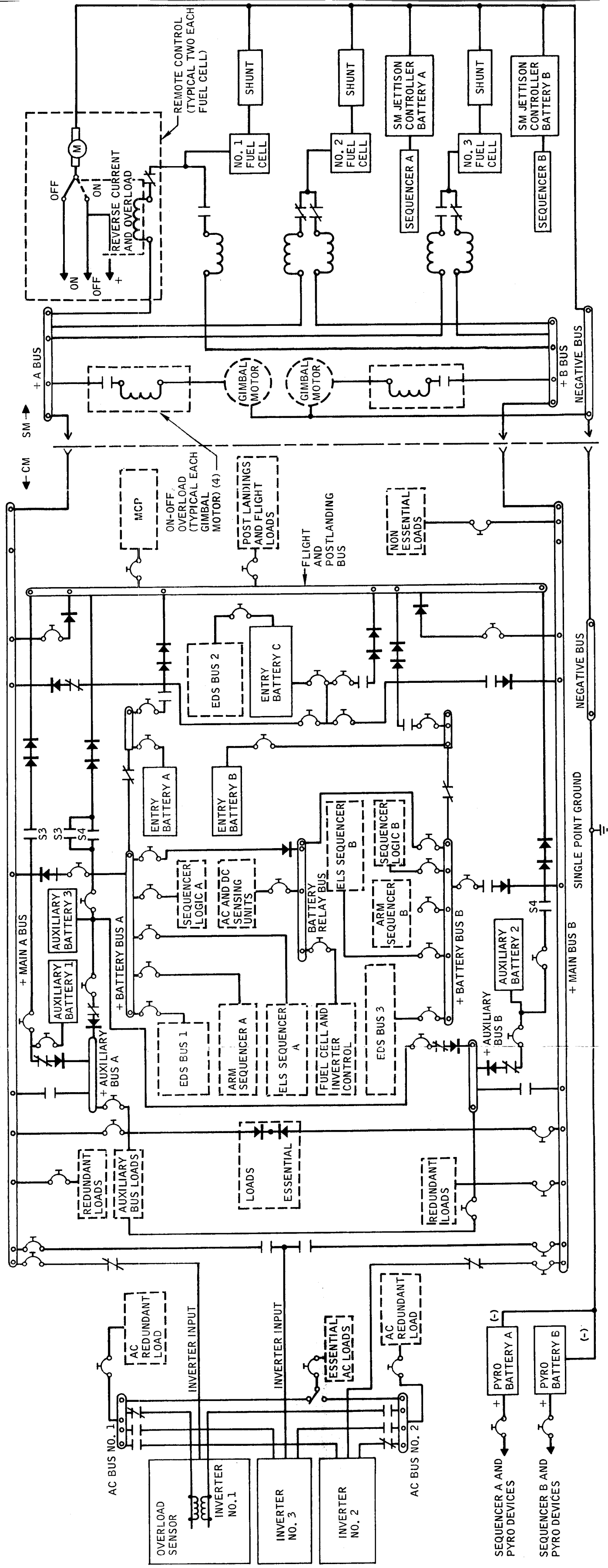
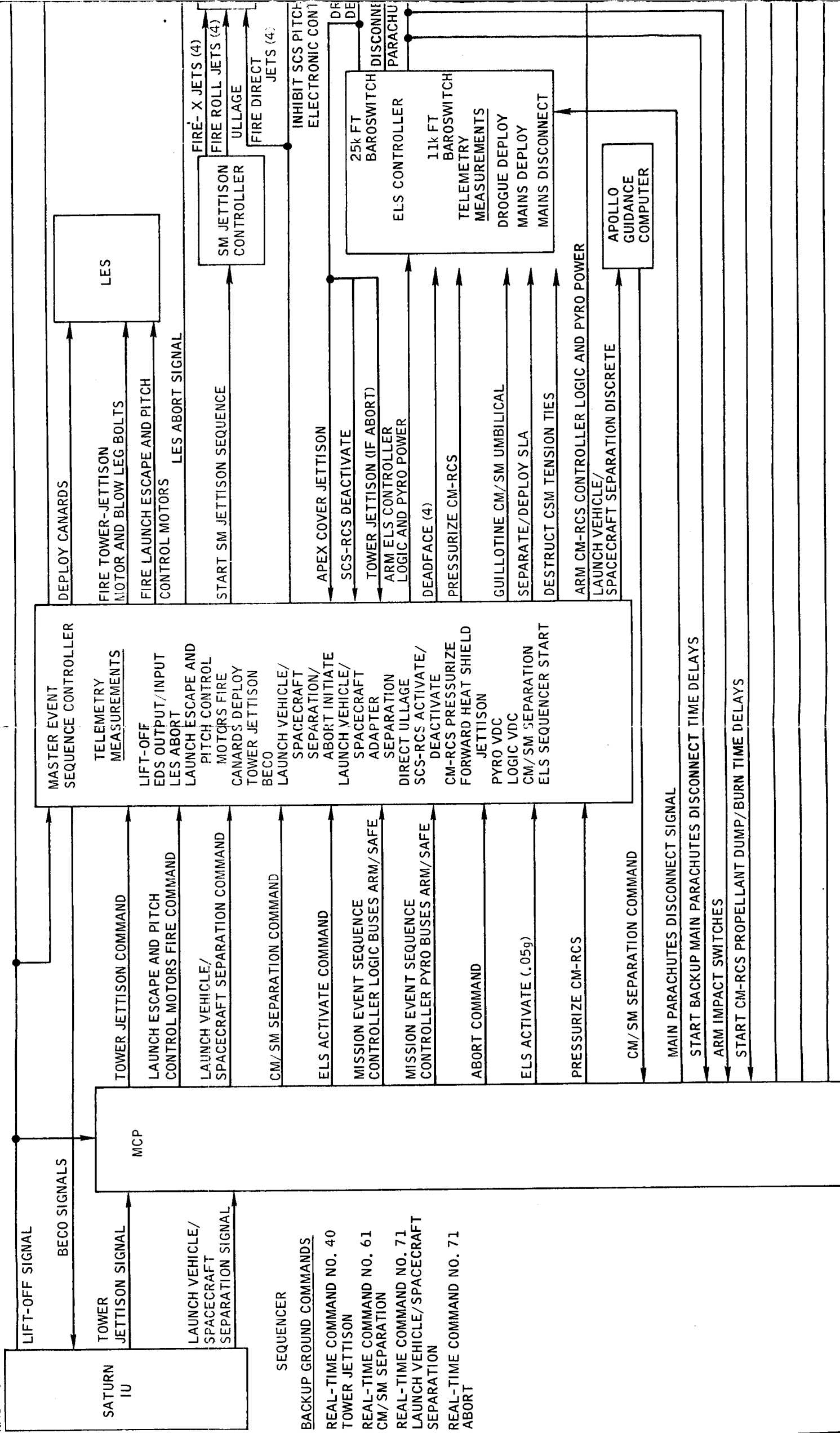


FIGURE 13.1-5.- ELECTRICAL POWER DISTRIBUTION SUBSYSTEM.

~~CONFIDENTIAL~~



Fold-out #1

~~CONFIDENTIAL~~

13-25

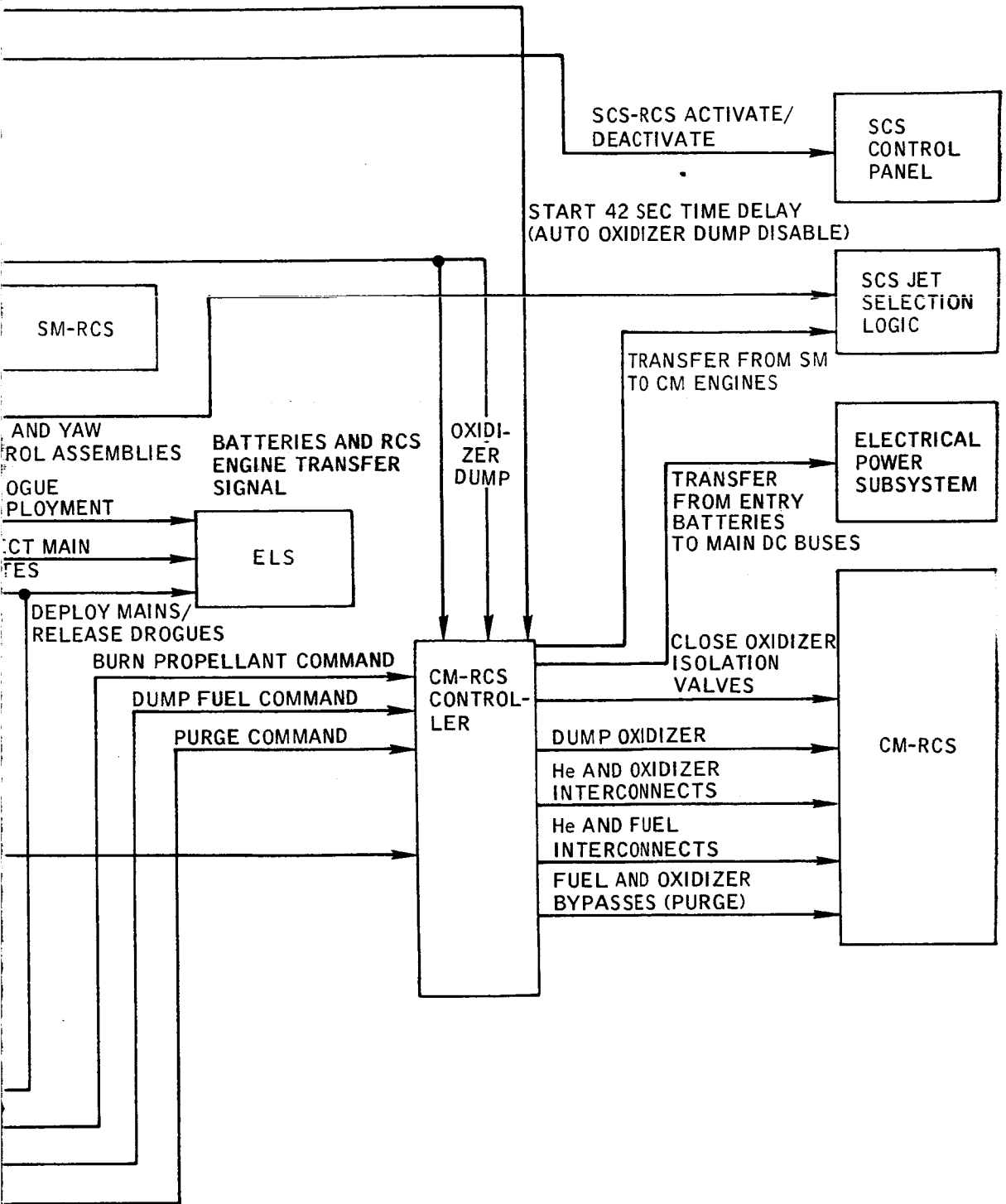


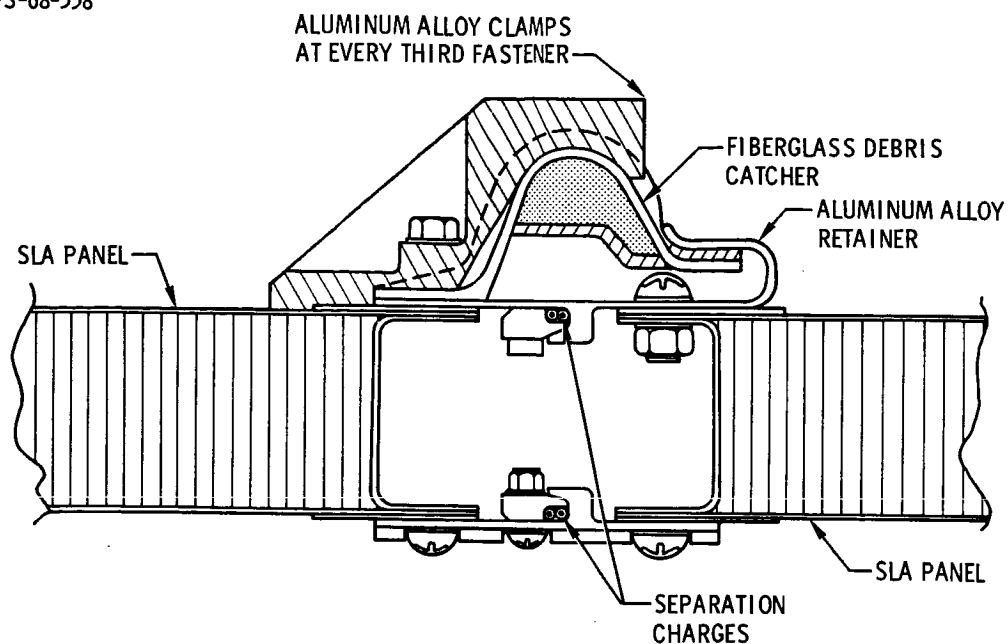
FIGURE 13.1-6.- SEQUENTIAL EVENTS CONTROL SUBSYSTEM  
FUNCTIONAL BLOCK DIAGRAM.

FOLD-OUT #2

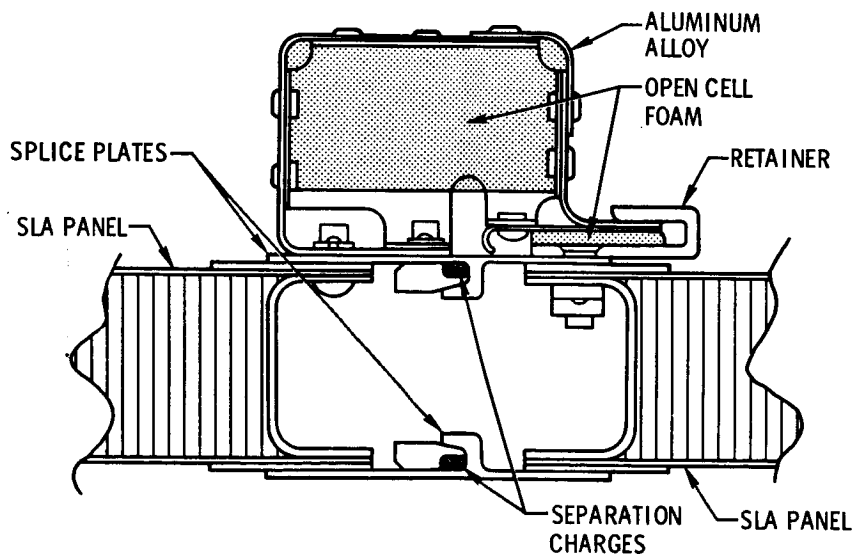
~~CONFIDENTIAL~~

~~CONFIDENTIAL~~

NASA-S-68-558



SPACECRAFT 011



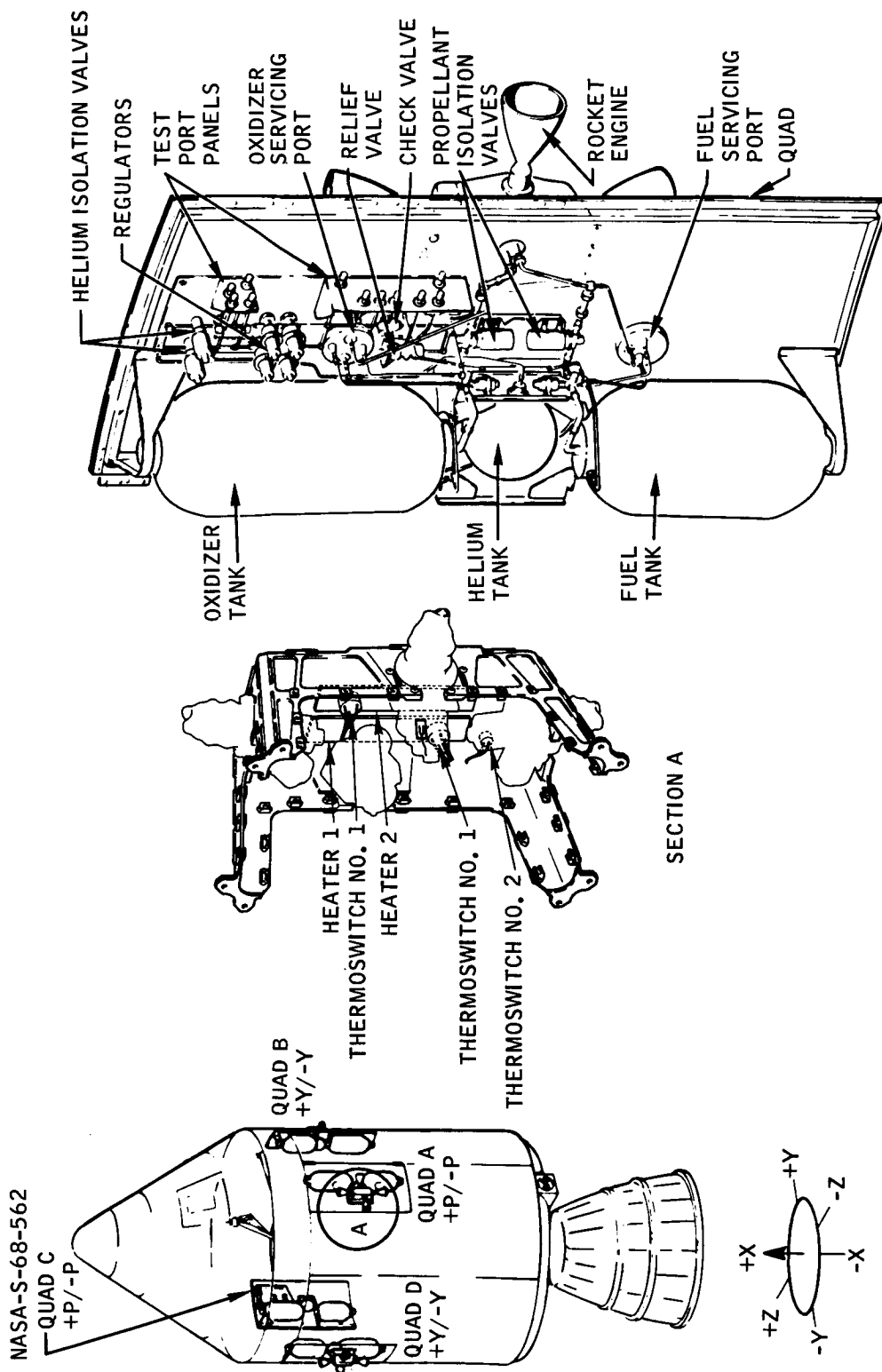
SPACECRAFT 017

FIGURE 13.1-7. - DEBRIS CATCHER CONFIGURATION ON SPACECRAFT LUNAR MODULE ADAPTER.

~~CONFIDENTIAL~~



~~CONFIDENTIAL~~



~~CONFIDENTIAL~~

FIGURE 13.1-11.- SERVICE MODULE REACTION CONTROL SUBSYSTEM COMPONENT LOCATION.

~~CONFIDENTIAL~~

13-31

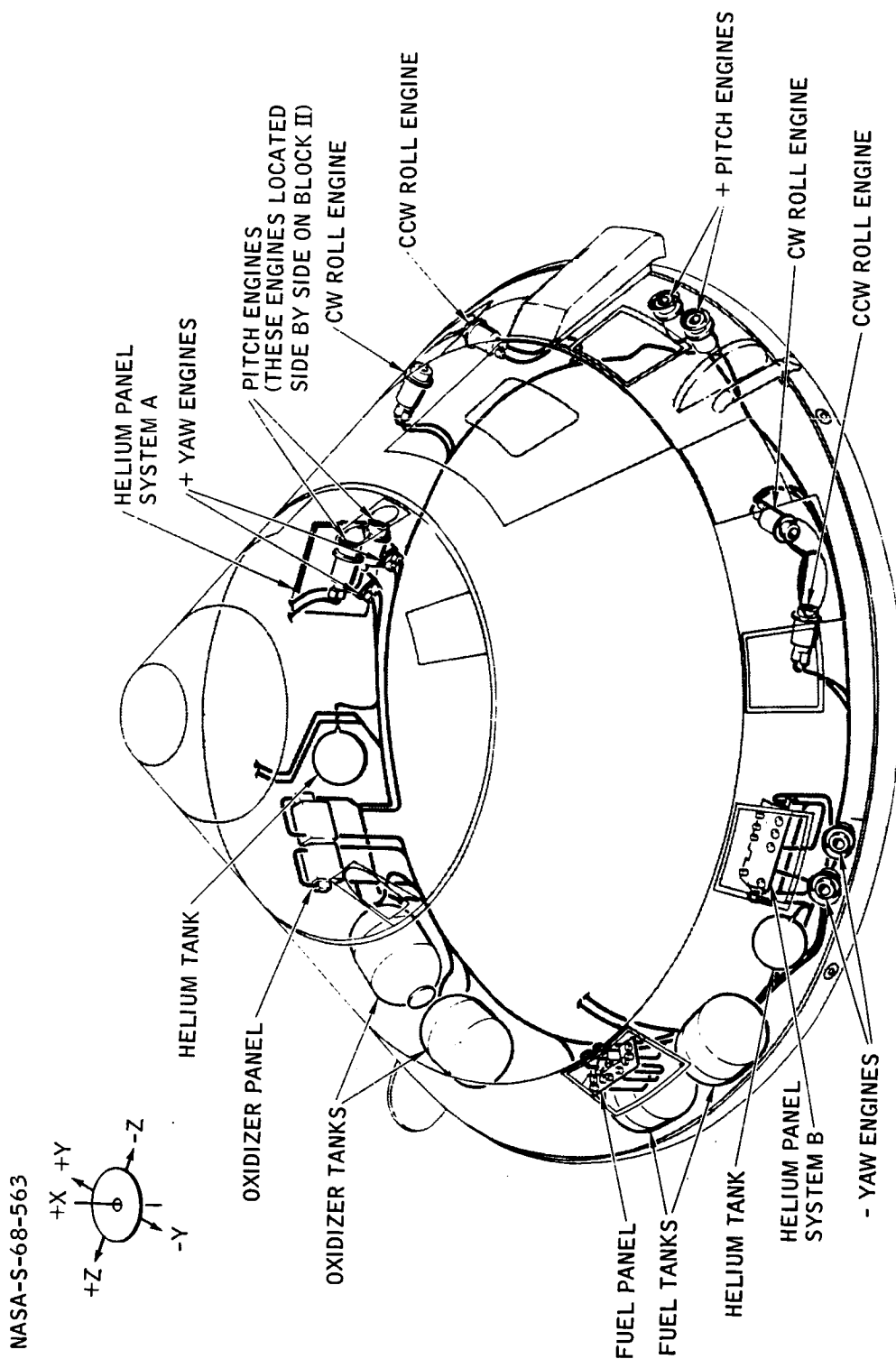


FIGURE 13.1-12. - COMMAND MODULE REACTION CONTROL SUBSYSTEM.

~~CONFIDENTIAL~~

~~CONFIDENTIAL~~

NASA-S-68-564

(P) PRESSURE  
(T) TEMPERATURE

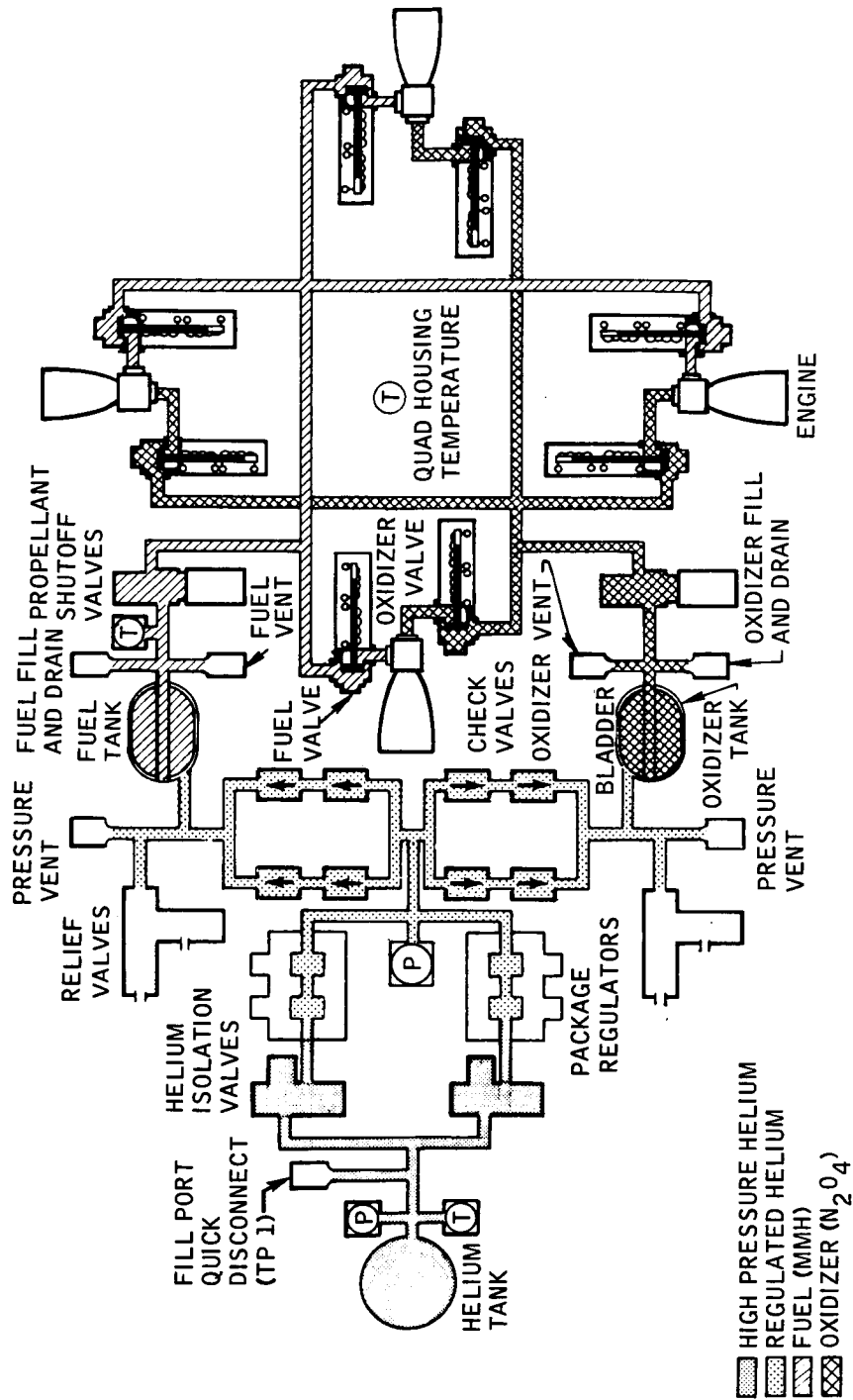


FIGURE 13.1-13.- SERVICE MODULE REACTION CONTROL SUBSYSTEM PROPELLANT FEED SUBSYSTEM.

~~CONFIDENTIAL~~



~~CONFIDENTIAL~~

NASA-S-68-565

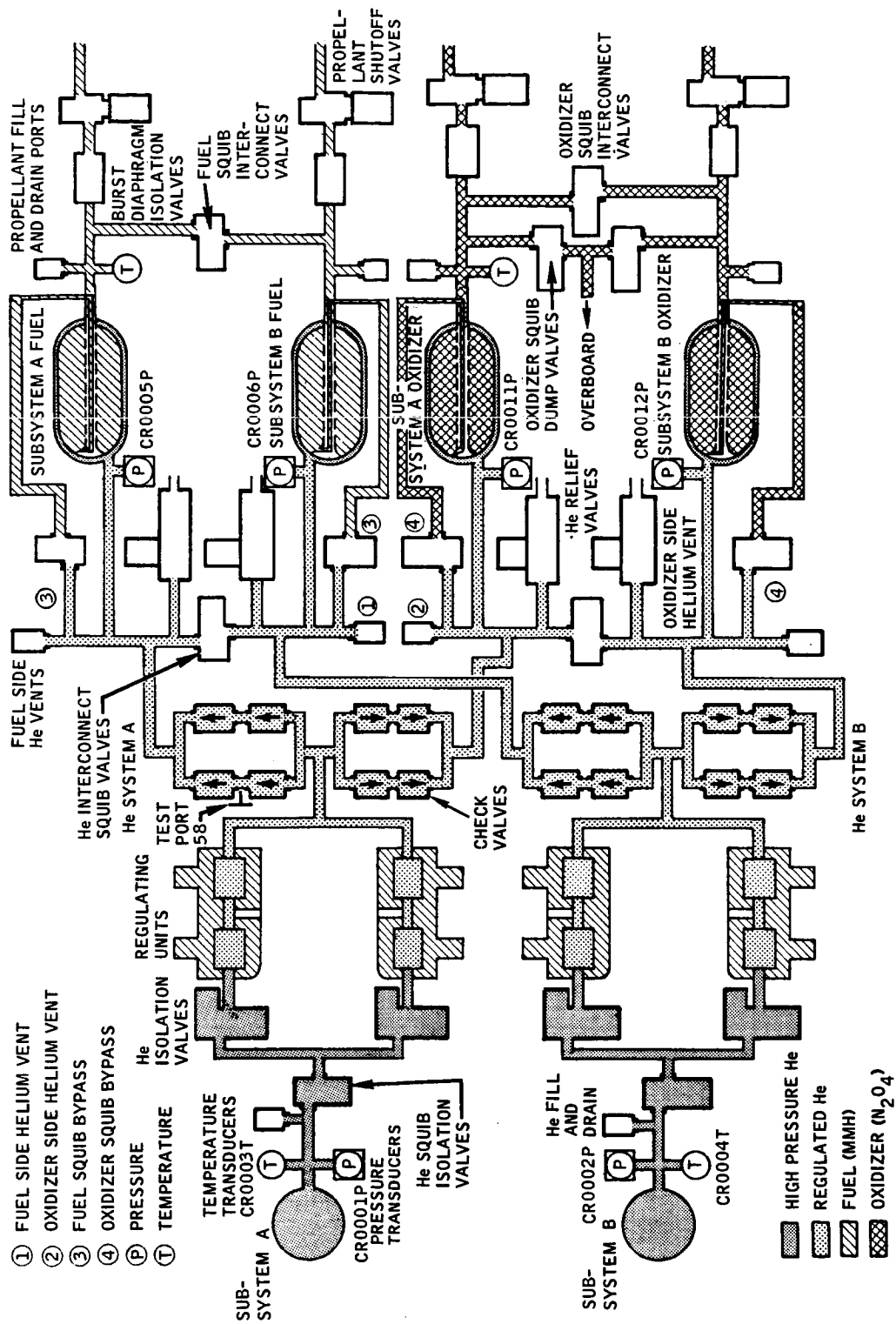


FIGURE 13.1-14 - COMMAND MODULE REACTION CONTROL SUBSYSTEM PROPELLANT DISTRIBUTION.

~~CONFIDENTIAL~~

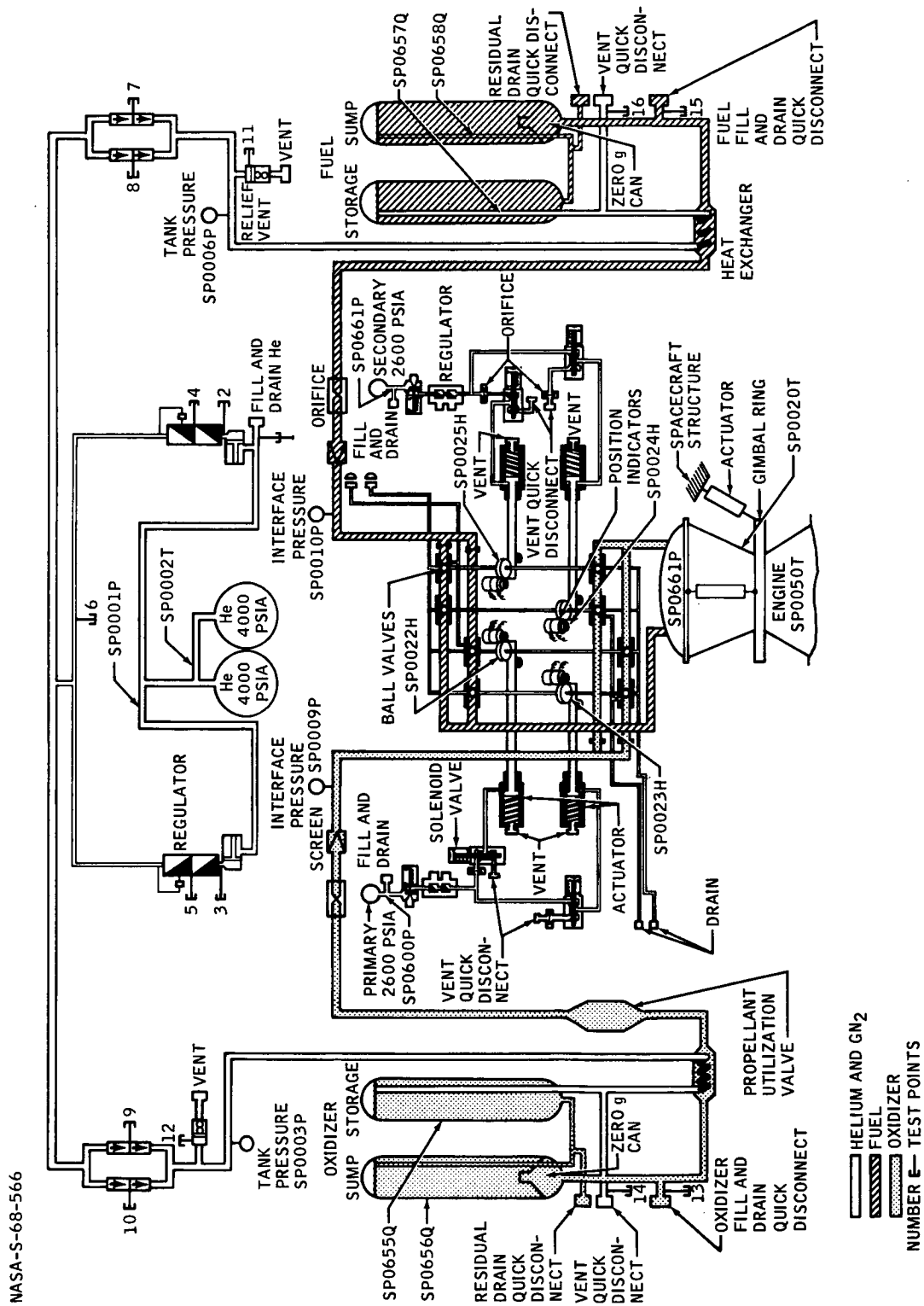
~~CONFIDENTIAL~~

FIGURE 13.1-15.- SERVICE PROPUSSION SUBSYSTEM FUNCTIONAL FLOW DIAGRAM.

~~CONFIDENTIAL~~

~~CONFIDENTIAL~~

13-35

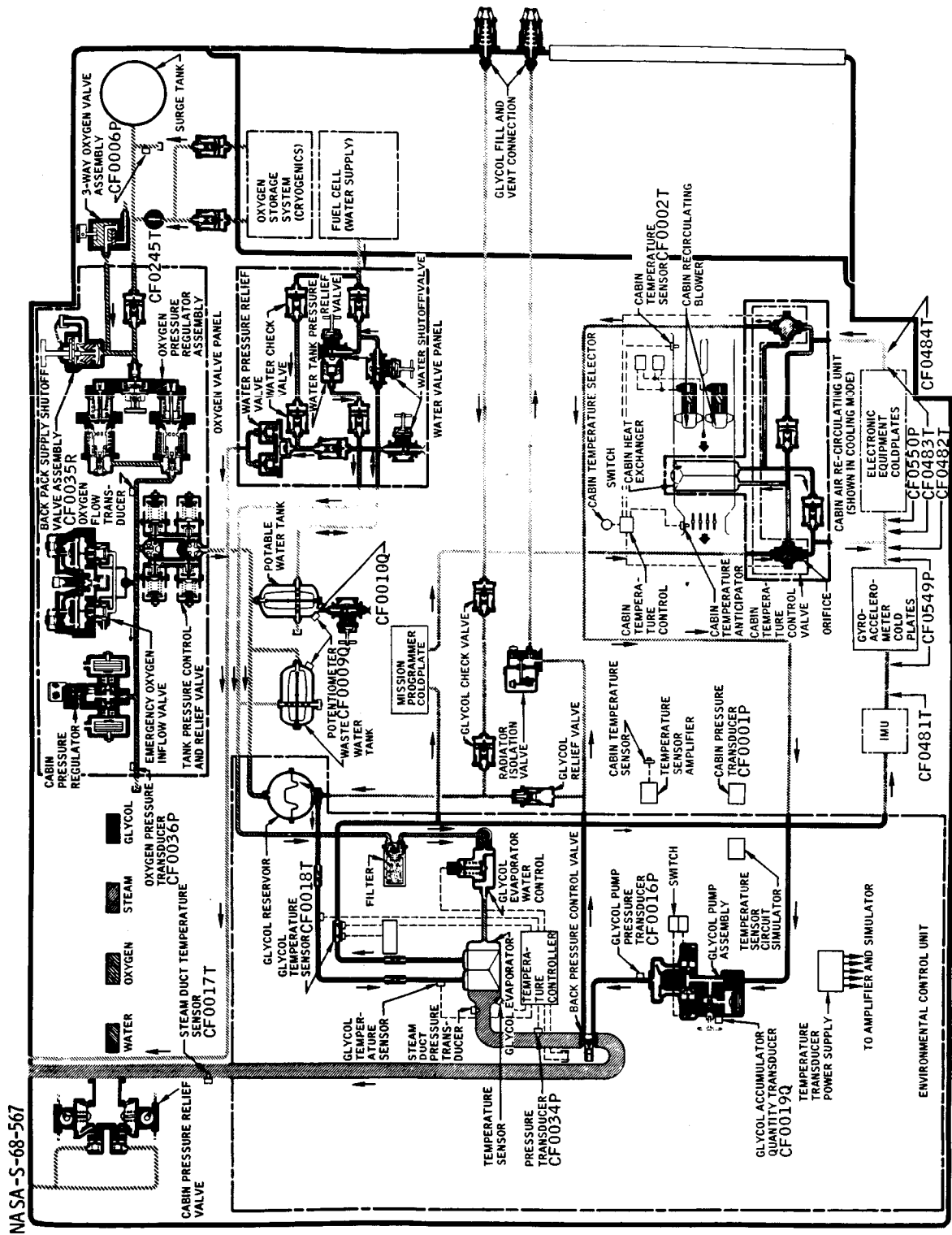
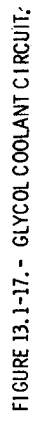


FIGURE 13.1-16. - ENVIRONMENTAL CONTROL SUBSYSTEM SCHEMATIC.

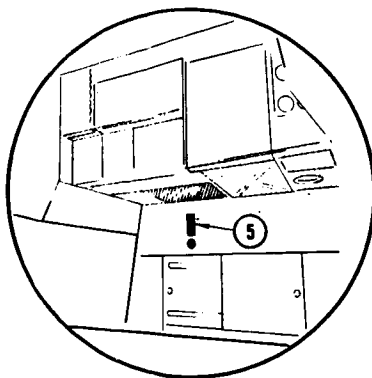
~~CONFIDENTIAL~~



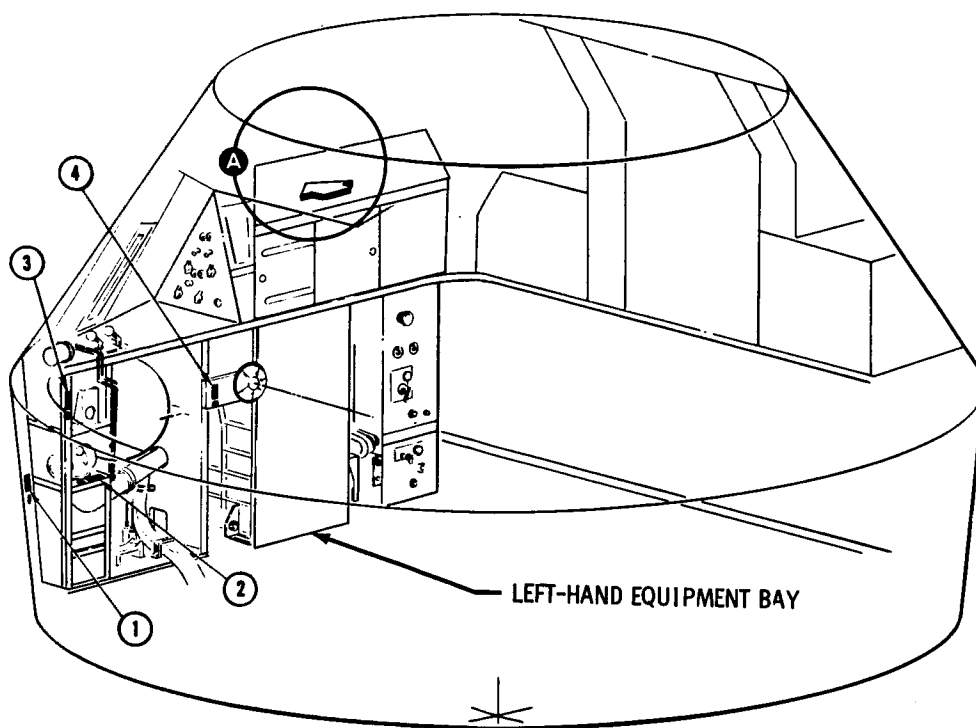
~~CONFIDENTIAL~~

13-37

NASA-S-68-569



VIEW A



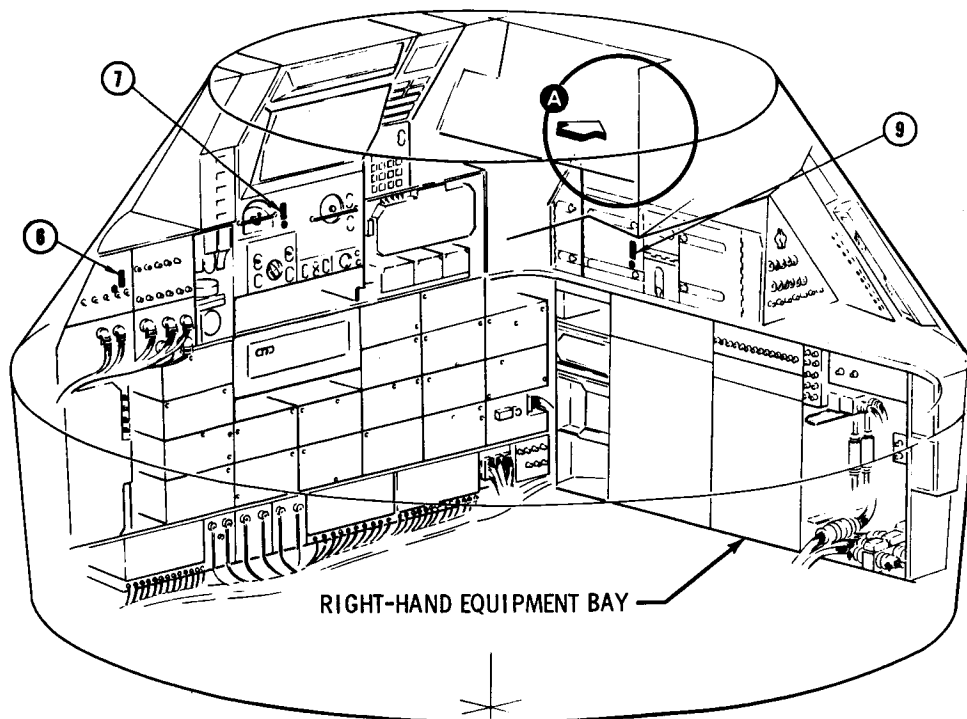
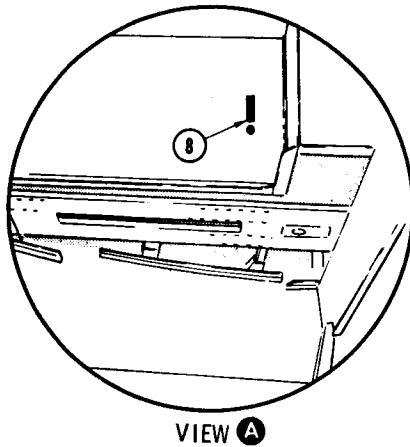
(A) TAPE LOCATIONS 1-5.

FIGURE 13.1-18. - VAPOR SENSITIVE TAPE LOCATIONS.

~~CONFIDENTIAL~~

~~CONFIDENTIAL~~

NASA-S-68-570



(B) TAPE LOCATIONS 6-9.

FIGURE 13.1-18. - CONTINUED.

~~CONFIDENTIAL~~

~~CONFIDENTIAL~~

13-39

NASA-S-68-571

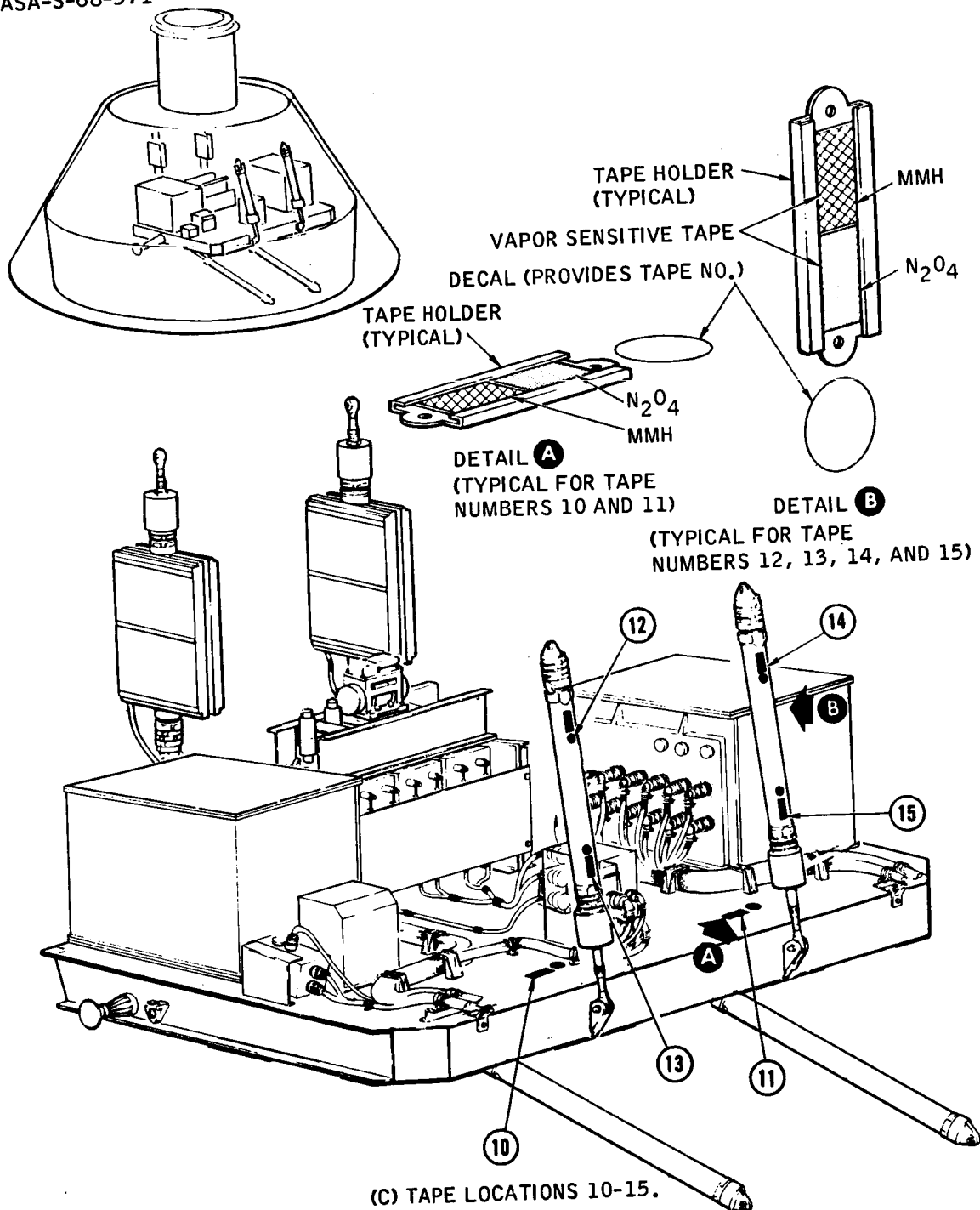


FIGURE 13.1-18.- CONCLUDED.

~~CONFIDENTIAL~~

~~CONFIDENTIAL~~

## 13.2 LUNAR MODULE TEST ARTICLE

## 13.2.1 General Description

The lunar module test article (LTA-10R) flown on the Apollo 4 mission consisted of a preproduction heavyweight descent stage and a mass representation of the ascent stage.

The descent stage (fig. 13.2-1) consisted of the basic cruciform structure, similar to LM-1; outriggers; propellant tanks; and a burned-out descent engine. The structural members were, in general, heavier than the normal lunar module (LM) structure. The propellant tanks, filled with deionized water to simulate propellant ballast, were fabricated of titanium and were of similar design to LM propellant tanks. The LTA-10R tanks were approximately 65 inches long and LM descent propellant tanks are approximately 70 inches long.

The LTA-10R ascent stage (fig. 13.2-2) consisted of an aluminum structural frame arranged to simulate the weight, center of gravity, and moment of inertia of the LM ascent stage. The ascent stage propellant tanks were represented by metal blocks arranged to simulate the desired mass properties and ballast was incorporated to represent the reaction control subsystem and aft equipment bay.

The test article was ballasted to 29 500 pounds. The center of gravity and moments of inertia approximated those of the LM. A development flight instrumentation package was mounted in the open quadrants of the descent stage. To satisfy cooling requirements, heat-sink mounting of portions of the development flight instrumentation (DFI) package were provided. Flight objectives required acquisition of data through the end of the first S-IVB stage burn.

## 13.2.2 Instrumentation and Communication

Two vhf telemetry antennas were supplied for the DFI as an integral part of the spacecraft/lunar module adapter and were mounted on heat sinks. The telemetry portion of the DFI package required passive cooling during prelaunch operations, and was, therefore, heat-sink mounted. Power for the package was provided by two 28 Vdc 9 A-hr batteries. The package provided 38 telemetered measurements consisting of five acceleration, nine vibration, 16 strain, six temperature, and two acoustical measurements.

~~CONFIDENTIAL~~



~~CONFIDENTIAL~~

13-41

NASA-S-68-572

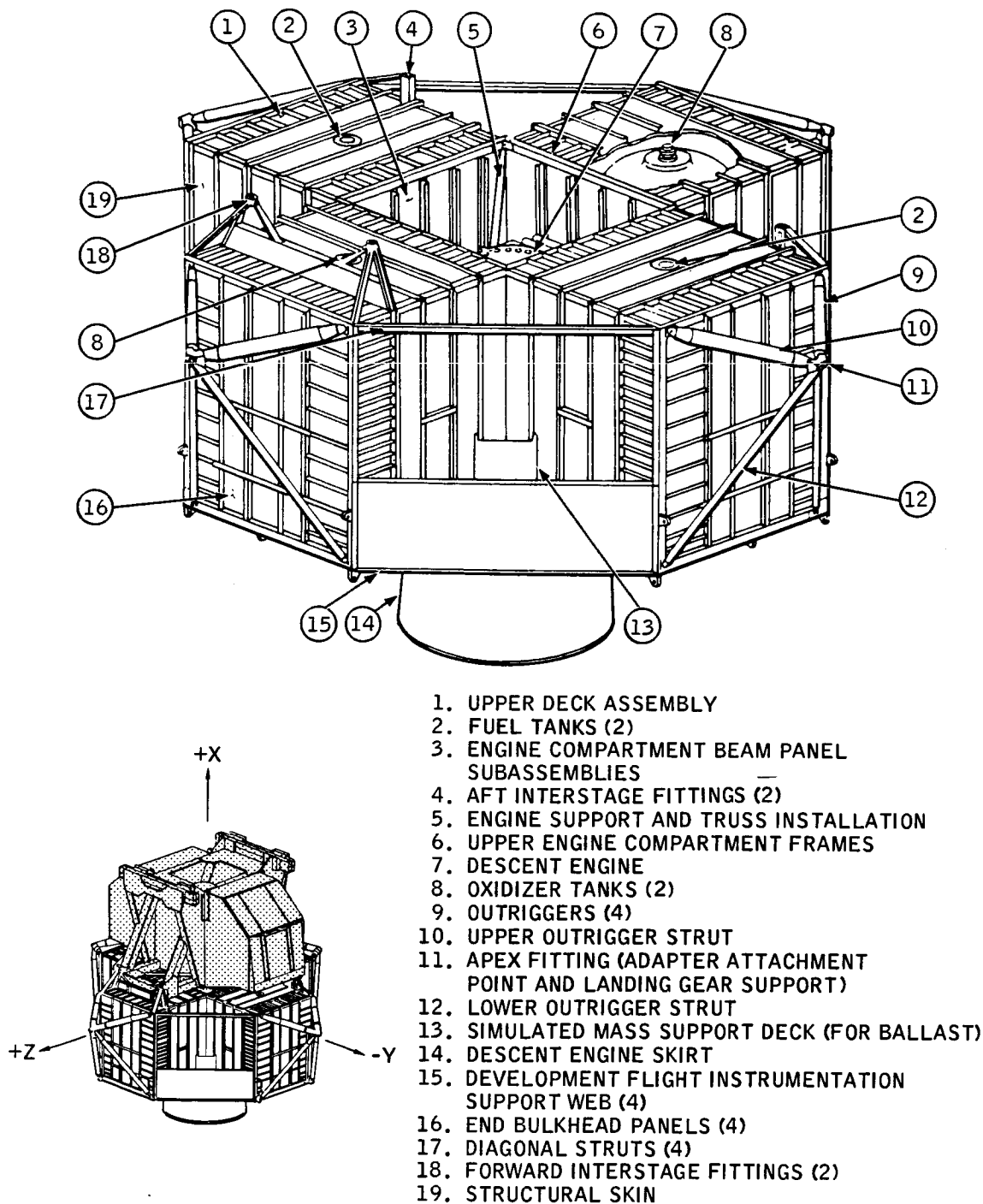


FIGURE 13.2-1.- LTA-10R, DESCENT STAGE.

~~CONFIDENTIAL~~

~~CONFIDENTIAL~~

NASA-S-68-573

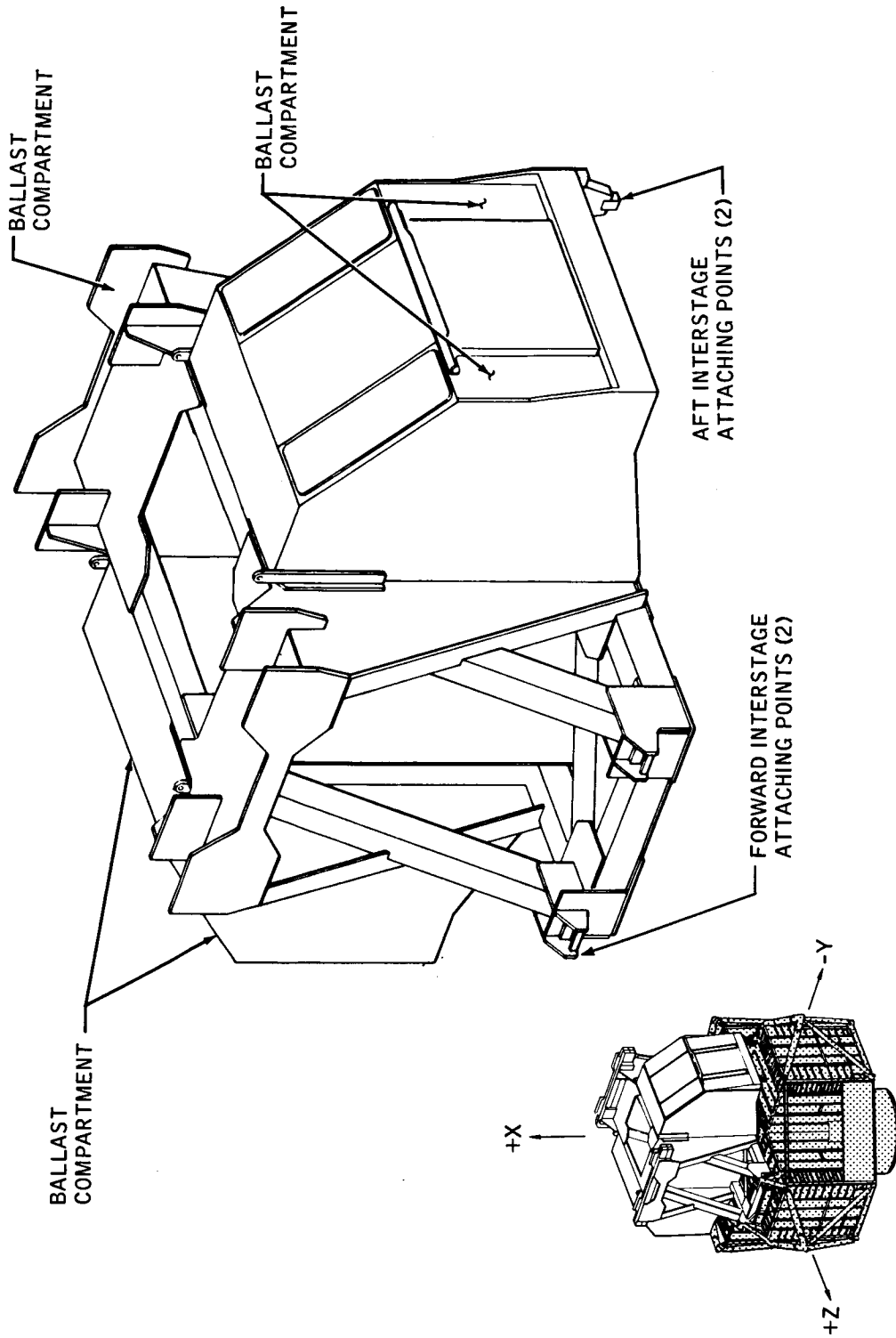


FIGURE 13.2-2.- LTA-10R, ASCENT STAGE.

~~CONFIDENTIAL~~

~~CONFIDENTIAL~~

13-43

### 13.3 LAUNCH VEHICLE DESCRIPTION

The Saturn V launch vehicle (fig. 13.3-1) consisted of three propulsive stages (S-IC, S-II, S-IVB) and an instrument unit.

The S-IC stage was approximately 138 feet long and 33 feet in diameter and had five liquid-fueled F-1 engines, which generated a total thrust of 7 500 000 pounds. The engines were supplied by a bi-propellant system of liquid oxygen (LOX) as the oxidizer and RP-1 as the fuel. The stage consisted of a thrust structure to which the engines were attached, an RP-1 fuel tank, a LOX tank, an intertank structure separating the LOX and fuel tanks, and a forward skirt structure which provided an interface surface for the S-II stage.

Each of the four outboard F-1 engines was gimbal-mounted on the stage thrust structure to provide engine thrust vectoring for vehicle attitude control and steering. Two hydraulic actuators are utilized to gimbal each engine in response to signals from the flight control computer located in the instrument unit.

The S-IC stage propellant system was composed of one LOX tank, one RP-1 tank, propellant lines, control valves, vents, and pressurization subsystems. Loading of the LOX and RP-1 tanks was controlled by ground computers. RP-1 loading was completed at a considerable time prior to start of LOX loading. LOX bubbling began and continued through the LOX tank loading to prevent possible LOX geysering. Approximately 90 seconds prior to ignition command, the RP-1 tank was pressurized from a ground source. Prior to start of automatic sequence and up to 72 seconds before lift-off, ground source helium was bubbled through the LOX lines and tank to prevent stratification in engine LOX suction lines. After lift-off the LOX tank pressurization was maintained by gaseous oxygen converted from LOX in the heat exchanger. The RP-1 tank was pressurized with helium stored in bottles in the LOX tank and heated by passing the helium through the heat exchanger.

The S-II stage structure included an aft interstage, an aft skirt and thrust structure, a heat shield, a LOX tank, a liquid hydrogen (LH<sub>2</sub>) tank, and a forward skirt. The stage had five J-2 engines which generated a total thrust of 1 000 000 pounds. The four outboard engines were gimbal-mounted to provide attitude control during powered flight. Attitude control was maintained by gimbaling one or more of the engines. Power for gimbaling was supplied by four independent engine-mounted hydraulic control systems. The S-II stage propellant system was composed of integral LOX/LH<sub>2</sub> tanks, propellant links, control valves, vents, and prepressurization subsystems. Loading of propellant tanks and flow of

~~CONFIDENTIAL~~

~~CONFIDENTIAL~~

propellants were controlled by the propellant utilization systems. The LOX/LH<sub>2</sub> tanks were prepressurized by ground source gaseous helium.

During powered flight of the S-II stage, the LOX tank was pressurized by gaseous oxygen bleed from the LOX heat exchanger. The LH<sub>2</sub> tank was pressurized by gaseous hydrogen bleed from the thrust chamber hydrogen injector manifolds. Pressurization was maintained by the LH<sub>2</sub> pressure regulator.

The propellant utilization system controlled loading and engine mixture ratios (LOX to LH<sub>2</sub>) to assure balanced consumption of LOX and LH<sub>2</sub> during flight. Capacitance probes mounted in the LOX and LH<sub>2</sub> containers monitored the mass of the propellants during powered flight. At propellant utilization system activation (5.5 seconds after J-2 ignition), the capacitance probes sensed the LOX to LH<sub>2</sub> imbalance and commanded the engine to burn at the high rate engine mixture ratio of 5.5:1. When the high mixture ratio was removed, the propellant utilization system then commanded the engine to burn the reference mixture ratio of 4.7:1, to achieve simultaneous depletion of LOX and LH<sub>2</sub> for maximum stage performance. Engine cutoff was initiated when any two of the five capacitance probes in either tank indicated dry.

The S-IVB stage structure consisted of an aft interstage, an aft skirt, a thrust structure, an LH<sub>2</sub> tank, a LOX tank, and a forward skirt. The single 200 000 pounds nominal thrust J-2 engine was gimbal mounted on the longitudinal axis of S-IVB stage. Power for gimbaling was supplied by a hydraulic control system mounted on the engine. Pitch and yaw control, during powered flight, was maintained by actuator control of the engine thrust vector. Roll control of the stage was maintained by properly sequencing the pulse-fired hypergolic propellant thrust motors in the auxiliary propulsion system (APS). When the stage enters the coast mode, the APS thrust motors control the stage in all three axes. The APS consisted of two self-contained attitude control modules mounted 180 degrees apart on the aft skirt of the S-IVB stage. Each attitude control module contained four thrust motors, which used hypergolic propellants — nitrogen tetroxide (N<sub>2</sub>O<sub>4</sub>) and monomethylhydrazine (MMH). The thrust motors were pulse-fired and no ignition system was required. Three thrust motors in each module provided pitch, yaw, and roll control during the S-IVB coast mode of operation, and roll control during S-IVB powered flight. An ullage engine was added to each module to settle propellants prior to engine restart.

The S-IVB stage propellant system was composed of integral LOX/LH<sub>2</sub> tanks, propellant lines, control valves, vents, and pressurization

~~CONFIDENTIAL~~

~~CONFIDENTIAL~~

13-45

subsystems. Loading of the propellant tanks and flow of propellants was controlled by the propellant utilization system. Both propellant tanks were initially pressurized by ground source cold helium. LOX tank pressurization during the S-IVB burns was maintained by helium supplied from spheres in the LH<sub>2</sub> tank; and expanded by passing through the helium heater. The helium maintained positive pressure across the common tank bulkhead and satisfied engine net positive suction head. The LH<sub>2</sub> pressurization strengthened the stage in addition to satisfying net positive suction head requirements. After engine ignition the pressure was maintained by gaseous hydrogen tapped from the engine supply.

The propellant utilization system monitored mass propellant loading and engine mixture ratios (LOX to LH<sub>2</sub>) to insure balanced consumption of LOX and LH<sub>2</sub>. Capacitance probes mounted in the LOX and LH<sub>2</sub> containers monitored the mass propellants during powered flight. At propellant utilization activation (6.3 seconds after first-time J-2 ignition and 5.0 seconds after second-time J-2 ignition) the capacitance probes sensed the LOX to LH<sub>2</sub> imbalance and commanded the engine to burn at the high rate engine mixture ratio of 5.5 to 1. When the high mixture ratio was removed, the propellant utilization system then commanded the engine to burn the reference mixture ratio of 4.7:1. The first and second cutoffs of the J-2 engine were velocity cutoffs initiated by a signal from the flight computer.

The instrument unit structure consisted of three arc segments (numbered 601, 602, and 603) of sandwiched honeycomb. The three arc segments were joined with splice plates bolted to the skin and the channel ring segments, thus forming a single unit of honeycomb construction. This construction formed an assembly 260 inches in diameter and 36 inches high. Brackets were bonded to the inner skin to provide mounting surfaces for 16 cold plates, which were 30 inches square. A coolant fluid was circulated through the cold plates to dissipate heat generated by the electrical components mounted on them.

Prior to vehicle launch, a temperature controlled atmosphere was forced from a ground source into the instrumentation unit and S-IVB forward skirt to maintain a temperature of 60° F to 80° F. Compressed air was used as a purging medium up to 30 minutes before the S-IVB stage was loaded with propellant, then the air purge was replaced with a nitrogen purge. The compartment purge was disconnected at vehicle lift-off by retraction of the instrument unit umbilical service arm.

~~CONFIDENTIAL~~

13-46

NASA-S-68-574

~~CONFIDENTIAL~~



FIGURE 13.3-1.- SATURN V LAUNCH VEHICLE  
WITH APOLLO SPACECRAFT 017.

~~CONFIDENTIAL~~

~~CONFIDENTIAL~~

13-47

#### 13.4 WEIGHT AND BALANCE DATA

The spacecraft mass properties for the Apollo 4 mission are summarized in tables 13.4-I and 13.4-II. These data represent the actual conditions as determined from postflight analyses of expendable loading and usage during the flight.

The weight and center of gravity were measured for each module prior to stacking. Inertia values were calculated for the actual weight data obtained. Mass properties of the ring retained with the service module following separation of the spacecraft lunar module adapter were calculated from the measured data. All engineering change activity subsequent to weight and center-of-gravity measurement prior to launch was monitored and the spacecraft mass properties were revised as required.

The spacecraft mass properties at launch (table 13.4-I) did not vary significantly from the predicted values used for the operational trajectory calculations. The final mission trajectory data were based on spacecraft mass properties which were adjusted for all changes including actual expendables loading.

The command module (CM) mass properties during the entry phase are shown in table 13.4-II; the usage of expendable materials is based on postflight data. Center-of-gravity data are calculated for significant phases of the entry to facilitate correlation with aerodynamic data.

The CM center of gravity considered in the operational trajectory calculations was equivalent to a predicted nominal lift-to-drag ratio of 0.355 at entry. Aerodynamic uncertainties, alignment tolerances, and center-of-gravity uncertainties resulted in tolerances of +0.066 and -0.028, applicable to the nominal ratio. The absolute minimum lift-to-drag ratio limitation of 0.30 was based on the guidance system performance capability and the requirement to assure attached flow on the windward side of the command module. The absolute maximum of 0.430 was based on thermal system capability. Prelaunch data adjusted for an excess of approximately 9 pounds of reaction control subsystem propellant indicated a nominal lift-to-drag ratio of 0.358. Application of the +0.066 lift-to-drag tolerance resulted in a maximum possible lift-to-drag ratio of 0.424. To provide additional margin as compared to the maximum lift-to-drag limit of 0.43, a container of simulated LiOH canisters was removed from the CM crew compartment. The spacecraft mass properties were adjusted for this change and final prelaunch data were provided to the flight controllers. The resultant entry lift-to-drag ratio was predicted to be 0.350.

~~CONFIDENTIAL~~

~~CONFIDENTIAL~~

Table 13.4-II shows the lift-to-drag ratios as determined by the center-of-gravity data based on postflight analysis of loading and utilization of expendable material. The data are consistent with final launch predictions and variations during the entry phase and are well within the established tolerances and limitations.

~~CONFIDENTIAL~~



~~CONFIDENTIAL~~

13-49

TABLE 13.4-I.- SPACECRAFT MASS PROPERTIES AT LAUNCH AND DURING ORBITAL FLIGHT

Launch	Weight, lb	Center of gravity, in.			Moment of inertia, slug-ft <sup>2</sup>		
		X	Y	Z	I <sub>xx</sub>	I <sub>yy</sub>	I <sub>zz</sub>
CM	11 985.9	1039.5	0.3	6.8	6 035	5 532	4 687
SM	9 536.6	912.1	-0.2	0.8	6 461	10 811	10 453
SPS propellant	30 068.0	901.6	14.8	-6.3	14 012	18 274	22 537
Lunar module (LTA-LOR)	29 500.0	587.3	0.1	0.0	19 183	21 005	21 450
Spacecraft lunar module adapter (SLA)	3 880.5	644.1	0.6	-2.1	9 704	13 515	13 377
Launch escape system	8 710.1	1303.1	0.0	0.6	666	24 883	24 870
Total spacecraft at launch	93 681.1	848.0	4.8	-1.1	57 368	1 072 230	1 076 114
Less: Launch escape system	-8 710.1	1303.1	0.0	0.6	666	24 883	24 870
Circular Orbit Insertion							
Total spacecraft at insertion	84 971.0	801.4	5.3	-1.3	56 651	618 476	622 335
Less: SLA	-3 789.5	639.5	0.6	-2.1	9 591	12 709	12 573
LTA-LOR	-29 500.0	587.3	0.1	0.0	19 183	21 005	21 450
Cryogenics - Hydrogen tank no. 1	-0.2	933.9	42.4	-42.4	0	0	0
Hydrogen tank no. 2	-0.2	858.4	42.4	-42.4	0	0	0
Oxygen tank no. 1	-5.0	971.5	23.0	-29.7	0	0	0
Oxygen tank no. 2	-3.8	896.0	23.0	-29.7	0	0	0

~~CONFIDENTIAL~~

TABLE 13.4-I.- SPACECRAFT MASS PROPERTIES AT LAUNCH AND DURING ORBITAL FLIGHT - Continued

Weight, lb	Center of gravity, in.			Moment of inertia, slug-ft <sup>2</sup>		
	X	Y	Z	I <sub>xx</sub>	I <sub>yy</sub>	I <sub>zz</sub>
SM-RCS propellant	959.0	0.0	0.0	0	0	0
Waste water	1022.6	-19.7	62.5	0	0	0
Plus: Potable water	1022.6	-63.5	-16.4	0	0	0
<u>Elliptical Orbit Insertion</u>						
Total spacecraft at insertion	935.4	8.6	-2.0	27 589	71 816	75 075
Less: SM-RCS propellant	959.0	0.0	0.0	0	0	0
Total spacecraft - Prior to first SPS burn	935.4	8.6	-2.0	27 562	71 744	75 000
Less: SPS propellant	880.1	-28.3	8.7	863	378	782
Cryogenics - Hydrogen tank no. 1	933.9	42.4	-42.4	0	0	0
Hydrogen tank no. 2	858.4	42.4	-42.4	0	0	0
Oxygen tank no. 1	971.5	23.0	-29.7	0	0	0
Oxygen tank no. 2	896.0	23.0	-29.7	0	0	0
SM-RCS propellant	959.0	0.0	0.0	0	0	0
Waste water	1022.6	-19.7	62.5	0	0	0

~~CONFIDENTIAL~~~~CONFIDENTIAL~~



~~CONFIDENTIAL~~

TABLE 13.4-II.- COMMAND MODULE MASS PROPERTIES AT ENTRY

	Weight, lb	Center of gravity, in.			Moment of inertia, slug-ft <sup>2</sup>		
		X	Y	Z	I <sub>xx</sub>	I <sub>yy</sub>	I <sub>zz</sub>
Command module at launch	11 985.9	1039.49	0.3	6.80	6 035	5 532	4 687
Less: Waste water	-43.4	1022.6	-19.7	62.5	0	0	0
Plus: Potable water	+16.4	1022.6	-63.5	-16.4	0	0	0
CM/SM at separation	11 958.9	1039.53	0.3	6.57	6 017	5 515	4 673
Less: RCS propellant	-10.0	1022.6	-5.6	57.0	2	0	2
Command module at entry (0.5g)	11 948.9	1039.54	0.3	6.52	(Lift-to-drag = 0.353)		
Less: RCS propellant	-8.0	1022.6	-5.6	57.0			
Command module at first peak g	11 940.9	1039.55	0.3	6.49	(Lift-to-drag = 0.350)		
Less: RCS propellant	-7.0	1022.6	-5.6	57.0			
Command module at up- control	11 933.9	1039.56	0.3	6.44	(Lift-to-drag = 0.349)		
Less: RCS propellant	-2.0	1022.6	-5.6	57.0			
Waste water	-0.5	1022.6	-19.7	62.5			
Command module at final entry	11 931.4	1039.57	0.3	6.45	(Lift-to-drag = 0.347)		
Less: RCS propellant	-12.5	1022.6	-5.6	57.0			
Waste water	0.5	1022.6	-19.7	62.5			
Command module at sec- ond peak g	11 918.4	1039.59	0.3	6.39	(Lift-to-drag = 0.343)		
Less: RCS propellant	-51.5	1022.6	-5.6	57.0			
Ablator burn- off	-261.0	1011.6	0.0	6.7			
Forward heat shield	-423.0	1011.7	-0.4	0.4			
Drogue	-63.0	1090.3	0.0	-20.9			
Waste water	-0.5	1022.6	-19.7	62.5			

~~CONFIDENTIAL~~

~~CONFIDENTIAL~~

13-53

TABLE 13.4-II.- COMMAND MODULE MASS PROPERTIES AT ENTRY - Concluded

	Weight, lb	Center of gravity, in.			Moment of inertia, slug-ft <sup>2</sup>		
		X	Y	Z	I <sub>xx</sub>	I <sub>yy</sub>	I <sub>zz</sub>
Command module at main parachute deploy Less: RCS propellant Main parachutes Waste water	11 119.4	1037.71	0.4	6.53			
	-152.8	1022.6	-5.6	57.0			
	-424.0	1090.5	-0.8	6.4			
	-2.0	1022.6	-19.7	62.5			
Command module at land- ing	10 540.6	1035.81	0.5	5.80			

~~CONFIDENTIAL~~

~~CONFIDENTIAL~~

THIS PAGE INTENTIONALLY LEFT BLANK

~~CONFIDENTIAL~~

~~CONFIDENTIAL~~

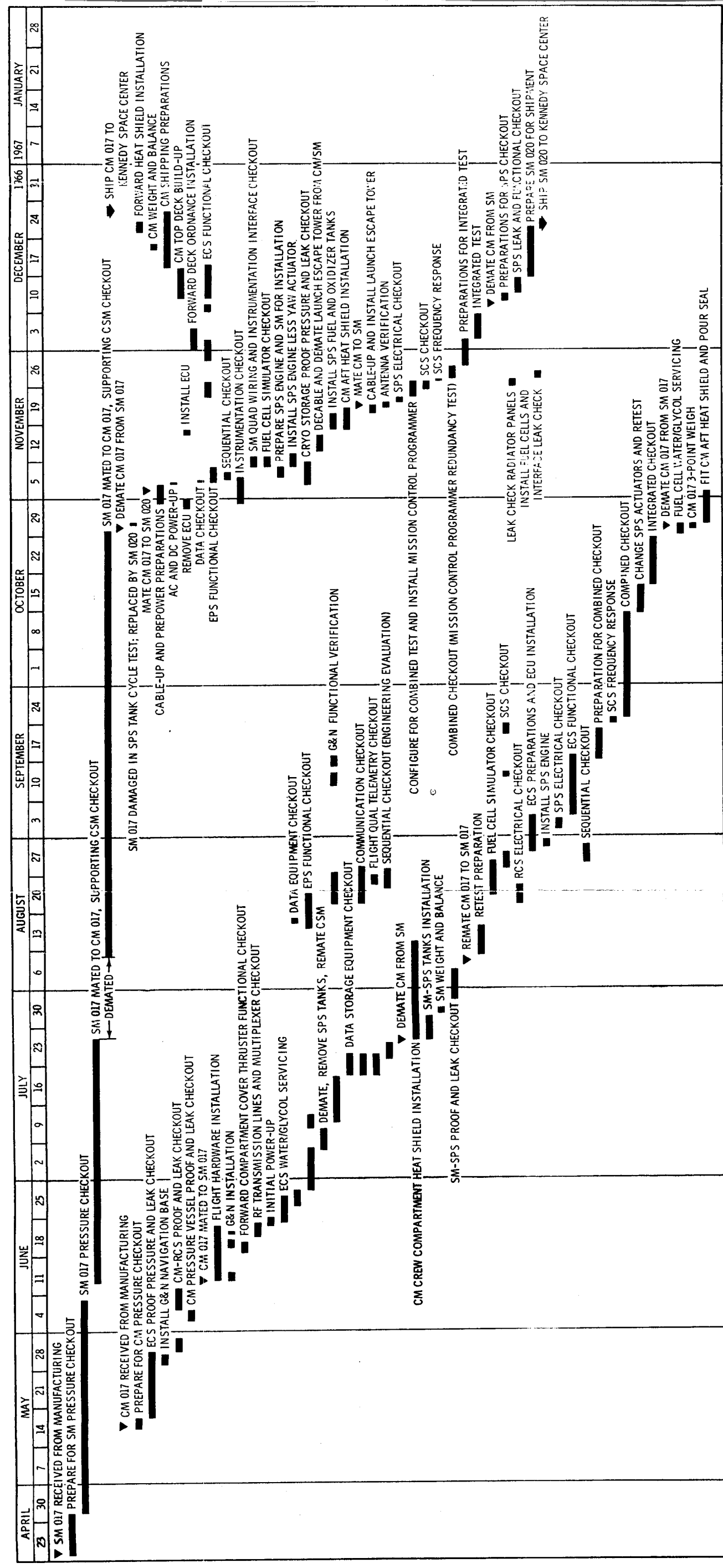
14-1

#### 14.0 SPACECRAFT HISTORIES

##### 14.1 COMMAND MODULE AND SERVICE MODULE

The factory checkout flow history of the command module and service module (Spacecraft 017) at the contractor's facility in Downey, California, is shown in figure 14.1-1. The prelaunch checkout flow history of Spacecraft 017 at Kennedy Space Center, Florida, is shown in figure 14.1-2.

~~CONFIDENTIAL~~





~~CONFIDENTIAL~~

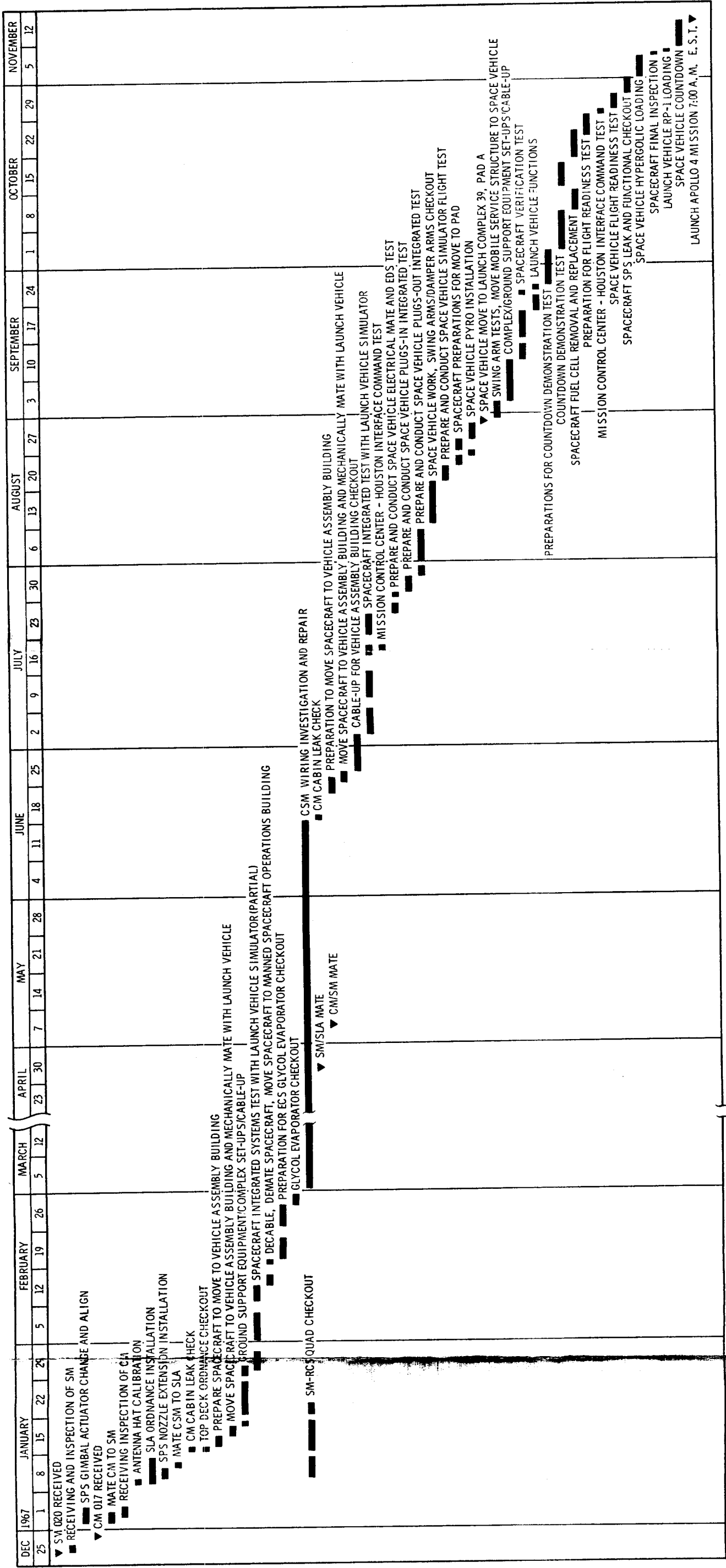


FIGURE 14. 1-2. - PRELAUNCH CHECKOUT FLOW FOR COMMAND AND SERVICE MODULE AT KENNEDY SPACE CENTER.

~~CONFIDENTIAL~~

~~CONFIDENTIAL~~

## 14.2 LUNAR MODULE TEST ARTICLE

The factory refurbishment, modification, and checkout flow history of the lunar module test article (LTA-10R) at the contractor's facility at Bethpage, New York, is shown in figure 14.2-1. The prelaunch checkout flow history of LTA-10R at Kennedy Space Center, Florida, is shown in figure 14.2-2.

~~CONFIDENTIAL~~



~~CONFIDENTIAL~~

THIS PAGE INTENTIONALLY LEFT BLANK

~~CONFIDENTIAL~~

~~CONFIDENTIAL~~

15-1

15.0 REFERENCES

1. Marshall Space Flight Center: Apollo 4 Mission Report. (This report has not yet been released; therefore, no report number can be cited, and the title may not be correct.)
2. Hillje, Ernest R.: Entry Flight Aerodynamics from Apollo Mission AS 202. NASA TN D-4185, August 1967.
3. Anon.: U.S. Standard Atmosphere Supplements, 1966. COESA, 1966.
4. Manned Spacecraft Center: Postlaunch Report for Mission AS 202 MSC-A-R-66-5, October 1966.
5. North American Aviation, Inc.: RCS Deactivation Procedures Handbook for NASA Landing Safing Team. SID 66-1893, 1966.

~~CONFIDENTIAL~~

~~CONFIDENTIAL~~

THIS PAGE INTENTIONALLY LEFT BLANK

~~CONFIDENTIAL~~

~~CONFIDENTIAL~~

16-1

16.0 DISTRIBUTION

<u>Addressee</u>	<u>Number of copies</u>
National Aeronautics and Space Administration Washington, D. C. 20546	
M/G. E. Mueller	1
MA/S. C. Phillips	1
MA/G. H. Hage	1
MA/L. B. James	1
MAO/J. K. Holcomb	1
MAP/Program Control Director	1
MAR/G. C. White	1
MAT/L. Day	1
MAT-1/W. A. Summerfelt	1
MAT-2/M. Behun	1
MAT-4/I. Davids	1
MAT-1/E. F. Mollenberg	1
MAT-1/W. A. Lucas	1
MC/MSF Field Center Development Director	1
MD/E. Cortright	1
ML/C. W. Mathews	1
MLT/M. Savage	1
MT/Advance Manned Missions Program Director	2
R/M.C. Adams	1
S/J. E. Naugle	1
T/E. C. Buckley	1
USS-10/NASA Headquarters Library	2
National Aeronautics and Space Administration Manned Spacecraft Center Houston, Texas 77058	
Office of Director	
Attention: AA/R. R. Gilruth	1
AB/G. S. Trimble	1
AC/P. E. Purser	1
AG/D. Collins	1
Legal Office	
Attention: AL3/M. F. Matthews	1
Public Affairs Office	
Attention: AP/P. Haney	1
AP/J. Riley	1

~~CONFIDENTIAL~~

~~CONFIDENTIAL~~

<u>Addressee</u>	<u>Number of copies</u>
AP6/Historical Office	1
AP8/Mission Planning and Operations Office	1
Director of Administration	
Attention: BA/W. L. Hjernevik	2
BF6/Reproduction Services Branch	1
BF66/Distribution Operation Section	90
BM4/Security Branch	1
BM5/Technical Information Preparation Branch	4
BM6/Library Processes Office	16
Director of Flight Crew Operations	
Attention: CA/D. K. Slayton	1
CB/Chief, Astronaut Office	4
CF/Chief, Flight Crew Support Division	8
Director of Medical Research and Operations	
Attention: DA/C. A. Berry, M.D.	4
DB/Chief, Biomedical Research Office	2
DD/Chief, Medical Operations Office	1
Director of Engineering and Development	
Attention: EA/M. A. Faget	5
EB/Chief, Information Systems Division	15
EC/Chief, Crew Systems Division	6
ED/Chief, Computation and Analysis Division	4
EE/Chief, Instrumentation and Electronic Systems Division	9
EG/Chief, Guidance and Control Division	7
EP/Chief, Propulsion and Power Division	12
ES/Chief, Structures and Mechanics Division	15
ET/Chief, Advanced Spacecraft Technology Division	3

~~CONFIDENTIAL~~



~~CONFIDENTIAL~~

16-3

<u>Addressee</u>	<u>Number of copies</u>
Director of Flight Operations	
Attention: FA/C. C. Kraft, Jr.	1
FC/Chief, Flight Control Division	7
FL/Chief, Landing and Recovery Division	5
FM/Chief, Mission Planning and Analysis Division	4
FL/Chief, Flight Support Division	3
Apollo Applications Program Office	
Attention: KA/R. F. Thompson	1
KA/J. E. Roberts/W. B. Mitchell	1
KF/Manager, Future Missions Project Office	1
KM/Manager, Mission Operations Office	2
KP/Manager, Program Control Office	1
KS/Manager, Systems Engineering Office	1
KT/Manager, Test Operations Office	1
KW/Manager, Orbital Workshop Project Office	1
Reliability and Quality Assurance Office	
Attention: NA/A. C. Bond	1
Apollo Spacecraft Program Office	
Office of Program Manager	
Attention: PA/G. M. Low	1
PA/E. F. M. Rees	1
PA/K. S. Kleinknecht	1
PA/C. H. Bolender	1
PA/S. H. Simpkinson	1
PA/J. T. Markley	1
PA/G. W. S. Abbey	1
PA/H. W. Tindall	1
PA/Apollo Files	1
PD/Chief, Systems Engineering Division	14
PE/Chief, LM Project Engineering Division	3
PF/Chief, C & SM Project Engineering Division	3

~~CONFIDENTIAL~~

~~CONFIDENTIAL~~

<u>Addressee</u>	<u>Number of copies</u>
PT/Chief, Test Division	27
PP/Chief, Program Control Division	3
NASA-RASPO Grumman Aircraft Engineering Corporation Bethpage, New York 11714 Attention: PB/J. H. Johansen	2
NASA-RASPO North American Rockwell Corporation 12214 Lakewood Blvd. Downey, California 90241 Attention: PC/W. H. Gray	13
Flight Safety Office Attention: SA/A. C. Bond	10
Director of Science and Applications Attention: TA/W. C. Hess	1
TD/Manager, Lunar Surface Project Office	1
TF/Manager, Test and Operations Office	2
TG/Chief, Space Physics Division	1
ASPO Assistant Manager, KSC Kennedy Space Center, Florida Attention: PSK/W. J. Kapryan	2
Goddard Space Flight Center Liaison Office, GSF-L Attention: GSF-L/W. B. Easter	1 1
Marshall Space Flight Center Resident Liaison Office Attention: RL/J. T. Hamilton	1
Langley Research Center Liaison Office Attention: RAA/A. T. Mattson	1
NASA Ames Research Center Moffett Field, California 94035 Attention: G. Goodwin	1
H. J. Allen	1
Ames Research Center Library	6

~~CONFIDENTIAL~~

~~CONFIDENTIAL~~

16-5

<u>Addressee</u>	<u>Number of copies</u>
Eastern Test Range	
Patrick Air Force Base, Florida	
Attention: Major General V. G. Huston	1
Colonel R. Olson, DOD Manager	1
 NASA Electronics Research Center	
565 Technology Square	
Cambridge, Massachusetts 02139	
Attention: J. C. Elms	1
 NASA Flight Research Center	1
Post Office Box 273	
Edwards, California 93523	
Attention: P. F. Bikle	1
 NASA Goddard Space Flight Center	
Greenbelt, Maryland 20771	
Attention: DIR/John F. Clark	1
506/M. F. Thompson	1
506/W. P. Varson	1
550/T. Roberts	1
Goddard Space Flight Center Library	3
 John F. Kennedy Space Center, NASA	
NASA Kennedy Space Center, Florida 32899	
Attention: AP/R. O. Middleton	1
AP-SCO/S. T. Beddingfield	1
AT-SCO/H. E. McCoy	1
CD/Dr. K. H. Debus	1
DE/G. M. Preston	1
IN/K. Sandler	1
LO/R. A. Petrone	1
LS/J. J. Williams	1
LS/A. M. Busch	1
LS-ENG/G. T. Sasseen	1
IS-CAS-42/John F. Kennedy Space Center	
Library	6

~~CONFIDENTIAL~~

~~CONFIDENTIAL~~

<u>Addressee</u>	<u>Number of copies</u>
NASA Lewis Research Center 2100 Brookpark Road Cleveland, Ohio 44135 Attention: Director	1
Lewis Research Center Library	6
NASA George C. Marshall Space Flight Center Huntsville, Alabama 35812 Attention: M-Dir/W. von Braun	1
I-MO/F. A. Speer	1
R-Aero-F/J. P. Lindberg	6
Marshall Space Flight Center Library	6
NASA MSC White Sands Missile Range Office of the Manager P. O. Drawer MM Las Cruces, New Mexico 88001 Attention: RA/M. L. Raines	5
NASA-RASPO Massachusetts Institute of Technology 75 Cambridge Parkway Cambridge, Massachusetts 02142 Attention: EG442/A. C. Metzger	2
Massachusetts Institute of Technology 75 Cambridge Parkway Cambridge, Massachusetts 02142 Attention: D. C. Hoag	3
NASA-RASPO AC Electronics Division Milwaukee, Wisconsin 53200 Attention: EG443/W. Swingle	1
AC Electronics Division, General Motors Corporation Milwaukee, Wisconsin 53200 Attention: H. Brady	3
Arnold Engineering Development Center Arnold Air Force Station, Tennessee 37389 Attention: General Gossick	1

~~CONFIDENTIAL~~

~~CONFIDENTIAL~~

16-7

<u>Addressee</u>	<u>Number of copies</u>
Bellcomm Inc. 1100 17th Street NW Washington, D.C. Attention: Information Systems Analysis Department Head	1
Grumman Aircraft Engineering Corporation Bethpage, New York 11714 Attention: J. G. Gavin, Jr.	25
Grumman Aircraft Engineering Corporation Kennedy Space Center, Florida Attention: G. M. Skurla	5
Grumman Aircraft Engineering Corporation 1740 NASA Boulevard Houston, Texas 77058 Attention: J. M. Buxton	1
TRW, Incorporated Space Park Drive Houston, Texas 77058 Attention: H1-2058/A. Rosenbloom	6
Jet Propulsion Laboratory Pasadena, California Attention: DIR/W. H. Pickering	1
North American Rockwell Corporation 12214 Lakewood Blvd. Downey, California 90240 Attention: D. D. Myers	30
North American Rockwell Corporation Kennedy Space Center, Florida Attention: B. Hello	10
North American Rockwell Corporation 1840 NASA Boulevard Suite 201 Houston, Texas 77058 Attention: W. T. Short	3

~~CONFIDENTIAL~~

~~CONFIDENTIAL~~

<u>Addressee</u>	<u>Number of copies</u>
The Boeing Company Space Division-Houston P. O. Box 58747 Houston, Texas 77058 Attention: W. R. Andrews	10
General Electric Company 1830 NASA Boulevard P. O. Box 58408 Houston, Texas 77058 Attention: L. W. Warzecha	10

~~CONFIDENTIAL~~